University of Southampton

Faculty of Environmental and Life Sciences

School of Biological Sciences

Molecular characterization of rice GTG/GPHR reveals a conserved role as an anion channel that regulates endomembrane pH

by

Tania Garcia Becerra

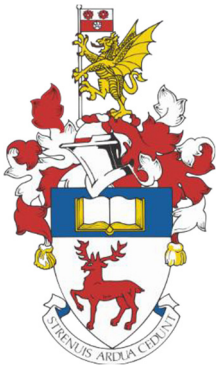

Thesis for the degree of Doctor of Philosophy

September 2020

University of Southampton

Abstract

Faculty of Environmental and Life Sciences

School of Biological Sciences

Thesis for the degree of Doctor of Philosophy

Molecular characterization of GTG/GPHR reveals a conserved role as an anion channel that regulates endomembrane pH

Tania Garcia Becerra

Membrane proteins mediate processes that are fundamental for the survival of the organism. Expanding the knowledge of how those membrane proteins function in the cell will allow us to improve crop survival and seed yield that is critical for future food security. G protein-coupled receptor type-G proteins (GTGs)/Golgi pH regulator proteins (GPHRs) are a conserved family of membrane proteins in eukaryotes, which are yet to be fully characterized. In mammalian cells they are described as anion channels regulating Golgi pH (Maeda et al., 2008), whereas in plants GTGs have been shown to interact with the Gα subunit of G proteins and have been described as plasma membrane abscisic acid receptors (in *Arabidopsis*) or as cold receptors (in rice) (Pandey et al., 2009; Ma et al., 2015). This study determines whether there is a conserved physiological function for GTGs in plants through the analysis of rice and Arabidopsis GTGs.

Arabidopsis contains two GTGs, and the deletion of both genes generates defects in growth, development and fertility (Jaffé et al., 2012). A functional complementation approach demonstrated that rice GTG rescued the defects seen in root length, biomass, hypocotyl growth, cell shape and ER body number in the Arabidopsis *gtg1gtg2* double mutant. This and the observation that rice GTG (OsGTG), like Arabidopsis GTG1, localises to the endoplasmic reticulum (ER) and Golgi, supports a conserved function for these proteins. OsGTG restored the increased pH observed in the ER and Golgi of the *gtg1gtg2* Arabidopsis mutant to wild-type levels, indicating that OsGTG is also able to regulate pH at the endomembrane system. Similar to the Arabidopsis *gtg1gtg2* mutant, knocking out *OsGTG* in rice led to several developmental defects, including

increased tiller number, delayed senescence and reduced grain production. Recombinant OsGTG synthesised using a cell-free expression system and incorporated into a planar lipid bilayer, displayed single-channel events that were inhibited by the anion channel blocker, DIDS.

The interaction between GTGs with the Gα subunit was also explored. Although no evidence for protein-protein interaction was found using BiFC, a *gtg1gtg2gpa1.4* triple mutant showed reduced hypocotyl growth and open cotyledons in the dark, and a reduced plant height in normal conditions, in comparison with WT, *gtg1gtg2* and *gpa1.4* mutants, suggesting a genetic interaction under particular conditions. The results of this thesis indicate that GTG/GPHRs have a conserved function across plant species as anion channels that regulate endomembrane pH. This thesis contributes to extend the knowledge of plant physiology by the characterization of this family of membrane proteins from its fundamental to its physiological role in the cell.

Table of Contents

Table of Tables

Table of Figures

Research Thesis: Declaration of Authorship

Print name: Tania Garcia Becerra

Title of thesis: Molecular characterization of rice GTG/GPHR reveals a conserved role as an anion channel that regulates endomembrane pH

I declare that this thesis and the work presented in it are my own and has been generated by me as the result of my own original research.

I confirm that:

1. This work was done wholly or mainly while in candidature for a research degree at this University;
2. Where any part of this thesis has previously been submitted for a degree or any other qualification at this University or any other institution, this has been clearly stated;
3. Where I have consulted the published work of others, this is always clearly attributed;
4. Where I have quoted from the work of others, the source is always given. With the exception of such quotations, this thesis is entirely my own work;
5. I have acknowledged all main sources of help;
6. Where the thesis is based on work done by myself jointly with others, I have made clear exactly what was done by others and what I have contributed myself;
7. None of this work has been published before submission

Signature: Date:

Acknowledgements

I would like to thank my supervisors Lorraine E. Williams and Matthew J. Terry for giving me this opportunity and for their knowledge and constant support and guidance. A special thanks to Lorraine to always be there, ready to help and guide me throughout this journey. Thank you to the Gerald Kerkut Charitable Trust for funding my thesis and allowing me to achieve this goal. I would like to thank Dr. Maurits de Planque for his help with the planar lipid bilayer assays. Thank you also to Chris Hawe for the ManI-RFP *cis* Golgi marker and John Runions for the ST-RFP and LT16b-mOrange.

A big thank you to all past and present LEW and MJT lab members. Thanks to Emily, Adam, Nick, Zul, Nancy, Franz, Roohi, Becca, David, Przemek, Matthew, Ellie, Ben, Mike and Sylwia to made me feel welcomed when I joined the lab and for all the help during this time. In special I would like to say thank you to Ilectra, for your friendship in and out the lab, what would I have done without you? Thanks to Kate and Jess, for the laughs and for making this experience more enjoyable. To the people of building 85 and specially the level 6 (Roberto, Felipe, Maria, Marcela, Marc, Ollie, Manal, Asia, Evelyn, Fabrizia, Connor, Billy, Suzie and Jasmine), to make all these years less hard and funnier. I also appreciated the help received by the technical team of building 85 (Mike, Dave, Marilyn, Karen, Rachael, Ben and Mark), and specially by Mark Dixon, thanks for your help, everything would have been much harder without you here.

I really want to thank my friends to keep me mentally healthy and to be always there, in the good and bad times. To Ilectra, George and Aragorn, thanks for everything, the friendship, chats, dinners, parties... To 'La family', Emilio, Maria, Laura, Mimi, Edu, Rocío, Elena, Mª Elena, Míriam and Inma, thank you to always be ready to meet when I went back home. To 'Los super-riquis', Bea, Juanma, Victor, Paula, George, Zaida, Andrea, Juanan, Fotis, Cecilia and Patri, I loved our meetings in Spain and around Europe.

Muchísimas gracias a toda mi familia, en especial a mi hermana, mi padre y mi madre que siempre me han apoyado y animado a seguir y a mejorar como persona. Esta tesis va dedicada a ella. Y al que más le debo agradecer es a Joan, por quererme, por aguantarme todos los días, por hacerme reír y por aceptarme tal y como soy. Sin ti no hubiera sido lo mismo. Deseando de ver lo que nos depara el futuro!

Definitions and Abbreviations

Abbreviations

°C	Degrees Celsius
A	Adenine
ABA	Abscisic acid
Ag/AgCl	Silver/silver chloride
AGB1	Arabidopsis Gβ subunit of G protein
AGG	Arabidopsis Gγ subunit of G protein
ALMT	Aluminium activated malate transport
ANOVA	Analysis of variance
At	*Arabidopsis thaliana* prefix
ATP	Adenosine triphosphate
BAK1	BRI1-Associated Receptor Kinase 1
BCECF-AM	2′,7′-bis(2-carboxyethyl)-5,6-carboxyfluorescein acetoxymethyl ester
BiFC	Bimolecular Fluorescence complementation
BIP	Binding immunoglobulin protein
BGLU	β-Glucosidase
BODIPY	Boron-dipyrromethene
bp	Base pair
BR	Brassinosteroid
bri1	BR-insensitive 1 mutant
BSA	Bovine serum albumin

CaMV	Cauliflower mosaic virus
CAX	Calcium/proton exchange
CBF	C-repeat binding factor
CBL	Calcineurin B-like protein
CCC	Cation-chloride cotransporter
cDNA	Complementary DNA
CDPK	Calcium-regulated protein kinase
CDS	Coding DNA sequence
Ce	*Caenorabditis elegans* prefix
Cel-GPHR	*Caenorabditis elegans* GPHR
CFPS	Cell-free protein synthesis
CHO	Chinese hamster ovary cells
CHX	Cation/proton exchanger
CIPK	CBL-interacting protein kinase
ClC	Chloride channel family
CLIC	Chloride intracellular channel
CNX6	Molybdopterin synthase large subunit
Co-IP	Co-immunoprecipitation assay
Col	Columbia *Arabidopsis thaliana* ecotype
COLD1	Chilling tolerance divergence 1
CORs	Cold-responsive genes
CRISPR/Cas9	Clustered regularly interspaced short palindromic repeats/CRISPR associated protein 9
d1	*Daikoku*, Rice Gα subunit mutant

DAPI	4′,6-diamidino-2-phenylindole
DdGPHR^{-}	*Dictyostelium discoideum* GTG/GPHR
DEP1	Dense and erect panicle 1
DET1	Deetiolated 1
DIDS	4,4'-Diisothiocyano-2,2'-stilbenedisulfonic acid
Dm	*Drosophila melanogaster* prefix
dGPHR^{-}	*Drosophila melanogaster* GPHR mutant
DMSO	Dimethyl sulfoxide
DNA	Deoxyribose nucleic acid
dNTPs	2′-deoxynucleotide-5′-triphosphate
DOPC	1,2-dioleoyl-sn-glycero-3-phosphocholine
DREB	Dehydration responsive element binding
DTX	Detoxification efflux carrier
ECR	Environmentally control rooms
EMS	Ethyl methanesulfonate
ER	Endoplasmic reticulum
ERL	ERECTA-LIKE genes
*Es*GPCR89	*Eriocheir sinensis* GPR89
FHAT	Flag-Histidine affinity tag
g	Gravitational force equivalent
G	Guanine
GA	Gibberellins
GAP	GTPase accelerating protein

GDP	Guanosine-5′-diphosphate
GEF	Guanine-nucleotide exchange factors
GFP	Green fluorescent protein
GID1	GA insensitive dwarf 1
Gly/G	Glycine
Glu/E	Glutamic acid
GnTI	N-acetylglucosaminyltransferaseI
GOLAC	Golgi anion channel
GPA1	Arabidopsis Gα subunit of G protein
GPCR	G protein-coupled receptor
GPHR	Golgi pH regulator
GPP130	Golgi integral membrane protein
GPR	Orphan G-protein coupled receptor
GS3	Grain size 3
GTG	G-protein coupled receptors type G-protein
GTP	Guanosine-5′-triphosphate
GUS	β-glucuronidase
HDEL	Endoplasmic reticulum signal peptide (His, Asp, Glu, Leu)
HEK293	Human kidney cells 293
HEPES	4-(2-hydroxyethyl)-1-piperazineethanesulfonic acid
H^+-PPase	Proton pyrophosphatase
HR	Hypersensitivity response
Hs	*Homo sapiens* prefix

IND	*Oryza sativa indica*
JA	Jasmonate
JAP	*Oryza sativa japonica*
kb	Kilobase
KcsA	Potassium channel of streptomyces A
LB	Luria-Bertani broth medium
Le	*Lycopersicon esculentum* prefix
Lys/K	Lysine
MΩ	MegaOhms
ManI	Mannosidase I
MAPK	Mitogen-activated protein kinase
Met/M	Methionine
MS	Murashige and Skoog
mV	Millivolt
n	Number of samples
NASC	Nottingham Arabidopsis Stock Centre
NHX	K^+/H^+ antiporter
NRT/NPF	Nitrate transporter/Peptide transporter family
OD	Optical density
Os	*Oryza sativa* prefix
OsGGC2	G protein γ subunit type C 2
pA	Picoampere
pA/pF	Picoampere per picofarad

PBS	Phosphate buffered saline
PCR	Polymerase chain reaction
PEG	Polyethylene glycol
PIN	PIN-FORMED genes
POPC	1-palmitoyl-2-oleoyl-sn-glycero-3-phosphocholine
pS	Picosiemens
P-type ATPase	Plasma membrane H^+-ATPase
PVC	Pre-vacuolar compartment
PVDF	Polyvinylidene difluoride
PXLG	Rice extra-large Gα subunit
PYR/PYL	Pyrabactin resistant receptor/PYR-like
QTL	Quantitative trait loci
RFP	Red fluorescence protein
RGA1	Rice G protein α subunit
RGB1	Rice G protein β subunit
R-GECO	Red fluorescent genetically encoded Ca^{2+} indicator for optical imaging
RGG1/RGG2	Rice G protein γ subunit 1 and 2
RGS	Regulator of G protein signalling
RNA	Ribonucleic acid
RNAi	RNA interference
rpm	Rotations per minute
ROS	Reactive oxygen species
RT-PCR	Retrotranscriptase polymerase chain reaction

SDS	Sodium dodecyl sulphate
SDS-PAGE	Sodium dodecyl sulphate polyacrylamide gel electrophoresis
SEM	Standard error of the mean
Sf9	*Spodoptera frugiperda*
SNP	Single nucleotide polymorphism
SOC	Super Optimal Broth with Catabolite repression medium
ST	Sialyltransferase
T	Thymine
Ta	*Triticum aestivum* prefix
TAE	Tris-acetate-EDTA
TAIR	The Arabidopsis Information Resource
TbGPR89	*Trypanosoma brucei* GPR89
TBST	Tris-buffered saline with Tween 20
T-DNA	Transfer-DNA
TGN	*Trans*-Golgi network
Ti	Tumour-inducing plasmid
TMEM165	Transmembrane protein 165
TRP-ML1	Mucolipin transient receptor potential channel 1
UPR	Unfolded protein response
V	Volt
V-ATPase	Vacuolar H^+-ATPase
VCCN1	Voltage-activated chloride channel 1
VHA	Vacuolar H^+-ATPase subunit

VSR	Vacuolar sorting receptor
Ws	Wassilewskija *Arabidopsis thaliana* ecotype
WT	Wild type
v/v	Volume/volume
w/v	Weight/volume
XLG	Extra-large Gα subunit
YFP	Yellow fluorescent protein

Chapter 1. General introduction

1.1. Membrane proteins in plants

Membrane proteins have important physiological roles that are vital for plant growth, development and response to stress. They can act as transporters across various membranes, in perception and transmission of signals and, in some cases, in biosynthetic activities (Cournia et al., 2015). In general, 20-30% of the genome encodes membrane proteins (Krogh et al., 2001, Komatsu et al., 2007, Engel and Gaub, 2008). More specifically, 25% of the *Arabidopsis thaliana* (Arabidopsis from herein) genome is predicted to be membrane proteins, where the plasma membrane is the more complex organelle (Komatsu et al., 2007). Although membrane proteins are essential in all organisms, the function of many of these proteins remains unknown.

This thesis focuses on the study of a family of membrane proteins called GTG/GPHR (G-protein-coupled receptors type G-protein/ Golgi pH regulator). Various functions have been proposed for these proteins in different organisms, which will be fully described in the following sections. In mammalian cells, they have been suggested to function as anion channels regulating endomembrane pH (Maeda et al., 2008). However, in plants, GTG/GPHRs have been shown to interact with the Gα subunit of the heterotrimeric G protein acting as an abscisic acid (ABA) receptor in Arabidopsis and as a cold sensor in rice (Pandey et al., 2009, Ma et al., 2015). Recent work in our laboratory has shown that Arabidopsis GTG/GPHR functions as an anion channel that regulates endomembrane pH (Adam, Terry and Williams, unpublished; Dorey, 2019). The data from this thesis reveal that rice GTG also functions as an anion channel regulating endomembrane pH, confirming that the function is conserved between Arabidopsis and rice. The capacity of GTG to be involved in cold tolerance, to interact with Gα or to work through G proteins to regulate the same signalling pathway are also addressed in this thesis. This introductory chapter covers topics required to provide a background to the questions addressed in this thesis.

1.2. Anion channels and carriers in plants

Ion channels are a type of membrane protein that allows the movement of ions across membranes down their electrochemical potential gradient. Anion channels are present in animals and plants and are responsible for the transport of negatively charged ions through the membrane. In some families the distinction between ion channels and exchangers is blurred and so, where relevant, these are discussed. In animals, anion channels are involved in cell excitability, synaptic transmission, pH regulation, cell volume, cell proliferation and migration (Schroeder and Keller, 1992, Jentsch and Günther, 1997, Lang et al., 2005, Mao et al., 2007, Graves et al., 2008, Maeda et al., 2008, Pasantes-Morales, 2016). Many families of anion channels have already been characterized in animals including the Cl^- intracellular channels (CLICs); the cystic fibrosis transmembrane conductance regulator (CFTR); the calcium activated Cl^- channels (CaCCs) and the volume-regulated anion channel (VRAC) (Gregory et al., 1990, Nilius et al., 1997, Valenzuela et al., 1997, Kuruma and Hartzell, 2000, Warton et al., 2002, Hartzell et al., 2004, Hagen et al., 2005, Picollo and Pusch, 2005, Scheel et al., 2005, Jentsch, 2008, Edwards and Kahl, 2010, Dickson et al., 2014, Ettorre et al., 2014, Jentsch, 2016). In addition, mammalian GTG/GPHR has been characterized as a Cl^- channel regulating Golgi pH (Maeda et al., 2008). Mutations in some of those channels produce different human diseases that affect different systems, such as the cardiovascular, nervous, respiratory and immune system (Gregory et al., 1990, Edwards and Kahl, 2010, Poroca et al., 2017).

In plants, anions such as Cl^- or NO_3^- need to be taken up by the roots and transported to the leaves and into the different organelles where they play specific roles. Several Cl^- channels and carriers are responsible for transporting Cl^- to its final destination. Under non-salt stress conditions, the Cl^- concentration inside the cell is higher than outside, therefore, Cl^- is acquired in the roots from the soil by active transport provided by H^+/Cl^- symporters present in the membrane (Colmenero-Flores et al., 2019). In Arabidopsis one candidate for Cl^- uptake is the Nitrate transporter 1 (NRT)/Peptide transporter family (NPF), where AtNPF6.3 is a low affinity NO_3^-/H^+ symporter with a $2H^+:NO_3^-$ ratio that can transport Cl^- when NO_3^- is less abundant or not present (Tsay et al., 1993, Wen and Kaiser, 2018). Another candidate is the Cation-Cl^- Cotransporter (CCC) channel, that transports K^+, Na^+ and Cl^- in Arabidopsis in a $2Cl^-:Na^+:K^+$ ratio and is found to regulate the uptake and the long distance transport of Cl^- (Colmenero-Flores et al., 2007).

The efflux of Cl^- is proposed to occur down the electrochemical gradient, mediated by anion channels (White and Broadley, 2001). These anion channels have not yet been identified but some possible candidates have been suggested. One is the aluminium-activated malate transporter (ALMT), an anion channel that in maize (ATLM1) is mainly expressed in the root tissue and is selective for SO_4^-, NO_3^- and Cl^- (Piñeros et al., 2008). The S-type (slow current) anion channel SLAH3 is highly expressed in roots and is involved in Cl^- release from root epidermal cells in the presence of ABA (Planes et al., 2015).

The root to shoot translocation of Cl^- seems to be carried out by the two S-type anion channels SLAH1 and SLAH3. These channels, which localise at the xylem pericycle in Arabidopsis roots, function as a complex and can transport NO_3^- and Cl^- (Cubero-Font et al., 2016). This SLAH1/SLAH3 complex plays a role introducing Cl^- into the xylem for shoot translocation. Also, the previously mentioned CCC channels help to retrieve Cl^- from the xylem in salt stress conditions and are involved in long distance Cl^- transport (Colmenero-Flores et al., 2007). Three different types of anion channel conductances have been identified in the root xylem of barley and maize, namely: X-IRAC, a xylem inward rectifying channel activated by membrane hyperpolarization; X-SLAC, a xylem S-type channel with slow activation and X-QUAC, a quick activated channel. The three channels are permeable to Cl^- and seem to play a role in root to shoot Cl^- translocation in crops (Köhler and Raschke, 2000, Gilliham and Tester, 2005, Colmenero-Flores et al., 2019).

Once the Cl^- reaches the leaf cells, it is compartmentalised to avoid toxic levels in the cell. Several Cl^- channels and carriers are localised at the tonoplast. In Arabidopsis, the Detoxification efflux carrier (DTX)/Multidrug and toxic compound Extrusion (MATE) transporters, AtDTX33 and AtDTX35, are suggested to serve this function. These are voltage-dependent channels that allow the influx of Cl^- into the vacuole contributing to the control of cell turgor and stomata movement when expressed in guard cells (Zhang et al., 2017). In Arabidopsis, the NO_3^-/H^+ antiporters, AtClCa and AtClCc, which also localise at the tonoplast, can transport Cl^- and play an important role in stomata movement (De Angeli et al., 2006, Wege et al., 2014, Hu et al., 2017). The tonoplast localised AtALMT9 contributes to the influx of Cl^- in the vacuole and is also involved in stomatal opening (De Angeli et al., 2013). Nitrate transporter, NRT1.1, in Arabidopsis has been found to be also involved in the transport of NO_3^- into the guard cells for controlling stomata aperture (Guo et al., 2003, Saito and Uozumi, 2019).

In guard cells, the anion efflux for stomata closure is mediated by R-type (rapid activation) and S-type (lower activation) anion channels. Both types of channels, with different electrophysiology characteristics, can transport various types of anions, such as Cl^-, NO_3^- and malate^{2-} and mediate the efflux of anions for stomata closure (Schroeder and Keller, 1992). S-type channels are major components of the depolarisation of the guard cell membrane that closes the stomata (Schroeder and Keller, 1992, Pandey et al., 2007). In Arabidopsis, one of the S-type channels is slow anion channel-associated 1 (SLAC1) that functions in stomata closure (Vahisalu et al., 2008). R-type channels act at more negative voltages, promoting the efflux of anions and activating the depolarisation of the guard cell membrane for stomata closure (Schroeder and Keller, 1992, Roelfsema and Hedrich, 2005, Pandey et al., 2007, Diatloff et al., 2010). R-type and S-type channels can be activated by ABA producing stomata closure (Roelfsema et al., 2004).

Cl^- can be transported into various organelles to contribute to the regulation of membrane potential and pH. In the Golgi, Cl^- functions as a counterion conductance for Golgi pH regulation (Demaurex, 2002, Schumacher, 2014). In Arabidopsis, AtCLCd and AtCLCf are Cl^-/H^+ exchangers that localise at the *trans* and *cis* Golgi, respectively, and play a role in pH regulation working as a counterion balance for the H^+ ions (Fecht-Bartenbach et al., 2007, Marmagne et al., 2007). Very few anion channels and carriers have been characterized in the endoplasmic reticulum (ER) in plants. In tobacco, ClC-Nt1, a putative Cl^-/H^+ antiporter was found in the ER and plays a role in luminal pH regulation (Sun et al., 2018). In soybean there is an ER localised cation/proton antiporter that regulates Cl^- exclusion from the shoot, however the mechanism remains unknown (Liu et al., 2016).

In the chloroplast, Cl^- functions as a micronutrient playing a role in the oxygen-evolving complex of photosystem II (Colmenero-Flores et al., 2019). Several anion channels have been found in Arabidopsis chloroplasts. AtClCe localises at the thylakoid membrane and plays a role exporting Cl^- to the thylakoid lumen (Marmagne et al., 2007, Herdean et al., 2016a). The voltage-activated Cl^- channel VCCN1 also localises at the thylakoid membrane where it fine-tunes the proton motive force across the thylakoid membrane contributing to photosynthesis (Herdean et al., 2016b).

1.3. Chloride and nitrate as plant nutrients

Although Cl^- has been traditionally considered a toxic element due to its effect in saline soils, recent studies have shown that Cl^- has a beneficial impact in plants within a specific concentration range (Franco-Navarro et al., 2016, Franco-Navarro et al., 2019). Cl^- is required in the plant cell at low concentrations, acting as a micronutrient. Cl^- is important for several functions including: a role in the oxygen-evolving complex of photosystem II; stomata movements; osmotic cell pressure and cell turgor; membrane potential and pH regulation (Marschner, 1995, White and Broadley, 2001, Kawakami et al., 2009, Teakle and Tyerman, 2010, Colmenero-Flores et al., 2019). Cl^- also functions as a cofactor for a limited number of enzymes, such as asparagine synthetase (Rognes, 1980) and the vacuolar H^+-ATPase (Churchill and Sze, 1984).

It is well-known that at higher concentrations, Cl^- is toxic to the cell, and therefore the cellular accumulation of Cl^- needs to be reduced when plants are exposed to saline soils. In salt tolerant plants, to protect photosynthesis, Cl^- is prevented from over accumulating in leaves by a reduction of transport of this anion through the xylem (Teakle and Tyerman, 2010). To avoid toxic levels of Cl^- building up in the cytosol, this anion is accumulated in the vacuole, where it can be stored (Teakle and Tyerman, 2010, Colmenero-Flores et al., 2019). Although at higher concentrations Cl^- can be toxic, recent studies from Franco-Navarro et al. (2016 and 2019), showed that treatment with non-toxic levels of Cl^- (between 1-5 mM) in tobacco plants produced a higher leaf cell size, higher fresh weight and higher dry weight. The Cl^- treatment improved water usage efficiency in the plant by a reduction of stomata density and therefore, stomata conductance and an increase in the photosynthesis rate (Franco-Navarro et al., 2016). The increase in photosynthesis in the Cl^- treated plants was due to an increase in the chloroplast number in the mesophyll cells that produced an increase in mesophyll diffusion conductance (Franco-Navarro et al., 2016). This indicates that at non-toxic levels, Cl^- can regulate leaf size and water efficiency in tobacco plants suggesting that Cl^- can function as a macronutrient. In rice it has been shown that Cl^- was able to promote root length since the root growth of the plant increased in the presence of ammonium chloride and not in the presence of ammonium sulfate (Kimura et al., 2004).

Nitrate (NO_3^-) is the most abundant source of nitrogen (N) in the soil, and for plants, N is an essential macronutrient that is required for growth and development (Crawford and Glass, 1998). NO_3^- is absorbed from the roots and transported and distributed throughout the plants by nitrate transporters (Dechorgnat et al., 2010). NO_3^-

can be stored in the vacuole to be used as a reservoir of nitrogen when the supply of this macronutrient is low (Richard-Molard et al., 2008). NO_3^- is reduced to nitrite (NO_2^-) by the nitrate reductase enzyme and to ammonium (NH_4^+) by nitrite reductase. Ammonium is assimilated into amino acids, nucleic acids and other nitrogen compounds (Masclaux-Daubresse et al., 2010). Therefore, nitrogen is an essential factor for plant growth because it is a component of proteins, nucleic acids, phytohormones, chlorophyll and secondary metabolites (Marschner, 1995). Since most of the nitrate transporters are NO_3^-/H^+ exchanges or symporters, NO_3^- is transported in combination with H^+ and therefore pH can have an effect in NO_3^- transport (Miller et al., 2007).

Many studies have shown that NO_3^- can affect the growth and development of the plant. It has been observed that NO_3^- can affect root growth in Arabidopsis, as the plants produced more lateral roots in the presence of NO_3^- and the Arabidopsis mutant of the nitrate transporter NRT1.1 showed a reduction of lateral roots when grown with a higher concentration of NO_3^- (Zhang and Forde, 2000, Remans et al., 2006). It has been shown that tobacco plants can grow larger using NO_3^- as a nitrogen source instead of NH_4^+, exhibiting larger shoots and roots, a higher leaf number and area, a greater cell number per leaf and increased cell size (Walch-Liu et al., 2000). This increase in leaf growth has also been observed in tomato and Arabidopsis plants when they were grown in the presence of NO_3^- (Alboresi et al., 2005, Rahayu et al., 2005). In rice, an increase of plant growth was also observed, as well as an increase of grain yield, when NO_3^- was applied together with NH_4^+ in comparison with plants that were grown with NH_4^+ only (Ying-Hua et al., 2006). NO_3^- is also involved in seed germination, flowering and hormone biosynthesis and transport (Alboresi et al., 2005, Rubio et al., 2008, Castro Marín et al., 2011, Krouk, 2016). All the above demonstrate the importance of NO_3^- for plant growth and development.

1.4. Regulation of endomembrane pH

pH is an important factor that regulates the function of different organelles in the cell. Many enzymes are pH sensitive, therefore the pH of the compartment will determine which enzymes are active and which processes are carried out in each organelle (Demaurex, 2002). The pH is regulated by the influx and efflux of protons across the membrane. During the active pumping of protons, an ATP is consumed, and this process generates energy that activates secondary transport (Demaurex, 2002, Beyenbach and Wieczorek, 2006). The lower pH of endomembrane compartments is

primarily generated by the Vacuolar H^+-ATPase, or V-ATPase. This is a proton pump present in all eukaryotes in intracellular compartments and in some cases the plasma membrane (Herman et al., 1994, Robinson et al., 1996, Kluge et al., 2004). The electrogenic activity of the proton pump creates an electrical potential across the cell that is used for the movement of other ions (Finbow and Harrison, 1997, Sze et al., 1999, Beyenbach and Wieczorek, 2006). V-ATPase consumes one ATP for the translocation of two H^+ (Tomashek and Brusilow, 2000) and is formed by two parts: the soluble V_1 subunit that interacts with ATP, ADP and inorganic phosphate, and the membrane-associated V_0 subunit which is responsible for the proton translocation (Finbow and Harrison, 1997, Toei et al., 2010, Marshansky et al., 2014). This V-ATPase is important, not only for pH regulation, but also for secretory/protein trafficking and its activity is critical for Golgi function (Dettmer et al., 2005, Gaxiola et al., 2007).

In plants there are three types of H^+-ATPases; apart from the previously mentioned V-ATPase, there is also the plasma membrane H^+-ATPase, or P-type H^+-ATPase, and the H^+-Pyrophosphatase (H^+-PPase) (Gaxiola et al., 2007). In plants, P-type H^+-ATPase is a principal component that energizes the cell allowing secondary transport to function at the plasma membrane. However, in animals this function is primarily carried out by the Na^+/K^+ ATPase (Buch-Pedersen et al., 2008). The P-type H^+-ATPase can be activated by different types of stresses, such as salt, cold, sugar depletion and fungal elicitors and it is regulated by a phosphorylation/dephosphorylation mechanism (Gaxiola et al., 2007). It has been shown that these proton pumps are involved in nutrient uptake and pathogen defence (Sondergaard et al., 2004, Elmore and Coaker, 2011). The H^+-PPase is a single subunit protein that generates a proton gradient across the membrane using the energy of the bond from pyrophosphate (Baltscheffsky et al., 1999). This proton pump is present only in higher plants and protozoa and it has been localised at the tonoplast mainly but also at the Golgi and in certain cases the plasma membrane (Ratajczak et al., 1999, Mitsuda et al., 2001, Li et al., 2005, Gaxiola et al., 2007). The H^+-PPase has been found to play a role in plant growth and development (Li et al., 2005).

To regulate and fine-tune the intracellular pH of organelles, a counterion conductance and proton leak are required. Generally, a pump and leak model has been accepted where the rate of protons pumped by the V-ATPase is balanced by the rate of H^+ efflux, called the proton leak. However, as both systems are electrogenic, a

movement of compensating charges is required. This is carried out by the counterion conductance that allows the regulation of the membrane potential (Demaurex, 2002, Schumacher, 2014). Cl^- and K^+ are the main ions that function in counterion conductance. The balance between the proton gradient generated by the proton pump, the proton leak and the counterion conductance, fine-tune the pH of each compartment. pH plays an important role in the secretory pathway, being involved in protein modification and sorting (Paroutis et al., 2004). In animals and plants, there is a gradual acidification from the ER to the lysosome/vacuole. The pH of the cytosol and ER is around 7.2-7.5, at the *cis* Golgi it is 6.9-6.7, at the *trans* Golgi network (TGN) it is 6.5-6, and it reaches pH 5-5.5 at the endosome and vacuole (Demaurex, 2002, Martinière et al., 2013a, Shen et al., 2013). This reduction of pH regulates protein modification and sorting through the secretory pathway. The different abundance of V-ATPase pumps in each compartment can contribute to the pH regulation of each organelle. Therefore, an increase in the number of V-ATPase pumps towards the more acidic compartments and a reduction of proton leakage can be involved in the acidification detected in the secretory pathway (Demaurex, 2002).

Several ion/H^+ exchangers have been suggested to play a role in pH regulation. In animals, the Na^+/H^+ exchangers, NHE, that localise at the Golgi, TGN and endosomes are involved in the maintenance of the luminal pH in those organelles (Nakamura et al., 2005). In plants, the tonoplast K^+/H^+ antiporters, NHX1 and NHX2, are involved in stomata movements and also play a role in pH regulation (Andrés et al., 2014). The Arabidopsis *nhx1nhx2* double mutant exhibited a more acidic vacuole in comparison with the wild type (WT) (Bassil et al., 2011b, Andrés et al., 2014). In addition, the *nhx1* single mutant had altered expression of genes involved in vesicular trafficking and protein sorting (Sottosanto et al., 2004). NXH5 and NHX6 localise at the *trans* Golgi and TGN and are involved in growth and vacuolar trafficking (Bassil et al., 2011a). The Ca^{2+}/H^+ antiporter, CAX, and the cation/H^+ exchangers in general, CHX, are also involved in pH regulation (Pittman, 2012, Chanroj et al., 2012). It was shown that the Arabidopsis *cax3* mutant is hypersensitive at low pH and has reduced plasma membrane H^+-ATPase activity (Zhao et al., 2008a). In the CHX family, AtCHX16-AtCHX20 were able to rescue the alkaline pH sensitivity of the *chx* yeast mutant (Chanroj et al., 2011).

Anion transporters also play a role in pH regulation. The tonoplast NO_3^-/H^+ exchangers, AtClCa and AtClCb provide counterion conductance and at the same time contribute to the proton gradient (De Angeli et al., 2006, Fecht-Bartenbach et al., 2007).

For pH homeostasis in the secretory pathway, two candidates are AtClCd and AtClCf that localise at the Golgi and TGN (Fecht-Bartenbach et al., 2007, Marmagne et al., 2007). While the *clc-d* mutant exhibited hypersensitivity to the V-ATPase blocker Concanamycin A and showed reduced growth at lower pH, the involvement of AtClCf in pH regulation has not yet been assessed (Fecht-Bartenbach et al., 2007, Schumacher, 2014). However, both proteins have been able to rescue the pH-dependent growth phenotype of the yeast *clc* mutant (Fecht-Bartenbach et al., 2007, Marmagne et al., 2007).

1.5. GTG/GPHRs are a family of conserved membrane protein with a range of proposed functions

G-protein-coupled receptors type G-protein/ Golgi pH regulator (GTG/GPHR) is a membrane protein family that was identified as an orthologue of GPR89, a putative orphan G protein-coupled receptor (GPCR) in humans (Maeda et al., 2008, Pandey et al., 2009, Jaffé et al., 2012). This family of proteins is predicted to have between 8 to 10 transmembrane domains and is conserved in eukaryotes. These proteins are found throughout the eukaryotic kingdom, from protists and fungi to animals and plants (Jaffé et al., 2012). The name GTG or GPHR refers to the function that has been reported for various members. Originally, the name GPHR was given as in Chinese hamster ovary cells these proteins were involved in pH regulation in the Golgi (see section 1.5.1) (Maeda et al., 2008). However, in plants they have been annotated as GTGs because of the suggested similar predicted topology with GPCRs and due to a mechanism of action that involves characteristics of GPCR and G proteins (see section 1.5.4). They were reported to interact with the Gα subunit of the heterotrimeric G protein (Pandey et al., 2009). In rice, this protein was called COLD1 since it was proposed to function as a cold receptor and interact with the rice Gα subunit (see section 1.5.8) (Ma et al., 2015). A summary of the GTG/GPHR nomenclature is given in Table 1.1 and a summary of GTG/GPHR proposed functions and localisations in different organisms is shown in Table 1.2.

Table 1.1. Nomenclature of genes encoding GTG/GPHR in different organisms

Gene name	Organism	Mutant name	References
GPHR	Chinese hamster	*gphr*	(Maeda et al., 2008)
GPHR	Mice (skin-specific)	K5-Cre:*GPHR*$^{f/f}$	(Tarutani et al., 2012)
GPHR	*Drosophila melanogaster*	*dGPHR*$^{-}$	(Charroux and Royet, 2014)
GPHR	*Dictyostelium discoideum*	*DdGPHR*$^{-}$	(Deckstein et al., 2015)
GPHR1 and *GPHR2*	*Caenorhabditis elegans*	*Cel-gphr*	(Wong, 2014)
GPR89	*Homo sapiens*	N/A	
GPCR89	*Eriocheir sinensis*	*dsEsGPCR89* (knockdown)	(Qin et al., 2019)
GPR89	*Trypanosoma brucei*	N/A	(Rojas et al., 2019)
GTG1 and *GTG2*	*Arabidopsis thaliana*	*gtg1* and *gtg2*	(Pandey et al., 2009)
COLD1	*Oryza sativa*	*cold1*	(Ma et al., 2015)
COLD1	*Triticum aestivum*	N/A	(Dong et al., 2019)
COLD1	*Lycopersicon esculentum* Mill.	*LeCOLD1*-RNAi (knockdown)	(Zhang et al., 2020)

Table 1.2. Summary of GTG/GPHR proposed functions and localisations

Name	Species	Function/physiological role	Localisation	References
GPHR	Chinese hamster	Golgi pH regulator acting as an anion channel	Golgi-TGN	(Maeda et al., 2008)
GPHR	*Drosophila melanogaste*r	Golgi pH regulator	Golgi and ER	(Charroux and Royet, 2014)
GPHR	*Dictyostelium discoideum*	Development	Golgi and ER	(Deckstein et al., 2015)
GPCR	*Eriocheir sinensis*	Cerebral antimicrobial peptide regulation	N/A	(Qin et al., 2019)
GPR	*Trypanosoma brucei*	Quorum sensing for stumpy formation	N/A	(Rojas et al., 2019)
GTG	*Arabidopsis thaliana*	ABA receptor acting as GPCR-type G protein	Plasma membrane	(Pandey et al., 2009)
GTG	*Arabidopsis thaliana*	Development and fertility	Golgi and ER	(Jaffé et al., 2012)
COLD1	*Oryza sativa*	Cold tolerance acting as possible calcium channel	ER and plasma membrane	(Ma et al., 2015)
COLD1	*Triticum aestivum*	Plant height regulator	ER and plasma membrane	(Dong et al., 2019)
COLD1	*Lycopersicon esculentum* Mill.	Cold tolerance	Plasma membrane	(Zhang et al., 2020)

1.5.1. GTG/GPHR acts as a Golgi pH regulator in mammalian cells with voltage-dependent anion channel activity

In mammalian cells, it was demonstrated with Chinese hamster ovary (CHO) cell mutants that GTG/GPHR proteins play a role in Golgi acidification (Maeda et al.,

2008). When GTG/GPHR was mutated using ethyl methanesulfonate (EMS), a delay in protein transport was observed. The CHO mutant cell lines also exhibited a defect in protein glycosylation in comparison to the WT (Maeda et al., 2008). The defects in protein transport were rescued by expressing the human GTG/GPHR in the mutant cells. GTG/GPHR was localised at the Golgi and TGN (Maeda et al., 2008). Golgi disorganization and an increase in pH of 0.35-0.50 in the Golgi and TGN were also observed in the mutant cell lines. No differences in pH were observed in the lysosomes between the mutant and the WT lines, indicating that the pH defect was specific to the Golgi (Maeda et al., 2008). Further *in vitro* electrophysiology assays showed that GTG/GPHR exhibited a voltage-dependent channel activity in the presence of KCl. GTG/GPHR was more permeable to Cl^- than K^+ and the current was inhibited by the anion blocker 4,4'-Diisothiocyano-2,2'-stilbenedisulfonic acid (DIDS) (Maeda et al., 2008). GTG/GPHR was also permeable to other anions such as I^-, Br^- and F^-. It was concluded that hamster GTG/GPHR functions as a voltage-dependent anion channel that generates a counterion conductance that regulates the pH of the Golgi (Maeda et al., 2008).

1.5.2. GTG/GPHR play an important role in growth and development in vertebrates and invertebrates

Knocking out GTG/GPHR specifically in the skin of mice demonstrated it had an important function in skin barrier development and in the formation of the lamellar granules (Tarutani et al., 2012). The skin-specific mice *GPHR* knockout mutant (called K5-Cre:*GPHR*$^{f/f}$) exhibited high mortality, slower growth and a defective skin barrier with skin inflammation, hypopigmentation, a defect in earlobes, genitals and hair loss (Figure 1.1 A-B) (Tarutani et al., 2012). In a more detailed examination, some additional abnormal differentiation, such as follicular dysplasia, expanded basal cells and impaired keratinocyte maturation was observed (Tarutani et al., 2012). This defect in keratinocyte maturation led to an abnormal lamellar body. Lamellar granules are secretory organelles that contain different proteins and lipids and are generated in the keratinocytes. It was suggested that the defect in the lamellar granules could be due to a problem in the acidification of the Golgi apparatus (Tarutani et al., 2012). Half of the mutants died one month after birth, showing the importance of GTG/GPHR in mice survival (Tarutani et al., 2012).

An orthologue of the mammalian GTG/GPHR has been characterized in *Drosophila melanogaster* (*Drosophila* from herein). An EMS mutagenesis was carried out in *Drosophila* and a mutant isolated with a point mutation in GTG/GPHR, where a conserved proline was changed for a lysine in the 91st amino acid position (Charroux and Royet, 2014). The *Drosophila* GPHR mutant (*dGPHR*$^{-}$) exhibited high mortality at the late larval stage and reduced growth of the pupae and adults (Charroux and Royet, 2014). DmGPHR was localised in the ER and the Golgi apparatus and those organelles were disorganized in the *dGPHR*$^{-}$ mutant (Charroux and Royet, 2014). This localisation differs from the mammalian GTG/GPHR which was reported to only localise at the Golgi (Maeda et al., 2008). The *dGPHR*$^{-}$ mutant also displayed defects in growth, such as smaller wings, and reduced cell size and cell number in the adults compared with WT flies (Figure 1.1 C). These phenotypes were rescued by complementing with DmGPHR. Human and hamster *GTG/GPHR* genes were also able to rescue the defective phenotype of the *dGPHR*$^{-}$ mutant, suggesting that human, hamster and *Drosophila* GTG/GPHRs are functional orthologues (Charroux and Royet, 2014).

A homolog of GPR89 in *Eriocheir sinensis* (*Es*GPCR89) was shown to be involved in the regulation of immune-related genes expression in the brain (Qin et al., 2019). *Es*GPCR89 was upregulated in the brain and hemocytes of the Chinese mitten crab after it was infected with *Staphylococcus aureus.* The expression of some immune-related genes, such as those encoding cerebral antimicrobial peptides, were also upregulated after infection. Silencing of *Es*GPCR89 in hemocytes using RNAi produced a reduction of cerebral antimicrobial peptides after infection, indicating that *Es*GPCR89 is involved in cerebral antimicrobial function via hemocytes (Qin et al., 2019).

Caenorhabditis elegans has two *GTG/GPHR* genes (Cel-*GPHR1* and Cel-*GPHR2*) and the *gphr-1gphr-2* double mutant, similar to the *Drosophila* mutant, exhibited a defect in growth and fertility (Wong, 2014). The *Cel-gphr-1gphr-2* mutant showed reduced movement and egg laying and, in most of the cases, the eggs did not pass the 30-cell stage (Figure 1.1 D). For the eggs that were laid, a significant reduction in hatching occurred in comparison to the WT, suggesting a strong egg development and egg-hatching defect. For those eggs that hatched, none reached an adult stage, exhibiting larval arrest. The pharyngeal pumping rate of the larvae in the mutant was lower than the WT larvae, which may have contributed to the larval arrest phenotype. None of the *Cel-gphr* single mutants exhibited this impaired phenotype, suggesting the two genes are functionally redundant (Wong, 2014).

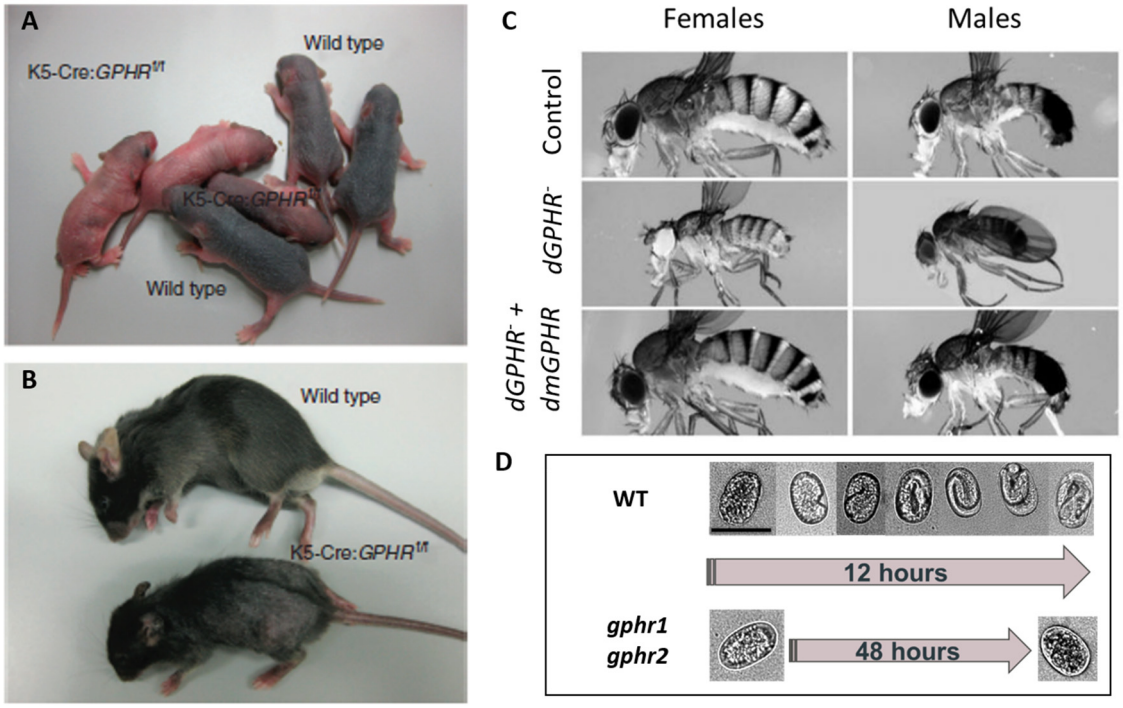

Figure 1.1. Skin-specific *GPHR* knockout mice (K5-Cre:*GPHR*$^{f/f}$), *Drosophila melanogaster* and *C. elegans GPHR* knockout mutants phenotypes

Skin-specific *GPHR* knockout mice at 5 days after birth A) or at one month old B). Images taken from Tarutani et al. (2012). C) *Drosophila melanogaster GPHR* knockout mutants (*dGPHR*$^{-}$) compared with WT and GPHR complementary lines (*dGPHR*$^{-}$ + dmGPHR) at 3 days old. Images taken from Charroux and Royet (2014). D) Defect in egg development in *Cel-gphr-1gphr-2* double mutant compared with WT. After 48 hours, the double mutant did not reach the final stage in comparison with the WT that completed development by 12 hours. Image taken from Wong (2014).

1.5.3. GTG/GPHRs are present in the protozoa kingdom

The amoeba *Dictyostelium discoideum* GTG/GPHR (DdGPHR), which shares 41% homology with the mouse protein and 32% with *Arabidopsis thaliana,* is reported to be involved in growth and development (Deckstein et al., 2015). The *DdGPHR*$^{-}$ mutant exhibited a reduction of growth due to a reduction of cell size. The mutant displayed several changes during development, such as loss of the normal cigar-like shape, defects in mobility and lack of formation of multicellular structures (Deckstein et al., 2015).

Although DdGPHR is localised in the ER and Golgi, the mutant did not show any abnormal ER or Golgi structures or a difference in pH in those compartments. The proteins that are processed through the Golgi were correctly synthesized in the mutant. However, the ER distribution in the *DdGPHR*$^{-}$ mutant was more sensitive to acidification (Deckstein et al., 2015).

Trypanosoma brucei, the parasite that causes trypanosomiasis in humans and animals, also has a homolog of GPR89 (*Tb*GPR89) (Rojas et al., 2019). This organism exhibits a proliferative slender form in the bloodstream. After a quorum-sensing response, it changes its state to a stumpy form which is a non-proliferative and transmissible stage (Seed and Wenck, 2003). *Tb*GPR89 is expressed at the surface of the slender form and ectopic expression of *Tb*GPR89 produced growth arrest and stumpy formation in the trypanosome. *Tb*GPR89 seems to be an essential protein since the attempts to create a complete knockout were unsuccessful (Rojas et al., 2019). *Tb*GPR89 exhibited some structural similarity to the proton-coupled oligopeptide transporters (POT) and further analysis showed that the *Tb*GPR89 was able to transport oligopeptides (Rojas et al., 2019). This was performed by expressing *Tb*GPR89 in *Escherichia coli* and measuring the uptake of fluorescent dipeptide β-Ala-Lys-AMCA (Rojas et al., 2019). A mutation of the tyrosine in the 48th position to histidine produced a 40% reduction of the fluorescence dipeptide uptake. It was suggested that *Tb*GPR89 functions as an oligopeptide transporter involved in stumpy formation of the trypanosomes (Rojas et al., 2019).

1.5.4. GTG/GPHR as a GPCR-type G protein in plants

In *Arabidopsis thaliana*, there are two GTG/GPHR proteins, called AtGTG1 and AtGTG2. Pandey et al. (2009) described these as GTGs due to a predicted GPCR-like topology and their ability to interact with G proteins. They were also purported to act as plasma membrane ABA receptors. The Arabidopsis GTGs have 45% identity and 68% similarity sequence to the orphan GPCR from human, GPR89. The Arabidopsis GTGs have 90% amino acid sequence identity and were predicted *in silico* analysis to have nine transmembrane domains instead of seven as usually seen for GPCRs (Pandey et al., 2009, Jaffé et al., 2012).

GPCR receptors are a group of membrane proteins involved in several important physiological responses. In mammalian cells these receptors play essential roles in

response to hormones and neurotransmitters (Rosenbaum et al., 2009). Typically, these receptors have seven transmembrane domains with an intracellular and extracellular domain. In the human genome, there are over 800 GPCRs, composing the biggest membrane protein family (Kling et al., 2013). They are able to transmit information downstream because of their association to a heterotrimeric G protein that changes conformation when a ligand binds to the receptor and activates other targets (Urano et al., 2013). In plants, some candidates have been proposed to be GPCRs, such as GCR1, GCR2, GTG1 and GTG2. The prediction was based on a partially similar transmembrane topology and a G protein-related phenotype (Urano et al., 2013). However none of them have been confirmed, as they do not exhibit GEF activity (Urano et al., 2013, Taddese et al., 2014, Pandey, 2019).

1.5.4.1. G protein signalling

The heterotrimeric G proteins sense differences in the environment and transmit extracellular signals into intracellular components, such as hormones and neurotransmitters (Urano et al., 2013). The G proteins have three subunits, α, β and γ and form a complex with GPCRs, which are transmembrane receptors that work as guanine-nucleotide exchange factors (GEF). In animal cells this complex works in every cell of the organism and is responsible for mediating GPCR signalling (Offermanns, 2003). In mammals, the complex is activated by the GPCR. In an inactivated basal state, the Gα subunit has GDP bound and generates a complex with Gβγ subunits. When a ligand binds to the GPCR, this stimulation promotes the exchange of the nucleotide in the Gα subunit, from GDP to GTP. Gα with GTP bound changes conformation and dissociates from the Gβγ subunits, forming an active state. The active Gα-GTP bound and Gβγ complex activate downstream effectors and regulate their activities. By hydrolysis of GTP, Gα returns to an inactive state and can again bind the Gβγ dimer. In animals there are proteins that accelerate the GTP hydrolysis activity of Gα such as regulators of G protein signalling (RGS) proteins (Figure 1.2 A) (Urano et al., 2013).

In plants, there is more controversy about the G protein mechanism; this is partly due to the capacity of the Gα subunit to spontaneously release GDP and bind GTP, without requiring the presence of the GPCR. Moreover, Gα has more affinity for GTP than GDP, suggesting that Gα binds GTP constitutively and therefore does not need GPCR or GEF (Johnston et al., 2007, Jones et al., 2011). Gα has intrinsic GTPase activity and hydrolyses GTP to return to an inactivated state. Interestingly, Gα can

change guanine nucleotides very fast but cannot hydrolyse GTP at the same speed (Johnston et al., 2007, Urano et al., 2013). In Arabidopsis it has been shown that the regulator of G protein signalling 1 (AtRGS1), a seven transmembrane protein, was able to accelerate the GTP hydrolysis rate of the Gα subunit (Johnston et al., 2007, Jones et al., 2011, Urano et al., 2012). Due to a very quick guanine nucleotide exchange rate, it has been suggested that Gα in plants has GTP bound by default and therefore is in a constitutively active form. After a stimulus occurs, AtRGS1 is phosphorylated and this allows dissociation from the G protein, releasing an active Gα-GTP that will activate some other downstream effectors (Stateczny et al., 2016). This indicates that plants may have a different system to animals for G protein signalling (Figure 1.2 B).

The human genome encodes 23Gα, 5Gβ and 12Gγ subunits (Chakravorty et al., 2015), however, in Arabidopsis, there is only one Gα subunit (AtGPA1) (Ma et al., 1990), one Gβ (AtAGB1) (Weiss et al., 1994) and three Gγ (AtAGG1, AtAGG2, AtAGG3) (Mason and Botella, 2000, Mason and Botella, 2001, Chakravorty et al., 2011). In rice, there is one Gα (RGA1), one Gβ (RGB1) and five Gγ (RGG1, RGG2, GS3, DEP1, GGC2) (Chakravorty et al., 2015). AtGPA1 protein shares approximately 30% identity with mammalian Gα proteins; AtAGB1 shares 42% and AtAGGs share 25-35% identity with mammalian orthologous (Wang et al., 2008b). In Arabidopsis, Gα is localised at the plasma membrane whereas Gβ has been localised at the plasma membrane and the endomembrane, for example ER (Wang et al., 2008b).

The Arabidopsis genome contains three extra-large Gα proteins called, XLG1-3, which are plant specific and can interact with Gβ subunit and Gβγ complex (Zhu et al., 2009, Chakravorty et al., 2015, Stateczny et al., 2016). A recent study has shown the presence of four extra-large Gα proteins in the rice genome, called PXLG1-4, where only PXLG2 was able to interact with the rice Gβ subunit in a two-yeast hybrid assay (Cui et al., 2020).

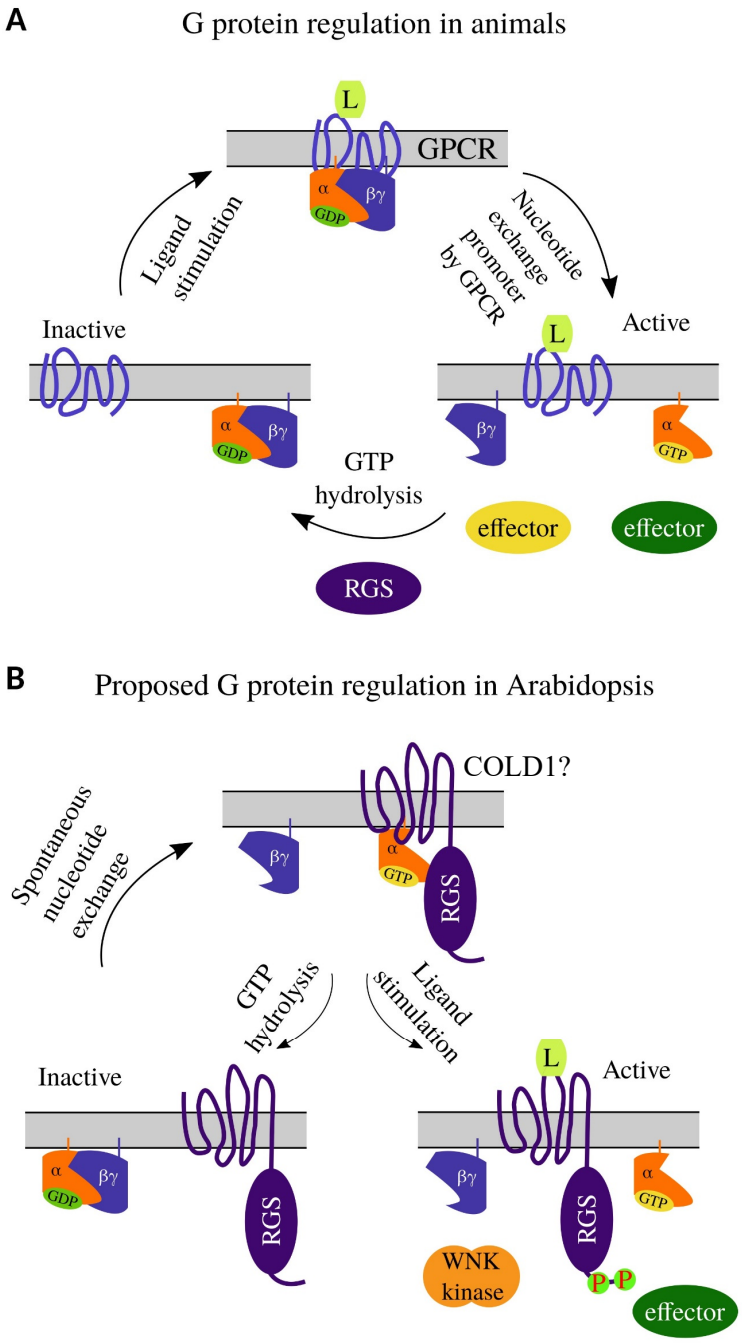

Figure 1.2. G protein signalling in animals and plants

A) In animal cells, upon ligand binding to the GPCR, the Gα subunit exchanges GDP for GTP and dissociates from Gβγ subunit. Activated Gα and Gβγ modulate the activity of downstream effectors. Gα hydrolyses GTP and re-binds to Gβγ subunit creating an inactive stage. B) In plant cells, Gα can spontaneously release GDP and activate itself. Upon activation, Gβγ dissociates from Gα and both subunits activate downstream effectors. Gα hydrolyses GTP and this is accelerated by RGS. RGS are not present in certain crops and COLD1 (rice GTG/GPHR) was proposed to function as a GTPase activating protein. Image taken from Urano et al. (2013).

1.5.4.2. GTGs interact with Gα subunit in plants

It was shown that both AtGTGs are able to interact with the Gα subunit using both the split ubiquitin system in yeast and co-immunoprecipitation (Co-IP) using transgenic Arabidopsis plants (Pandey et al., 2009). In the split ubiquitin system, AtGTGs were tagged with the N-terminal part of ubiquitin (NUb), whereas AtGPA1 was tagged with the C-terminal part (CUb), and the interaction was observed with the tags in both orientations (Figure 1.3) (Pandey et al., 2009). In the Co-IP assay, transgenic Arabidopsis plants expressing AtGTGs tagged with FLAG were used. In this assay, AtGTGs-FLAG were immunoprecipitated using anti- FLAG antibodies and AtGPA1 was detected in the total microsomal fraction (Pandey et al., 2009). Furthermore, it was observed that the interaction between AtGTGs and AtGPA1 enhanced the GTP binding activity and inhibited the GTPase activity of the AtGTGs (Pandey et al., 2009).

The interaction between GTGs and Gα subunit has not only been seen in Arabidopsis but also in rice. An orthologue of Arabidopsis GTG was found in the rice genome that was named COLD1 in relation to its function proposed in cold tolerance (further described in section 1.5.8) (Ma et al., 2015). Rice GTG, was able to interact with rice Gα subunit and this was tested by Co-IP and Bimolecular Fluorescence Complementation (BiFC) assay (Ma et al., 2015). For the Co-IP assays, transgenic plants expressing COLD1-GFP and FLAG-RGA1 were used. Extracts of transgenic plants were immunoprecipitated using anti-FLAG antibodies and GFP-COLD1 was detected using anti-GFP antibodies. This interaction was confirmed by a BiFC assay where the N terminus of YFP was tagged to GTG/COLD1 and the C terminus was tagged to RGA1. The fluorescence signal was observed at the plasma membrane. (Figure 1.3) (Ma et al., 2015). The GTPase activity of RGA1 increased when GTG/COLD1 from *japonica* rice was present (Ma et al., 2015).

A recent study showed that wheat GTG/COLD1 was also able to interact with wheat Gα subunit (Dong et al., 2019). The wheat genome contains three Gα sequences and, using firefly luciferase complementation and pull-down assays, it was shown that the central hydrophilic loop of GTG/COLD1 was able to interact with one of the three Gα genes of wheat. It was also shown that the C-terminal region of the Gα subunit was required for the interaction with wheat GTG/COLD1 (Dong et al., 2019).

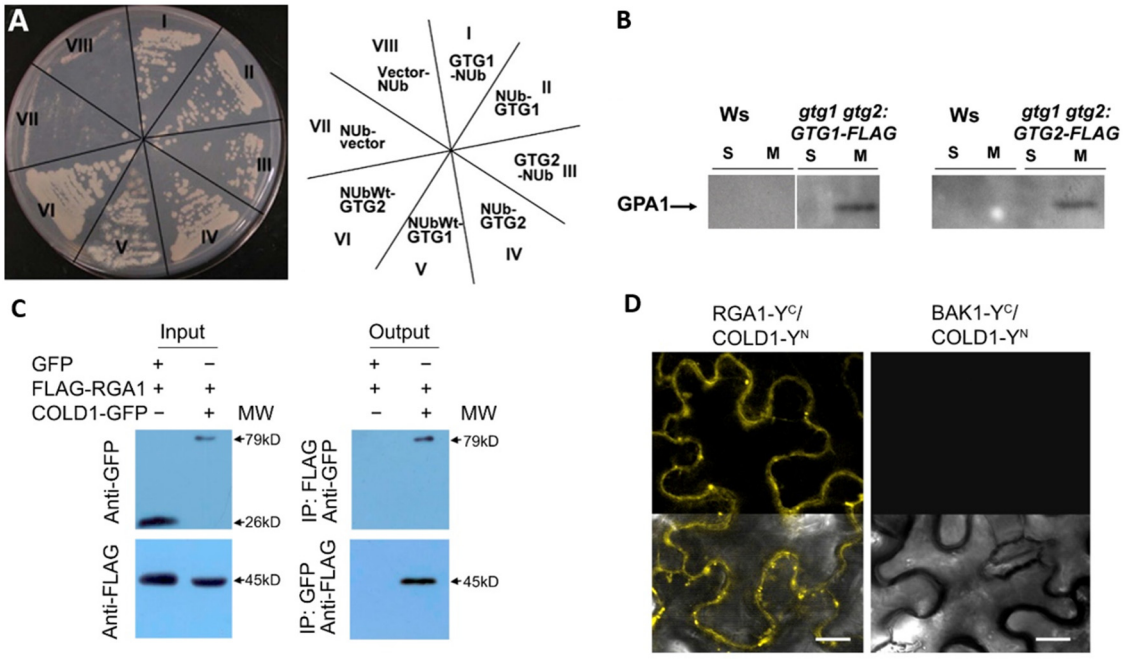

Figure 1.3. Interaction of GTGs with the Gα subunit in Arabidopsis and rice

A) Split ubiquitin system in yeast for AtGTGs and AtGPA1 interaction. On the right is the different fusion proteins used in the assay, that were expressed with AtGPA1-CUb (C-terminal part of ubiquitin). On the left is the yeast growth assay that indicates the interaction. B) Co-IP in Arabidopsis. Proteins were isolated from WT and *gtg1gtg2* expressing GTG1-FLAG or GTG2-FLAG and precipitated with anti-FLAG antibody. AtGPA1 was detected using anti-GPA1 antibodies. Images taken from Pandey et al. (2009). C) Co-IP in tobacco leaves co-expressing rice COLD1-GFP and RGA1-FLAG. COLD1-GFP was detected in complexes precipitated with anti-FLAG antibodies. D) BiFC assay. Positive interaction between COLD1-YFP^N and RGA1-YPF^C on the left. Negative control using BAK1-YFP^C with COLD1-YFP^N on the right. Images taken from Ma et al. (2015).

1.5.5. Arabidopsis GTGs as ABA receptors

As previously mentioned, AtGTG proteins were proposed to function as ABA receptors, in part due to the GPCR-like topology as well as the hyposensitivity to ABA observed in the *gtg1gtg2* double mutant (Pandey et al., 2009). It was also reported that both GTGs were able to bind ABA and this binding was increased in the presence of GDP (Pandey et al., 2009). ABA is a phytohormone that plays an important role in different biological processes, working as an endogenous signal in biotic and abiotic stresses and playing a key role in drought stress and regulation of germination

(Finkelstein et al., 2002, Raghavendra et al., 2010). Another ABA receptor that has been reported in plants is the pyrabactin resistant receptor (PYR)/PYR-like (PYL)/regulatory components of ABA (RCAR) receptors (PYR/PYL/RCARs) (Cutler et al., 2010), that has been shown to negatively regulate the ABA pathway by inhibition of the phosphatase PP2C (Ma et al., 2009).

In Pandey et al. (2009), the Arabidopsis *gtg1gtg2* double mutant, generated by crossing both *gtg1* (*gtg1-1*) and *gtg2* (*gtg2-1*) singles mutants in the Wassilewskija (Ws) ecotype, exhibited hyposensitivity to ABA in germination and post-germination assays. This hyposensitivity was not seen in any of the single *gtg* mutants, due to functional redundancy. The germination percentage of the *gtg1gtg2* double mutant in the presence of ABA was higher than the WT; at 1 μM ABA only 50% of the WT seeds germinated but about 80% of the double mutant germinated (Pandey et al., 2009). Even after germination, *gtg1gtg2* mutant seedlings exhibited more green cotyledons than WT or any single *gtg* mutant under ABA treatment. *gtg1gtg2* exhibited 100% green cotyledons in contrast to the WT that had only 60% in the presence of ABA. It was observed that the roots were less inhibited in the double mutant in the presence of ABA comparing with the WT or any single *gtg* mutants (Pandey et al., 2009). However, an independent study performed with three different *gtg1gtg2* double mutant alleles (see section 1.5.6), including the same one that was used in Pandey et al. (2009), showed that all the double mutants had the same root inhibition in the presence of ABA as the WT. Also, it was shown that there was no difference in germination in the presence of ABA between any *gtg1gtg2* double mutant and WT (Jaffé et al., 2012). Interestingly, the endogenous ABA level in the double mutant was similar to the WT and no differences were found between the *gtg1gtg2* double mutant and WT in the expression level of some ABA receptors (Pandey et al., 2009, Jaffé et al., 2012).

The hypothesis that AtGTGs could be ABA receptors was further tested by ABA binding assays. It was observed that both AtGTGs were able to specifically bind ABA and that this binding was increased in the presence of GDP comparing with GTP or ATP (Pandey et al., 2009). This role of the AtGTGs in ABA responses was also tested by a quantitative proteomics analysis that was conducted in Arabidopsis roots (Alvarez et al., 2013). In this study, the proteome of WT roots was compared to the proteome of roots from *gtg1gtg2* mutant plants, in the presence and absence of ABA. The results showed that the lack of GTG proteins generated an effect on the ABA response with two-thirds of ABA regulated-proteins dependent on the presence of GTG1 and GTG2.

However, 25% of ABA-regulated gene expression was independent of GTGs (Alvarez et al., 2013). Some PYR/PYL receptors were downregulated in the WT under ABA conditions but not in the *gtg1gtg2* mutant, suggesting an interference between ABA receptors (Alvarez et al., 2013). In Jaffé et al. (2012), a microarray analysis was performed in Arabidopsis WT and the *gtg1gtg2* mutant, where, interestingly, only one gene involved in ABA regulation, the Abscisic Acid Responsive Elements Binding Factor 3 (*ABF3/DPBF5*), was downregulated in the mutant (Jaffé et al., 2012). Genes involved mainly in transport, development, hormone metabolism and cell wall formation were altered in the *gtg1gtg2* mutant in comparison to the WT (Jaffé et al., 2012).

1.5.6. GTGs are involved in growth, development and fertility in Arabidopsis

A study on Arabidopsis GTG/GPHRs using new mutant alleles for AtGTG1 and AtGTG2, different from those used previously by Pandey et al. (2009), was carried out. The new single mutants were from Columbia (Col) (*gtg1-2* and *gtg2-2*) and Wassilewskija (Ws4) (*gtg1-3* and *gtg2-3*) background (Jaffé et al., 2012). In the process of generating a double mutant, during the isolation of homozygous from heterozygous, a defect in the segregation ratio was observed. The progeny of the double heterozygous (*gtg1* (+/-) and *gtg2* (+/-)) cross did not follow a Mendelian segregation of 1 in 16. This impaired segregation ratio occurred in both ecotypes (Jaffé et al., 2012).

The *gtg1gtg2* double mutants displayed growth defects, such as a short root length and reduced fresh weight in the absence of sucrose in comparison with the WT (Figure 1.4). The hypocotyl length of the *gtg1gtg2* double mutants was also reduced under low white light but not under dark conditions, suggesting a role in light-dependent seedling growth (Jaffé et al., 2012). The *gtg1gtg2* double mutant for both ecotypes exhibited a defect in fertility, with a reduced silique length and seed yield. The fertility impairment was due to a pollen defect (Jaffé et al., 2012). Pollen germination *in vitro* was reduced for both double mutants and pollen tubes extended less *in vivo*, compared to WT, not penetrating more than half way along the pistil. The reduced seed yield was due to the higher proportion of aborted ovules probably due to lack of fertilization and undeveloped seeds in the silique of *gtg1gtg2* double mutant in comparison with WT siliques (Figure 1.4) (Jaffé et al., 2012).

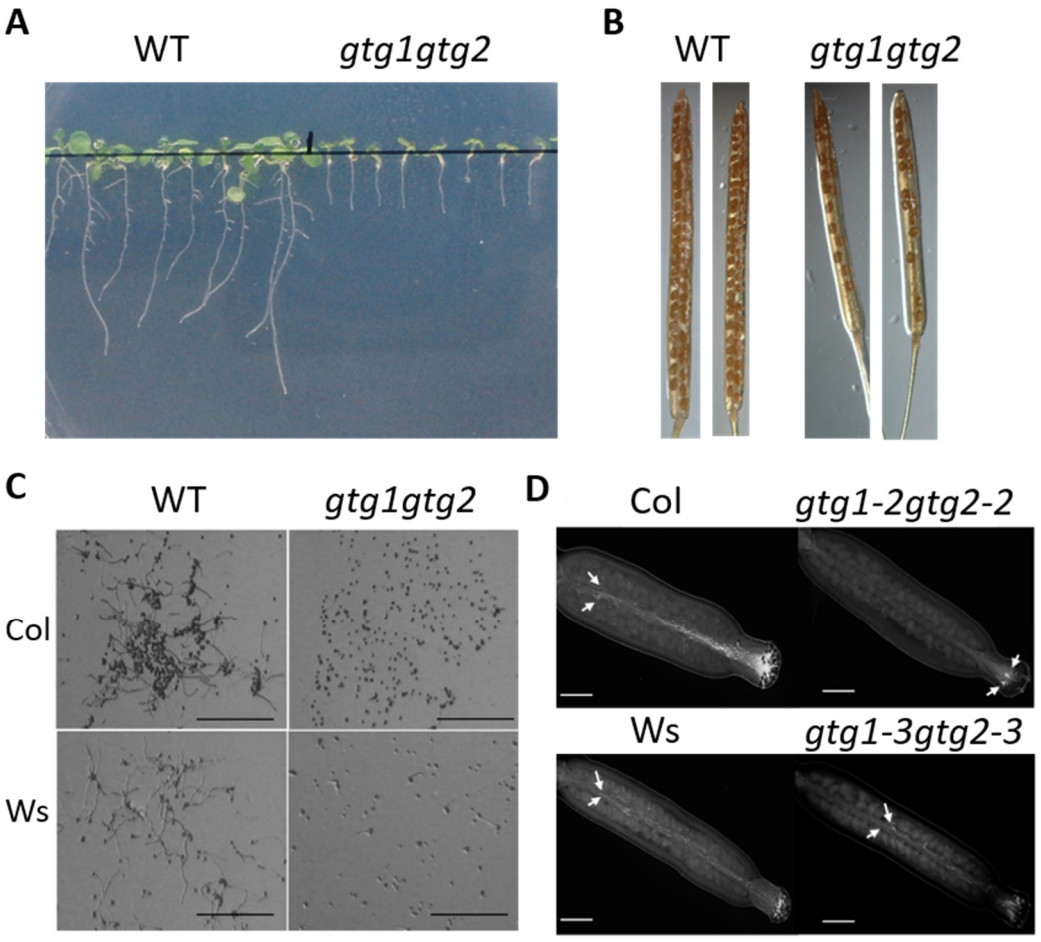

Figure 1.4. *gtg1gtg2* mutant displays a defect in growth and fertility

A) Reduce root length of the *gtg1gtg2* mutant in comparison to the WT in absence of sucrose. B) Shorter silique length in *gtg1gtg2*. Reduced pollen germination *in vitro* observed in the *gtg1gtg2* mutant, in Col and Ws backgrounds (C) and shorter pollen tube growth *in vivo* in both *gtg1gtg2* double mutants (D). Images A and B taken from Wong (2014) and C and D from Jaffé et al. (2012).

A microarray assay showed that the expression of 295 genes was altered in the *gtg1gtg2* mutant, with 194 genes upregulated and 101 downregulated. Those genes are involved in cell wall formation and modification, lipid and amino acid metabolism, sugar transport and hormone regulation. Interestingly, as mentioned above, only one gene involved in ABA regulation was found to be downregulated in the *gtg1gtg2* mutant (Jaffé et al., 2012).

It was shown that GTG is also involved in growth in wheat (*Triticum aestivum*). Overexpression of wheat GTG (TaCOLD1), containing a lysine in the 187th amino acid position, produced plants with reduced height. The plants exhibited shorter internodes and reduced cell length (Dong et al., 2019). This indicates that GTG is involved in growth and development in different plant species.

1.5.7. AtGTG1 functions as an anion channel that regulates endomembrane pH

Previous work in our laboratory has shown that AtGTG1 also functions as an anion channel that regulates endomembrane pH (Adam, Terry and Williams, unpublished; Dorey, 2019). These experiments were carried out using whole-cell patch clamping in Human Embryonic Kidney 293 (HEK293) cells that expressed AtGTG1. The HEK293 cells that expressed AtGTG1 exhibited more current activity than the cells transformed with the empty vector (Dorey, 2019). The current was observed in the presence of Cl^- and it was blocked by the specific anion channel inhibitor, DIDS. In addition, channel activity was independent of ABA and pH and AtGTG1 was also permeable to NO_3^-, F^- and Br^- ions (Dorey, 2019).

These results were further confirmed by a single-channel activity assay in an artificial lipid bilayer. AtGTG1 protein was expressed in an *in vitro* cell-free system and was inserted into an artificial membrane of POPC (1-palmitoyl-2-oleoyl-sn-glycero-3-phosphocholine) lipids. Current activity was observed when AtGTG1 was inserted into the membrane in a symmetrical and asymmetrical gradient of KCl. Moreover, in the asymmetrical gradient of KCl, AtGTG1 was more permeable to Cl^- than K^+. In addition, AtGTG1 current activity was inhibited by the addition of the anion blocker DIDS, indicating that AtGTG1 functions as an anion channel in the same manner as the mammalian GTG/GPHR (Dorey, 2019). Whole-cell patch clamping in HEK293 and the planar lipid bilayer assay were also carried out for CeGTG1, showing that the *C. elegans* protein also functions as an anion channel (Dorey, 2019). This, together with the fact that mammalian GTG/GPHR also acts as an anion channel, indicates that the function of the protein as an anion channel is conserved in different species (Dorey, 2019).

pH analysis performed in WT plants and the *gtg1gtg2* mutant *in vivo* showed that Arabidopsis GTG can regulate endomembrane pH (Adam, Terry and Williams, unpublished). A pHluorin pH sensor tagged with different organelle sequences was used

for pH measurements. pHluorin was tagged to several organelle markers: HDEL sequence for ER, ManI (Mannosidase I) for *cis* Golgi, the vacuolar sorting receptor BP80 for *trans* Golgi, and VSR2 for pre-vacuolar compartment (PVC) (Shen et al., 2013). All pHluorins tagged with the different organelle sequences were expressed in WT and *gtg1gtg2* plants. The pH of the ER and the *cis* Golgi in the *gtg1gtg2* mutant was higher than the WT compartments (Table 1.3; data from Adam, Terry, Williams, unpublished), but no pH difference was found in the *trans* Golgi and the PVC. The pH was restored to normal when AtGTG1 was expressed in the *gtg1gtg2* mutant (Adam, Terry and Williams, unpublished). These results indicate that Arabidopsis GTG/GPHR regulates endomembrane pH in a similar manner to the mammalian GTG/GPHR.

Table 1.3. pH values of different organelles in 7-day-old WT and *gtg1gtg2* seedlings using pHluorin

Organelle	WT pH	*gtg1gtg2* pH
ER	7.21 ± 0.04	7.33 ± 0.04 *
cis Golgi	6.78 ± 0.02	6.85 ± 0.02 *
trans Golgi	6.34 ± 0.03	6.38 ± 0.04
PVC	6.5 ± 0.02	6.51 ± 0.01

* significant differences between the pH of WT and the *gtg1gtg2* mutant.

1.5.8. GTG is involved in cold tolerance in rice and tomato

In rice (*Oryza sativa*) and tomato (*Lycopersicon esculentum* Mill.), GTG has been suggested to be involved in cold tolerance (Ma et al., 2015, Zhang et al., 2020). Cold tolerance is a complex quantitative trait controlled by multiple genes (Zhao et al., 2016). Several quantitative trait loci (QTLs) have been identified to be involved in cold tolerance in rice following Genome-wide association study (GWAS), an approach that allows the identification of genes associated with specific traits (Adamski et al., 2016, Lv et al., 2016, Wang et al., 2016, Zhao et al., 2016, Shakiba et al., 2017, Zhang et al., 2018a). GTG was identified in rice as one of the QTLs involved in chilling tolerance and was called COLD1 (Ma et al., 2015). The implications of GTG/COLD1 in rice and

tomato cold tolerance are described in more detail in section 1.5.8.2 after a review of cold stress signalling in plants.

1.5.8.1. Cold stress signalling in plants

Plants are affected by different environmental factors such as salinity, drought and high and low temperature that induce stress in the organism (Lichtenthaler, 1998). *Oryza sativa* is a tropical and subtropical crop that is important economically. In contrast to wheat or barley, rice is more severely affected by low temperatures, which can cause a reduction in seed yield and productivity (Zhao et al., 2016). In rice, damage from cold stress causes 3-5 million tons of annual losses (Zhang et al., 2013). Low temperature also affects the chlorophyll content and photosynthesis rate, produces an increase of reactive oxygen species (ROS) and impairs metabolism (Zhang et al., 2014). During reproductive stages, cold stress leads to spikelet sterility causing a defect in grain maturation (Dametto et al., 2015, Adamski et al., 2016). Due to global environment changes, there is an urgent need to understand the genetic mechanism of plant responses to cold so that we can improve low temperature tolerance in crops (Lv et al., 2016).

Plants sense low temperatures by changes in the fluidity and composition of membranes and some metabolite concentrations are affected, such as amino acids, organic acids and sugars (Zhao et al., 2013). Under adverse conditions, such as biotic and abiotic stresses, cytosolic calcium (Ca^{2+}) increases due to an influx of Ca^{2+} through the plasma membrane (Knight and Knight, 2001, Romeis et al., 2001). This increase is mediated by mechano-sensitive Ca^{2+} channels or by ligand-activated Ca^{2+} channels such as Cyclic nucleotide-gated channels (CNGCs) and Glutamate receptor-like channels (GLRs) (Swarbreck et al., 2013, Zhang et al., 2013, Jha et al., 2016). Cytosolic free Ca^{2+} acts as a second messenger in many abiotic and biotic stresses and functions as a central response for such environmental changes (Rentel and Knight, 2004, Lecourieux et al., 2005, Tracy et al., 2008, Boudsocq et al., 2010, Kudla et al., 2010, Dubiella et al., 2013, Li et al., 2014b). Ca^{2+} is also required as a nutrient as it is involved in certain cellular processes, such as photosynthesis and plays a structural role in the cell wall and membranes (Hepler, 2005, Hochmal et al., 2015). Due to all these functions, the elevation of Ca^{2+} required in each part of the cell at any one time has to be very tightly regulated (McAinsh and Hetherington, 1998, Ng and McAinsh, 2003).

Cytosolic Ca^{2+} binds to calcium sensors that amplify the signal and activate downstream effectors involved in cold responses. Examples of these sensors are Calmodulins (CaM), Calmodulin-like proteins (CMLs) and Calcineurin B-like proteins (CBLs), that activate specific kinases such as CBL-interacting protein kinases (CIPKs) and Calcium-regulated protein kinases (CDPKs) (Kudla et al., 2010, Zhang et al., 2013, Wilkins et al., 2016) (Figure 1.5). The latter is a serine/threonine kinase that has been shown to play a role in cold tolerance in rice and OsCDPK7 and OsCDPK13 overexpressor lines showed enhanced cold tolerance and higher recovery rates after cold stress treatment (Zhang et al., 2013). Most of the downstream effectors involved in cold tolerance are transcription factors. The most well-known comprise the DREB-CBF/DRE (Drought-responsive element-C-repeat binding factor/Drought-responsive element binding factor) pathway, found in Arabidopsis and rice (Dubouzet et al., 2003, Agarwal et al., 2006, Wang et al., 2008a, Zhang et al., 2009, Zhang et al., 2013, Adamski et al., 2016). In rice, DREBs/CBFs are identified as being involved in cold stress as their expression is induced within a short period of exposure to cold, and overexpression of the transcription factors improves cold tolerance and increases the expression of cold-responsive genes at normal temperature (Agarwal et al., 2006, Chinnusamy et al., 2010). The expression of *OsDREB1B* is increased under chilling treatment and overexpression of *OsDREB1F* enhances cold tolerance in rice and Arabidopsis transgenic plants (Gutha and Reddy, 2008, Wang et al., 2008a). MYBs are another class of transcription factors involved in cold tolerance. MYBS3 responds slowly to cold stress, a difference from DREB1 that acts quicker and in a shorter term (Zhang et al., 2009, Zhang et al., 2013, Adamski et al., 2016). *OsMYB2* is highly induced after cold stress (Yang et al., 2012, Lv et al., 2016), although it has been reported to also be involved in other stress responses, such as to salt and drought (Yang et al., 2012). The activation of all these transcription factors regulates downstream effectors, activating or repressing gene expression in response to low temperature but also to drought and salinity stress (Zhu, 2016).

Ca^{2+} is not the only factor involved in low temperature signalling; the accumulation of ABA regulates the transcription factor ABF (ABA-responsive elements- binding bZIP transcription factor) that also triggers a cold response in the cell (Tuteja, 2007, Miura and Furumoto, 2013, Zhang et al., 2013). The exposure of plants to abiotic stress also produces ROS that activate the Mitogen-Activated Protein Kinase (MAPK) cascade (Figure 1.5). MAPKs regulate cell division, development and differentiation in response to stress and are involved in cold stress, but also in response to drought,

pathogens, ROS and wounding (Rodriguez et al., 2010). In Arabidopsis, AtMPK4 and AtMPK6 are rapidly activated by cold stress (Ichimura et al., 2000, Sinha et al., 2011) and in rice, some MAPKs have been shown to be involved in cold tolerance, such as OsMPK3 and OsMPK6, and their overexpression enhances cold tolerance in plants (Zhang et al., 2013).

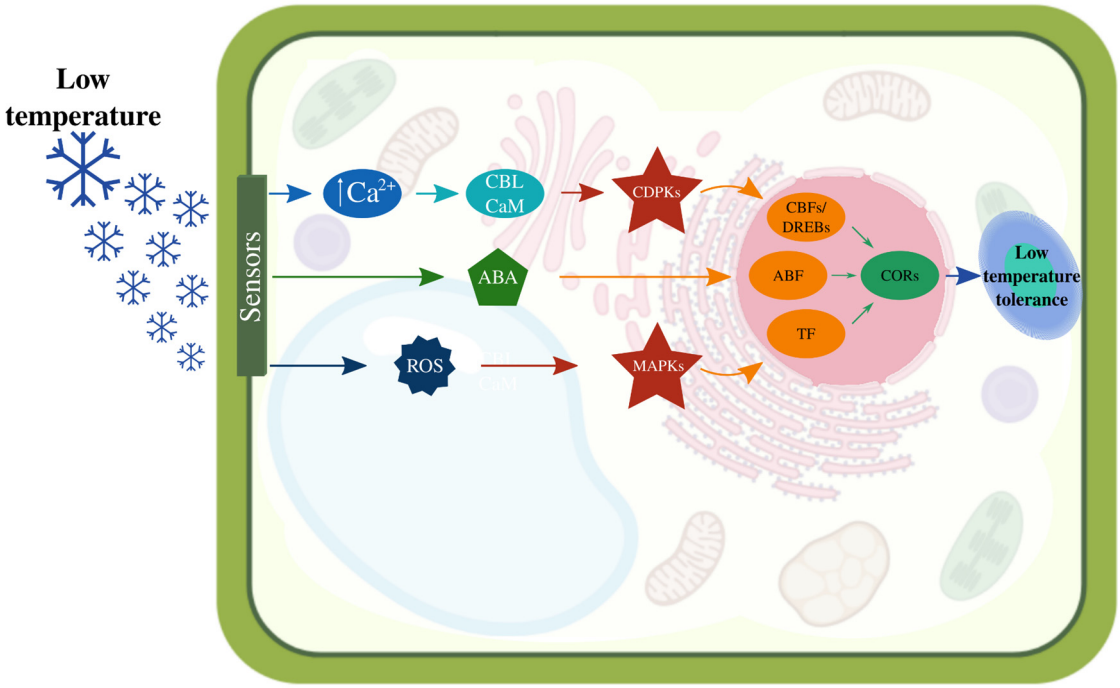

Figure 1.5. Diagram of the response to low temperature stress in plants

Low temperature is detected by plasma membrane sensors followed by an increase of $[Ca^{2+}]_{cyt}$. This Ca^{2+} is detected by Ca^{2+} sensors, such as calmodulins (CaM) or Calcineurin-B-like (CBL) proteins that activate specific kinases, such as calcium-regulated protein kinase (CDPKs). These kinases phosphorylate the C-repeat binding factor/Dehydration responsive element binding (CBFs/DREBs) transcription factors that induce cold-responsive genes (CORs). Under low temperatures, ABA levels and ROS also increase, activating ABA-responsive elements-binding bZIP transcription factors (ABF) and the MAPK cascade respectively that also regulates the expression of CORs genes. This cascade generates a cold tolerance response in the plant. Image modified from Zhang et al. (2013) and Noman et al. (2017).

In a transcriptomic analysis performed in rice, 1,361 genes had different expression levels under cold stress in cold tolerant plants relative to sensitive plants (Dametto et al., 2015). In cold tolerant plants, upregulated genes were related to cell division and cell growth and cold tolerant seedlings exhibited large epidermal cells and a higher percentage of mitotic cells in comparison with sensitive plants (Dametto et al., 2015). Some of those upregulated genes included aquaporins to improve efficiency in water uptake during germination; ion transporters, such as K^+ and Cl^- channels, to maintain the ionic balance of the cell; cellulose synthase and other cell wall-related genes to maintain the cell wall structure under low temperature; fatty acid desaturases to increase the amount of unsaturated fatty acids and therefore to increase the fluidity of the membrane; and antioxidant-related genes such as peroxidase, ascorbate peroxidase and monodehydroascorbate reductase to reduce the levels of ROS generated under stress (Dametto et al., 2015).

1.5.8.2. GTG/COLD1 is involved in cold tolerance in rice and tomato

Oryza sativa has two major subspecies, *indica* and *japonica* and both were domesticated from the ancestor *O. rufipogon* (Londo et al., 2006). *Japonica* can grow in areas with lower temperature, due to higher cold tolerance in comparison to *indica* varieties (Dametto et al., 2015, Ma et al., 2015, Wang et al., 2016, Zhao et al., 2016, Shakiba et al., 2017). Latitude distribution of rice is associated with cold adaptation (Lv et al., 2016), suggesting that latitude could be an environmental factor for cold tolerance domestication and could be involved in *indica-japonica* differentiation (Wang et al., 2016). As previously mentioned, GTG was identified in rice as one of the QTLs involved in chilling tolerance (Ma et al., 2015). The QTL analysis was carried out using inbred lines generated from a cross of a *japonica* with an *indica* variety that were exposed to low temperature treatment. GTG/COLD1 was one of the QTL identified in the screening to confer cold tolerance. Genomic DNA sequence in the region where *GTG/COLD1* is localised (on chromosome 4) was performed to compare the parental sequences, in this case Nipponbare (*japonica* cold tolerance) and 93-11 (*indica* chilling sensitive). The results indicated that the sequence of *GTG/COLD1* in *japonica* had one different nucleotide in the 4th exon (adenine (A) instead of thymine (T)) in comparison to *indica*, which generated a change in the amino acid sequence, lysine in *japonica* and methionine in *indica*. There were other single nucleotide polymorphisms (SNP) between these two ecotypes, one synonymous polymorphism in the first exon that did

not produce an amino acid change at the protein level and five substitutions in introns. Out of all the accessions of rice cultivars that were sequenced, all the *japonica* varieties and the *O. rufipogon* (*O. sativa* ancestor) had the SNP with an adenine, leading to a lysine in the 4th exon; however, all *indica* varieties analysed had a thymine or cytosine in that position, generating a methionine in the protein sequence (Ma et al., 2015).

It was shown that plants lacking the *GTG/COLD1* gene were more sensitive to cold (2-4°C), and those in which *GTG/COLD1* was overexpressed were more resistant (Ma et al., 2015). Furthermore, it was shown that transgenic lines generated with *GTG/COLD1* from *japonica* (*COLD^{jap}*) in the *cold1* mutant background had the same response as WT under cold stress. However, transgenic lines created with *GTG/COLD1* gene from *indica* variety (*COLD1^{ind}*) in *cold1* were not able to rescue the phenotype under low temperature conditions and exhibited a low cold tolerance, similar to the *cold1* mutant phenotype (Figure 1.6) (Ma et al., 2015).

Since Ca^{2+} is a key factor involved in cold stress, the level of Ca^{2+} influx in the transgenic lines was investigated. It was observed that the transgenic lines expressing COLD1^{jap} had a higher Ca^{2+} influx in comparison with WT plants after cold treatment. The opposite occurred in transgenic plants expressing COLD1^{ind}, where the Ca^{2+} influx after cold treatment was lower than WT plants (Ma et al., 2015). This difference was also observed when *japonica* Nipponbare and *indica 93-11* were analysed. The latter had lower Ca^{2+} influx after cold exposure than Nipponbare. In addition to these results, the *cold1* mutant showed similar levels of Ca^{2+} influx to the *indica 93-11* variety. Although the mutant had a smaller increase in cytosolic Ca^{2+} than the WT, this was rescued in the COLD1^{jap} complementary lines, where WT levels of Ca^{2+} were observed. Rice *cold1* mutant lines that were expressing COLD1^{ind} did not show rescued Ca^{2+} levels (Ma et al., 2015).

Using a two-electrodes voltage clamp in *Xenopus* oocytes, it was shown that after cold treatment an inward current was observed in the cells that co-expressed COLD1^{jap} and the Gα subunit, RGA1 (Ma et al., 2015). No significant differences in current were found between the cells expressing COLD1^{jap} or COLD1^{ind}. However, the ion being transported was not characterized. The fact that *cold1* mutant plants showed lower resting Ca^{2+} and lower influx levels of Ca^{2+} upon cold stress, together with the inward current observed when COLD1^{jap} and RGA1 were co-expressed, led Ma et al. (2015) to speculate that "COLD1 itself possibly represents a potential calcium permeable channel or a subunit of such a channel". A model for COLD1 in response to chilling is shown in

Figure 1.7 (Manishankar and Kudla, 2015). Another hypothesis proposed was that the low temperature produces a change in the fluidity of the plasma membrane and this produces perturbations in GTG/COLD1 structure that induces the interaction observed between GTG/COLD1 and RGA1 and activates downstream effectors involved in cold responses (Ma et al., 2015).

Interestingly, COLD1 has not been identified in subsequent genetic screen performed for the identification of cold tolerance QTLs (Shakiba et al., 2017, Lv et al., 2016, Wang et al., 2016, Song et al., 2018, Zhang et al., 2018a). However other QTLs identified in the Ma et al. (2015) study have also been identified in other genetic screens, such as COLD2 (on chromosome 8; Lv et al., 2016), COLD3 (on chromosome 1; Shakiba et al., 2017), COLD4 (on chromosome 6; Lv et al., 2016, Shakiba et al., 2017, Schlappi et al, 2017). So far the causative genes for these QTLs are unknown.

In tomato (*Lycopersicon esculentum* Mill.), LeCOLD1, was also reported to be involved in cold tolerance (Zhang et al., 2020). Tomato plants that overexpressed LeCOLD1 were taller and more resistant to low temperature in comparison with WT plants, whereas the RNAi lines that expressed less LeCOLD1 (*LeCOLD1*-RNAi) were shorter and more sensitive to cold stress than the WT (Zhang et al., 2020). Following the cold treatment, the overexpressor lines had higher fresh weight and higher survival rate than the WT, whereas the *LeCOLD1*-RNAi lines exhibited lower survival rate. The plants that overexpressed LeCOLD1 exhibited less damage after the cold stress since the malondialdehyde (MDA) content and the electrolyte leakage in those lines was lower than the WT and the *LeCOLD1*-RNAi lines. In addition, the overexpressor lines displayed a higher expression of antioxidant related-genes, higher activity of antioxidant enzymes and a reduction of ROS, that together indicate less oxidative stress after the cold treatment (Zhang et al., 2020).

1.6. The expression pattern and localisation of GTGs

GTG/GPHRs in Arabidopsis are expressed in all tissues throughout the plant. This was analysed using β-glucuronidase (GUS) staining that showed expression in guard cells, rosette leaves, stems, flowers, siliques, cotyledons, hypocotyl and roots, where it was higher at the root tip (Pandey et al., 2009, Jaffé et al., 2012). High expression was detected in the stigma, stamen, pollen and base of the carpel in the flower (Figure 1.8) (Jaffé et al., 2012).

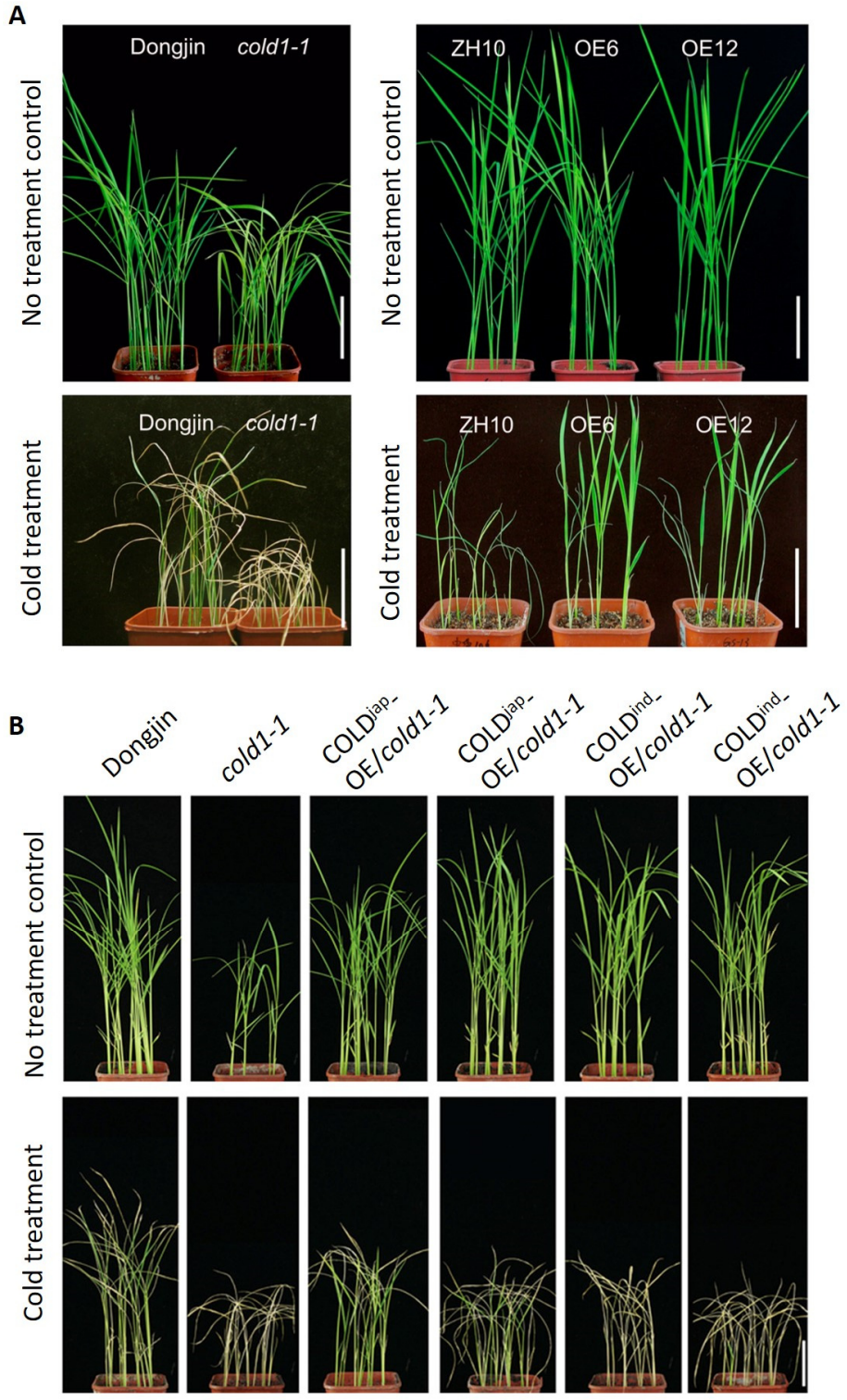

Figure 1.6. The effect of COLD1 on cold tolerance in rice

A) The *cold1-1* mutant shows chilling sensitivity in comparison with WT (Donjing) and rice COLD1 overexpression lines (OE6 and OE12) showed chilling tolerance in comparison with the WT (ZH10). B) Transgenic lines expressing $COLD^{jap}$ in *cold1-1* mutant background showed a better recovery after cold treatment than transgenic lines expressing $COLD^{ind}$ in *cold1-1*. Images taken from Ma et al. (2015).

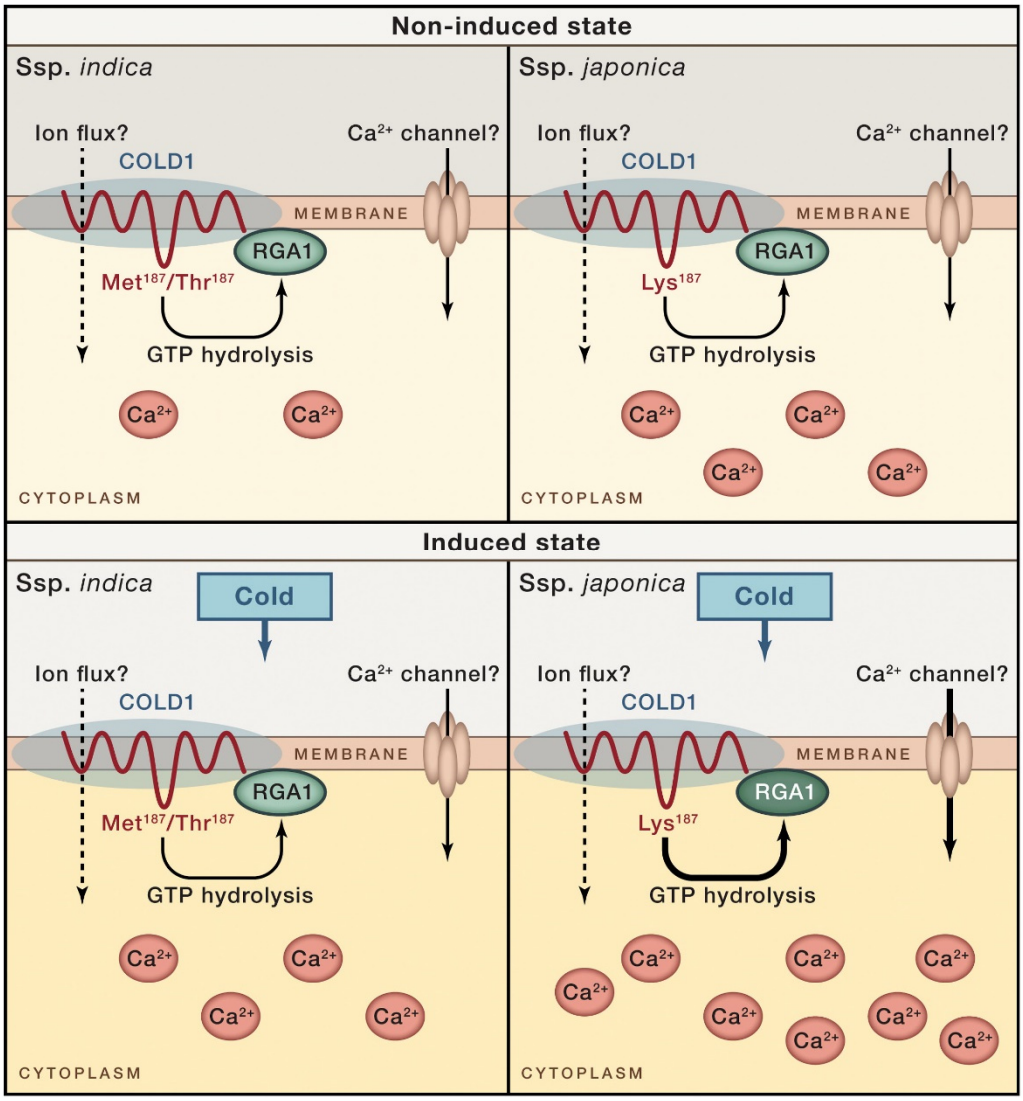

Figure 1.7. Model of rice COLD1 function in cold stress

The cold sensitive *indica* variety contains a methionine in the 187th residue of the COLD1 protein whereas *japonica* contains a lysine. This difference produces a higher Ca^{2+} concentration in the cytoplasm and a higher increase of cytoplasmic Ca^{2+} concentration after cold stress in *japonica* in comparison to the *indica* cultivar. Under cold stress, the GTPase activity of the Gα subunit (RGA1) is accelerated after RGA1 interacts with COLD1^{jap} but not with COLD1^{ind}. COLD1 functions as a Ca^{2+} channel or forms part of a Ca^{2+} channel. Figure from Manishankar and Kudla (2015).

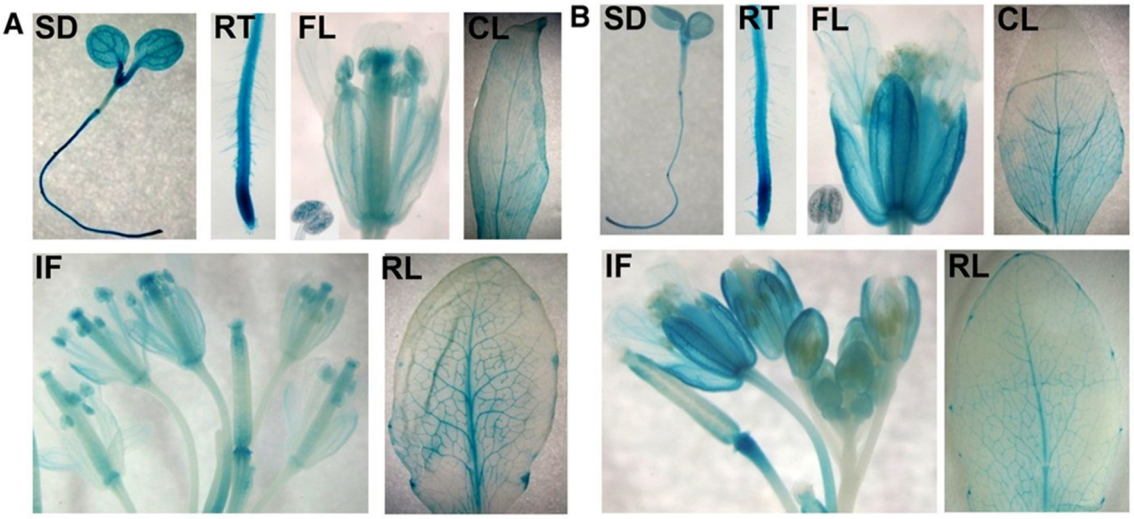

Figure 1.8. GUS staining showing the spatial expression of AtGTGs

A) AtGTG1 expression under control of the AtGTG1 promoter and B) AtGTG2 expression under the AtGTG2 promoter. SD= seedling, RT= root tip, FL= flower, CL= cauline leaf, IF= inflorescence, RL= rosette leaf. Image taken from Jaffé et al. (2012).

To analyse the subcellular localisation of GTG/GPHRs, green fluorescent protein (GFP) has been used and different localisations have been reported in different species (Table 1.4). In CHO cells, GTG/GPHR localises at the Golgi-TGN (Maeda et al., 2008) whereas in *Drosophila* and the amoeba *Dictyostelium discoideum* it localises at the ER and Golgi (Charroux and Royet, 2014, Deckstein et al., 2015). In plant however, there has been more controversy about the localisation of GTGs. Both AtGTGs have been reported at the plasma membrane in Arabidopsis protoplasts, however, no plasma membrane marker was used to corroborate this localisation (Figure 1.9) (Pandey et al., 2009). In an independent study, AtGTG1 showed ER and Golgi localisation when it was expressed transiently in tobacco cells, and co-localised with the ST (sialyltransferase) *trans* Golgi marker (Figure 1.9) (Jaffé et al., 2012).

Rice GTG localisation was analysed using two different plant species. ER localisation was observed in Arabidopsis protoplasts, where the rice GTG was co-localised with the BIP ER marker (Ma et al., 2015). Plasma membrane localisation was reported using a transient expression in tobacco protoplasts and in this case rice GTG was co-localised with the PIP2-cherry plasma membrane marker (Figure 1.9) (Ma et al., 2015). However, the PIP2 marker has been previously reported to also localise to the

ER (Lee et al., 2009). In wheat protoplasts, wheat GTG localised at the ER and plasma membrane and co-localised with the PIP2 marker (Dong et al., 2019). In tomato (*Lycopersicon esculentum* Mill.), LeGTG localised at the plasma membrane in Arabidopsis protoplasts and co-localised with the PM-rk marker (Zhang et al., 2020).

Table 1.4. The localisation of GTGs in different organisms

Organism	**Localization**
Chinese hamster ovary cells	Golgi-TGN (Maeda et al., 2008)
Drosophila melanogaster	ER and Golgi (Charroux and Royet, 2014)
Dictyostelium discoideum	ER and Golgi (Deckstein et al., 2015)
Arabidopsis thaliana	Plasma membrane in Arabidopsis protoplasts (Pandey et al., 2009) ER and Golgi in tobacco transient expression (Jaffé et al., 2012)
Oryza sativa (rice)	Plasma membrane in tobacco protoplast cells and ER in Arabidopsis protoplasts (Ma et al., 2015)
Triticum aestivium (Wheat)	Plasma membrane and ER in wheat mesophyll protoplasts (Dong et al., 2019)
Lycopersicon esculentum Mill. (Tomato)	Plasma membrane in Arabidopsis protoplasts (Zhang et al., 2020)

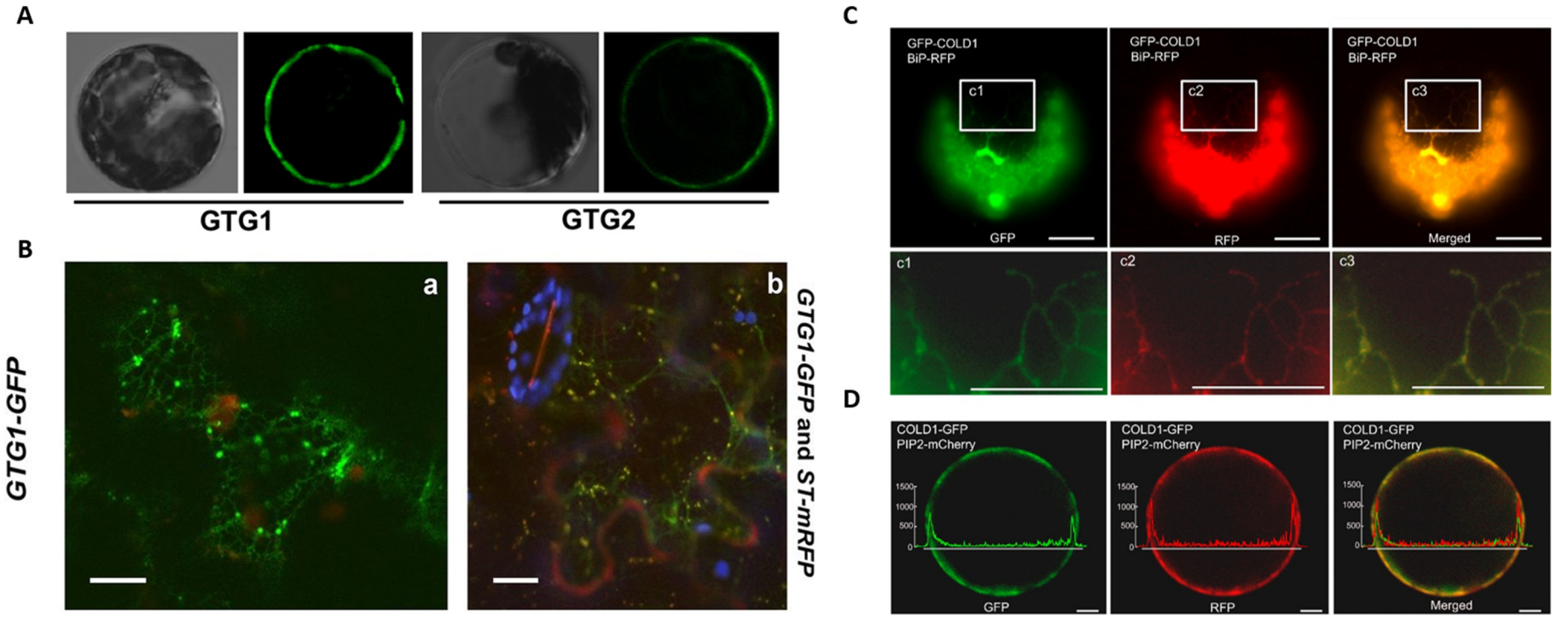

Figure 1.9. Arabidopsis and rice GTGs localisation in different studies

A) Transient expression of AtGTG1-GFP and AtGTG2-GFP in Arabidopsis protoplasts showing plasma membrane localisation (Pandey et al., 2009). B) Transient expression of AtGTG1-GFP in tobacco leaf cells showing ER and Golgi localisation in green and chloroplasts in red on the left and co-localisation of AtGTG1-GFP with Golgi marker ST-RFP in yellow, chloroplasts in blue and apoplast in red on the right (Jaffé et al., 2012). C) Transient expression of rice COLD1-GFP in Arabidopsis protoplasts co-localised with BIP-RFP ER marker. D) Transient expression of rice COLD1-GFP in tobacco protoplasts co-expressed with PIP2-mcherry marker (Ma et al., 2015).

1.7. Arabidopsis and rice as plant model systems

In this thesis, Arabidopsis and rice plants have been used to study the function of GTG/GPHR in plants, and to discover whether its function is conserved between both species. Arabidopsis is a dicotyledonous member of the *Brassicaceae* family and it was the first plant to have its genome sequenced (AGI, 2000). Arabidopsis has several advantages as a model organism, such as a short life cycle (approximately 6-7 weeks from germination to mature seeds), small size, large number of offspring and a relatively small genome of 125MB (containing 25,498 protein-encoding genes) (AGI, 2000). Thanks to the fully sequenced genome, many genes have been characterized and many families of proteins have already been discovered and studied. Since Arabidopsis is relatively easy to manipulate genetically, T-DNA insertion mutants have been generated to help identify the role of many proteins involved in different processes (AGI, 2000). All of the above make Arabidopsis a useful plant model organism to study gene function in plants.

The Arabidopsis life cycle has three main stages: vegetative, reproductive and embryogenesis (Figure 1.10). Vegetative growth starts with seed germination, followed by seedling formation. The first two embryonic leaves, known as cotyledons, and the roots are formed and the seedling develops to a fully mature plant. The reproductive period starts when the plant develops flowers and reproductive organs and continues during pollination. The fertilized ovule develops into a seed and siliques are formed at the final stage (Figure 1.10) (Vivian-Smith and Koltunow, 1999, Zeiger, 2006). Embryogenesis occurs after fertilization where two groups of meristem cells, the root and shoot apical meristems are developed (Zeiger, 2006). When the mature embryo is formed, the seed enters a dormancy phase in which germination is delayed until the environmental conditions are favourable (Nonogaki, 2014).

Rice (*Oryza sativa*) is the most widely consumed crop in the world. It is an annual monocotyledon and requires a temperate climate to grow, being more abundant in tropical and subtropical areas. The rice genome sequence became available during the Rice Genome Annotation Project, which provided a high quality annotation with 40,000-60,000 genes (Kawahara et al., 2013). Since then, T-DNA insertion mutant lines have been created making rice a popular model organism.

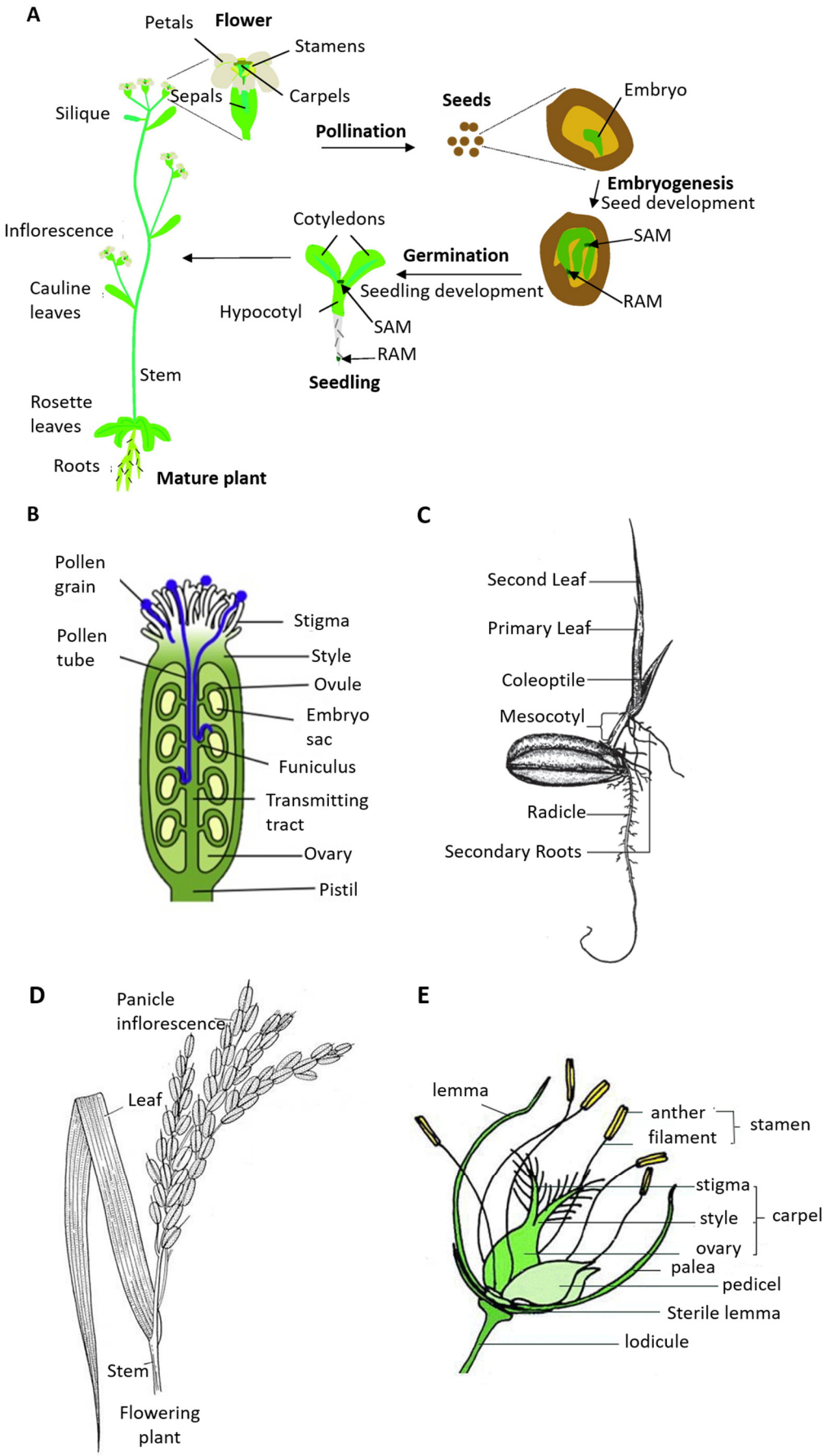

Figure 1.10. Arabidopsis and rice anatomy and life cycle diagram

A) Diagram showing Arabidopsis anatomy and life cycle. Mature plants have roots, rosette leaves, stems, cauline leaves, inflorescence, flower and siliques. Flowers contain sepals, petals, stamens and carpels. Seeds contain the embryo and during embryogenesis, the embryo grows and develops the shoot meristem (SAM) and root meristem (RAM). After germination, the seedling is produced with the hypocotyl and cotyledons. Figure taken from Diévart and Clark (2004). B) Schematic diagram of pollen tube growth in Arabidopsis. Pollen grains interact with the stigma and grow to reach the different ovules of the flower. Figure taken from Kanaoka and Higashiyama (2015). C) Diagram of a germinating seed in rice, showing the root and the shoot with the mesocotyl, coleoptile and leaves. Diagram taken from Hardke and Service (2013). D) Diagram of a rice flowering stem and panicle. Taken from www.cdn.biologydiscussion.com. E) Spikelet of a rice flower, which includes the stamens and carpel. Figure taken from www.pbl.ucdavis.edu.

Rice also has three main growth stages: vegetative, that includes germination and growth, reproductive, with panicle initiation and flowering, and ripening, that includes embryo and seed formation and maturation (Hardke and Service, 2013). As with Arabidopsis, under favourable environmental conditions, seeds that contain the endosperm and the embryo, germinate after imbibition of water. This action activates the embryo, producing two main structures: the radicle and the coleoptile that emerges, grows and elongates (Figure 1.10). A seedling then develops and the primary leaf appears. The plant continues to grow and develops more leaves and as new leaves are produced, older leaves senesce (Saichuk et al., 2009). During the reproductive stage, the panicle develops, flowering begins and pollination occurs. After the ripening phase begins, the embryo and grain are formed and matured and become ready to be harvested (Saichuk et al., 2009).

1.8. Aims of the thesis

The GTG/GPHRs are a conserved family of membrane proteins that are present in all eukaryotes. GTG/GPHRs have been shown to be involved in growth, development and fertility in mice (Tarutani et al., 2012), *Drosophila* (Charroux and Royet, 2014), *C. elegans* (Wong, 2014) and Arabidopsis (Jaffé et al., 2012). However, there is still much controversy regarding GTG/GPHR function since they have been associated with diverse functions in different organisms. GTG/GPHRs have been suggested to play roles as Golgi pH regulators in mice cell lines (Maeda et al., 2008), as ABA plasma membrane receptors in Arabidopsis (Pandey et al., 2009) and also as chilling tolerance sensors in rice (Ma et al., 2015). Due to these function differences, it is necessary to further investigate this protein family to fully understand their mechanism of action and whether they have a unified fundamental role. The aims of this thesis are:

Chapter 3: To study whether GTG/GPHRs have a conserved function between Arabidopsis and rice. This will be addressed by:

i) determining whether rice GTG can rescue the Arabidopsis *gtg1gtg2* double mutant defective growth phenotype. Since a mutation in a conserved glutamic acid in the 9th residue was found in the cloned sequence of rice GTG, the involvement of this polymorphism in the function and localisation of the protein will be also studied.
ii) investigating the localisation of rice GTG using Arabidopsis stable lines and transient expression in tobacco leaves to determine whether rice and Arabidopsis GTG exhibited the same intracellular localisation.
iii) analysing the proposed involvement of the lysine/methionine 187th residue of OsGTG in cold stress, that will be investigated using Arabidopsis plants. In addition, the cold tolerance of the Arabidopsis *gtg1gtg2* knockout mutant compared to WT plants will be studied. The involvement of the lysine/methionine amino acid difference in the 187th residue of OsGTG in the function and localisation of the protein will be also studied.
iv) investigating the phenotypic characteristics of a rice *gtg* knockout mutant and determining whether the rice *gtg* mutant has a similar growth and fertility defect as the Arabidopsis double mutant.

Chapter 4: To elucidate the function of rice GTG in the cells by:

i) studying whether OsGTG functions as an anion channel. This will be carried out using two electrophysiological approaches: whole-cell patch clamping in HEK293

cells expressing OsGTG and a planar lipid bilayer assay using OsGTG protein synthesised in a cell-free system.

ii) determining whether OsGTG plays a role in regulating endomembrane pH using WT and *gtg1gtg2* lines expressing the pH sensor pHluorin targeted to different endomembrane organelles.

Chapter 5: To study whether GTGs work through G proteins by:

i) determining whether rice GTG interacts with rice Gα *in vivo* using a bimolecular fluorescence complementation assay.

ii) investigating whether there is a genetic interaction between Arabidopsis GTGs and AtGPA1 by generating plants lacking *GTG1*, *GTG2* and *GPA1* genes by crossing *gtg1gtg2* with the *gpa1.4* mutant. The growth phenotype of the *gtg1gtg2gpa1.4* triple mutant will be analysed in comparison with WT, *gpa1.4* and the *gtg1gtg2* double mutant to test whether GTGs and GPA1 are involved in the same processes.

Chapter 2. Materials and methods

2.1. Plant growth

2.1.1. Soil growth conditions for *Arabidopsis thaliana* and *Oryza sativa*

Arabidopsis thaliana plants were grown in 8 cm pots (Desch, UK) in a soil containing Levingtons F5 no 2 (Green-Tech, UK), John Innes no 2 (John Innes Manufacturers Association, UK) and Sinclair vermiculite Medium Grade (Scot plants Direct, UK), in 1:1:1 ratio. Soil was sterilized autoclaving at 121°C for 15 minutes at one bar pressure and 0.28 g/L of Imidasect 5GR insecticide (Bayer Environmental Sciences SAS, UK) was added before used. Arabidopsis was grown in environmentally controlled rooms (ECRs), with 16 hours light at 120 μmol m^{-2} s^{-1} light intensity, 23°C temperature and 60% humidity, and 8 hours dark, at 18°C and 55% humidity. After the first flower was developed, plants were bagged in 60 x 30 x 10 cm flower sleeves (Geerings, UK) to avoid cross-pollination. Siliques were harvested after approximately 3 months. For the Arabidopsis long day growth experiment pictures were taken and were analysed using ImageJ software for plant height and rosette diameter measurements. Bolting and flowering times were calculated based on the number of days from planting. After plant maturity, all the seeds were harvested at the same time and seed yield was calculated by using the fresh weight of all the seeds harvested per line.

Oryza sativa was grown in 20 cm diameter pots (Desch, UK) in a soil containing Jack's Magic compost (Westland, UK) and horticultural sand (Westland, UK) in 1:0.5 ratio. The soil was previously sterilized autoclaving at 121°C for 15 minutes at one bar pressure and 0.28 g/L of Imidasept insecticide (Bayer Environmental Sciences SAS, UK) and Miracle-Gro all-purpose continuous-release (Micracle-Gro, UK) were added before used. Rice plants were grown in ECRs with 12 hours light at 150 μmol m^{-2} s^{-1}, 28°C temperature, 70% humidity and 12 hours dark, at 25°C, and 65% humidity. Rice seeds were pre-heated at 50°C for 3 days. Pericarp was removed before germination and the seeds were imbibed on wet filter paper in a petri dish for 6-7 days in the ECR conditions previously described. Germinated seeds were transferred to the previously described soil mix for the remaining of their growth. Seeds were harvested after

approximately 8-10 months. For the rice growth experiment, the height, number of leaves, tillers and panicles were measured throughout the growth of the plants. The number of seeds per panicles was counted after the plants were harvested. Rice WT and *gtg* mutant were obtained from Dr Gynheung An (Kyung Hee University, Crop Biotech Institute, Korea) (Jeon et al., 2000, Jeong et al., 2006).

2.1.2. Growth of Arabidopsis seedlings in plates

Arabidopsis seeds were sterilized with 15% (v/v) bleach (Domestos) for 15 minutes and were washed with sterilised distilled water five times. Seeds were individually sown onto plates containing 0.5x Murashige and Skoog (MS) medium (Duchefa), 1% (w/v) sucrose and 0.8% (w/v) agar (Sigma). Plates were sealed using 3M Micropore^{TM} tape (3M, UK), wrapped in aluminium foil and kept at 4°C for 48 hours. Plates were transferred to a Fitotron Plant Growth Chamber (Weiss Gallenkamp, UK) with 16 hours light/8 hours dark, at 23°C, 60% humidity and 120 µmol m^{-2} s^{-1} light intensity during the day and 18°C and 55% humidity during the night.

For root length experiments, sterilized seeds were plated individually onto 0.5x Murashige and Skoog media containing 0.8% (w/v) agar (Sigma Aldrich). Plates were kept at 4°C wrapped in aluminium foil for 48 hours and were transferred vertically to plant growth cabinets and grown for 14 days in the conditions described above. Pictures were taken at day 7, 10, 12 and 14. Root length was measured at day 10 using ImageJ software. At day 14, the fresh weight of the seedlings was weighted using a 5dp balance. For hypocotyl length experiments, seeds were sterilized and plated individually onto 0.5x Murashige and Skoog media containing 1% (w/v) sucrose (Fisher Scientific, UK) and 0.8% (w/v) agar (Sigma Aldrich). After 48 hours at 4°C in the dark, plates were transferred horizontally to plant growth cabinets with a light intensity of 120 µmol m^{-2} s^{-1} for 2 hours. After this period, in the low white light assays, plates were covered with a neutral density filter 211/210 (Lee Filters, Hampshire, UK) to generate 10 µmol m^{-2} s^{-1} light intensity, whereas in the dark experiments plates were wrapped in aluminium foil and transferred to a dark cabinet (0 µmol m^{-2} s^{-1}, 23°C constant temperature). Plants were grown for 5 or 7 days and photographs were taken at those time points after hypocotyls were placed against the agar in the plate. For hypocotyl length and cotyledons angle measurements, images were analysed using ImageJ software.

2.1.3. Generating Arabidopsis *gtg1gtg2gpa1.4* triple mutant

To generate the *gtg1gtg2gpa1.4* triple mutant, 5-6 weeks-old soil-grown plants were crossed by emasculating the maternal plant (*gtg1gtg2* double mutant) and transferring the pollen from the paternal plant (*gpa1.4* single mutant) onto the maternal stigma two days post emasculation. Crossed siliques were harvested after 4 weeks and were dried at room temperature before sowing the first generation. Seeds harvested from the cross were sown onto soil and heterozygosity was confirmed in the F1 generation plants by PCR (see section 2.3.5). After self-pollination of F1 heterozygous generation, the F2 generation was harvested, sown onto soil and screened for homozygous. Since no homozygous plants were found in this generation, double homozygous for *gtg1gtg2* and heterozygous for *gpa1.4* (*gtg1* (-/-), *gtg2* (-/-), *gpa1.4* (+/-)) was self-fertilized and the F3 generation was harvested. Seeds of the F3 generation were sown onto soil and screened to identify a triple homozygous.

2.1.4. Arabidopsis transformation

For Arabidopsis transformation, the vector of interest was first transformed into *Agrobacterium tumefaciens* strain GV3101 (section 2.2.4). The first inflorescence of 5-weeks-old Arabidopsis was clipped to increase the proliferation of secondary bolts and 6-week-old plants were transformed using the floral dip method (Clough and Bent, 1998). A positive colony of *Agrobacterium* carrying the vector of interest was grown into 5 mL of LB medium (section 2.2.1) containing 25 μM kanamycin, 30 μM gentamicin and 25 μM rifampicin and was incubated at 28°C, 225 rpm agitation overnight. This pre-culture was inoculated in 250 mL of LB medium containing the same antibiotic concentrations as above. This second culture was incubated at 28°C, 225 rpm agitation overnight. Acetosyringone (3',5'-dimethoxy-4'-hydroxyacetophenone, Sigma Aldrich) was added to the culture to a final concentration of 100 μM, leaving the culture to grow for 3 hours at the same conditions as before. Cultures were centrifuged at 4,560 rpm for 15 minutes. Each pellet was resuspended in 250 mL of 5% (w/v) sucrose and Silwet L-77 (Van Meeuwen Chemicals BV, NL) was added to a final concentration of 0.05% (v/v). Aerial parts of 6-week-old plants, with the first inflorescent previously clipped, were immersed into this solution with gentle agitation for 3 seconds. Plants were sealed with a plastic bag to maintain high humidity

and were placed in the shade for 24 hours. After this period, plants were returned to long day conditions (section 2.1.1) and first-generation seeds were harvested after 6-8 weeks.

For the positive transformant selection, seeds harvested from the dipped plants (T1 generation) were plated onto 0.5x MS media containing 1% (w/v) sucrose and 1% (w/v) agar with 50 μM hygromycin (Sigma Aldrich) antibiotic selection. Plates were incubated as previously described in section 2.1.2 and after two weeks, the positive transformants were transferred to soil (section 2.1.1) and allowed to self-fertilise. The T2 generation was harvested from those plants and was plated in the previously described media and grown in the same conditions for 2 weeks. Lines with a survival rate of 75% were transplanted onto soil for self-fertilisation. The T3 generation was harvested from those plants and was plated and grown in the conditions described above. Lines with a 100% survival rate were characterized as homozygous for the transformed construct. Three independent lines for each construct were generated. RNA was extracted from the T3 homozygous lines and RT-PCR was performed to confirm the presence of the transgene (see sections 2.3.2 to 2.3.5).

2.1.5. Arabidopsis cold stress experiment

The lines used for this experiment (WT Col-8, *gtg1gtg2* Col-8, WT Ws4, *gtg1gtg2* Ws4, *gtg1gtg2* expressing AtGTG1, *gtg1gtg2* expressing OsGTGe^{187K}, *gtg1gtg2* expressing OsGTGg^{187K} *gtg1gtg2* expressing OsGTGe^{187M} *gtg1gtg2* expressing OsGTGg^{187M}) were grown in soil (see section 2.1.1) using 35 x 22 x 5 cm trays. Six trays were used and 8 seeds per line per tray were planted. Each tray contained all the lines used in the experiment. Plants were grown at 23°C, with 16 hours light and 8 hours dark period for 19 days. Afterwards, three of the trays were transferred to 4°C for 10 days whereas the other three were kept at 23°C. After the cold treatment, the three trays that were at 4°C were transferred back to 23°C for a 7 day recovery period. The number of leaves, rosette diameter and stem length were measured throughout the experiment.

2.2. Bacterial growth

DH5α, DB3.1 and One Shot™ TOP 10 chemically competent strains for *Escherichia coli* (*E. coli*) and GV3101 strain for *Agrobacterium tumefaciens* (*Agrobacterium*) were used in this thesis (Table 2.1).

Table 2.1. Bacterial strains used in this thesis

Bacterial strain	Usage	Source
E. coli DB3.1	Propagation of destination vector containing *ccdB* gene	Homemade chemically competent
E. coli DH5α	Propagation of entry and expression vectors	Homemade chemically competent
E. coli TOP10	TOPO pENTR/D vector transformation	Invitrogen (USA)
Agrobacterium GV3101	Stable expression in Arabidopsis and transient expression in tobacco	Homemade chemically competent

2.2.1. Culture of bacteria

All bacteria strains were grown in Luria-Broth (LB) medium (1% (w/v) tryptone (Sigma Aldrich), 1% (w/v) NaCl (Sigma Aldrich), 0.5% (w/v) yeast extract (Bioshop), pH 7.0) or on LB agar plates (1.5% (w/v) agar Sigma Aldrich) prepared in sterile 18 MΩ H_2O. Both mediums were sterilized for 20 minutes at 121°C at one bar pressure. *E. coli* was incubated at 37°C and *Agrobacterium* at 28°C in Innova™ 4300 Incubator Shaker (New Bruskwick Scientific Ltd., UK) with 225 rpm agitation for liquid cultures. For agar plates, a Classic incubator (LEEC, UK) at 37°C was used for *E. coli* and a Gallenkamp Cooled Illuminated Incubator at 30°C was used for *Agrobacterium* strains.

2.2.2. Chemically competent *E. coli* preparation

E. coli was streaked onto non-selective LB agar plates and was incubated overnight at 37°C (section 2.2.1). A single well-isolated colony was inoculated into 5 mL LB medium and was grown overnight at 37°C with 225 rpm agitation. This pre-culture was

inoculated into 250 mL LB and incubated with moderated agitation (160 rpm) at 23°C for 8-14 hours until OD_{600} of 0.5 to 0.8 was obtained. The cultures were cooled for 10 minutes on ice before being centrifuged at 4,000 rpm for 10 minutes at 4°C in a Sorvall legend RT table-top centrifuge (Thermo Fisher Scientific, USA). Cells were washed twice with 20 mL of ice-cold transformation buffer (10 mM PIPES (piperazine-1, 2-bis [2-ethyanesulfonic acid]), pH 6.7, 250 mM KCl, 55 mM $MnCl_2.4H_2O$, 15 mM $CaCl_2.2H_2O$, Sigma Aldrich). Each pellet was resuspended in 1 mL of ice-cold transformation buffer containing 0.075 µl/mL (v/v) DMSO (Sigma Aldrich) and it was divided into 50 µL aliquots and immediately snap-frozen in liquid nitrogen before storage at -80°C.

2.2.3. *Agrobacterium* chemically competent cells preparation

Agrobacterium GV3101 strain was grown on selective LB agar plate with chromosomal and Ti plasmid antibiotics (25 µM rifampicin and 30 µM gentamicin) for 3 days at 28°C. A single isolated colony was inoculated into 5 mL of selective LB medium and grown at 28°C overnight with 225 rpm agitation. This culture was inoculated into 500 mL of selective LB and incubated at 28°C with 225 rpm agitation until an OD_{600} of 0.5 to 0.8. The culture was centrifuged twice at 4,000 rpm for 10 minutes at 4°C in a Sorvall legend RT table-top centrifuge (Thermo Fisher Scientific, USA) and the pellet was resuspended in 50 mL ice-cold sterile 18 MΩ H_2O in the first wash and in 5 mL of 10% (v/v) ice-cold sterile glycerol (Sigma Aldrich) in the second wash. Cells were divided into 50 µL aliquots and snap-frozen in liquid nitrogen before storage at -80°C.

2.2.4. Transformation of Chemically Competent *E. coli* and *Agrobacterium*

For *E. coli* cells transformation, 1 µL of plasmid DNA was added into the cells that were incubated on ice for 30 minutes followed by a heat shock at 42°C for 30 seconds. Cells were returned to ice for 2 minutes before adding 250 µL SOC media (2% (w/v) tryptone, 0.5% yeast extract, 10 mM NaCl, 2.5 mM KCl, 10 mM $MgCl_2$, 10 mM $MgSO_4$ and 20 mM glucose, Sigma Aldrich) for TOPO cloning transformation system or 800 µL of LB for the other transformations. The cells were incubated at 37°C for 1 hour with 225 rpm agitation. After the incubation, the cells were spread on selective LB

plates and grown overnight at 37°C. Colony PCRs were performed to confirm transformation success (section 2.3.5).

For GV3101 *Agrobacterium* transformation, 100 ng of the purified vector was added into the cells and were snapped-frozen into liquid nitrogen followed by a 5 minutes incubation at 30°C. 1 mL of LB was added and the cells were incubated for 3 hours at 28°C with 225 rpm agitation. Cultures were spread in selective LB plates with Ti plasmid, chromosomal and vector antibiotic selections. Colony PCRs were performed to confirm transformation success (section 2.3.5).

2.2.5. Plasmid DNA purification from bacterial cells

An isolated colony from the *E. coli* containing the vector of interest was inoculated into 5 mL selective LB media, containing the appropriate antibiotic, and was grown at 37°C with 225 rpm agitation overnight (section 2.2.1). Plasmid DNA was extracted using Qiagen Spin Mini-prep kit (Qiagen) following manufacturer's instructions. The DNA was eluted in 20 µL sterile 18 MΩ H_2O and quantified by spectrophotometry (section 2.3.3).

2.3. Molecular methods

2.3.1. Genomic DNA extraction from Arabidopsis and rice

For genomic DNA extraction from plant tissues, DNAmite plant genomic DNA extraction kit (Microzone, UK) was used according to manufacturer's instructions. A couple of leaves from Arabidopsis were added into tubes containing 300 µL of cell lysis (LA) solution and tissues were ground using a pestle in the tube. For rice, one leaf was ground to fine powder using liquid nitrogen in a pestle and mortar, and the same amount of lysis solution was added. 30 µL of protein denaturation (PA) buffer were added and the suspension was centrifuged at 10,000 rpm for 5 minutes. 200 µL supernatant were transferred into a new tube and centrifuged at 10,000 rpm for 5 minutes. 175 µL of supernatant were transferred into a new tube containing 175 µL of microCLEANg (CA) solution before they were incubated at room temperature for 5 minutes. The solution was centrifuged at 13,000 rpm for 7 minutes and the pellet was resuspended in 20 µL of

sterile 18 MΩ H_2O. The DNA concentration was determined by spectrophotometry (section 2.3.3).

2.3.2. RNA extraction from Arabidopsis and rice

For all RNA methods, buffers and plasticware were autoclaved for 90 minutes at 121°C prior to usage at one bar pressure. Arabidopsis and rice tissues were snap-frozen into liquid nitrogen and ground to a fine powder using a prechilled pestle and mortar. The tissue was homogenised using 1 mL of Trizol reagent (Invitrogen, USA) and 200 µL chloroform (Sigma Aldrich). The solution was incubated at room temperature for 3 minutes and was centrifuged at 12,000 *g* at 4°C for 15 minutes. The upper phase was transferred into a new tube and 50% (v/v) isopropyl alcohol was added. The sample was incubated at room temperature for 10 minutes and was centrifuged at 12,000 *g* at 4°C for 10 minutes. The pellet was washed twice with 75% (v/v) ethanol and was centrifuged at 7,600 *g* at 4°C for 5 minutes. Air-dried RNA pellet was resuspended in 30 µL TE buffer (1 mM Na_2EDTA and 10 mM Tris/HCl, pH 7.0) and RNA concentration was measure by spectrophotometry (section 2.3.3). Additionally, RNA quality was determined by running 1 µg of RNA on a 1% (w/v) agarose electrophoresis gel (section 2.3.6).

2.3.3. DNA/RNA quantification using NanoDrop

The quantity and purity of DNA and RNA were determined using a NanoDrop ND-1000 spectrophotometer (Thermo Fisher Scientific, USA) using the program ND-1000 V3.7.1. One µL of DNA or RNA sample was loaded onto the pedestal and absorbance was measured over 200-300 nm. The program used the Beer-Lambert equation ($A=Ɛ \times b \times c$) to calculate the nucleic acid concentration from the absorbance reading at 260nm.

2.3.4. cDNA synthesis

To synthesise cDNA, 1 µg of RNA was used and 1 µL of 10 µM dT18 primer (Sigma Aldrich) was added in a total volume of 3.6 µL using sterile 18 MΩ H_2O. RNA was denatured at 72°C for 5 minutes. To synthesise the first strand, ImPromII RT reverse transcriptase (Promega) was used. 1x buffer (Promega), 8 mM $MgCl_2$, 2 nM dNTPs (containing 2 nM each of dATP, dTTP, dCTP and dGTP) and 1 µL ImPron-II™

reverse transcriptase were added in a final volume of 20 µL with sterile 18 MΩ H_2O. The samples were incubated at 25°C for 5 minutes, 42°C for 60 minutes and 70°C for 15 minutes using a peqSTAR 96 Universal PCR machine (peqLAB, DE). cDNA was stored at -20°C.

2.3.5. PCR and RT-PCR amplification

PCR was used to amplify DNA using genomic or plasmid DNA as a template whereas RT-PCR was used to amplify RNA using cDNA as a template. PCR tubes (Starlab Ltd) and peqSTAR 96 Universal PCR machine (peqLAB, DE) were used. For reactions that did not need a non-proofreading enzyme, the Taq polymerase Biomix Red (Bioline) was used whereas for reactions that needed a proofreading enzyme, *Pfu* (Promega) was used. See reagent concentrations and cycle conditions in Table 2.2 and Table 2.3 respectively. Colony PCRs were performed to confirm successful bacteria transformation. To do so, instead of the DNA template, a small fraction of the colony was picked with a sterile pipette tip and dipped into the PCR tube containing the rest of reagents. To amplify products for cloning or sequencing, the proofreading enzyme *Pfu* (Promega) was used. Primers were obtained from Integrated DNA technologies and Sigma Aldrich. The primers used for cloning, colony PCR and sequencing are shown in Table 2.4.

The homozygosity of the rice *gtg* mutant was determined by PCR using genomic DNA of the plants extracted with DNAMITE plant Kit (Microzone Ltd, UK) according to the manufacturer's instructions (section 2.3.1). For the PCRs, Biomix Taq (Bioline) and two sets of primers were used: one that binds to the gene of interest, to confirm the absence of the gene in the mutant, and another set that binds to both the T-DNA vector and the gene to confirm the presence of the T-DNA insertion in the mutants. Gene expression of the homozygous lines was analysed by RT-PCR using full-length primers for *OsGTG*. The primers used for the genotype of the rice *gtg* mutant and the analysis of the full-length transcripts are shown in Table 2.5.

Table 2.2. PCR reagent concentrations

	Biomix red reaction	***Pfu* reaction**
Reagent	**Concentration**	**Concentration**
2X Biomix buffer	1x	-
10X *Pfu* buffer	-	1x
10 mM dNTPs	-	200 µM
10 µM forward primer	0.2 µM	1 µM
10 µM reverse primer	0.2 µM	1 µM
Template DNA	0.1-0.5 µg/colony trace	0.1-0.5 µg
Pfu polymerase	-	1 Unit
Sterile 18 MΩ H_2O	Up to 10 µL	Up to 25-50 µL

Table 2.3. PCR cycle conditions

	Biomix Red Reaction	***Pfu* reaction**
Step	**Temperature and duration**	**Temperature and duration**
Initial denaturation	94 °C 2 minutes	95 °C 2 minutes
Denaturation	94°C 30 seconds	95 °C 1 minutes
Annealing	55-62 °C 1 minute	55-62 °C 30 seconds
Extension	72 °C 1 minutes /1kb	72 °C 1.5 minutes /1kb
Repeat cycle	38 cycles (semi-quantitative, 25-30 cycles)	35 cycles
Final extension	72 °C 5 minutes	72 °C 5 minutes
Storage	4 °C indefinite	4 °C indefinite

Table 2.4. Primers used for TOPO cloning, colony PCRs and sequencing

Primer name	Sequence
Primers used for cloning	
OsGTG topo F1	CACCATGGGTTGGGGC
OsGTG stop R1	TCAATCAATTGGGTGCTTGTC
OsGTG no stop R1	ATCAATTGGGTGCTTGTCTG
OsGPA topo F2	CACCATGTCCGTGCTTACCTG
OsGPA no stop R1	AGTTCCTTCCCTGGAGCGTC
Primers used for colony PCRs and sequencing	
M13 F	GTAAAACGACGGCCAG
M13 R	CAGGAAACAGCTATGAC
pMDC35S	GTAAAACGACGGCCAG
MDCnos R	AAGACCGGCAACAGGATTC
GFP R	CTGTTGACGAGGGTGTCTCC
T7	TAATACGACTCACTATAGGG
PIVEX 5 F2	TTCACACAGGAAACAGCTATGA
PIVEX 3 R	TTTATTATGCATCTTGACTACCTCAAGTTG

Table 2.5. Primers used for rice *gtg* mutant genotype and full-length transcript

Primer name	Sequence
OsGTG F (cold1 RP)	TCTGTTCGAGGTTTCTTGGC
OsGTG R (cold1 LP)	CATCACGATGCAAAGCATTC
RBpGA	AACGCTGATCAATTCCACAG
OsGTG topo F1	CACCATGGGTTGGGGC
OsGTG stop R1	TCAATCAATTGGGTGCTTGTC
UBQ F	CCGCAAGAAGAAGTGTGGTC
UBQ R	ACGATTGATTTAACCAGTCCATGA

To confirm the heterozygosity or homozygosity of the *gtg1gtg2gpa1.4* triple mutants, genomic DNA was extracted from plants using DNAMITE plant Kit (Microzone Ltd, UK) (section 2.3.1) and two sets of primers were used for the PCRs (Biomix Taq (Bioline)) as previously described, one to confirm the presence or absence of the gene and the other to confirm the presence of the T-DNA. After self-pollination of F1 heterozygous generation, the F2 generation was harvested, sown onto soil and screened for homozygous by genomic DNA PCR. Since no homozygous plants were found in this generation, double homozygous for *gtg1gtg2* and heterozygous for *gpa1.4* (*gtg1* (-/-), *gtg2* (-/-), *gpa1.4* (+/-)) was self-fertilized and the F3 generation was harvested. Seeds of the F3 generation were sown onto soil and screened to identify a triple homozygous plant by genomic DNA PCR. Three triple homozygous plants were found in this generation and were confirmed three times by PCR. Gene expression of those lines was analysed by RT-PCR using full-length primers for each of the genes. The primers used for the genotyping of the *gtg1gtg2gpa1.4* mutant and the analysis of the full-length transcripts are shown in Table 2.6.

2.3.6. DNA/RNA electrophoresis gel

RNA, PCR products and restriction digests (section 2.3.9) were analysed on 1% (w/v) agarose in TAE buffer (1 mM EDTA, 40 mM Tris/acetate, pH 8.0) gel containing 2.5 μL/100 mL NANCY-520 dye (Sigma Aldrich) for DNA detection. The PCR or restriction digest reactions were loaded into the wells alongside 5 μL of Hyperladder 1kb (Bioline) molecular weight marker to assess the product size. Gels were run in 1x TAE buffer at 100-120 V for an hour using Power Pac 200/2.0 (Bio-Rad, USA). Gel products were visualized using a UV transilluminator (Syngene).

2.3.7. DNA purification from agarose gels

To purify the DNA from agarose gel, the agarose band was cut out from the gel under UV light using a clean scalpel blade and was purified using Qiaquick Gel Extraction kit (Qiagen, USA) according to the manufacturer's instructions. Buffer QG was added to the tube containing the agarose gel in a 3:1 ratio (v/w) and was incubated at 50°C for 10 minutes. One volume of 100% isopropanol (v/v) (Sigma Aldrich) was added and the sample was loaded into a column prior to centrifugation at 13,000 rpm

for 1 minutes. 500 µL of GQ buffer were added into the column and was centrifuged at 13,000 rpm for 1 minute. The column was washed by adding 750 µL of PE buffer and centrifuging the sample at 13,000 rpm for 5 minutes. The column was eluted into a new tube using 20 µL sterile 18 MΩ H_2O by centrifuging at 13,000 rpm for 1 minutes. DNA concentration was quantified by spectrophotometry (section 2.3.3).

Table 2.6. Primers used for Arabidopsis *gtg1gtg2gpa1.4* mutant genotype and full-length transcripts

Primer name	Sequence (5'- 3')
GTG1 2F	ATTGGGATGTTGATTGTGA
GTG1 1R	TTACTCGATGGCGTGCTTAT
LBa1	TGGTTCACGTAGTGGGCCATCG
FR2 RT F	GGCTATGCGTGTTCCATTTAC
FR2 RT R	TCGTCAAGAATCCCCTCAC
GTG2 1R	AAGTGAAAGCCTCCGTCTA
AtGPA1 F	CACCATGGGCTTACTCTGCAGTAGA
AtGPA1 R_S	TCATAAAAGGCCAGCCTCCAGT
FR1 F	ATGAGTTACGGATGGGCG
AtGTG1 R	TTACTCGATGGCGTGCTTATC
Actin F	GGTAACATTGTGCTCAGTGGTGG
Actin R	CTCGGCCTTGGAGATCCACATC

2.3.8. Gateway ® cloning

TOPO® cloning system (Invitrogen, USA) was used to clone the gene of interest into the entry vector. The forward primers were designed to contain the CACC (5'-3') sequence prior to the start codon of the gene of interest (primers in Table 2.4). A proofreading enzyme *Pfu* polymerase (Promega) was used for the PCR reaction to amplify the gene of interest. After amplification and purification of the gene of interest (section 2.3.5 to 2.3.7), the fragment was cloned into TOPO® pENTR/D entry vector (Invitrogen, USA) according to manufacturer's instructions. 20 ng of the purified PCR

product of interest were added to 1 µL of salt solution and 10 ng of TOPO® pENTR/D entry vector, reaching a total volume of 3 µL with sterile 18 MΩ H_2O. The reaction was incubated for 3 hours at room temperature and transformed into One Shot® TOP 10 chemically-competent *E. coli* cells as described in section 2.2.4. The culture cells were spread on LB agar plates containing 50 µM kanamycin. Colony PCRs (section 2.3.5) were performed to select the positive colonies that contained the gene of interest inserted into TOPO® pENTR/D entry vector. This was further confirmed with restriction digest analysis after the plasmid DNA was extracted using Qiagen Mini-prep kit (Qiagen, USA) following the manufacturer's instructions (section 2.2.5 and 2.3.9). To introduce the gene of interest, cloned into pENTR/D entry vector, into a destination vector, the LR Clonase™ reaction (Invitrogen, USA) was applied following the manufacturer's instructions. For destination vectors that contain the kanamycin resistant gene, 500 ng of the pENTR/D entry vector cloned with the gene of interest were digested with *Pvu*I restriction enzyme prior to the LR clonase recombination. For the LR reaction, 75 ng of the destination vector were mixed with 75 ng of digested or undigested cloned pENTR/D entry vector in a final volume of 4 µL with TE (pH 8.0). One µL of Clonase™ II enzyme was added and the reaction was incubated at 25°C for 8-10 hours. The reaction was halted by the addition of 0.5 µL of Proteinase K followed by incubation at 37 °C for 10 minutes. The reaction was transformed into chemically competent DH5α *E. coli* cells (section 2.2.4) and the culture was spread in LB plates with the appropriated antibiotic selection (100 µM kanamycin or 100 µM ampicillin). See Table 2.7 for destination vectors and their antibiotic selection. Colony PCR and restriction enzyme digest were performed to confirm the correct insert location and orientation (sections 2.3.5 and 2.3.9).

2.3.9. Restriction enzyme digest analysis

Restriction enzyme digestions were performed in 10 µL reaction, where 500 ng of isolated DNA (section 2.2.5) were added to 1x buffer, 1 mM BSA and 5 units of restriction enzyme, making a final volume of 10 µL with sterile 18 MΩ H_2O. The whole reaction was incubated for 2 hours at 37°C. Samples were visualized by 1% agarose (w/v) gel electrophoresis (section 2.3.6). The product sizes were predicted using pDRAW32 software.

Table 2.7. List of destination vectors used in this thesis

Destination vector	Organism of transformation	Bacterial antibiotic selection
pMDC32	*Arabidopsis thaliana*	Kanamycin
pMDC83	*Arabidopsis thaliana*	Kanamycin
pDEST GwVYNE	*Nicotiana tabacum*	Kanamycin
pDEST GwVYCE	*Nicotiana tabacum*	Kanamycin
pcDNA-DEST47	Mammalian cells	Ampicillin
pIVEX1.3	Wheat germ CFPS	Ampicillin

2.3.10. Restriction-ligation cloning

Restriction-ligation cloning was used for expression vectors that were not Gateway compatible, such as pIVEX1.3 vector. To clone the gene of interest into pIVEX1.3, the restriction sites *Nde*I and *Sac*I were added to *OsGTG* at the 5' and 3' end respectively, and *Not*I and *Xho*I were added to *RGA1*. For the amplification, the proofreading enzyme *Pfu* polymerase was used (section 2.3.5) with primers that were designed to amplify the full-length of the gene adding in the forward and the reverse *Nde*I and *Sac*I or *Not*I and *Xho*I restriction sites sequences (primers in Table 2.8). After amplification and gel purification (section 2.3.7), the fragment and the empty destination vector were digested for 4 hours using the *Nde*I and *Sac*I restriction enzymes (section 2.3.9). Dephosphorylation of the digested destination vector was done using Anza^{TM} alkaline phosphatase (Thermo Fisher, USA), where 17 µL of the purified digested vector were mixed with 2 µL phosphatase Anza buffer plus 1µL phosphatase Anza enzyme. The reaction was incubated for 1 hour at 37°C followed by 20 minutes at 80°C for inactivation of the enzyme. The ligation of the digested insert with the dephosphorylated vector was done in a 3:1 ratio (insert: vector). 5 µL of Anza^{TM} T4 ligase master mix (Thermo Fisher, USA) were added making a final volume of 20 µL with sterile 18 MΩ H_2O. The ligation reaction was incubated overnight at 4°C. 5 µL of the ligation reaction mix were transformed into *E. coli* DH5α cells (section 2.2.4) and cells were spread in LB plates with 100 µM ampicillin and incubated overnight at 37°C.

Colony PCR and restriction digest analysis of the purified plasmid DNA were performed to select and confirm the positive transformant (sections 2.3.5 and 2.3.9).

Table 2.8. Primers used in restriction-ligation cloning

Primer name	Sequence
OsGTGe NdeI F	GGAACTACATATGGGTTGGGGCGCGGTGGTGTACGAGG
OsGTGg NdeI F	GGAACTACATATGGGTTGGGGCGCGGTGGTGTACGGTG
OsGTG SacI NS	TAGGAGCTCTATCAATTGGGTGCTTGTCTG
OsGPA NotI F	GATTCTGCGGCCGCATGTCCGTGCTTACCTGTGTG
OsGPA XhoI NS	ATAACTCGAGAGTTCCTTCCCTGGAGCGTCT

2.3.11. Site-directed mutagenesis by overlapping PCR

All the site-directed mutagenesis presented in this thesis was achieved by overlapping PCR. Primers that included the base pair mutation were designed in the forward and reverse strand (see Table 2.9 for primer used for mutagenesis by overlapping PCR). These primers have enough overlap sequence of the gene to allow the full-length of the gene to be amplified. For mutagenesis by overlapping PCR, three independent PCRs using the proofreading enzyme *Pfu* (Promega) were carried out (section 2.3.5). In one PCR, a forward primer that binds at the beginning of the gene and a reverse primer that includes the mutation were used. In the second PCR, a forward primer that includes the mutation and a reverse primer that binds at the end of the gene were used. The products of both PCRs were run in an agarose gel, purified (sections 2.3.6-2.3.7) and used in a third PCR to allow both fragments to anneal to each other. In this third PCR, both purified fragments and the TOPO gene primers for full-length amplification were used. The PCR reagent composition and conditions for the three PCRs are shown in Table 2.10 and Table 2.11 respectively. The new product was purified from an agarose gel and was transformed into TOPO® pENTR/D entry vector (section 2.3.8). Colony PCR and restriction digest of the cloned pENTR/D (sections 2.3.5 and 2.3.9) confirmed the success of the cloning and the gene was then sequenced in forward and reverse directions to confirm the presence of the mutation.

Table 2.9. Primers used for overlapping PCR mutagenesis

Primer name	Sequence
OsGTG E9G F2	GCGGTGGTGTACGGTGGCGGCGTGGTGG
OsGTG E9G R2	CCACCACGCCGCCACCGTACACCACCGC
OsGTG K187M F	CACTGTTTATCAGGGAAATTGATGAAATGGACATCAAAA CATTGG
OsGTG K187M R	CCAATGTTTTGATGTCCATTTCATCAATTTCCCTGATAAA CAGT

2.3.12. DNA sequencing

Plasmid DNA or purified DNA from gels were sent for Sanger sequencing (Source Bioscience Limited and Eurofins genomics) with a specific forward and reverse primers for each DNA. The sequences were visualised using BioEdit Sequence Alignment Editor Program and aligned using Muscle Omega website (http://www.ebi.ac.uk/Tools/msa/muscle/).

Table 2.10. Overlapping PCR reagent composition

Reagent in first and second PCRs	Volume used in first and second PCRs	Reagent in third PCR	Volume used in third PCR
10X *Pfu* buffer	5 µL	10X *Pfu* buffer	2.5 µL
10 mM dNTPs	1 µL	10 mM dNTPs	0.5 µL
10 µM forward primer	5 µL	Purified template 1	5 µL
10 µM reverse primer	5 µL	Purified template 2	5 µL
Template DNA (unmutated sequence, 50-100 ng/ µL concentration)	2 µL	10 µM forward and reverse primers	2.5 µL each
Pfu polymerase	0.4 µL	*Pfu* polymerase	0.2 µL
Sterile 18 MΩ H_2O	31.6 µL	Sterile 18 MΩ H_2O	8.43 µL

Table 2.11. Overlapping PCR conditions

Step	Conditions first and second PCR	Conditions third PCR
Initial denaturation	95°C 2 minutes	95°C 2 minutes
Denaturation	95°C 1 minute	95°C 1 minute
Annealing	55°C 30 seconds	60°C 30 seconds
Extension	72°C 2 minutes	72°C 2 minutes
Repeat cycle	35 cycles	15 cycles (using the overlap of both fragments as primers)
Initial denaturation		95°C 2 minutes
Denaturation		95°C 1 minute
Annealing		55°C 30 seconds
Extension		72°C 2.5 minutes
Repeat cycle		25 cycles (after adding forward and reverse full-length primers)
Final extension	72°C 5 minutes	72°C 5 minutes
Storage	4°C indefinite	4°C indefinite

2.4. Protein methods

2.4.1. SDS-PAGE

Proteins were run and separated in 10% (v/v) acrylamide SDS-PAGE (sodium dodecyl sulphate polyacrylamide gel electrophoresis) gels. Running and stacking gels were prepared following the composition shown in Table 2.12. The running gel was prepared first and left to set, followed by the staking gel that was set on top of the running gel. A gel comb was inserted into the stacking gel for the formation of the wells. After the gel was polymerized, the gel was inserted into a gel tank (BioRad), was covered with running buffer (25 mM Tris, 192 mM Glycine, 0.1% (w/v) SDS) and the comb was removed. The protein sample (2 µL) was mixed with 1/3 of 4x loading buffer (0.5 M Tris-HCl pH 6.6, 10% (w/v) SDS, 50% (w/v) glycerol, bromophenol blue, 0.4 mL β-mercaptoethanol) and loaded into the well. 5 µL of SDS-6B molecular marker

(Sigma) was used per gel, which was pre-heated for 2 minutes at 90°C prior used. The gel was run at 80 mV for 15 minutes until the samples reached the running gel section and at 150 mV for 50 minutes until the samples reached the end of the gel. Once the electrophoresis was finished, the gel was removed from the tank, disassembled and the stacking gel was discarded. Two gels were run in parallel each time and they were used for subsequent assays: Coomassie staining or western blot analysis (sections 2.4.2 and 2.4.3 respectively).

2.4.2. Coomassie staining

After the proteins were run in a SDS-PAGE electrophoresis gel (section 2.4.1), one of the gels was used for Coomassie staining to see the proteins that were present in the extract. The gel was incubated with Coomassie blue staining (methanol, acetic acid and water in a 4:1:5 ratio with 0.25 g of Coomassie Brilliant Blue) for 1 hour on a slow speed shaker. The Coomassie staining was then removed and the gel was incubated with destaining solution (methanol, acetic acid and water in a 4:1:5 ratio) for 1 hour on a slow speed shaker. The old destaining solution was replaced with fresh one several times until the Coomassie staining background was removed. The gel was revealed using Odyssey fluorescence scanner (Li-Cor, USA) at 700 nm intensity.

Table 2.12. 10% SDS-PAGE gels buffer composition

Running gel	**Stacking gel**
3.6 mL 30% acrylamide (Sigma)	1 mL 30% acrylamide (Sigma)
4.5 mL water	4.2 mL water
2.7 mL Lower Tris buffer 1.5 M Tris pH 8.8 0.4% SDS (Fisher Scientific)	1.75 mL Upper Tris buffer 1 M Tris pH 6.8 0.4% SDS (Fisher Scientific)
5 µL TEMED (Sigma)	5 µL TEMED (Sigma)
40 µL 40% APS (sigma)	40 µL 40% APS (Sigma)

2.4.3. Western blot

After the proteins were run in a SDS-PAGE electrophoresis gel (section 2.4.1), one of the gels was used for western blot analysis to visualise the protein of interest. The acrylamide gel was transferred into a PVDF (Polyvinylidene difluoride) hybond-P membrane (Amersham Pharmacia biotech) previously hydrated in methanol for 30 seconds. Two sets of filter paper, sponge pads and the PVDF membrane were soaked in transfer buffer (25 mM Tris pH 7.8, 190 mM Glycine, 20% (v/v) methanol) and placed with the acrylamide gel. The setup was inserted in a wet transference system (Biorad) and the transference was run at 100 mV for 1 hour. After the transference, the membrane was blocked for 1 hour using 5% milk in TBST buffer (20 mM Tris-Cl pH 7.5, 150 mM NaCl. 0.1% (v/v) Tween 20). The membrane was incubated overnight at 4°C in a 1/500 dilution of mouse anti-His antibody (R&D system) in 5% milk in TBST buffer (with slow agitation). The next day the antibody solution was removed and the membrane was incubated with 1/15,000 dilution of fluorescence anti-mouse 800 secondary antibody for 1 hour on a slow speed shaker. The antibody solution was removed and the membrane was washed five times with TBST buffer for 5 minutes at a time on a slow speed shaker. The membrane was revealed using Odyssey fluorescence scanner (Li-Cor, USA) at 800 nm intensity for the antibody signal and at 700 nm for the ladder signal.

2.5. Localisation studies

2.5.1. Transient expression in tobacco

A positive colony of GV3101 *Agrobacterium* transformed with the plasmid of interest (section 2.2.4) was used for transient expression in tobacco leaves. A single well-isolated *Agrobacterium* colony was inoculated in 5 mL LB medium containing 25 µM of rifampicin, 30 µM of gentamicin and 25 µM of kanamycin. The cultures were incubated at 28°C overnight (section 2.2.1) and were then centrifuged at 4,000 rpm for 5 minutes and resuspended in 2 mL infiltration medium (2 mM Na_3PO_4, 50 mM MES (2-(N-morpholino)ethanesulfonic acid), pH 5.6, 0.5% (w/v) D-glucose, 60 mg/L acetosyringone in DMSO). The cells were incubated at room temperature for 2 hours and centrifuged at 4,000 rpm for 5 minutes. The pellet was resuspended to a final OD_{600} of 0.5 with infiltration medium. For co-expression or bimolecular fluorescence

complementation (BiFC) assays, cultures for both plasmids were mixed at the same OD_{600} of 0.5. 4-6 weeks-old leaves from tobacco plants (*Nicotiana tabacum*) were infiltrated with the culture as described in Sparkes et al. (2006). Infiltrated leaves were grown in normal conditions in the glasshouse for 48 hours before they were analysed by confocal microscopy (section 2.5.2).

2.5.2. Confocal fluorescence microscopy

Samples of 1 cm of plant leaf disc were mounted in water on microscope slides with coverslips. Fluorescence was detected in a Leica SP8 confocal laser scanning microscope. GFP excitation was at 488 nm, emission at 550-550 nm; YFP excitation at 514 nm, emission at 520-560 nm; RFP excitation at 561 nm, emission at 565-600 nm; mOrange excitation at 561 nm, emission at 563-590 nm; chlorophyll autofluorescence excitation at 633 nm, emission at 650-700 nm. HyD3 detector and 40x and 63x objectives with specific immersion oil were used.

For HEK293 cells confocal analysis, the transfected cells (section 2.6) were fixed into a glass coverslip using 4% paraformaldehyde in PBS (137 mM NaCl, 2.7 mM KCl, 10 mM Na_2HPO_4, 1.8 mM KH_2PO_4, pH 7.4 with HCl) and incubated for 7 minutes at room temperature. The paraformaldehyde was removed and washed with 1 mL PBS. A drop of DAPI and a drop of lectin staining were added to the slide and was then covered with the coverslip and sealed with nail polish. The cells were analysed using a Leica SP8 confocal laser microscope with HyD3 detector, 63x objective and the conditions described above, with a resolution of 512 x 512. DAPI staining excitation was at 405 nm and lectin staining excitation was at 561 nm.

2.5.3. ER and Golgi bodies quantification

The number of ER bodies per cell was quantified using WT, *gtg1gtg2* and *gtg1gtg2* expressing OsGTG lines that all contained HDEL pHluorin marker (section 2.8). Golgi bodies per cell were quantified using *gtg1gtg2* expressing several versions of OsGTG protein tagged with GFP. Videos of the different lines were taken using a Leica SP8 confocal microscopy with 488 nm excitation and 500-550 nm emission. HyD3 detector and 63x objective were used. The ER and Golgi body numbers were counted from those videos using ImageJ software.

2.6. Patch-clamping in HEK293 cells

2.6.1. HEK239 cells culture

The HEK293 cells were cultured in Dulbecco's Modified Eagle's Medium-High glucose (Sigma Aldrich). 500 mL of this medium was completed by the addition of 50 mL heat inactivated FBS (fetal bovine serum) Qualified H+ (Gibco) plus 5 mL penicillin streptomycin solution (Pen Strep) (Invitrogen, USA). The cells were grown in a T75 flask (Corning®) with 12 mL of complete medium in an incubator set at 37°C in 5% CO_2 and were kept between 10% and 90% confluency. The cells were transferred into a new flask every two days or when the cells reached a confluency of 80% -100%. To passage the cells, the medium was removed from the flask and 1 mL of trypsin (Trypsin-EDTA solution (Sigma-Aldrich)) was added into the flask. This trypsin was aspirated, and 3 mL of new trypsin were added and the flask was incubated for 5 minutes at 37°C in 5% CO_2. After the incubation, 5 mL of the complete medium were added into the flask and the cells were collected into a 15 mL tube. The cells were centrifuged at 1,400 rpm for 3 minutes and the pellet was then resuspended in a complete medium depending on the confluency observed before splitting the cells. For example, for a 70% confluency, the pellet was resuspended in 7 mL of complete medium. To split the cells into a new T75 flask, 2 mL of resuspended cells were added and the flask was filled up to 12 mL using a complete medium. To pass the cells into 6-well plates (Corning®) for transfections, 400 µL of the resuspended cells were added into each well, which was filled up to 2 mL with complete medium. The T75 flask and 6-well plates were placed in an incubator at 37°C in 5% CO_2.

2.6.2. Transfecting HEK293 cells

For transfection, HEK293 cells were grown in 6-well plates (section 2.6.1) and jetPEI® DNA transfection reagent (Polyplus transfection®) was used. Purified plasmid DNA (1-5 µg) was added into a tube containing 50 µL NaCl. In another tube, 350 µL of NaCl plus jetPEI® DNA transfection reagent (2 µL for each µg of plasmid DNA used) were added. Both reactions were vortexed vigorously. The jetPEI® DNA transfection reaction was added into the DNA reaction tube and was vortexed for 10 seconds. The reaction mix was incubated at room temperature for 30 minutes. Each reaction mix was used only in one of the 6-wells. After the incubation period, the reaction mixture was

added into the 6-well plate containing the HEK293 cells. The cells were incubated with the reagent for 4 hours at 37°C in 5% CO_2. Afterwards, the media of each well was removed and 2 mL of fresh complete medium were added into the wells. The plate was incubated overnight at 37°C in 5% CO_2. The success of the transfection was analysed the next day using a fluorescence microscope (AxovisionSE64).

2.6.3. Whole-cell patch clamping in transfected HEK293 cells

For the patch clamping assays, HEK293 cells were grown in a 6-well plate and were transfected with jetPEI® DNA transfection kit (sections 2.6.1 and 2.6.2). The old medium of each well was removed and two drops of trypsin were added in each well. The trypsin was aspirated and the cells were washed with 500 µL of trypsin and incubated for 5 minutes at 37°C in 5% CO_2. After the incubation, the cells of each plasmid DNA transfection were collected from the wells and placed into a 15 mL tube. For each well containing the same plasmid DNA transfection, 2 mL of complete medium were added into the tube. For example, for 2 wells used for the same plasmid DNA transfection, 4 mL of complete medium were added. 1 mL of the cells and 1 mL of complete medium were added into 35 mm plates with a circular coverslip inside. The cells were incubated for 3 hours at 37°C in 5% CO_2 before the patch clamping assay to allow the cells to adhere to the coverslip.

The cells were visualised using an Olympus BX51 fluorescent microscope (Olympus, USA) and the patch was performed using polished glass pipettes over an Ag/AgCl electrode. The borosilicate glass pipettes (1.5/1.0 mm, World Precision Instruments, USA) were generated using a two step-glass microelectrode puller (Narisige PP-830) and were polished using a microforge (Narishige's MF-830). The pipette resistance obtained was around 6-10 MΩ. The pipette was positioned in a micromanipulator (Axon Instruments CV-7B) connected to an Axon AxoPatch 200B amplifier (Molecular Devices, USA) that was connected to a Digidata 1440A digitiser (Molecular Devices, USA). pCLAMP™ software was used to acquire the signal and analyse the data. The microscope, bath chamber and perfusion system were placed on top of a vibration control table, inside of a Faraday cage.

The coverslip with the HEK293 cells was inserted into the bath chamber on the Olympus BX51 fluorescent microscope (Olympus, USA). The cells were washed with 10 mL of extracellular solution and the glass pipette was filled with the intracellular

solution and tighten onto the Ag/AgCl electrode. The composition of the intracellular and extracellular solutions used for chloride and calcium experiments are shown in Table 2.13 and Table 2.14 respectively. For the whole-cell configuration, the pipette containing the Ag/AgCl electrode was placed into the extracellular solution and was lowered using the micromanipulator until the tip touched the surface of the cell. Then, a suction was applied using a syringe that was attached to the pipette, until a seal was created and the pipette resistance reached one giga-ohm. A second pulse of suction was applied to rupture the cell membrane inside the pipette to form the whole-cell configuration (Figure 2.1). Currents were recorded at each voltage from -100 mV to 90 mV over a 250 ms window. Multiple cells per transfection event were recorded with this method. Three recordings were done per cell and the average was used as the data point for the cell. The currents were analysed using pCLAMP™ software and the graphs were done using GraphPad Prism 7. Current density was calculated dividing the current at each voltage by the capacitance of the cell.

Table 2.13. Chloride patch clamping solutions.

Chloride extracellular solution (bath)	**Chloride intracellular solution (pipette)**
135 mM NaCl	130 mM N-methyl-D-glucamine
1.2 mM $MgSO_4$	95 mM L-glutamic acid
1.2 mM $CaCl_2$	2 mM $MgCl_2$
10 mM TES (pH 7.3 with NaOH)	1 mM EGTA Cs
5 mM D-glucose	1 mM MgATP
	5 mM TES (pH 7.3 with HCl (41 mM)

* Expected Nernst potential for Cl^- is -30 mV

Table 2.14. Calcium patch clamping solutions

Calcium extracellular solution (bath)	Calcium intracellular solution (pipette)
95 mM NaCl	120 mM CsCl
5 mM CsCl	20 mM TEA-Cl
20 mM TEA-Cl	2 mM $MgCl_2$
0.6 mM $MgCl_2$	10 mM EGTA
20 mM $CaCl_2$	2 mM NaATP
5 mM HEPES (pH 7.3 with NaOH/HCl)	10 mM HEPES (pH 7.3 with CsOH)
5 mM D-glucose	

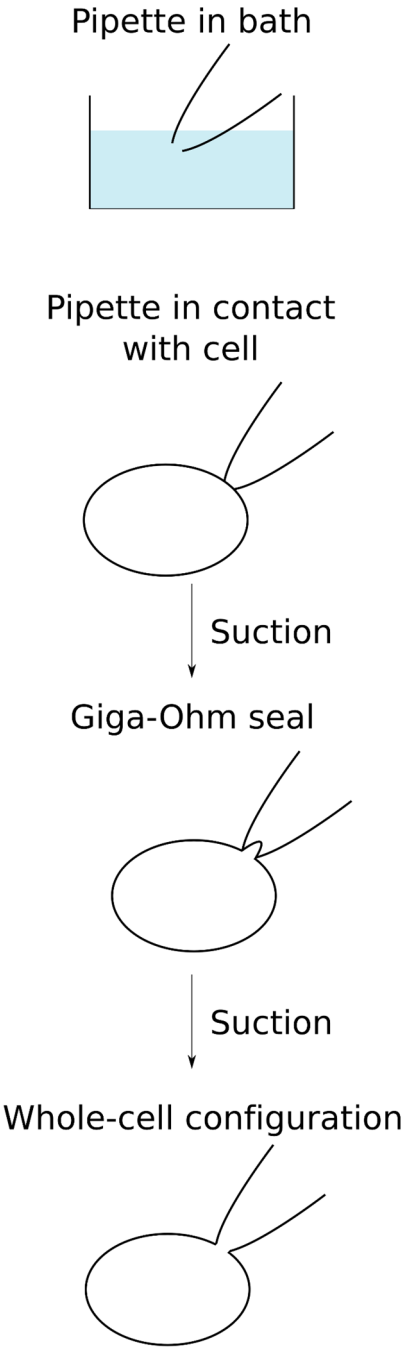

Figure 2.1. Diagram of the formation of whole-cell configuration

The tip of the pipette is inserted into the bath solution and is lowered until it reaches the surface of the cell. A first suction is applied to obtain one giga-ohm seal and a second suction is applied to rupture the membrane of the cell to form a whole-cell configuration.

2.7. Planar lipid bilayer assays

2.7.1. Protein synthesis by cell-free system kit

The synthesis of the protein was achieved by using the RTS 100 Wheat germ lysate kit (5 PRIME). The gene of interest was previously cloned into pIVEX1.3 His_6 tag vector using restriction site-ligation cloning system (section 2.3.10). The lyophilised reagents from RTS 100 Wheat germ lysate kit were reconstituted before use as per instructions and were kept at -20°C except for the Wheat Germ lysate that was kept at -80°C. OsGTG proteins were synthesized in the presence of DOPC (1, 2-dioleoyl-sn-glycero-3-phosphocholine) lipids. For the lipid formation, 1 mL of chloroform (Sigma-Aldrich) was added to 20 mg of DOPC (Avanti, Polar Lipids, INC) in a glass vial. The mixture was stirred until the lipids were completely dissolved. The chloroform was removed using a stream of nitrogen gas until a dry film of lipid was formed around the surface of the vial. The glass vial containing the lipid was exposed to high vacuum for 2 hours. 1 mL of 50 mM HEPES pH 7.5 (with KOH) was added into the vial and was mixed until a cloudy/milky solution was formed. Five rounds of freeze in dry ice and thaw at 60°C were carried out with the lipids solution to create vesicles of the same size. The lipids solution was passed several times (approximately 20 times) through an extruder (Avanti Polar Lipids, INC) with 200 nm filter membrane placed inside (Figure 2.2 A). A clearer cloudy solution containing unilamellar vesicles was formed that was kept at 4°C until use.

The RTS 100 Wheat germ lysate kit (5 PRIME) for protein synthesis, uses a continuous-exchange cell-free modules formed by the feeding and the reaction compartments. In the feeding compartment 900 µL feeding mix, 80 µL amino acids and 20 µL of methionine were added. In the reaction compartment, 15 µL reaction mix, 4 µL amino acid, 1 µL methionine, 15 µL Wheat Germ Lysate and 15 µL of sterile water containing 2 µg of the plasmid DNA were added. For the proteins that were synthesised with DOPC lipids, 50 µL of the lipid solution were also added into the reaction compartment for a 1:1 ratio. The reaction was incubated in a thermomixer at 24°C for 24 hours with 900 rpm agitation (Multi-therm, Benchmark). After the incubation period, the samples were collected and stored at 4°C if they were synthesised in the presence of lipids or at -80°C if they were synthesised without lipids. The expression of the protein was confirmed by western blot analysis (sections 2.4.1 and 2.4.3).

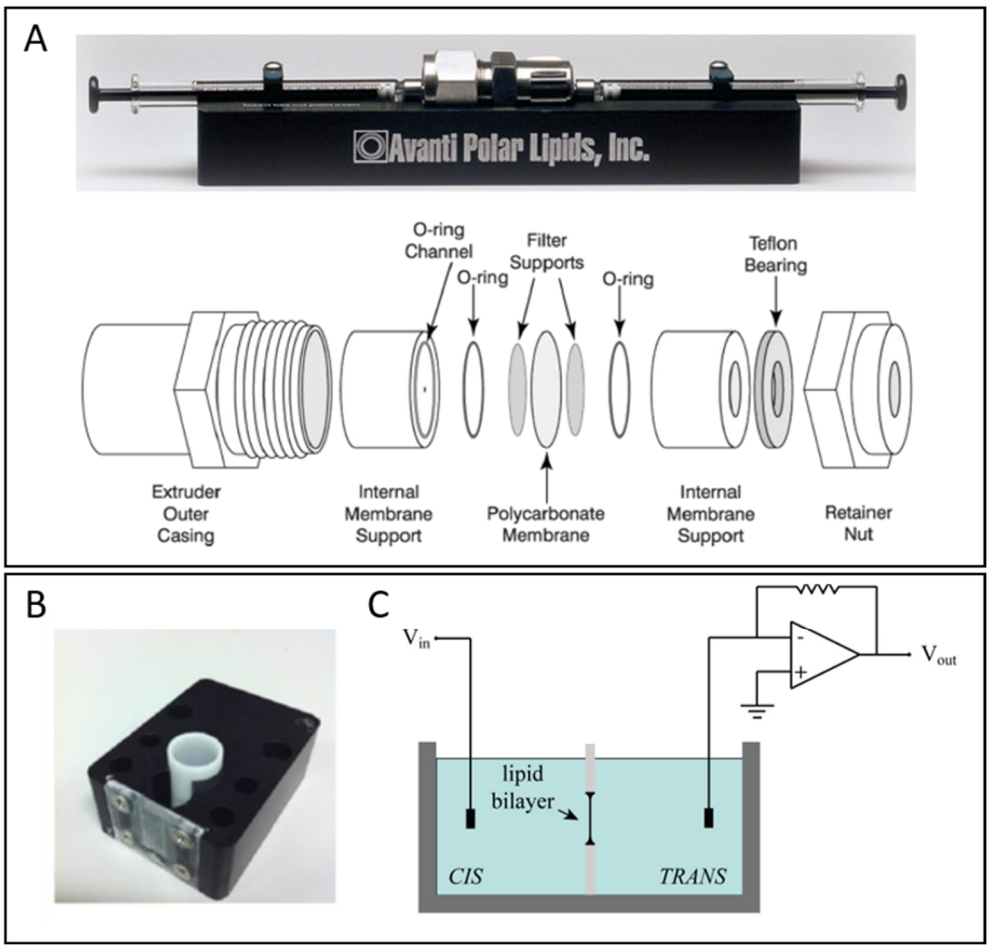

Figure 2.2. Extruder set-up and planar lipid bilayer method

A) Setup of the Avanti extruder (Avanti Polar Lipids, INC). 200 nm of polycarbonate membrane was used to produce unilamellar vesicles for incorporation in cell-free system reaction. B) Image of bilayer chamber (black) and cuvette (white) containing the aperture where the lipid bilayer is formed. C) Diagram of the lipid bilayer method, showing the Ag/AgCl electrodes inserted in each compartment and the formation of the lipid bilayer that separates both chambers. Image modified from Shlyonsky et al., (2014).

2.7.2. Planar lipid bilayer technique

In this technique, an artificial membrane is created between two chambers that contain two electrodes inside where the current can be measured. POPC (1-palmitoyl-2-oleoyl-sn-glycero-3-phosphocholine) lipids were used for the formation of the artificial membrane. 10 mg of POPC (Avanti, Polar Lipids, INC) were added into a glass vial containing 500 µL of chloroform. The chloroform was removed using a stream of nitrogen gas until a dry film of lipid was formed around the surface of the vial. The vial

containing the lipids was exposed to a high vacuum for 1 hour. The lipids were dissolved in 500 µL of decane (Sigma Aldrich) and were kept at room temperature until use. The artificial membrane was created between the two chambers using the painting method, where a small tip was coated with the lipid solution and was applied across the aperture of the cup. The cup was inserted into the chamber and was tightened properly. One mL of the desired buffer was added into both chambers (*cis* and *trans*) and an Ag/AgCl electrode was inserted into each chamber (Figure 2.2 B-C). For the chloride experiments, the symmetrical gradient was formed with 100 mM of KCl, 10 mM HEPES, pH 7.0 that was added into each chamber. For the asymmetrical gradient, 300 mM of KCl, 10 mM HEPES, pH 7.0 was added into the *cis* chamber and 100 mM of KCl, 10 mM HEPES, pH 7.0 was added into the *trans* chamber. In experiments where DIDS was added, DIDS (Sigma, Missouri, USA) was dissolved in DMSO, before being diluted to 20 µM in the KCl solution. For the calcium experiments, the asymmetrical gradient was formed adding 300 mM of $CaCl_2$, 10 mM HEPES, pH 7.0 into the *cis* chamber and 100 mM of $CaCl_2$, 10 mM HEPES, pH 7.0 into the *trans* chamber. For the calcium gluconate experiments, 100 mM of calcium gluconate, 10 mM HEPES, pH 7.0 was added into both chambers. For the selectivity assay, KCl was substituted for KI, KBr or KNO_3^-. For the asymmetrical gradients, agar bridges were used to protect the Ag/AgCl electrodes. 2% (w/v) agar was added to 3 M KCl and was heated in a microwave. The heated solution was poured into pipette tips which were left to set. The agar bridges were stored into 3 M KCl. When an asymmetrical gradient was applied, a silicon bung was inserted into the open part of the agar bridges and the electrodes were inserted into the agar filled tips.

Current measurements were obtained using an Axon AxoPatch 200B amplifier (Moleular Devices, USA) that was connected to a Digidata 1440A digitiser (Molecular Devices, USA). The amplifier and digitiser were placed on top of a Faraday cage (50 cm x 82 cm x 50 cm). Inside of the Faraday cage a retort stand held the CV 203BU headstage (Molecular Devices, USA) that was connected to the amplifier. pCLAMP™ software was used to acquire the signal and analyse the data. Bilayer formation was indicated using capacitance measurements of 50-70 pF. For each experiment, 2-5 µL of the protein expressed through the cell-free system were added into the *cis* compartment and voltages ranging from -100 mV to 100 mV were applied. The currents were analysed using pCLAMP™ software and the graphs were created using GraphPad Prism 7. Nernst's equation was used to calculate the reversal potential of the ions,

$$V_{Eq} = \frac{RT}{zF} \ln\left(\frac{[X]out}{[X]in}\right).$$

Goldman-Hodgkin-Katz equation was used to calculate the permeability ratio between different ions,

$$E_{REV} = \frac{RT}{zF} \ln\left(\frac{P_X[K]_o + P_{Cl}[Cl]_i}{P_X[K]_i + P_{Cl}[Cl]_o}\right).$$

2.8. Intracellular pH analysis

The pH analysis was performed using a pHluorin pH sensor tagged to different signal sequences for specific organelle localisation. HDEL signal peptide was used for ER localisation, ManI protein for *cis* Golgi localisation and BP80 for *trans* Golgi localisation (Gomord et al., 1997, Nebenführ et al., 1999, Li et al., 2002, Shen et al., 2013). Arabidopsis WT and *gtg1gtg2* mutant Wassilewskija background plants were previously transformed with these constructs using the floral dipping technique and homozygous lines were obtained for all the lines and used for the pH analysis (Adam, Terry, Williams, unpublished). In addition, *gtg1gtg2* homozygous lines expressing HDEL pHluorin and ManI pHluorin were also transformed with *OsGTG* (cloned in the plant destination vector pMDC32) by the floral dipping method (section 2.1.4) (Clough and Bent, 1998). Homozygous lines were isolated (section 2.1.4) and used for intracellular pH analysis.

For pH measurements analysis, pure pHluorin was used to calibrate a Leica SP8 confocal microscope. To achieve this, pure pHluorin was bound to Ni^{2+} agarose bead and was placed under different pH solutions: 5.0, 5.5, 6.0, 6.5, 7.0, 7.5 and 8.0 that were generated using a combination of 1M K_2HPO_4 and 1M KH_2PO_4 until the desired pH was acquired. Images of the pHluorin bound to Ni^{2+} agarose bead were taken at those pH values using 405 nm and 488 nm excitation wavelength at 2% and 500-550 nm emission for both lasers. HyD3 detector and 63x objective were used for both lasers. After the images of the pure pHluorin at different pH were taken, the 405/488 ratio was calculated using ImageJ software. The 405/488 ratio was plotted against pH using GraphPad Prism 7 and a Boltzmann curve was used to fit the values,

$$Y = Bottom + \frac{Top - Bottom}{(1 + 10^{((LogIC50 - X) \cdot HillSlope)})}.$$

To measure the intracellular pH of the transgenic lines, 7 day-old plants grown on 0.5x Murashige and Skoog (MS) medium (Duchefa) and 0.8% (w/v) agar (Sigma) (section 2.1.2) were imaged with the microscope settings described above. The 405/488 ratio was determined for each cell (for ER pH measurements) or for each foci (for Golgi pH measurements) using ImageJ, and the pH values were calculated using the Boltzmann equation obtained previously.

2.9. Bioinformatics

Arabidopsis gene sequences were obtained from TAIR website (www.arabidopsis.org). *Oryza sativa* sequences were obtained from Rice Genome Annotation Project (Ouyang et al., 2007, Tanaka et al., 2008, Kawahara et al., 2013), where OsGTG sequence was from LOC_ Os04g51180 and RGA1 was from LOC_ Os05g0333200. Homologues of Arabidopsis GTGs were found using BLAST database (https://blast.ncbi.nlm.nih.gov/Blast.cgi). Multiple alignments were performed by Muscle Omega website (http://www.ebi.ac.uk/Tools/msa/muscle/). The GenBank accession number of the proteins used in the alignments are shown in Table 2.15. To predict introns and exons of a gene of interest, genomic and cDNA sequences were aligned. Exons were assigned as the genomic sequence that aligned with cDNA sequence whereas introns were the sequence that did not align. Membrane topologies were predicted using TMHMM server v.2.0 and the diagram was created using Protter tool (Omasits et al., 2013). Protein sequences were obtained from ExPASy Bioinformatics Resource Portal (http://web.expasy.org/translate/) using cDNA sequences.

2.10. Statistical analysis

For all statistical analyses, Minitab software was used. Analysis of variance (ANOVA) was applied for parametric test, using normally distributed data. *Anderson-Darling* test was applied to determine whether the data followed a normal distribution.

Johnson transformation was performed for any data that required normalization. With the normalized data, One-way ANOVA was applied. Tukey *post-hoc* comparison was used to analyse significant differences between groups by analysing differences between the means. This is one of the most common *post-hoc* tests used to compare all groups by analysing all possible pairwise comparisons. Means not sharing a letter are significantly different. Statistical tests are reported in the figure legends.

Table 2.15. GenBank accession number of the proteins used for the sequence alignments

Organism	Accession number
Arabidopsis thaliana 1	NP_176679
Arabidopsis thaliana 2	NP_194493
Oryza sativa (Rice)	EAZ31870
Zea mays (Maize)	ACR34497
Vitis vinifera	XP_002270494
Ricinus communis	XP_002520085
Brachypodium distachyon	XP_003580421.1
Populus trichocarpa	XP_002319243
Medicago truncatula	XP_003610649.1
Sorghum bicolour	XP_002448458
Hordeum vulgare (Barley)	AK251496.1
Triticum aestivum (Wheat)	AK332997.1
Caenorhabditis elegans 1	CAA22103
Caenorhabditis elegans 2	CAA94117
Drosophila melanogaster	NP_611016
Homo sapiens (Human)	NP_057418
Mus musculus (Mouse)	NP_080505
Rattus norvegicus (Brown rat)	NP_001132958
Cricetulus griseus (Hamster)	BAG41890

Chapter 3. Functional analysis of OsGTG

3.1. Introduction

Elucidating the function of GTG has been challenging as several roles have been proposed (Table 1.2). The main aim of this thesis is to understand whether GTGs could have a general role and a conserved function. More specifically, this chapter focuses on the characterisation of rice GTG and explores whether the function of Arabidopsis and rice GTGs is conserved.

3.1.1. Transgenic lines as tools for functional studies

Arabidopsis is a plant model organism widely used to study the function of proteins and their roles in various cellular processes. Plants lacking or overexpressing a gene of interest have been extensively used to understand the function of proteins in plants (Krysan et al., 1996, Østergaard and Yanofsky, 2004, Bolle et al., 2011). Several different mutagenesis methods, such as EMS (Maple and Møller, 2007), radiation (Shirley et al., 1992) and T-DNA insertion (Krysan et al., 1999) have been developed in Arabidopsis. A new gene-editing technique called CRISPR/Cas9 has also been applied in Arabidopsis (Li et al., 2014a, Bortesi and Fischer, 2015). T-DNA insertion mutants have also been developed in rice to characterize a range of genes (An et al., 2005). One example is rice GTG, which was studied using a T-DNA insertion mutant called *cold1* as discussed later (Ma et al., 2015). Genes involved in growth and chlorophyll biosynthesis have also been characterized in rice by T-DNA insertion mutagenesis (Jung et al., 2003, Liu et al., 2009). Therefore, T-DNA insertion mutants are a good method in Arabidopsis and rice to study protein function. Complementation assays can be carried out to test whether a mutant phenotype can be rescued by incorporating a specific gene. For example, the Arabidopsis Na^+ transporter *hkt1* mutant exhibited a hypersensitivity to NaCl that was restored by the expression of AtHKT1 in the mutant (Berthomieu et al., 2003). The cation-Cl^- cotransporter mutant, *ccc*, exhibited a strong growth defect, with a reduced size and an absence of inflorescence development. These defects were rescued by the expression of CCC in the mutant (Colmenero-Flores et al., 2007). Previous work on AtGTGs showed that the expression of AtGTG1 or AtGTG2

in the *gtg1gtg2* double mutant background rescues the defective growth phenotype observed in the mutant (Jaffé et al., 2012).

Heterologous expression can be used to study the conservation of function of orthologue proteins. This aids the study of the cellular function of gene families between species. For example, an Arabidopsis double mutant of two gibberellin receptors called GID1A and GID1C (GA insensitive dwarf1) displayed a dwarf phenotype. This mutant phenotype was rescued by the expression of GID1A from *Vitis vinifera*, suggesting the conserved function of the protein across these plant species (Acheampong et al., 2015). Therefore, transgenic plants can be generated to study a gene of interest where the gene can be cloned into a plant expression vector, with specific promoters based on the expression levels required. Reporter genes, such as fluorescent or luminescent proteins, can also be used to tag to the gene of interest in order to study subcellular localisation and tissue expression patterns.

To generate transgenic lines in Arabidopsis, *Agrobacterium tumefaciens* (*Agrobacterium*) has been commonly used due to its capacity to transfer foreign DNA into plant genomes. *Agrobacterium* introduces the T-DNA randomly in the genome, interrupting the transcription and translation of a gene producing a knockout mutant or introducing a specific gene of interest. *Agrobacterium* uses a tumour-inducing plasmid called Ti that contains the T-DNA and the virulence *vir* genes. These latter genes are required for the introduction of the T-DNA into the genome (Chilton et al., 1977, Garfinkel and Nester, 1980, Ooms et al., 1980, Ooms et al., 1982). For the creation of transgenic plants, a specific binary plasmid system has been developed (Figure 3.1 A). In this system two plasmids are required, one that contains the *vir* genes and another one that contains the T-DNA (Hoekema et al., 1983). For the generation of transgenic lines, the T-DNA is replaced by the gene of interest. The vector containing the T-DNA is transformed into *Agrobacterium* that already contains a vector with the *vir* genes. The *Agrobacterium* with the two vectors is consequently used to transform Arabidopsis, usually by the floral dip method (Clough and Bent, 1998).

A Gateway binary destination vectors system has been developed for expression in plants (Curtis and Grossniklaus, 2003). In our study, pMDC32 and pMDC83 have been used where the gene of interest is driven by the constitutive CaMV 35S promoter, which allows constitutive expression in plants (Figure 3.1 B) (Odell et al., 1985, Karimi et al., 2002). In the pMDC83 vector, a GFP is tagged at the C terminus of the gene of interest.

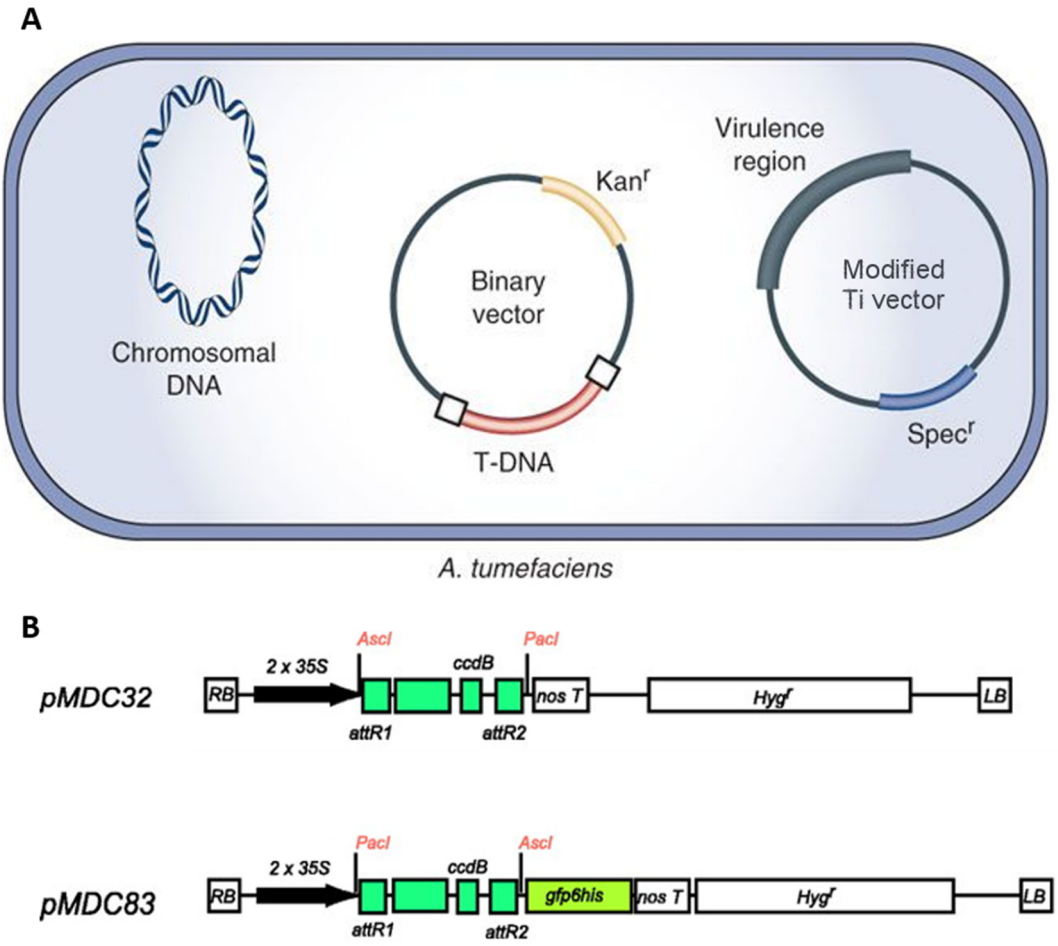

Figure 3.1. *Agrobacterium* binary system for plant transformation and schematic of the Gateway Arabidopsis destination vectors

A) *Agrobacterium* binary system containing the two vectors required for plant transformation. On the right the modified Ti vector that contains spectinomycin (*Spec*^{r}) as a resistance marker and the *vir* genes, and in the middle the manipulated T-DNA vector that contains the gene of interest and kanamycin resistance (*Kan*^{r}) are shown. Figure adapted from Michielse et al. (2008). B) Structure of the destination pMDC32 and pMDC83 vectors showing the recombination sites flanked by attR1 and attR2 recognition sites, with hygromycin resistance (*Hyg*^{r}) for selection in Arabidopsis. LB = left border, RB = right border sequences of the T-DNA region. Both vectors contain 2x35S plant promoter for constitutive expression, and pMDC83 also contains a C-terminal GFP-6His tag. Adapted from Curtis and Grossniklaus (2003).

The pMDC vectors have been widely used in Arabidopsis for intracellular localisation and functional analysis (Vahisalu et al., 2008, Li et al., 2016, Oda et al., 2016, Ortega-Amaro et al., 2015). pMDC32 and pMDC83 have been successfully used to study Arabidopsis GTG1 and *C. elegans* GTG1 function and localisation (Jaffé et al., 2012, Wong, 2014).

3.1.2. The function of GTG/GPHRs

GTG/GPHR is a family of membrane protein that is structurally conserved in all eukaryotes (section 1.5). Different functions and intracellular localisations have been proposed for this protein in mammalian, Arabidopsis and rice species (Maeda et al., 2008, Pandey et al., 2009, Jaffé et al., 2012, Ma et al., 2015) (Table 1.2). Mammalian GTG/GPHR has been proposed to function as an anion channel that regulates Golgi pH (Maeda et al., 2008). The function seems conserved between vertebrates and invertebrates since the hamster and human GTG/GPHRs were able to rescue the growth defects observed in *Drosophila GPHR*$^{-}$ mutant (Charroux and Royet, 2014). Rice GTG is 80% identical and 90% similar to the Arabidopsis GTG at the amino acid level (Figure 3.2). However, it remains unclear whether the fundamental function of this protein is conserved between the two species.

In Arabidopsis, T-DNA mutants have been used to investigate the role of GTG in plants. Two independent *gtg1gtg2* double mutants have been generated by crossing *gtg1* and *gtg2* single mutants from Flag and Salk T-DNA mutant collections, in Wassilewskija and Columbia Arabidopsis ecotypes respectively (Pandey et al., 2009, Jaffé et al., 2012). A previous study in Arabidopsis proposed that GTGs could function as an ABA receptor (see section 1.5.5) due to the hyposensitivity to ABA that the *gtg1gtg2* mutant exhibited in germination and growth assays (Pandey et al., 2009). However, repetition of those experiments using the same *gtg1gtg2* mutant and double mutants utilizing different alleles showed a normal response to ABA (Jaffé et al., 2012, Wong, 2014).

A role of GTG in growth and fertility has also been proposed since the *gtg1gtg2* mutant showed a reduced root, hypocotyl and silique length, as well as fresh weight, seed yield and seed number per silique (Jaffé et al., 2012). Impaired developmental phenotypes were rescued by the introduction of AtGTG1 or AtGTG2 back into the double mutant (Jaffé et al., 2012). Interestingly, only the double mutant showed a

defective phenotype whereas the single mutants exhibited a WT phenotype, suggesting function redundancy between these two proteins (Pandey et al., 2009, Jaffé et al., 2012). *C.elegans* GTG1 (CeGTG1), which shares 39% identity with AtGTG1, can also rescue the defective Arabidopsis mutant phenotype, suggesting a conservation of function between these two species (Wong, 2014).

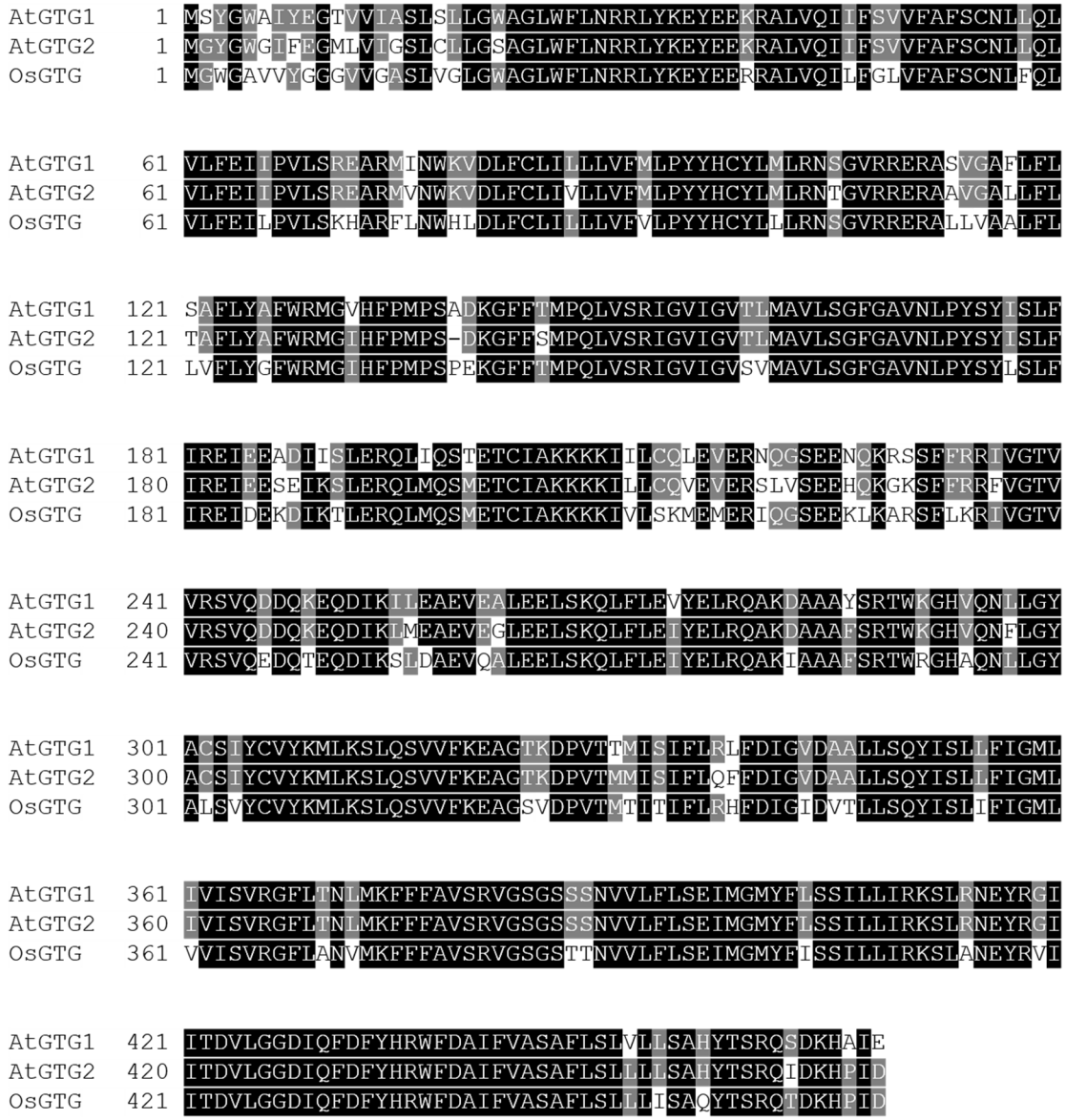

Figure 3.2. Protein sequence alignment of *Arabidopsis thaliana* GTGs with *O. sativa* GTG

Protein sequence alignment of AtGTG1, AtGTG2, OsGTG using ClustalW algorithm and represented by BoxShade. In the sequences: black = conserved residues, grey = conserved in both organisms.

A rice *gtg* mutant was recently characterised and OsGTG was proposed to play a role in cold tolerance acting as a cold sensor (Ma et al., 2015). It was reported that the rice *gtg* mutant showed a reduced cold tolerance in comparison to WT plants. Moreover, it was suggested that the 187th residue of the protein was responsible for the cold tolerance, since the OsGTG with lysine in that position was able to rescue the cold sensitivity of the mutant, whereas OsGTG with a methionine did not (Ma et al., 2015). In tomato, GTG was also proposed to be involved in cold tolerance and in wheat it was suggested to function as a plant height regulator (Dong et al., 2019, Zhang et al., 2020).

3.1.3. Intracellular localisation of Arabidopsis and rice GTGs

The subcellular localisation of GTGs also generates controversy (see section 1.6 and Figure 1.9). Determining the subcellular localisation of GTG is important in order to elucidate its possible cellular roles. AtGTG1 has been shown to be targeted to different localisations in different studies. It was reported at the plasma membrane in Arabidopsis protoplasts by Pandey et al. (2009), but no organelle-specific marker was used to confirm this localisation, and at the ER and Golgi in tobacco leaves by Jaffé et al. (2012), where the Golgi localisation was confirmed by co-expression with the ST-RFP *trans* Golgi marker. Rice GTG was localised at the plasma membrane in tobacco protoplasts, and co-localised with the PIP2-mcherry marker, that as they mentioned, also localised at the ER (Lee et al., 2009, Ma et al., 2015). In addition, rice GTG was also localised at the ER in Arabidopsis protoplasts and co-localised with the ER marker BIP-RFP (Ma et al., 2015).

3.1.4. Mutagenesis analysis to study protein function

To identify which residues are important for the function and localisation of the protein, site-directed mutagenesis can be used. Changes in the DNA sequence can produce changes at the protein level. The mutated gene can be expressed in Arabidopsis plants and the rescue of knockout mutant phenotypes can be studied. In this thesis, several amino acids of the rice GTG sequence have been mutated using overlapping PCR. In this technique two fragments are generated, each including the mutation and a second PCR is performed to combine both fragments to generate the full gene that will contain the mutated nucleotides. Mutagenesis has been used in plants to study protein function. In the Arabidopsis voltage-gated K^+ channel, KAT1, a change of threonine to

glutamine in position 256 in the pore was shown to reduce the conductance and modify the gating properties of the channel (Moroni et al., 2000). In Arabidopsis α-tubuline 6 (TUA6), the conserved lysine in the 40th amino acid position was mutated to alanine or glutamine. The mutated TUA6 versions were expressed in Arabidopsis where several growth defects were observed (Xiong et al., 2013). In *Drosophila* GTG/GPHR, a mutation in the conserved proline in the 91st amino acid residue produced flies with reduced growth and high mortality at the late larvae stage (Charroux and Royet, 2014).

3.1.5. Aims

In order to elucidate whether the function and the localisation of rice GTG and Arabidopsis GTGs is conserved, the aims of this chapter are:

1. To clone *OsGTG* into different plant expression vectors to test whether OsGTG can rescue the defective phenotype of the Arabidopsis *gtg1gtg2* mutant in order to study a possible conservation of function.
2. To study the role of the conserved glutamic acid residue in the 9th amino acid position found in all plant GTGs by generating a mutant with glycine in the same position. Both protein versions will be expressed in the *gtg1gtg2* mutant to study whether they can rescue the defective phenotype.
3. To investigate the subcellular localisation of OsGTG both by stable expression of these proteins tagged with GFP in Arabidopsis and by transient co-expression with different organelle markers in tobacco cells.
4. To study the role of the lysine present at the 187th amino acid position by mutating it to a methionine to test whether this residue is involved in cold tolerance. Also, to investigate whether this amino acid plays a role in the function and localisation of the protein.
5. To isolate and characterize a rice *gtg* mutant to investigate whether the defective growth and fertility phenotypes of the Arabidopsis mutant are also observed in rice knockout plants.

3.2. Results

3.2.1. Cloning *OsGTG* from rice Nipponbare ecotype

To study the conservation of function of OsGTG, the gene was cloned into vectors suitable for expression in Arabidopsis. CDS sequences from the Nipponbare ecotype were obtained from the Rice Genome Annotation Project database (LOC_ Os04G51180 in http://rice.plantbiology.msu.edu/) and the TOPO® cloning system was used to clone *OsGTG* into an entry vector which was used to create a destination vector (section 2.3.8). The *OsGTG* full CDS sequence was amplified with and without the stop codon to allow for C-terminal GFP tagging. Total RNA extracted from rice Nipponbare leaves was used to synthesise cDNA. As shown in Figure 3.3, *OsGTG* CDS, with and without the stop codon, were amplified successfully.

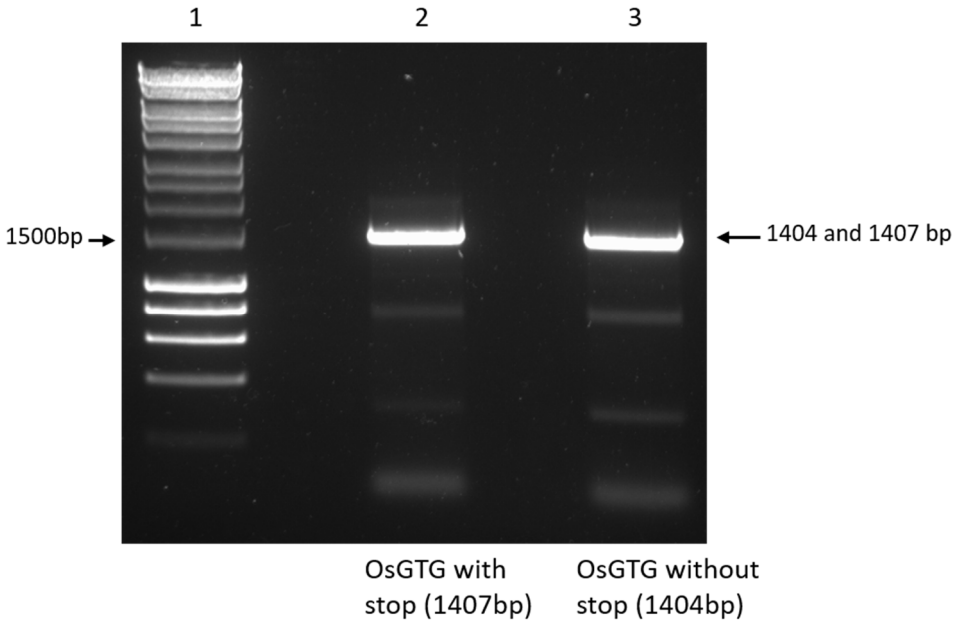

Figure 3.3. *OsGTG* products amplified from Rice Nipponbare cDNA

OsGTG gene products with and without the stop codon were amplified by PCR from rice Nipponbare cDNA. *OsGTG* with and without the stop codon was amplified using primers OsGTG topo F1 + OsGTG Stop R1 (lane 2) and OsGTG OsGTG topo F1 + OsGTG no stop R1 (lane 3) respectively. Predicted product sizes are on the right and the molecular marker sizes are indicated on the left (lane 1).

Both CDS of *OsGTG* were individually cloned into the pENTR/D vector to create pENTR/D *OsGTG* with and without the stop codon. These pENTR/D vectors were transformed into *E.coli* cells and colony PCRs were carried out followed by a restriction enzyme analysis on the isolated plasmid DNA. The PCR and the restriction analysis results confirmed that *OsGTG* was successfully cloned in the right orientation (Figure 3.4). Sequencing of both vectors in forward and reverse directions confirmed that the CDS of *OsGTG* was inserted correctly and the sequence corresponded to the CDS predicted in the Rice Genome Annotation Project database apart from two nucleotides. The CDS sequence from the database, in the 25-26 nucleotide position had a guanine + thymine (GT) whereas the CDS sequence that was amplified in this study had adenine + guanine (AG) in that position (Figure 3.5).

To confirm that the polymorphism found was not due to a technical error, *GTG* from Donjing, another rice ecotype, was amplified and sequenced and also showed the same AG nucleotide mutation. In addition, the same AG mutation was found in the cDNA and genomic sequence of rice Nipponbare. As a result, this polymorphism generated a difference in the amino acid sequence in the 9th residue; instead of the glycine (Gly/G) as per the database sequence, our amplified gene contained a glutamic acid (Glu/E) in that position (Figure 3.6). From now on the gene version with the glycine in the 9th residue will be called OsGTGg and the version amplified in this study with the glutamic acid in that position will be called OsGTGe.

3.2.2. Mutating glutamic acid in the 9th amino acid position into glycine

The polymorphism found in the *OsGTG* sequence cloned here resulted in one amino acid difference, a glutamic acid instead of glycine in the 9th residue. Analyses of GTG sequences in other plant species revealed that in the database all plants examined have a glutamic acid in that position. In addition to AtGTGs that have a glutamic acid in that position, other crops such as wheat, barley and maize also contain a glutamic acid in their GTG sequences (Figure 3.7). This suggests that this glutamic acid seems to be a highly conserved residue in plant GTG proteins. In *C. elegans*, *Drosophila* and mammalian GTGs, such as human, mouse or hamster there is an aspartic acid in that position (Figure 3.8).

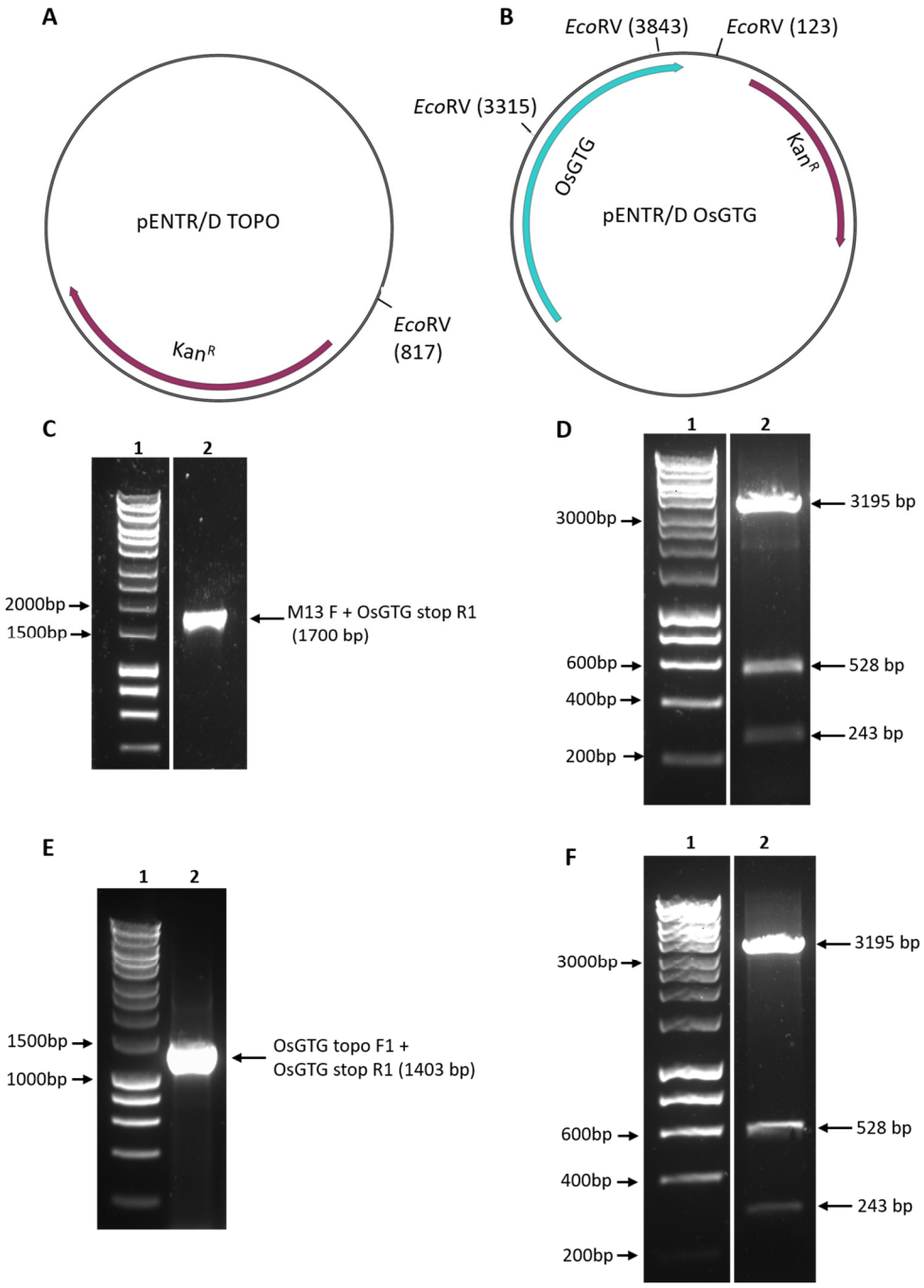

Figure 3.4. PCR and diagnostic restriction analysis of pENTR/D *OsGTG* entry vectors

Vector map of empty pENTR/D showing *Eco*RV digestion sites (A) and vector map of pENTR/D *OsGTG* showing the three *Eco*RV restriction sites (B). Colony PCR of pENTR/D *OsGTG* with the stop codon using M13F + OsGTG stop R1 primers (lane 2) in C) and without the stop codon using OsGTG topo F1 + OsGTG stop R1 primers (lane 2) in E). Restriction digest of pENTR/D *OsGTG* with the stop codon D) and without the stop codon F) using *Eco*RV (lane 2). Predicted product sizes are on the right and molecular markers are on the left (lane 1).

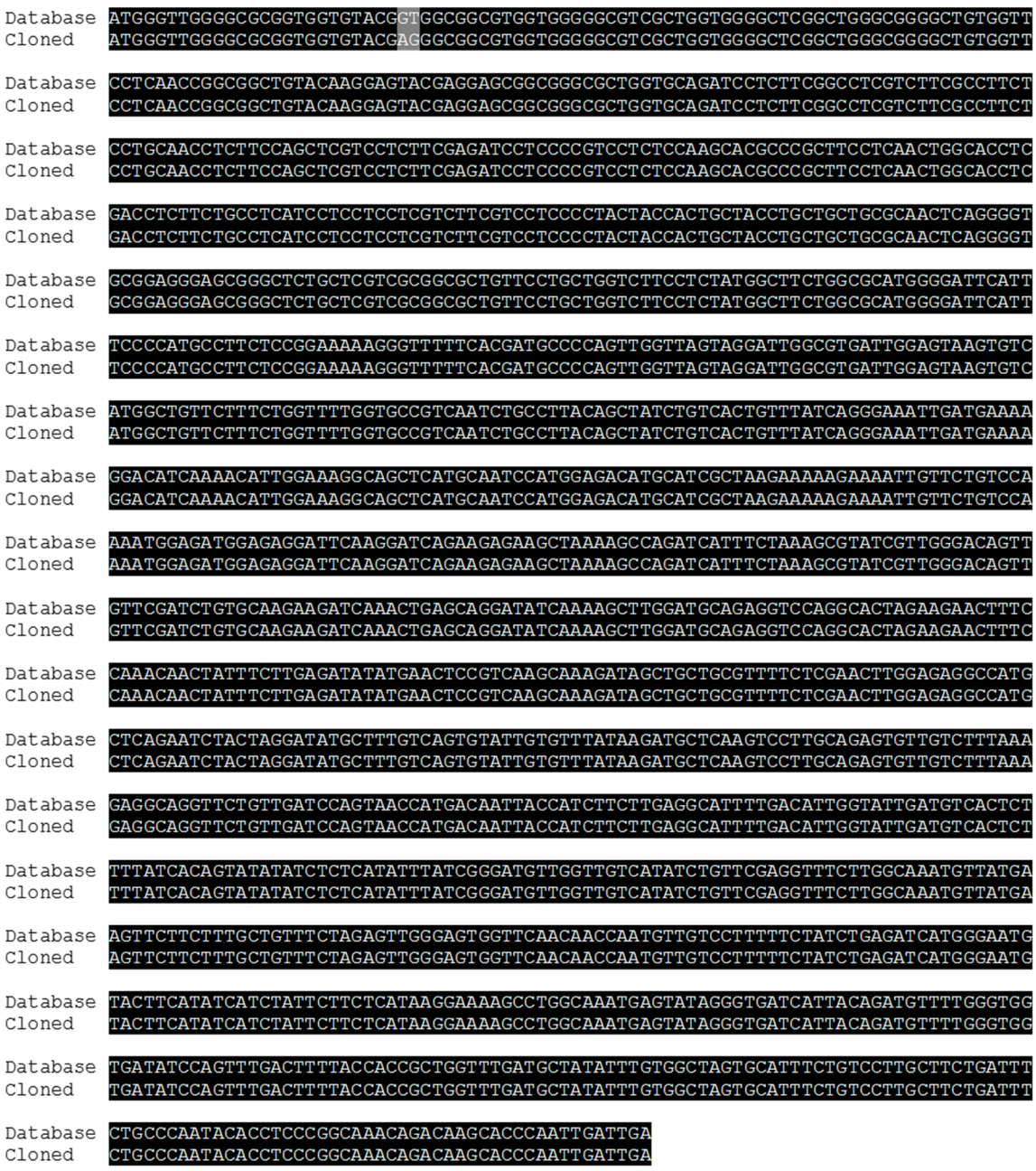

Figure 3.5. Alignment of *OsGTG* database CDS with *OsGTG* amplified and sequenced in this study

Highlighted in black is the sequence alignment between the database CDS (http://rice.plantbiology.msu.edu/) and the *OsGTG* cloned in this study. Highlighted in grey are the differences in two nucleotides in these sequences.

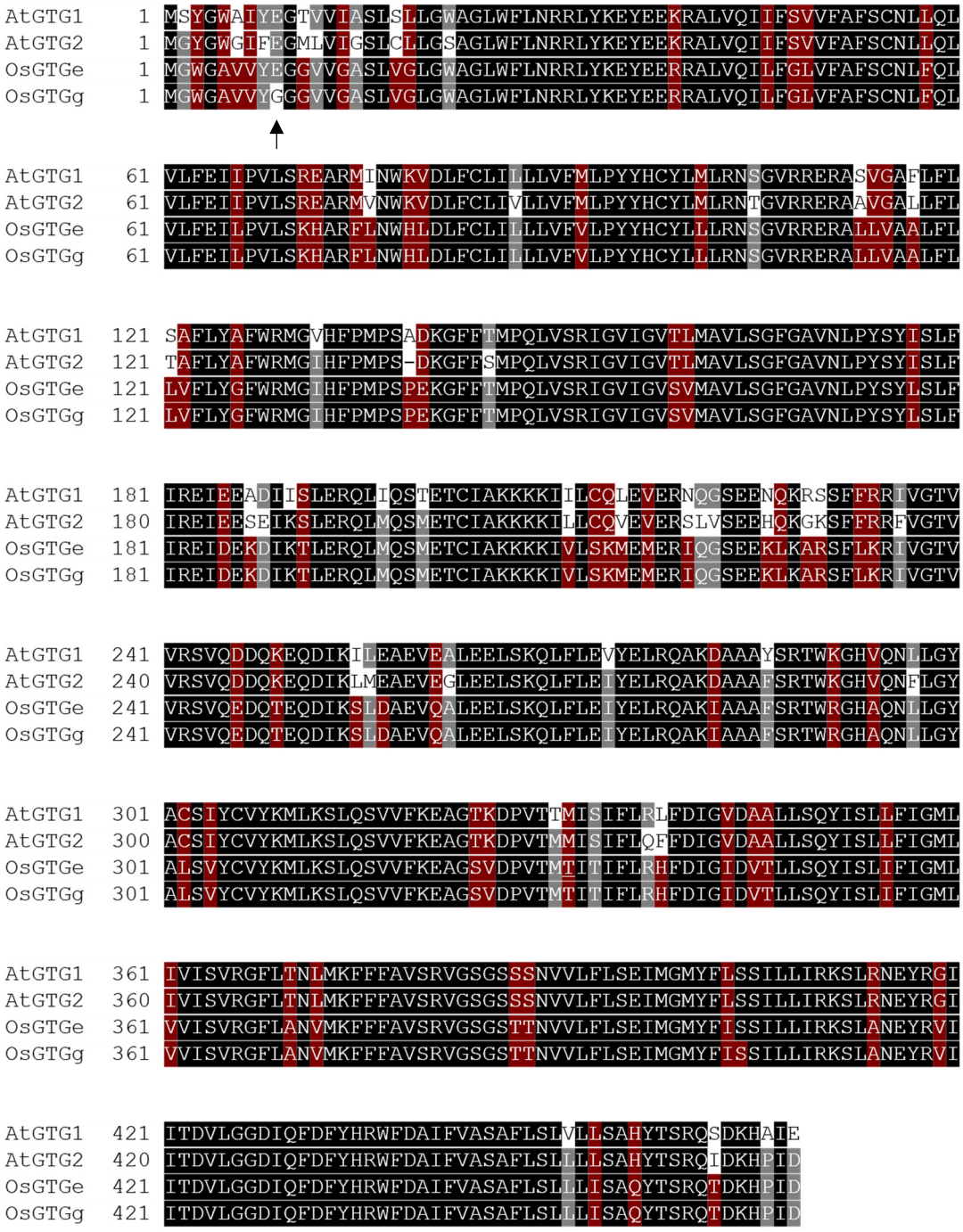

Figure 3.6. Alignment comparing protein sequences of both Arabidopsis GTGs with *O. sativa* GTGs

Protein sequence alignment of AtGTG1, AtGTG2, OsGTGe (glutamic acid in the 9th amino acid position) and OsGTGg (glycine in the 9th amino acid position) using ClustalW algorithm and represented by BoxShade. In the sequences: black = conserved residues, grey = conserved in three organisms and red = conserved in two organisms. Black arrow marks the 9th amino acid.

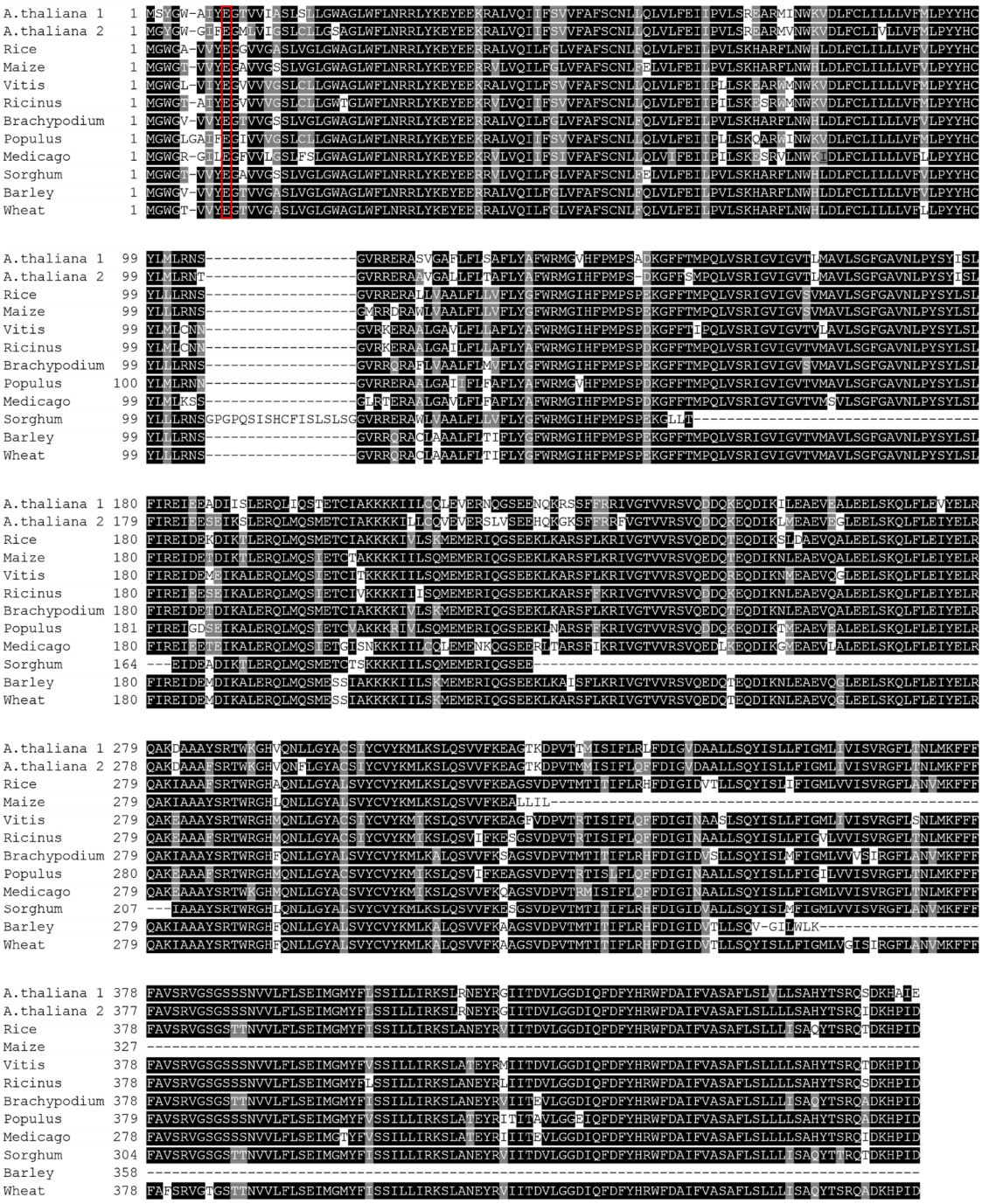

Figure 3.7. Alignment comparing protein sequences of plant GTGs

Protein sequence alignment of several plant GTGs using ClustalW algorithm and represented by BoxShade. In the sequences: black = conserved residues, grey = conserved in at least in three organisms. Red square marks the 9th amino acid residue. The GenBank accession number of the proteins used are shown in Table 2.15.

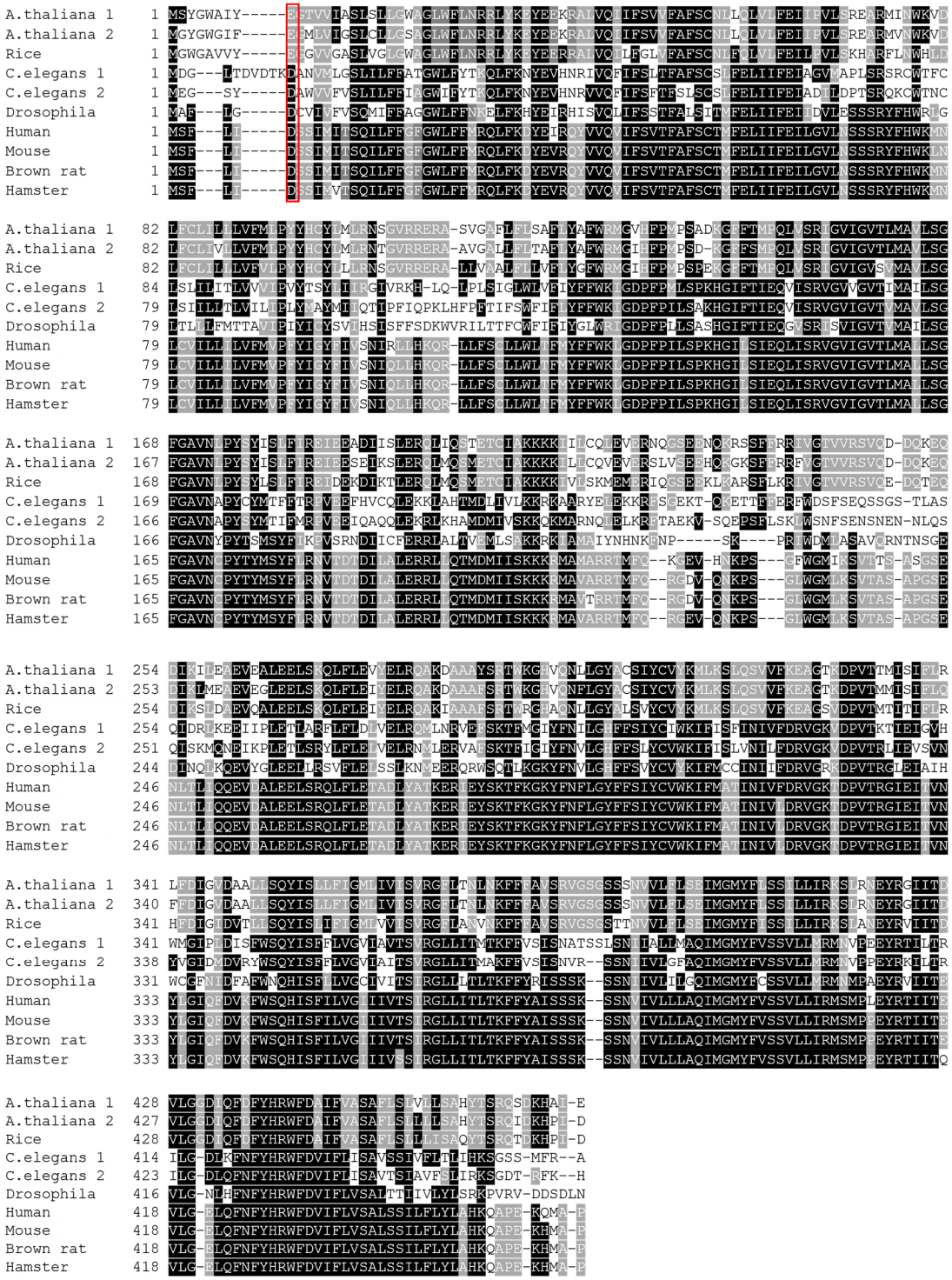

Figure 3.8. Alignment comparing protein sequences of plant, invertebrate and vertebrate GTGs

Protein sequence alignment of Arabidopsis, rice, *C. elegans*, *Drosophila*, human, mouse, brown rat and Chinese hamster GTGs using ClustalW algorithm and represented by BoxShade. In the sequences: black = conserved residues, grey = conserved in 3-4 organisms. Red square marks the 9th amino acid residue. The GenBank accession number of the proteins used are shown in Table 2.15.

This residue is predicted to be part of the first transmembrane domain and the change of amino acid does not seem to affect the predicted protein topology (Figure 3.9). Interestingly, previous work done in OsGTG by Ma et al. (2015) did not show the presence of this polymorphism, indicating that the protein that was used for their assays contained a glycine in that position.

To analyse the importance of this amino acid, the glutamic acid was mutated to a glycine (E9G) by overlapping PCR using pENTR/D *OsGTG* with stop codon as a template. Primers were designed across the mutation site including the E9G nucleotide change. Since the mutation was 25 bp after the start codon, a longer sequence had to be amplified to allow two fragments to be generated and overlapped by PCR in the next step. After the two fragments were generated, a second PCR was carried out to amplify the *OsGTG* full-length sequence. This process is summarised in a diagram in Figure 3.10 A and the results are shown in Figure 3.10 B-D. The final fragment generated was cloned into the pENTR/D entry vector as described in section 2.3.8. The entry vector was sequenced in forward and reverse directions to confirm that the mutation was introduced in the sequence. Once the presence of a glycine in the 9th amino acid position was confirmed (Figure 3.10 E), the *OsGTG E9G* (*OsGTGg* from herein) without the stop codon was created. Table 3.1 shows the pENTR/D vectors generated for this study.

3.2.3. Expressing *OsGTGe* and *OsGTGg* in Arabidopsis

To clone both *OsGTG* versions into plant expression vectors, LR recombination was performed with pENTR/D *OsGTGe* and pENTR/D *OsGTGg*, both with and without the stop codon. Two plant expression vectors, pMDC32 and pMDC83, were used. *OsGTGs* with and without the stop codon were inserted into pMDC32 and pMDC83 destination vectors respectively by LR recombination and transformed into *E. coli* cells (section 2.3.8). Colony PCR and restriction digest were performed to confirm that *OsGTGs* were cloned in the right orientation in the destination vectors. The results in Figure 3.11 C-G indicate that both *OsGTGs* were inserted successfully into pMDC32 and pMDC83. Both expression vectors were sequenced in forward and reverse directions and the analysis confirmed that *OsGTGs* were inserted correctly into both destination vectors.

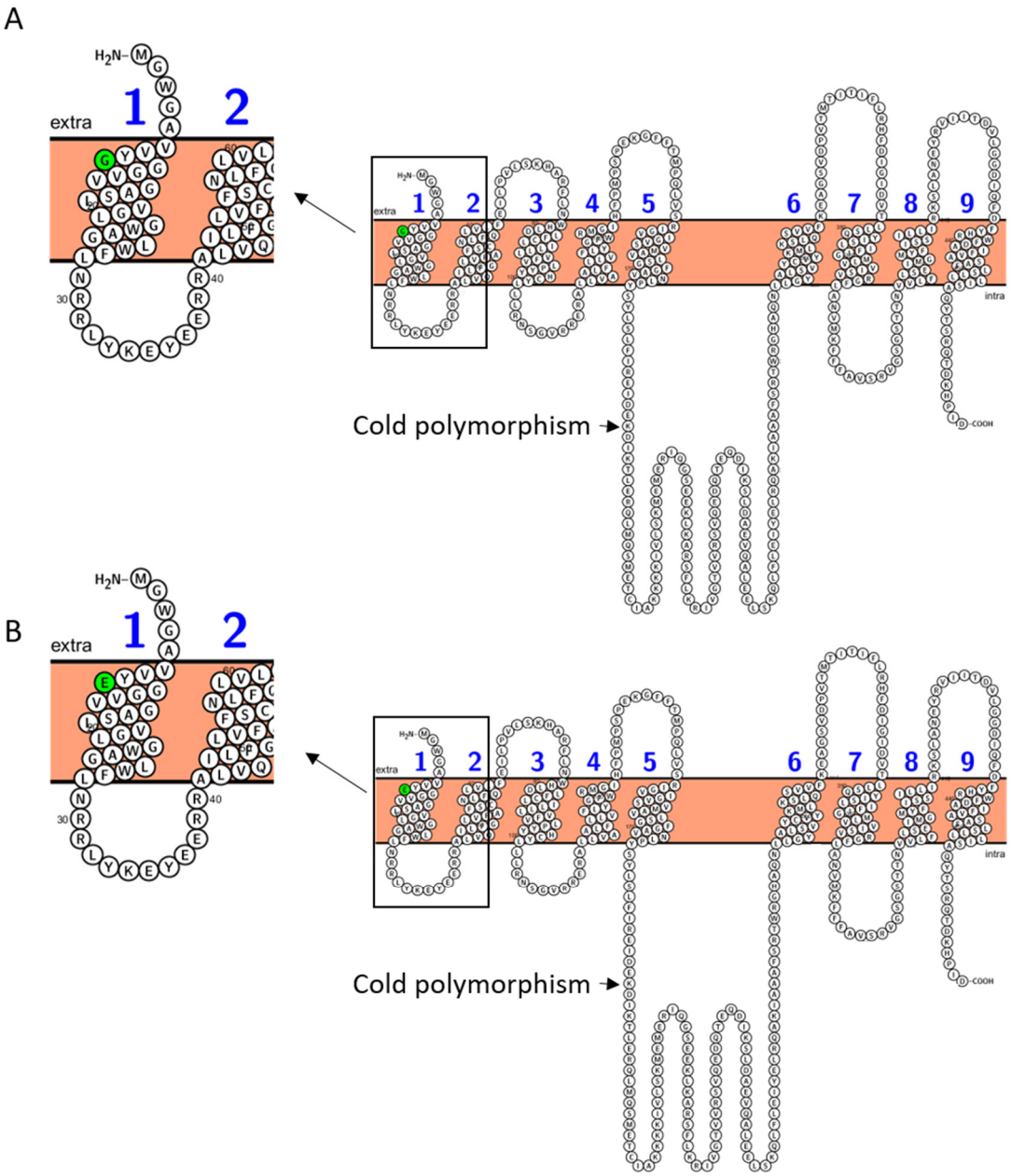

Figure 3.9. Predicted membrane protein topology of OsGTGe and OsGTGg

Predicted topology of OsGTGg (A) and OsGTGe (B). In green the 9th amino acid showing a glycine or glutamic acid. Topology prediction was made it by TMHMM (Sonnhammer et al., 1998). Diagrams were drawn using Plotter (Omasits et al., 2013).

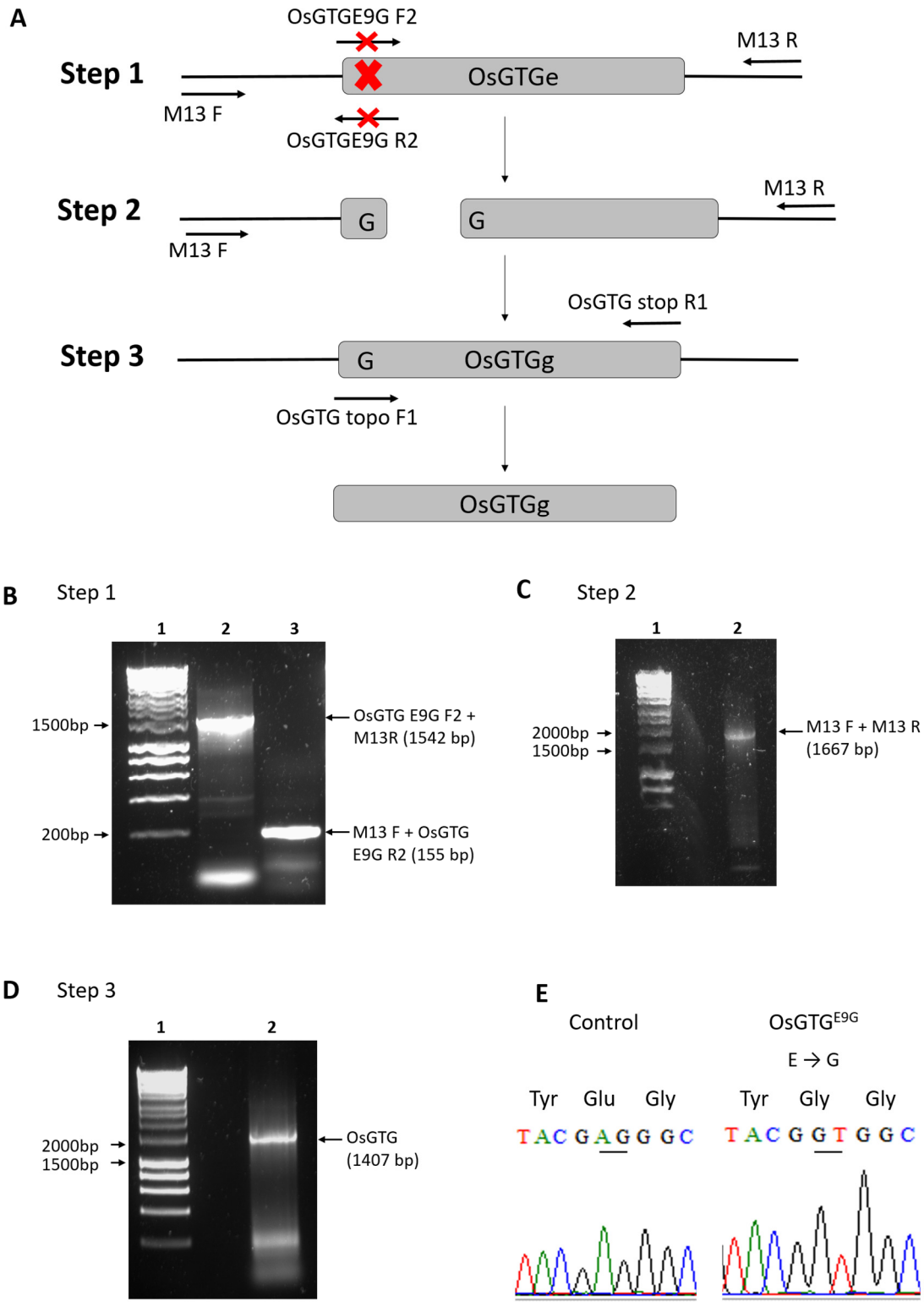

Figure 3.10. Site-directed mutagenesis by overlapping PCR to generate *OsGTGE9G* from *OsGTGe*

A) Diagram showing the mutagenesis strategy for the three steps (1-3) of the process. The location of the mutation is represented by a red cross. B) Step 1, pENTR/D *OsGTG* was used as a template and two independent fragments were generated using M13F + OsGTG E9G R2 (lane 3) and OsGTG E9G F2 + M13R (lane 2) primers. C) Step 2, overlapping PCR using both fragments from step 1 and primers M13F + M13R (lane 2). D) Step 3, PCR using overlapped product from step 2 and primers OsGTG topo F + OsGTG stop R1 (lane 2). E) Sequencing of pENTR/D *OsGTGg* confirming the presence of the mutation (GAG → GGT). Predicted sizes are shown on the right and molecular markers on the left (lane 1 in all gels).

Table 3.1. The entry vectors generated in this study

Plasmid	Description
pENTR/D *OsGTGe* with stop codon	CDS of *OsGTG* containing Glu in the 9th amino acid position
pENTR/D *OsGTGe* without stop codon	CDS of *OsGTG* containing Glu in the 9th amino acid position that can be C-terminally tagged
pENTR/D *OsGTGg* with stop codon	CDS of *OsGTG* where Glu was mutated to Gly in the 9th amino acid position
pENTR/D *OsGTGg* without stop codon	CDS of *OsGTG* where Glu was mutated to Gly in the 9th amino acid position that can be C-terminally tagged

The expression vectors were transformed into *Agrobacterium* for Arabidopsis transformation. To confirm that the *Agrobacterium* transformation was successful, colony PCRs were performed (Figure 3.12). The vectors that were transformed into *Agrobacterium* are listed in Table 3.2. *Agrobacterium* containing all the destination vectors generated were used to transform Arabidopsis WT and *gtg1gtg2* double mutant plants by the floral dip method (section 2.1.4). T3 generation plants were subsequently obtained and homozygosity was analysed. Table 3.3 shows the different independent homozygous lines generated for each vector in each background.

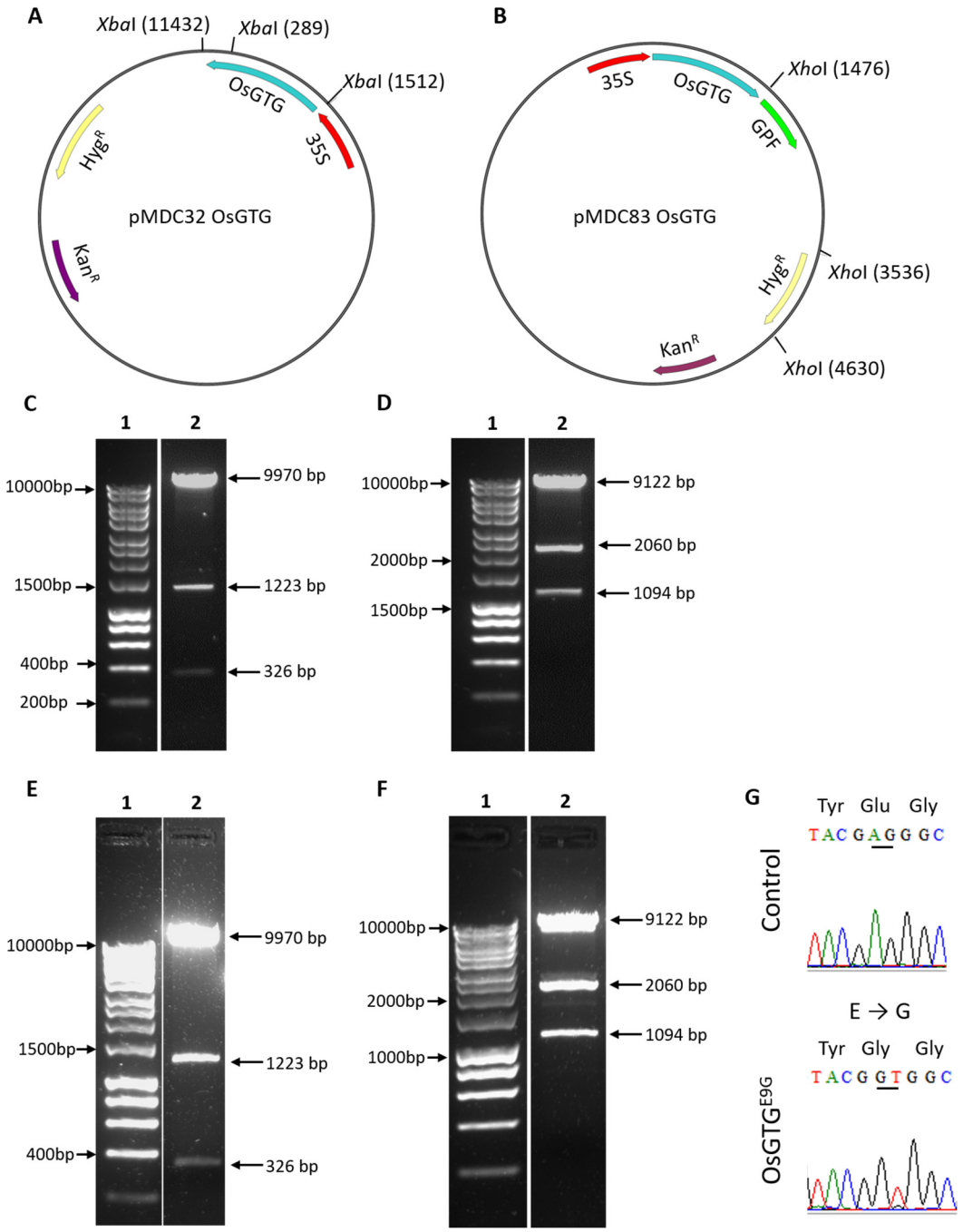

Figure 3.11. Diagnostic restriction analysis of *OsGTGe* and *OsGTGg* cloned into plant expression vectors

Analysis of *OsGTGe* and *OsGTGg* in plant expression vectors pMDC32 and pMDC83. Vector map of pMDC32 *OsGTG* with *Xba*I restriction sites (A) and pMDC83 *OsGTG* with *Xho*I restriction sites (B). Restriction digest of pMDC32 *OsGTGe* (C) and pMDC32 *OsGTGg* (E) with *Xba*I (lane 2). Digestion of pMDC83 *OsGTGe* (D) and pMDC83 *OsGTGg* (F) with *Xho*I (lane 2). G) Sequencing of pMDC83 *OsGTGg* confirming the presence of the mutation (GAG → GGT). Predicted product sizes are indicated on the right and molecular marker sizes on the left (lane 1).

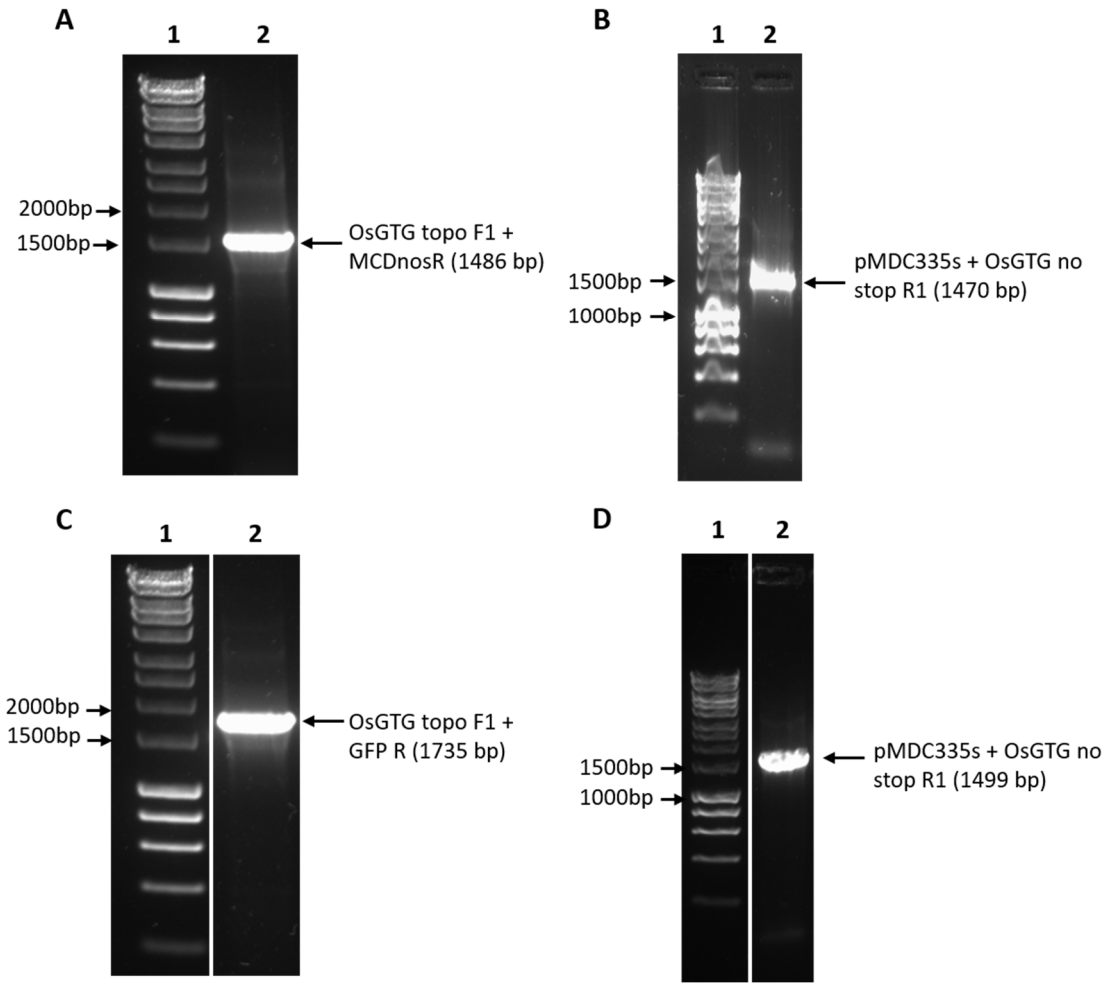

Figure 3.12. *Agrobacterium* transformed with *OsGTGe* and *OsGTGg* in pMDC32 and pMDC83

Colony PCR of *Agrobacterium* GV3101 transformed with pMDC32 *OsGTGe* (A), pMDC32 *OsGTGg* (B), pMDC83 *OsGTGe* (C) and pMDC83 *OsGTGg* (D) Arabidopsis expression vectors (lane 2). Primers OsGTG topo F1 and MDCnos R in A), pMDC35s and OsGTG no stop R1 in B), OsGTG topo F1 and GFP R in C) and pMDC35s and OsGTG no stop R1 in D) were used. Predicted sizes are indicated on the right and molecular marker sizes on the left (lane 1).

Table 3.2. Plasmids transformed into *Agrobacterium*

Plasmid	Description
pMDC32 *OsGTGe*	P35S::*OsGTGe*
pMDC83 *OsGTGe*	P35S::*OsGTGe*::*GFP*
pMDC32 *OsGTGg*	P35S::*OsGTGg*
pMDC83 *OsGTGg*	P35S::*OsGTGg*::*GFP*

Table 3.3. The homozygous T3 transgenic Arabidopsis lines created with OsGTGs

Plasmid	Construct	Plant Transformed	# T3 lines
pMDC32 *OsGTGe*	P35S::*OsGTGe*	WT	4
pMDC32 *OsGTGe*	P35S::*OsGTGe*	*gtg1gtg2*	4
pMDC83 *OsGTGe*	P35S::*OsGTGe*::*GFP*	WT	3
pMDC83 *OsGTGe*	P35S::*OsGTGe*::*GFP*	*gtg1gtg2*	3
pMDC32 *OsGTGg*	P35S::*OsGTGg*	WT	3
pMDC32 *OsGTGg*	P35S::*OsGTGg*	*gtg1gtg2*	3
pMDC83 *OsGTGg*	P35S::*OsGTGg*::*GFP*	WT	4
pMDC83 *OsGTGg*	P35S::*OsGTGg*::*GFP*	*gtg1gtg2*	2

3.2.4. Expression of OsGTG rescues Arabidopsis *gtg1gtg2* double mutant growth phenotype

The Arabidopsis *gtg1gtg2* double mutant is characterized by a defective growth phenotype (Jaffé et al., 2012). Double mutant plants exhibit a reduced root length and fresh weight and a shorter hypocotyl length with distended epidermal cells (Jaffé et al., 2012). To study the conservation of function of the GTG family, *OsGTGe* and *OsGTGg* were expressed in the Arabidopsis *gtg1gtg2* double mutant to determine whether they could rescue these growth defects. WT plants were also transformed. RT-PCR was used to confirm *OsGTG* expression (Figure 3.13). The transgenic lines showed clear expression of *OsGTG* whereas in the control WT and *gtg1gtg2* plants no expression was observed. *ACTIN* was used as a control gene for cDNA quality and showed expression in all lines with no genomic contamination observed (Figure 3.13).

Both OsGTGe and OsGTGg were able to rescue the short root length observed in the Arabidopsis *gtg1gtg2* double mutant (Figure 3.14 B and Figure 3.15 B). An *AtGTG1* transformed line, used as a control, also showed rescue. Plant biomass, which was also reduced in the *gtg1gtg2* double mutant compared to WT, was also rescued by expression of both OsGTGe and OsGTGg (Figure 3.14 C and Figure 3.15 C). This confirmed that both OsGTGs can rescue the root length and fresh weight defective phenotypes observed in *gtg1gtg2* mutant plants indicating a likely conservation of protein function between these plant species. The root length was also analysed in *gtg1gtg2* plants expressing OsGTGe and OsGTGg tagged with GFP. These plants were transformed with pMDC83 *OsGTGe* and pMDC83 *OsGTGg*. Both OsGTGs tagged with GFP were able to rescue the defective root length and fresh weight phenotype of the *gtg1gtg2* mutant (Figure 3.16 and Figure 3.17). This indicates that the addition of GFP did not affect the functioning of the protein.

As mentioned previously, *gtg1gtg2* mutant exhibits a short hypocotyl in comparison to WT when grown in low light conditions (Jaffé et al., 2012). Both versions of OsGTG were able to rescue the defective hypocotyl growth of the Arabidopsis *gtg1gtg2* double mutant (Figure 3.18). Whereas *gtg1gtg2* showed a short hypocotyl, *gtg1gtg2* lines expressing both OsGTGs exhibited the same hypocotyl length as the WT and the *AtGTG1* transformed line. All these results suggest that the function of GTG is conserved between Arabidopsis and rice.

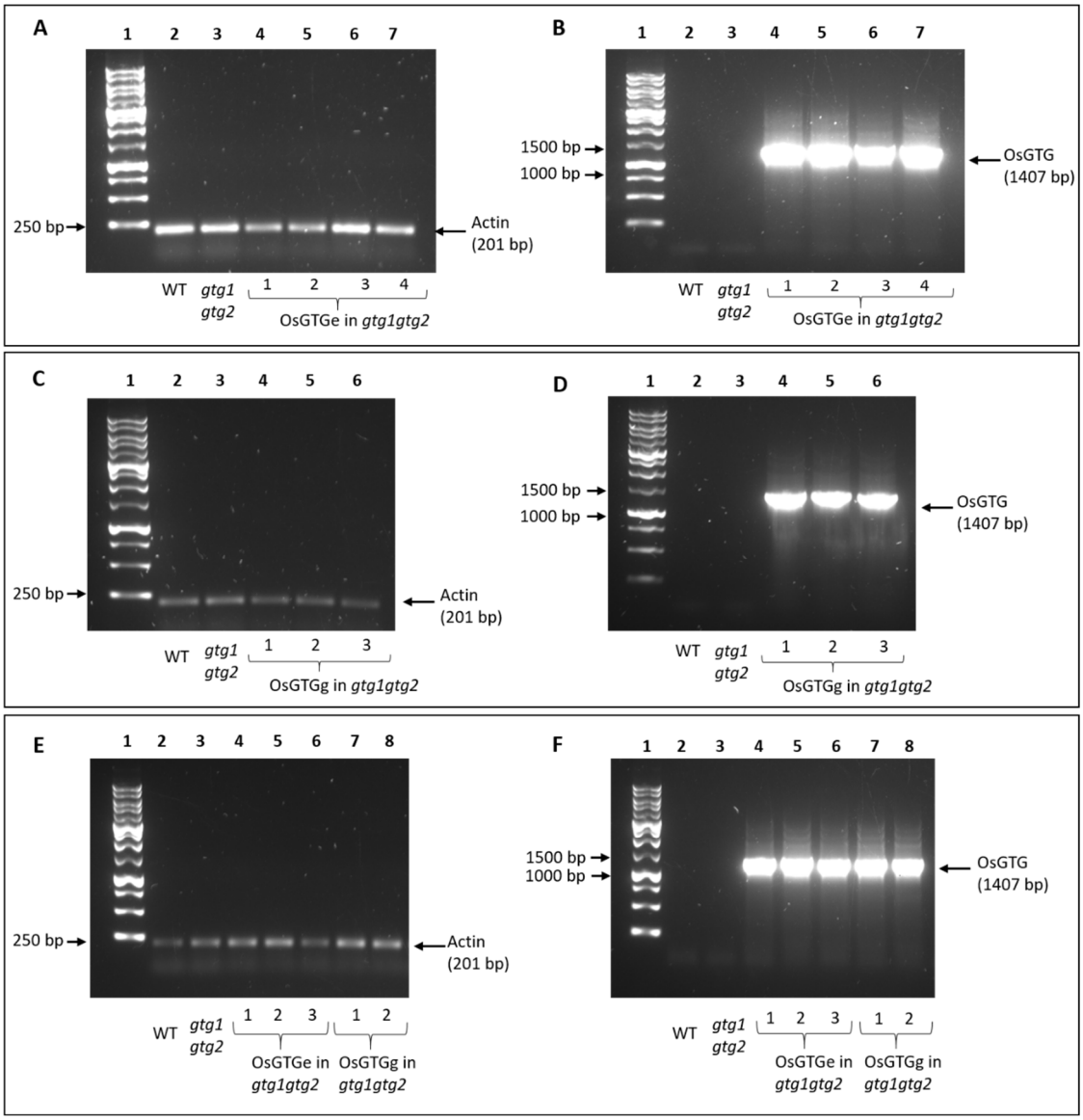

Figure 3.13. Expression of *OsGTGe* and *OsGTGg* in *gtg1gtg2* mutant background

RT-PCR using cDNA generated from WT, *gtg1gtg2* and *gtg1gtg2* expressing *OsGTGe* or *OsGTGg*. On the left panels, Actin F and Actin R (predicted 201 bp) primers were used and on the right panels OsGTG topo F1 and OsGTG stop R1 (predicted 1407 bp). For all gels WT (lane 2), *gtg1gtg2* (lane 3). A and B) Four independent pMDC32 *OsGTGe* transformed *gtg1gtg2* lines (lanes 4-7); C and D) Three independent pMDC32 *OsGTGg* transformed *gtg1gtg2* lines (lanes 4-6); E and F) Three independent pMDC83 *OsGTGe* transformed *gtg1gtg2* lines (lanes 4-6) and two independent pMDC83 *OsGTGg* transformed *gtg1gtg2* lines (lanes 7-8). Predicted products are shown on the right and molecular markers on the left (lane 1).

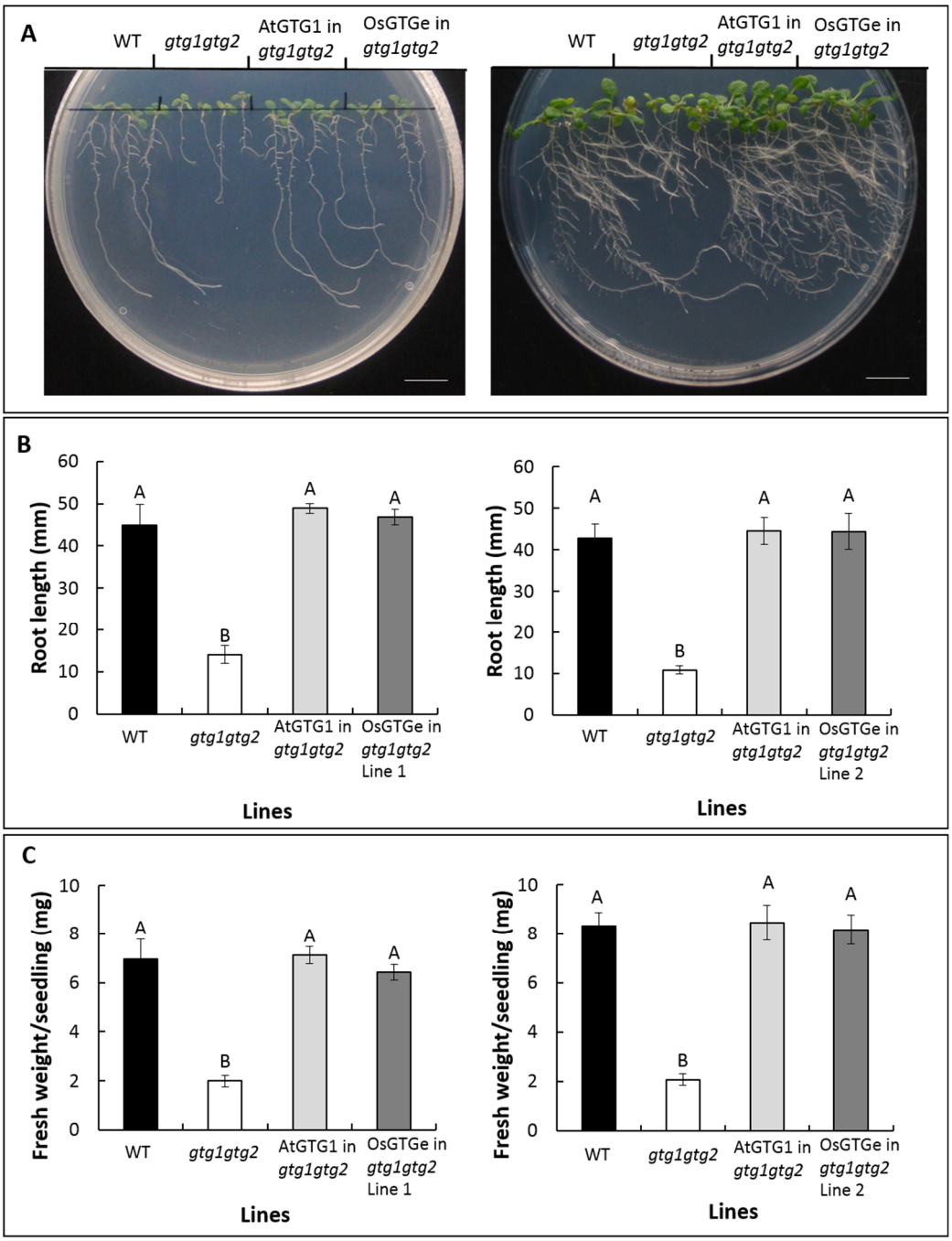

Figure 3.14. OsGTGe rescues the root length and fresh weight defects of the Arabidopsis *gtg1gtg2* double mutant

A) Representative images of seedlings at day 10 (left) and at day 14 (right); scale bar 1 cm. Root length at 10 days (B) and fresh weight per seedling at 14 days (C) of WT (black), *gtg1gtg2* (white), *AtGTG1* transformed lines (light grey) and *OsGTGe* transformed lines (dark grey) grown on 0.5 MS in the absence of sucrose. Data represent the mean (±SEM) of six plates with four seedlings per line per plate (B, n=24 and C, n=6). One-way ANOVA ($p < 0.05$). Means not sharing a letter are significantly different; Tukey *post-hoc* test.

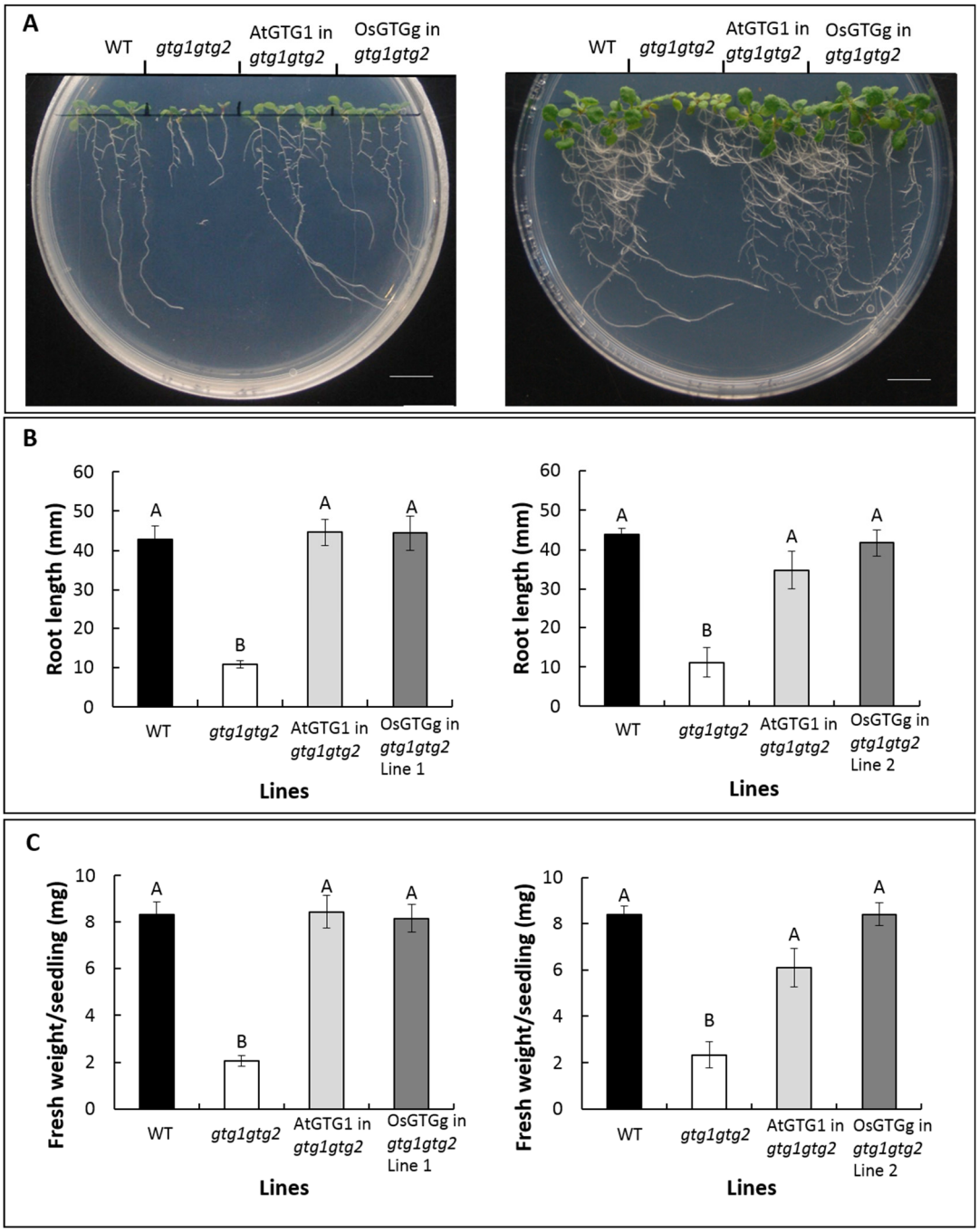

Figure 3.15. OsGTGg rescues the root length and fresh weight defects of the Arabidopsis *gtg1gtg2* double mutant

A) Representative images of seedlings at day 10 (left) and at day 14 (right); scale bar 1 cm. Root length at 10 days (B) and fresh weight per seedling at 14 days (C) of WT (black), *gtg1gtg2* (white), *AtGTG1* transformed lines (light grey) and *OsGTGg* transformed lines (dark grey) grown on 0.5 MS in the absence of sucrose. Data represent the mean (±SEM) of six plates with four seedlings per line per plate (B, n=24 and C, n=6). One-way ANOVA ($p < 0.05$). Means not sharing a letter are significantly different; Tukey *post-hoc* test.

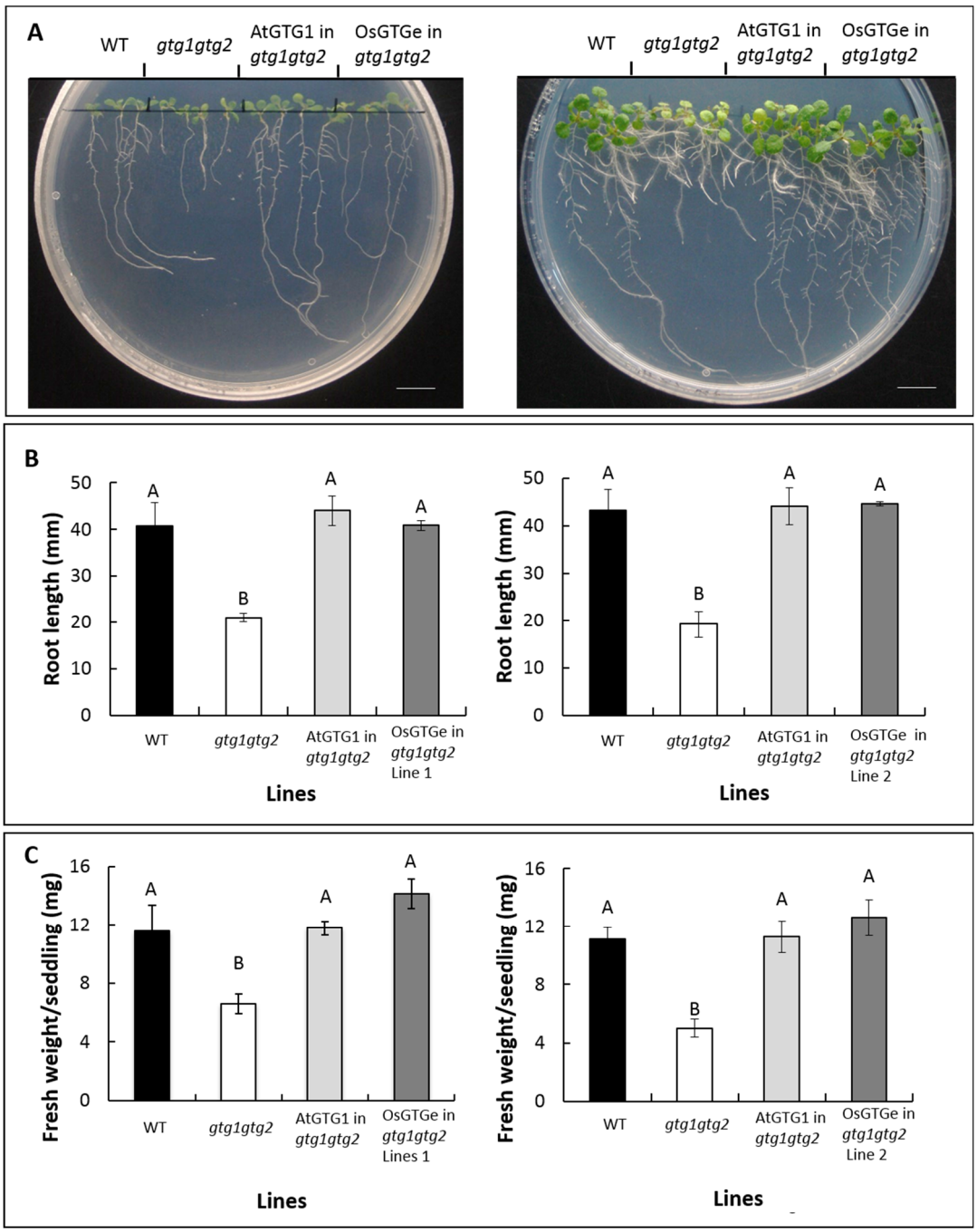

Figure 3.16. OsGTGe::GFP rescues the root length and fresh weight defects of the Arabidopsis *gtg1gtg2* mutant

A) Representative images of seedlings at day 10 (left) and at day 14 (right); scale bar 1 cm. Root length at 10 days (B) and fresh weight per seedling at 14 days (C) of WT (black), *gtg1gtg2* (white), *AtGTG1::GFP* transformed lines (light grey) and *OsGTGe::GFP* transformed lines (dark grey) grown on 0.5 MS in the absence of sucrose. Data represent the mean (±SEM) of six plates with four seedlings per line per plate (B, n=24 and C, n=6). One-way ANOVA ($p < 0.05$). Means not sharing a letter are significantly different; Tukey *post-hoc* test.

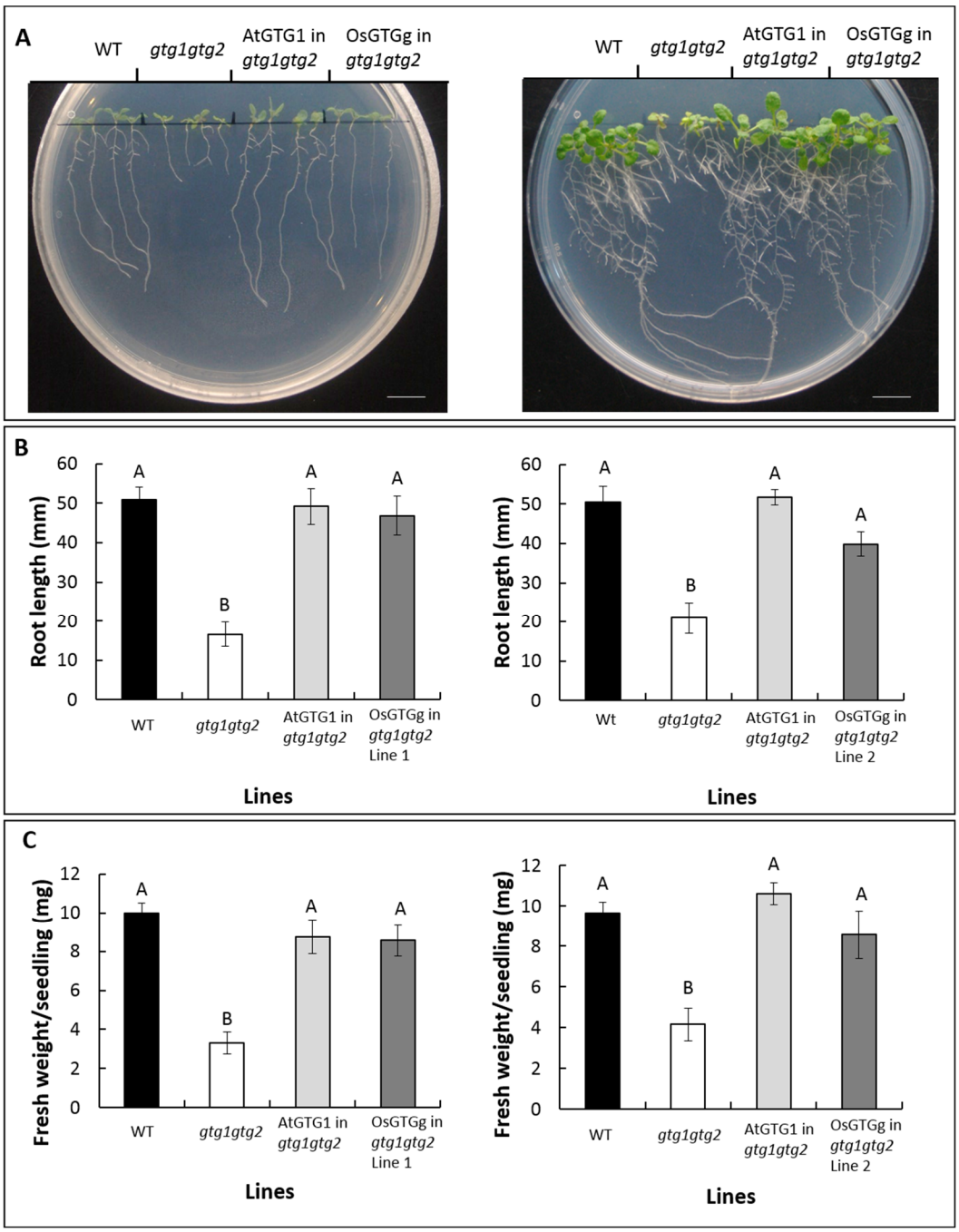

Figure 3.17. OsGTGg::GFP rescues the root length and fresh weight defects of the Arabidopsis *gtg1gtg2* mutant

A) Representative images of seedlings at day 10 (left) and at day 14 (right); scale bar 1 cm. Root length at 10 days (B) and fresh weight per seedling at 14 days (C) of WT (black), *gtg1gtg2* (white), *AtGTG1::GFP* transformed lines (light grey) and *OsGTGg::GFP* transformed lines (dark grey) grown on 0.5 MS in the absence of sucrose. Data represent the mean (±SEM) of six plates with four seedlings per line per plate (B, n=24 and C, n=6). One-way ANOVA ($p < 0.05$). Means not sharing a letter are significantly different; Tukey *post-hoc* test.

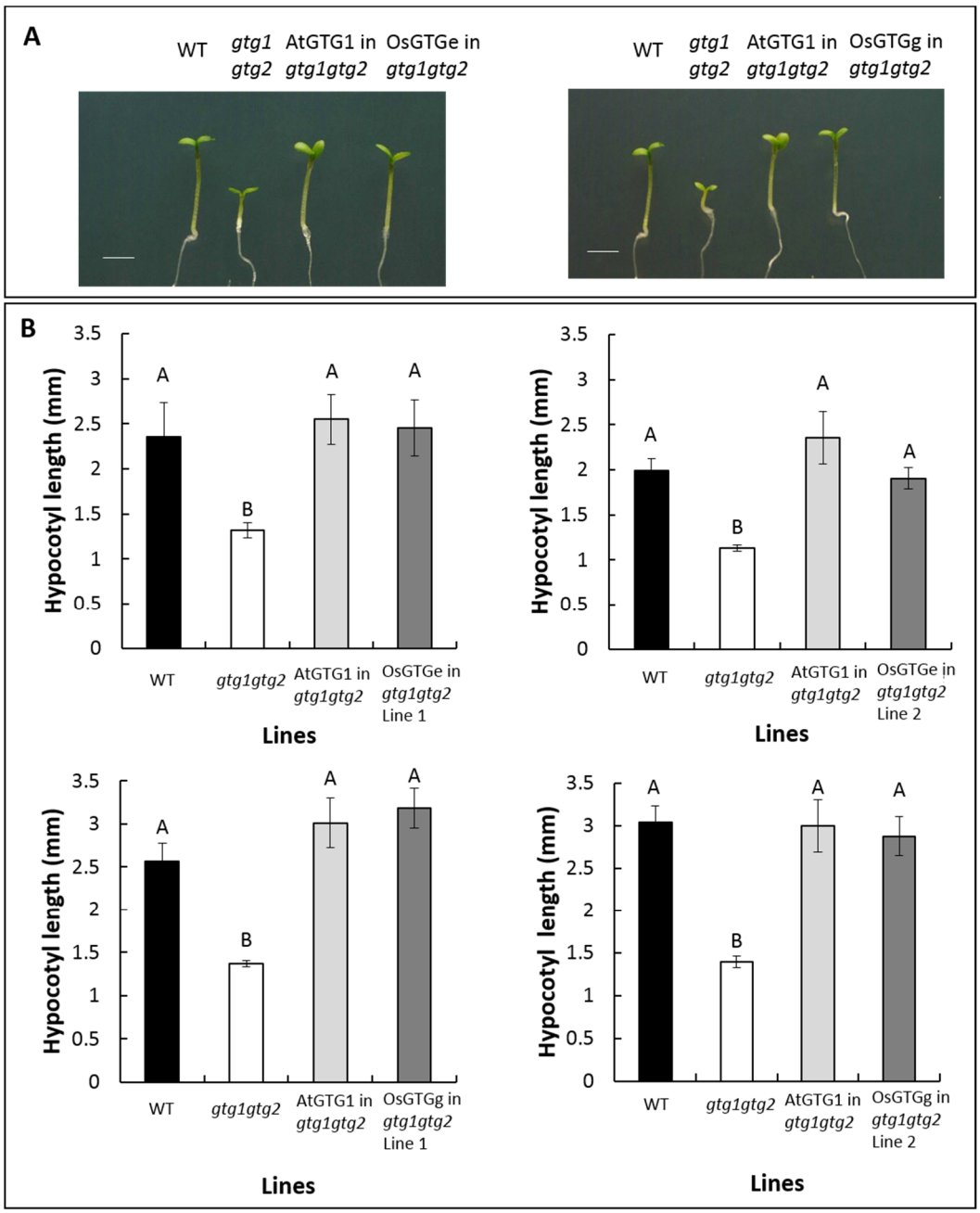

Figure 3.18. OsGTGe and OsGTGg rescue the defective hypocotyl growth of the *gtg1gtg2* mutant in low light conditions

A) Representative images of seedlings at day 5 of *OsGTGe* transformed lines (left) and *OsGTGg* transformed lines (right); scale bar 1mm. B) Hypocotyl length of WT (black), *gtg1gtg2* (white), *AtGTG1* transformed lines (light grey), *OsGTGe* transformed lines (dark grey, top) and *OsGTGg* transformed lines (dark grey, bottom) grown on 0.5 MS with 1% sucrose at 10 µmol m^{-2} s^{-1} light intensity for 5 days. For *OsGTG* transformants data from two independent lines are shown (line 1 and line 2). Data represent the mean (±SEM) of six plates with 15 seedlings per line per plate (n=75-85). One-way ANOVA ($p < 0.05$). Means not sharing a letter are significantly different; Tukey *post-hoc* test.

3.2.5. OsGTG rescues the defective ER body number and cell morphology of Arabidopsis *gtg1gtg2* mutant

Previous work in our laboratory has shown that the *gtg1gtg2* mutant had a defective cell morphology with a reduced number of ER bodies. This was shown using the pH sensor pHluorin with an HDEL sequence to retain it in the ER. HDEL pHluorin was expressed in both WT and the *gtg1gtg2* mutant (Adam, Terry, Williams, unpublished). The pH sensor pHluorin, is a modified GFP that can be detected by confocal microscopy. The defective cell shape and ER body number were restored when AtGTG1 was expressed in the mutant (Adam, Terry, Williams, unpublished).

To test whether OsGTG is also able to rescue this defect in cell shape, both OsGTGs (pMDC32 *OsGTGe* and pMDC32 *OsGTGg* vectors) were expressed in the *gtg1gtg2* mutant that already contained the pH sensor pHluorin tagged to the ER retention signal HDEL. The lines generated for this study are shown in Table 3.4. Unfortunately, silencing occurred in some of the T3 homozygous *OsGTGe* transformed lines, and thus T2 lines were also used for the analysis. The shape of the epidermal cells in Arabidopsis was analysed by confocal microscopy. The *gtg1gtg2* mutant plants that expressed OsGTGe and OsGTGg rescued the defective cell shape of the mutant (Figure 3.19). The cells of the *gtg1gtg2* double mutant showed an abnormal shape, however, the cell shape of the *gtg1gtg2* mutant expressing any of the OsGTGs was similar to the WT cell shape. This is another indication that the function of Arabidopsis and rice GTG is conserved.

Table 3.4. Generation of Arabidopsis lines containing HDEL pHluorin and transformed with *OsGTGs*

Arabidopsis background	Gene inserted	Organelle pH sensor	T2 lines with signal	T3 homozygous lines with signal
gtg1gtg2 Ws2	*OsGTGe*	HDEL (ER)	2	1
gtg1gtg2 Ws2	*OsGTGg*	HDEL (ER)	7	4

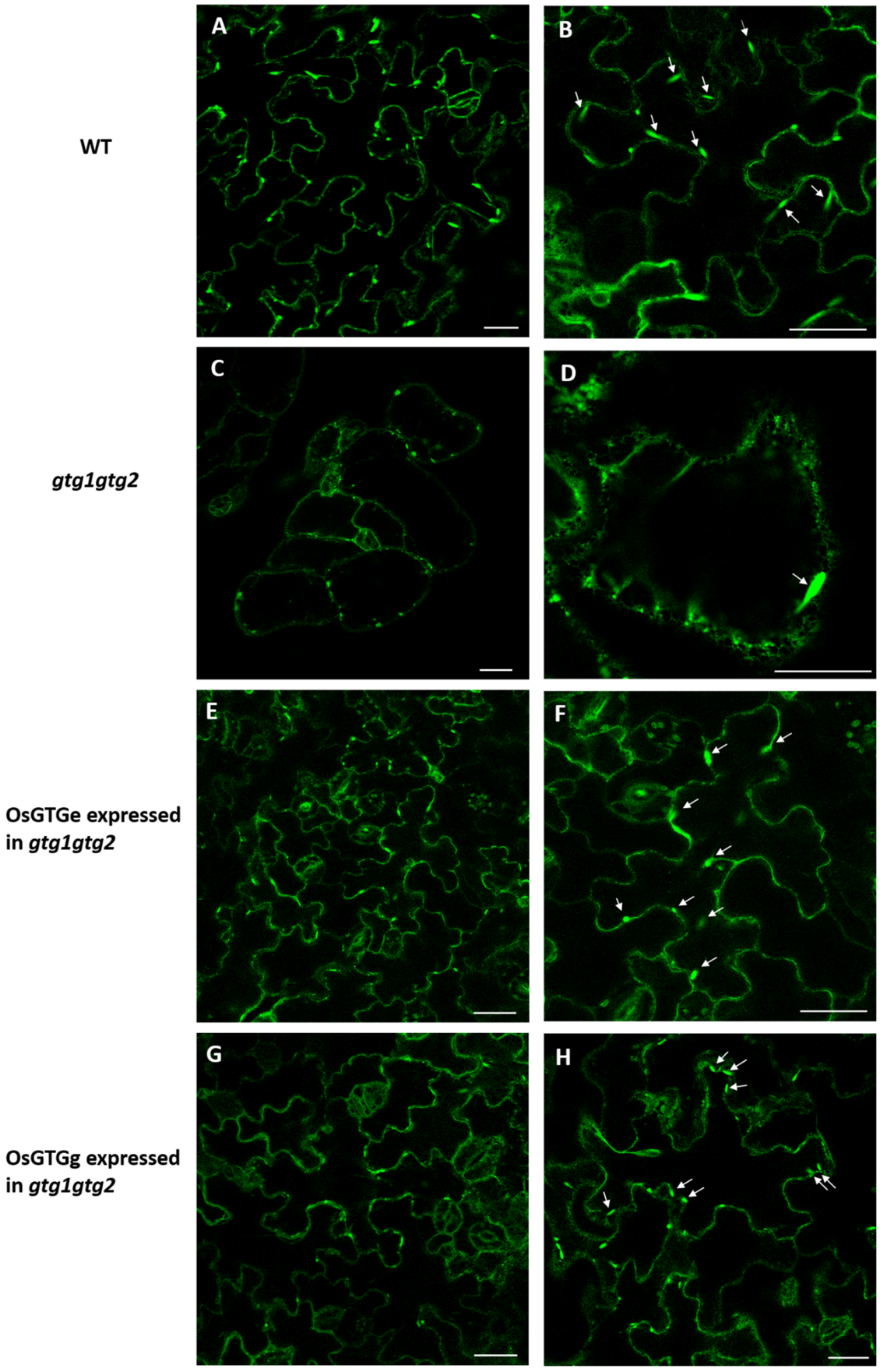
WT
gtg1gtg2
OsGTGe expressed in gtg1gtg2
OsGTGg expressed in gtg1gtg2
A
B
C
D
E
F
G
H

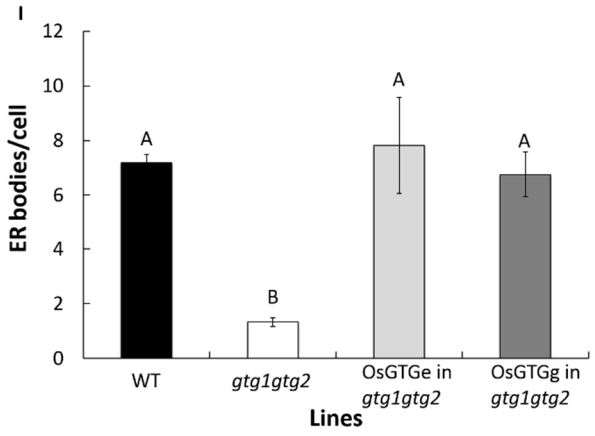

Figure 3.19. OsGTG rescues the defective cell shape and ER body number of the *gtg1gtg2* mutant

Confocal microscopy was used to analyse the epidermal cell shape (left) and ER body number (right) of WT (A and B), *gtg1gtg2* (C and D), and *gtg1gtg2* lines expressing OsGTGe (E and F) and OsGTGg (G and H), all containing HDEL pHluorin. White arrows represent ER bodies. Scale bar 25µm. I) Graph representing the number of ER bodies found per cell in each of the genotypes analysed. Three independent lines per genotype were used and 4-20 cells per line were analysed (n=12-60). One-way ANOVA ($p < 0.05$). Means not sharing a letter are significantly different, Tukey *post-hoc* test.

Another observation was that the *gtg1gtg2* double mutant produced less ER bodies than the WT (Adam, Terry, Williams, unpublished). ER bodies are Brassica-specific cigar-shape organelles that are derived from the ER (Matsushima et al., 2003a, Yamada et al., 2009, Nakano et al., 2014). WT cells contained around seven ER bodies in each cell (Figure 3.19 I), but the *gtg1gtg2* mutant only had approximately one ER body per cell. Thus the reduction in ER bodies is confirmed in this study. Most of the cells in the double mutant did not contain ER bodies and in some of them, only one or two were detected. When OsGTGe and OsGTGg were expressed in the mutant, the ER body count was similar to WT. This shows that OsGTG can rescue this defect in ER body number in the *gtg1gtg2* mutant and further confirms the conserved function of GTG between these two plant species.

3.2.6. Determining the subcellular localisation of OsGTG

The subcellular localisation of OsGTG was examined by fusing the cDNA of both *OsGTGs* with GFP. The constructs pMDC83 *OsGTGe* and pMDC83 *OsGTGg* generated previously were used. Two approaches were taken: transient expression of these constructs in tobacco leaves and stable expression in Arabidopsis plants. For the stable line generation, WT Arabidopsis plants were transformed with pMDC83 *OsGTGe* and pMDC83 *OsGTGg*. RT-PCR demonstrated that there was a high expression of *OsGTG* in the transgenic lines whereas no gene expression was observed in WT un-transformed control lines (Figure 3.20). The localisation of OsGTG was analysed in all lines using confocal microscopy. Fluorescence from the GFP with both OsGTGs was consistently observed mainly at the periphery of the cell and in a tubular network across the Arabidopsis cells (Figure 3.21 A-D). OsGTG seemed to also localise in punctuate structures similar to Golgi bodies (Ueda et al., 2014). The dynamic movement of the punctuate structures resembled Golgi organelles. The dynamic tubular network resembled the characteristic ER plant structure (Nelson et al., 2007, Griffing et al., 2017).

While stable expression of OsGTGe::GFP in WT Arabidopsis plants showed a pattern consistent with localisation in the ER and the Golgi, OsGTGg::GFP seemed to localise predominantly to the ER (Figure 3.21 C-D). Using the same focal plane, Golgi localisation was observed in the OsGTGe transgenic lines, but not many Golgi bodies were found in the WT lines expressing OsGTGg. The number of Golgi bodies was quantified in cells expressing OsGTGe and OsGTGg. As shown in Figure 3.21 E, cells expressing OsGTGe exhibited more Golgi bodies than cells expressing OsGTGg, suggesting that OsGTGe localises more at the Golgi than OsGTGg. This indicates that the 9th amino acid could play a role in the localisation of the protein.

In the epidermal cells of plants, the vacuole expands and occupies most of the cell space; confining the cytoplasm and the ER close to the plasma membrane (Marty, 1999). To confirm the localisation of OsGTG, specific organelle markers were used and transient expression in tobacco leaves was carried out by co-expressing both OsGTGs::GFP with different organelle markers tagged with RFP. To confirm ER localisation, the HDEL marker tagged with RFP was used (Gomord et al., 1997). As shown in Figure 3.22, RFP fluorescent signal overlapped with signals from both OsGTGs::GFP, generating the yellow colour in the overlay images. Since Golgi has *cis*, *medial* and *trans* compartments (Dupree and Sherrier, 1998), Golgi localisation was

confirmed using different markers. For *cis-medial* Golgi ManI (Mannosidase I) tagged with RFP was used (Nebenführ et al., 1999). For OsGTGe a clear overlap was observed with the ManI *cis* Golgi marker for some Golgi bodies (Figure 3.23 A-C). For OsGTGg Golgi localisation was also observed but it was less abundant in comparison to OsGTGe. The *trans* Golgi localisation was confirmed using the ST::RFP (Sialyltransferase) marker (Boevink et al., 1998). Both OsGTG proteins co-localised with the marker in some of the Golgi bodies, being more abundant in OsGTGe expressing cells (Figure 3.24).

To determine whether OsGTG localises to the plasma membrane, the LT16b plasma membrane marker tagged to a mOrange fluorophore was used (McGavin et al., 2012). As shown in Figure 3.25, the signal of the plasma membrane marker did not co-localise with OsGTGe::GFP or with OsGTGg::GFP, suggesting that OsGTGs mostly localises in the endomembrane system of the plant cells, mainly in ER and in the Golgi apparatus, and not at the plasma membrane.

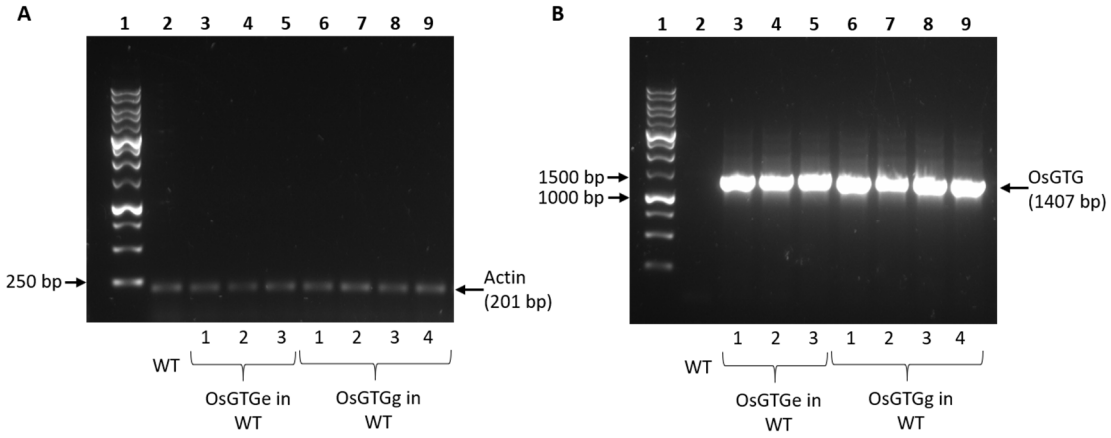

Figure 3.20. Expression of *OsGTGe* and *OsGTGg* in WT Arabidopsis

RT-PCR of WT (lane 2), three independent lines of *OsGTGe::GFP* expressed in WT (lanes 3-5) and four independent lines of *OsGTGg::GFP* expressed in WT (lanes 6-9). Actin F and Actin R primers were used (predicted 201 bp) in A) and OsGTG topo F1 and OsGTG stop R1 (predicted 1407 bp) in B). Predicted products sizes are shown on the right and molecular markers on the left (lane 1).

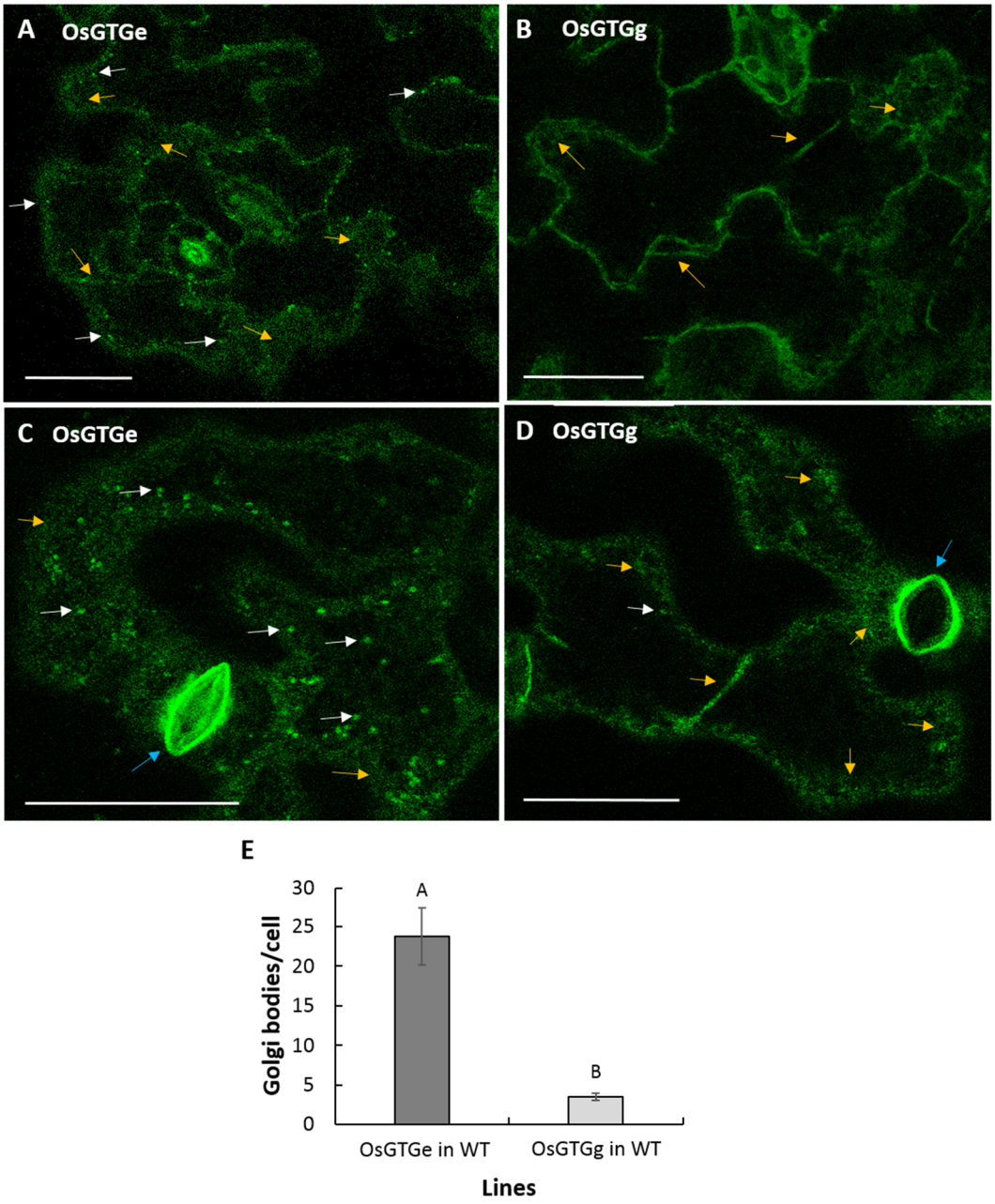

Figure 3.21. Subcellular localisation of OsGTGe and OsGTGg in Arabidopsis stable lines

Confocal microscopy images showing OsGTGe::GFP (A and C) and OsGTGg::GFP (B and D) localisation in WT Arabidopsis lines. Yellow arrows represent ER localisation and white arrows Golgi localisation. Blue arrows indicate stomata cells. Scale bar 25 µm. E) The number of Golgi bodies per cell. Three independent lines per genotype and 5-10 cells per line were analysed (n=15-30). One-way ANOVA ($p < 0.05$). Means not sharing a letter are significantly different, Tukey *post-hoc* test.

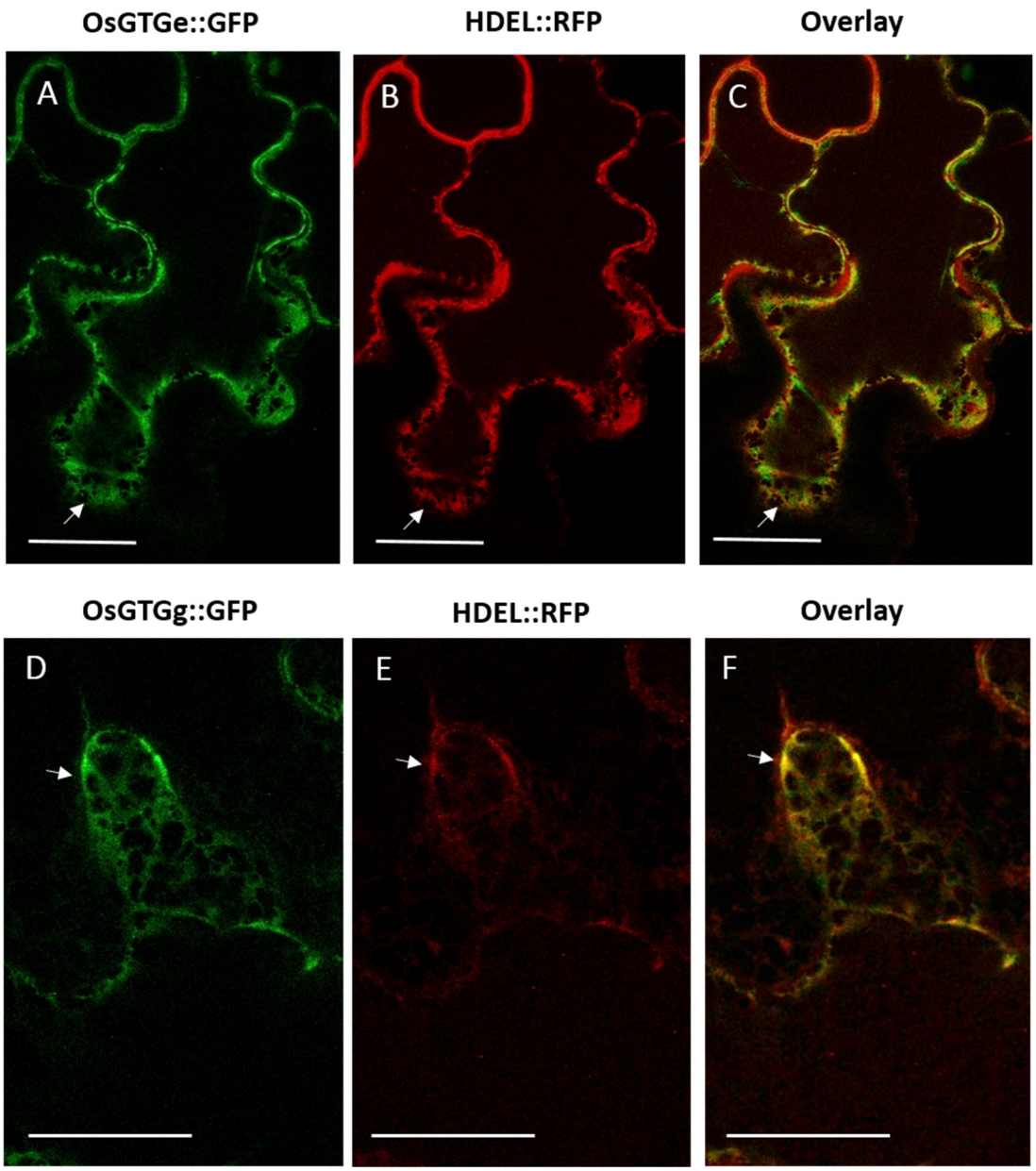

Figure 3.22. OsGTGe and OsGTGg co-localise with the HDEL::RFP ER marker

Confocal microscopy images showing that OsGTGe::GFP (A-C) and OsGTGg::GFP (D-F) co-localise with the HDEL::RFP ER marker when transiently expressed in tobacco cells. OsGTGe::GFP and OsGTGg::GFP expression pattern in green in A and D. HDEL::RFP marker in red in B and E. Merged images showing co-localisation in yellow in C and F. White arrows = ER network. Scale bar 25 µm.

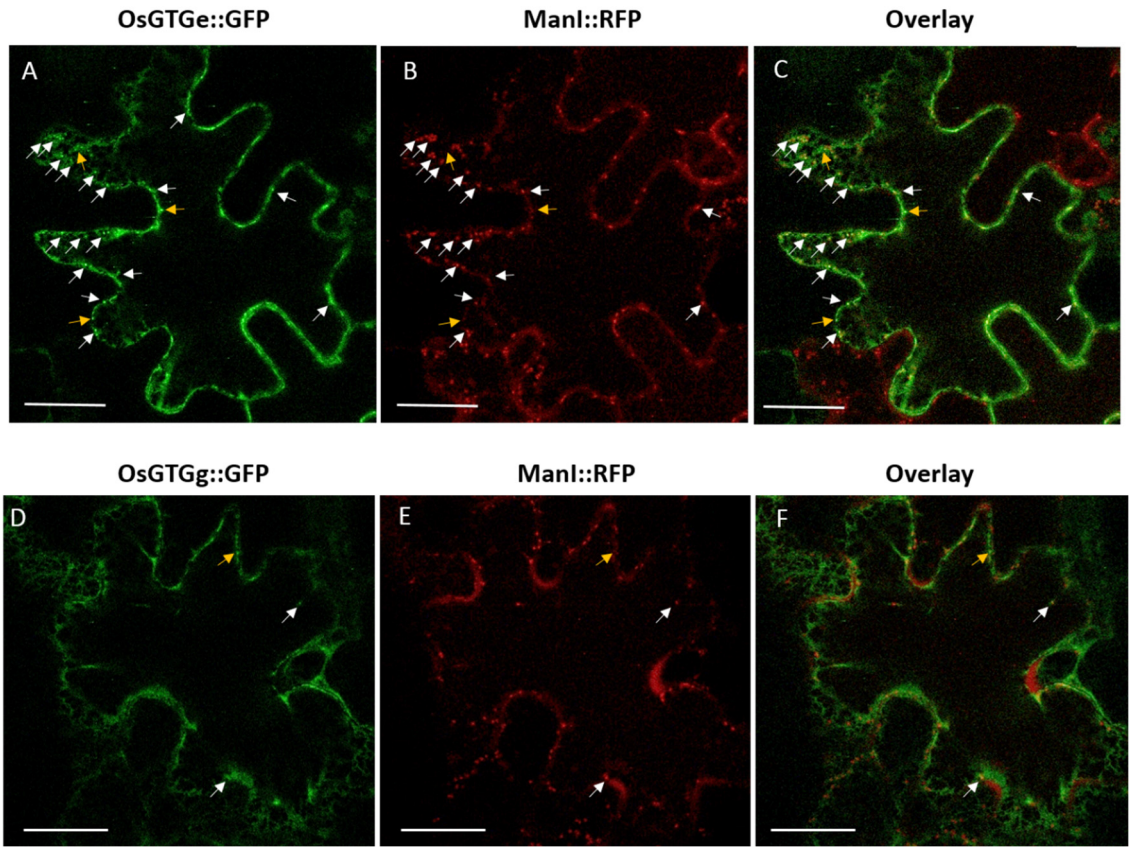

Figure 3.23. OsGTGe showed more abundant *cis* Golgi localisation than OsGTGg using the ManI marker

Confocal microscopy images showing that OsGTGe::GFP (A-C) and OsGTGg::GFP (D-F) co-localise with the ManI::RFP *cis* Golgi marker when transiently expressed in tobacco cells. OsGTGe::GFP and OsGTGg::GFP expression pattern in green in A and D. ManI::RFP marker in red in B and E. Merged images showing co-localisation in yellow in C and F. White arrows = co-localisation, yellow arrows = OsGTGe or OsGTGg::GFP localisation only. Scale bar 25 µm.

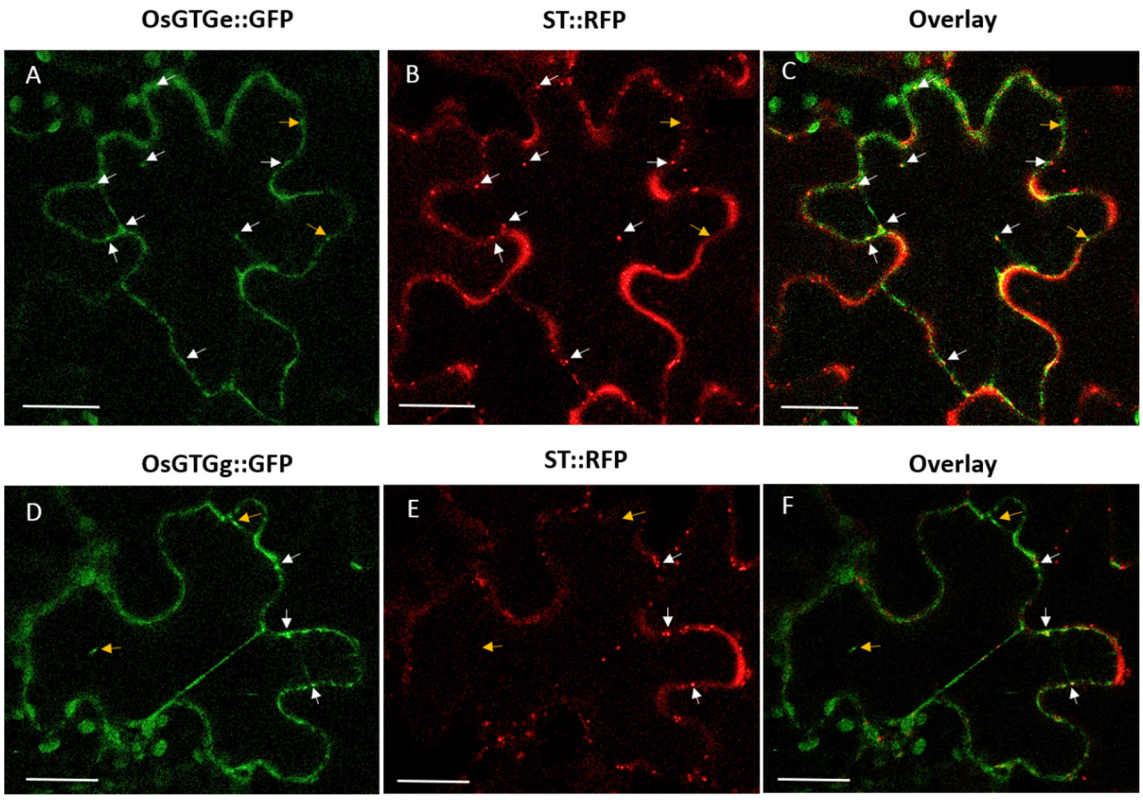

Figure 3.24. OsGTGe and OsGTGg exhibit *trans* Golgi localisation

Confocal microscopy images showing that OsGTGe::GFP (A-C) and OsGTGg::GFP (D-F) co-localise with the ST::RFP *trans* Golgi marker when transiently expressed in tobacco cells. OsGTGe::GFP and OsGTGg::GFP expression pattern in green in A and D. ST::RFP marker in red in B and E. Merged images showing co-localisation in yellow in C and F. White arrows = co-localisation, yellow arrows = OsGTGe or OsGTGg::GFP localisation only. Scale bar 25 µm.

3.2.7. Analysis of the Lys/Met residue at the 187th amino acid position of the OsGTG protein

A previous study has reported that the lysine (Lys/K) in the 187th amino acid position of OsGTG is involved in rice cold tolerance (Ma et al., 2015). It was shown that the cold tolerant rice variety *japonica* had a lysine in the 187th amino acid position in contrast to the cold sensitive *indica* variety, which had methionine (Met/M) instead. To study whether this residue is involved in cold tolerance, a mutated version of OsGTG with methionine in the 187th amino acid position was generated.

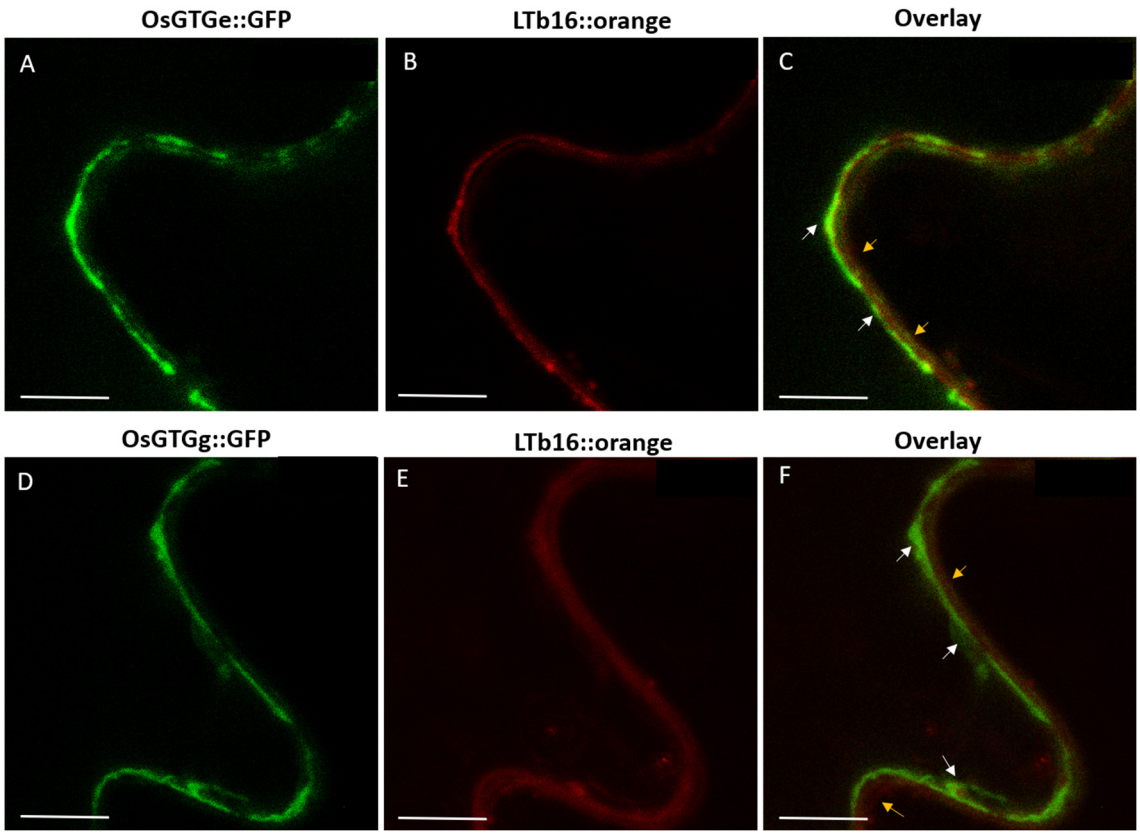

Figure 3.25. OsGTGs do not co-localise with the LT16b mOrange plasma membrane marker

Confocal microscopy images showing that OsGTGe::GFP (A-C) and OsGTGg::GFP (D-F) do not co-localise with the LT16b mOrange plasma membrane marker when transiently expressed in tobacco cells. OsGTGe::GFP and OsGTGg::GFP expression pattern in green in A and D. LT16b marker in red in B and E. Merged images showing no co-localisation in C and F. White arrows = OsGTGe::GFP or OsGTGg::GFP localisation, yellow arrows = LT16b marker localisation. Scale bar 7.5 µm.

The original *OsGTG* sequence that was amplified from the *japonica* variety contained a lysine at position 187. The objective was to generate Arabidopsis transgenic plants that contained both OsGTG versions and test whether this amino acid change had any effect on cold tolerance in Arabidopsis. At the same time, it can also be determined whether this residue could be involved in the function and localisation of OsGTG. Overlapping PCRs were performed to introduce the 187th methionine mutation. For the mutation of the lysine to methionine, an adenine at 560 bp was changed to a thymine. The constructs pENTR/D *OsGTGe* and pENTR/D *OsGTGg*, both with and without the

stop codon, were used as a template. Two fragments were generated using primers that included the mutation. A PCR using the full-length sequence was carried out to overlap both fragments. This process is summarised in Figure 3.26 A and an example of the cloning is shown in Figure 3.26 B-F. The fragment generated was cloned into pENTR/D entry vector (section 2.3.8) and this vector was sequenced in forward and reverse directions to confirm that the mutation was introduced in the sequence. Following this process, the rest of the constructs were generated. This mutation was generated in both OsGTGe and OsGTGg. The different entry vectors produced to study the role of the 187th Lys/Met residue are shown in Table 3.5.

The mutated gene with the stop codon was cloned into pMDC32 destination vector and the gene without the stop codon was cloned into pMDC83 for GFP tagging (section 2.3.8). The cloned product was transformed into *E.coli*. Colony PCRs and restriction analysis were carried out to confirm that the genes were inserted correctly in the destination vectors. The list of constructs generated is shown in Table 3.5. The vectors were introduced into *Agrobacterium* and Arabidopsis WT and *gtg1gtg2* mutant plants were transformed with those constructs by the floral dipping method (section 2.1.4). In Table 3.6 the list of transgenic plants that have been generated for this study is shown.

3.2.7.1 The 187th Lys/Met mutation does not affect the function and localisation of OsGTG in Arabidopsis plants

To test whether the 187th amino acid residue was involved in the function of OsGTG, OsGTGe K187M (OsGTGe^{187M}) and OsGTGg K187M (OsGTGg^{187M}) were expressed in Arabidopsis *gtg1gtg2* mutant plants. RT-PCRs were carried out to determine whether *OsGTG* was expressed in those transgenic lines. All the transgenic lines showed a high expression of *OsGTG* whereas no gene expression was observed in the WT and *gtg1gtg2* control lines (Figure 3.27). *ACTIN* was also analysed as a control gene for cDNA quality and showed a clear signal in all lines with no genomic contamination observed.

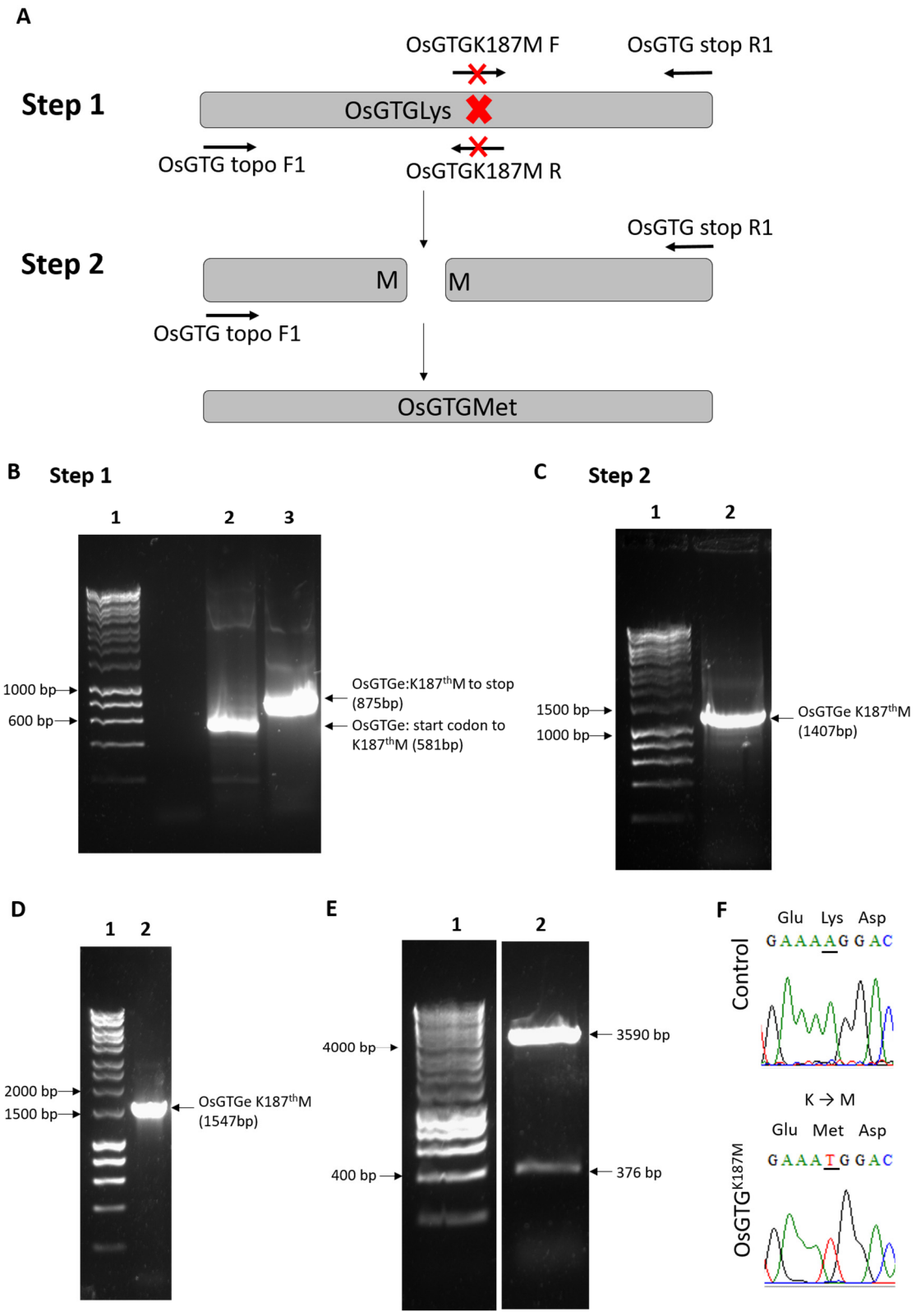

Figure 3.26. Mutagenesis by overlapping PCR to introduce methionine in the 187th amino acid position of OsGTGe

Diagram of the mutagenesis steps in A). The mutation point is marked by a red cross. B) Step 1, OsGTG topo F1 + OsGTG K187M R (581 bp in lane 2) and OsGTG K187M F + OsGTG stop R1 (875 bp in lane 3) primers in pENTR/D *OsGTGe*. C) Step 2, overlapping PCR using fragments from step 1 and OsGTG topo F1 + OsGTG stop R1 (1407 bp in lane 2) primers. Colony PCR of pENTR/D *OsGTGe K187M* using M13 F + OsGTG stop R1 primers (1547 bp lane 2) in D), restriction digest with *Xba*I + *Hind*III (lane 2) in E) and sequencing confirming the presence of the mutation (AAG → ATG) in F). Predicted sizes are shown on the right and molecular markers on the left (lane 1).

Table 3.5. Entry vectors and destination vectors generated to study the 187th Lys/Met residue

pENTR	Destination	Description
pENTR *OsGTGe-S K187M*	pMDC32 *OsGTGe K187M* (P35S::*OsGTGe K187M*)	Glu in the 9th, Met in the 187th residue. With stop codon
pENTR *OsGTGe-NS K187M*	pMDC83 *OsGTGe K187M* (P35S::*OsGTGe K187M*::*GFP*)	Glu in the 9th, Met in the 187th residue. Without stop codon
pENTR *OsGTGg-S K187M*	pMDC32 *OsGTGg K187M* (P35S::*OsGTGg K187M*)	Gly in the 9th, Met in the 187th residue. With stop codon
pENTR *OsGTGg-NS K187M*	pMDC83 *OsGTGg K187M* (P35S::*OsGTGg K187M*::*GFP*)	Gly in the 9th, Met in the 187th residue. Without stop codon

Table 3.6. The transgenic Arabidopsis lines created with the Lys/Met 187th mutation

Plasmid	Construct	Plant Transformed	# T1 lines	# T3 lines
pMDC32 *OsGTGe K187M*	P35S::*OsGTGe K187M*	WT	10	-
pMDC32 *OsGTGe K187M*	P35S::*OsGTGe K187M*	*gtg1 gtg2*	7	3
pMDC83 *OsGTGe K187M*	P35S::*OsGTGe K187M*::*GFP*	WT	15	4
pMDC83 *OsGTGe K187M*	P35S::*OsGTGe K187M*::*GFP*	*gtg1 gtg2*	12	4
pMDC32 *OsGTGg K187M*	P35S::*OsGTGg K187M*	WT	10	-
pMDC32 *OsGTGg K187M*	P35S::*OsGTGg K187M*	*gtg1 gtg2*	11	3
pMDC83 *OsGTGg K187M*	P35S::*OsGTGg K187M*::*GFP*	WT	11	5
pMDC83 *OsGTGg K187M*	P35S::*OsGTGg K187M*::*GFP*	*gtg1 gtg2*	15	3

To test whether this mutated version of OsGTG was able to rescue the defective growth phenotype observed in the mutant, root length and hypocotyl length were measured in the transgenic lines. OsGTGe^{187M} and OsGTGg^{187M} were able to rescue the defective root length and reduced fresh weight exhibited by the *gtg1gtg2* double mutant (Figure 3.28 and Figure 3.29). The plants expressing OsGTG^{187M} showed a similar root length and fresh weight to the WT and the plants expressing OsGTG^{187K}. This indicates that both OsGTG versions can produce a functional protein. Similar results were observed when the hypocotyl growth was analysed. Both OsGTG^{187M} lines were able to restore to normal the defective hypocotyl growth of the *gtg1gtg2* mutant (Figure 3.30).

The hypocotyl length observed in the lines expressing OsGTG^{187M} was similar to the length of the WT and the OsGTG^{187K} expressing lines. This is a further confirmation that this amino acid does not play a key role in the function of the protein.

To study whether this amino acid is involved in the localisation of the protein, stable Arabidopsis WT plants expressing OsGTGe^{187M} and OsGTGg^{187M} were analysed by confocal microscopy. OsGTGe^{187M} exhibited a clear ER and Golgi localisation (Figure 3.31). This was similar to the localisation found in cells expressing OsGTGe^{187K}. However, cells expressing OsGTGg^{187M} showed mostly ER localisation and barely any Golgi localisation. A similar localisation pattern was observed for OsGTGg^{187K} (Figure 3.21). The number of Golgi bodies per cell found in each line was quantified and showed that OsGTGe localises more at the Golgi in comparison to OsGTGg (Figure 3.32). The difference in the 187th amino acid did not seem to affect the localisation of the protein. However, the 9th amino acid residue seems to play an important role in the localisation of OsGTG.

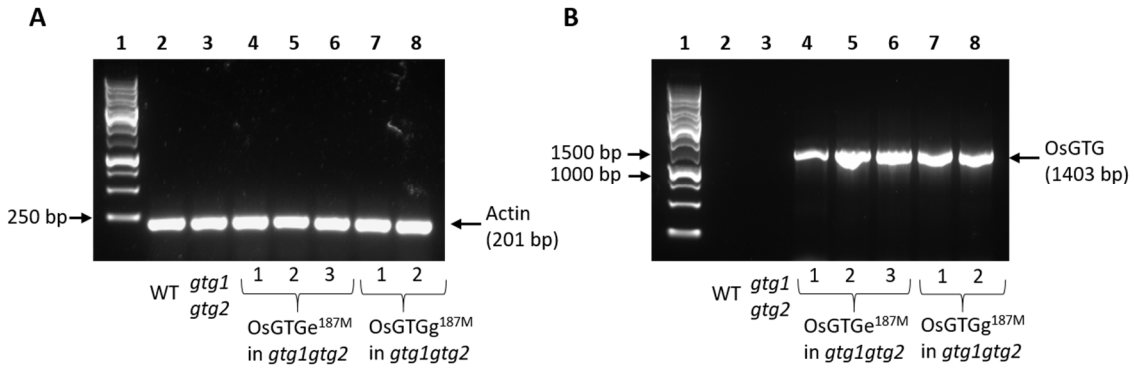

Figure 3.27. Expression of *OsGTG* in *gtg1gtg2* lines transformed with *OsGTGe^{187M}* and *OsGTGe^{187M}*

RT-PCR of WT (lane 2), *gtg1gtg2* (lane 3), three independent lines of *OsGTGe* expressed in *gtg1gtg2* (lanes 4-6) and two independent lines of *OsGTGg* expressed in *gtg1gtg2* (lanes 7-8). Actin F and Actin R primers were used (predicted 201 bp) in A) and OsGTG topo F1 and OsGTG stop R1 (predicted 1407 bp) in B). Predicted products are shown on the right and molecular markers on the left (lane 1).

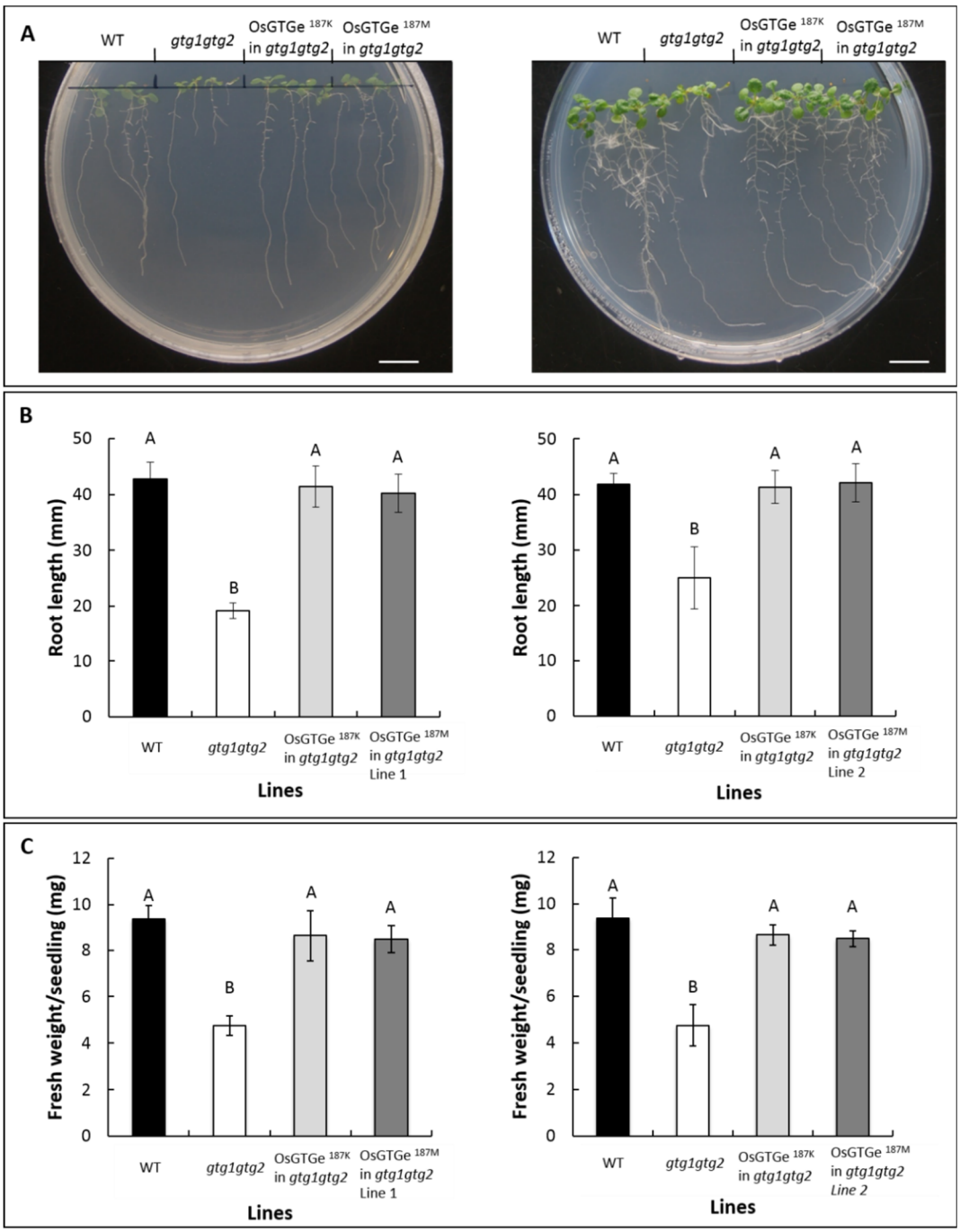

Figure 3.28. OsGTGe with Met in the 187th amino acid position also rescues the defective root length and fresh weight of the *gtg1gtg2* Arabidopsis mutant

A) Representative images of seedlings at day 10 (left) and at day 14 (right); scale bar 1 cm. Root length at 10 days (B) and fresh weight per seedling at 14 days (C) of WT (black), *gtg1gtg2* (white), *OsGTGe*^{187K} transformed lines (light grey) and *OsGTGe*^{187M} transformed lines (dark grey) grown on 0.5 MS in the absence of sucrose. Data represent the mean (±SEM) of six plates with four seedlings per line per plate (B, n=24 and C, n=6). One-way ANOVA ($p < 0.05$). Means not sharing a letter are significantly different; Tukey *post-hoc* test.

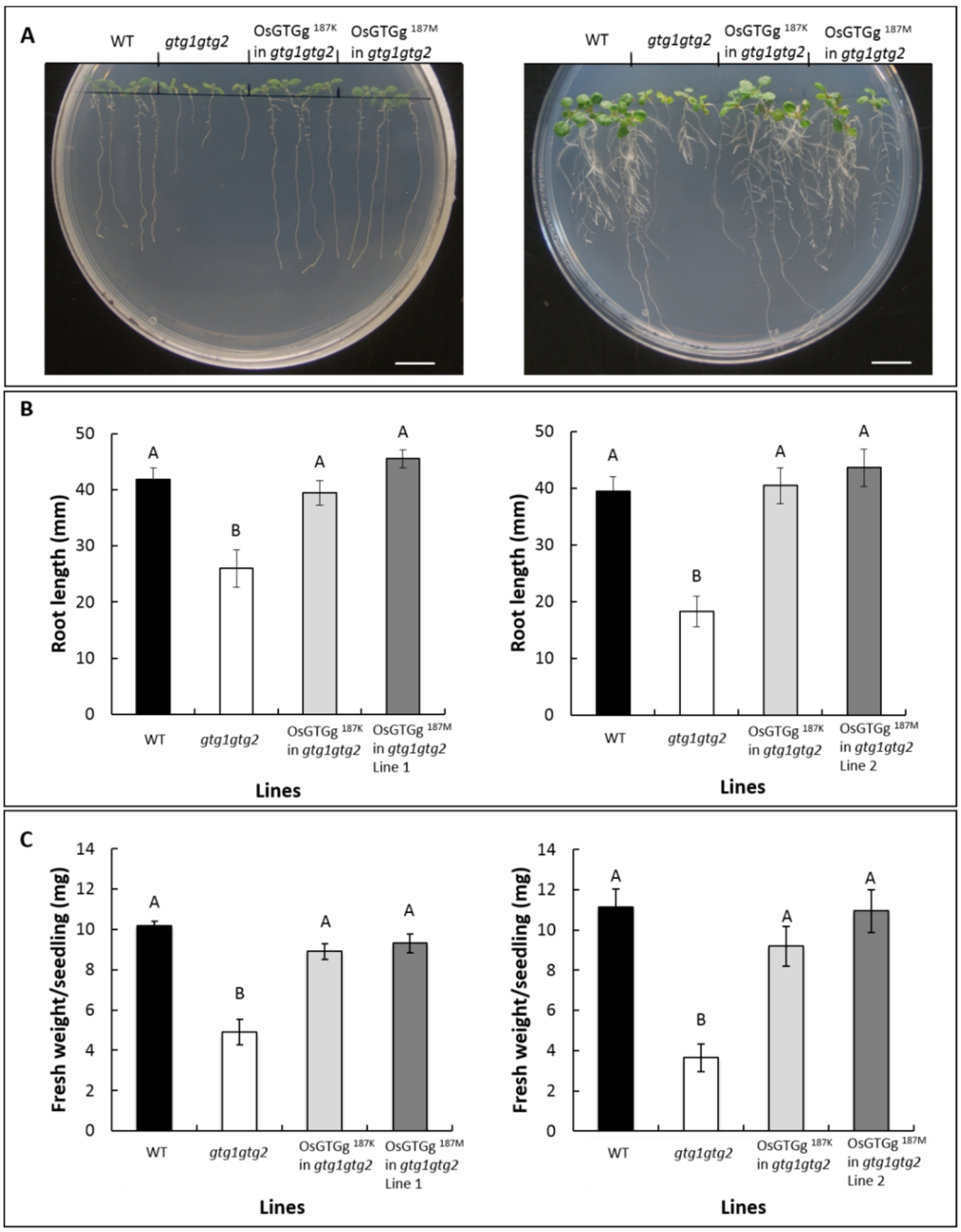

Figure 3.29. OsGTGg with Met in the 187th amino acid position also rescues the defective root length and fresh weight of the *gtg1gtg2* Arabidopsis mutant

A) Representative images of seedlings at day 10 (left) and at day 14 (right); scale bar 1 cm. Root length at 10 days (B) and fresh weight per seedling at 14 days (C) of WT (black), *gtg1gtg2* (white), *OsGTGg*^{187K} transformed lines (light grey) and *OsGTGg*^{187M} transformed lines (dark grey) grown on 0.5 MS in the absence of sucrose. Data represent the mean (±SEM) of six plates with four seedlings per line per plate (B, n=24 and C, n=6). One-way ANOVA ($p < 0.05$). Means not sharing a letter are significantly different; Tukey *post-hoc* test.

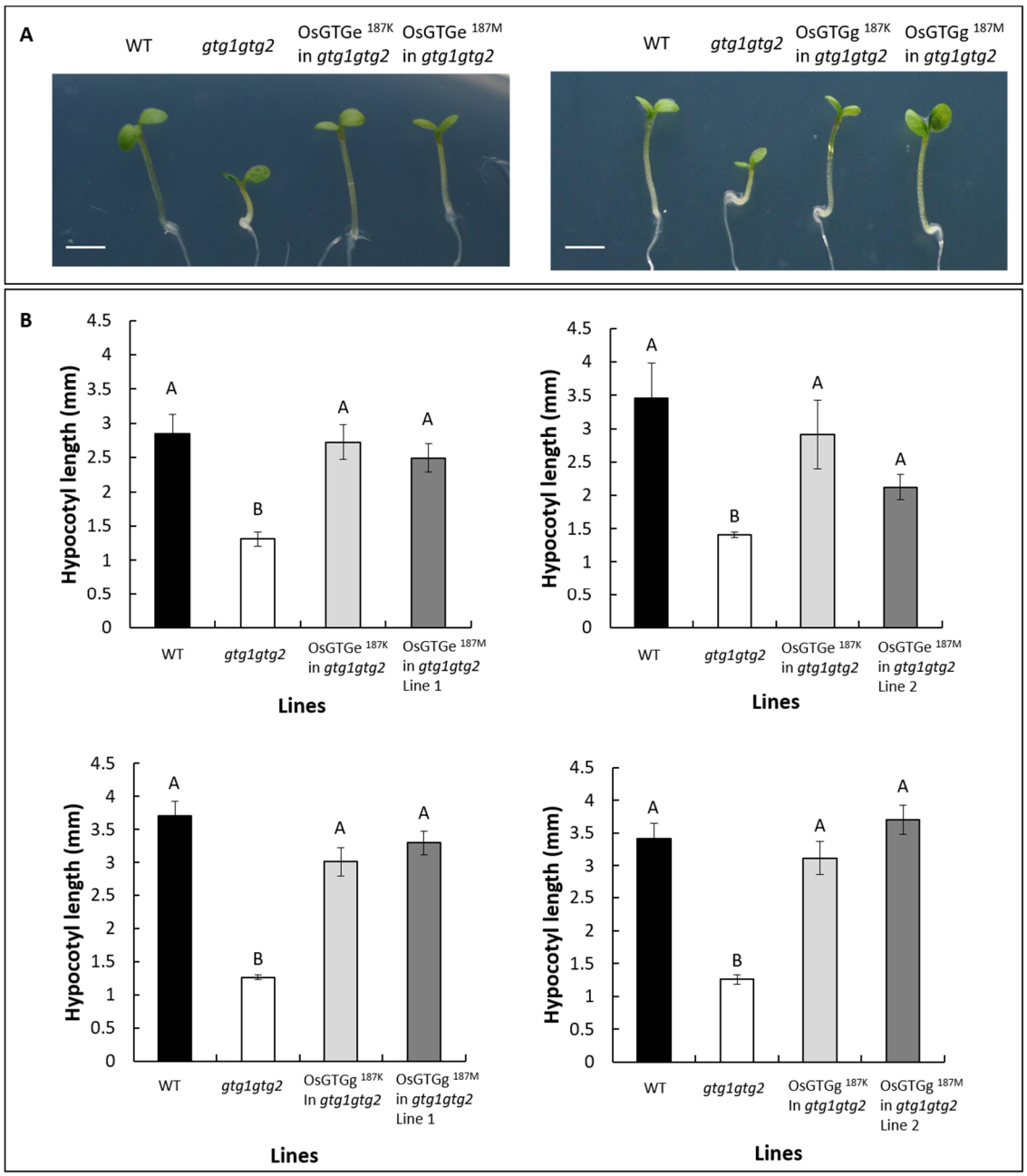

Figure 3.30. OsGTG^{187M} rescues the defective hypocotyl growth of the Arabidopsis *gtg1gtg2* mutant

A) Representative images of hypocotyl at day 5 of *OsGTGe^{187M}* transformed lines (left) and *OsGTGg^{187M}* transformed lines (right); scale bar 1mm. B) Hypocotyl length of WT (black), *gtg1gtg2* (white), *OsGTGe^{187K}* transformed lines (light grey, top), *OsGTGe^{187M}* transformed lines (dark grey, top), *OsGTGg^{187K}* transformed lines (light grey, bottom) and *OsGTGg^{187M}* transformed lines (dark grey, bottom) grown on 0.5 MS with 1% sucrose at 10 µmol m^{-2} s^{-1} light intensity for 5 days. For *OsGTG^{187K}* transformants data from two independent lines are shown (line 1 and line 2). Data represent the mean (±SEM) of six plates with 15 seedlings per line per plate (n=75-90). One-way ANOVA ($p < 0.05$). Means not sharing a letter are significantly different; Tukey *post-hoc* test.

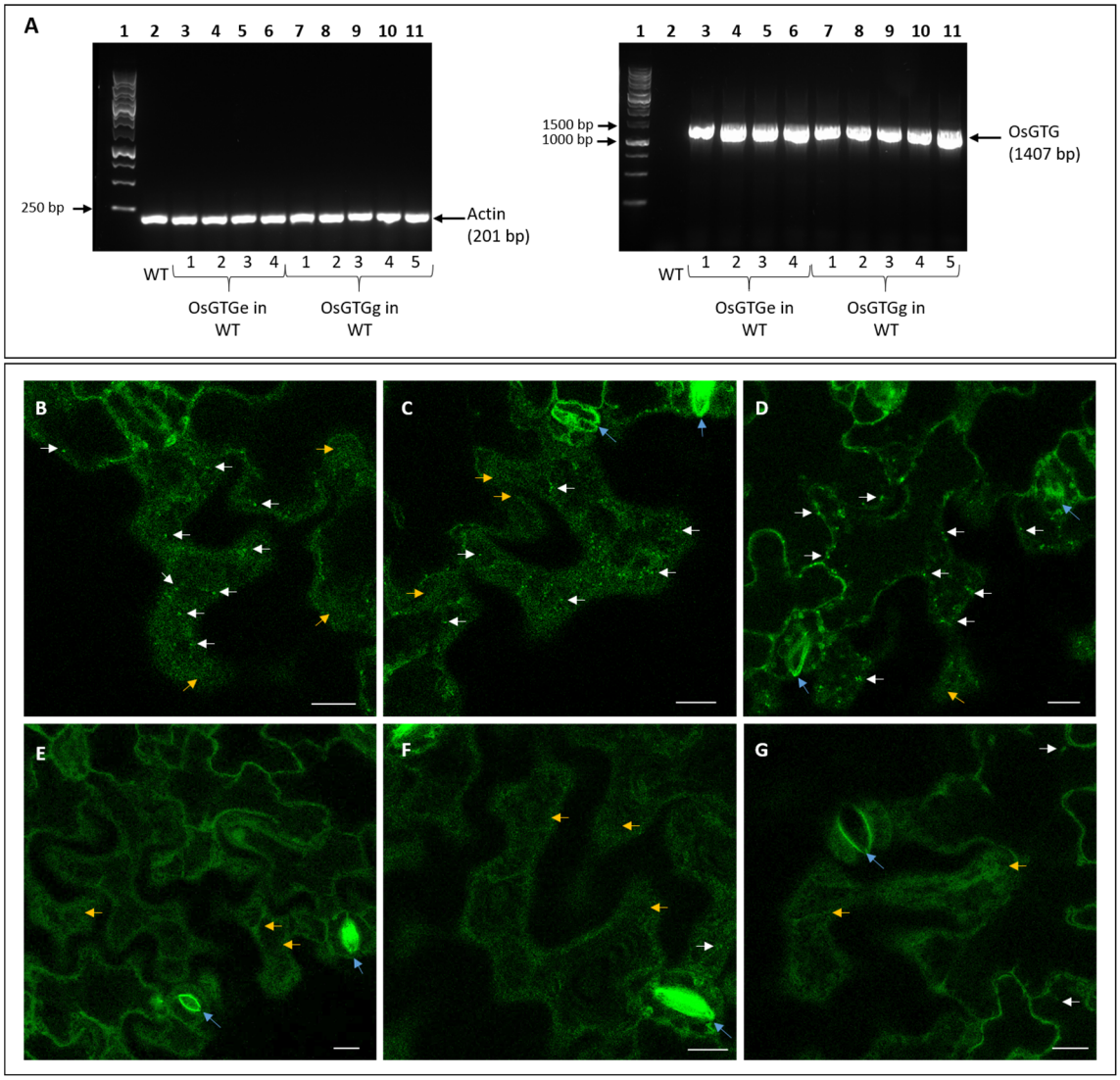

Figure 3.31. *OsGTG* gene expression and subcellular localisation of OsGTGe^{187M} and OsGTGg^{187M} in Arabidopsis stable lines

A) RT-PCR of WT (lane 2), four lines of *OsGTGe^{187M}::GFP* expressed in WT (lanes 3-6) and five lines of *OsGTGg^{187M}::GFP* expressed in WT (lanes 7-11). Actin F and Actin R (left, predicted 201 bp) and OsGTG topo F1 and OsGTG stop R1 (right, predicted 1403 bp) primers were used. Predicted products are shown on the right and molecular markers on the left (lane 1). Confocal microscopy images showing OsGTGe^{187M}::GFP (B-D) and OsGTGg^{187M}::GFP (E-G) localisation in WT Arabidopsis lines. Yellow arrows indicate ER, white arrows, Golgi localisation and blue arrows, stomata cells. Scale bar 10 µm.

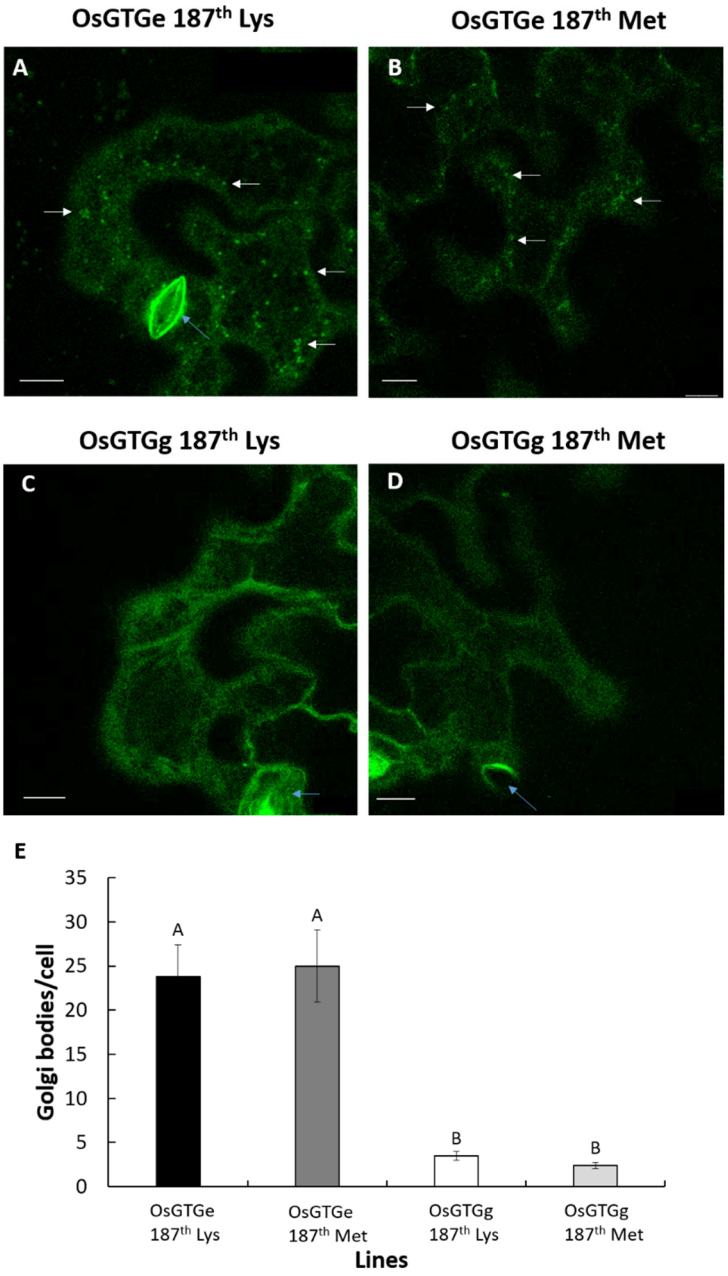

Figure 3.32. OsGTGe^{187M} showed more Golgi localisation than OsGTGg^{187M}

Representative confocal microscopy images of showing OsGTGe^{187K}::GFP (A), OsGTGe^{187M}::GFP (B), OsGTGg^{187K}::GFP (C) and OsGTGg^{187M}::GFP (D) localisation in WT Arabidopsis lines. White arrows show Golgi localisation and blue arrows represent stomata cells. Scale bar 10 µm. E) Golgi body number per cell analysed in WT lines expressing OsGTGe^{187K}, OsGTGe^{187M}, OsGTGg^{187K} and OsGTGg^{187M}. Three independent lines per genotype were used and 5-10 cells per line were analysed (n=15-30). One-way ANOVA ($p < 0.05$). Means not sharing a letter are significantly different, Tukey *post-hoc* test.

3.2.7.2 The 187th amino acid residue of rice GTG does not play a role in cold stress in Arabidopsis

As previously mentioned, it has been proposed that OsGTG functions as a cold receptor and that the 187th amino acid residue plays an important role in cold stress (Ma et al., 2015). In that previous study it was proposed that in the *japonica* variety, the lysine present in the 187th amino acid position of rice GTG was responsible for the cold tolerance observed in this variety. In contrast, the methionine present in *indica* was responsible for the cold sensitivity of that ecotype. In this chapter, using Arabidopsis plants, it was tested whether GTG is involved in cold tolerance and whether the 187th amino acid residue plays a key role in that function.

Using WT, *gtg1gtg2* and some of the transgenic lines described in Table 3.3 and Table 3.6, the effect of cold stress was examined. The plants were grown for 19 days at 23°C and then half of the plants were transferred to 4°C for 10 days whereas the other half were kept at 23°C as a control. After the cold treatment, the plants were placed back to 23°C for 7 days for recovery. During the experiment, several plant characteristics were measured, such as rosette diameter, number of leaves and primary stem length.

To study whether GTG could be involved in cold stress, the growth of WT and *gtg1gtg2* mutant at 4°C in comparison to the growth of the plants at 23°C was analysed. This was done using WTs and double mutants in both the Ws4 and Col-8 background lines for comparison. *gtg1gtg2* exhibited a smaller rosette diameter and leaf number in comparison to WT (Figure 3.33 C-F). It can also be observed that the growth of both lines was reduced under cold stress treatment (data represented between the two back arrows). The reduction of growth of the *gtg1gtg2* mutant in comparison to WT under 4°C treatment is similar to the reduction of growth between these two lines in the control conditions. It is likely that the differences seen in the *gtg1gtg2* mutant under cold stress are due to these genes being involved in growth rather than GTG being involved in cold tolerance. Both lines were able to recover after the cold treatment. The differences in rosette diameter and number of leaves between WT and *gtg1gtg2* mutant are seen in both Ws4 and Col-8 backgrounds, corroborating the importance of GTG in growth rather than cold tolerance. In addition, it was also observed that the primary stem length of the mutant was shorter than the WT, even under control conditions (Figure 3.33 G-H).

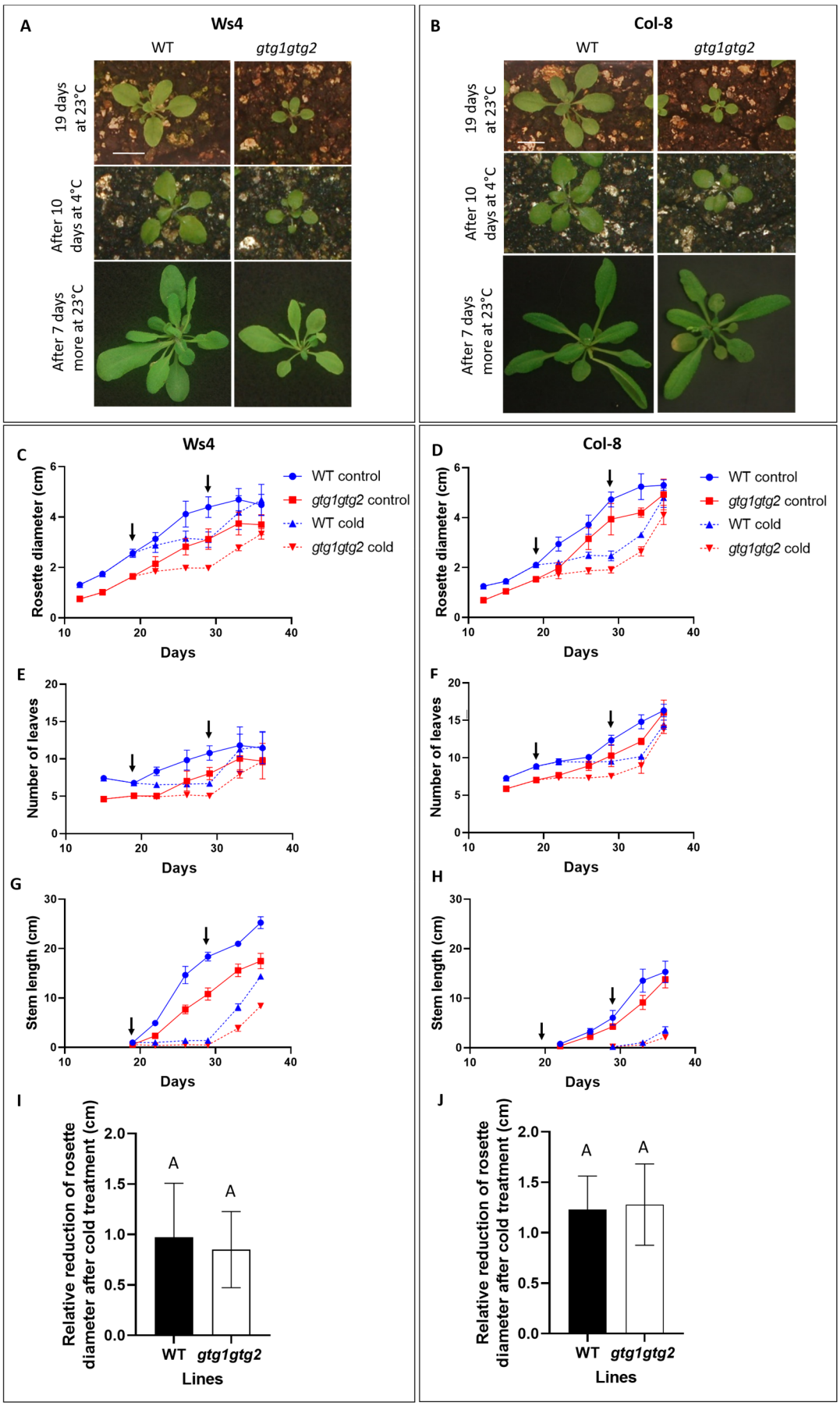

Figure 3.33. GTG does not play a role in cold tolerance in Arabidopsis

Cold stress experiment using WT and *gtg1gtg2* mutant lines in Ws4 (left) and Col-8 (right) backgrounds. 24 plants per line were grown at 23°C for 19 days, transferred to 4°C for 10 days and then given 7 day recovery period at 23°C. The black arrows mark the beginning and end of the cold treatment. Plants grown at 23°C (continuous line) are shown with plants treated at 4°C (discontinuous line). Representative pictures of WT and *gtg1gtg2* mutants in Ws4 (A) and in Col-8 background (B); scale bar 1 cm. Rosette diameter in Ws4 (C) and in Col-8 (D). Number of leaves in Ws4 (E) and in Col-8 (F). Primary stem length in Ws4 (G) and in Col-8 (H). Reduction of rosette diameter in cold treated plants (7 days at 4°C) relative to the control plants for Ws4 (I) and Col-8 (J). The data represent the mean (±SEM) of 24 plants. One-way ANOVA ($p > 0.05$). Means sharing a letter are not significantly different by Tukey *post-hoc* test.

To test whether the lysine residue at position 187 plays a role in cold tolerance, different mutated versions of OsGTG were used in the cold stress experiment. The different OsGTG mutated versions that were expressed in the *gtg1gtg2* mutant Ws4 background and used in this experiment were: OsGTGe^{187K}, OsGTGe^{187M}, OsGTGg^{187K} and OsGTGg^{187M}. The Arabidopsis *AtGTG1* transformed line was used as a control. All the OsGTG expressing lines showed a rosette diameter, number of leaves and primary stem length similar to WT (Figure 3.34). This was observed in the control plants that were kept at 23°C but also in the plants that were exposed to cold treatment. It can also be observed that the reduction of growth during the cold period for all the transgenic lines was similar to the WT. There were no growth differences between the *gtg1gtg2* mutant lines expressing OsGTG^{187M} and the lines expressing OsGTG^{187K} in any of the conditions. This suggests that the 187th amino acid residue of OsGTG is not involved in cold tolerance when expressed in Arabidopsis. As is shown in Figure 3.34, at 23°C and 4°C the double mutant showed a reduced rosette diameter, number of leaves and primary stem length compared to the rest of the lines. The reduced rosette diameter and number of leaves observed in the *gtg1gtg2* mutant in comparison to the WT and the rest of the transgenic lines after the cold treatment was also observed in the *gtg1gtg2* control lines. This indicates that the lack of GTG affects the growth of the plant rather than the cold tolerance. All the lines were able to recover after the cold treatment. These results indicate that the lysine present in the 187th amino acid position of OsGTG does not play a role in cold tolerance in Arabidopsis.

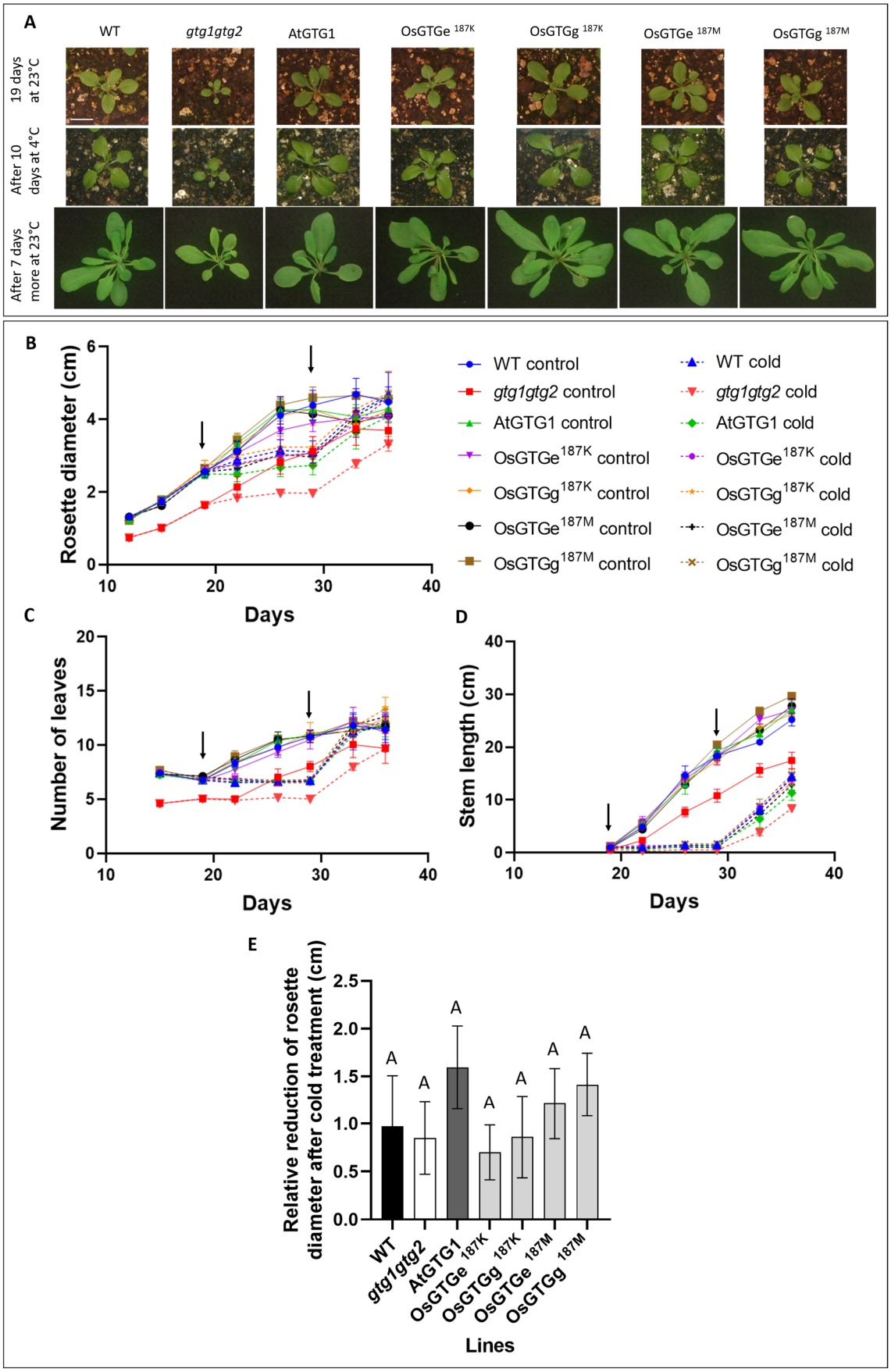

Figure 3.34. The 187th amino acid of OsGTG does not play a role in cold tolerance in Arabidopsis

Cold stress experiment using WT, *gtg1gtg2*, *gtg1gtg2* expressing AtGTG1, *gtg1gtg2* expressing OsGTGe^{187K}, *gtg1gtg2* expressing OsGTGe^{187M}, *gtg1gtg2* expressing OsGTGg^{187K} and *gtg1gtg2* expressing OsGTGg^{187M}. 24 plants per line were grown at 23°C for 19 days, transferred to 4°C for 10 days and the given 7 day recovery period at 23°C. The black arrows mark the beginning and end of the cold treatment. Plants grown at 23°C (continuous line) are shown with plants treated at 4°C (discontinuous line). A) Representative pictures of the lines through the experiment; scale bar 1 cm. Rosette diameter (B). Number of leaves (C). Primary stem length (D). E) Reduction of rosette diameter in cold treated plants (7 days at 4°C) relative to the control plants. The data represent the mean (±SEM) of 24 plants. One-way ANOVA ($p > 0.05$). Means sharing a letter are not significantly different by Tukey *post-hoc* test.

3.2.8. Isolation and characterization of a rice *gtg* mutant

To study whether the function of OsGTG is conserved, a rice *gtg* mutant was isolated and characterized. The rice *gtg* homozygous T-DNA mutant was isolated from the PFG collection in the Donjing background. The homozygosity of the isolated line was confirmed at genomic and RNA levels. The presence of the T-DNA in three rice *gtg* plants is shown in Figure 3.35 A. No amplification of *OsGTG* was detected in these mutant plants. In the WT Donjing line, there was clear amplification of *OsGTG* gene whereas no T-DNA was detected.

This homozygosity at the DNA level was also confirmed by gene expression. RNA was extracted from leaves and cDNA was synthesised. PCR using the cDNA with the full-length gene primers was carried out. No band for *GTG* gene was observed in the *gtg* mutant plants, however the WT Donjing sample showed clear *OsGTG* expression (Figure 3.35 C). *Ubiquitin* was used as a control gene for cDNA quality.

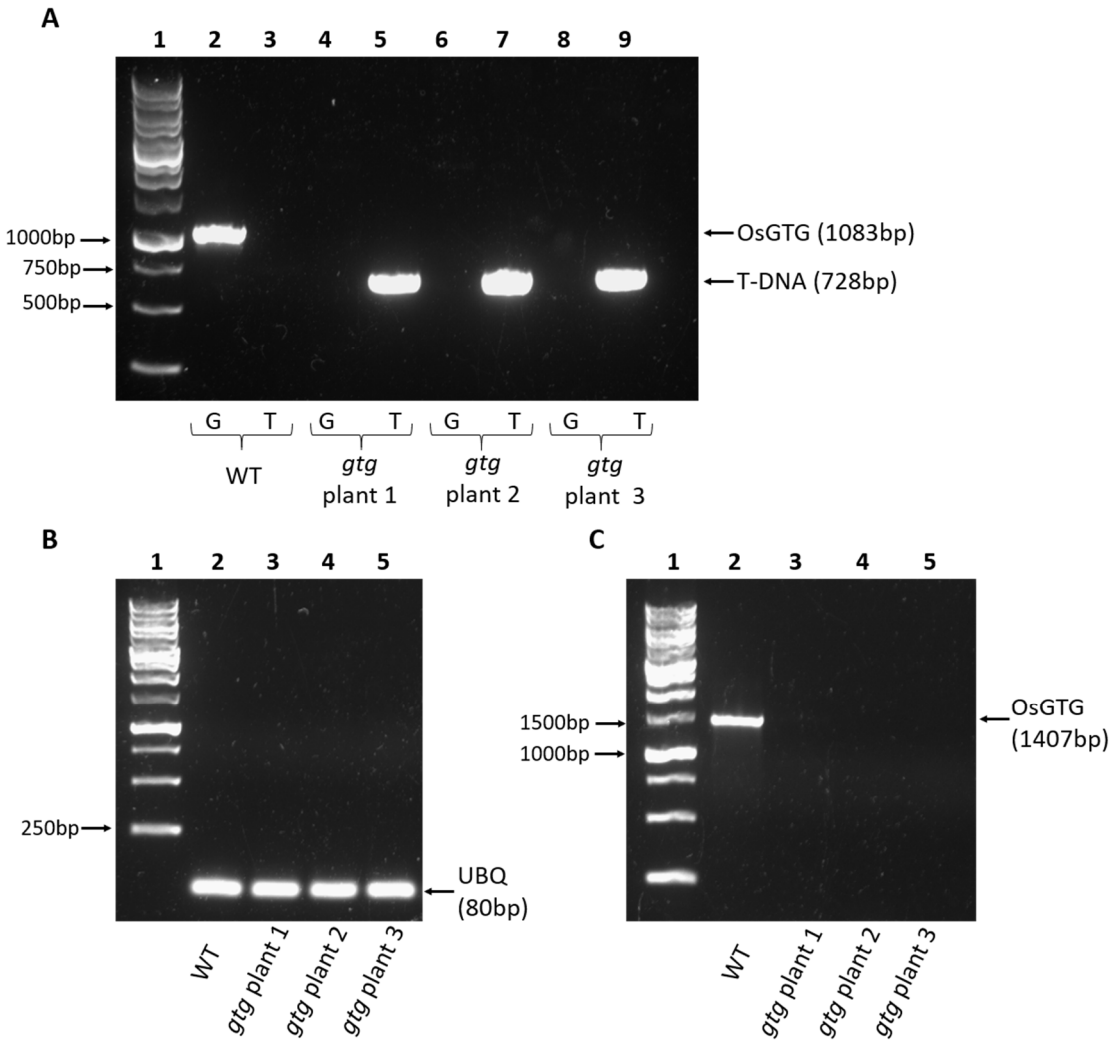

Figure 3.35. Confirmation of rice *gtg* mutant homozygous plants

PCR using genomic DNA (A) and cDNA synthesized from RNA (B and C) extracted from WT Donjing and three T-DNA *gtg* mutant plants. A) In G, COLD1 RP + COLD1 LP primers were used (lane 2, 4, 6 and 8, predicted band 1083 bp) and in T, COLD1 RP + RBpGA primers (lane 3, 5, 7 and 9, predicted 728 bp). WT (lanes 2-3); *gtg* plant 1 (lanes 4-5); *gtg* plant 2 (lanes 6-7); *gtg* plant 3 (lanes 8-9). RT-PCR using UBQ F and UBQ R primers (predicted 80 bp) in B) and OsGTG topo F and OsGTG stop R1 (predicted 1407 bp) in C) of WT (lane 2) and *gtg* (lane 3, 4 and 5). Predicted products are shown on the right and molecular markers on the left (lane 1).

The Arabidopsis *gtg1gtg2* double mutant plant exhibits a defect in growth, development and fertility (Jaffé et al., 2012). To study whether the absence of rice GTG can cause similar effects, the growth of the rice *gtg* mutant was analysed. The rice *gtg* mutant exhibited a reduced height in comparison to WT plants (Figure 3.36 B). Interestingly, rice *gtg* mutant produced a higher number of leaves, tillers (rice stems) and panicles (rice inflorescences) than the WT plants (Figure 3.36 C-E). It was observed that the *gtg* mutant continued to produce leaves, tillers and panicles even at older stages, whereas the WT lines reached a point where senescence set in and the production of new leaves, tillers and panicles slowed. This is a similar phenotype to what was observed for the Arabidopsis *gtg1gtg2* mutant as it too had more branching in comparison to WT lines (see Figure 5.15 C in chapter 5).

The fertility of the rice *gtg* mutant was also analysed, to study whether this mutant displayed a similar fertility defect as the Arabidopsis mutant (Jaffé et al., 2012). Interestingly, although the rice *gtg* mutant produced more panicles than the WT, most of the seeds of the panicles were unfilled (Figure 3.37 A, E). The *gtg* mutant was unable to form full grains. The total number of spikelets was analysed per panicle and per plant. A spikelet was considered as the individual unit of the flower that has the potential to become a seed. The spikelet includes all of the seed components, the floret (rice flower) and the glume (Figure 1.10). The rice *gtg* mutant has less spikelets per panicle (Figure 3.37 B), however, because it exhibited more panicles than WT, the total number of spikelets in the mutant is higher than the WT (Figure 3.37 C).

Since most of the *gtg* mutant seeds were unfilled, the seed-setting rate was calculated as:

$$\frac{\text{number of filled seeds}}{\text{number of filled seeds} + \text{number of unfilled seeds}} \cdot 100$$

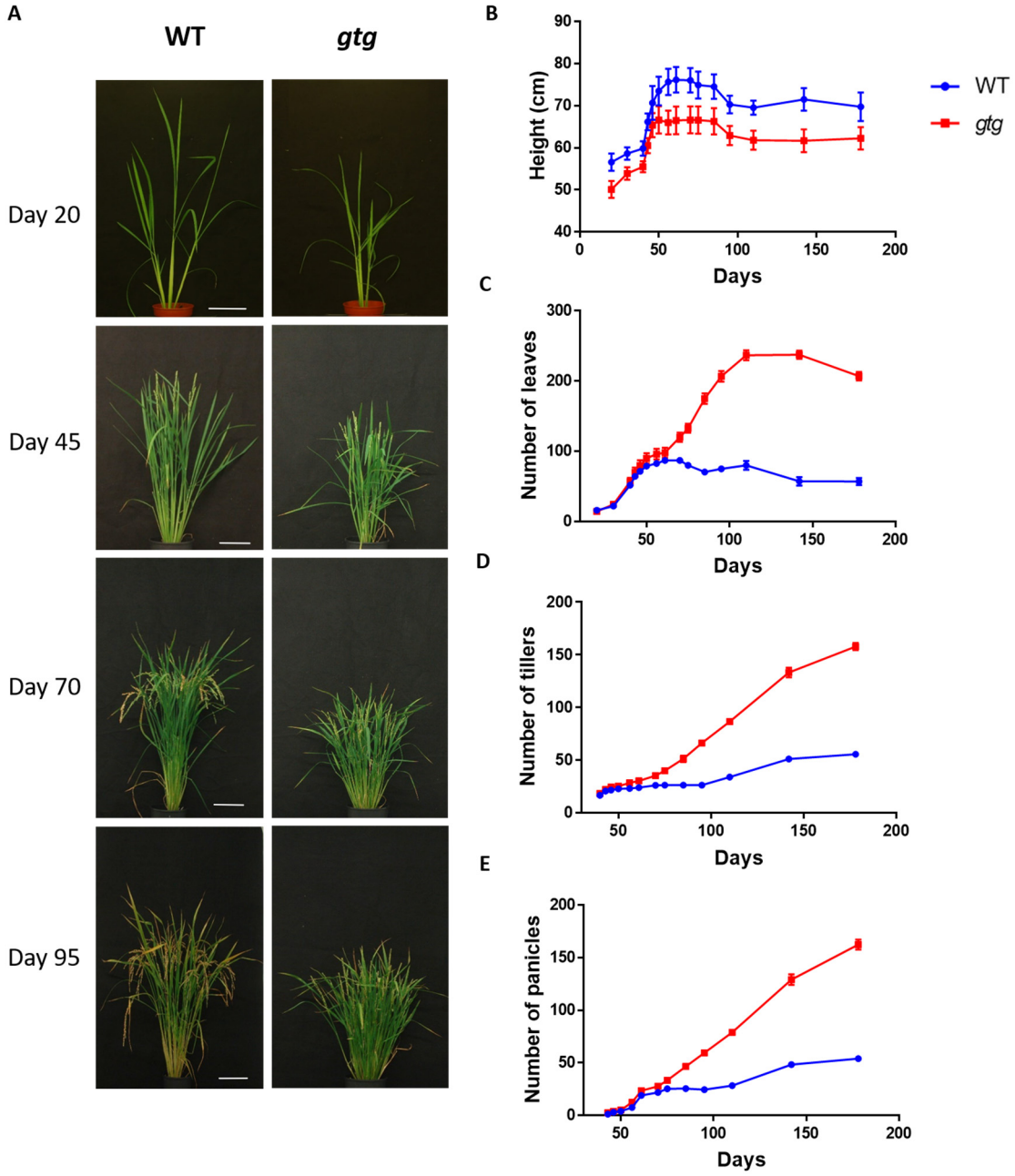

Figure 3.36. The rice *gtg* mutant is shorter than WT but produces more leaves, tillers and panicles

Growth of the rice *gtg* mutant in comparison to WT. 6 WT and 8 *gtg* mutant plants were analysed and the average (±SEM) is represented. A) Representative images of WT Donjing ecotype (left) and *gtg* mutant lines (right) at 20, 45, 70 and 95 days old. Scale bar 10 cm. B) Height of plants. C) Number of leaves. D) Number of tillers. E) Number of panicles. WT is represented in blue and the *gtg* mutant in red.

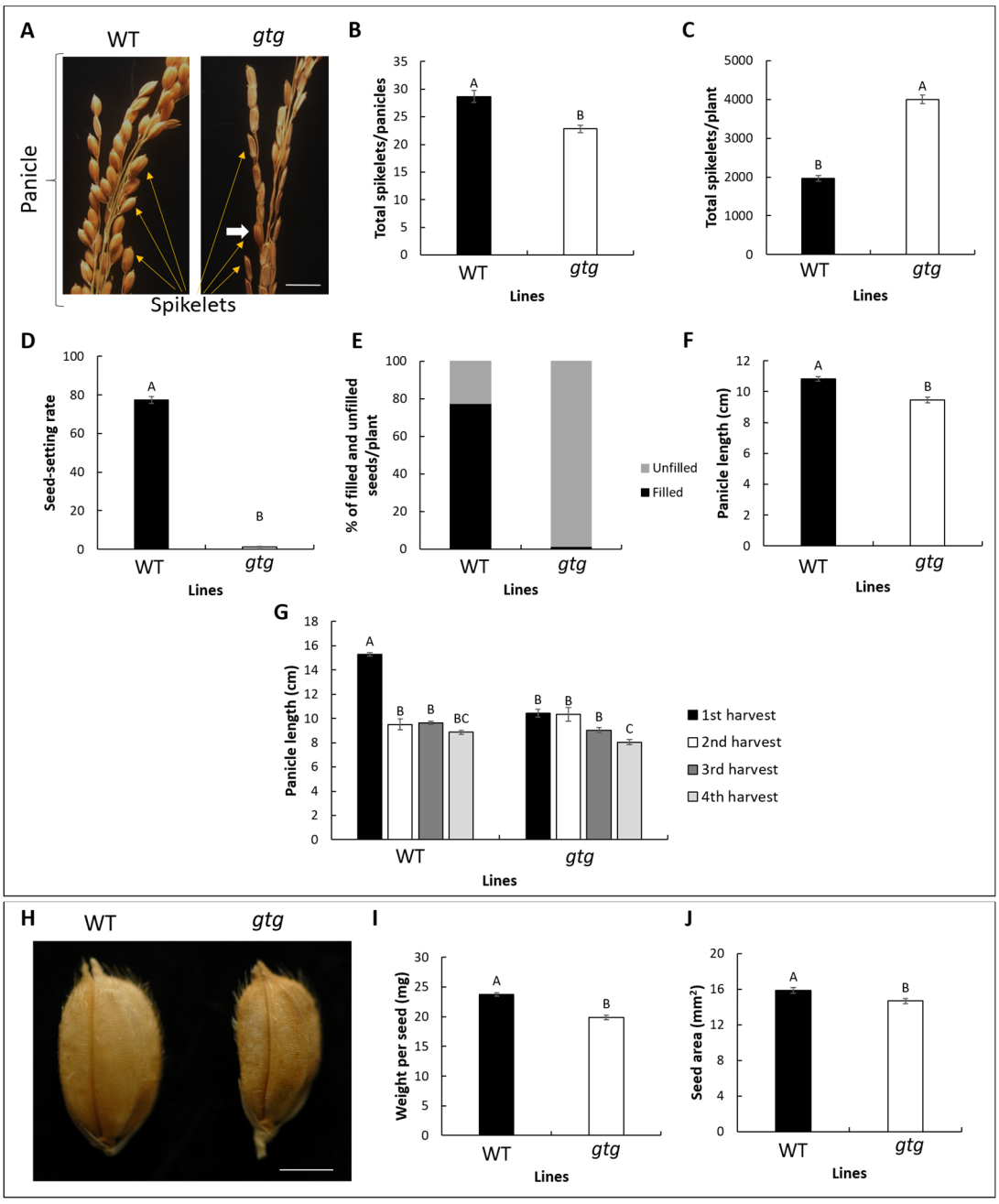

Figure 3.37. The rice *gtg* mutant is defective in fertility

A) Representative pictures of WT (left) and *gtg* (right) panicles. White arrow shows the only filled grain in that panicle and yellow arrow shows different spikelets; scale bar 1 cm. 6 WT Donjing and 8 *gtg* mutant were analysed and mean (±SEM) is represented. Total number of spikelets per panicle (B) and per plant (C). D) Seed-setting rate. E) Percentage of filled/unfilled seeds per plant. Total panicle length (F) and per harvest event (G). H) Representative images of WT (left) and *gtg* mutant (right) seed; scale bar 2 mm. Weight per seed (I) and seed area (J). 30 seeds were analysed per line. One-way ANOVAs and two-way ANOVA in G were performed, ($p < 0.05$). Means not sharing a letter are significantly different, Tukey *post-hoc* test.

The percentage of filled/unfilled seeds of each genotype was also calculated. As shown in Figure 3.37 D and E, the number of filled seeds produced for the *gtg* mutant was very small in comparison to WT. This is an indication that the *gtg* mutant is defective in the ability to produce viable seeds, suggesting a defect in fertility. It was also observed that the panicle of the *gtg* mutant was shorter than the WT (Figure 3.37 F). This reduction of panicle length is mostly observed in the first harvest event as shown in Figure 3.37 G. It is apparent that the first panicles produced by the plants are significantly reduced in length in the mutant plants. Furthermore, it was observed that the seeds were smaller and showed a reduced weight in comparison to WT (Figure 3.37 I-J). These results indicate that the rice *gtg* mutant exhibits the growth, development and fertility defects that resemble the defects previously reported for the Arabidopsis *gtg1gtg2* mutant (Jaffé et al., 2012). These results indicate a conserved physiological role between Arabidopsis and rice GTGs.

3.3. Discussion

3.3.1. Polymorphism in the *OsGTG* sequence

After the cDNA of *GTG* was amplified from *O. sativa* Nipponbare ecotype, a non-synonymous polymorphism was identified. In the sequence that was amplified in this study, two alternative nucleotides were detected when compared to the sequence available in the Rice Genome Annotation Project database. These nucleotide changes resulted in a different residue in the protein sequence. In the 9th amino acid position, a glycine was changed to a glutamic acid. Amplifications from Donjing, another rice ecotype and with different enzymes were carried out to confirm that the polymorphism was not due to a technical error. The database sequence seems to be confirmed in a previous study where *O. sativa* GTG was amplified independently and no mention of a polymorphism in that residue was reported (Ma et al., 2015). Interestingly, a sequence conflict was discovered in the Universal protein resource database (Uniprot) where a glycine was changed to a glutamic acid in the 9th amino acid position. It seems that this difference in amino acid was previously reported in a study where improved whole genome shotgun sequences for the analysis of *indica* and *japonica* varieties was used (Uniprot) (Yu et al., 2005). This indicates that this polymorphism has been previously found in rice.

Analysis of this residue in the orthologue GTG sequences of other plants revealed that the glutamic acid was a conserved residue in that position in all the species analysed apart from rice (Figure 3.7). These other species included Arabidopsis, *Medicago truncatula*, *Populus trichocarpa* and most of the grasses such as *Hordeum vulgare*, *Triticum aestivum*, *Brachipodium distachyon* and *Zea mays*. This indicates that this glutamic acid is a highly conserved residue in plant GTGs. To study the importance of this residue in the function and localisation of the protein, OsGTG with a glycine in the 9th amino acid position of the protein was created by mutagenesis. This residue is predicted to be part of the first transmembrane domain of the protein, and this change in the amino acid sequence does not seem to affect the predicted topology of the protein (Figure 3.9).

These two amino acids possess completely different characteristics. Glutamic acid is a polar, hydrophilic amino acid that is negatively charged and glycine is a simple, non-polar, hydrophobic amino acid with no charge (Cooper, 2000, Betts and Russell,

2003). These differences could affect the electrostatic charges between amino acids and potentially affect the structure of the protein. Charged amino acids are often important for the function of the protein, therefore, this amino acid difference would allow us to study how important this residue is for the function or localisation of the protein. This glutamic acid seems to be a conserved amino acid across the plant GTGs and it has been shown that polar amino acids are more conserved when they are present in a transmembrane domain of a protein (Illergård et al., 2011, McKay et al., 2018). Glutamate is frequently involved in protein active and binding site (Betts and Russell, 2003). Glycine residues are important for helix-helix interaction and therefore for maintaining the structure of the protein (Javadpour et al., 1999). As mentioned previously, AtGTG1 was previously characterized in our laboratory as an anion channel (Dorey, 2019), therefore, if the function of rice GTG is conserved, the glutamic acid residue could potentially be involved in the activity of the protein.

Single point amino acid mutations can have consequences for the structure and function of the protein. In sickle cell anaemia, a glutamate of the haemoglobin is mutated to a valine producing a low solubility protein that causes the formation of long fibres in the red blood cells and the characteristic cell shape of the disease (Serjeant, 1997, Fitzsimmons et al., 2016). Changes in an aspartic acid and glutamic acid in a ryanodine receptor, a family of Ca^{2+} release channels that are similar to the bacterial K^{+} channel KcsA, produced changes in the conductance and selectivity of the channel. This indicates that these residues can be important for ion conductance and selectivity (Wang et al., 2005).

3.3.2. The localisation of OsGTGs

The localisation of both OsGTG proteins was studied using two approaches: stable expression of OsGTGs in Arabidopsis lines and transient expression in tobacco leaves. In Arabidopsis stable lines there was a different pattern in the localisation of OsGTGe and OsGTGg. OsGTGe localises to the ER and Golgi whereas OsGTGg localises predominately to the ER (Figure 3.21). Not many ‘Golgi-like compartments’ were found in the Arabidopsis epidermal cells expressing OsGTGg although the same focal area was scanned for both samples. This is clearly seen in Figure 3.21 C when OsGTGe is expressed in a punctuate structure resembling Golgi bodies while in Figure 3.21 D those structures are not regularly observed where OsGTGg was expressed. Analysis of

the Golgi body number revealed a strong difference between the lines expressing OsGTGe and OsGTGg.

The localisation pattern of OsGTGe is similar to AtGTG1 showing ER and Golgi localisation (Jaffé et al., 2012). Interestingly AtGTG1 also has a glutamic acid in the 9th residue of the protein, suggesting a possible role of that conserved amino acid in the Golgi localisation of the protein. Since in Arabidopsis lines expressing OsGTGg there was not much Golgi localisation, this could indicate that this glutamic acid is required for Golgi targeting. The different characteristics of these two amino acids could be the reason for the difference in subcellular localisation. The fact that the amino acid difference is in the 9th amino acid position, close to the N-terminal of the protein, can justify the effect of a single amino acid change interfering with the potential Golgi target signal sequence of the protein and could indicate that this residue forms part of such a signal sequence. However more in-depth analysis needs to be carried out to determine this. Whereas HDEL and KDEL are well-stablished ER retention signals, no clear signal sequences have been proposed for Golgi localisation (Banfield, 2011). In the mammalian autophagy-related protein, ATG9A, it was shown that a conserved glycine was required for the protein to be transported to the Golgi; mutation of the glycine in the 516th position impaired the transport of the protein (Staudt et al., 2016). A conserved glutamine in the single transmembrane domain of N-acetylglucosaminyltransferaseI, GnTI, was essential for *cis/medial* Golgi localisation; mutation of that residue produced mis-localisation of the protein (Schoberer et al., 2019). Although no signal peptide was found in any of the two OsGTGs sequences using *in silico* analysis, it is possible that the difference in charge and structure of the amino acids can affect the structure of the protein or its interaction with the lipids of the organelle membrane to change the localisation of the protein.

To confirm the exact localisation of both OsGTGs, organelle markers were used. Transient expression in tobacco leaves was carried out, co-expressing both OsGTGs tagged with GFP along with different organelles markers tagged with RFP. The organelles markers used in this project were LT16b mOrange for plasma membrane, HDEL for ER, ManI for *cis* Golgi and ST for *trans* Golgi (Gomord et al., 1997, Boevink et al., 1998, Nebenführ et al., 1999). OsGTG was seen to localise to the ER and Golgi network (*cis* and *trans* Golgi). A strong overlap was observed of both OsGTGs with the HDEL ER marker, confirming the ER localisation observed previously in Arabidopsis plants expressing both OsGTGs (Figure 3.22). The *trans*

Golgi localisation was confirmed for both OsGTGs by the co-localisation with the ST::RFP marker, and *cis* Golgi localisation was confirmed using the ManI marker with a clear overlap between OsGTGs::GFP and the marker (Figure 3.23 and Figure 3.24). Similar to what was observed in the Arabidopsis stable lines, more Golgi localisation was found in tobacco cells when OsGTGe was expressed. This corroborates that glutamic acid is an important residue for Golgi localisation. In Ma et al. (2015) the OsGTG version that was used contained glycine in the 9th amino acid position and no Golgi localisation was reported. In this thesis it was observed that OsGTGs did not localise at the plasma membrane as it was reported previously (Ma et al., 2015). In that study the plasma membrane marker used was PIP2, an aquaporin isoform that, as they reported, also localises to the ER (Lee et al., 2009, Ma et al., 2015). Although the ER localisation was later confirmed by a second ER marker, the plasma membrane localisation was not confirmed with an independent marker. This raises the doubt of whether the plasma membrane localisation described it is in fact ER that was difficult to distinguish since in epidermal plants cells the ER is pushed out and squeezed against the plasma membrane due to the size of the vacuole (Marty, 1999). To overcome this issue, LT16b, a different plasma membrane marker, was used in this thesis. The green signal from the OsGTGs is adjacent to the red signal of the plasma membrane marker, but they do not overlap. This marker was not observed in the ER network or ER strands unlike PIP2, which was clearly seen in those locations. The use of the organelle markers confirmed the ER and Golgi localisation observed in the Arabidopsis stable lines expressing OsGTG.

The ER is a complex of the endomembrane system and is involved in the secretory pathway. Although the ER also connects with other organelles in the cell, it is well-established that it interacts with Golgi bodies (Sparkes et al., 2009b). Both organelles together are involved in the secretory and trafficking pathway. The main functions of the ER include protein production, folding, quality control and lipid biosynthesis (Hawes et al., 2015). Since the Golgi is responsible for the transport, targeting and sorting of the proteins, the ER-Golgi interaction is very important for protein production and trafficking (Dupree and Sherrier, 1998). ER is a very dynamic organelle that can be remodelled depending on the environmental conditions of the cell. ER movements are driven by actin tubules and their main component myosin (Sparkes et al., 2009a). The fact that OsGTG localises at the ER and Golgi, indicates that this protein could be involved in the protein trafficking and secretory pathway.

Future work would be required to confirm OsGTG localisation in rice cell protoplasts. The fact that AtGTG1 and OsGTG exhibit the same subcellular localisation could indicate that there is a conservation of function of GTGs between different plant species.

3.3.3. OsGTG rescues *gtg1gtg2* defective phenotype

As previously described, the Arabidopsis *gtg1gtg2* mutant exhibits various growth and developmental defects when grown under certain conditions, such as reduced root and hypocotyl growth, reduced fresh weight and defective hypocotyl epidermal cells (Jaffé et al., 2012). This defective phenotype was restored when AtGTG1 or AtGTG2 were expressed back in the double mutant, suggesting functional redundancy of the proteins (Jaffé et al., 2012). In our group it has been reported that GTG1 protein from *C.elegans* was able to rescue the defective root, biomass and hypocotyl phenotypes of the Arabidopsis *gtg1gtg2* double mutant (Wong, 2014). In this thesis it is shown that the expression of OsGTG also rescued the root, fresh weight and hypocotyl defective phenotype of the *gtg1gtg2* mutant (Figure 3.14 to Figure 3.18). Four independent *gtg1gtg2* lines expressing OsGTGe and three independent lines expressing OsGTGg were analysed and showed the same result. Similar *OsGTG* gene expression was found in all the transgenic lines expressing *OsGTG* although this was not a quantitative measurement. The functional complementation by OsGTG suggests that Arabidopsis and rice GTGs proteins have a similar function. Since the CeGTG1 protein was able to rescue the mutant phenotype when sharing only 39% protein identity to AtGTG1, it is not surprising that OsGTG, sharing 90% identity, was able to do so. The fact that the defective root and fresh weight phenotype were restored to WT levels when CeGTG1 and OsGTG were expressed suggests that the function between orthologues is completely conserved. The conservation of GTG function has also been addressed in another study where it was shown that human and hamster GTG/GPHR were able to rescue the defective growth and development of the *Drosophila* mutant (Charroux and Royet, 2014). The rescue of the defective root and biomass growth of the *gtg1gtg2* mutant by OsGTG was also observed when the protein was tagged with GFP at the C-terminal (Figure 3.16 and Figure 3.17). This indicates that the GFP did not affect or interfere with the function of the protein. No differences were found between OsGTGe and OsGTGg expressing lines, indicating that the difference in amino acid did not affect

the function of the protein and therefore this specific residue does not play a key role in GTG function.

The hypocotyl and root defects observed in the *gtg1gtg2* mutant could be caused by defects in cell wall synthesis. Cellulose, hemicellulose (which the most abundant is xyloglucans) and pectin are all cell wall components (Heredia et al., 1995, Houston et al., 2016). Hemicellulose and pectin are synthesised in the Golgi and transported to the plasma membrane (Zhang and Staehelin, 1992, Worden et al., 2012, Sinclair et al., 2018). Although cellulose is synthesized in the plasma membrane by the cellulose synthase complexes, these complexes are assembled at the Golgi and transported to the plasma membrane (McFarlane et al., 2014, Polko and Kieber, 2019). For these reasons, Golgi impairment could lead to defects in cell wall synthesis and this could affect cell elongation. Mutants of the *PROCUSTE1* gene (*PCR1*), encoding a cellulose synthase subunit, exhibited a reduced root and hypocotyl length due to a decrease in cell elongation (Desnos et al., 1996, Fagard et al., 2000). *pcr1* mutants also produced swollen and distorted hypocotyl epidermal cells in the same manner as *gtg1gtg2* mutant (Desnos et al., 1996, Fagard et al., 2000). Many cell wall formation and modification genes were found to be altered in *gtg1gtg2* (Jaffé et al., 2012), supporting the growth defect observed in the mutant. Since the function between AtGTG1 and OsGTG seems to be conserved, it is possible that OsGTG is capable of restoring the Golgi morphology and therefore the cell wall components required for cell elongation in the roots and the hypocotyl. Although OsGTGg is less abundant in the Golgi, the amount is presumably sufficient for the function since it was able to fully rescue the growth defects of *gtg1gtg2* mutant.

OsGTG was also able to rescue the defective cell shape and ER body number observed in the *gtg1gtg2* mutant. Previous work in our laboratory has showed that AtGTG1 was also able to rescue these defective traits (Adam, Terry, Williams, unpublished). Cell shape is also regulated by cell wall expansion (Ivakov and Persson, 2013). As mentioned above, cell wall component are synthesised by the Golgi (Zhang and Staehelin, 1992), therefore, Golgi defects can also lead to cell shape alterations. ER bodies are spindle-shaped organelles derived from the ER that are present in seedlings and mature roots in Brassica plants (Haseloff et al., 1997, Matsushima et al., 2003a). There are two major types of ER bodies: constitutive in epidermal cells of seedlings, and wound-inducible in rosette leaves (Nakano et al., 2014). Recently, constitutive ER bodies have also been identified in the marginal cells of rosette leaves (Nakazaki et al.,

2019). ER bodies are involved in plant defence and accumulate β-glucosidase, specifically BGLU18 and PYK10. The transcription factor NAI1 is responsible for ER body formation. This was observed in the *nai1* mutant, where no transcript of *PYF10* was produced and no ER bodies were present (Matsushima et al., 2003b). An independent single point mutation in PYK10, where a cysteine in mutated to a tyrosine in the 29th amino acid position, generated Arabidopsis plants that produce less ER bodies (Nagano et al., 2009). Interestingly, the *NAI1* transcription factor is downregulated in the *gtg1gtg2* mutant (Jaffé et al., 2012), and this could be the reason for the low number of ER bodies produced by the mutant. Because ER bodies are derived from ER membrane, the characteristics of the ER network could also play a role in the capacity of the plant to form ER bodies. Defects in the ER network could contribute to the reduction of ER bodies found in the mutant. OsGTG can restore the ER network to normal and this could contribute to the higher number of ER bodies. It would be interesting to analyse transcript levels of *NAI1* in the OsGTG expressing lines to see whether there was any alteration of gene expression.

Since both OsGTGs were able to rescue the root length, hypocotyl length, cell shape and ER body number in the same way, it indicates that this amino acid residue does not play a key role in the function of the protein. It seems that the change of a negatively charged amino acid to a non-charge one did not affect the structure and function of the protein, or if it did, it reduced activity rather than eliminating it. Not all the amino acids that form a protein play an essential role in its function. In the QacA multidrug transporter from *Staphylococcus aureus* it was shown that mutation of some of the prolines that were predicted to be in the transmembrane region did not affect the expression of the protein, maintaining the catalytic transport activity (Hassan et al., 2006). It could be interesting to analyse the effect of other conserved residues in GTG, such as the proline in the 91st position that was found to be important for function in *Drosophila* where mutation of this residue produced flies with reduced growth and a high lethality at the larval stage (Charroux and Royet, 2014).

3.3.4. Rice *gtg* mutant exhibited a growth, development and fertility defect

The next step was to study whether the rice *gtg* mutant exhibits the same defective growth and development phenotype that the Arabidopsis mutant displays. In Ma et al. (2015) a rice *gtg* mutant was characterised, and it was found that the plant was more sensitive to cold stress, proposing that OsGTG could be involved in cold sensing and

tolerance. Analysis of the images of the rice *gtg* mutant from that study revealed that the mutant has a reduced height in comparison to WT plants under normal conditions (Ma et al., 2015). In this thesis, the same T-DNA insertion rice *gtg* mutant has been isolated and characterized. A knockout line with no expression of *OsGTG* was generated (Figure 3.35). The mutant showed a reduced height in comparison to WT. Interestingly the rice mutant produced more leaves, tillers and panicles than WT plants, suggesting some developmental defects (Figure 3.36). Some of those defects resemble the growth and development defects observed in the *gtg1gtg2* Arabidopsis mutant (Jaffé et al., 2012). Although the mature Arabidopsis *gtg1gtg2* mutant does not seem to be shorter than the WT, it exhibited an increase in branching (Figure 5.15 C), similar to the rice *gtg* mutant. This indicates that GTG in rice and Arabidopsis both play a similar role in plant development. Shoot and stem development are regulated by hormones, specifically by auxin and cytokinin (Evers et al., 2011). In the *gtg1gtg2* Arabidopsis mutant, several genes involved in hormone metabolism are downregulated (Jaffé et al., 2012). Since some of those downregulated genes were involved in auxin and cytokinin synthesis, this could be one of the reasons for the increased branching observed in the mutant. One example is the PIN auxin export carriers proteins, where PIN1 plays a role controlling shoot branching (Zhou and Luo, 2018). Interestingly, *PIN3*, another auxin efflux protein, is downregulated in *gtg1gtg2* mutant (Jaffé et al., 2012), possibly indicating some defect in hormone transport in the mutant, which therefore can affect the shoot development of the plant. Future gene expression analysis in the rice *gtg* mutant would help us to understand whether expression of similar genes is also altered in rice.

The Arabidopsis *gtg1gtg2* mutant exhibited a strong fertility defect with reduced seed yield, seed number per silique and silique length (Jaffé et al., 2012). In the rice *gtg* mutant, analysis of the seed yield also indicates a strong fertility defect. In the rice mutant most of the spikelets remained unfilled, in comparison to WT that had most of them filled, forming grain (Figure 3.37). The fertility defect observed in the Arabidopsis double mutant was due to a reduction in pollen tube germination and pollen tube length, which led to a reduction in seed production. Arabidopsis flowers contain several ovules per flower, which is why inhibition of pollen tube growth produces less fertilised ovules in the flower. This in turn produces shorter siliques with less seeds in the mutant. In contrast to Arabidopsis, rice has only one ovule in each floret, so if the pollen tube does not germinate or grow the required distance, the ovule will not be fertilised and the grain will not be produced (Yoshida and Nagato, 2011). This is consistent with what we observed in the rice *gtg* mutant, where most of the spikelets were unfilled. However,

similar in vitro pollen tube germination and elongation assays need to be done with the rice *gtg* mutant to see whether the lack of filled grain is due to a defect in pollen.

Defects in pollen tube extension can be caused by ER alterations as observed in the *chx21chx23* Arabidopsis mutant. The lack of these ER localised cation/H^+ exchangers produced a pH and cation imbalance that led to defects in the pollen tube and male sterility (Lu et al., 2011). Additionally, the impairment of V-ATPase activity led to defects in Golgi morphology that produced pollen maturation dysfunction and male gametophytic lethality (Dettmer et al., 2005). This indicates that impairment of ER and Golgi could affect pollen regulation and can explain the fertility defect observed in the rice and Arabidopsis *gtg* mutants. Future work in rice using more advance microscopy, such as electron microscopy, would help us to study whether the structure and distribution of these organelles are affected in the *gtg* mutant.

3.3.5. The 187th residue does not play a key role in the function and localisation of OsGTG and its role in cold tolerance is questioned

In a previous study it was suggested that GTG could be involved in cold tolerance in rice since the rice *gtg* mutant, called *cold1*, showed a reduction of cold tolerance in comparison to the WT (Ma et al., 2015). Furthermore, a QTL analysis of rice sequences showed that a difference in the 187th amino acid of GTG was responsible for the cold tolerance trait. The *japonica* variety of rice, that it is cold tolerant, contains a lysine at position 187, while the *indica* variety, that is cold sensitive, contains a methionine. It was shown that OsGTG with a lysine was able to rescue the cold tolerance in the *gtg* mutant whereas OsGTG with a methionine could not (Ma et al., 2015). To test whether this residue could be involved in chilling tolerance in Arabidopsis, but also in the function and localisation of the protein, OsGTG with lysine and methionine in the 187th amino acid position were generated and expressed in the Arabidopsis *gtg1gtg2* mutant. The mutagenesis was performed in both the OsGTGe and OsGTGg backgrounds. OsGTGe^{187M} and OsGTGg^{187M} were able to rescue the defective root length, fresh weight and hypocotyl length of the *gtg1gtg2* mutant in the same way as OsGTGe^{187K} and OsGTGg^{187K} (Figure 3.28 to Figure 3.30). This indicates that both residues generated a functional protein, but that they did not play a key role in protein function.

Similar localisation patterns were found when OsGTG^{187K} and OsGTG^{187M} were tagged to GFP and expressed in Arabidopsis WT lines. Both OsGTGe showed an ER

and Golgi localisation. However, OsGTGg lines exhibited mostly ER localisation (Figure 3.32). The number of Golgi foci found in the lines that expressed OsGTGe was higher than in the lines that expressed OsGTGg, independent of the residue 187. It seems that the 187th amino acid is not involved in the localisation of the protein in the same way that the 9th amino acid is. In the predicted topology, the 187th residue is not localised in a transmembrane domain, it is located in the large loop, between the 5th-6th transmembrane domains, whereas the 9th amino acid residue is in the first transmembrane domain, close to the N-terminal of the protein where it could be part of a signal sequence.

Low temperature is an important environmental factor that affects plant growth (Zhang et al., 2013). During cold stress, plants activate a signal transduction pathway that creates a response to that stress. As a summary (see section 1.5.8 for a full description), after the cold stimulus is applied, the low temperature is sensed in the cell producing a decrease in the fluidity of the plasma membrane that activates specific calcium channels. These channels produce an influx of Ca^{2+} that will be sensed by Ca^{2+}-binding proteins. These Ca^{2+}-binding proteins activate specific kinases which will trigger a downstream response including the expression of specific transcription factors, such as CBFs, producing the cold response in the plant (Guo et al., 2018, Yadav, 2010, Miura and Furumoto, 2013).

In Ma et al. (2015) it was proposed that OsGTG could function as a cold receptor, sensing the low temperature through changes of plasma membrane fluidity, which activate the influx of Ca^{2+} into the cytosol. It was observed that the resting levels of Ca^{2+} prior to the stress and the influx of Ca^{2+} after the cold treatment was reduced in the mutant in comparison to the WT (Ma et al., 2015). To test whether GTG is involved in cold tolerance in Arabidopsis, WT and *gtg1gtg2* lines in Ws4 and Col-8 backgrounds were exposed to cold stress. The plants were grown at 23°C and transferred to 4°C for the cold stress treatment. The *gtg1gtg2* mutants in both backgrounds exhibited reduced growth and number of leaves compared to their respective WTs in normal conditions and under cold treatment (Figure 3.33). The growth of the *gtg1gtg2* mutant was reduced before the cold treatment. Reduction of growth was observed during the cold treatment in *gtg1gtg2* but also in WT plants. Both lines were able to recover during the recovery period. The fact that the mutant and WT were able to recover after the cold treatment indicates that the *gtg1gtg2* mutant lines were not more affected than the WT lines during the cold treatment. All this indicates that GTG is not involved in cold tolerance

in Arabidopsis. In Ma et al. (2015) it was shown that OsGTG was involved in cold tolerance, however analysis of the pictures from the experiment showed that the rice *gtg* plants were smaller than WT, even prior the cold treatment, and this defect in growth could affect the cold sensitivity observed in the mutant after the cold treatment. Future cold stress experiments with the rice *gtg* mutant need to be performed to study whether OsGTG could regulate cold tolerance in rice. In addition, experiments using Ca^{2+} sensors, such as R-GECO or Cameleon, would allow us to study whether the resting Ca^{2+} levels or the Ca^{2+} influx in the Arabidopsis *gtg1gtg2* mutant after the cold stress is reduced in comparison to WT. Since plasma membrane Ca^{2+} channels are synthesised through the ER-Golgi network (Roden and Kupershmidt, 1999, Taylor et al., 2009, Lazniewska and Weiss, 2017), it is possible that the reduction of the Ca^{2+} influx and resting levels observed in the rice *gtg* mutant could be due to a defect or reduction of plasma membrane Ca^{2+} channels due to ER and Golgi impairment.

This study also tested whether the 187th amino acid in OsGTG could affect cold tolerance in Arabidopsis plants. *gtg1gtg2* mutant plants transformed either with *OsGTG^{187K}* or *OsGTG^{187M}* were subjected to the same cold stress treatment. Lines expressing AtGTG1 were also used as a control. All the transgenic lines exhibited similar growth and number of leaves to the WT. *gtg1gtg2* showed a reduced rosette diameter and number of leaves in comparison to WT and all the *OsGTG* transformed lines when grown in normal conditions and prior to the cold treatment. There was a reduction of growth in the mutant during the cold treatment that was also observed in the WT and the rest of the OsGTG expressing lines. No differences were found between the lines transformed either with *OsGTGe^{187K}*, *OsGTGe^{187M}*, *OsGTGg^{187K}* or *OsGTGg^{187M}*, indicating that both residues form a functional protein. This result also suggests that the 187th amino acid, and also the 9th residue, are not involved in cold tolerance in Arabidopsis. The growth defects observed in the mutant seem to be due to GTG being involved in growth rather than cold tolerance. A different cold experiment with a lower temperature or longer treatment could be carried out to see whether there is any specific response in the *gtg1gtg2* mutant plants. In addition, to finally confirm whether OsGTG is involved in cold tolerance, a cold experiment using rice WT, *gtg* mutant, and *gtg* mutant expressing OsGTG^{187K} and OsGTG^{187M} also needs to be performed to test whether the results of Ma et al. (2015) can be replicated.

Chapter 4. Investigating the function of OsGTG as an anion channel regulating endomembrane pH

4.1. Introduction

It has been proposed that mammalian GTG/GPHR functions as an anion channel regulating Golgi pH in mammalians cells (Maeda et al., 2008) (section 1.5.1). Work in our laboratory (section 1.5.7) has indicated that AtGTG1 and CeGTG1 also function as anion channels and that AtGTG1 may regulate endomembrane pH in a similar manner to mammalian GTG/GPHR (Adam, Dorey, Terry and Williams, unpublished; Dorey, 2019). In this chapter, the aim was to explore whether OsGTG could play the same role. Anion channel activity was investigated using two different electrophysiology approaches: patch-clamping in HEK293 cells expressing OsGTG; and single-channel activity analysis in a planar lipid bilayer system using cell-free expressed OsGTG. Additionally, the role of OsGTG in regulating pH in the endomembrane system was tested by using a ratiometric pH-dependent GFP called pHluorin.

4.1.1. Patch clamping using HEK293 cells to measure channel activity

HEK293 cells are used extensively for expression and electrophysiological analysis of ion channels (He and Soderlund, 2010, Ooi et al., 2016). Voltage-current analysis performed using a whole-cell patch clamping technique allows for the recording of ion current passing through the plasma membrane of the cell under a predetermined membrane potential (Sakmann and Neher, 1984, Fuchs et al., 2005, Elter et al., 2007). For whole-cell patch clamping, a pipette is placed on the surface of the cell creating a high resistance seal, and a pulse of suction is applied to rupture the membrane producing a continuity between the cell and the pipette. This allows the recording of multiple channels at the same time and produces lower resistance and better electrical access inside the cell. The pipette is filled with an electrolyte solution and an Ag/AgCl electrode is placed inside. The second Ag/AgCl electrode is connected to the ground maintaining the voltage across the membrane and facilitates the recording of the current (Kornreich, 2007, Zhao et al., 2008b). HEK293 cells are commonly used for patch-

clamping due to their high transfection efficiency and high cell division rate, easy maintenance and low expression of native channels (Wurm, 2004, Backliwal et al., 2008, Ooi et al., 2016).

Several transporters have been characterized by whole-cell patch clamping in HEK293 cells. A Golgi localised protein has been shown to be involved in Ca^{2+} and pH homeostasis in yeast and human cells using this system (Demaegd et al., 2013). A limitation of the whole-cell technique is the requirement for the protein of interest to localise at the plasma membrane. However, high expression of proteins can result in endomembrane channels being expressed at the plasma membrane, as is the case with several transporters, such the Golgi Ca^{2+} channel previously mentioned (Demaegd et al., 2013) and the lysosomal cation channel TRP-ML1 (Kiselyov et al., 2005).

Acid activated Cl^- channels from human cells have also been identified by this technique (Capurro et al., 2015). These Cl^- channels are pH-dependent, being specifically activated at very low pH that is mainly reached in the lysosome and endosome, which suggests they might be active in organelles with acidic pH that are involved in protein trafficking (Capurro et al., 2015). The Arabidopsis Cl^- channel, which is homologous to the mammalian intracellular Cl^- channel (CLIC), was expressed in HEK293 cells and characterized using whole-cell patch clamping, and showed an inward rectifying current with no ion selectivity (Elter et al., 2007). Rice channels have also been identified and characterized using this technique, such as OsAKT1, a voltage-dependent K^+ channel that is involved in salt stress responses (Fuchs et al., 2005).

Other electrophysiology techniques, such as two-electrode voltage clamp in *Xenopus* oocytes have also been used to characterise several channels in plants, like the long distance Cl^- transporter AtNPF2.4 from Arabidopsis (Li et al., 2016) and the high affinity K^+ channel, OsHKT2 from rice (Lan et al., 2010). Electrode voltage clamp in *Xenopus* oocytes was used in a previous study that characterized rice GTG/COLD1 (Ma et al., 2015). In that study a strong inward current was observed after cold treatment when rice GTG/COLD1 was expressed along with the rice Gα subunit, indicating a potential activation of GTG/COLD1 by Gα (Ma et al., 2015). Interestingly, the ion being transported by GTG/COLD1 was not determined, although it was suggested that GTG/COLD1 could function as a calcium channel due to the reduction of the resting levels and temporal elevation of Ca^{2+} in the *cold1* rice mutant (Ma et al., 2015).

4.1.2. Lipid bilayer assay for measuring channel activity using cell-free expressed protein

Proteins can be expressed and purified using different organisms. One of the most commonly used organisms for the production of recombinant proteins is *E.coli.* The addition of a C or N-terminal tag facilitates the purification of the protein (Nallamsetty and Waugh, 2007, Gräslund et al., 2008, Rosano and Ceccarelli, 2014, Tripathi, 2016). However, not all proteins, including some membrane proteins and proteins toxic to the cell, can be expressed and purified successfully using a host cell. A cell-free protein synthesis (CFPS) system allows the expression of membrane proteins in an *in vitro* system that contains cell extracts with the ribosomal machinery, together with the amino acids and the metabolic energy needed to synthesize proteins (Carlson et al., 2012). Extracts from different organisms can be used for CFPS, such as *E.coli*, rabbit reticulocytes, insect cells or wheat germ lysate (Sitaraman and Chatterjee, 2009, Takai et al., 2010, Toru et al., 2010). The advantage of this system is that there is less equipment required and it is less time consuming because the expression of the protein is achieved in a continuous exchange cell-free chamber over 24 hours (Zemella et al., 2015). One disadvantage of CFPS is the potential degradation of DNA by endogenous nucleases present in the extract. This is more common when linear expression templates are used and can be overcome by the use of circular plasmids where no DNA end is present (Zemella et al., 2015). Proteins such as malaria proteins, polio virus proteins and ion channels have been studied using a CFPS system (Villa-Komaroff et al., 1975, Tsuboi et al., 2008, Friddin et al., 2013, Herdean et al., 2016b).

Following expression and purification through CFPS, proteins can be inserted into a planar lipid bilayer to undertake single-channel current measurements. The planar lipid bilayer system is an electrophysiology technique used to analyse single-channel activity in an artificial membrane created in a controlled environment. The membrane functions as an electrical insulator through which current cannot pass. Therefore, this assay can provide controlled transport of ions across the membrane due to the insertion of a channel into that membrane (Zakharian, 2013). In cells, membranes separate the external space from the inside and allow eukaryotic organisms to have different compartments or organelles (Walter, 1989). Ion channels are present in all biological membranes and allow different ions to pass through. They usually have a central pore that opens and closes depending on conformational changes of the protein structure and they can exhibit a selectivity for specific ions, such as Na^+, Ca^{2+}, K^+, Cl^- etc. (Bezanilla,

2008, Minor, 2010). In the planar lipid bilayer technique an artificial membrane is created in a small aperture that separates two chambers containing Ag/AgCl electrodes in electrolytic solutions (Zakharian, 2013). A protein is inserted into that membrane and current activity is measured. This technique allows for the characterization of ion channels that do not localise at the plasma membrane or are more difficult to record by whole-cell patch clamping.

The validation of this technique has been confirmed using well-characterised ion channels, such as KcsA (Friddin et al., 2013). KcsA is a bacterial proton-gated K^+ channel that was expressed in a cell-free system from *E.coli* lysate and added to an artificial lipid bilayer made of soybean asolectin lipids. The recordings of the current events were made at different voltage values, validating this method for ion channel characterization (Friddin et al., 2013). It has also been reported that KcsA synthesised in the cell-free system with liposomes, generates a functional tetramer and integrates into the membrane in the correct form (Ando et al., 2016). In the extracts used for the CFPS system there are no membranes or lipids present, eliminating the hydrophobic environment required for the proper folding of membrane proteins. For this reason, the addition of detergent, lipids or liposomes to the lysate or the reaction has been recommended and applied (Zemella et al., 2015).

The mammalian GTG/GPHR protein was confirmed as an anion channel using a lipid bilayer technique. The protein was first tagged with FHAT (Flag-Histidine affinity tag) and then expressed and purified by a cell-free system using a Sf9 insect cell extract (Maeda et al., 2008). The protein was inserted into lipid vesicles prior to being introduced into an artificial membrane of soybean lecithin lipids created between two chambers where single-channel activity was analysed. GTG/GPHR exhibited a voltage-dependent current activity with five or six subconductance states. Using an asymmetrical gradient of 150/300 mM KCl it was shown that the channel was more permeable to Cl^- than K^+ and, that the activity was inhibited by the anion channel blocker DIDS. The selectivity of the channel was $I^- > Cl^- = Br^- > F^-$; however NO_3^- was not measured in this study (Maeda et al., 2008).

Other plant channels have been characterized using this technique, such as VCCN1, a thylakoid protein that functions as a voltage-dependent Cl^- channel that is involved in the proton motive force across the membrane (Herdean et al., 2016b). VCCN1 was first expressed in an *in vitro* system using a wheat germ lysate and was then inserted into a lipid bilayer. When the single-channel activity was measured, VCCN1 showed activity

in the presence of KCl and KNO_3. VCCN1 was more selective for Cl^-, however it was also able to transport NO_3^- (Herdean et al., 2016b). It was proposed that VCCN1 transports Cl^- into the thylakoid lumen to counterbalance the protons introduced by the H^+ pump (Herdean et al., 2016b).

4.1.3. Regulation of endomembrane pH

The pH in the secretory pathway is regulated by proton pumps and other transporters (Martinière et al., 2013a, Shen et al., 2013). V-ATPases are critical for the generation of proton gradients that, apart from causing the acidic pH of the organelles, also regulate the activation of secondary transport (Figure 4.1) (Demaurex, 2002). V-ATPases are present in all the compartments of the secretory pathway and play an important role in protein trafficking and Golgi function (Beyenbach and Wieczorek, 2006, Dettmer et al., 2006, Gaxiola et al., 2007, Maxson and Grinstein, 2014). In animals, the endosomal/lysosomal trafficking depends on the acidification generated by V-ATPase (Finbow and Harrison, 1997). In Arabidopsis, mutants of the tonoplast V-ATPase subunit VHA-a exhibited an increase in vacuolar pH of 0.5 units (Krebs et al., 2010). Similarly, *avp1* mutant of the H^+ pyrophosphatase (H^+-PPase) also showed an increase in pH of 0.25 in the vacuole (Ferjani et al., 2011, Li et al., 2005). The influx of protons causes an increase of membrane potential and this can limit the activity of the V-ATPase. Therefore, the action of a counterion is required to dissipate the rise in membrane potential allowing the V-ATPase to keep pumping protons inside the lumen of the organelles (Schumacher, 2014, Demaurex, 2002). Cl^-, K^+ and Na^+ fluxes play a potential role as counterions, but the channels involved in pH regulation are yet to be definitively identified. In a study performed in HeLa cells, it was shown that Cl^- contributed to H^+ fluxes in regulating Golgi pH. When Cl^- was removed from the solution and replaced with gluconate, the pH of the Golgi increased rapidly (Llopis et al., 1998). This indicated that Cl^- functions as a counterion in pH regulation.

Accurate pH is maintained by the influx and efflux of protons. K^+/H^+ antiporters are good proton leak candidates (Sze and Chanroj, 2018). NHX1 and NHX2 play a role in vacuolar pH regulation. The *nhx1nhx2* double mutant exhibited a lower vacuole pH than WT (Andrés et al., 2014). K^+/H^+ antiporters also can regulate pH in rice. OsNHX5, a protein that localises at the Golgi, TGN and PVC plays a role in the pH regulation of those organelles. It was shown that the rice *nhx5* mutant exhibited more acidic compartments than the WT (Zhu et al., 2019). The CAX proteins, which are Ca^{2+}/H^+

exchangers, are also candidates for ion homeostasis and pH regulation (Pittman, 2012). A mutant lacking the vacuolar CAX1 and CAX3 proteins displayed a reduction of V-ATPase activity (Cheng et al., 2005). In addition, the cation/H^+ exchangers can also play a role in pH homeostasis. The cation/H^+ antiporters AtCHN16-AtCHX20, can rescue the alkaline pH sensitivity growth phenotype of the corresponding yeast mutant and increase vacuole pH in yeast (Chanroj et al., 2011). Therefore there is a range of proteins involved in the regulation of endomembrane pH in plants (Figure 4.1).

Intracellular pH homeostasis is critical for the correct function of the cell and different organelles since pH fluctuations can affect several processes in the cell (Casey et al., 2009). In humans, defects in pH homeostasis lead to various diseases, such as acidosis, cancer associated with glycosylation defects and cutis laxa (Rivinoja et al., 2006, Rivinoja et al., 2011, Aoi and Marunaka, 2014). This is because pH regulation is crucial for the correct function of the secretory pathway and protein trafficking (Carnell and Moore, 1994, Wu et al., 2001, Paroutis et al., 2004, Huang and Chang, 2011). GTG/GPHR has been shown to regulate Golgi pH in mammalian cells. By using the pH sensor pHluorin it was shown that CHO cells that did not have a functional GTG/GPHR, exhibited an increase in pH in the lumen of the Golgi of 0.35-0.52 (Maeda et al., 2008).

To measure pH values *in vivo*, genetically encoded biosensors, such as pHluorin, have been used. This is based on variants of fluorescent proteins that are pH-sensitive and permit pH measurement in living cells (Gjetting et al., 2012). In general, the chromophore of modified GFP is used to measure fluorescence absorption at two different wavelengths, 395nm and 475nm, and the differences in the ratio of the two wavelengths indicate the changes in the pH. The range of pH of those sensors extends from pH 5.4 to 8.4 (Miesenböck et al., 1998, Martinière et al., 2013b). pHluorin can be directed to different organelles by adding the appropriated targeting sequence (Martinière et al., 2013b). These genetically encoded pH sensors have been used to measure intracellular pH in plant cells. Two independent studies have measured the pH of different compartments in plant cells using two pHluorin variants, ratiometric and ecliptic, and in both studies a gradual acidification from the ER to the vacuole was observed (Table 4.1) (Martinière et al., 2013a, Shen et al., 2013). The gradual acidification observed in plant cells is in agreement with what has been reported in animals, where there is a gradual acidification from the ER to the late endosomes and

lysosomes. This acidification determines the enzymes and the processes that are carried out in each organelle (Demaurex, 2002).

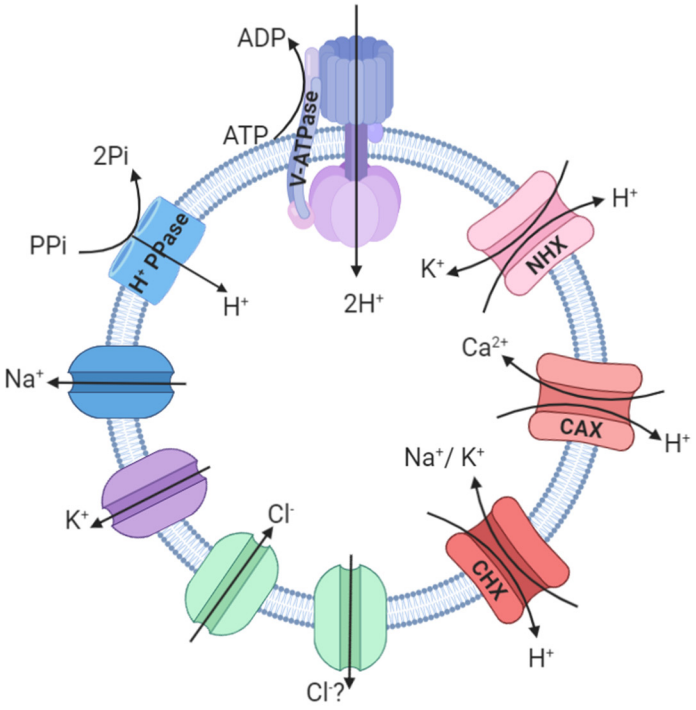

Figure 4.1. Diagram of possible channels involved in pH regulation

Schematic diagram of the channels involved in pH regulation in a hypothetical endomembrane organelle. V-ATPase and H^+-PPase generate the proton gradient and regulate secondary transport. Na^+, K^+ and Cl^- channels function as a counterion balance reducing the membrane potential generated for the proton pump and regulating pH. K^+/H^+ antiporters (NHX), Ca^{2+}/H^+ exchangers (CAX) and cation/H^+ antiporters (CHX) are potential proton leaks to fine-tune the pH of the organelle. The mechanism of Cl^- exclusion in intracellular organelles remains unknown, however in order to avoid chloride to be built up inside the organelle, the presence of an efflux chloride channel may be possible.

Table 4.1. pH values obtained in different plant cell organelles

Organelle	Targeting method	Plant tissue	pH	Reference
Cytosol	pHluorin	Tobacco epidermal cells and Arabidopsis root cells	7.8	(Martinière et al. 2013a)
		Arabidopsis protoplast	7.3	(Shen et al. 2013)
ER	HDEL	Tobacco epidermal cells and Arabidopsis root cells	7.5	(Martinière et al. 2013a)
		Arabidopsis protoplast	7.1	(Shen et al. 2013)
cis Golgi	ManI	Arabidopsis protoplast	6.8	(Shen et al. 2013)
trans Golgi	ST	Tobacco epidermal cells and Arabidopsis root cells	6.8	(Martinière et al. 2013a)
	BP80	Arabidopsis protoplast	6.3	(Shen et al. 2013)
PVC	VSR2	Tobacco epidermal cells and Arabidopsis root cells	6.7	(Martinière et al. 2013a)
		Arabidopsis protoplast	6.2	(Shen et al. 2013)
Vacuole	BCECF-AM Dye	Tobacco epidermal cells and Arabidopsis root cells	6.0	(Martinière et al. 2013a)
	Aleurain	Arabidopsis protoplast	5.2	(Shen et al. 2013)

4.1.4. Aims

This chapter investigates whether rice GTG can function as an anion channel regulating pH in the endomembrane system, with the following aims:

1. To determine whether OsGTGe and OsGTGg function as channels. Two approaches will be taken to measure channel activity: a patch clamping technique using HEK293 cells and a planar lipid bilayer electrophysiological assay using proteins expressed in a cell-free system.
2. To determine whether both OsGTGs play a role in regulating endomembrane pH. Arabidopsis pH sensor lines, produced previously (these lines were produced by: Adam, Terry, Williams, unpublished), will be used in which the pH sensor, pHluorin, was targeted to specific organelles (ER and *cis* Golgi). Here, OsGTGe and OsGTGg will be expressed in these pH sensor Arabidopsis lines and the pH of the compartments will be analysed to determine whether OsGTG plays a role in regulating the ER and *cis* Golgi pH.

4.2. Results

4.2.1. Cloning both *OsGTG* versions into mammalian expression vectors to measure channel activity in HEK293 cells by patch clamping

To analyse channel activity in a HEK293 cell system the gene of interest needs to be cloned into a suitable expression vector, transformed into HEK293 cells and then analysed using whole-cell patch clamping. The results from these steps are covered here.

4.2.1.1. Generating expression vectors for *OsGTGe* and *OsGTGg* for HEK293 expression

OsGTGe and *OsGTGg* were cloned into a pDEST47 Gateway vector. This vector contains a Cytomegalovirus (CMV) promoter and a C-terminal GFP tag. LR recombination reactions were carried out to introduce *OsGTGe* and *OsGTGg* from the pENTR/D vector into a pDEST47 destination vector. The constructs, pENTR/D *OsGTGe* without stop codon and pENTR/D *OsGTGg* without stop codon, were used as entry vectors for each recombination reaction so that the final product would be tagged with GFP (section 2.3.8). The reaction was transformed into *E.coli* DH5α cells. To identify positive clones and confirm that both *OsGTGs* were inserted correctly into the destination vector, colony PCR and restriction digests were performed. Figure 4.2 shows that both *OsGTGs* were inserted successfully into the destination pDEST47 vector. The predicted product sizes are indicated. The resulting vectors were sequenced in forward and reverse directions to confirm that the correct CDS sequence of both *OsGTGs* were inserted in the correct orientation and that both had the GFP attached. The destination vectors (Table 4.2) were transformed into HEK293 cells (section 2.6.2). The transfection was confirmed using fluorescence microscopy. Cells that have been transfected with *OsGTGe* and *OsGTGg* exhibited a clear GFP signal, which indicated that the transfection was achieved (Figure 4.3).

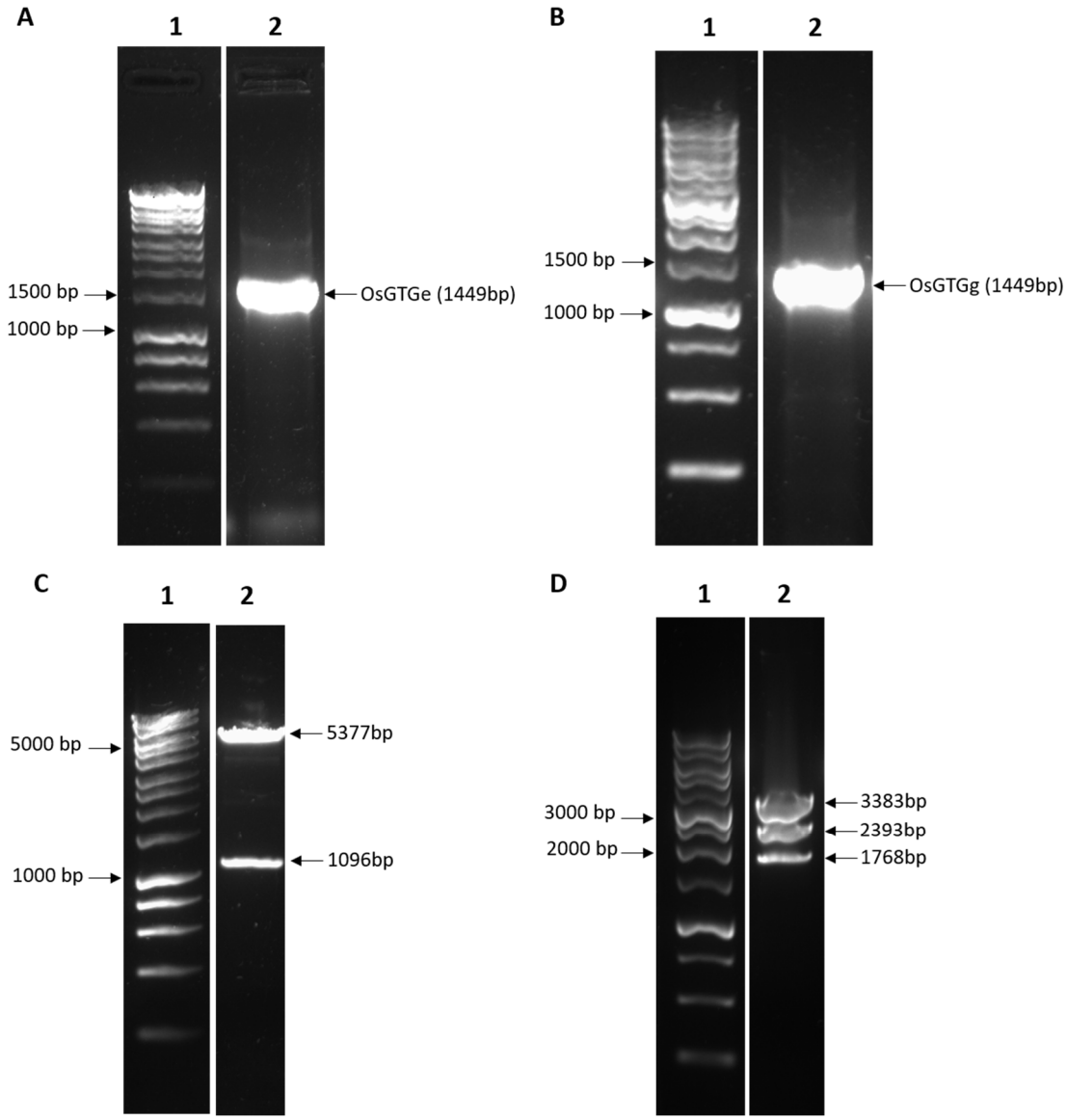

Figure 4.2. Cloning of *OsGTGe* and *OsGTGg* into the pDEST47 mammalian expression vector

Colony PCR (top) and restriction digest analysis (bottom) of pDEST47 *OsGTGe* and pDEST47 *OsGTGg*. Colony PCR of pDEST47 *OsGTGe* (A) and pDEST47 *OsGTGg* (B) using primers T7 promoter + OsGTG no stop R1 (lane 2, predicted size 1449 bp). Restriction digest of pDEST47 *OsGTGe* (C) and pDEST47 *OsGTGg* (D) using restriction enzymes *Pvu*II and *Xmn*I respectively (lane 2). Predicted product sizes are indicated on the right and molecular markers are indicated on the left (lane 1).

Table 4.2. Plasmids generated for patch clamping assay

Plasmid	Description	System
pDEST47 *OsGTGe*	CMV::*OsGTGe*::GFP	Mammalian expression vector used for patch clamping system
pDEST47 *OsGTGg*	CMV::*OsGTGg*::GFP	Mammalian expression vector used for patch clamping system

4.2.1.2. Intracellular localisation of OsGTGs and AtGTG1 in HEK293 cells

For current recordings using whole-cell patch clamping in HEK293 cells some plasma membrane localisation is necessary. As seen in Chapter 3, OsGTG is not observed at the plasma membrane when expressed in plants. However, when highly expressed in mammalian cells, it has been reported that secretory pathway proteins can be found at the plasma membrane (Demaegd et al., 2013) and therefore, that was investigated here for OsGTG expression in HEK293 cells. OsGTGe and OsGTGg were mainly observed around the nucleus in the endomembrane system (Figure 4.4). DAPI staining was used to stain the nucleus. No clear plasma membrane localisation was detected when OsGTGe or OsGTGg were expressed in HEK293 cells, although it cannot be ruled out that some may occur because of the resolution of the system (section 2.5.2).

AtGTG1 was also tested in HEK293 cells and this again localises mostly around the nucleus in the endomembrane system (Figure 4.5). In this case, lectin was used as a plasma membrane stain and it was observed that AtGTG1 seemed to be present in some contact sites between the endomembrane system and the plasma membrane. These contact sites could be the reason for the channel activity observed in HEK293 cells when AtGTG1 is expressed (Dorey, 2019).

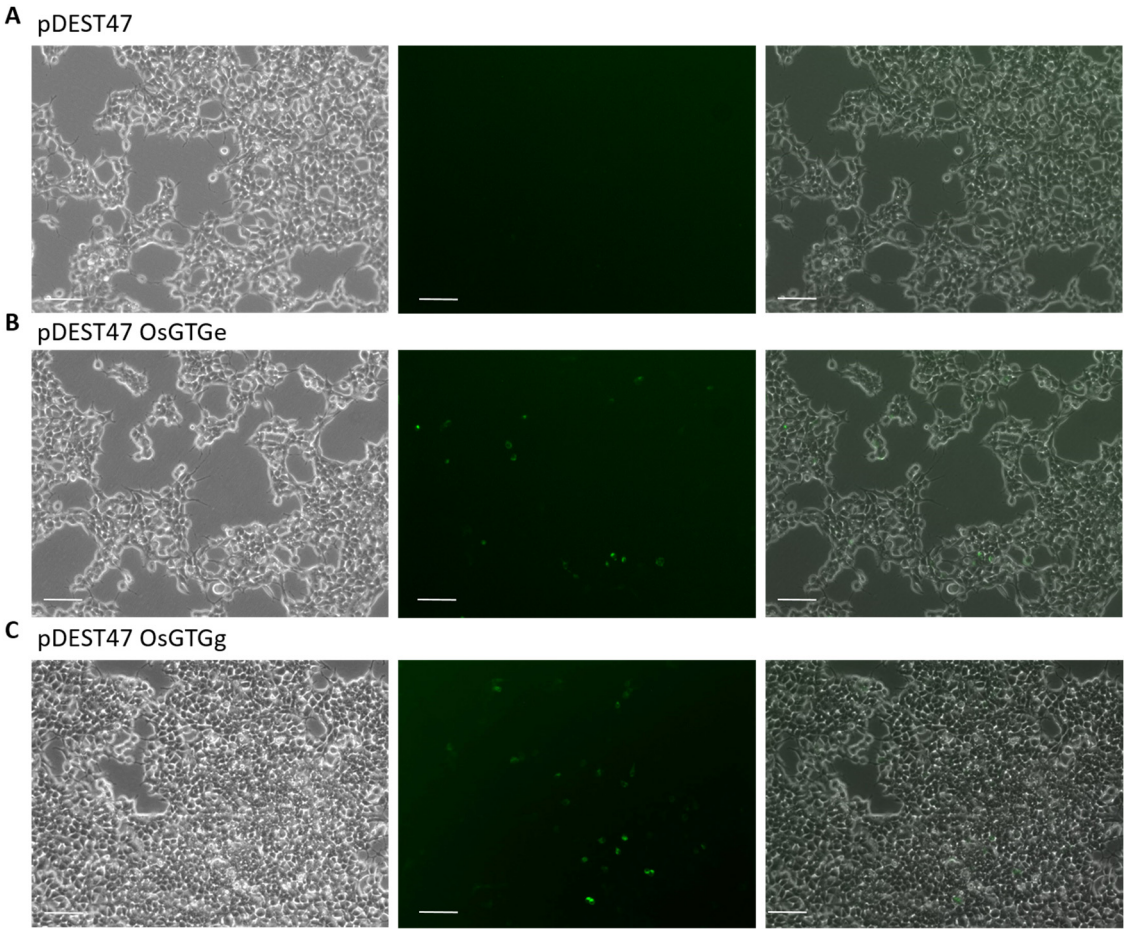

Figure 4.3. Expression of OsGTGe and OsGTGg in HEK293 cells after transfection

Fluorescence microscopy images showing GFP in HEK293 cells transfected with pDEST47 empty vector (A), with GFP tagged *OsGTGe* (B) and *OsGTGg* (C). Brightfield is shown on the left and fluorescence on the middle and overlay on the right. Scale bar 100µm.

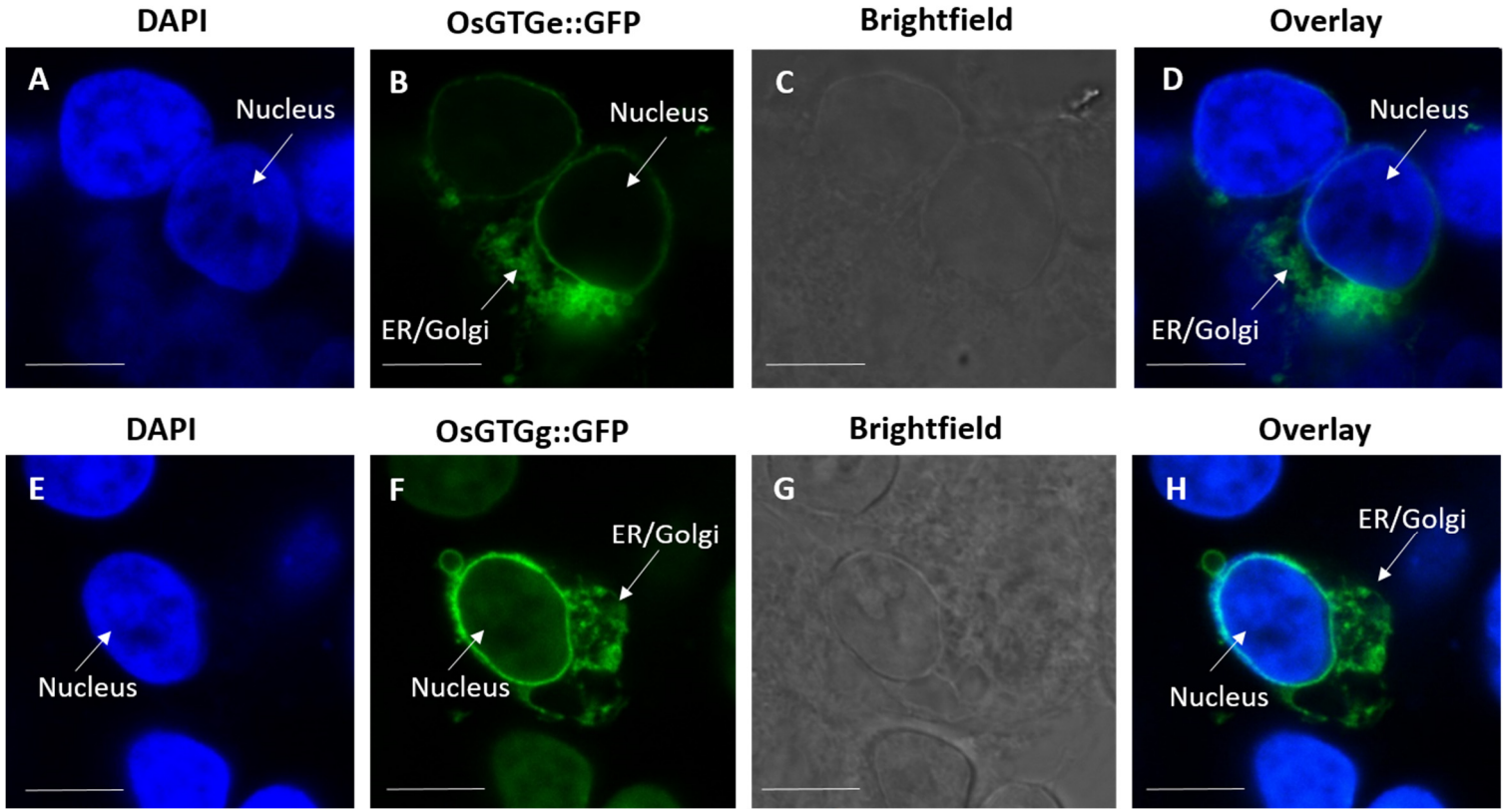

Figure 4.4. OsGTGe and OsGTGg show endomembrane localisation around the nucleus in HEK293 cells

Confocal microscopy images showing GFP-tagged OsGTGe (A-D) and OsGTGg (E-H) localised to the endomembrane system in HEK293 cells fixed using 4% paraformaldehyde. A) and E) DAPI staining (blue) of nucleus. Laser 405 for DAPI excitation. B) and F) GFP (green) using excitation at 488 nm and emission at 500-550 nm. C) and G) Brightfield images. D) and H) Overlay images showing GFP and DAPI. Scale bar 10µm. The experiment was performed once, and same preparation was imaged twice.

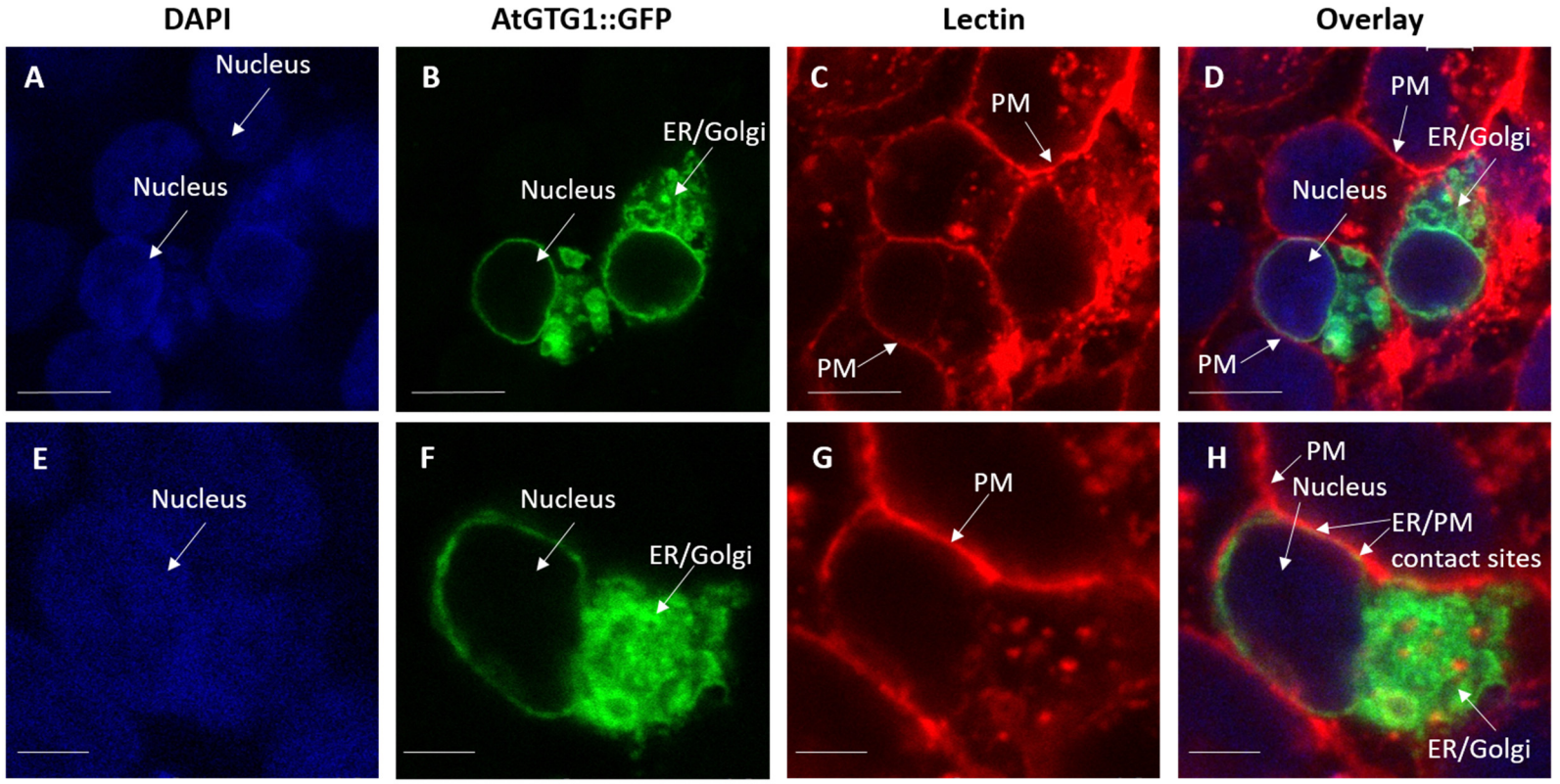

Figure 4.5. AtGTG1 shows endomembrane localisation in HEK293 cells

Confocal microscopy images showing GFP-tagged AtGTG1 localised in the endomembrane system when expressed in HEK293 cells fixed using 4% paraformaldehyde. Scale bar 10 µm for A-D) and 4µm for E-H). A) and E) DAPI staining (blue) of nucleus. Laser 405 for DAPI staining excitation. B) and F) GFP (green) using excitation at 488 nm and emission at 500-550 nm. C) and G) Lectin staining (red) of plasma membrane. RFP excitation at 561 nm and emission at 580-600 nm D) and H) Overlay images showing GFP, DAPI and lectin. Performed once, and the preparation imaged twice.

4.2.1.3. Measuring current activity in HEK293 cells expressing OsGTGs

To test whether OsGTG could function as an anion channel, whole-cell patch clamp recordings were carried out using a chloride solution. For the whole-cell patch clamping assay, HEK293 cells were transfected with pDEST47 empty vector (control), pDEST47 *OsGTGe* or pDEST47 *OsGTGg*. Multiple cells (40 cells for the empty vector, 60 for *OsGTGe* and 47 for *OsGTGg*) were patched for each transfection reaction.

HEK293 cell recordings are shown with the pDEST47 empty vector (Figure 4.6 A-B), pDEST47 *OsGTGe* (Figure 4.6 C-D) and pDEST47 *OsGTGg* (Figure 4.6 E-F). In those I-V graphs it can be observed that the range of current produced from HEK293 cells that were transfected with the empty vector is lower than the range of current generated from HEK293 cells expressing OsGTGe and OsGTGg. Both current and current density are represented for comparison purposes. The average current obtained at the highest voltages from the HEK293 cells transfected with the empty vector ranged between 25.6 ± 1.6 pA and -33.2 ± 2.5 pA, with a maximum current recorded of 40 and -50 pA respectively. However, the analogous average current obtained from cells expressing OsGTGe was between 38.5 ± 3.1 pA and -47.1 ± 3.8 pA, with a maximum current recorded of 138 and -75 pA respectively, and from cells expressing OsGTGg the average current obtained was between 39.4 ± 2.9 pA and -53.2 ± 4.3 pA where the maximum current observed was 94 and -106 pA respectively.

The current average from all the cells that were recorded indicated that there is a higher current in the cells transfected with OsGTGe and OsGTGg than in the cells transfected with the empty vector (Figure 4.7). This difference became smaller when current density was represented against the voltages. One of the reasons could be that the microscope used for patch clamping did not have the appropriate fluorescence settings, so it was impossible to identify which cells were fluorescent and therefore expressing OsGTG. Most of the patch clamping was performed blindly without any knowledge of whether a cell was transfected. However, as shown in Figure 4.7 A, some cells that expressed OsGTGe or OsGTGg showed higher current than the cells transfected with the empty vector.

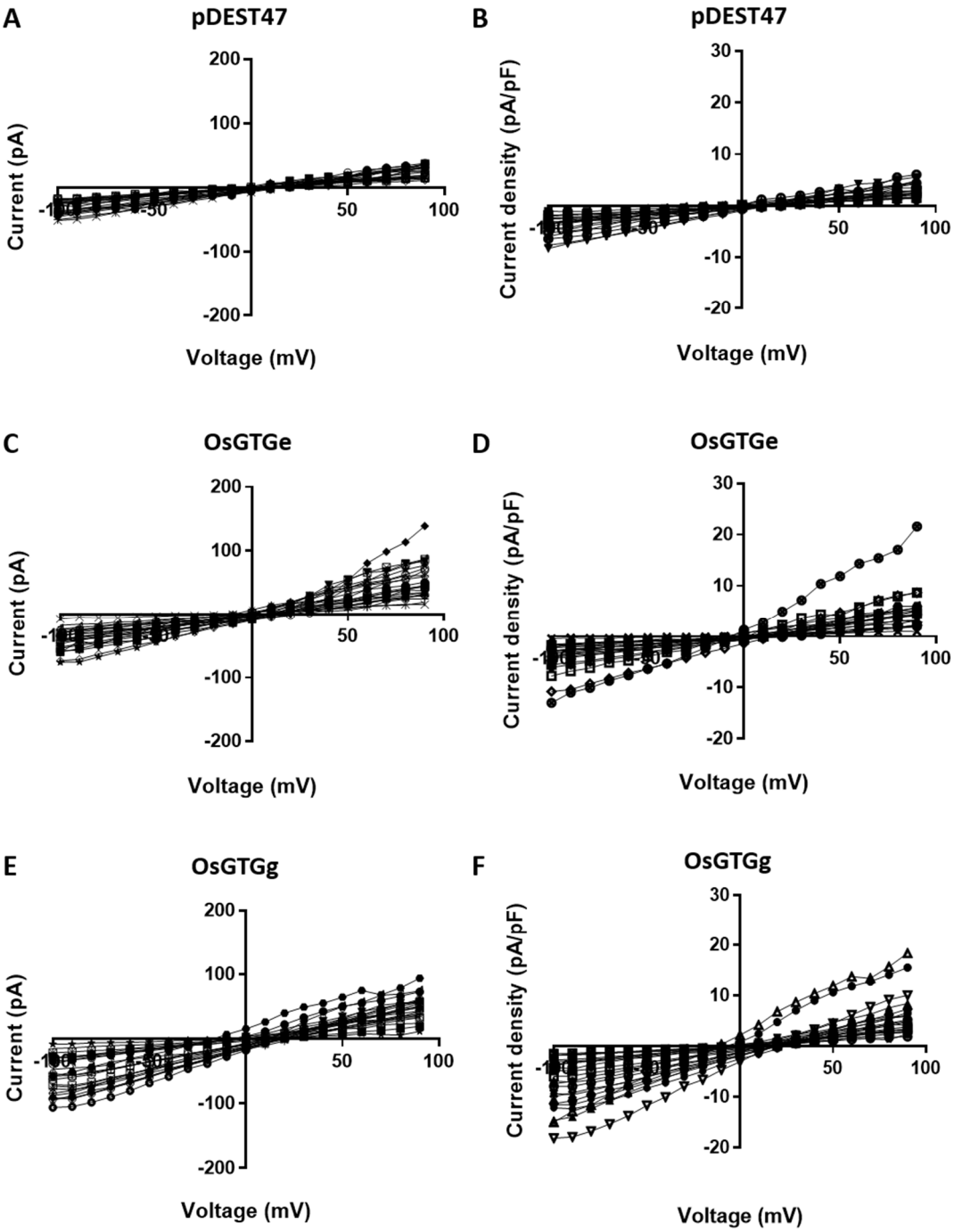

Figure 4.6. Whole-cell patch clamping recordings of HEK293 cells transfected with pDEST47 empty vector, pDEST47 *OsGTGe* and pDEST47 *OsGTGg* using a chloride solution

Voltage against current (left) and current density (right) is represented for whole-cell patch clamping recordings in several HEK293 cells transfected with pDEST47 empty vector (A-B) (n=20), pDEST47 *OsGTGe* (C-D) (n= 22) and pDEST47 *OsGTGg* (E-F) (n= 22).

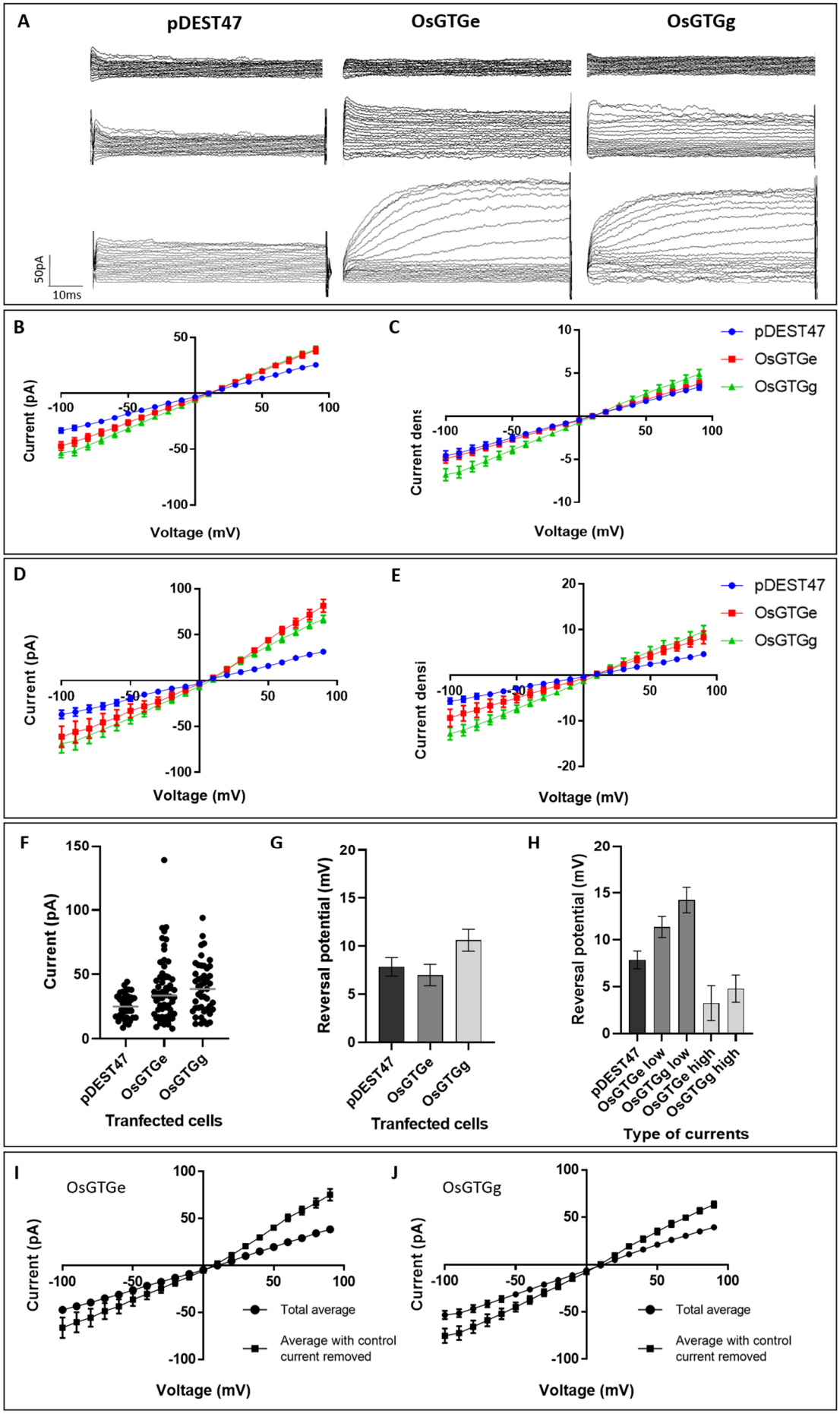
A
pDEST47
OsGTGe
OsGTGg
50pA
10ms
B
Current (pA)
Voltage (mV)
C
pDEST47
OsGTGe
OsGTGg
Current dens
Voltage (mV)
D
Current (pA)
Voltage (mV)
E
pDEST47
OsGTGe
OsGTGg
Current densi
Voltage (mV)
F
Current (pA)
pDEST47
OsGTGe
OsGTGg
Tranfected cells
G
Reversal potential (mV)
pDEST47
OsGTGe
OsGTGg
Tranfected cells
H
Reversal potential (mV)
pDEST47
OsGTGe low
OsGTGg low
OsGTGe high
OsGTGg high
Type of currents
I
OsGTGe
Current (pA)
Total average
Average with control current removed
Voltage (mV)
J
OsGTGg
Current (pA)
Total average
Average with control current removed
Voltage (mV)

Figure 4.7. HEK293 cells expressing OsGTGe and OsGTGg showed a higher current activity than the control cells using a chloride solution

Whole-cell patch clamping recordings in HEK293 cells that expressed OsGTGe and OsGTGg. A) Sample traces of the patch clamping recording from HEK293 cells transfected with pDEST47 empty vector, pDEST47 *OsGTGe* and pDEST47 *OsGTGg*. Total current average (±SEM) (n=40 for control, n=60 for OsGTGe and n=47 for OsGTGg) for voltage plotted against current in B) (significant differences between pDEST47 and OsGTGe and OsGTGg transfected cells at 90 mV; One-way ANOVA ($p < 0.05$)) and voltage against current density in C) (significant differences between OsGTGg in comparison with pDEST47 and OsGTGe transfected cells at 90 mV; One-way ANOVA ($p < 0.05$). Current average (±SEM) of cells with the highest currents (cells above the 99% confidence interval of the mean) in D and E) (n = 10). F) Current obtained at 90 mV. Higher currents observed in cells transfected with OsGTGe and OsGTGg in comparison with the cells transfected with the pDEST47 empty vector. Reversal potential (±SEM) obtained from cells transfected with pDEST47 empty vector, OsGTGe and OsGTGg in G) and separated in low and high current cells in relation to the control cells (inside and outside the 99% confidence interval) in H). Total current average (±SEM) for OsGTGe (I) or OsGTGg (J) (same data than B) and the average without the cells that showed a similar current to the control cells (n=13) is represented.

The maximum current observed for the control cells at 90 mV was always below 50 ± 1.6 pA, which is outside the 99% confidence interval. In addition, 20% of the cells transfected with *OsGTGe,* which are the ones outside the 99% confidence interval, exhibited higher current than the control cells, with an average of 77.4 ± 6.3 pA, whereas for OsGTGg the percentage was 25% of ones outside the 99% confidence interval and an average of 65.6 ± 3.5 pA (Table 4.3 and Figure 4.7 F). Taking these cells that have a higher current than the control (outside the 99% confidence interval), it can be observed that there is an increase in the current measured for the cells transfected with *OsGTGs* in comparison to the cells transfected with the empty vector (Figure 4.7 D-E).

Table 4.3. Percentage of HEK293 cell that showed a current higher than 50 pA at 90 mV

Transfected gene	Total cells analysed	Total cells with current > 50pA	Percentage (%) of cells with current > 50 pA
pDEST47 *OsGTGe*	60	12	20%
pDEST47 *OsGTGg*	47	12	25%
pDEST47 empty vector	40	0	0

Similarly, when the current values that were higher than the negative control were taken into account only, this same current pattern appeared in cells expressing OsGTG and in this case a current increase in the HEK293 cells expressing OsGTGs was observed (Figure 4.7 I-J). This indicates that there are some cells in the OsGTGe or OsGTGg batches that exhibit some current activity. However, many other cells did not have current and were more similar to the control cells. This could be due to the fact that the transfection efficiency was low and many cells were not transfected. Alternatively, it could indicate that OsGTG localisation to the plasma membrane only occurs in a proportion of cells and therefore this technique would not detect activity in cells where plasma membrane localisation had not occurred. To address this issue a plasma membrane signal peptide could be cloned in the OsGTG sequence to be certain that the protein can localise at that particular membrane.

The statistical analysis of the reversal potential showed that the reversal potential obtained when all the cells transfected with OsGTGe and OsGTGg were analysed (7.8 ± 1 mV and 10.62 ± 1.2 mV respectively) was within the 99% confidence interval obtained for the reversal potential of the cells transfected with the empty vector (7.8 ± 1 mV) (Figure 4.7 G). Separating the high and low current cells as described above (Table 4.3 and Figure 4.7 F), the reversal potential obtained for the low current cells that were transfected with OsGTGe (11.37 ± 1.1 mV) was within the 99% confidence interval of the reversal potential obtained with the empty vector (7.8 ± 1 mV). While the reversal potential obtained for the low current OsGTGg transfected cells was higher (14.24 ± 1.3 mV), it was also within the 99% confidence interval of the control (Figure 4.7 H). The

reversal potential obtained for the high current cells when OsGTGe or OsGTGg were transfected (3.2 ± 1.8 mV and 4.8 ± 1.4 mV respectively) was within the 99% confidence interval of the reversal potential obtained with the empty vector (7.8 ± 1 mV) (Figure 4.7 H). Nevertheless, the reversal potential obtained for the cells transfected with OsGTGs was different from the reversal potential for the Cl^- ion (-30 mV), since it was outside of the 99% confidence interval, indicating that the current was not produced by a Cl^- selective ion channel.

A recent study proposed that OsGTG may function as a calcium channel (Ma et al., 2015), so this hypothesis was tested using a calcium containing medium in the whole-cell patch clamping assays. There were no differences between the current obtained in the vector control cells compared to the current seen in the cells transfected with either *OsGTGe* or *OsGTGg*. Similar results were obtained when current density was represented (Figure 4.8 A-B). Several cells exhibited a higher current than the control cells which were outside the 99% confidence interval. If these cells that showed the higher currents were the only cells taken into account from the transfected cells, it can be observed that there are no differences between the control cells and the cells expressing OsGTGg (Figure 4.8 C). The fact that there is a slight increase of current in the cells expressing OsGTGe in comparison to the control cells could be due to the Cl^- that was present in these solutions. Further experiments are required to confirm whether OsGTG could transport Ca^{2+}. However, these results indicate that, in the presence of a calcium solution, there is no significant current increase in the HEK293 cells when OsGTG is expressed. Therefore, this suggests that OsGTG does not show a strong calcium channel activity in the patch clamping system.

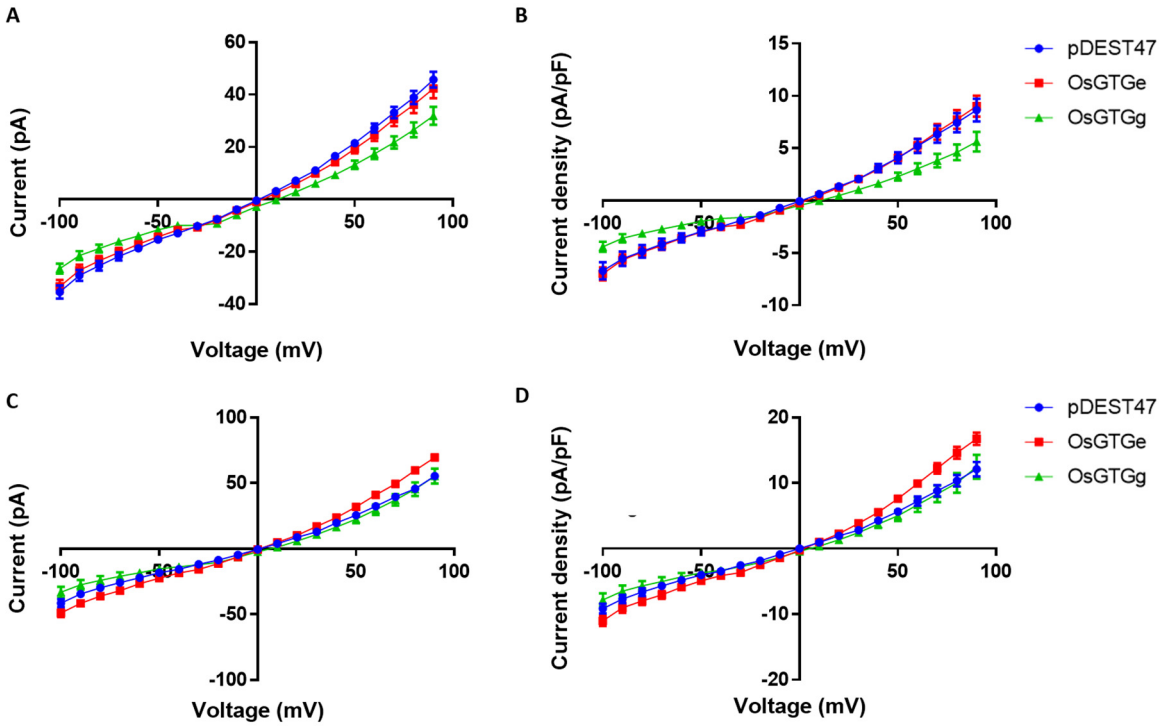

Figure 4.8. HEK293 cells transfected with *OsGTGe* and *OsGTGg* did not exhibit a strong current activity in whole-cell patch clamping using a calcium solution

Patch clamping recordings in HEK293 cells that expressed OsGTGe and OsGTGg using a calcium solution. Total current average (±SEM) (n=19 for control, n=34 for OsGTGe and n=33 for OsGTGg) for voltage plotted against current in A) (significant differences between pDEST47 and OsGTGg transfected cells at 90 mV; One-way ANOVA ($p < 0.05$) and voltage against current density in B) is represented (significant differences between OsGTGg in comparison with pDEST47 and OsGTGe transfected cells at 90 mV; One-way ANOVA ($p < 0.05$). Current average (±SEM) of ten cells that exhibited the highest currents in C) and D).

4.2.2. Cloning *OsGTGs* into cell-free system vectors for planar lipid bilayer assays

To further investigate the potential function of OsGTG to act as a channel, a second electrophysiology assay was carried out. In this approach, an *in vitro* system was used to overcome the potential localisation issues faced during the patch clamping experiments. This involves cloning the gene of interest in an appropriate expression

vector, generating the protein using a cell-free system and then recording channel activity using the planar lipid bilayer technique.

4.2.2.1. Generating pIVEX1.3 expression vectors

OsGTGs were cloned into a specific expression vector, pIVEX1.3 that contains a T7 promoter and a C-terminal His_6 tag. Both *OsGTGs* cDNAs were amplified by PCR introducing *Nde*I and *Sac*I restriction sites to the N-terminal and C-terminal respectively, to allow the cloning of both *OsGTGs* into the vector. Colony PCR and restriction digests confirmed that the cDNA was cloned in the correct orientation. Figure 4.9 shows the cloning of *OsGTGe* and *OsGTGg* into the pIVEX1.3 vector. Sequencing of both in forward and reverse directions confirmed the sequence and the right orientation. Table 4.4 shows the plasmids generated.

4.2.2.2. Expression of OsGTGe and OsGTGg proteins using a cell-free system

Measuring channel activity in the planar lipid bilayer requires the protein of interest to first be synthesised. This was achieved by using the CFPS system kit that uses a wheat germ lysate to provide a synthetic transcription and translation system (section 2.7). The pIVEX1.3 vector, designed to be used in this system, contains a T7 promoter and a His_6-tag for antibody detection of the protein. To improve the incorporation of OsGTG into an artificial membrane the proteins were synthesized in the presence of 1, 2-dioleoyl-sn-glycero-3-phosphocholine (DOPC) lipids. The pIVEX1.3 empty vector was used as a control.

Following the synthesis of OsGTGe and OsGTGg, the expression of both proteins was assessed by western blotting. One SDS-PAGE gel was used for Coomassie staining analysis to detect the total amount of protein loaded in the gel while the other gel was transferred onto a PVDF membrane for western blot analysis. The membrane was incubated with a mouse anti-His primary antibody and a secondary fluorescent anti-mouse antibody, which was detected at 800 nm wavelength using an Odyssey Licor scanner. Both OsGTG proteins were successfully expressed in the CFPS system (Figure 4.10).

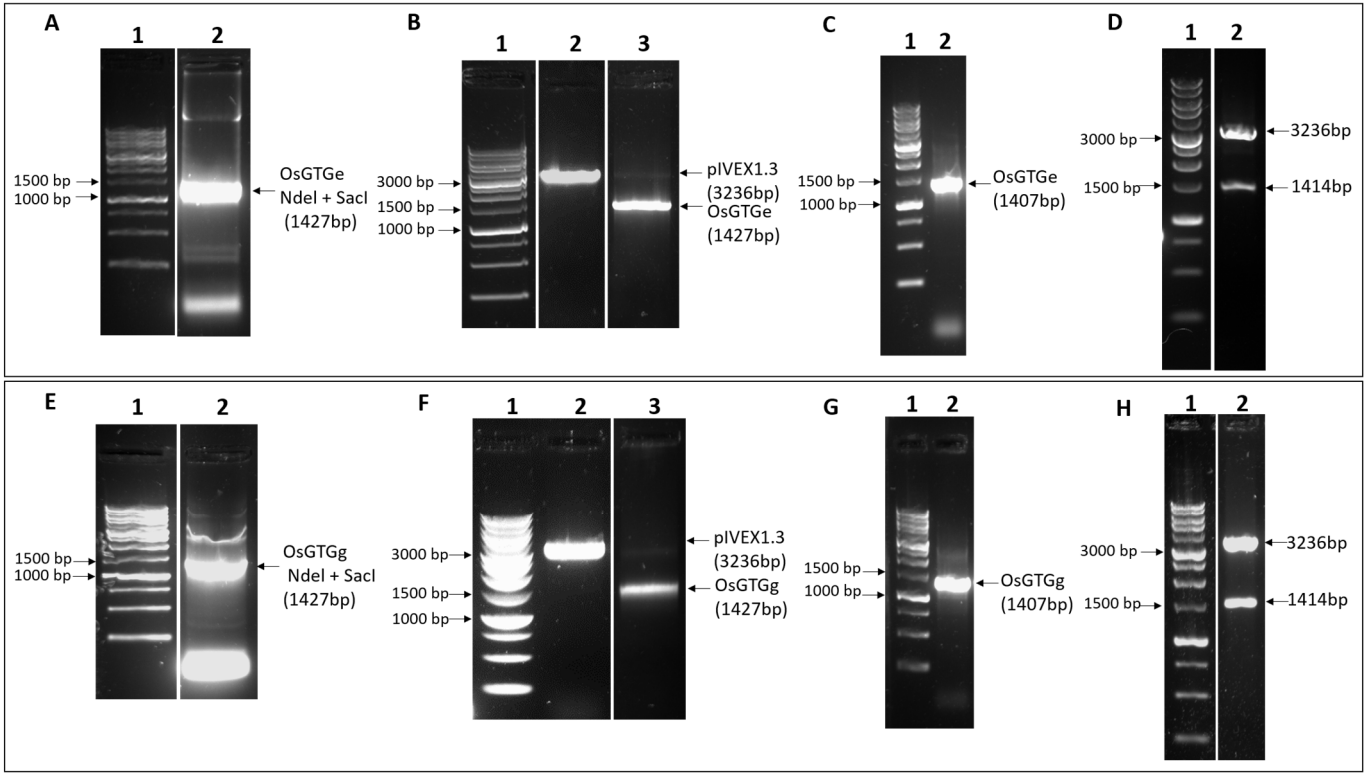

Figure 4.9. Cloning of *OsGTGe* and *OsGTGg* into the pIVEX1.3 expression vector

A) Amplification of *OsGTGe* (A) and *OsGTGg* (E) to add *Nde*I and *Sac*I restriction sites using OsGTGe *Nde*I + OsGTG *Sac*I NS primers (lane 2). Restriction digest of *OsGTGe* (B), *OsGTGg* (F) and pIVEX1.3 vector using *Nde*I and *Sac*I enzymes. Colony PCR of pIVEX1.3 *OsGTGe* (C) and pIVEX1.3 *OsGTGg* (G) using primers OsGTG topo F1 + OsGTG no stop R1 (lane 2). Restriction digest of pIVEX1.3 *OsGTGe* (D) and pIVEX1.3 *OsGTGg* (H) using enzyme *Nde*I and *Sac*I (lane 2). Predicted product sizes are on the right and molecular markers are on the left (lane 1).

Table 4.4. Plasmids generated for the cell-free expression of OsGTG to be used in the planar lipid bilayer assays

Plasmid	Description
pIVEX1.3 *OsGTGe*	T7::*OsGTGe*::His_6
pIVEX1.3 *OsGTGg*	T7::*OsGTGg*::His_6
pIVEX1.3 *RGA1*	T7::*RGA1*::His_6

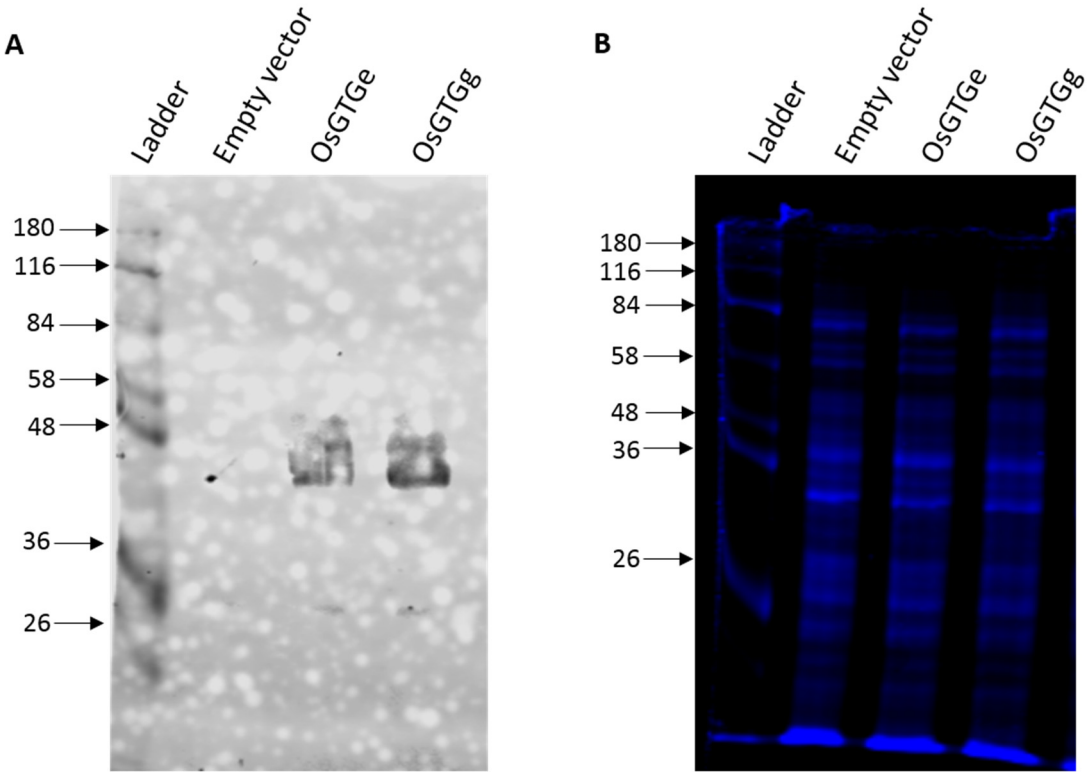

Figure 4.10. OsGTG protein expression using a cell-free protein synthesis system in the presence of DOPC

OsGTGe and OsGTGg expression was achieved using the wheat germ kit and products detected by western blotting (A) using a mouse anti-His as the primary antibody and fluorescent anti-mouse as the secondary antibody. The pIVEX1.3 empty vector was used as a negative control. Fluorescence detection of the second antibody was at 800 nm and detection of the ladder (on the left) was at 700 nm. Coomassie staining showing the total protein loaded in the SDS-PAGE gel (B).

4.2.2.3. OsGTG shows current activity in a planar lipid bilayer system

The planar lipid bilayer technique was used to test whether OsGTG can function as a channel. Both OsGTGs were expressed in the presence of the DOPC lipids and were inserted into the artificial membrane for current measurements. One Ag/AgCl electrode was inserted in each chamber and a symmetrical gradient using 100 mM KCl was applied in both chambers to study whether OsGTG was able to conduct current through the membrane. Current recordings were analysed at different voltages, from -100 mV to +100 mV. The recording patterns obtained when the pIVEX1.3 empty vector was added to one of the chambers are shown in Figure 4.11. No current was observed at any of the voltages applied, indicating that no component from the wheat germ lysate used for the synthesis of the proteins has the ability to generate current activity.

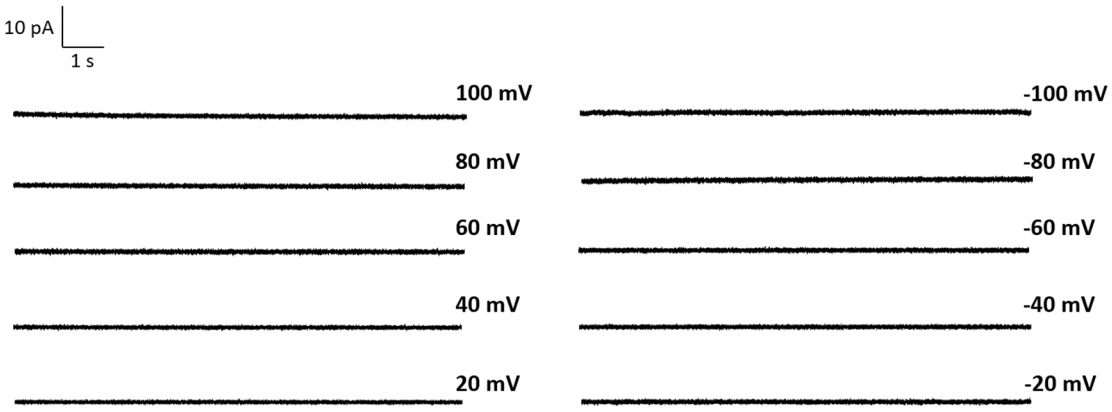

Figure 4.11. No current was observed when the negative control was added to the planar lipid bilayer in a KCl symmetrical gradient

Traces of the planar lipid bilayer recordings when the CFPS system containing the pIVEX1.3 empty vector was added in a POPC membrane in a 100 mM KCl symmetrical gradient. No current was seen at any of the voltages applied.

Recordings of the current at different voltages are shown for OsGTGe (Figure 4.12 A) and OsGTGg (Figure 4.13 A). Both OsGTGe and OsGTGg produced a square-wave pattern that represents the opening and closure of the channel and therefore indicates single-channel activity. These square patterns were observed at all the voltages applied.

Analysis of the current events generated I-V curves (Figure 4.12 B and Figure 4.13 B). Interestingly, the current activity produced from the two different OsGTG proteins increased to some extent as the voltage was increased. Similar ion conductance and maximum current were observed for both proteins. The conductance, that indicates how easily current passes through an electrical conductor, was 75 ± 0.04 pS for OsGTGe and 88 ± 0.12 pS for OsGTGg, whereas the maximum current observed for OsGTGe was -6 pA and +6.5 pA and -7.5 pA and +7 pA for OsGTGg. The linear regression for both I-V curves crossed through zero, which is the reversal potential for K^+ or Cl^- in the symmetrical gradient. This indicates that OsGTG functions as a channel moving ions across the membrane; however, it does not distinguish between the two types of ions, K^+ or Cl^- and so an asymmetrical gradient, with different KCl concentration in each chamber, was then tested.

In an asymmetrical gradient, where the *cis* chamber had 300 mM KCl, and the *trans* chamber had 100 mM KCl, a square-wave like pattern was observed when OsGTGe or OsGTGg were inserted into the membrane (Figure 4.14 A and Figure 4.15 A). The reversal potential was calculated using the Nernst equation (section 2.7.2). Under our experimental conditions, the calculated reversal potential for Cl^- would be +27 mV and the reversal potential of the K^+ would be -27 mV. The I-V curves shown in Figure 4.14 B and Figure 4.15 B were calculated using all the current events recorded at all the voltages applied for each protein. The best-fitting regression line crosses through +2 ± 1.3 mV for OsGTGe and through +1 ± 1.1 mV for OsGTGg. These differ from the calculated reversal potential for Cl^- (they are outside of the 99% confidence interval). Using the Goldman-Hodgkin-Katz equation, (section 2.7.2) the P_{Cl}/P_K permeability ratio calculated was 1.17 ± 0.12 for OsGTGe and 1.1 ± 0.11 for OsGTGg, indicating that both OsGTGs were more selective for Cl^- than K^+. The I-V curves obtained for OsGTGe and OsGTGg were very similar (Figure 4.16 A) (no significant differences, *t* test, $p = 0.91$), indicating that the amino acid difference does not significantly affect the activity of the channel.

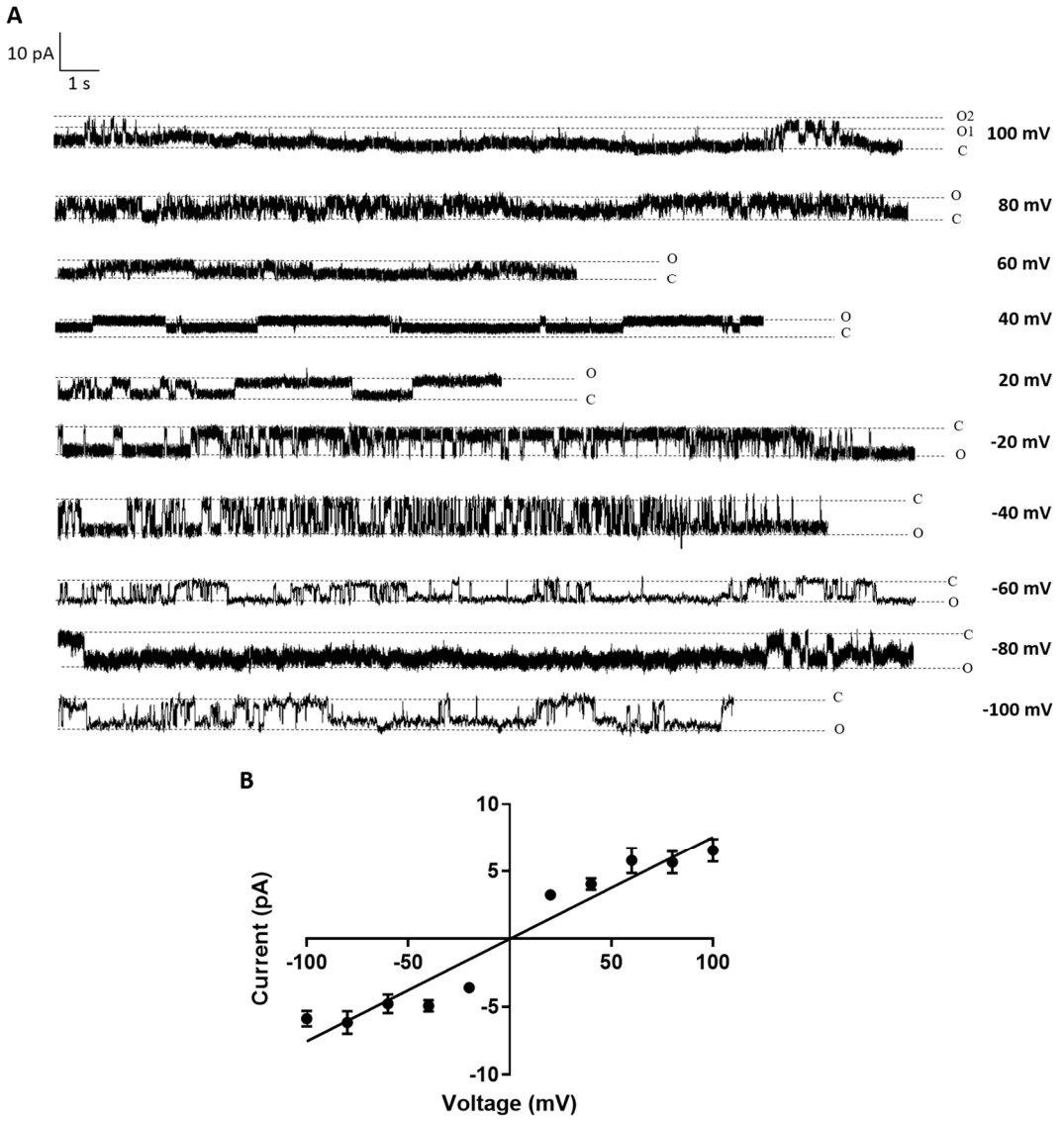

Figure 4.12. OsGTGe showed single-channel activity in a KCl symmetrical gradient

Planar lipid bilayer recordings of OsGTGe protein expressed in DOPC lipids and inserted into a POPC artificial membrane in a symmetrical gradient of 100 mM KCl. A) Representative traces showing OsGTGe ion activity at different voltages. B) I-V curve with the average current obtained at each voltage (±SEM) fitting a linear regression (R^2 = 0.934, $p < 0.0001$) (n per voltage = 7-20).

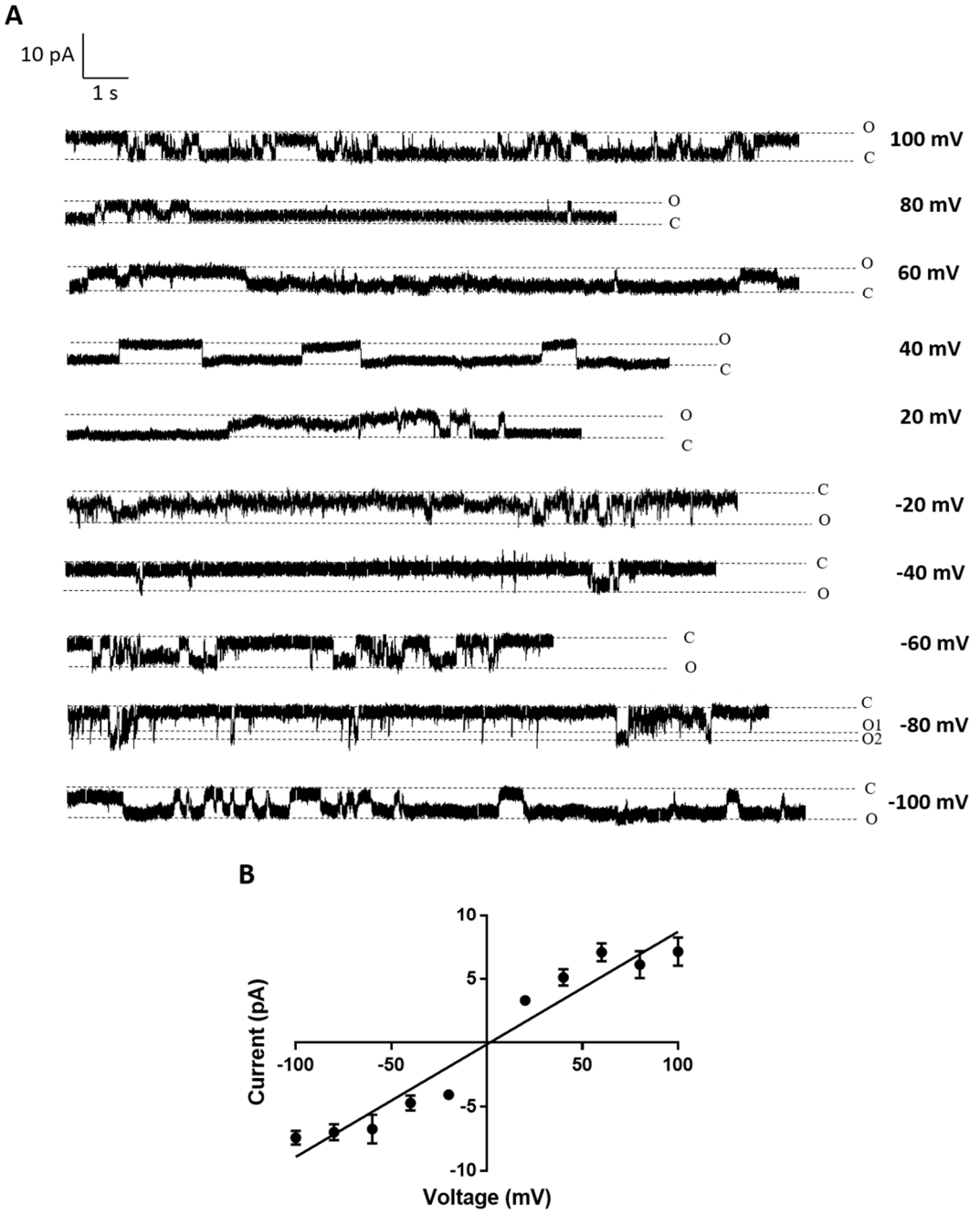

Figure 4.13. OsGTGg showed single-channel activity in a KCl symmetrical gradient

Planar lipid bilayer recordings of OsGTGg protein expressed in DOPC lipids and inserted into a POPC artificial membrane in a symmetrical gradient of 100 mM KCl. A) Representative traces showing OsGTGg ion activity at different voltages. B) I-V curve with the average current obtained at each voltage (±SEM) fitting a linear regression (R^2 = 0.938, $p < 0.0001$) (n per voltage = 4-24).

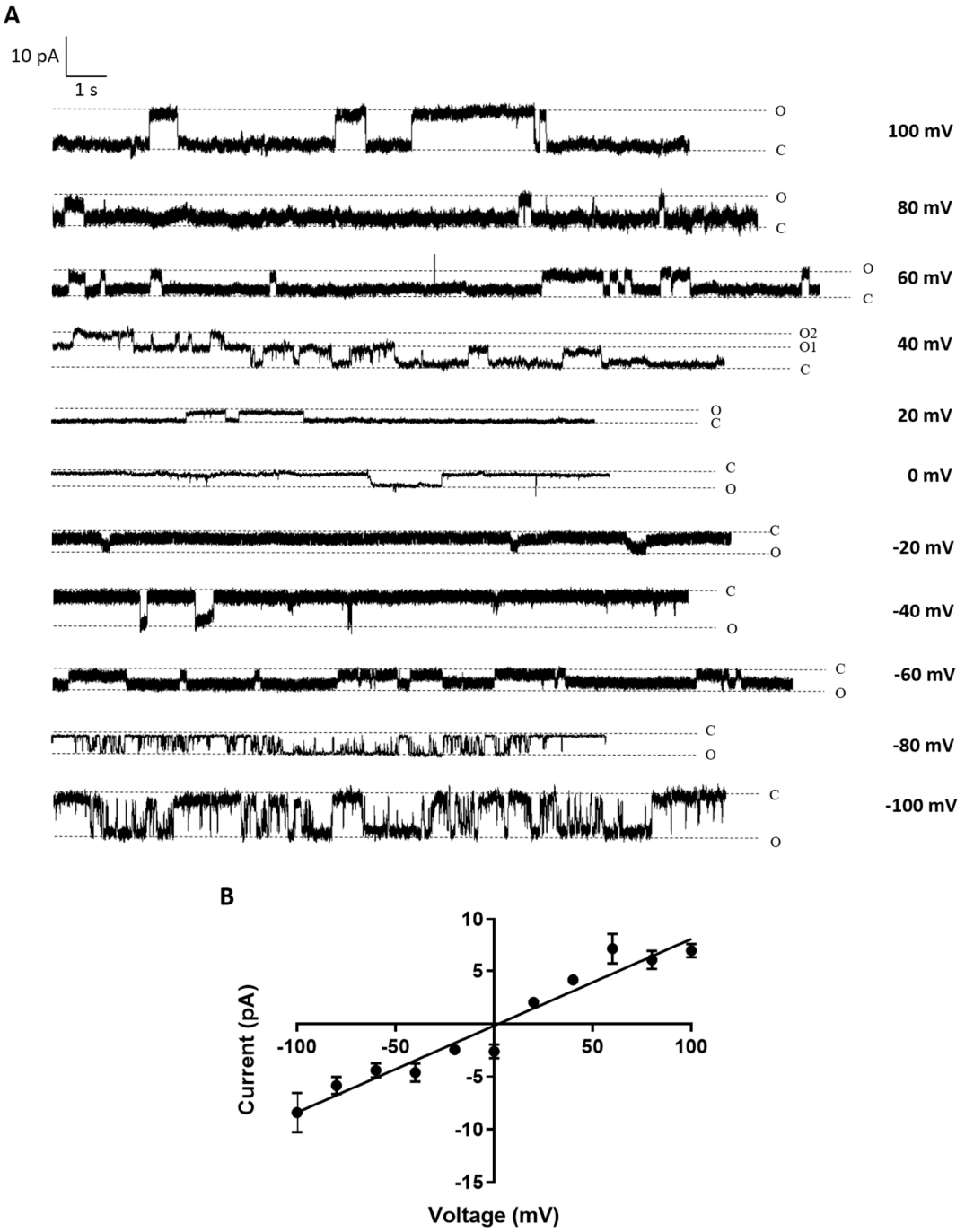

Figure 4.14. Single-channel activity of OsGTGe detected in the planar lipid bilayer in an asymmetrical gradient of KCl

Planar lipid bilayer recordings of OsGTGe protein expressed in DOPC lipid and inserted into a POPC artificial membrane in an asymmetrical gradient of 300/100 mM KCl. A) Representative traces showing OsGTGe ion activity at different voltages. B) I-V curve with the average current obtained at each voltage (±SEM) fitting a linear regression ($R^2 = 0.945$, $p < 0.0001$) (n per voltage = 4-12).

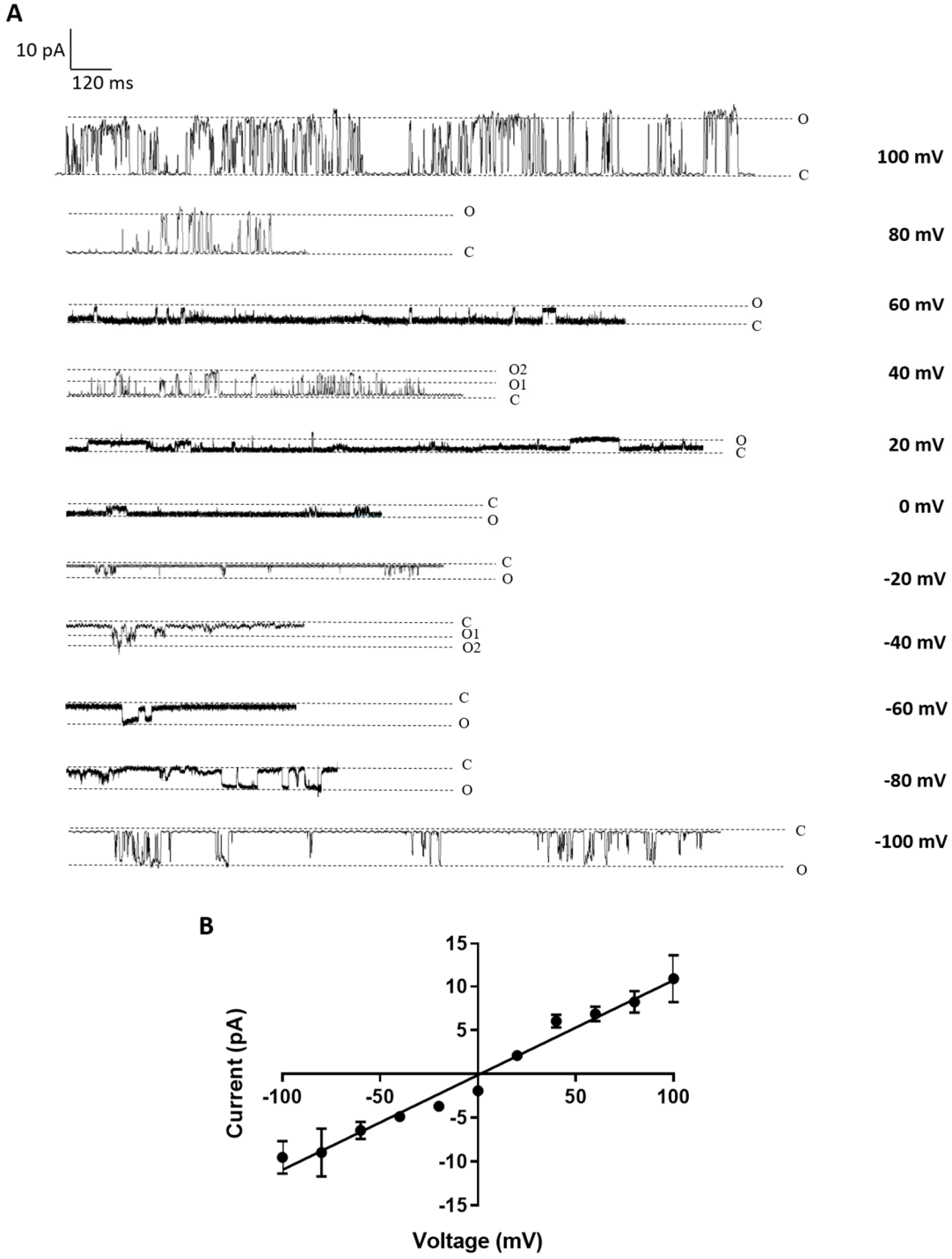

Figure 4.15. Single-channel activity of OsGTGg detected in the planar lipid bilayer in an asymmetrical gradient of KCl

Planar lipid bilayer recordings of OsGTGg protein expressed in DOPC lipid and inserted into a POPC artificial membrane in an asymmetrical gradient of 300/100 mM KCl. A) Representative traces showing OsGTGg ion activity at different voltages. B) I-V curve with the average current obtained at each voltage (±SEM) fitting a linear regression ($R^2 = 0.979$, $p < 0.0001$) (n per voltage = 3-11).

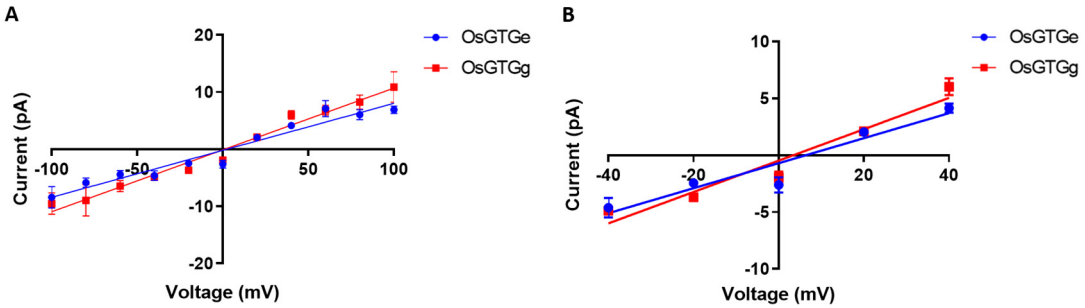

C

	OsGTGe	OsGTGg
Conductance -100mV to 100mV	82 ± 0.2 pS	108 ± 0.1 pS
Reversal potential -100mV to 100mV	2 mV	1 mV
Conductance -40mV to 40mV	110 ± 0.6 pS	138 ± 0.5 pS
Reversal potential -40mV to 40mV	6 mV	3 mV

Figure 4.16. Comparison of OsGTGe and OsGTGg current activity in KCl asymmetrical gradient

Single-channel activity of OsGTGe and OsGTGg expressed in DOPC and recorded in a POPC membrane using an asymmetrical gradient of 300/100 mM KCl. A) I-V curve with the average current (±SEM) obtained from -100 to 100 mV fitting a linear regression (R^2 = 0.945 for OsGTGe and R^2 = 0.979 for OsGTGg, $p < 0.0001$ for both) (no significant differences, *t* test, $p = 0.91$). B) Same data than A) with the average current (±SEM) obtained at voltages from -40 to +40 mV fitting a linear regression (R^2 = 0.914 for OsGTGe and R^2 = 0.944 for OsGTGg, $p < 0.05$ for both) (no significant differences, *t* test, $p = 0.93$). C) Table with the conductance and the reversal potential data obtained from I-V curves A and C.

The conductance obtained in the asymmetrical gradient was 82 ± 0.2 pS for OsGTGe and 108 ± 0.1 pS for OsGTGg. The maximum current observed was -8.5 pA and +7 pA for OsGTGe and -9.5 pA and +10.8 pA for OsGTGg. The conductance of the OsGTGe and OsGTGg seems saturated at higher voltages. To determine whether the reversal potential was affected by this saturation of the channel activity, a new I-V curve was plotted using the values obtained from voltages ranging from -40 mV to +40 mV. As seen in Figure 4.16 C, the conductance of both OsGTGs increased using lower

voltages only. OsGTGe conductance increased from 82 to 110 pS and OsGTGg from 108 to 138 pS. The reversal potential also increased slightly when the lower voltages were used. The OsGTGe reverse potential in this case was +6 ± 1.2 mV and for OsGTGg it was +3 ± 1.2 mV. Using the Goldman-Hodgkin-Katz equation it was calculated that the P_{Cl}/P_K permeability ratio was 1.61 ± 0.17 for OsGTGe and 1.26 ± 0.13 for OsGTGg. This indicates that OsGTG is more permeable to Cl^- than K^+ at lower voltages than at higher voltages.

4.2.2.4. OsGTGs do not transport calcium in the planar lipid bilayer system

An asymmetrical gradient assay was carried out using 300/100 mM $CaCl_2$ to determine whether OsGTG could function as a calcium channel instead of a Cl^- channel. In this case, 300 mM $CaCl_2$ was added in the *cis* chamber and 100 mM $CaCl_2$ in the *trans* chamber. OsGTGe and OsGTGg were added to the system and current activity was recorded at a voltage range from -100 mV to +100 mV (Figure 4.17 A-B). The regression line did not cross through the calculated reversal potential for the Cl^- ion, which was +27 mV, although it still crossed through the positive X-axis. The reversal potentials were +7 ± 1.1 mV for OsGTGe and +12 ± 1.4 mV for OsGTGg, indicating that calcium was not transported by OsGTG. Using the Goldman-Hodgkin-Katz equation the P_{Cl}/P_{Ca} permeability ratio calculated was 2.14 ± 0.25 for OsGTGe and 3.64 ± 0.56 for OsGTGg, indicating that both OsGTGs were more selective to Cl^- than Ca^{2+}. A similar conductance as before was obtained for both proteins, 85 ± 0.6 pS for OsGTGe and 90 ± 1.0 pS for OsGTGg. The maximum current value observed for OsGTGe was -8 pA and +8 pA and -9.8 pA and +6.4 pA for OsGTGg. As previously noted, the channel activity of OsGTGs was saturated at high voltage. For this reason, the I-V curve was produced with the lower voltages and the reversal potential was calculated from that graph. As shown in Figure 4.18, the reversal potential from -40 mV to +40 mV was +8 ± 0.9 mV for OsGTGe and +10 ± 1.2 mV for OsGTGg. The P_{Cl}/P_{Ca} permeability ratio was 2.38 ±0.22 for OsGTGe and 2.94 ± 0.37 for OsGTGg, indicating that both OsGTGs were more selective to Cl^- than Ca^{2+}. The conductance of the channel increased at lower voltages; OsGTGe conductance increased to 116 ± 0.95 pS and OsGTGg to 132 ± 1.3 pS (Figure 4.18 C).

To further confirm that OsGTG does not function as a calcium channel, a single-channel recording was carried out using equal values of calcium gluconate in each chamber. No current was observed when either of the OsGTGs were added in the

system (Figure 4.17 C-D). This indicates that OsGTG does not function as a calcium channel in this system.

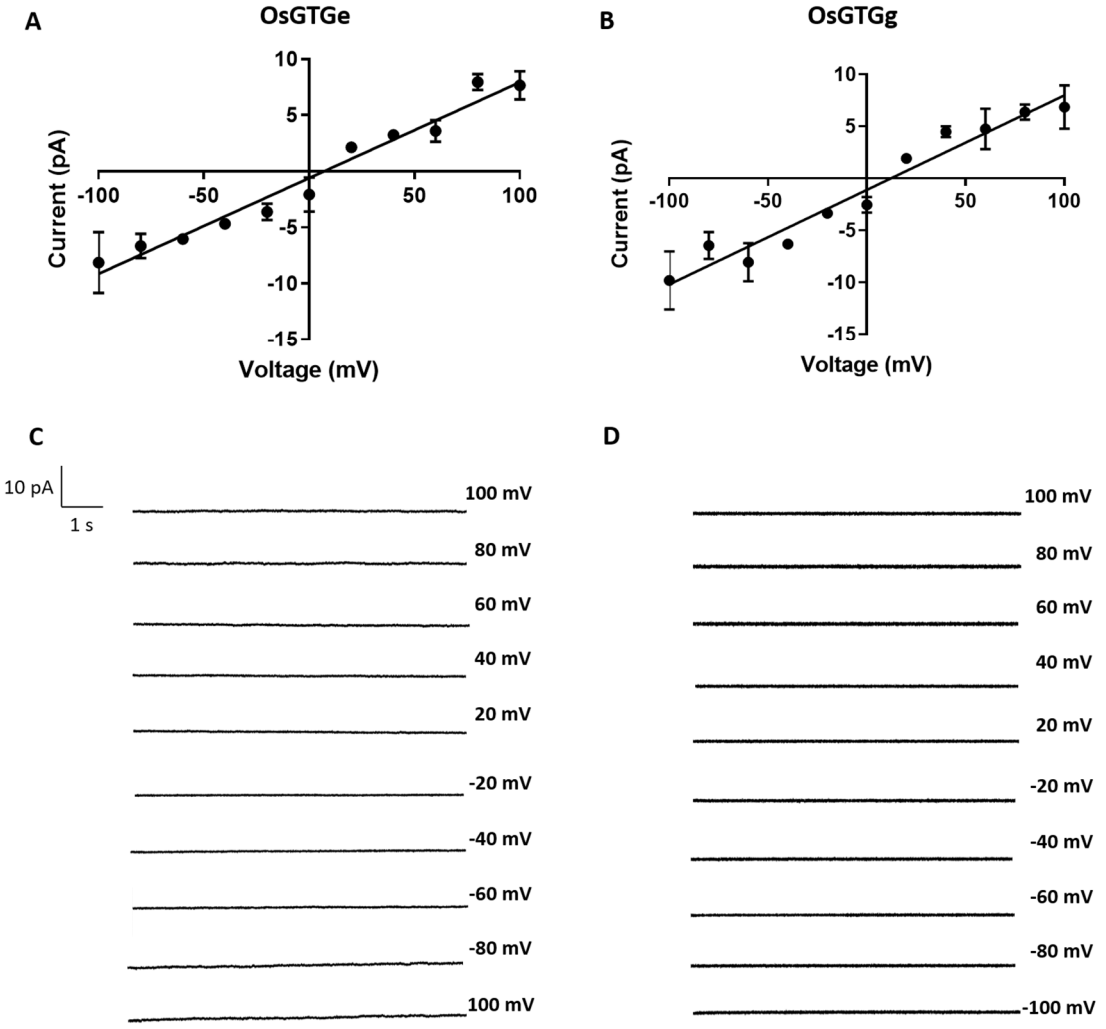

Figure 4.17. OsGTGe and OsGTGg do not transport calcium

Planar lipid bilayer results of OsGTGe and OsGTGg expressed in DOPC lipids and inserted into a POPC membrane in an asymmetrical gradient of 300/100 mM $CaCl_2$ and in 100 mM calcium gluconate. I-V curve with the average current (±SEM) obtained using 300/100 mM $CaCl_2$ with OsGTGe (A) and OsGTGg (B) fitting a linear (R^2 = 0.963 for OsGTGe and R^2 = 0.954 for OsGTGg, $p < 0.0001$ for both) (n per voltage = 3-9 for OsGTGe and 3-6 for OsGTGg). Representative traces showing no current activity at different voltages using 100 mM calcium gluconate when OsGTGe (C) or OsGTGg (D) were added.

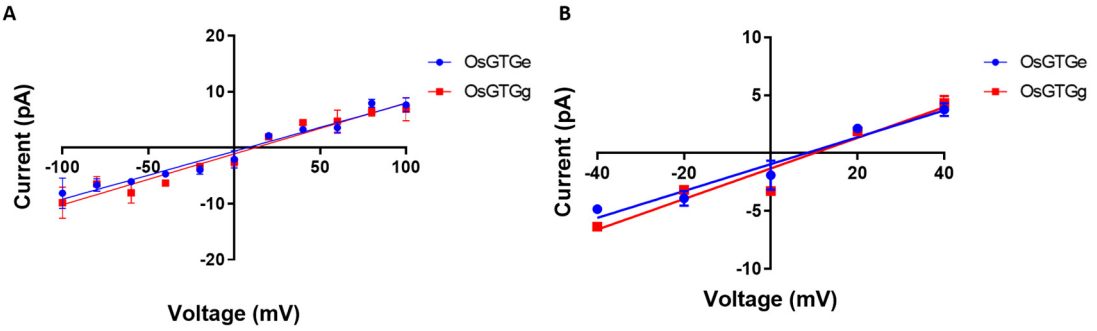

C

	OsGTGe	OsGTGg
Conductance -100mV to 100mV	85 ± 0.6 pS	90 ± 1.0 pS
Reversal potential -100mV to 100mV	7 mV	12 mV
Conductance -40mV to 40mV	116 ± 0.9 pS	132 ± 1.3 pS
Reversal potential -40mV to 40mV	8 mV	10 mV

Figure 4.18. Comparison of OsGTGe and OsGTGg current activity in $CaCl_2$ asymmetrical gradient

Single-channel activity of OsGTGe and OsGTGg expressed in DOPC and recorded in a POPC membrane using an asymmetrical gradient of 300/100 mM $CaCl_2$. I-V curve with the average current (±SEM) obtained from -100 to 100 mV fitting a linear regression ($R^2 = 0.963$ for OsGTGe and $R^2 = 0.954$ for OsGTGg, $p < 0.0001$ for both) in A) (no significant differences, *t* test, $p = 0.86$). B) Same data than in A), with the average current (±SEM) obtained from -40 to +40 mV fitting a linear regression ($R^2 = 0.956$ for OsGTGe and $R^2 = 0.934$ for OsGTGg, $p < 0.005$ for both) (no significant differences, *t* test, $p = 0.69$). C) Table with the conductance and the reversal potential data obtained from I-V curves A and C.

4.2.2.5. The anion blocker DIDS inhibits OsGTG channel activity

Since our previous data suggested that OsGTG does not function as a calcium channel, but in fact functions as an anion channel, a more in depth confirmation was required. DIDS (4,4'-Diisothiocyano-2,2'-stilbenedisulfonic acid) is a channel inhibitor that specifically blocks anion channels (Lyons et al., 1993, Takahashi et al., 2005). In an asymmetrical gradient of 300/100 mM of KCl, after current events were observed, DIDS was added into the *cis* chamber. The current activity of both OsGTGs was

inhibited after the addition of DIDS (Figure 4.19 A-B). A solvent control using DMSO confirmed that the absence of current was not due to the solvent (Figure 4.19 C-D). This is confirmation that OsGTG functions as an anion channel when is expressed in the planar lipid bilayer system.

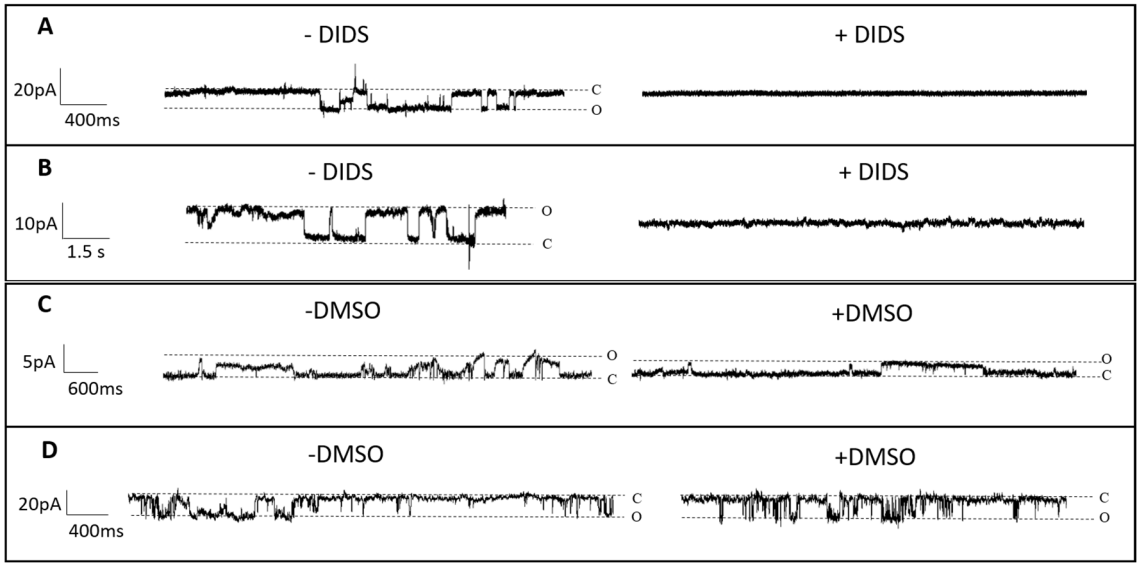

Figure 4.19. OsGTGe and OsGTGg channel activities are inhibited by anion blocker DIDS

DIDS was added when the current event was observed in a POPC planar lipid bilayer with OsGTGe and OsGTGg using an asymmetrical gradient of 300/100 mM KCl. Traces on the left show current activity with OsGTGe (A and C) or OsGTGg (B and D). In A and B) the traces on the right show the inhibition of the current activity after the addition of 20 μM of DIDS. In C and D) the traces on the right show current activity when DMSO was added.

4.2.2.6. OsGTG is more selective to chloride than other anions

The selectivity of the OsGTG channel was also studied using I^-, Br^- and NO_3^-. The I-V curves generated for each anion, supplied as a potassium salt, are shown in Figure 4.20. Both OsGTGs showed higher selectivity to Cl^- than the rest of the anions tested. The selectivity sequence detected for OsGTGe and OsGTGg was $Cl^- > I^- > Br^- > NO_3^-$. The reversal potential of all the anions was shifted to the right, indicating less permeability. The conductance obtained in the presence of Cl^- was 82 pS for OsGTGe

and 108 pS for OsGTGg, however the conductance observed for the rest of the anions was between 33 pS to 56 pS for both OsGTGs. This indicates that both OsGTGs are more selective to Cl^- than I^-, Br^- and NO_3^-. The conductance and reversal potential data for each ion are shown in Table 4.5.

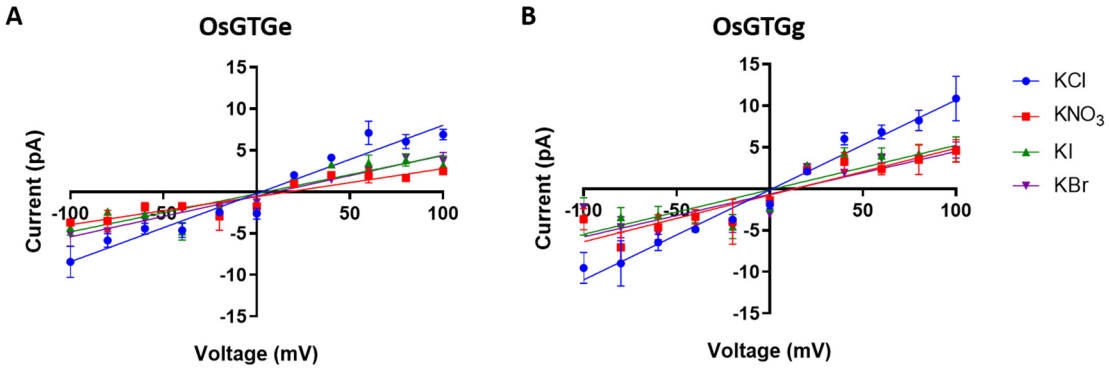

Figure 4.20. OsGTGe and OsGTGg are more selective to chloride than to other anions tested

OsGTGe (A) and OsGTGg (B) expressed in DOPC were inserted into a POPC membrane and single-channel activity was analysed using KCl, KNO_3, KI and KBr solutions. I-V curves with the current average (±SEM) obtained at each voltage fitting a linear regression for OsGTGe in A) (R^2 = 0.945 for KCl, 0.835 for KI, 0.976 for KBr, 0.863 for KNO_3, $p < 0.0001$ for all) and for OsGTGg in B) (R^2 = 0.979 for KCl, 0.770 for KI, 0.755 for KBr, 0.860 for KNO_3, $p < 0.0005$ for all), or a non-linear regression in B) and D) (n per voltage for OsGTGe = 4-12 for KCl, 3-9 for KI, 3-6 for KBr, 3-6 for KNO_3 and for OsGTGg = 3-11 for KCl, 3-7 for KI, 3-5 for KBr, 3-7 for KNO_3).

4.2.2.7. OsGTGe activity did not increase in the presence of RGA1

Ma et al. (2015) proposed that the rice Gα subunit can induce OsGTG channel activity. This was observed in an electrophysiology assay carried out in *Xenopus* oocytes where the current activity detected when both proteins were co-expressed was higher than when OsGTG was expressed alone (Ma et al., 2015). To assess this effect, the Gα subunit (RGA1) was also included with OsGTG in the planar lipid bilayer assay. *RGA1* from Nipponbare was amplified and cloned into pIVEX1.3 vector and was added

in the cell-free wheat germ kit where the protein was synthesised. As RGA1 is a soluble protein that does not need to be inserted in a membrane, no DOPC lipids were added into the synthesis of the protein. After the synthesis of the protein was confirmed, OsGTGe and RGA1 were added sequentially into a POPC artificial membrane for a single-channel activity assay.

Using an asymmetrical gradient of KCl as previously, currents were recorded when RGA1 was present. As shown in Figure 4.21 A, the average current at +80 mV when OsGTGe was inserted in the membrane was around 5 pA. However, when RGA1 was added to the chamber in the presence of OsGTGe, the current activity observed was around 3 pA. This indicates that RGA1 did not activate OsGTGe. More recordings need to be carried out at different voltages to further confirm this result. The fact that the current observed when both proteins were together was lower than the current recorded when only OsGTGe was present could be due to instability when two proteins are present at the same time in this system or due to an inhibitory effect of RGA1.

To test whether the presence of RGA1 can activate OsGTGe as a calcium channel, recordings were carried out using calcium gluconate as a buffer. No current activity was observed at any of the voltages (Figure 4.21 B). This indicates that the presence of RGA1 does not activate the movement of calcium across the membrane, suggesting that OsGTGe in the presence of RGA1 does not function as a calcium channel.

Table 4.5. Conductance and reversal potential of OsGTGe and OsGTGg in the presence of different anions

		KCl	**KI**	**KBr**	**KNO_3**
Conductance	OsGTGe	82 ± 0.2 pS	46 ± 0.2 pS	45 ± 0.4 pS	33 ± 0.5 pS
	OsGTGg	108 ± 0.1 pS	53 ± 0.1 pS	51 ± 0.6 pS	56 ± 0.7 pS
Reversal potential	OsGTGe	+2.2 mV	+4.5 mV	+6.8 mV	+16.65 mV
	OsGTGg	+1 mV	+1.9 mV	+12.2 mV	+12.9 mV

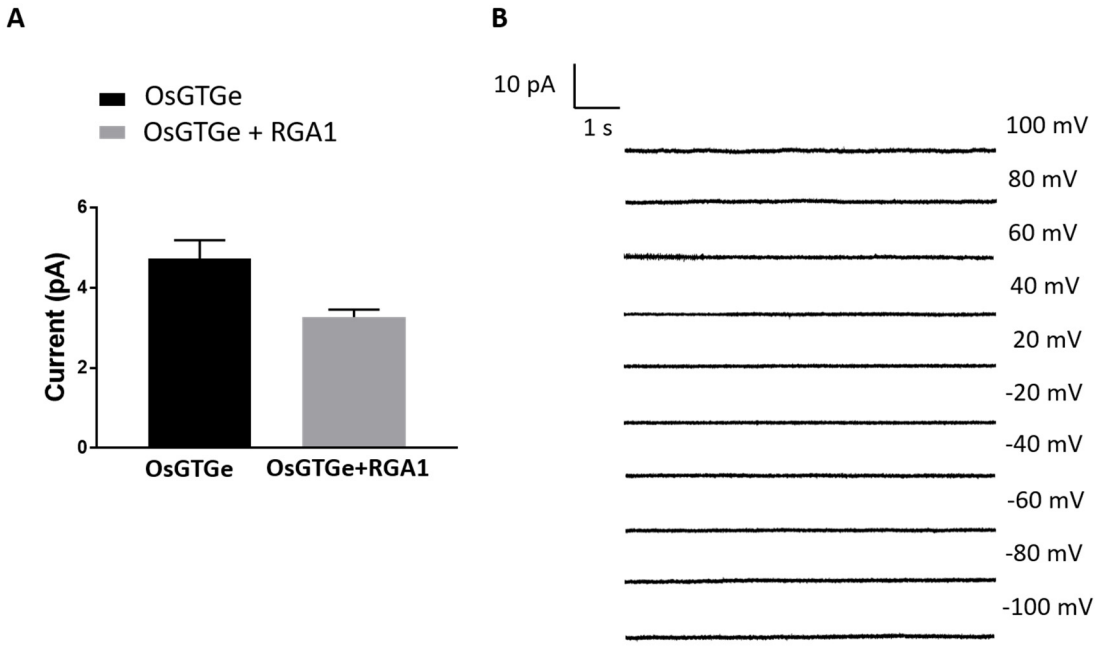

Figure 4.21. RGA1 does not induce the activity of OsGTGe

Planar lipid bilayer assays using OsGTGe and RGA1 in a POPC membrane. A) Average current activity (±SEM) recorded at 80 mV with OsGTGe or OsGTGe with RGA1 in an asymmetrical gradient of 300/100 mM KCl (n=13). Significant difference, *t* test, $p < 0.005$. B) Representative traces showing no current when OsGTGe and RGA1 were added in a 100 mM calcium gluconate solution.

4.2.3. OsGTG can regulate endomembrane pH in Arabidopsis cells

As described previously, GTG regulates Golgi pH in mammalian cells (Maeda et al., 2008). Stable Arabidopsis WT and *gtg1gtg2* mutant lines expressing the pH sensor pHluorin were generated in our laboratory and pH measurements were carried out. This pHluorin was targeted to different intracellular compartments by the use of different organelle signal peptide tags. pHluorin was tagged with the signal peptide HDEL for ER, with mannosidase I enzyme ManI for *cis* Golgi and with a plant vacuolar sorting receptor BP80 for *trans* Golgi localisation (Gomord et al., 1997, Nebenführ et al., 1999, Li et al., 2002). Prior to measuring and comparing pH values in the different lines, the confocal microscope was calibrated by using purified pHluorin. A calibration curve showing the ratio of fluorescence intensity at 500-550 nm after excitation with lasers at

405 and 488 nm was calculated for each buffer pH and is shown in Figure 4.22. A Boltzmann curve was used to fit the values, and a Boltzmann equation (section 2.8) was used to consequently calculate the pH for the rest of the Arabidopsis lines.

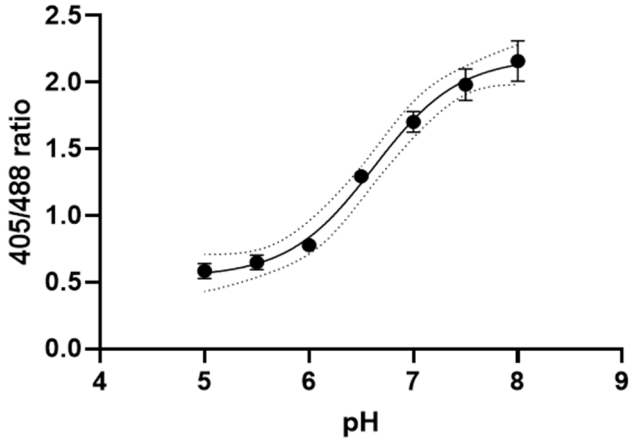

Figure 4.22. pHluorin calibration curve

Confocal images of fluorescence after excitation at 405 and 488 nm of pure pHluorin at different pH values ranging from 5 to 8 were taken. The 405/488 ratio was plotted against pH (n=5) and a Boltzmann curve was used to fit the values. The values obtained for the curve ($Y = Bottom + \frac{Top-Bottom}{(1+10^{((LogIC50-X)\cdot HillSlope)})}$) were: 2.186 for *Top*, 0.5393 for *Bottom*, 6.621 for *LogIC50* and 1.062 for *Hillslope*.

The *gtg1gtg2* mutant plants expressing HDEL or ManI pHluorin pH sensors were transformed with pMDC32 *OsGTGe* and pMDC32 *OsGTGg* to study whether OsGTG is involved in Arabidopsis pH homeostasis. OsGTG was not expressed in *gtg1gtg2* plants expressing BP80 pHluorin. The lines generated for this study are shown in Table 4.6. Unfortunately, gene silencing was observed in some of the lines and as a result there was no signal of the pH sensor after the second generation. This has been previously observed in our laboratory when proteins were expressed in the double mutant. In this instance the *gtg1gtg2* ManI pHluorin sensor lines expressing OsGTGe showed no fluorescence signal in the second or third generation. In addition, second generation lines were also used for *gtg1gtg2* HDEL pHluorin lines expressing OsGTGe.

Homozygous plants were obtained for the rest of the lines and confocal imaging was carried out for pH analysis. Images of the different Arabidopsis lines that contain the HDEL (ER) pHluorin and ManI pHluorin were taken in the confocal microscope after excitations at 405 and 488 nm with 500-550 nm emission for both lasers (Figure 4.23). Analyses of those images were carried out to obtain the 405/488 intensity ratio of each cell (for ER pH measurement) or each foci (for Golgi pH measurement). Using the Boltzmann equation obtained from the calibration curve, the organelle pH was calculated for each line and organelle. The expression of *OsGTG* was also analysed with the lines containing the pHluorin tagged with HDEL and ManI. RT-PCR was performed in those lines and it was shown that *OsGTG* was expressed in all the lines that were transformed either with *OsGTGe* and *OsGTGg* (Figure 4.24). *ACTIN* expression was analysed as a control.

Table 4.6. List of transgenic plants co-expressing the different organelle pH sensors with the OsGTGs

Arabidopsis background	**Gene inserted**	**Organelle pH sensor**	**T2 lines with signal**	**T3 homozygous lines with signal**
gtg1gtg2 Ws2	*OsGTGe*	ManI (*cis* Golgi)	-	-
gtg1gtg2 Ws2	*OsGTGg*	ManI (*cis* Golgi)	6	4
gtg1gtg2 Ws2	*OsGTGe*	HDEL (ER)	2	1
gtg1gtg2 Ws2	*OsGTGg*	HDEL (ER)	7	4

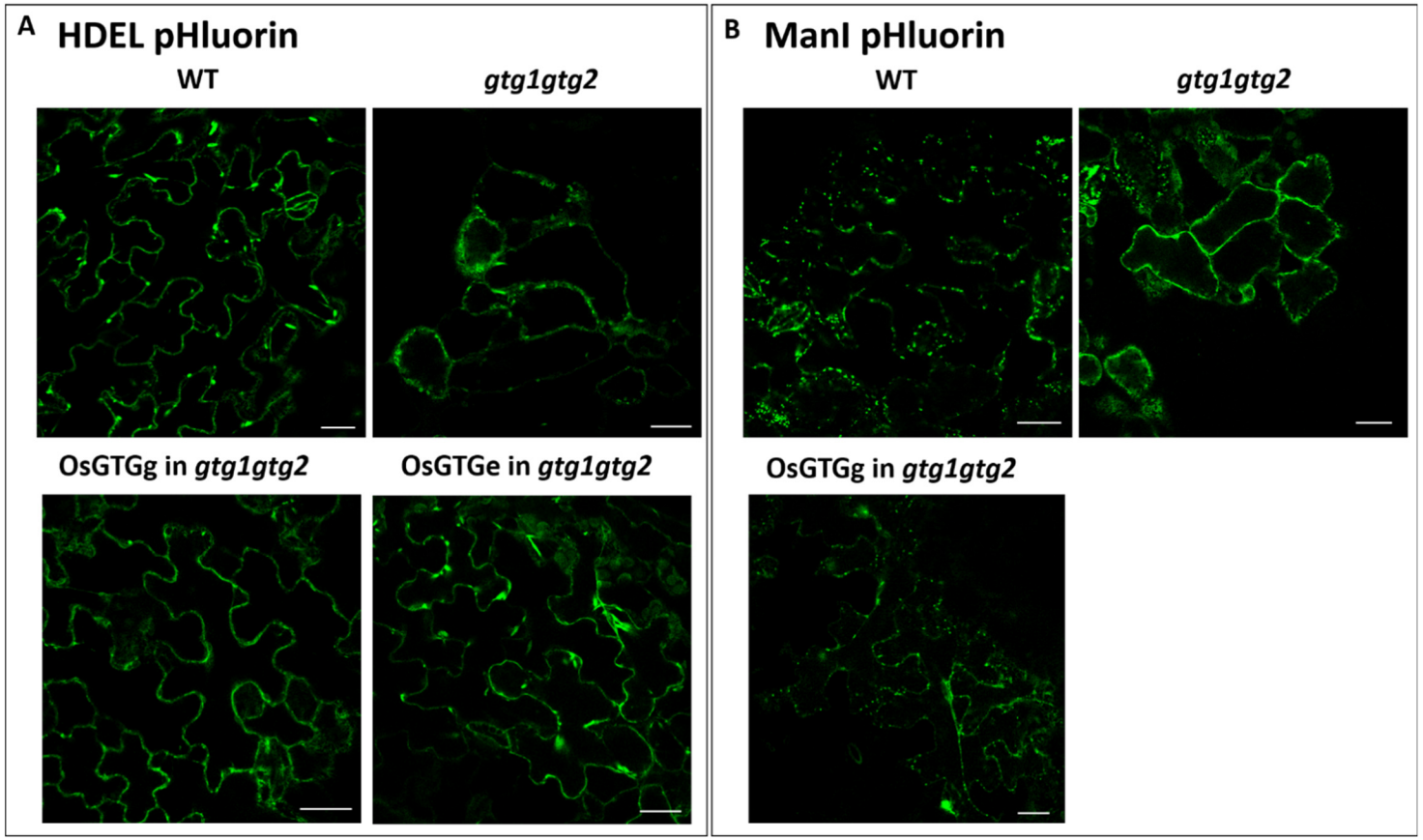

Figure 4.23. Localisation of the ER and *cis* Golgi pH sensors in Arabidopsis plants

Confocal microscopy images showing the localisation of the pHluorin pH sensor lines in different Arabidopsis lines. Representative images of HDEL pHluorin sensor expressed in WT, *gtg1gtg2*, and *gtg1gtg2* expressing OsGTGg and OsGTGe lines (A) and ManI pHluorin sensor expressed in WT, *gtg1gtg2*, and *gtg1gtg2* expressing OsGTGg lines (B). Scale bar 25 µm. Three independent lines per each transgenic were analysed and imaged twice.

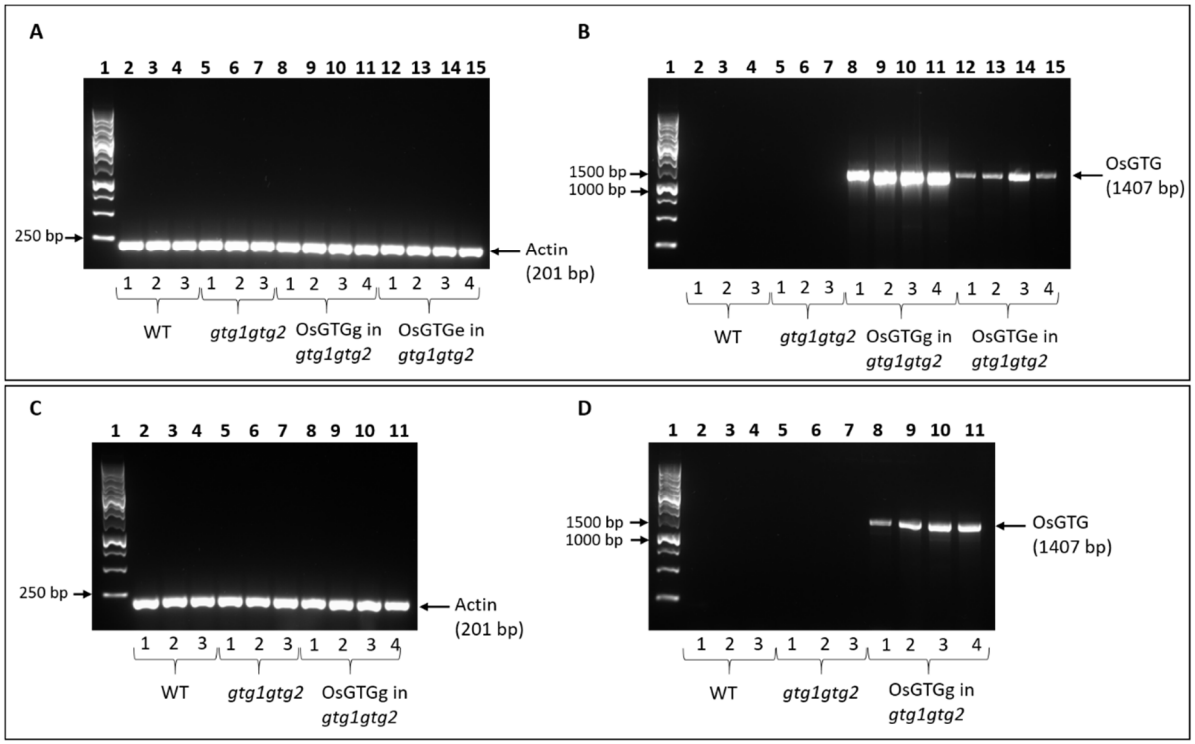

Figure 4.24. Expression of *OsGTGe* and *OsGTGg* in the *gtg1gtg2* mutant containing pHluorin tagged with HDEL and ManI

RT-PCR using RNA extracted from pHluorin tagged with HDEL (top) and ManI (bottom) lines. On the left, Actin F and Actin R (predicted 201 bp) primers were used and on the right, OsGTG topo F1 and OsGTG stop R1 (predicted 1407 bp) primers. A and B) HDEL pHluorin lines in WT (lanes 2-4), *gtg1gtg2* (lanes 5-7), *gtg1gtg2* expressing *OsGTGg* lines (lanes 8-11) and *gtg1gtg2* expressing *OsGTGe* lines (lanes 12-15). C and D) ManI pHluorin lines in WT (lane 2-4), *gtg1gtg2* (lane 5-7), *gtg1gtg2* expressing *OsGTGg* lines (lanes 8-11). Predicted products are shown on the right and molecular markers are shown on the left (lane 1).

The pH value for the ER in the WT background was 7.26 ± 0.04, but was slightly higher for the *gtg1gtg2* mutant with a pH of 7.38 ± 0.03 (Table 4.7 and Figure 4.25). The *gtg1gtg2* lines that expressed OsGTGe and OsGTGg exhibited a pH value of 7.19 ± 0.01 and 7.21 ± 0.02 respectively in the ER, which indicates a restoration to WT pH levels when OsGTG is expressed. The *cis* Golgi pH for WT cells was 6.74 ± 0.02 whereas for *gtg1gtg2 cis* Golgi pH was slightly higher, 6.81 ± 0.02. Again, the expression of OsGTGg rescued pH levels, reaching 6.72 ± 0.01 in the *cis* Golgi of the transgenic lines. Similar pH values were found in the *trans* Golgi of WT (6.36 ± 0.02) and *gtg1gtg2* mutant (6.37 ± 0.01). Statistical analysis showed that there were significant differences between the pH of the ER and *cis* Golgi in the *gtg1gtg2* lines in comparison to the pH obtained in those organelles for WT and *gtg1gtg2* expressing OsGTG lines. This indicates that OsGTG is capable of regulating endomembrane pH in a similar manner to HsGPHR and AtGTG1. Besides confirming the conservation of function of GTG between species, these results also suggest that the physiological function of GTG in plants is to fine-tune the pH in ER and Golgi organelles.

Table 4.7. ER and *cis* Golgi pH values for WT, *gtg1gtg2* and *gtg1gtg2* expressing OsGTG

Organelle	**WT pH**	***gtg1gtg2* pH**	**OsGTGe in *gtg1gtg2* pH**	**OsGTGg in *gtg1gtg2* pH**
ER	7.26 ± 0.04	7.38 ± 0.03 *	7.19 ± 0.01	7.21 ± 0.02
cis Golgi	6.74 ± 0.02	6.81 ± 0.02 *	-	6.72 ± 0.01
trans Golgi	6.36 ± 0.02	6.37 ± 0.01	-	-

* significant differences between the pH of the *gtg1gtg2* double mutant in comparison to WT and *gtg1gtg2* lines expressing OsGTGe and OsGTGg. The significant differences are seen in the ER and the *cis* Golgi (n = 45-90). One-way ANOVA; ($p < 0.0001$).

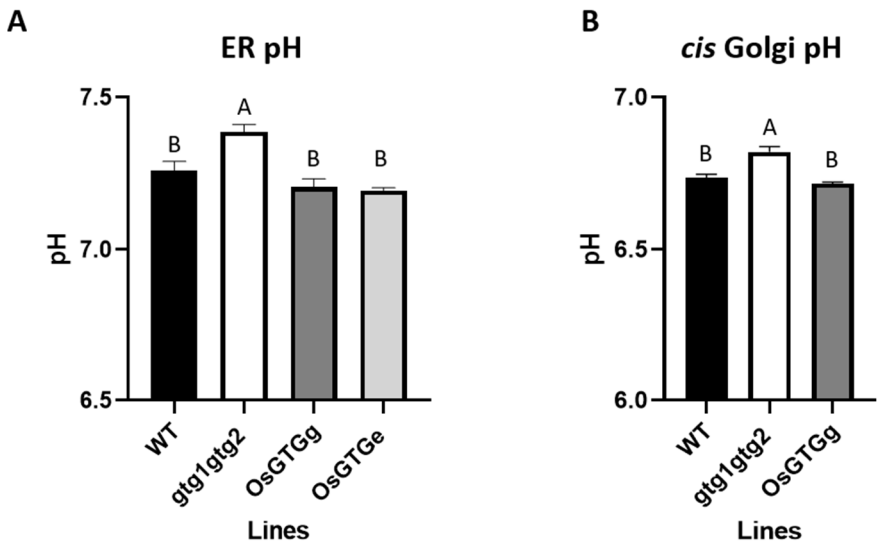

Figure 4.25. The Arabidopsis *gtg1gtg2* mutant exhibited a higher pH at the ER and at the *cis* Golgi and this was restored by the expression of OsGTG

Graphical representation of same data from Table 4.7 showing the ER and *cis* Golgi pH obtained for WT, *gtg1gtg2*, *gtg1gtg2* expressing OsGTGe and *gtg1gtg2* expressing OsGTGg plants. A) ER pH values obtained using the HDEL pHluorin pH sensor lines. B) *cis* Golgi pH values obtained using the ManI pHluorin pH sensor lines. The data represent the mean (±SEM) of three seedlings per independent line with 5-10 cells per seedling (n = 45-90). One-way ANOVA; ($p < 0.0001$). Tukey *post-hoc* test where means not sharing a letter are significantly different ($p < 0.0001$ between *gtg1gtg2* and the rest of the lines).

4.3. Discussion

4.3.1. OsGTG functions as an anion channel

In mammalian cells it has been demonstrated that GTG/GPHR functions as an anion channel that regulates endomembrane pH (Maeda et al., 2008). In our laboratory it has been shown that the function of GTG is conserved between species and that AtGTG1 and CeGTG1 also function as anion channels regulating endomembrane pH (Adam, Terry, Williams, unpublished; Dorey, 2019). In this study, OsGTG was tested to see whether this protein could have the same function as the Arabidopsis homologue.

To study this, a planar lipid bilayer technique was used. With this technique, a single-channel activity can be measured, allowing the study of membrane proteins that do not localise at the plasma membrane and also allowing the study of different properties of a channel (Zakharian, 2013). To do so, a purified protein is required, which was obtained through a cell-free system. Protein expression and purification systems have been well-established and widely used. In those systems an organism, most commonly *E.coli*, is used to produce high amounts of the protein of interest followed by a purification approach. This conventional method of obtaining proteins is costly, time-consuming and requires certain laboratory equipment to produce high protein yields to account for the loss of protein throughout the process (Wingfield, 2015). Cell-free systems on the other hand, allow the production of proteins in a short time and with less laboratory equipment. These systems allow the expression of proteins that are toxic to living cells or that are difficult to express and purify in other organisms, such as membrane proteins. In this study, a commercially available cell-free system kit from wheat germ lysate was used for the expression of OsGTGs. DOPC lipids were added to the cell-free system to improve protein folding (Zemella et al., 2015). The production of proteins in lipids using a commercial cell-free system kit has been previously tested using the well-characterized K^+ channel KcsA, which could be expressed as a functional protein when it was inserted into a planar lipid bilayer system (Friddin et al., 2013). Different lipids have been used successfully in the production of different proteins, such as DOPC, 1,2-di-dimyristoyl-sn-glycero-3-phosphocholine (DMPC) and soybean lipids (Kalmbach et al., 2007, Goren and Fox, 2008, Nomura et al., 2008). DOPC has been successfully tested previously for the characterization of AtGTG1 in the planar lipid bilayer system (Dorey, 2019) and for this reason, in this study, DOPC was selected and added to the cell-free reaction for OsGTG synthesis.

After the protein was synthesized, an electrophysiological assay in a planar lipid bilayer was carried out. In this technique an artificial membrane is created in a small aperture that separates two chambers. OsGTG was inserted into the membrane and the current was recorded by the electrodes that are inserted into the chambers. In previous work with AtGTG1, POPC and different percentages of PC asolectin were used for the creation of the artificial membrane. Stable membranes were formed with POPC and 95% PC asolectin. However, the activity of the channel seemed to hold longer in the POPC membranes (Dorey, 2019). Thus, in this study, POPC lipids were also used for artificial membrane formation.

Once it was confirmed that no components of the wheat germ lysate were able to produce current (Figure 4.11), OsGTGe and OsGTGg were characterized and single-channel currents were observed when the proteins were inserted into the system in a symmetrical gradient of KCl. A similar conductance was obtained for both proteins, 75 pS for OsGTGe and 88 pS for OsGTGg. Apart from the similar conductance values, it can also be observed that both OsGTGs showed a similar I-V curve pattern. An increase of current with changes in voltages was observed for both OsGTGs (Figure 4.12 and Figure 4.13). This indicates that both proteins can function as a channel in a similar manner, suggesting that the difference in the 9th amino acid residue does not affect the function of the protein.

To decipher which ion was being transported by OsGTG, an asymmetrical gradient of KCl was applied and showed that both OsGTGs were more selective to Cl^- than K^+. On average OsGTG was 1.14 times more selective to Cl^- than to K^+. The conductance obtained for both proteins was similar to the conductance obtained previously for the symmetrical gradient, which was 82 pS for OsGTGe and 108 pS for OsGTGg. The conductance observed for OsGTG has been seen in other Cl^- channels in plants. The chloroplast Cl^- channel VCCN1 that is involved in the proton motive force across the thylakoid membrane, exhibited a conductance of 96 pS at positive voltages and 60 pS at negative voltages with a maximum current of 11 pA and -8 pA at positive and negative voltages, respectively (Herdean et al., 2016b). Nevertheless, the conductance obtained for OsGTGs was lower than the conductance obtained for AtGTG1, that was 136 pS, and much smaller than the conductance for CeGTG1 and HsGPHR that was 200 pS and 400 pS respectively (Maeda et al., 2008, Dorey, 2019). Although AtGTG1 and OsGTG show similar intracellular localisation (Jaffé et al., 2012) and the function between these two homologous proteins seems to be conserved, the sequence similarity between them

is 80%, suggesting that there are some amino acid differences that could affect the channel properties. Several of these amino acid differences are concentrated in the big loop present in the protein between the 5^{th} and 6^{th} transmembrane domain. Although the structure of the protein has not been deciphered yet, this big loop could potentially form the channel pore and therefore those amino acid differences between AtGTG1 and OsGTG could affect the capacity of ion transport through the channel.

In the case of AtGTG1 and OsGTG characterization, the experimental conditions were similar. However, in the case of HsGPHR, there were several experimental differences. Instead of a C-terminal His_6 tag, the GPHR protein was tagged with FHAT, a Flag-HAT tandem that is a longer tag (Maeda et al., 2008). Additionally, HsGPHR was expressed and purified through Sf9 insect cells and the protein was reconstituted into liposomes using egg phosphatidylcholine and bovine brain phosphatidylserine, and the lipids used for the artificial membrane were from soybean lecithin (Maeda et al., 2008). All those differences can improve the integration of more proteins into the artificial membrane producing the increase of conductance and current observed for HsGPHR.

In the asymmetrical gradient, the reverse potential of OsGTGe and OsGTGg was +2 ± 1.3 mV and +1 ± 1.1 mV respectively when the data for higher voltages were included. However, the reversal potential shifted to +6 ± 1.2 mV and +3 mV ± 1.2 respectively when lower voltages were used. Nevertheless, these values are within the 99% confidence interval of the reversal potentials obtained for OsGTGs with the higher voltages included. However the reversal potential obtained is close to zero and far from the theoretical reverse potential for Cl^- in those conditions, which is +27 mV. The fact that the reversal potential is different from the theoretical could be due to the fact that another ion is transported in the opposite direction. However, the P_{Cl}/P_K permeability ratio indicates that OsGTG is more permeable to Cl^- than K^+. It is not uncommon that the calculated reversal potential differs from the measured one. In other Cl^- channels like GOLAC-1 and GOLAC-2, the calculated reverse potential differs from the obtained one by 48 mV and 32 mV, respectively (Nordeen et al., 2000, Thompson et al., 2002). However, in both cases the reversal potential obtained was positive and the permeability of the channels to Cl^- was higher than to K^+ (Nordeen et al., 2000, Thompson et al., 2002). For GOLAC-1 the permeability to Cl^- was even higher than to Na^+ (Nordeen et al., 2000). This was similar to OsGTG, where the permeability to Cl^- was higher than to K^+ but it was even higher than to Ca^{2+}. This difference in reversal potential is also

observed in some endomembrane ClC channels that function as H^+/Cl^- antiporters, such as the mammalian endosomal voltage-dependent Cl^-/H^+ exchangers, ClC4 and ClC5 (Scheel et al., 2005). Additionally, the *E.coli* ClC channel, which functions as a H^+/Cl^- antiporter also showed a difference of 15 mV between the expected and the obtained reversal potential (Accardi and Miller, 2004). Therefore, the possibility that OsGTG could function as an antiporter cannot be discarded.

Nevertheless, the confirmation that OsGTG functions as an anion channel came from the fact that OsGTG activity was inhibited by DIDS (Figure 4.19). DIDS specifically blocks anion channels, and the inhibition depends on the sulfonate groups present in the molecule. These groups have a strong negative charge and are attracted to the highly positive residues that are usually present in the pore of anion channels (Nordeen et al., 2000). It has been shown that DIDS can alkylate lysine and thiol residues (Lu and Boron, 2007, Benítez-Rangel et al., 2015). OsGTG has four lysine residues in the large loop of the protein, between the 206-209th amino acid. This loop could form part of the potential pore of the channel and the positive residues from the lysine could be attracted to the negative charge of DIDS and therefore block the channel. The irreversible inhibition of DIDS is produced by the fact that this molecule can covalently bond to amines (Lu and Boron, 2007, Matulef and Maduke, 2005). The inhibition of GTGs by DIDS has been shown before for AtGTG1 activity, in whole-cell patch clamping and in a planar lipid bilayer system (Dorey, 2019) and for HsGPHR activity in planar lipid bilayers (Maeda et al., 2008).

It was also observed that OsGTG was more selective to Cl^- than to the other anions tested. Both OsGTGs exhibited the following selectivity sequence: $Cl^- > I^- > Br^- > NO_3^-$, another indication that the 9th amino acid residue does not play a key role in the function of the protein. The conductance and the current were reduced in the presence of the other anions (Figure 4.20). The selectivity sequence observed for OsGTG is not too different from the selectivity found in the mammalian GPHR, which was $I^- > Cl^- = Br^- > F^-$ (Maeda et al., 2008). The selectivity of AtGTG1 and CeGTG1 was tested in whole-cell patch clamping using HEK293 cells and both showed a similar ion selectivity pattern, that was $Cl^- > NO_3^- > F^- > SCN^- > I^- > Br^-$ (Dorey, 2019). The discrepancy in the selectivity sequence between AtGTG1, OsGTG and HsGPHR could be due to the difference in the techniques that were used in each case. Although OsGTG and HsGPHR selectivity was analysed in a planar lipid bilayer system, the protein purification system, the liposomes and the lipids used for the artificial membrane were

different. This could account for the differences in the permeability sequence obtained for these two proteins. However, the selectivity of AtGTG1 and CeGTG1 were analysed in whole-cell patch clamp following heterologous expression in HEK293 cells. In this case, an average cell current is measured with completely different solutions and techniques. This could explain the differences in selectivity observed in OsGTG in comparison to AtGTG1 and CeGTG1. Nevertheless, in these three homologues, Cl^- has the highest selectivity.

The fact that OsGTG functions as a channel was previously suggested in an independent study where channel activity was observed when OsGTG from the *japonica* variety and rice Gα subunit were co-expressed together in *Xenopus* oocytes (Ma et al., 2015). This indicates a possible interaction or even activation of OsGTG by Gα. However, the type of ion transported was not directly tested in that system. The indication that the ion could be Ca^{2+} came from the rice *gtg* mutant showing a reduced Ca^{2+} resting level and a reduced peak of Ca^{2+} after it was exposed to cold stress (Ma et al., 2015). In this thesis, in order to test whether OsGTG could be a Ca^{2+} channel, an asymmetrical gradient of $CaCl_2$ was applied in the planar lipid bilayer system. Similar I-V curves were obtained with $CaCl_2$ as with KCl, including a positive reversal potential. OsGTGe and OsGTGg were also observed to be more permeable to Cl^- than Ca^{2+}. On average, the P_{Cl}/P_{Ca} permeability ratio was 2.89. The conductance obtained for both OsGTGs in the presence of $CaCl_2$ was similar to the conductance obtained in the presence of KCl (Figure 4.16 and Figure 4.18), suggesting that the presence of Ca^{2+} did not affect the activity of the channel. The lack of current observed when calcium gluconate was applied also supports the idea that OsGTG is not a calcium channel. Calcium gluconate has been used previously to characterize Ca^{2+} channels in the planar lipid bilayer system. Single-channel activity has been observed in the presence of calcium gluconate when Ca^{2+} channels have been inserted into an artificial membrane. More specifically, this was shown in the study of the plant Mitochondrial Calcium Uniporter, MCU, which also exhibited a negative reversal potential in an asymmetrical gradient with $CaCl_2$ (Teardo et al., 2017). In addition, the activity of OsGTG together with rice Gα subunit was also assessed, to study whether the activity of OsGTG was dependent of RGA1. In a preliminary experiment, the activity of OsGTG did not increase after the addition of RGA1. In fact, the activity when both proteins were expressed was reduced when compared to the activity shown by OsGTG alone (Figure 4.21). These preliminary data indicate that RGA1 does not activate OsGTG, but further experiments are required to fully test this.

The capacity of OsGTG to transport Ca^{2+} was also tested in this thesis by the patch-clamping technique in HEK293 using a calcium solution. The current obtained when OsGTGg was expressed in HEK293 cells was similar to the current obtained with the negative control, and there was a slight current increase in the OsGTGe expressing cells. Nevertheless, as just described above, this hypothesis was addressed in the planar lipid bilayer assay, where by using $CaCl_2$ and calcium gluconate it was shown that OsGTGe does not transport Ca^{2+} and does not function as a Ca^{2+} channel. The slight increase of current observed in HEK293 cells that expressed OsGTGe could be due to the chloride present in the solution. Also, the current could be produced by endogenous Ca^{2+} channels, which have been characterized in the plasma membrane of HEK293 cells using patch clamping assays (Berjukow et al., 1996). Four types of Ca^{2+} plasma membrane influx channels have been reported in HEK293 cells. I_{CRAC} channels that are highly selective to Ca^{2+}; I_{min} and I_{max} which can be activated by InsP3 and I_{NS} that are non-selective channels (Bugaj et al., 2005). Nevertheless, our results indicate that OsGTG does not seem to function as a calcium channel.

Patch clamping in HEK293 cells was also used to test the channel activity of OsGTG. When using a chloride solution for OsGTGe and OsGTGg HEK293 cells, an increase of current was observed in comparison to the cells transfected with the empty vector (Figure 4.7 D). The average of the maximum current recorded in cells transfected with OsGTG reached 81 ± 6.3 pA for OsGTGe and 67 ± 3.5 pA for OsGTGg, with the negative control giving a maximum current average of 32 ± 1.6 pA. However, the current produced by OsGTG was not as strong as the current observed when AtGTG1 was expressed in the same type of cells, which reached up to ~150 pA (Dorey, 2019). One reason for the lack of very high current could be that the GFP fluorescence produced from the transfected cells could not be detected in the microscope used for the patch clamping. As a result, patch clamping had to be performed blindly, without knowing whether the cell analysed had been successfully transfected. This may have led to a reduction in the current activity if the proportion of cells not transfected was higher.

Another reason for the lack of strong current observed in the *OsGTG* transfected cells could due to less localisation of OsGTG at the plasma membrane, and thus the current produced by OsGTG in HEK293 cells would not be detected by patch clamping. Previous work done with OsGTG suggested that the protein localised at the plasma membrane and ER in tobacco protoplasts and Arabidopsis protoplasts respectively (Ma et al., 2015). However the marker used in that study to corroborate the plasma

membrane localisation, PIP2, also localises at the ER (Lee et al., 2009). In this thesis, the localisation of OsGTG has been addressed using specific intracellular organelle markers: HDEL for ER, ManI for *cis* Golgi and ST for *trans* Golgi (Gomord et al., 1997, Boevink et al., 1998, Nebenführ et al., 1999), and co-localisation with OsGTG in transient expression in tobacco leaves was confirmed with each of the three markers (Figure 3.22 to Figure 3.24). Interestingly, no co-localisation was detected when a specific plasma membrane marker, LT16b, was co-expressed with OsGTG, indicating that OsGTG is not targeted to the plasma membrane (Figure 3.25). This observation raised some doubts on whether OsGTG could localise at the plasma membrane in HEK293 cells, which is necessary to analyse current measurements across that membrane. The localisation of OsGTGe and OsGTGg was analysed by confocal microscopy in HEK293 cells and a clear endomembrane localisation was observed, mostly around the nucleus and inside the cell (Figure 4.4), which indicates ER localisation (Herpers and Rabouille, 2004). The localisation observed resembles the localisation of the ER tracker marker and the Golgi stain BODIPY TR C5 ceramide (Yadav et al., 2013, Ghosh et al., 2017). No clear plasma membrane localisation was observed when OsGTGs were expressed in HEK293 cells. A similar pattern was observed when AtGTG1 was expressed in the HEK293 cells. Previous studies have shown different localisations for AtGTG1, at the plasma membrane in Arabidopsis protoplasts (Pandey et al., 2009) and at the ER and Golgi in tobacco cells (Jaffé et al., 2012). The confocal studies in HEK293 cells expressing AtGTG1 also showed the endomembrane localisation previously observed in plants. When a plasma membrane stain was applied in those cells, no co-localisation with AtGTG1 was observed (Figure 4.5). However, as mentioned before, an increase in current activity was observed in HEK293 cells that expressed AtGTG1 in comparison to the cells that were transfected with the empty vector (Dorey, 2019). This increase of current was not seen in every cell, with only 27% of the cells analysed showed a current activity higher than 100 pA. This could be due to the fact that AtGTG1 does not primarily localise at the plasma membrane. However, several cells showed strong current activity potentially produced through the ER-plasma membrane contact sites (ER-PM contact sites). Although the ER is a very dynamic organelle, it is also anchored to the plasma membrane at specific sites. These ER-PM contact sites are involved in lipid trafficking and homeostasis in the cell and allow for quick transmission of signals from outside the cell to the intracellular compartments (Bayer et al., 2017, McFarlane et al., 2017, Perico and Sparkes, 2018, Wu et al., 2018). Thus, the current activity observed when AtGTG1 was expressed in

HEK293 cells could have been produced through these contact sites. It is also possible that the high currents observed in HEK293 cells expressing AtGTG1 could be due to the gene being expressed under the T7 constitutive promoter, which produces high expression of the protein that can lead to leakage of the protein into the plasma membrane. This has been seen previously for other intracellular channels, like TMEM165, a Golgi Ca^{2+}/H^{+} antiporter that was able to localise at the plasma membrane in HeLa cells due to the overexpression of the protein under the constitutive triose-phosphate isomerase, TPI1 promoter (Demaegd et al., 2013). However, OsGTG was also expressed under the T7 promoter and did not seem to produce high current activity. This could be due to differences in the protein sequence. This localisation issue has been already observed with mammalian GTG/GPHR, where the patch clamp assay failed because the protein did not localise to the plasma membrane (Maeda et al., 2008). In the future it may be interesting to target GTGs to the plasma membrane in HEK293 cells and determine whether higher channel activity can be detected.

In summary, the data from this chapter indicate that OsGTG functions as an anion channel which localises in the endomembrane system, mostly in the ER and the Golgi (see chapter 3). Two major anion channels that have been identified in the Golgi of animal cells are GOLAC-1 and GOLAC-2. Both channels were identified in isolated Golgi fractions from rat liver and were introduced into a lipid bilayer system. Two different conductances were found, a large one that was identified as GOLAC-2 and a lower one that was identified as GOLAC-1 (Nordeen et al., 2000, Thompson et al., 2002). GOLAC-2 is a large conductance channel, 328 pS, that exhibited 5 subconductance states and was inhibited by DIDS (Thompson et al., 2002). This channel shows some resemblance to the mammalian GTG/GPHR, which apart from the high conductance of 400 pS, also showed 5-6 subconductance states and was also inhibited by DIDS (Thompson et al., 2002, Maeda et al., 2008). The selectivity sequence was also similar; GOLAC-2 selectivity was $I^{-} > Br^{-} > Cl^{-} > F^{-}$, whereas GTG/GPHR selectivity was $I^{-} > Cl^{-} = Br^{-} > F^{-}$ (Thompson et al., 2002, Maeda et al., 2008). The differences found between these two channels could be due to the lipids used in each experiment or the structural differences between the proteins. In GTG/GPHR electrophysiology assays, soybean lecithin was used as the lipid for the artificial membrane, whereas for GOLAC-2, 1-palmitoyl-2-oleoyl-*sn*-glycerol-3-phosphoethanolamine (POPE) and 1-palmitoyl-2-oleoyl-*sn*-glycerol-3-phospho-L-serine (POPS) were used. Also in GOLAC-2, isolated rat liver membrane was added to the system whereas in GTG/GPHR a mixture of PC and bovine brain was added to the

protein. All those experimental variations can account for the differences observed in the conductance and selectivity for other ions (Thompson et al., 2002, Maeda et al., 2008).

Similarly, GOLAC-1 is a DIDS sensitive channel with a lower conductance of 130 pS. This resembles the conductance of AtGTG1 that was 136 pS, and OsGTG, which was 110-130 pS at lower voltages and 90-100 pS at higher voltages. GOLAC-1 also exhibited 5-6 subconductance states (Nordeen et al., 2000). However, GOLAC-1 showed a higher conductance when pH between 5.2 to 7.2 was applied, whereas AtGTG1 did not seem to be regulated by pH in patch clamp assays performed in HEK293 cells (Nordeen et al., 2000, Dorey, 2019). Interestingly GOLAC-2 activity, in a similar manner to AtGTG1, does not seem to be regulated by pH (Thompson et al., 2002, Dorey, 2019). Future experiments at different pH values could be carried out with OsGTG to determine whether this channel is regulated by pH. More experiments are needed to confirm whether GTGs are indeed plant GOLAC channels or another novel type of anion channel.

In the ER, a Cl^- intracellular channel CLIC4 has been found in HEK293 cells (Duncan et al., 1997). This protein showed an outward rectifying current with a conductance of 42 pS when vesicles from transfected cells were inserted into an artificial lipid bilayer (Duncan et al., 1997, Edwards et al., 1998). Bestrophin1, a Ca^{2+} activated Cl^- channel, has also shown ER localisation and controls Ca^{2+} signalling in animals (Barro-Soria et al., 2010). No channel solely for Cl^- has been identified to date in the ER in plants (Colmenero-Flores et al., 2019). ClC-Nt1 is a putative Cl^-/H^+ antiporter that localises in the ER in tobacco cells and plays a role in luminal pH regulation (Sun et al., 2018). Previous electrophysiology work indicated that ClC-Nt1 functions as a Cl^- channel. That was based on the inward Cl^- current that was produced when ClC-Nt1 was expressed in *Xenopus* oocytes (Lurin et al., 1996). However, ClC-Nt1 was later characterised as a Cl^-/H^+ antiporter, due to the similarity of its sequence with the mammalian Cl^-/H^+ antiporter ClCs and also to the presence of two key glutamates, E213 and E280, that are conserved residues in the Cl^-/H^+ antiporters and have been shown to be involved in the gating and proton transport activity of the protein (Sun et al., 2018).

The data presented in this chapter indicates that there is a conserved anion channel function of GTGs from mammalian to plants cells. It is possible that GTG functions as an anion channel in the plant endomembrane system, and could be involved in protein

trafficking, consequently producing the several growths and developmental defects observed in the *gtg1gtg2* mutant (Jaffé et al., 2012). Further experiments need to be carried out to study whether GTG is involved in protein trafficking and in the secretory pathway.

4.3.2. GTGs are involved in pH homeostasis in plants

As previously mentioned, mammalian GTG/GPHR has been shown to regulate Golgi pH (Maeda et al., 2008). In this thesis, using WT and *gtg1gtg2* lines expressing the pH sensor pHluorin tagged to the ER (HDEL tag) and to *cis* Golgi (ManI tag), the pH of those organelles was measured. It was observed that Arabidopsis plants lacking GTGs displayed more alkaline pH at the ER and Golgi in comparison to WT. Arabidopsis WT cells showed ER and *cis* Golgi values of 7.26 and 6.74, respectively. However, for the *gtg1gtg2* mutant, the pH was 7.38 for the ER and 6.81 for *cis* Golgi. The pH values obtained for the ER and *cis* Golgi in our laboratory were similar to the pH values reported by Shen et al. (2013), which were pH of 7.1 for ER and 6.8 for *cis* Golgi. Both analyses were performed using the same organelle markers in Arabidopsis but, in Shen et al. (2013), protoplasts were analysed and in this study epidermal cells of seedlings were used. A similar pH pattern was also found in an independent study that was performed in tobacco leaves (Martinière et al., 2013a). Interestingly, expression of OsGTG was able to restore the alkaline pH of the *gtg1gtg2* mutant in the ER and the *cis* Golgi. This indicates that OsGTG can regulate endomembrane pH. In a similar manner it was found that AtGTG1 was also able to restore the pH in those compartments (Adam, Terry and Williams, unpublished). These results corroborate the notion that there is a conserved function between AtGTG1 and OsGTG.

The analysis of the pH in different organelles done in our laboratory also confirmed the gradual acidification reported previously for the secretory pathway in plants, where the ER is closer to neutral pH and the TGN and vacuole are more acidic (Martinière et al., 2013a, Shen et al., 2013). As shown in Table 4.1, the pH of the cytosol is 7.8, more basic than the pH of the ER, which was of 7.5 in tobacco leaves and 7.1 in Arabidopsis protoplasts (Martinière et al., 2013a, Shen et al., 2013). In both studies the pH of the ER was measured by expressing a pHluorin construct tagged with the ER retention signal HDEL. The *cis* Golgi was measured in Arabidopsis protoplasts using mannosidase I as a targeting sequence and showed a pH value of 6.8. The *trans* Golgi exhibited a pH of 6.3 in Arabidopsis protoplasts using the vacuolar sorting receptor, BP80, and 6.8 in

tobacco leaves using the sialyltransferase targeting sequence (Martinière et al., 2013a, Shen et al., 2013). In our laboratory, the pH values obtained for the *trans* Golgi using the BP80 marker in Arabidopsis seedlings were 6.36 for WT and 6.38 for *gtg1gtg2*. These values were very similar to the values reported by Shen et al. (2013). In relation to the PVC, in Martinière et al. (2013) analysis in tobacco epidermal cells revealed a more acidic pH in the compartments closely associated with the TGN (pH 6.1), than in the compartments distant to the TGN (pH 6.7). In Shen et al. (2013), the pH reported in the PVC of Arabidopsis protoplasts was around 6.2.

This gradual acidification of the secretory pathway has also been observed in animals (Demaurex, 2002, Casey et al., 2009, Ohgaki et al., 2010). pH in the organelles is primarily generated by the V-ATPase and is regulated by a proton leak and counterions (Demaurex, 2002, Schumacher, 2014). In mammalian Golgi membranes, the Na^+/H^+ exchangers NHE7 and NHE8 can influx Na^+ or K^+ in exchange for H^+, which could contribute to the regulation of intracellular pH, and these are therefore good candidates for the proton leak needed for pH homeostasis (Numata and Orlowski, 2001, Ohgaki et al., 2010). In plants, as described previously (section 1.4), K^+/H^+ antiporters (NHX), Ca^{2+}/H^+ antiporters (CAX), cation/H^+ antiporters (CHX) and Cl^- or NO_3^-/H^+ exchangers (ClC) are involved in Golgi and vacuolar pH regulation (De Angeli et al., 2006, Fecht-Bartenbach et al., 2007, Fecht-Bartenbach et al., 2010, Bassil et al., 2011a, Chanroj et al., 2011, Pittman, 2012, Andrés et al., 2014).

For the analysis in mammalian cells, the pH of the Golgi was measured using pHluorin fused to the Golgi target signal GPP130 for *cis* Golgi, to the *N*-acetylglucosaminyltransferase I, GnTI, for the *medial-trans* Golgi and to TGN38 for the TGN (Maeda et al., 2008). The pH sensors were stably expressed in CHO WT and *gphr* mutant cells and the pH obtained in the mutant was higher than in the WT (0.35 to 0.52 pH higher). More specifically, the pH in the mutant was 6.88 in the *cis* Golgi in comparison to 6.36 in WT, 6.96 in *medial-trans* Golgi in comparison to 6.34 in WT and 6.59 in TGN in comparison to 6.19 in WT. No differences in pH were found in the early endosomes and lysosomes, indicating that the pH changes detected were Golgi specific (Maeda et al., 2008). In our laboratory, the increase in pH found in the *gtg1gtg2* double mutant was only significantly different in the *cis* Golgi, and not in the *trans*. The pH in the WT was 6.74 whereas in the mutant it was 6.81. In the *trans* Golgi, the pH was 6.36 in WT and 6.38 in *gtg1gtg2*. The fact that significant differences occurred in the pH of the *cis* Golgi and not of the *trans* Golgi could be due to AtGTG1 being more abundant

in the *cis* than in the *trans* Golgi, which may indicate that the protein plays a more central role in that part of the organelle. In addition, other channels that localise at the *trans* Golgi, such as AtClCd, NHX5 and NHX6 (Fecht-Bartenbach et al., 2007, Bassil et al., 2011a), could compensate for the lack of AtGTG1 in the regulation of pH. Nevertheless, the results obtained in this chapter indicate that GTG proteins are pH regulators and that their function is conserved in animals and plants.

Chapter 5. Functional characterisation of GTG and G alpha triple mutant

5.1. Introduction

5.1.1. GTGs and G protein in Arabidopsis and rice

G proteins allow plants to sense and respond to the environment and transfer information inside the cell. This mechanism generates a specific response in the cell after the recognition of a stimulus (Urano et al., 2013). G proteins are composed of α, β, and γ subunits forming a heterotrimeric protein and a complex with GPCR which in animals are responsible for the perception of the stimulus and the activation of G protein signalling (Urano et al., 2013). G protein signalling functions in a different manner in animals and plants (section 1.5.4). In animals, activation of the GPCR receptor causes the exchange of GDP for GTP in the Gα subunit (Offermanns, 2003). However, in plants, the Gα subunit can release GDP spontaneously and bind to GTP without the need of a guanine nucleotide exchange factor or the presence of a GPCR (Johnston et al., 2007). The Gα subunit in plants has more affinity for GTP than GDP and can exchange nucleotides very fast. However, the hydrolysis rate is very slow (Johnston et al., 2007, Urano et al., 2013). The Arabidopsis genome encodes a regulator of G protein signalling (RGS1), a seven transmembrane domain protein that accelerates the GTP hydrolysis rate of the Gα subunit (Johnston et al., 2007, Jones et al., 2011). Interestingly, many monocot plant genomes, such as rice, wheat, barley, maize and sorghum, do not code for RGS proteins (Urano et al., 2012, Hackenberg et al., 2017), but they must contain another protein with GTPase-accelerating properties (GAP) to promote the GTP hydrolysis rate of the Gα subunit. Rice GTG was proposed to function as a GAP protein in monocots since OsGTG caused an increase in the hydrolysis rate of rice Gα subunit (Ma et al., 2015). Moreover, it was proposed that only OsGTG with a lysine residue in the 187th amino acid position was able to accelerate the GTPase activity of rice Gα whereas OsGTG with methionine in that residue suppressed the activity (Ma et al., 2015).

In Arabidopsis, GTGs have been described as GPCR type G-proteins (section 1.5.4). This was based on the predicted GPCR like-topology and the capacity of the GTGs to interact with the Gα subunit (Pandey et al., 2009). However, GTGs are not predicted to have the classic GPCR seven transmembrane domain structure but instead contain eight or nine transmembrane domains (Pandey et al., 2009, Jaffé et al., 2012). GTGs were also classified as GPCRs due to their sequence similarity to human orphan receptor GPR89, which shares a 45% identity and 68% similarity with Arabidopsis GTGs (Pandey et al., 2009, Jaffé et al., 2012). However, there is no evidence that GPR89 functions as a GPCR but instead shares 96% identity with the mammalian homologue from Chinese hamster that exhibits a voltage-dependent anion channel activity and acts as a Golgi pH regulator (Maeda et al., 2008).

AtGTGs were able to interact with Arabidopsis Gα subunit by the ubiquitin-split system and by co-immunoprecipitation (section 1.5.4.2) (Pandey et al., 2009) and rice GTG was shown to interact with rice Gα in a co-immunoprecipitation and bimolecular fluorescence complementation assays (Ma et al., 2015). Wheat GTG was able to interact with wheat Gα subunit in a firefly luciferase complementation imaging in *N. benthamiana* (Dong et al., 2019).

Although in plants GTGs have been proposed to work as GPCRs, in other organisms such as Chinese hamster and *Drosophila*, they are proposed to play a role as Golgi pH regulators affecting protein trafficking (Maeda et al., 2008, Charroux and Royet, 2014). Since there are different functions proposed for GTGs (see Table 1.2), it is important to confirm whether GTGs can work through G proteins. To study this, reverse genetics was used here and a *gtg1gtg2gpa1.4* plant, lacking *AtGTG1*, *AtGTG2* and *AtGPA1* gene expression was created and analysed.

5.1.2. Arabidopsis Gα, Gβ and Gγ mutants

G proteins are involved in numerous plant responses and they regulate a wide range of developmental processes. Reverse genetics approaches have been employed to understand the diversity of the processes that are regulated by Gα, Gβ or Gγ. Using an AtGPA1 loss-of-function plant (*gpa1*), it was reported that G proteins regulate cell growth and differentiation (Ullah et al., 2001). The *gpa1* mutant exhibited a reduced hypocotyl length in the dark in comparison to WT due to a reduced number of cells, caused by a defect in cell division (Ullah et al., 2001). Under light conditions, *gpa1*

mutant displayed round shaped rosette leaves due to larger epidermal cells (Figure 5.1) (Ullah et al., 2001, Trusov et al., 2008). Nevertheless, the Gα subunit does not seem to regulate cell division in the roots, since the root phenotype of the mutant was similar to the WT (Ullah et al., 2001). The *gpa1* mutant had sorter pedicels and longer sepals than WT (Ullah, 2003). The *gpa1* mutant had a reduced stomata density and stomata index in cotyledons in comparison with the WT and this phenotype correlated with the fact that *gpa1* had less water loss in comparison with WT (Zhang et al., 2008).

The Gα subunit also plays a role in pollen germination by activation of Ca^{2+} channels in Arabidopsis pollen grain since the *gpa1* mutant showed reduced pollen germination, pollen tube length and cytosolic free Ca^{2+} in the pollen in comparison to WT, whereas the AtGPA1 overexpressor, exhibited longer pollen tubes (Wu et al., 2007). G proteins are involved in different hormones pathways since Arabidopsis *gpa1* mutants are altered in the response to different hormones, such as auxins, brassinosteroid (BR), ABA, giberellin (GA) and jasmonate (JA) (Wang et al., 2001, Ullah et al., 2002, Ullah et al., 2003, Pandey et al., 2006, Okamoto et al., 2009).

Apart from the canonical Gα, the Arabidopsis genome contains three extra-large Gα proteins called, XLG1-3, that have a C-terminal Gα-like domain with GTPase activity but they differ from canonical Gα in using Ca^{2+} as a cofactor instead of Mg^{2+} (Heo et al., 2012). XLG proteins can act like G proteins since they can interact with Gβ subunit and Gβγ complex and they are involved in the regulation of defence genes and plant immunity and in root morphogenesis (Ding et al., 2008, Zhu et al., 2009, Chakravorty et al., 2015, Maruta et al., 2015).

Gβ protein is also involved in cell proliferation, shown by the *agb1* mutant producing shorter and wider hypocotyls than WT in the dark, due to a reduction of epidermal cells and an increase in the diameter of cortical cells (Figure 5.1). The *agb1* mutant also displayed round rosette leaves with an island of small cells creating a wrinkly surface (Lease et al., 2001, Ullah et al., 2003, Trusov et al., 2008). The *agb1* exhibits a longer primary root, due to an increase in cell production in the root apical meristem, and a higher number of lateral roots due to an increase of primordia density (Ullah et al., 2003, Chen et al., 2006a). The *agb1* mutant had shorter and wider siliques than WT, and also had higher stomata density and stomata index and therefore higher water loss in comparison with WT and *gpa1* (Figure 5.1) (Lease et al., 2001, Trusov et al., 2008, Zhang et al., 2008, Chakravorty et al., 2011).

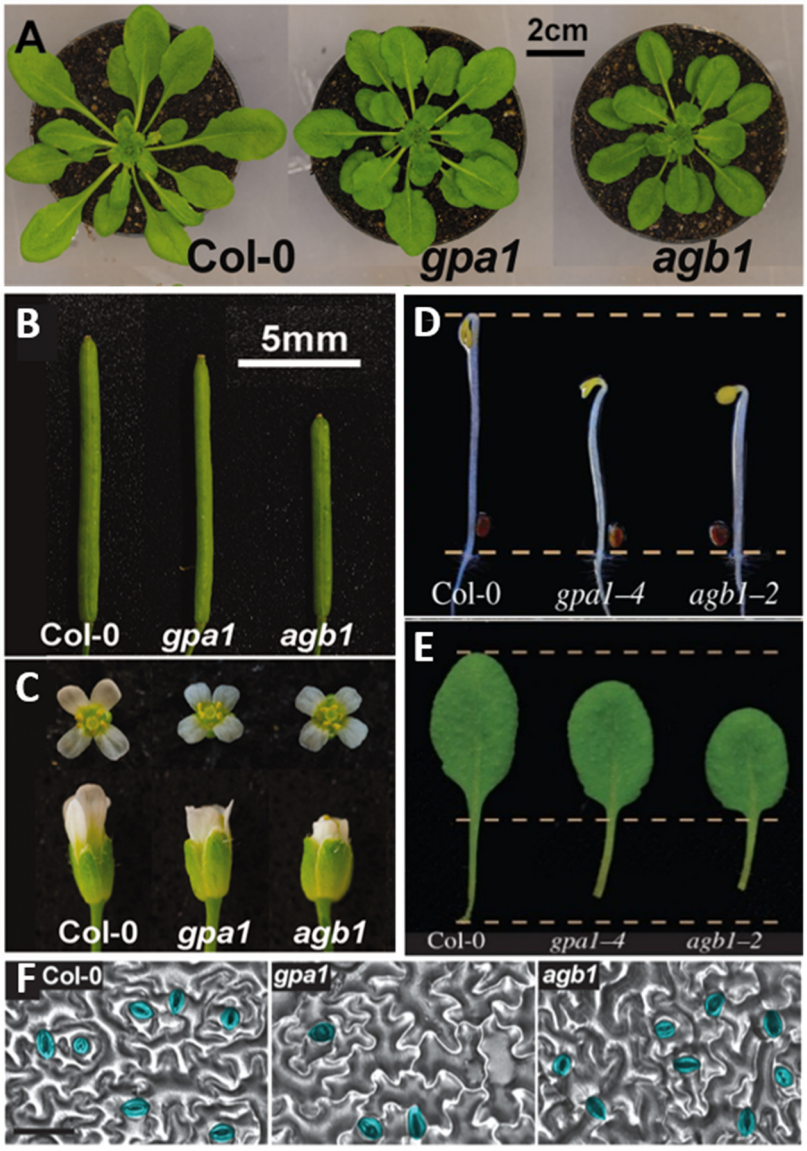

Figure 5.1. *gpa1* and *agb1* mutant phenotypes

A) *gpa1* and *agb1* mutants display round rosette leaves in comparison to WT plants. B) Silique length of WT and mutants, showing a reduced silique size in *agb1* mutant. C) Image of the flowers where *gpa1* mutant exhibits longer sepals and *agb1* shorter petals. D) Reduced hypocotyl length of *gpa1* and *agb1* mutants in comparison to the WT in darkness. E) Shorter pedicel in *gpa1* and *agb1* plants in comparison with WT. F) *gpa1* mutant has a reduced stomata density in comparison with WT whereas *agb1* has a higher stomata number than WT in the epidermis. Images A, B, C and F taken from Urano et al. (2016) and images D and E from Urano et al. (2013).

Arabidopsis Gβ subunit plays a role in salinity responses since the *agb1* mutant displays a hypersensitive phenotype under salt stress and a higher stomata conductance and transpiration (Zhang et al., 2008, Yu and Assmann, 2015). In biotic stress, G proteins are involved in pathogen resistance regulation (Zhang et al., 2012, Liu et al., 2013, Urano et al., 2013). AtAGB1 is required for cell death and immunity triggered by the pathogen-associated molecular pattern (PAMPs) and is also required for PAMP-triggered induction of ROS (Liu et al., 2013). *agb1* is more susceptible to necrotrophic fungal pathogens (Delgado-Cerezo et al., 2012, Zhang et al., 2012). Gβ subunit plays a role in cell death triggered by unfolded protein response (UPR) (Wang et al., 2007). A recent study showed that Gβ subunit is involved in BR signalling due to its interaction with BES1, a BR transcription factor, and that together they regulate cell elongation (Zhang et al., 2018b).

Arabidopsis has three genes coding for Gγ subunits, *AtGG1*, *AtGG2* and *AtGG3*. Plants lacking AtAGG1 and AtAGG2 exhibited the same hypocotyl size, leaf shape and silique length as WT (Trusov et al., 2008, Thung et al., 2012). AtAGG3 has lower homology with the other two Gγ subunits, but it has more affinity and binds strongly to AtAGB1 (Chakravorty et al., 2011). The Arabidopsis *agg3* mutant plants showed the same phenotype seen in *gpa1* and *agb1*, such as shorter petals, flat, shorter and wider siliques, rounder leaves, shorter hypocotyl under dark conditions and reduced plant height (Chakravorty et al., 2011, Li et al., 2012, Thung et al., 2012).

5.1.3. G protein mutants in rice

In rice, there is one Gα subunit (RGA1) and the knockout exhibits a dwarf phenotype. The mutant (called *Dikoku* (*d1*)) also displays reduced seed size (Wang et al., 2006). The small size phenotype is due to a reduced cell number in the leaf, internode, lemma or root, suggesting that Gα in rice is involved in cell proliferation (Izawa et al., 2010). An independent *rga1* mutant created by CRISPR/Cas9 technology also exhibited a dwarf phenotype with reduced seed yield, seed setting rate, panicle length and grain length (Cui et al., 2020). Rice Gα plays a role in GA signalling since the *d1* mutant seedlings are less responsive to exogenous GA treatment in comparison with WT (Ueguchi-Tanaka et al., 2000). Rice Gα is also involved in BR signalling since the mutant was less sensitive to brassinosteroid than WT (Wang et al., 2006).

The rice Gα subunit is also involved in responses to several abiotic and biotic stresses. Two independent *rga1* mutants exhibited a high drought tolerance in comparison with WT plants (Ferrero-Serrano and Assmann, 2016, Cui et al., 2020). *rga1* mutant also showed an increase in chilling and salt tolerance (Cui et al., 2020). A microarray study performed in the rice *d1* mutant showed that many stress-response genes were altered in the mutant, mostly involved in cold, heat, drought and salt stress (Jangam et al., 2016). Rice Gα mutant had a reduced hypersensitivity response (HR) under avirulent *Magnaporthe grisea* infection and produced less ROS following treatment with *M. grisea* elicitors (Suharsono et al., 2002, Urano et al., 2013).

Recently it has been found that the rice genome also contained four extra-large Gα proteins, called *PXLG1-4* (Cui et al., 2020). CRISPR/Cas9 mutants of these four genes exhibited earlier flowering than the WT. *pxlg1* mutant also showed a reduced height, shorter panicle, longer grains and an increase in seed yield; *pxlg2* and *pxlg3* exhibited a higher seed setting rate, with *pxlg3* also showing a reduced height (Cui et al., 2020). All four mutants were more tolerant to salt stress than WT, but in addition, *pxlg4* mutant was also more drought and chilling tolerant in comparison to WT. Interestingly, using a yeast two-hybrid it was shown that only PXLG2 was able to interact with the rice Gβ subunit (Cui et al., 2020).

The rice Gβ subunit (RGB1) seems to be more essential for the survival of the plant since to date no knockout plant for this gene has been reported, however not many publications have been released that address this issue. Nevertheless, an *rgb1* knockdown line using RNAi system showed some defects in growth, such as dwarfism, small size of panicle and browning of the lamina joint region and nodes (Utsunomiya et al., 2011, Utsunomiya et al., 2012). A recent study generated a three and six base deletion CRISPR/Cas9 *rgb1* mutant that showed a semi-dwarf phenotype with a reduced number of panicles in comparison with WT. The mutant also displayed a higher chilling sensitivity than WT and an increase in salt tolerance (Cui et al., 2020).

Rice has five Gγ subunits: RGG1, RGG2, GS3, DEP1 and OsGGC2 (Kato et al., 2004, Fan et al., 2006, Huang et al., 2009, Trusov et al., 2012). GS3 and DEP1 have been suggested to be a major QTL for grain density per panicle and grain size, where GS3 works as a regulator of grain size and DEP1 as a regulator of grain yield (Fan et al., 2006, Huang et al., 2009). Using CRISPR/Cas9 gene-editing technique, mutants of the five rice Gγ subunits have been created (Cui et al., 2020). The *rgg1* mutant exhibited longer panicles than WT, *rgg2* showed a reduced height, *gsc3* produced higher panicle

number with longer grain size and increase in seed yield, *dep1* had a reduced height however produced more grains but with smaller size, and *ggc2* exhibited a reduced height in comparison to WT (Cui et al., 2020). All Gγ mutants exhibited an increase in salt tolerance, but in addition, *dep1* mutant was more chilling and drought tolerant and *gs3* mutant also exhibited an increase in chilling tolerance in contrast to *ggc2* mutant that showed more chilling sensitivity in comparison to WT (Cui et al., 2020).

5.1.4. Reverse genetics and protein-protein interaction assays to study protein function

In reverse genetics, the study of protein function is carried out by the observation of phenotypes associated with the loss of the gene of interest. In Arabidopsis there are different methods to generate mutant plants. The most common method is generating T-DNA insertion lines that are created using *Agrobacterium tumefaciens* that transfers foreign DNA into the plant genome (Krysan et al., 1999). This can be used to generate mutants since the T-DNA integrates randomly into the genome interrupting different genes. T-DNA mutants have been generated in different Arabidopsis ecotypes with the most common ones being Columbia and Wassilewskija. In this study, the T-DNA mutants used were from the SALK collection in Columbia ecotype (Alonso et al., 2003). T-DNA express website (http://signal.salk.edu/cgi-bin/tdnaexpress) is a database used to identify the T-DNA mutants of interest. Those mutants have an inserted T-DNA fragment in the gene of interest disrupting the capacity of polymerases to transcribe the gene producing a knockout mutant that can be used for gene function analysis. Double or triple mutants are generated by crossing single mutants.

In this thesis, reverse genetic was used to create and study a *gtg1gtg2gpa1.4* triple mutant that lacks the endogenous *AtGTG1*, *AtGTG2* and *AtGPA1* genes, to understand whether GTG and Gα interact or whether they work independently to regulate the same process. The genetic mechanism in which the effect of a gene mutation depends on the presence of other genes is called epistasis. By epistasis studies, it can be analysed how the interaction of genes can affect the phenotype of the organism. The function of G proteins and their possible interaction has been extensively studied using reverse genetics and epistasis. Arabidopsis Gα subunit, AtGPA1, is involved in the BR pathway since the *gpa1.2bri1.5*, a Gα and BR receptor double mutant exhibited more severe dwarfism than the *bri1.5* single mutant, indicating that G protein and BR pathway function together to control cell proliferation (Gao et al., 2008). To test whether a

phospholipase Dα1 (PLDα1) was a component of the G protein signalling, several Arabidopsis double and triples mutants were generated. A *gpa1xrgs1xpldα1* triple mutant exhibited a smaller rosette diameter and hypocotyl length than the single or double mutants, indicating that these proteins function together controlling those specific plant development features (Choudhury and Pandey, 2016).

To study whether two proteins interact, several techniques have been developed and improved in recent years. Yeast two-hybrid and the split-ubiquitin system were the first methods to be used (Fields and Song, 1989, Johnsson and Varshavsky, 1994). To study protein-protein interaction in plants, several techniques have been developed, such as Co-IP, fluorescence resonance energy transfer (FRET), BiFC and split luciferase complementation (Pollok and Heim, 1999, Hu et al., 2002, Phee et al., 2006, Fujikawa and Kato, 2007). In this study, a BiFC technique was used to test whether OsGTG and rice Gα can interact. This is an *in vivo* technique based on the reconstitution of a fluorescence protein where YFP is most commonly used. Briefly, one of the proteins of interest is tagged with the N-terminal fragment of the YFP and the other protein is tagged with the C-terminal part of the YFP. When both proteins interact, the YFP protein is reconstituted and a yellow fluorescence signal is produced (Hu et al., 2002). This technique has been successfully used to study the interaction of different proteins in plants, such as the interaction of CBL proteins with CIPKs (Waadt et al., 2008) and the interaction of the Arabidopsis three extra-large Gα subunits with the Gβγ dimer (Chakravorty et al., 2015).

5.1.5. Aims

To determine whether GTG requires G proteins for its functions, these are the aims of this chapter:

1. To test whether there is a genetic interaction between Arabidopsis GTGs and Arabidopsis Gα, a triple mutant plant lacking *AtGTG1*, *AtGTG2* and *AtGPA1* genes will be generated. This will carry out crossing *gtg1gtg2* and *gpa1.4* mutants and several generations will be screen to isolate the triple homozygous mutant.
2. Analysing the phenotype of *gtg1gtg2gpa1.4* mutant to study whether the absence of AtGPA1 can affect the growth, development and fertility of the *gtg1gtg2* mutant. The growth, development and fertility of the new

gtg1gtg2gpa1.4 mutant will be compared with the growth of WT, *gtg1gtg2* and *gpa1.4* to study whether GTGs and GPA1 are be involved in the same process.

3. To investigate whether rice GTG interacts with rice Gα *in vivo* using a bimolecular fluorescence complementation assay.

5.2. Results

5.2.1. Generating a *gtg1gtg2gpa1.4* triple mutant

To generate the AtGTG1, AtGTG2 and AtGPA1 triple mutant, Arabidopsis *gtg1-2 gtg2-2* T-DNA double mutant was crossed with a *gpa1.4* T-DNA single mutant, all from the SALK collection in Columbia ecotype background (obtained from TAIR). The *gtg1-2 gtg2-2* double mutant was previously isolated in our laboratory and was originally generated from the cross of *gtg1-2* and *gtg2-2* T-DNA single mutants (Jaffé et al., 2012). A distortion in the segregation ratios was observed when the progeny of the *gtg1-2 gtg2-2* cross was analysed. The progeny of the *gtg1-2* (+/-) *gtg2-2* (+/-) double heterozygous did not follow a Mendelian segregation since only one double homozygous mutant was identified out of 24 progeny that were analysed (Jaffé et al., 2012). A *gtg1-2 gtg2-2* double mutant was isolated from the progeny, where no full-length *GTG1* and *GTG2* were amplified. However, a faint product was observed when the full-length of *AtGTG1* was amplified from *gtg1-2* and *gtg1-2 gtg2-2* mutants. Sequences analysis of the product showed a T-DNA excision, where part of the 11st to the 13th exon has been spliced out in *GTG1*, producing a shorter protein that lacked the last two predicted transmembrane domains (Jaffé et al., 2012).

In the cross for the generation of *gtg1gtg2gpa1.4* triple mutant, *gtg1-2 gtg2-2* (*gtg1gtg2* from herein) homozygous line was used as female whereas *gpa1.4* homozygous mutant was used as a male. For *gtg1-2* the T-DNA insertion is in the 12th exon, for *gtg2-2* in the 10th intron and for *gpa1.4* in the 12th intron (Figure 5.2). Each gene localises at different chromosomes: *AtGTG1* is localised at chromosome 1, *AtGTG2* at chromosome 4 and *AtGPA1* at chromosome 2. Following the cross of *gtg1gtg2* with *gpa1.4* mutant, genomic DNA PCRs were carried out in the first generation to confirm that the three T-DNA insertions were present. Five plants from independent cross events were analysed and, to confirm the presence of the T-DNA insertions, primers for the gene and the T-DNA border were used. All the plants analysed contained the three T-DNA inserts for the three mutations, indicating that they were heterozygous for each mutation (Figure 5.3). One of the triple heterozygous plants was selected and after self-fertilization, the second generation progeny of the cross was analysed. Out of 72 plants that were genotyped, no triple *gtg1gtg2gpa1.4* homozygous was found, although the expected ratio of a triple homozygous is one out of 64 (Table 5.1). However, out of those 72 plants, three were homozygous for *gtg1* and *gpa1.4*

mutations and heterozygous for *gtg2* (*gtg1* (-/-) *gtg2* (+/-) *gpa1.4* (-/-)), and only one was double homozygous for *gtg1* and *gtg2* and heterozygous for *gpa1.4* mutation (*gtg1* (-/-) *gtg2* (-/-) *gpa1.4* (+/-)) (Table 5.1). The double homozygous *gtg1gtg2* and heterozygous *gpa1.4* plant was self-fertilized and the third-generation progeny was analysed to find the triple *gtg1gtg2gpa1.4* homozygous. Out of 24 plants that were analysed in this third generation, three plants were found homozygous for *gtg1*, *gtg2* and *gpa1.4* mutations. Genomic DNA was extracted from WT, *gtg1gtg2*, *gpa1.4* and *gtg1gtg2gpa1.4* plants and PCRs were carried out to confirm the absence of the three genes using primers across the T-DNA insertion for each gene. To confirm the presence of the T-DNA insertions, primers for the gene and the T-DNA border were used. No bands for *AtGTG1*, *AtGTG2* or *AtGPA1* genes were observed in *gtg1gtg2gpa1.4* (Figure 5.4). However, the correct bands for *AtGTG1*, *AtGTG2* and *AtGPA1* gene products were observed in the WT sample. At the same time, the *gtg1gtg2gpa1.4* plants have a *gtg1*, a *gtg2* and a *gpa1.4* T-DNA bands. No T-DNA insertion bands were present in the WT sample. Correct bands were obtained for *gtg1gtg2* and *gpa1*.4 mutants (Figure 5.4).

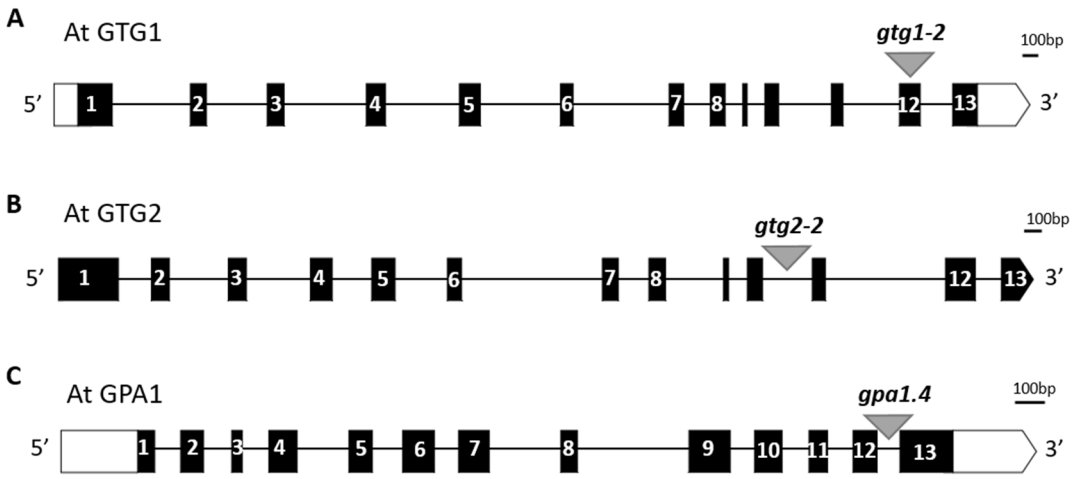

Figure 5.2. Diagram of the T-DNA insert sites for *AtGTG1*, *AtGTG2* and *AtGPA1.4*

The genomic structures of *AtGTG1* (A), *AtGTG2* (B) and *AtGPA1* (C) are represented in this diagram along with the T-DNA insertion sites (triangle above the gene). White boxes are the 5' and 3' UTR, black boxes are exons and black lines are introns.

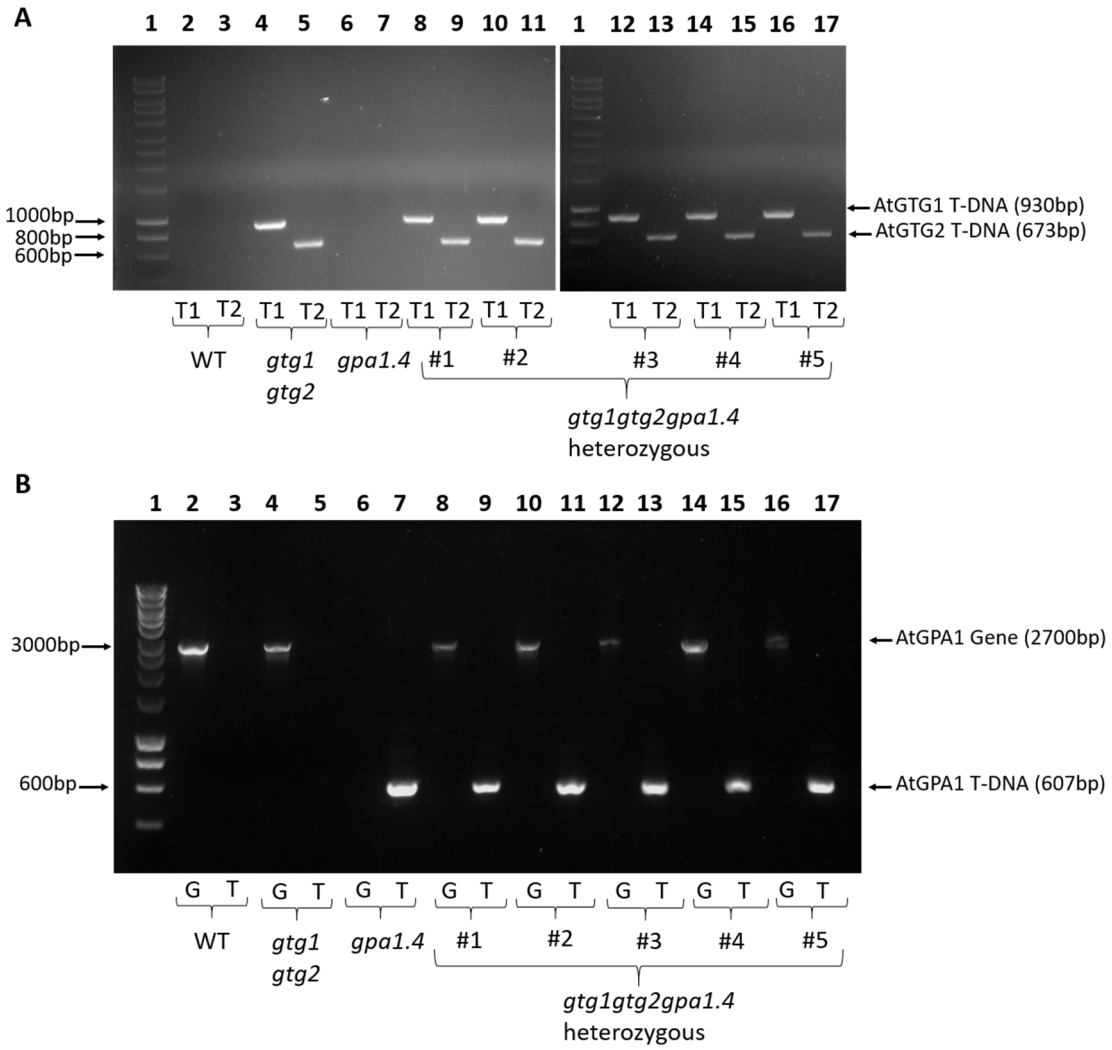

Figure 5.3. Genotype of the first generation of the *gtg1gtg2* and *gpa1.4* cross showing the three T-DNA insertions

PCR using genomic DNA for WT (lanes 2-3), *gtg1gtg2* (lanes 4-5), *gpa1.4* (lanes 6-7), and five *gtg1gtg2gpa1.4* heterozygous plants (lanes 8-17). A) For *AtGTG1* T-DNA insertion (T1 in the gel), primers GTG1 2F + Lba1 (predicted 930 bp) were used and for *AtGTG2* T-DNA insertion (T2 in the gel), primers GTG2 1R + Lba1 (predicted 673 bp) were used. B) For *AtGPA1* gene (G in the gel), primers AtGPA1 F + AtGPA1 R_S (predicted 2700 bp) were used and primers AtGPA1 R_S + LBa1 (predicted 678 bp) were used for the T-DNA insertion (T in the gel). Predicted products are shown on the right and molecular markers on the left (lane 1).

Table 5.1. Expected and obtained segregation ratios of the *gtg1gtg2* with *gpa1.4* cross

	1st Generation	**2nd Generation**	**3rd Generation**
Expected segregation ratio	**Of triple heterozygous = 1** *gtg1* (+/-) *gtg2* (+/-) *gpa1.4* (+/-)	**Of triple homozygous = 1/64** *gtg1* (-/-) *gtg2* (-/-) *gpa1.4* (-/-) **Of double homozygous and heterozygous =** **2/64** *gtg1* (-/-) *gtg2* (-/-) *gpa1.4* (+/-) **2/64** *gtg1* (-/-) *gtg2* (+/-) *gpa1.4* (-/-) **2/64** *gtg1* (+/-) *gtg2* (-/-) *gpa1.4* (-/-)	**Of triple homozygous = 1/4** *gtg1* (-/-) *gtg2* (-/-) *gpa1.4* (-/-)
Obtained segregation ratio	**Of triple heterozygous = 5/5 =1** *gtg1* (+/-) *gtg2* (+/-) *gpa1.4* (+/-)	**Of triple homozygous = 0/72** *gtg1* (-/-) *gtg2* (-/-) *gpa1.4* (-/-) **Of double homozygous and heterozygous =** **1/72** *gtg1* (-/-) *gtg2* (-/-) *gpa1.4* (+/-) **3/72** *gtg1* (-/-) *gtg2* (+/-) *gpa1.4* (-/-) **0/72** *gtg1* (+/-) *gtg2* (-/-) *gpa1.4* (-/-)	**Of triple homozygous = 3/24 = 1/8** *gtg1* (-/-) *gtg2* (-/-) *gpa1.4* (-/-)

(+/-) = heterozygous, (-/-) = homozygous

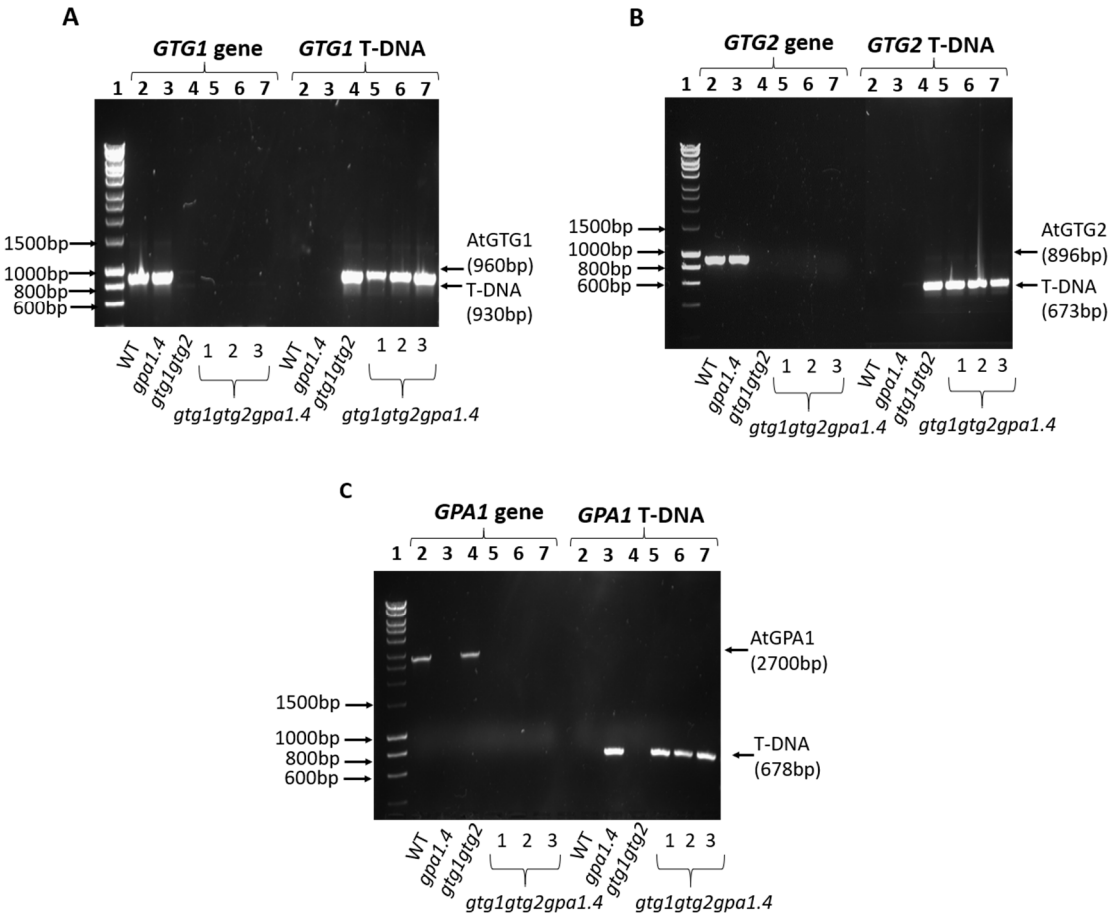

Figure 5.4. Genotype of *gtg1gtg2gpa1.4* mutant showing the three T-DNA insertions

PCR using genomic DNA for WT (lane 2), *gpa1.4* (lane 3), *gtg1gtg2* (lane 4) and the three *gtg1gtg2gpa1.4* plants (lane 5-7). A) For *AtGTG1*, primers GTG1 2F + GTG1 1R (predicted 960 bp) were used for the gene and GTG1 2F + Lba1 (predicted 930 bp) for T-DNA insertion. B) For *AtGTG2*, primers FR2 RT F + FR2 RT (predicted 896 bp) were used for the gene and GTG2 1R + Lba1 (predicted 673 bp) for the T-DNA insertion. C) For *AtGPA1*, primers AtGPA1 F + AtGPA1 R_S (predicted 2700 bp) were used for the gene and AtGPA1 R_S + LBa1 (predicted 678 bp) for the T-DNA insertion. Predicted products sizes are shown on the right and molecular marker sizes on the left (lane 1).

To further analyse whether the *gtg1gtg2gpa1.4* line was a knockout mutant, RNA was extracted from seedlings and cDNA was synthesised. PCRs were carried out to examine the expression of *AtGTG1*, *AtGTG2* and *AtGPA1* in the mutant. The *gtg1gtg2gpa1.4* plants did not show wild-type bands for *AtGTG1*, *AtGTG2* and *AtGPA1* genes whereas those products appeared in the control WT sample (Figure 5.5). This indicates that the *gtg1gtg2gpa1.4* lines did not express any of the three genes, confirming that *gtg1gtg2gpa1.4* is indeed a triple knockout mutant. *ACTIN*, which is constitutively expressed in Arabidopsis plants, was used as a control for cDNA quality and showed a clear signal in all lines with no genomic contamination observed.

5.2.2. Characterisation of *gtg1gtg2gpa1.4* mutant phenotype

To study whether AtGTGs could interact with the Gα subunit, several physiological experiments were carried out to compare the phenotype of WT, *gtg1gtg2, gpa1.4* and *gtg1gtg2gpa1.4* mutant. Here it is shown how the absence of AtGPA1 in the *gtg1gtg2* mutant background affects Arabidopsis growth, development and fertility.

5.2.2.1. *gpa1.4* mutation does not affect *gtg1gtg2* defective root growth.

As previously described in this thesis, the *gtg1gtg2* double mutant exhibits a strong reduction of root growth and fresh weight when grown on agar plates in absence of sucrose (Jaffé et al., 2012); however, *gpa1.4* mutant is reported not to display a reduced primary root (Ullah, 2003). The *gtg1gtg2gpa1.4* triple mutant showed a similar reduced root length and fresh weight per seedling to the *gtg1gtg2* double mutant (Figure 5.6). The *gtg1gtg2gpa1.4* and *gtg1gtg2* mutants exhibited reduced root length and fresh weight in comparison to WT and *gpa1.4*. The single *gpa1.4* mutant showed similar root length and fresh weight to WT. These results indicate that the lack of AtGPA1 in the *gtg1gtg2* lines does not affect the defective root growth phenotype of the double mutant.

As discussed in section 1.5.8, rice GTG has been proposed to play a role in cold tolerance (Ma et al., 2015). Therefore, it was considered that the low temperature treatment given during Arabidopsis seed plating should be explored. To test whether low temperature could affect root growth, the effect of the two days at 4°C pre-treatment before incubation at 23°C was also tested. To synchronise seed germination, plates are normally pre-treated for two days at 4°C before they are incubated at 23°C.

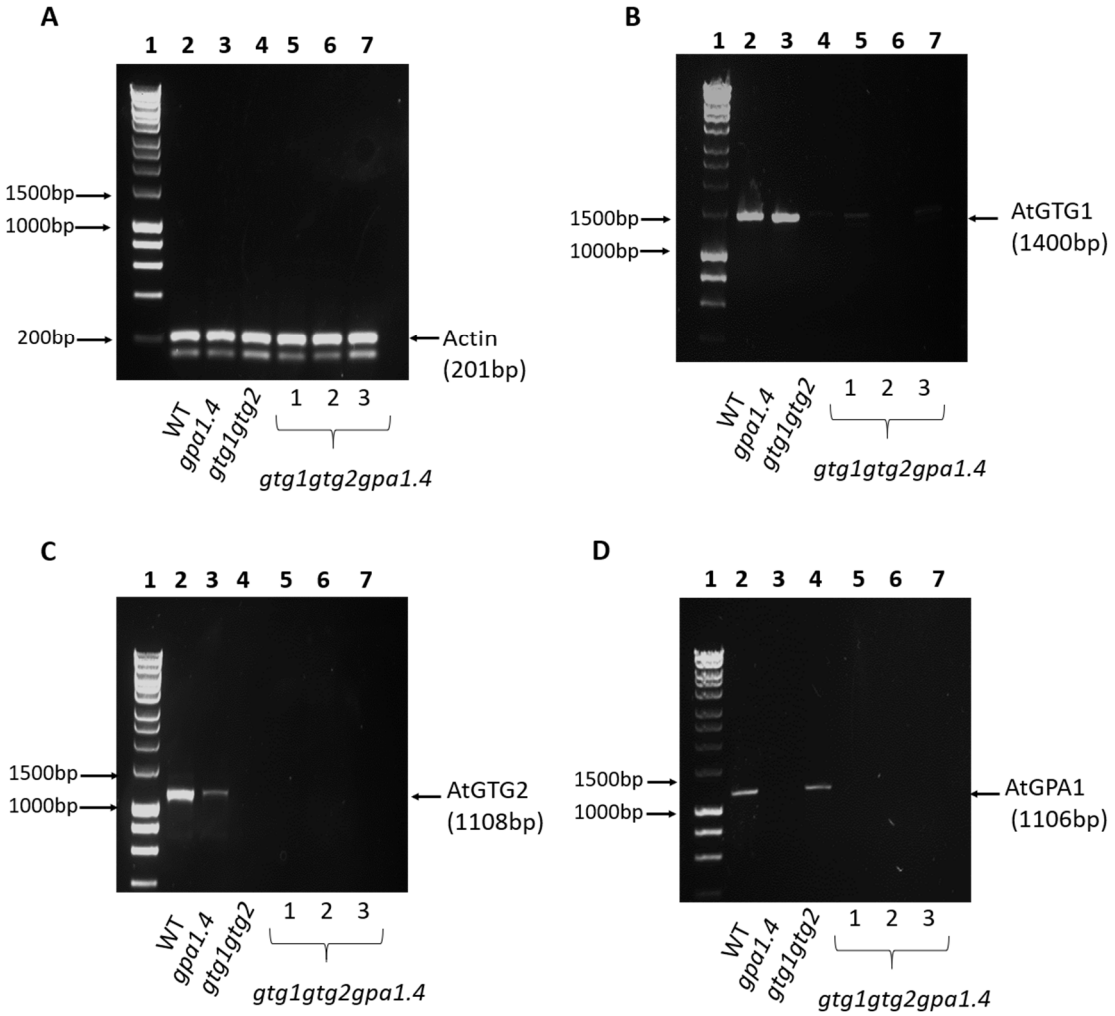

Figure 5.5. The *gtg1gtg2gpa1.4* lines are knockout for *AtGTG1*, *AtGTG2* and *AtGPA1* genes

RT-PCR of WT (lane 2), *gpa1.4* (lane 3), *gtg1gtg2* (lane 4) and the three *gtg1gtg2gpa1.4* plants (lane 5-7). Actin F + Actin R primers (predicted 201 bp) were used for *ACTIN* amplification (A), FR1 F + AtGTG1 R (predicted 1400 bp) for *AtGTG1* amplification (B), FR2 RT F + FR2 RT R (predicted 1108 bp) for *AtGTG2* amplification (C) and AtGPA1 F + AtGPA1 R_S (predicted 1106 bp) for *AtGPA1* amplification (D). Predicted products are shown on the right and molecular marker sizes on the left (lane 1).

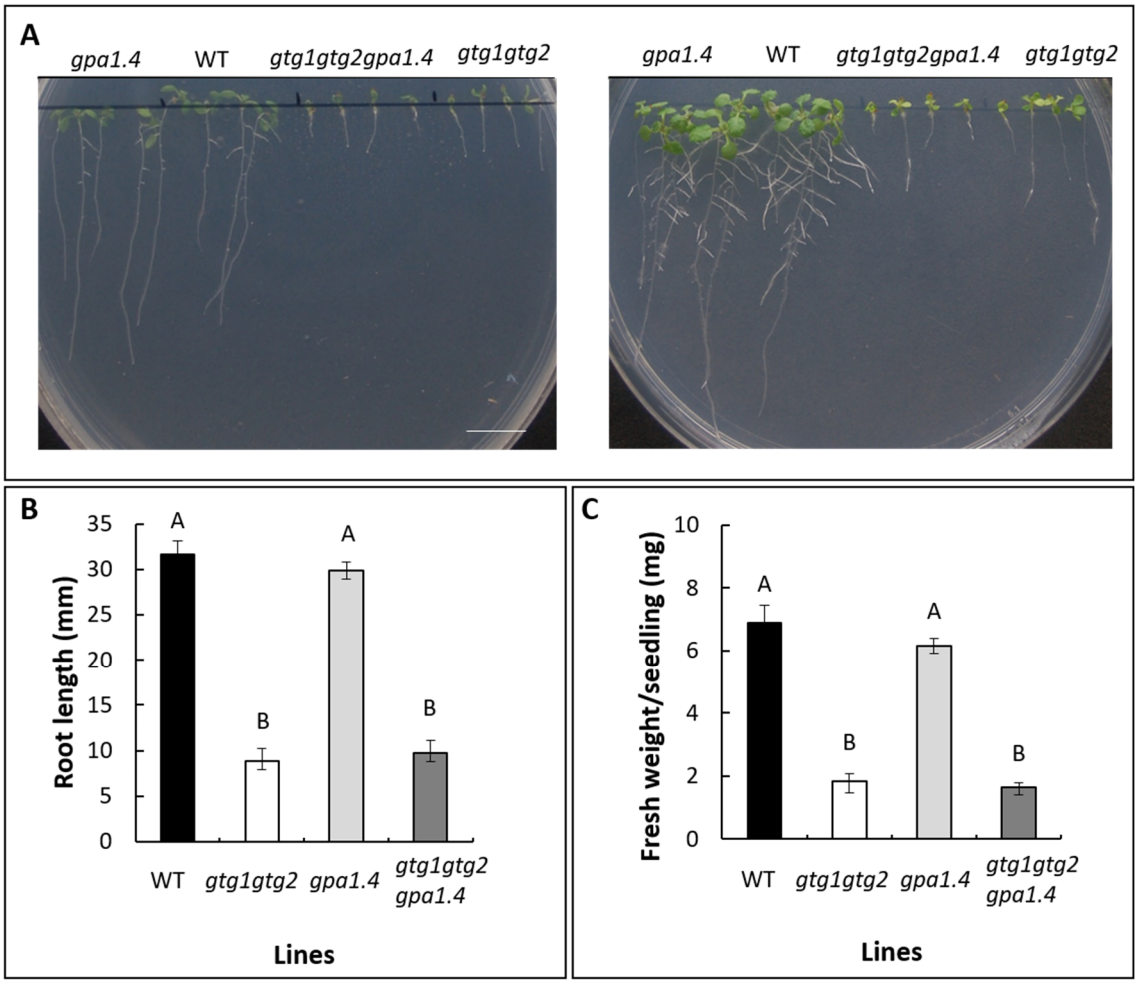

Figure 5.6. *gtg1gtg2gpa1.4* displays a similar root defective phenotype to *gtg1gtg2* in the absence of sucrose

A) Representative images of seedlings at day 10 (left) and at day 14 (right); scale bar 1 cm. Root length at 10 days (B) and fresh weight per seedling at 14 days (C) of WT (black), *gtg1gtg2* (white), *gpa1.4* (light grey) and *gtg1gtg2gpa1.4* (dark grey) grown on 0.5 MS in the absence of sucrose. Data represent the mean (±SEM) of six plates with four seedlings per line per plate (B, n=24 and C, n=6). One-way ANOVA ($p < 0.05$). Means not sharing a letter are significantly different; Tukey *post-hoc* test.

To test how the cold pre-treatment can affect root growth and fresh weight of the *gtg1gtg2* and *gtg1gtg2gpa1.4* mutants, the lines were subjected to three different pre-treatments: A) two days at 4°C in the dark before transfer to normal growth conditions (23°C) for 14 days; B) two days at 23°C in the dark followed by exposure to light for 14 days at 23°C; C) no pre-treatment and seeds were plated two days later and immediately

at normal growth conditions (23°C) for 14 days. It was observed that *gtg1gtg2* and *gtg1gtg2gpa1.4* mutants have reduced root growth in all conditions in comparison to WT and *gpa1.4* (Figure 5.7). The *gtg1gtg2* and *gtg1gtg2gpa1.4* mutants exhibited a reduced fresh weight in comparison to the WT when they were grown without cold pre-treatment, incubated those extra two days at 23°C (Figure 5.8 B, middle graph). In the plants that were exposed to two days 4°C pre-treatment, not significant differences were found between *gtg1gtg2*, *gtg1gtg2gpa1.4* and *gpa1.4* fresh weight. In the lines that were planted two days later, and did not receive the cold pre-treatment, they were no significant differences between WT, *gpa1.4* and *gtg1gtg2gpa1.4* fresh weight (Figure 5.8).

Comparing the root length of all the lines under the three pre-treatments, it was evident that the WT and *gpa1.4* lines were able to grow a longer primary root with the extra two days of growth at 23°C (Figure 5.7 C). However, *gtg1gtg2* and *gtg1gtg2gpa1.4* mutants were not able to grow longer roots even if they were incubated for a longer period. This was also observed with the fresh weight per seedling data (Figure 5.8 C), where *gtg1gtg2* and *gtg1gtg2gpa1.4* did not produce more biomass even when the growth period was prolonged. However, WT and *gpa1.4* produced higher fresh weight when they were grown for a longer time.

5.2.2.2. *gtg1gtg2gpa1.4* mutant displays a light-dependent hypocotyl defect

Along with the reduced primary root, the *gtg1gtg2* double mutant displays a defective hypocotyl growth under low light conditions (Jaffé et al., 2012). To test whether *gtg1gtg2gpa1.4* shows a similar response, WT, *gtg1gtg2*, *gpa1.4* and *gtg1gtg1gpa1.4* lines were subjected to different hypocotyl analysis experiments. Firstly, the hypocotyl growth under low light conditions was examined. WT, *gtg1gtg2*, *gpa1.4* and *gtg1gtg1gpa1.4* lines were grown at 10 µmol m^{-2} s^{-1} light intensity in the presence and absence of sucrose. In both conditions, *gtg1gtg2gpa1.4* exhibited the same reduced hypocotyl length as *gtg1gtg2* whereas *gpa1.4* displays the same phenotype as WT (Figure 5.9). This suggests that the lack of AtGPA1 does not affect the defective hypocotyl growth observed in the *gtg1gtg2* under low light.

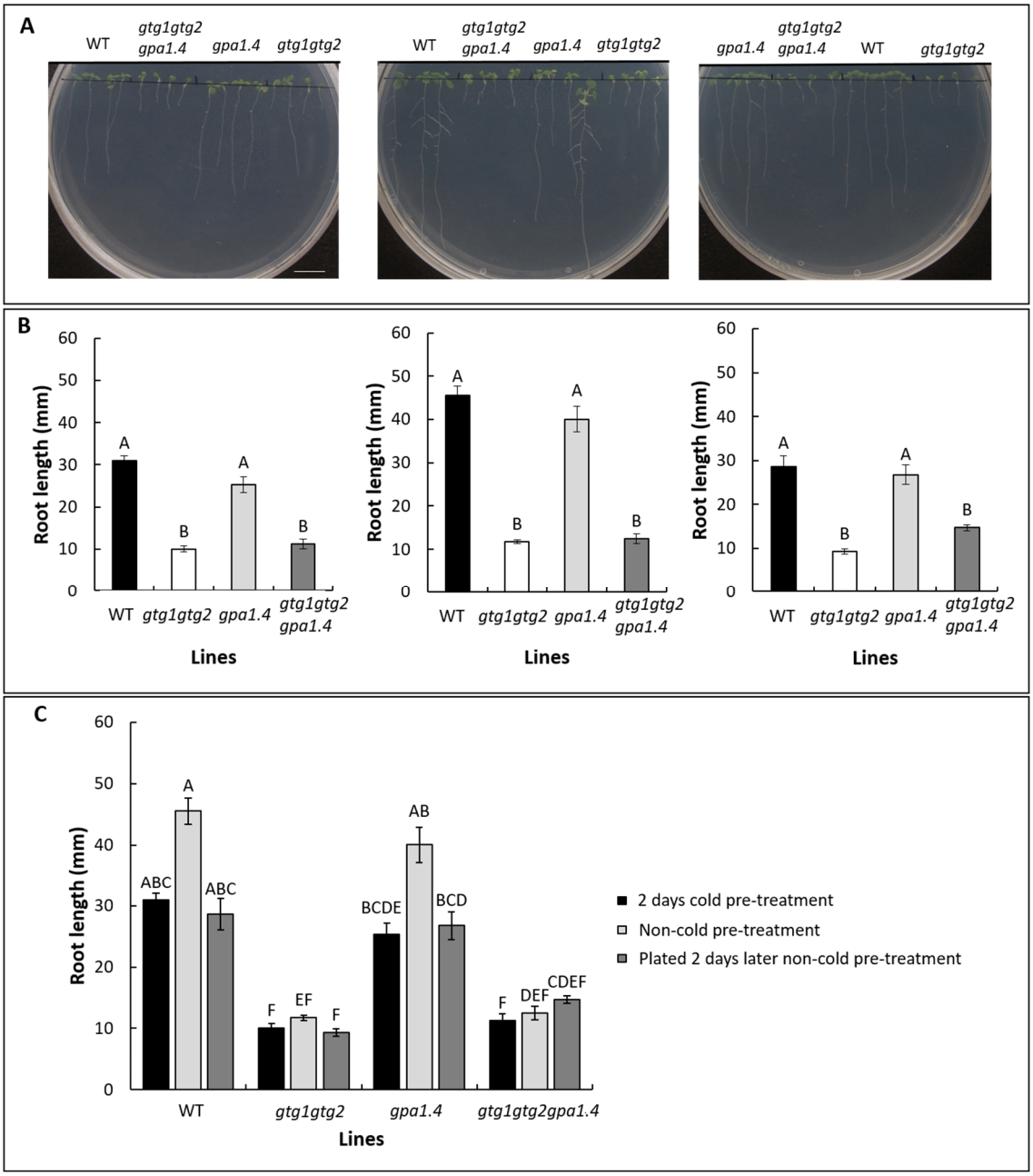

Figure 5.7. The cold pre-treatment does not affect the defective root phenotype in *gtg1gtg2* and *gtg1gtg2gpa1.4* mutants

A) Representative images of seedlings at day 10 with a 2 day at 4°C pre-treatment (left), no pre-treatment growing at 23°C for those 2 days (middle) and no pre-treatment seeds plated 2 days later (right); scale bar 1 cm. Root length at 10 days (B) of WT (black), *gtg1gtg2* (white), *gpa1.4* (light grey) and *gtg1gtg2gpa1.4* (dark grey) grown on 0.5 MS in the absence of sucrose with the three different pre-treatment as above. C) Comparison of the root length with the three pre-treatment conditions. Data represent the mean (±SEM) of four plates with four seedlings per line per plate (n=12). One-way ANOVA in B and Two-ways ANOVA in C ($p < 0.05$). Means not sharing a letter are significantly different; Tukey *post-hoc* test.

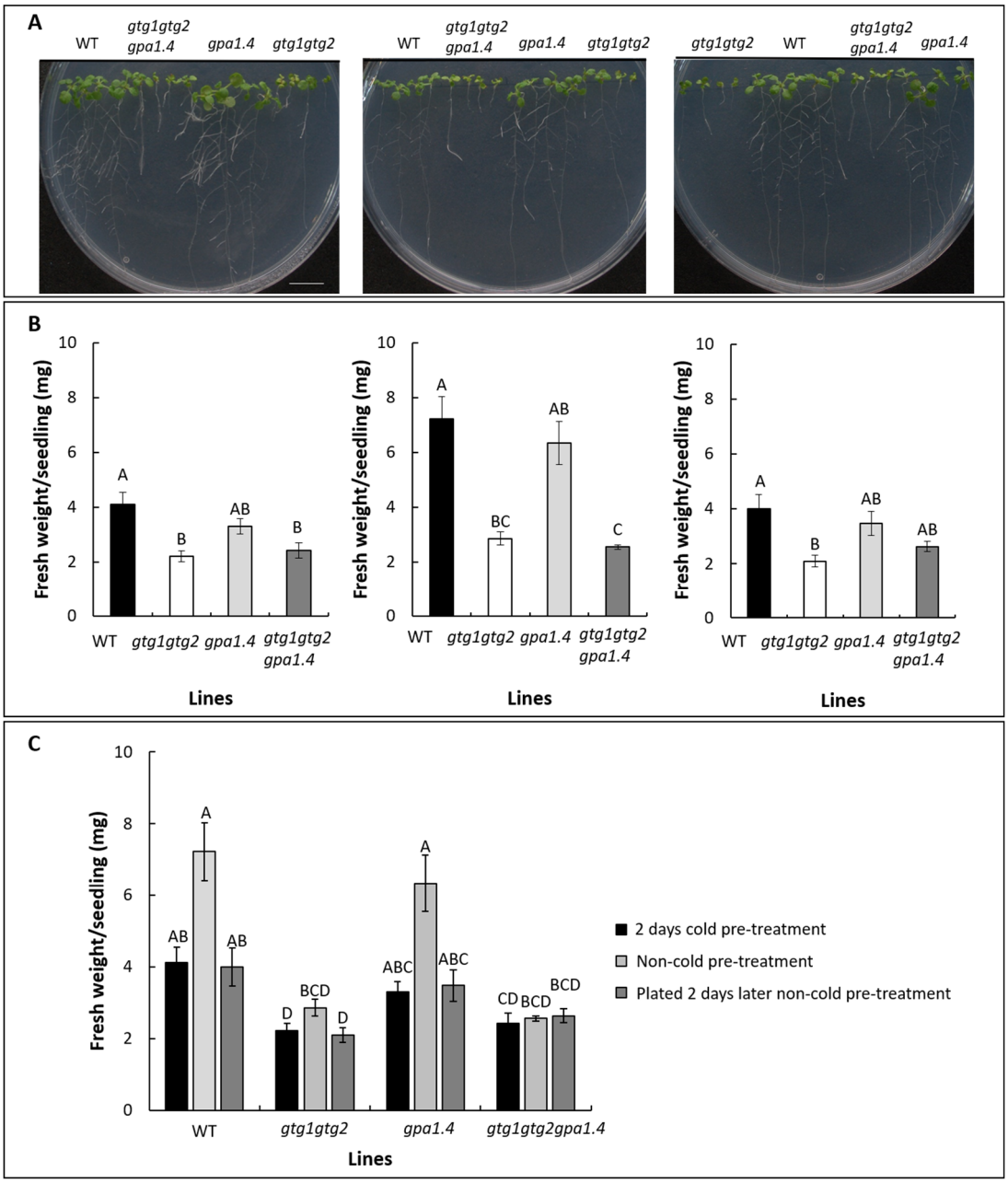

Figure 5.8. Fresh weight per seedling of WT, *gtg1gtg2, gpa1.4* and *gtg1gtg2gpa1.4* mutants in different cold pre-treatment conditions

A) Representative images of seedlings at day 14 with a 2 day at 4°C pre-treatment (left), no pre-treatment growing at 23°C for those 2 days (middle) and no pre-treatment seeds plated 2 days later (right); scale bar 1 cm. Fresh weight per seedling at 14 days (B) of WT (black), *gtg1gtg2* (white), *gpa1.4* (light grey) and *gtg1gtg2gpa1.4* (dark grey) grown on 0.5 MS in the absence of sucrose with the three different pre-treatment as above. C) Comparison of the fresh weight with the three pre-treatment conditions. Data represent the mean (±SEM) of four plates with four seedlings per line per plate (n=4). One-way ANOVA in B and Two-ways ANOVA in C ($p < 0.05$). Means not sharing a letter are significantly different; Tukey *post-hoc* test.

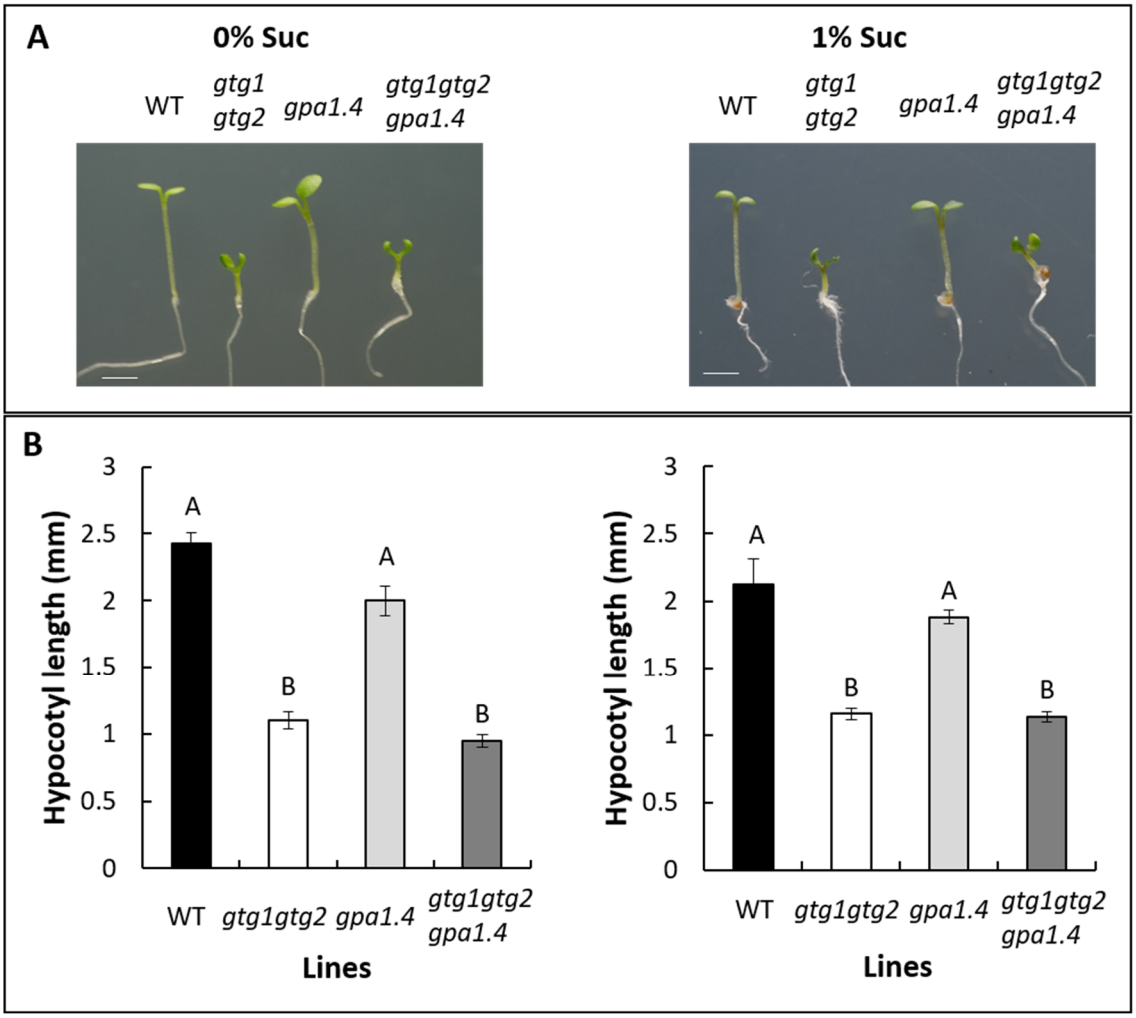

Figure 5.9. The *gpa1.4* mutation does not affect the defective hypocotyl growth of *gtg1gtg2* mutant in low white light conditions in the presence and absence of sucrose

A) Representative images of hypocotyl at day 5 in the absence (left) and presence of sucrose (right); scale bar 1mm. B) Hypocotyl length at 5 days of WT (black), *gtg1gtg2* (white), *gpa1.4* (light grey), *gtg1gtg2gpa1.4* (dark grey) grown in 0.5 MS without sucrose (left) and with 1% sucrose (right) at 10 µmol m^{-2} s^{-1} light intensity. Data represent the mean (±SEM) of six plates with 15 seedlings per line per plate (n=80-90). One-way ANOVA ($p < 0.05$). Means not sharing a letter are significantly different; Tukey *post-hoc* test.

However, when the seedling was grown in the dark, the *gtg1gtg2gpa1.4* mutant hypocotyl was more affected in comparison with the WT and *gpa1.4* but also more than *gtg1gtg2*. In the presence and absence of sucrose, *gtg1gtg2gpa1.4* displayed a

considerable reduction in hypocotyl length in comparison with the single and double mutant (Figure 5.10). This defect in hypocotyl growth in the *gtg1gtg2gpa1.4* mutant was observed at day 5 and 7 of growth in the dark. The *gtg1gtg2* and *gpa1.4* mutants also exhibited a reduced hypocotyl growth in comparison to WT in the presence and absence of sucrose. *gpa1.4* mutant has already been reported to display a shorter hypocotyl length when grown in the dark (Ullah et al., 2001, Chen et al., 2006a). However, in a previous study, the *gtg1gtg2* mutant did not show the reduced hypocotyl growth in dark conditions (Jaffé et al., 2012). This difference could be due to slight differences in conditions or growth media but as much as possible these had been kept the same.

To analyse whether this reduced hypocotyl growth in the *gtg1gtg2gpa1.4* mutant was an additive effect of *gtg1gtg2* and *gpa1.4* mutations, the differences of hypocotyl growth of the lines in reference to WT were calculated. Apart from the hypocotyl growth in the absence of sucrose at day 5, in the other cases, the reduction of the hypocotyl length of the *gtg1gtg2gpa1.4* was higher than the reduction of the hypocotyl growth of the *gtg1gtg2* and *gpa1.4* combined (Figure 5.11). This indicates that in the presence of sucrose and after 7 days of growth, the reduction in hypocotyl length of *gtg1gtg2gpa1.4* is more than an additive effect of *gtg1gtg2* and *gpa1.4* mutations.

To corroborate the *gtg1gtg2gpa1.4* defective hypocotyl phenotype, a further dark phenotype experiment was performed. To activate seed germination, in our previous experiments the seeds were exposed for two hours to white light prior to the dark treatment. To examine whether the phenotype observed in *gtg1gtg2gpa1.4* was dependent on this light treatment, a growth experiment in dark conditions was performed where no light pre-treatment was applied. In complete darkness, the *gtg1gtg2gpa1.4* hypocotyl was shorter in comparison to the WT, *gtg1gtg2* and *gpa1.4* lines (Figure 5.12). As shown in previous experiments (Figure 5.10), *gtg1gtg2* also exhibited a reduced hypocotyl growth in comparison to the WT, however the hypocotyl length is longer than the *gtg1gtg2gpa1.4* mutant. A similar observation was made with *gpa1.4*, which also displayed a shorter hypocotyl length than the WT. However, the inhibition of hypocotyl length in *gtg1gtg2gpa1.4* is higher than WT, *gtg1gtg2* and *gpa1.4*. This suggests that the lack of AtGPA1 is affecting the defective hypocotyl growth of the *gtg1gtg2* in the dark, indicating a possible connection between GTGs and GPA1 in the regulation of hypocotyl growth in the dark.

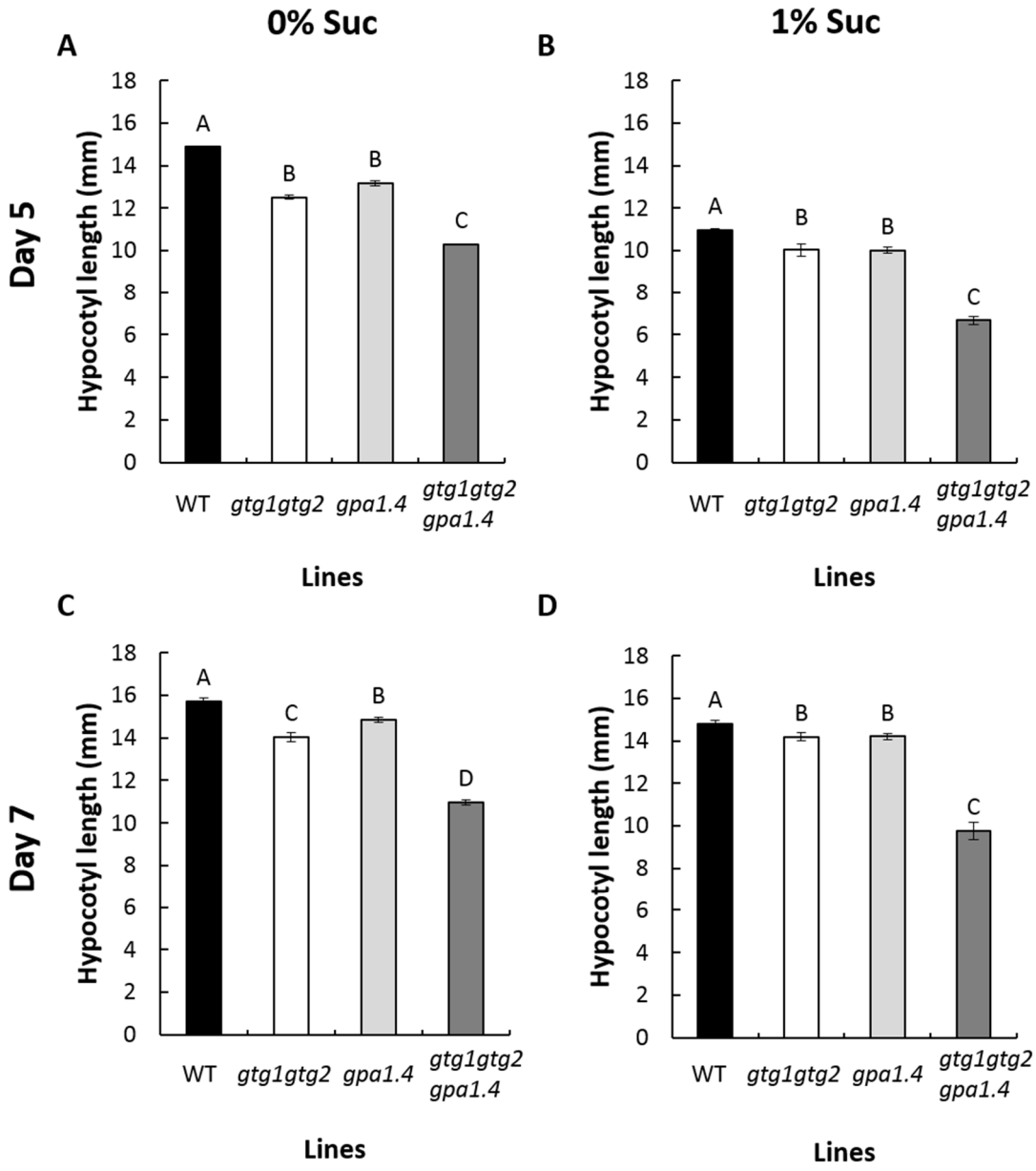

Figure 5.10. *gtg1gtg2gpa1.4* exhibits shorter hypocotyls in dark conditions in the presence and absence of sucrose

Hypocotyl length of WT (black), *gtg1gtg2* (white), *gpa1.4* (light grey), *gtg1gtg2gpa1.4* (dark grey) grown on 0.5 MS without sucrose (left) and with 1% sucrose (right) in darkness during day 5 (top) and 7 (bottom). Data represent the mean (±SEM) of six plates with 15 seedlings per line per plate (n=80-90). One-way ANOVA ($p < 0.05$). Means not sharing a letter are significantly different; Tukey *post-hoc* test.

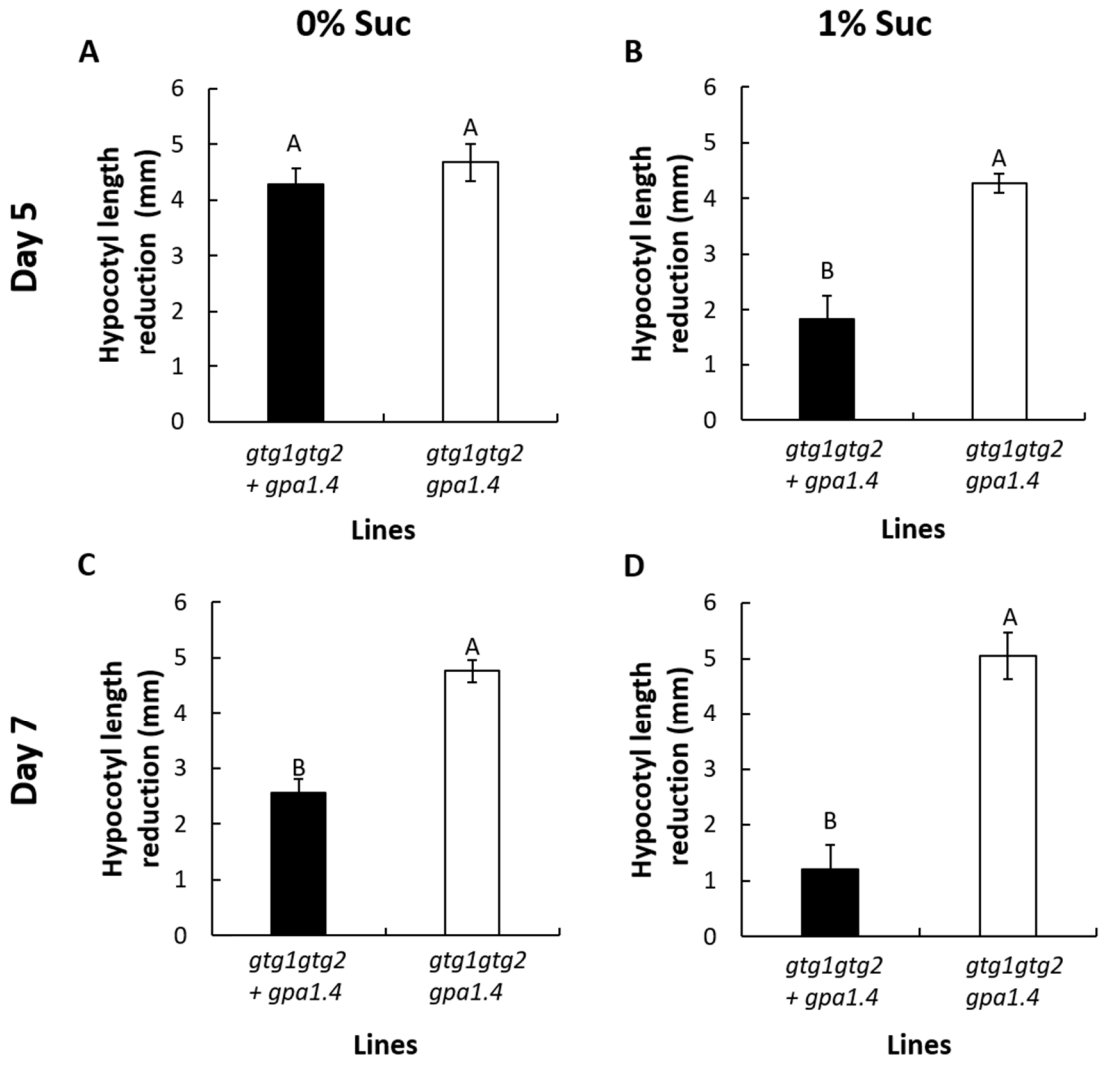

Figure 5.11. Inhibition of the hypocotyl growth in *gtg1gtg2gpa1.4* compared with the reduction of the hypocotyl growth in *gtg1gtg2* and *gpa1.4* combined

Reduction of hypocotyl growth *gtg1gtg2* and *gpa1.4* combined (black) and *gtg1gtg2gpa1.4* mutants (white) in relation to the WT grown 0.5 MS without sucrose (left) and with 1% sucrose (right) in darkness during day 5 (top) and 7 (bottom). Data represent the difference between the means (±SEM) of six plates with 15 seedlings per line per plate (n=6). One-way ANOVA ($p < 0.05$). Means not sharing a letter are significantly different; Tukey *post-hoc* test.

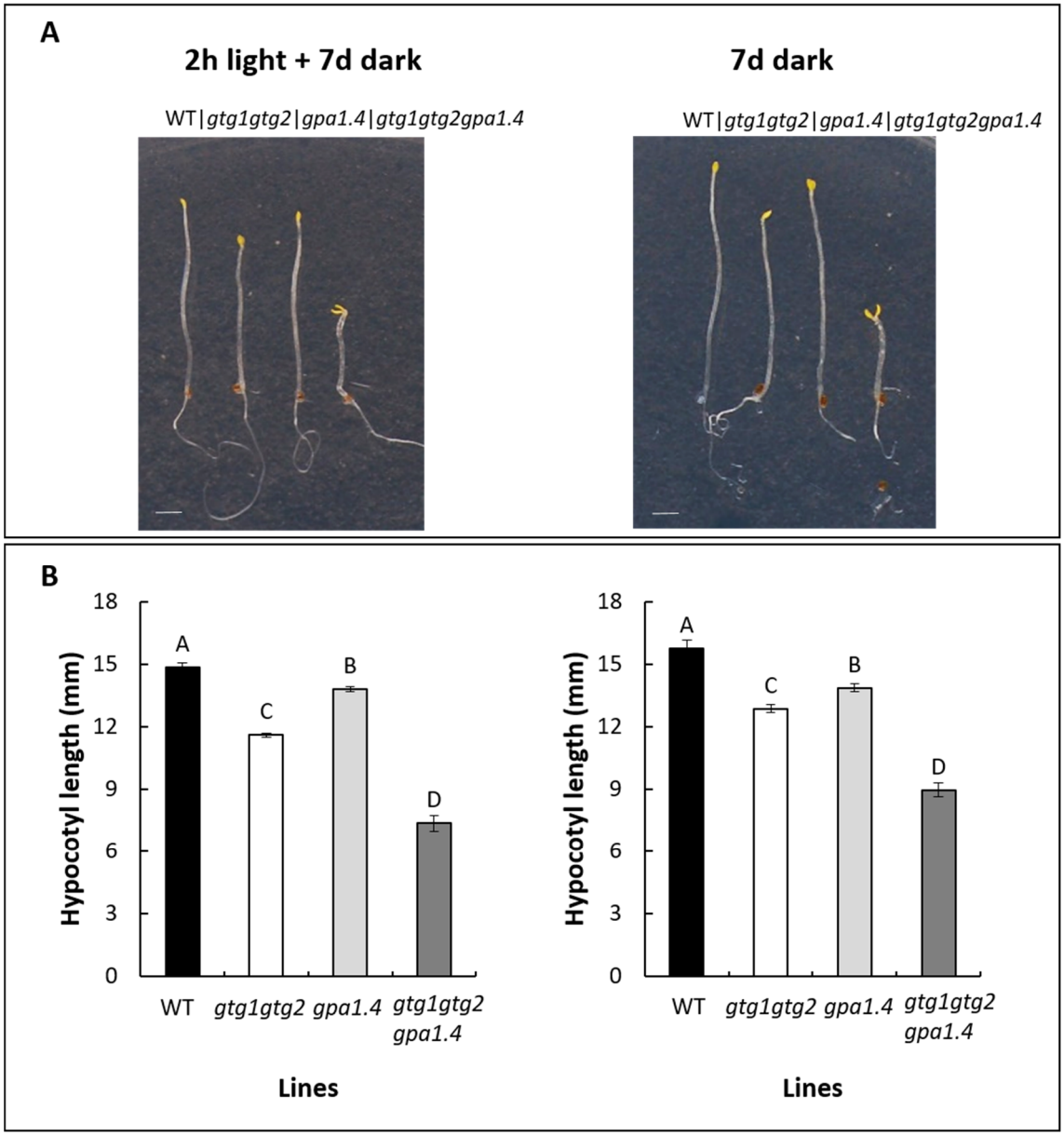

Figure 5.12. *gtg1gtg2gpa1.4* mutant displays a shorter hypocotyl when grown in complete darkness in the absence of sucrose

A) Representative images of hypocotyl at day 7 with 2 hours white light (left) and without white light (right); scale bar 1mm. B) Hypocotyl length at 7 days of WT (black), *gtg1gtg2* (white), *gpa1.4* (light grey), *gtg1gtg2gpa1.4* (dark grey) lines grown in 0.5 MS without sucrose in darkness with 2h of white light exposure at 120µmol m^{-2} s^{-1} light intensity (left) or without (right). Data represent the mean (±SEM) of six plates with 15 seedlings per line per plate (n=75-85). One-way ANOVA ($p < 0.05$). Means not sharing a letter are significantly different; Tukey *post-hoc* test.

Another characteristic observed in *gtg1gtg2gpa1.4* hypocotyls when grown under dark conditions, was that the cotyledons of the triple mutant were open in comparison to WT, *gpa1.4* and *gtg1gtg2*. Seeds that are grown in the dark develop a long hypocotyl with closed cotyledons that generate the characteristic apical hook of dark-grown seedlings. In the dark, the cotyledons of *gtg1gtg2gpa1.4* were open, whereas this effect was not observed in the WT or the *gpa1.4* single mutant (Figure 5.13). In *gtg1gtg2* a few seedlings with open cotyledons were occasionally observed but this effect was very rare and the cotyledon angle in those *gtg1gtg2* lines was smaller to the angle of *gtg1gtg2gpa1.4*. This indicates that the combined deletion of AtGPA1 and AtGTGs is producing an effect on cotyledon opening in the dark.

5.2.2.3. *gtg1gtg2gpa1.4* displays a similar phenotype to *gtg1gtg2* in long day conditions

gtg1gtg2 mutant display several other growth and fertility defects, such as short silique length and seed yield (Jaffé et al., 2012). To study whether the *gtg1gtg2gpa1.4* mutant exhibits similar defects, the growth of WT, *gtg1gtg2, gpa1.4* and *gtg1gtg2gpa1.4* plants was analysed under long day conditions (section 2.1.1). *gtg1gtg2* and *gtg1gtg2gpa1.4* mutants exhibited a reduced rosette diameter in comparison to WT and *gpa1.4* in this condition. The absence of AtGPA1 in the *gtg1gtg2* mutant background did not affect the reduced rosette growth of the mutant (Figure 5.14). This reduced rosette diameter was also observed at late stages of the plants, even at day 25 the *gtg1gtg2* and *gtg1gtg2gpa1.4* mutants still display a smaller rosette diameter compared to the WT and *gpa1.4* lines (Figure 5.14 C). In addition, it was observed that the *gtg1gtg2* and *gtg1gtg2gpa1.4* mutants developed more stems from the rosette than WT and *gpa1.4* plants (Figure 5.15 C). Significant differences were found between *gtg1gtg2* and *gtg1gtg2gpa1.4* in comparison to the WT at day 56 and 75. Interestingly, it was observed that the *gtg1gtg2gpa1.4* mutant was shorter in comparison to the rest of the lines. The *gtg1gtg2gpa1.4* mutant has a reduced height in comparison not only to WT and *gpa1.4* but also the *gtg1gtg2* mutant (Figure 5.15 A-B). This indicates that the absence of GTGs and GPA1 produced a stronger effect on the height of the plant.

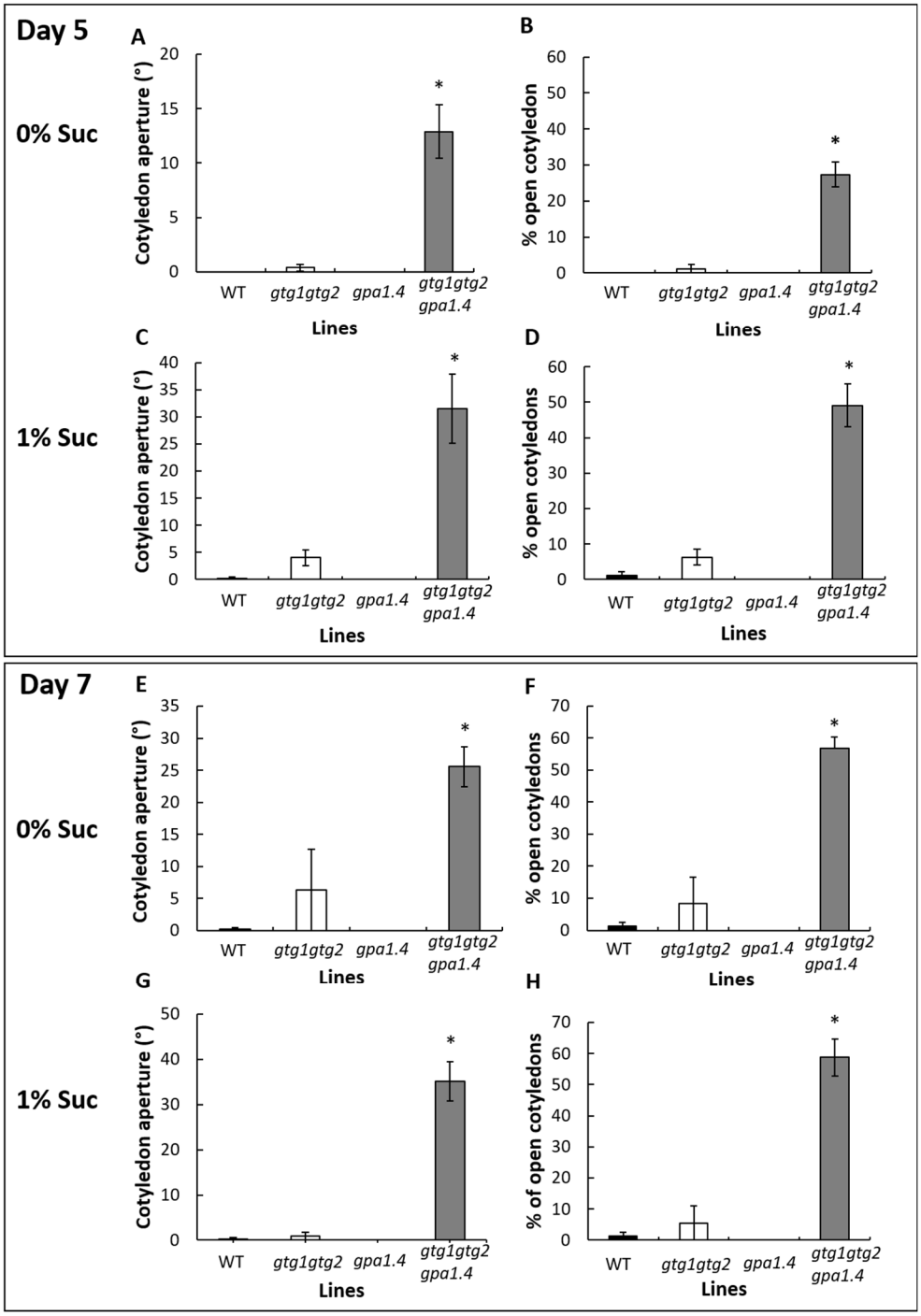

Figure 5.13. *gtg1gtg2gpa1.4* has open cotyledons when grown in darkness

Cotyledon angle of WT (black), *gtg1gtg2* (white), *gpa1.4* (light grey), *gtg1gtg2gpa1.4* (dark grey) grown on 0.5 MS without sucrose (A and E) and with sucrose (C and G) in the dark during 5 (top) and 7 days (bottom). Percentage of hypocotyls with open cotyledons without sucrose (B and F) and with sucrose (D and H) grown in the same conditions. The data represent the mean (±SEM) of six plates with 15 seedlings per line per plate (n=75-85). Kruskal-Wallis ($p < 0.05$); Asterisk means significant difference.

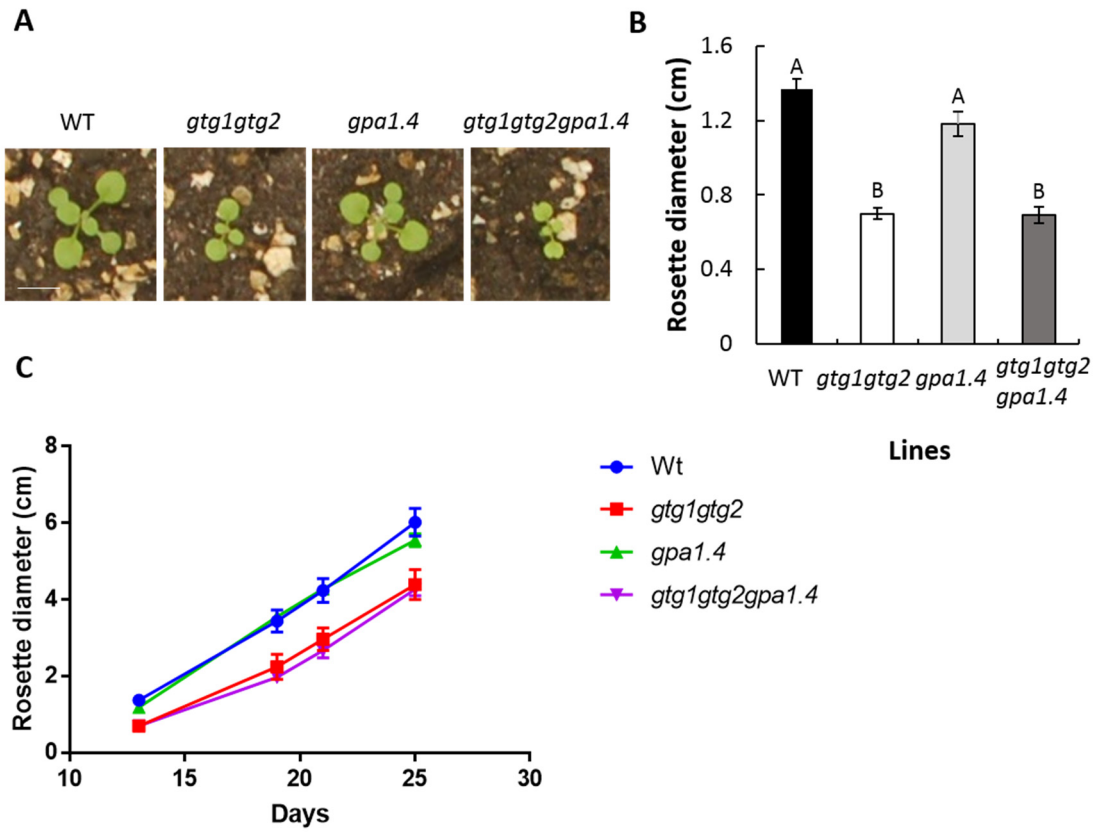

Figure 5.14. *gtg1gtg2gpa1.4* and *gtg1gtg2* mutants show a similar reduced rosette diameter

A) Representative picture of the rosette at day 13 of WT, *gtg1gtg2*, *gpa1.4* and *gtg1gtg2gpa1.4* under long day conditions; scaler bar 5 mm. B) Rosette diameter at day 13 of WT (black), *gtg1gtg2* (white), *gpa1.4* (light grey) and *gtg1gtg2gpa1.4* (dark grey). C) Rosette diameter of the lines at day 13, 19, 22 and 25 in long day conditions. Results represent the mean (±SEM) of 10 plants per line. One-way ANOVA ($p < 0.05$). Means not sharing a letter are significantly different; Tukey *post-hoc* test.

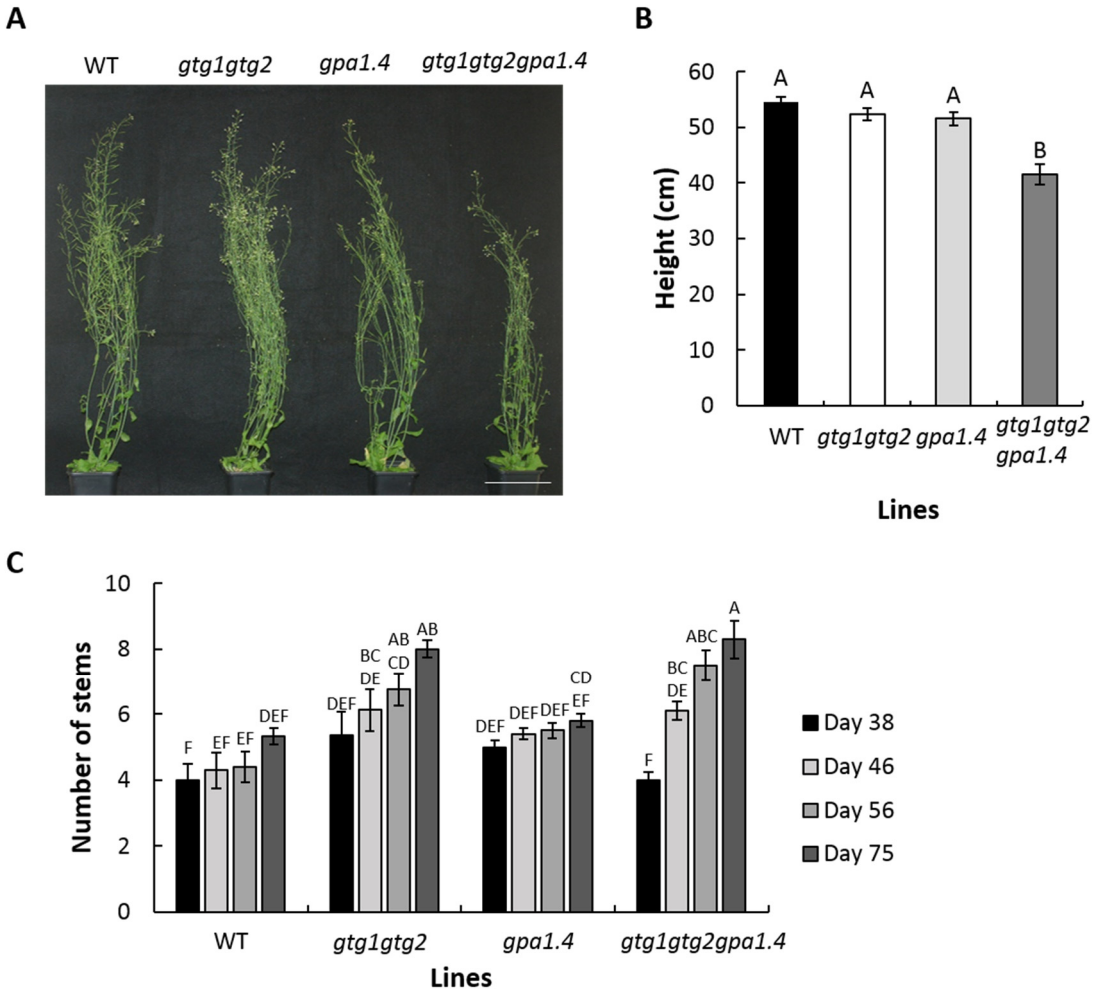

Figure 5.15. *gtg1gtg2gpa1.4* mutant shows a reduced height in long day conditions

A) Representative plants are shown for the lines growing in long day conditions. B) Height of WT (black), *gtg1gtg2* (white), *gpa1.4* (light grey) and *gtg1gtg2gpa1.4* (dark grey) at day 27 grown under long day conditions. C) Number of stems at day 38, 46, 56 and 75. Results represent the mean (±SEM) of 10 plants per line. One-way ANOVA (B) and two-way ANOVA (C) ($p < 0.05$). Means not sharing a letter are significantly different; Tukey *post-hoc* test.

The number of days to bolting was similar between *gtg1gtg2gpa1.4*, *gtg1gtg2* and *gpa1.4*, and the three mutants showed a delayed bolting time compared to WT (Figure 5.16). Analysis of the days until flowering, showed that *gtg1gtg2gpa1.4* has a flowering time similar to *gtg1gtg2* and *gpa1.4,* however it flowers later than WT. No significant differences were observed in the days to flowering between WT, *gtg1gtg2* and *gpa1.4*.

As described before, the g*tg1gtg2* mutant exhibits a fertility defect, showing a reduced silique and seed yield phenotype (Jaffé et al., 2012). The *gtg1gtg2gpa1.4* exhibited a similar defective fertility phenotype as the *gtg1gtg2* double mutant. The siliques of the triple mutant were shorter than the WT and *gpa1.4*; however they exhibited the same size as *gtg1gtg2* (Figure 5.16 D). The same observation was made with seed yield, where it was observed that *gtg1gtg2* and *gtg1gtg2gpa1.4* had a reduced amount of seeds in comparison to the WT and *gpa1.4* lines (Figure 5.16 C).

5.2.3. Studying the *in vivo* interaction of OsGTG with RGA1 by a bimolecular complementation assay

It has been proposed that GTGs interact with the Gα subunit of G protein (see section 1.5.4.2), and this has been shown in Arabidopsis and rice (Pandey et al., 2009, Ma et al., 2015). It is well-known that the Arabidopsis and rice Gα subunits localise to the plasma membrane (Kato et al., 2004, Chen et al., 2006a, Wang et al., 2008b); however, the fact that OsGTG did not localise at the plasma membrane (Figure 3.25) raised doubts as to whether OsGTG and RGA1 could actually interact. To address this issue, BiFC was used.

BiFC is an *in vivo* technique where one of the proteins of interest is tagged with the N-terminal part of YFP and the other protein is tagged with the C-terminal part and when both proteins are close together, the YFP protein is reconstituted producing a fluorescence signal. OsGTGe and OsGTGg were tested to see whether they were able to interact with RGA1 as seen previously (Ma et al., 2015). OsGTGe and OsGTGg were already cloned into the pENTR/D vector (sections 3.2.1 and 3.2.2), and for this assay *RGA1* needed to also be cloned. *RGA1* CDS sequence from *O. sativa* Nipponbare ecotype was obtained from the Rice Genome Annotation Project database (LOC_ Os05g0333200 in http://rice.plantbiology.msu.edu/). *RGA1* CDS amplification was carried out using RNA extracted from rice Nipponbare leaf followed by cDNA synthesis.

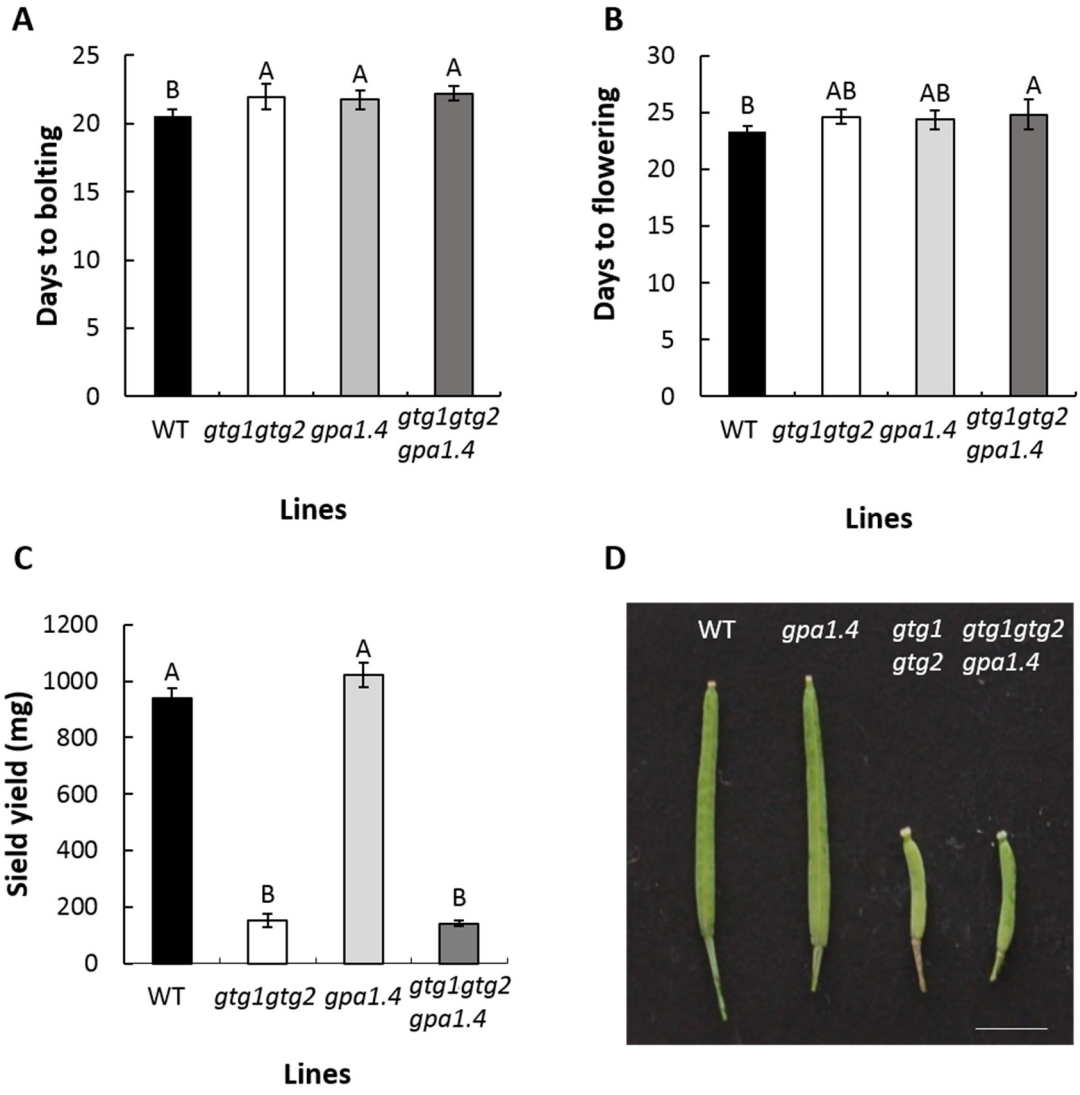

Figure 5.16. *gtg1gtg2gpa1.4* exhibits similar silique length and seed yield defects to the *gtg1gtg2* double mutant

Bolting day (A), flowering day (B) and seed yield per plant (C) of WT (black), *gtg1gtg2* (white), *gpa1.4* (light grey) and *gtg1gtg2gpa1.4* mutants (dark grey) growth on long day conditions. Results represent the mean (±SEM) of 10 plants per lines. One-way ANOVA ($p < 0.05$). Means not sharing a letter are significantly different; Tukey *post-hoc* test. D) Representative images of the siliques; scale bar 3mm.

Two versions were generated, with and without the stop codon and both versions were cloned into the pENTR/D entry vector (section 2.3.8) generating pENTR/D *RGA1*-stop and pENTR/D *RGA1*-no stop constructs (Figure 5.17 A). The entry vectors were transformed into *E.coli* and colony PCR and restriction digest of the plasmid were performed to confirm that the gene was cloned in the right direction (Figure 5.17 B). Both entry vectors were sequenced in forward and reverse directions and the sequencing results corroborated the sequence predicted by the Rice Genome Annotation Project database.

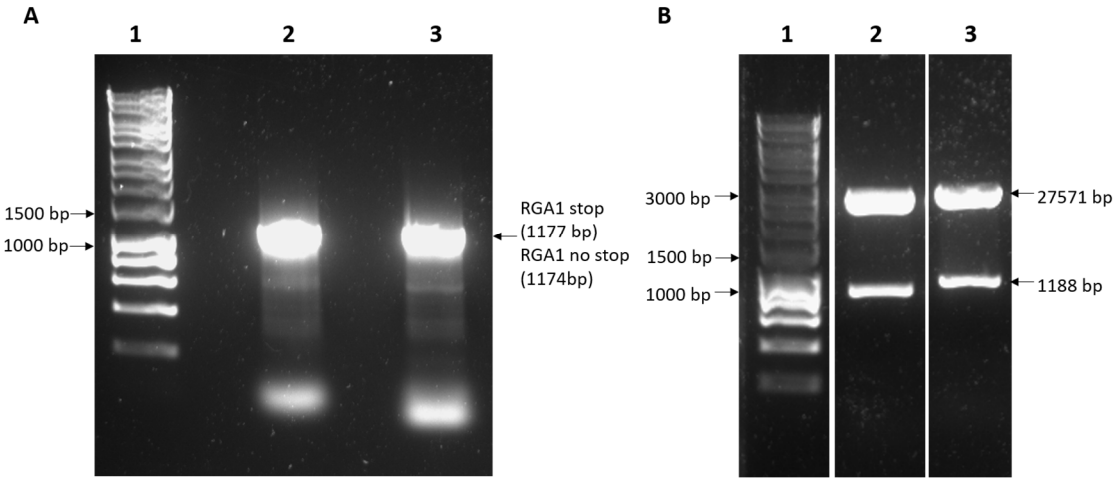

Figure 5.17. Amplification and cloning of *RGA1* with and without the stop codon into the pENTR/D vector

RGA1 gene products with stop codon (primers RGA1 topo F2 + RGA1 stop R2, predicted size 1177 bp, lane 2) and without the stop codon (RGA1 topo F2 + RGA1 no stop R1, predicted size 1174 bp, lane 3) were amplified by PCR from *O. sativa* Nipponbare cDNA in A). Restriction digest of pENTR/D *RGA1*-stop (lane 2) and pENTR/D *RGA1*-no stop (lane 3) using *Mlu*I in B). Predicted products are shown on the right and molecular markers on the left (lane 1).

For the BiFC assays, two specific vectors were used: pDEST GwVYCE and pDEST GwVYNE (Gehl et al., 2009). Both plasmids are driven by the 35S promoter and in both the YFP fragment is C-terminally tagged to the gene of interest. However, pDEST GwVYCE contains the C-terminal fragment of YPF and pDEST GwVYNE contains the N-terminal fragment (Figure 5.18 A). *OsGTGe* (pENTR/D *OsGTGe*-no stop) and *OsGTGg* (pENTR/D *OsGTGg*-no stop) were cloned into pDEST GwVYNE and *RGA1* (pENTR/D *RGA1*-no stop) was cloned into pDEST GwVYCE by LR recombination (section 2.3.8). The reactions were transformed into *E.coli* cells and colony PCR and restriction digest were performed to confirm the right orientation of the genes (Figure 5.18). The three clones were sequenced in forward and reverse directions to confirm the correct sequence. The list of plasmids generated for the BiFC assay is shown in Table 5.2.

For the BIFC assay, the constructs were transformed into *Agrobacterium* and a mixture of the two vectors was infiltrated into tobacco leaves (section 2.5.1). All the vector combinations for this experiment are shown in Table 5.3. The development of fluorescence signal was detected two days post infiltration. As a positive control CNX6 protein was used, which encodes for a molybdopterin synthase subunit that forms dimers producing the complex CNX6/ CNX6 in Arabidopsis (Gehl et al., 2009). This protein is required to synthesize a molybdenum cofactor that is involved in molybdenum metabolism (Schwarz and Mendel, 2006, Gehl et al., 2009). The expression of the two CNX6 proteins produced a clear YFP signal at the plasma membrane of the tobacco epithelial cell (Figure 5.19 A), indicating that the infiltration and the procedure were successful. To eliminate the possibility of false positives, several combinations of the empty vectors with the complementary vectors containing OsGTGs or RGA1 were tested (see Table 5.3 for all the negative control combinations). None of those negative controls produced a fluorescence signal, only the background fluorescence produced by the stomata cells (Figure 5.19 D-G). The combination of OsGTGe and RGA1 did not produce YFP signal (Figure 5.19 B). Similarly, when OsGTGg and RGA1 were co-expressed no YFP signal reconstitution was detected (Figure 5.19 C). This indicates that in our experimental conditions OsGTGs and RGA1 do not interact.

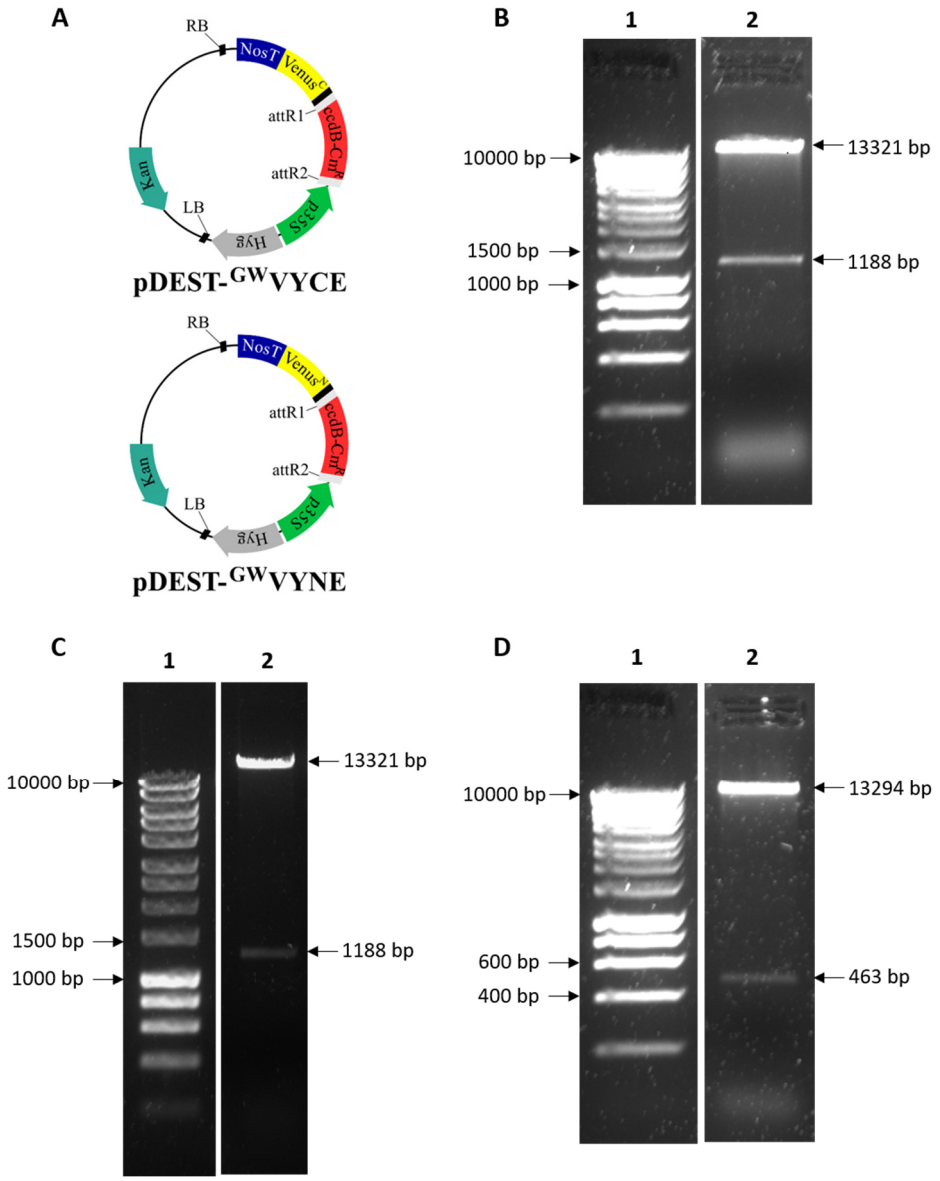

Figure 5.18. Restriction analysis of *OsGTGs* and *RGA1* cloned into the BiFC vectors

A) Diagram of pDEST GwVYCE (top) and pDEST GwVYNE (bottom) showing attR1 and attR2 recombination sites. Both vectors contain kanamycin (kan) resistance for bacteria selection, hygromycin (hyg) for plant selection, p35S promoter, Nos T terminator and *ccd*B-Cm^R killed gene. pDEST GwVYCE contains the C-terminal fragment of YFP-Venus and pDEST GwVYNE contains the N-terminal fragment. YFP is tagged in the C-terminal of the gene in both vectors. Image adapted from Gehl et al. (2009). Restriction digest of pDEST GwVYNE *OsGTGe* using *Xba*I (lane 2) (B), of pDEST GwVYNE *OsGTGg* using *Xba*I (lane 2) (C) and of pDEST GwVYCE *RGA1* using *Sac*I (lane 2) (D). Predicted products are shown on the right and molecular markers on the left (lane 1).

Table 5.2. Plasmids generated for BiFC assays

Plasmid	Description
pDEST GwVYNE *OsGTGe*	P35S::*OsGTGe*::*YFP* N-terminus
pDEST GwVYNE *OsGTGg*	P35S::*OsGTGg*::*YFP* N-terminus
pDEST GwVYCE *RGA1*	P35S::*RGA1*::*YFP* C-terminus

Table 5.3. Combinations of plasmids tested for the BiFC assay

Plasmid combinations	Description	Results
pDEST GwVYNE *CNX6* + pDEST GwVYCE *CNX6*	Positive control using a plasma membrane protein that forms dimers to confirm the infiltration process was successful.	YFP signal
pDEST GwVYNE *OsGTGe* + pDEST GwVYCE *RGA1*	To study the possible interaction between OsGTGe and RGA1	No signal
pDEST GwVYNE *OsGTGe* + pDEST GwVYCE empty vector	Negative control to check for false positives with pDEST GwVYNE *OsGTGe* construct	No signal
pDEST GwVYNE *OsGTGg* + pDEST GwVYCE *RGA1*	To study the possible interaction between OsGTGg and RGA1	No signal
pDEST GwVYNE *OsGTGg* + pDEST GwVYCE empty vector	Negative control to check for false positives with pDEST GwVYNE *OsGTGg* construct	No signal
pDEST GwVYCE *RGA1* + pDEST GwVYNE empty vector	Negative control to check for false positives with pDEST GwVYCE *RGA1* construct	No signal
pDEST GwVYNE empty vector + pDEST GwVYCE empty vector	Negative control to check for false positives with any of the empty vectors.	No signal

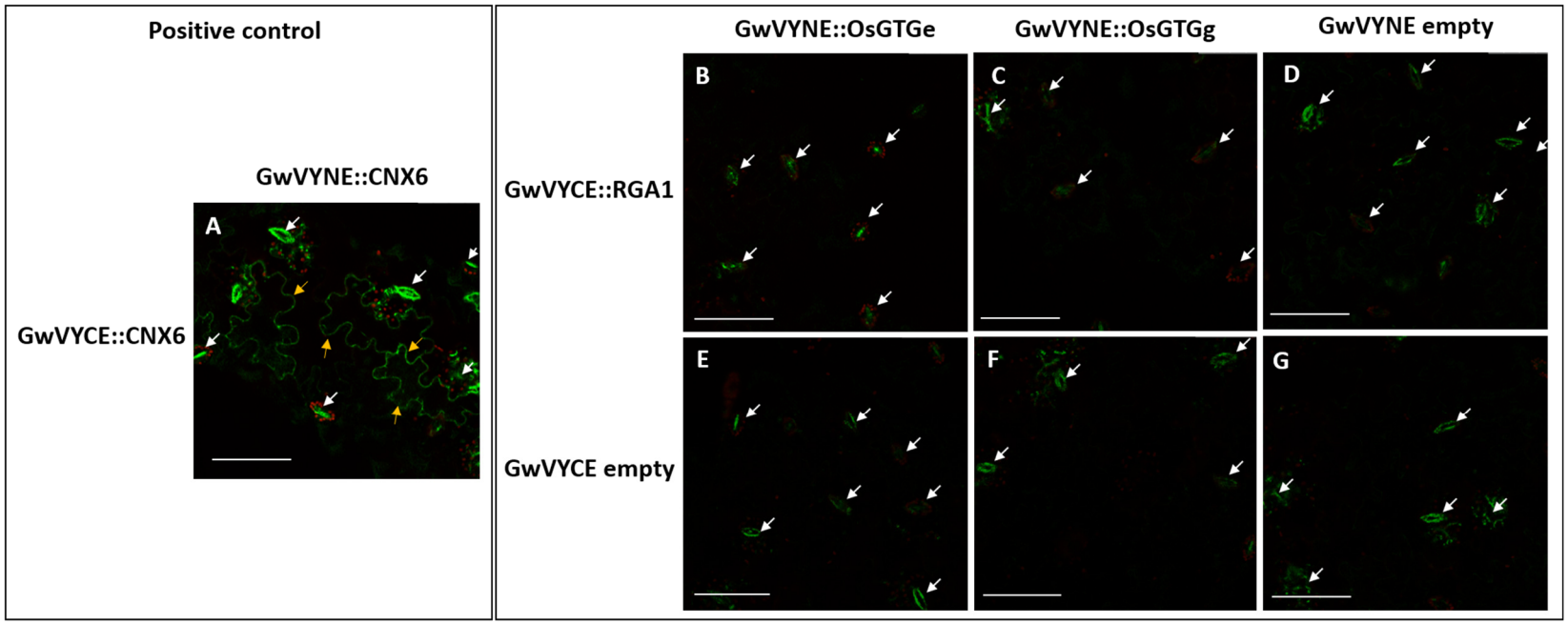

Figure 5.19. BiFC assay showed no interaction between OsGTGs and RGA1 proteins

Confocal images showing the BiFC assay where pDEST GwVYNE *OsGTGe* or pDEST GwVYNE *OsGTGg* were co-expressed with pDEST GwVYCE *RGA1* using transient expression in tobacco cells. A) Positive control expressing pDEST GwVYNE *CNX6* + pDEST GwVYCE *CNX6* (yellow arrows). Co-expression of pDEST GwVYNE *OsGTGe* + pDEST GwVYCE *RGA1* in B) and pDEST GwVYNE *OsGTGg* + pDEST GwVYCE *RGA1* in C). Negative controls co-expressing pDEST GwVYNE empty vector + pDEST GwVYCE *RGA1* in D), pDEST GwVYNE *OsGTGe* + pDEST GwVYCE empty vector in E), pDEST GwVYNE *OsGTGg* + pDEST GwVYCE empty vector in F) and pDEST GwVYNE empty vector + pDEST GwVYCE empty vector in G). Chloroplast autofluorescence in red. White arrows = stomata guard cells background. Scale bar 100 µm. The experiment was repeated three times.

5.3. Discussion

It has previously been reported that GTGs interact with the Gα subunit of the G protein complex (Pandey et al., 2009, Ma et al., 2015). However, in a study of the interactome of the Arabidopsis G proteins components, GTGs did not appear (Klopffleisch et al., 2011). To study in more depth whether GTGs could interact with Gα, a *gtg1gtg2gpa1.4* triple mutant was generated by crossing a *gtg1gtg2* with a *gpa1.4* mutant. The *gtg1gtg2gpa1.4* triple knockout was analysed to study whether the lack of Gα subunit in the *gtg1gtg2* background produced any additional defects.

5.3.1. *gtg1gtg2gpa1.4* mutant exhibits a stronger defective hypocotyl growth in dark conditions

As mentioned previously, Arabidopsis plants lacking both GTGs exhibit a light-dependent defective hypocotyl growth; under low white light conditions, the mutant displays a reduced hypocotyl length in comparison to WT (Jaffé et al., 2012). The *gtg1gtg2gpa1.4* triple mutant exhibited the same defect in hypocotyl growth under low light conditions as *gtg1gtg2* (Figure 5.9). The *gpa1.4* mutant, however, showed normal hypocotyl length in those conditions, similar to WT. Interestingly, in the dark, the *gtg1gtg2gpa1.4* mutant displayed a stronger reduction of hypocotyl length than WT, *gpa1.4* and *gtg1gtg2*. This reduction in length was more severe after 7 days of growth and in the presence of sucrose (Figure 5.10). Two different mechanisms control hypocotyl growth; one is in the dark (skotomorphogenesis) and another under light conditions (photomorphogenesis). In the dark, etiolated development is produced where cotyledons remain closed, the apical hook is formed and the hypocotyl increases in length. Under light conditions, seedlings are de-etiolated, the cotyledons open and expand, leaves are formed and hypocotyl extension is reduced. For the formation of the hypocotyl, the cell wall needs to be formed correctly for the cell to elongate (Gendreau et al., 1997). Plant growth is achieved by two main processes, biomass biosynthesis and cell expansion. The cell wall plays a critical role in both processes since it is the major component of biomass and limits cell expansion (Vandenbussche et al., 2005). Cellulose synthesis is controlled by cell trafficking and is an important factor for hypocotyl growth (Ivakov et al., 2017). Impaired cell wall formation and composition in the mutants could be one of the reasons for the reduced hypocotyl growth of the triple

mutant. It is well-known that the *gpa1* mutant has a reduced cell division and reduced cell number (Ullah et al., 2001). A study of the G protein interactome revealed important connections with cell wall biogenesis and metabolism. Some of those interactions involve xylose biosynthesis, suggesting a role for G proteins in cell wall formation (Klopffleisch et al., 2011). In addition, G protein mutants have altered the xyloglucan cell wall composition (Klopffleisch et al., 2011), which indicates that the *gpa1.4* mutant could have its cell wall formation and composition affected, contributing to the reduction of cell elongation observed in the *gtg1gtg2gpa1.4* hypocotyl.

Regarding to *gtg1gtg2*, a microarray study performed in our laboratory revealed that the expression of various cell wall synthesis genes was altered in the mutant (Jaffé et al., 2012). In addition, the hypocotyl of the double mutant displays swollen epidermal cells that resemble mutants affected in cell wall components (Desnos et al., 1996, Fagard et al., 2000, Shevell et al., 2000). All this can indicate a defect in cell wall formation and modification in *gtg1gtg2.* Since *gpa1.4* and *gtg1gtg2* mutants seem to have a defective cell wall formation and composition (Klopffleisch et al., 2011, Jaffé et al., 2012), it is possible that the combination of the three mutations could produce a stronger phenotype in the hypocotyls grown in the dark. This is clearly seen after seven days of growth and in the presence of sucrose, where the reduction of hypocotyl growth observed in the *gtg1gtg2gpa1*.4 mutant was greater than the reduction of growth of the single and double mutant together (Figure 5.11). These results suggest a possible synergistic interaction between AtGTGs and AtGPA1 in the regulation of hypocotyl growth in the dark.

Previous work in our laboratory suggested that AtGTGs could be involved in sucrose metabolism since the root length defect observed in the *gtg1gtg2* mutant was rescued in the presence of sucrose and genes involved in sugar transport were altered in the mutant (Jaffé et al., 2012). At the same time, it is known that G proteins are involved in sugar sensing since *gpa1* and *agb1* mutants are hypersensitive to glucose inhibition of germination, root elongation and seedling development (Ullah et al., 2002, Huang et al., 2006, Pandey et al., 2006). The hypocotyl length of the *gpa1* mutant was reduced in the presence of sucrose (Ullah et al., 2002). In addition, AtRGS1, the regulator of G protein signalling, was proposed to function as a glucose receptor (Grigston et al., 2008) and exhibits hyposensitivity to glucose and sucrose (Chen et al., 2006b, Johnston et al., 2007). This could suggest that the strong effect observed in the

gtg1gtg2gpa1.4 hypocotyls grown in the presence of sucrose could be due to AtGTGs and AtGPA1 being involved in sugar sensing and metabolism.

It was previously shown that *gtg1gtg2* exhibited a reduced hypocotyl growth under light conditions but this defect was not observed in hypocotyls grown in the dark (Jaffé et al., 2012). However, in this project it was observed that *gtg1gtg2* mutant also displays a reduced hypocotyl length in comparison to the WT under dark conditions (Figure 5.10, Figure 5.12). This could be due to a different set of seeds or slightly different experimental conditions. However, experiments were repeated under the same conditions using different seed batches and the same result was obtained. In addition, to ensure this was not due to a WT seed batch problem, a WT from *gtg1gtg2* and *gpa1.4* cross was isolated and experiments were carried out using this plant. Those phenotype experiments also revealed a reduced hypocotyl length for *gtg1gtg2* in comparison to the WT. Nevertheless, since AtGTGs are involved in cell wall formation and the hypocotyl of double mutant displays a cellular distortion with irregularly shaped cells (Jaffé et al., 2012), it is not surprising that the *gtg1gtg2* mutant also exhibits a reduced hypocotyl growth in the dark. It would be interesting to investigate whether that defective cell morphology is also seen in *gtg1gtg2gpa1.4* mutant hypocotyls.

In the *gtg1gtg2gpa1.4* mutant, the cotyledons of the hypocotyls grown in the dark were open in a high proportion (Figure 5.13). During skotomorphogenesis, the cotyledons are closed forming the apical hook (Gendreau et al., 1997). Hormones play an important role in the regulation of the cotyledon closure in the dark-grown seedlings. This light-grown characteristic observed in the *gtg1gtg2gpa1.4* hypocotyls grown in the dark has been observed in plants that have an impairment in hormone synthesis. One well-known mutant is the Arabidopsis deetiolated mutant (*det*), which is defective in the BR synthesis. The *det1* mutant displays open cotyledons in dark-grown hypocotyls (Wei and Deng, 1996). It was suggested that DET1 could positively regulate the phytochrome interactor factor PIFs that are responsible for blocking photomorphogenesis and repressing the opening of cotyledons in the dark (Dong et al., 2014). GA function may also be altered in the *det1* mutant since DET1 also regulates DELLA protein levels (Li et al., 2015). The *det2* mutant is also defective in BR biosynthesis and displays open cotyledons in seedlings grown in the dark (Li et al., 1996). The *dwf4* (Arabidopsis *dwarf 4*), is a mutant that also displays short and open cotyledons in seedlings grown in the dark and this phenotype can be rescued using BR, suggesting that BR could be involved in hypocotyl development (Azpiroz et al., 1998).

BR-insensitive 1 mutant, *bri1* also shows short and open cotyledons in dark-grown seedling (Clouse et al., 1996, Gou et al., 2012). BR and GA are hormones involved in hypocotyl elongation (Gendreau et al., 1997). The *gpa1.4* mutant exhibits reduced sensitivity to BR in hypocotyl growth and seed germination (Ullah et al., 2002). It has been reported that *gpa1.4* mutant has an enhanced cell division defect in *bri1-5*, a BR receptor mutant (Gao et al., 2008). In addition, *gtg1gtg2* mutant has altered gene expression that regulates plant hormones, some involved in BR and GA synthesis that can affect the development of the hypocotyls (Jaffé et al., 2012). It is possible that *gpa1.4* mutation is exacerbating the defect in hormone synthesis and therefore hormone balance in the *gtg1gtg2gpa1.4* mutant producing the open cotyledons feature observed hypocotyls grown in the dark.

5.3.2. Gα mutation does not affect the defective root growth seen in *gtg1gtg2* phenotype

The *gtg1gtg2* mutant also displays a shorter primary root and reduced biomass in comparison to WT (Jaffé et al., 2012). To study whether the *gtg1gtg2gpa1.4* mutant displays the same defective root phenotype, the mutant was grown vertically in the absence of sucrose. The *gtg1gtg2gpa1.4* line exhibited the same reduced root growth as the *gtg1gtg2* mutant, whereas *gpa1.4* displayed a normal root length similar to the WT (Figure 5.6). This indicates that the effect observed in root growth is mainly produced by the lack of GTGs and it is not affected by the deletion of *GPA1*. Although G proteins are well-known to be involved in cell proliferation (Urano et al., 2016) and their interactome contains important connections with cell wall biogenesis and metabolism (Klopffleisch et al., 2011), the *gpa1.4* mutant is not affected in root (Ullah, 2003). Therefore, the *gpa1.4* mutation does not affect the root growth of the *gtg1gtg2gpa1.4* mutant, indicating the reduced cell elongation and hence the reduced root growth observed in the triple mutant is due to the absence of AtGTGs. As discussed in the previous section, the involvement of AtGTGs in the expression of cell wall synthesis and modifications genes (Jaffé et al., 2012), can contribute to the defect in root growth observed in the double mutant.

In addition, auxins, which are hormones involved in root elongation (Overvoorde et al., 2010) are also impaired in the *gtg1gtg2* mutant. The double mutant has altered several auxin-related genes, such as auxin transporters and auxin-responsive genes (Jaffé et al., 2012). Although the *gpa1.4* mutant has a WT root phenotype, the

overexpressor exhibits inhibition of root growth (Ullah, 2003). The Gβ subunit negatively regulates auxin-induced genes that are involved in cell division, affecting several developmental processes. This is seen in Arabidopsis Gβ mutants that exhibit a small root (Ullah, 2003). It is possible that in the *gtg1gtg2gpa1.4*, the lack of GTGs and GPA1 can affect Gβ subunit, making it inactive. This Gβ inactivation could also affect the root growth of *gtg1gtg2gpa1.4.* Analysis of a quadruple mutant lacking GTGs, GPA1 and AGB1 could contribute to understanding the connection between those proteins.

5.3.3. *gtg1gtg2gpa1.4* is shorter at maturity than *gtg1gtg2* under long day conditions

Most of the *gtg1gtg2gpa1.4* phenotypes observed, such as rosette diameter, days to bolting and flowering and number of stems from the rosette, were similar to the *gtg1gtg2* mutant. However, one interesting distinct phenotype observed in *gtg1gtg2gpa1.4* was the reduced height in comparison to WT, *gpa1.4* and even *gtg1gtg2* lines (Figure 5.15). Since *gtg1gtg2* and *gpa1.4* mutants have a defective cell wall formation and cell elongation (Klopffleisch et al., 2011, Jaffé et al., 2012), this could affect not only the hypocotyl length as previously discussed; but also alter the size of the whole plant. It is known that hormones such as BR and GA regulate plant height (Chinnusamy et al., 2010). In the *bri1* mutant, which lacks a BR receptor, the *gpa1.4* mutation enhanced the cell division and elongation defect observed in the mutant. It was reported that although *gpa1.4* single mutant displays a normal height, the *gpa1.4bri1* double mutant exhibits a dwarf phenotype (Gao et al., 2008). Although *gtg1gtg2gpa1.4* does not display a dwarf phenotype, it has a reduced height in comparison to the WT, *gtg1gtg2* and *gpa1.4* plants. This could be due to the effect generated by the impaired hormone signalling in *gtg1gtg2* that can be exacerbated by the *gpa1.4* mutation.

It was observed that *gtg1gtg2* and *gtg1gtg2gpa1.4* mutants produced more stems from the base than WT and *gpa1.4* (Figure 5.15 C). Shoot formation requires a specific cytokinin and auxin ratio (Hwang and Sheen, 2001, Cary et al., 2002). It is possible that in *gtg1gtg2* and *gtg1gtg2gpa1.4* the levels of auxin and cytokinin are altered generating a hormone balance that enhances the formation of stems. Leaf development is also a process regulated by different hormones. The regulation of auxin fluxes in the meristem tissues is involved in leaf growth (Keuskamp et al., 2010, Rodriguez et al., 2014). PIN-FORMED (PIN), is an auxin transporter that regulates auxin fluxes in the meristem of

Arabidopsis (Rodriguez et al., 2014). PIN3 and other auxin transporters are downregulated in *gtg1gtg2* (Jaffé et al., 2012) and this can affect the auxin fluxes produced in the meristems and as a result, can affect the development and growth of the mutants.

5.3.4. *gtg1gtg2gpa1.4* mutant shows the same fertility defect as *gtg1gtg2*

The *gtg1gtg2* mutant has been reported to have a defective fertility phenotype, with reduced silique size and seed yield (Jaffé et al., 2012). The *gpa1.4* mutant does not have those defective phenotypes, it is mostly Gβ mutant which exhibits short and wide siliques (Ullah et al., 2003, Chen et al., 2006a). The *gtg1gtg2gpa1.4* mutant exhibited the same reduced silique and seed yield as *gtg1gtg2*, however, *gpa1.4* had a WT-like silique size and seed yield (Figure 5.16). The reason for the defect seen in silique size and seed yield in the *gtg1gt2* mutant was reduced pollen germination and pollen tube elongation. It would be interesting to study whether the triple mutant also exhibits the same pollen defects. Studies in *gpa1.4* mutants have shown lower germination and shorter pollen tubes, in comparison to overexpressor lines that had higher germination percentage and longer pollen tubes (Wu et al., 2007). Gα has been proposed to be involved in plasma membrane hyperpolarization by activating Ca^{2+} permeable channels in pollen cells (Wu et al., 2007) and Ca^{2+} is involved in pollen germination and elongation, and it is required for pollen tube growth (Dutta and Robinson, 2004). Ion channels are also involved in pollen growth; in tobacco, pollen localised Cl^- channels have been involved in pollen germination and tube elongation (Breygina et al., 2009, Gutermuth et al., 2013). As mentioned previously, work in our laboratory has demonstrated that AtGTG1 function as an anion channel, as proposed for the mammalian GTG/GPHR, and may be able to regulate the Cl^- homeostasis that is required for pollen growth.

5.3.5. Do GTGs and GPA interact?

In this chapter, it was shown that OsGTG and RGA1 did not interact in our BiFC experimental conditions (Figure 5.19). However, another protein-protein interaction technique, such as co-immunoprecipitation or split-luciferase complementation, should be used to confirm this result. It has been previously shown that OsGTG and RGA1 were able to interact in a BiFC assay (Ma et al., 2015), however this was performed

using a different set of vectors that could account for the differences observed. pSPYNE 173 and pSPYCE (M) were used in Ma et al. (2015), and the Gateway pDEST GwVYCE and pDEST GwVYNE were used in this thesis. Although both sets of vectors contained the 35S CaMV promoter, the YFP fragments were different for each set of vectors; the pSPYNE 173/pSPYCE (M) vectors use eYFP, an enhanced YFP, and the pDEST GwVYCE and pDEST GwVYNE used Venus, a modified YFP that exhibits brighter fluorescence and folding (Walter et al., 2004, Waadt et al., 2008, Gehl et al., 2009). In addition, in Ma et al. (2015) no set of negatives control combinations were reported. Only a combination of a different protein, OsBAK1, a BRI1-Associated Receptor Kinase 1, with OsGTG was reported as a negative control. It is known that in BiFC technique there is a high likelihood of a false positive due to spontaneous self-assembly of the fluorescence fragment (Kudla and Bock, 2016, Xing et al., 2016). In several studies, the presence of non-specific fluorescence background has been shown in the negative control due to high expression levels of YFP (Walter et al., 2004, Waadt et al., 2008). The most accurate control has been proposed to be the combination of one of the proteins of interest with a mutated version of the second protein or, if a mutation is not possible, a close family related protein can be used. However, if an unrelated protein is used, it is important to demonstrate that this protein is capable of interacting with another protein in a BiFC assay (Kudla and Bock, 2016). The orientation of the YFP tag is also an important factor because it can affect the intensity of the signal and can also increase the likelihood of a false positive (Kudla and Bock, 2016, Xing et al., 2016). In our case, both proteins were C-terminally tagged with the YFP fragments, in the same manner as in Ma et al. (2015). In this thesis all the different tag combinations were not carried out with rice proteins; however, this was performed with AtGTG1 and AtGPA1 in our laboratory and no signal or interaction was observed with any combination (Adam, Terry, Williams, unpublished).

It is possible that OsGTG and RGA1 do not interact in our conditions. Since Ma et al. (2015) suggested that OsGTG could function as a cold receptor, it would be interesting to carry out the BiFC experiment with OsGTG and RGA1 under cold treatment, to study whether these two proteins are able to interact under specific stress conditions.

Phenotypic analysis of *gtg1gtg2gpa1.4* showed that the mutant exhibited several similar characteristics to the *gtg1gtg2* double mutant. The same phenotype was observed in the triple mutant in reduced root growth, fresh weight per seedling,

hypocotyl length in light conditions, rosette diameter, number of stems from the rosette, silique length and seed yield. This indicates that mutation of *AtGPA1* does not additionally affect those specific characteristics. However, there were a few characteristics where *gtg1gtg2gpa1.4* exhibited a different phenotype to the *gtg1gtg2* and *gpa1.4* mutants. The hypocotyl length of the triple mutant grown in the dark was reduced in comparison to the WT, *gtg1gtg2* and *gpa1.4* (Figure 5.10). The difference was stronger after 7 days of growth in the dark and in the presence of sucrose. In addition, the *gtg1gtg2gpa1.4* mutant exhibited more open cotyledons in the seedlings that were grown in the dark in comparison to the rest of the mutants. This could indicate a synergistic interaction between AtGTGs and AtGPA1 to control hypocotyl growth and cotyledon closure in the dark. This genetic interaction between GTGs and GPA1 could indicate that the activity of both proteins converges in the same process to regulate hypocotyl length and cotyledon closure in the dark. Since AtGPA1 is involved in cell division and cell wall formation (Ullah et al., 2003, Klopffleisch et al., 2011) and AtGTGs are involved in cell wall formation and therefore cell elongation (Jaffé et al., 2012), it is also possible that the deletion of the three proteins can produce a stronger hypocotyl growth reduction in the triple mutant. Synergistic interaction has been observed between the transcription elongation factor Elongator complex, ELO3 and the positive photomorphogenesis regulator LONG HYPOCOTYL IN FAR-RED 1 (HFR1) in the regulation of hypocotyl growth under different light conditions (Woloszynska et al., 2018). The *elo3-6xhfr1-101* double mutant exhibited a longer hypocotyl than each of the single mutant under far-red light but not under darkness. This indicates that the activity of both proteins converged into the same pathway in hypocotyl elongation producing a strong effect in the double mutant under far-red light (Woloszynska et al., 2018).

Another synergistic interaction between AtGTGs and AtGPA1 was found in the regulation of plant height. The *gtg1gtg2gpa1.4* exhibited a reduced height in comparison to the WT, *gtg1gtg2* and *gpa1.4* mutants. Since AtGTGs and AtGPA1 are involved in cell elongation and division and also regulate different hormones involved in plant growth, it could be possible that the deletion of the three proteins activities can cause the reduced height of the *gtg1gtg2gpa1.4*. When the receptor-like kinase ERECTA, that regulates inflorescence morphology was crossed with ERL1 and ERL2, two ERECTA-LIKE genes, a synergistic interaction was detected between the three proteins in the regulation of flower development and cell proliferation (Shpak et al., 2004). The *erecta105xerl1-2xerl2-1* triple mutant showed a stronger reduction in height,

silique and pedicel length in comparison to the WT, *erecta105* or *erl1-2erl2-1* double mutant. The triple mutant also exhibited compact inflorescence cluster together at the tip of the flower buds. All this indicates a synergistic interaction between ERECTA, ERL1 and ERL2 to regulate plant and flower growth (Shpak et al., 2004). The results in this chapter indicate that although GTG and GPA1 do not seem to physically interact, it is possible that both proteins are involved in the regulation of some of the same processes, such as cell elongation and plant growth, producing the defects observed in the *gtg1gtg2gpa1.4* mutant.

Chapter 6. General discussion

6.1. GTG/GPHRs have a conserved function as anion channels regulating endomembrane pH

GTG/GPHR is a conserved family of membrane protein that is present in mammals, fungi and plants. Several functions are proposed for GTG/GPHRs in different organisms (Table 1.2). In mammalian cells, GTG/GPHR functions as an anion channel regulating Golgi pH, as CHO cells lacking GTG/GPHR display a delay in protein trafficking and an increase in Golgi pH (Maeda et al., 2008). However, a wider range of functions is proposed for GTG/GPHR in plants. In Arabidopsis, GTGs were reported as ABA receptors that interact with the Gα subunit of G proteins (Pandey et al., 2009), whereas in rice, GTGs were proposed to be involved in cold tolerance, working as a cold sensor that also interacts with the Gα subunit, affecting calcium concentration (Ma et al., 2015). Despite those differences in function, it has been shown that GTGs are strongly involved in growth, development and fertility in plants (Jaffé et al., 2012). The Arabidopsis *gtg1gtg2* mutant exhibits a reduced root, hypocotyl, pollen germination, pollen tube, silique length and seed yield (Jaffé et al., 2012). The involvement of GTG/GPHR in growth and development has also been observed in mice, *Drosophila* and in the amoeba *D. discoideum* (Tarutani et al., 2012, Charroux and Royet, 2014, Deckstein et al., 2015). Interestingly, recent work in our laboratory has shown that AtGTG1 also functions as an anion channel that regulates ER and Golgi pH (Dorey, 2019). These findings generate the following question: are GTGs a conserved protein family that function as anion channels regulating endomembrane pH?

In this thesis, further studies have been carried out to characterise rice GTG in more depth, to understand whether rice and Arabidopsis GTGs play a similar role in the cell and whether they can function as anion channels that regulate endomembrane pH. OsGTG sequence shares a 90% similarity and 80% identity to AtGTG1 and both proteins share a predicted topology of nine transmembrane domains. Electrophysiology assays (chapter 4) in single-channel planar lipid bilayer assays with OsGTG expressed via a cell-free synthesis kit revealed that OsGTG could function as a channel. OsGTG displayed square-wave like patterns that indicated single-channel activity when it was inserted into an artificial membrane. OsGTG was more permeable to Cl^- than K^+ or Ca^{2+} when the current activity was measured using an asymmetrical gradient of KCl or $CaCl_2$

respectively. OsGTG exhibited an average conductance of 88 pS. In addition, the single-channel activity observed was inhibited by the addition of the anion blocker DIDS. The ion selectivity sequence observed for OsGTG was $Cl^- > I^- > Br^- > NO_3^-$.

The results obtained for OsGTG were similar to what was observed for AtGTG1, CeGTG1 and HsGPHR, indicating that the function of these proteins as anion channels is conserved in animals and plants (Maeda et al., 2008, Dorey, 2019). Using the same single-channel planar lipid bilayer technique, the three GTG/GPHR homologues exhibited channel activity in an asymmetrical gradient of KCl, all being more selective for Cl^- than K^+. In addition, AtGTG1 and HsGPHR currents were inhibited by DIDS (Maeda et al., 2008, Dorey, 2019). The three orthologues were permeable to other anions; HsGPHR showed a selectivity sequence of $I^- > Cl^- = Br^- > F^-$ whereas AtGTG1 and CeGTG1 showed $Cl^- > NO_3^- > F^- > SCN^- > I^- > Br^-$. However, the latter were measured in whole-cell patch clamping using HEK293 cells expressing AtGTG1 or CeGTG1. The differences in the selectivity may be due to the differences in the technique used or be due to slight differences in the structure of these channels. The conductance of the channel was also different between the proteins. HsGPHR showed a conductance of 400 pS, CeGTG1 of 200 pS, AtGTG1 of 136 pS and OsGTG of 88 pS (Maeda et al., 2008, Dorey, 2019). Certainly, HsGPHR showed higher conductance than AtGTG1, and both exhibited a higher conductance than OsGTG. Differences in the protein sequence can account for the differences of the permeability and conductance, although AtGTG and OsGTG share an 80% identity. The recombinant proteins were also expressed with different protein tags; AtGTG1, CeGTG1 and OsGTG were expressed with a His_6 tag, whereas HsGPHR was expressed with Flag-HAT tandem, a longer tag that could affect the properties of the channel in the assay (Maeda et al., 2008, Dorey, 2019). Protein tags can affect the function or properties of the protein of interest. It was shown that a *myc* tag fused to the N or C-terminus of hERG, an alpha subunit of a K^+ channel, can affect the expression and the kinetics of the channel (Osterbur-Badhey et al., 2017). In future, the properties of the channels could be investigated with a variety of tags to see if this affects the properties of the GTG/GPHRs.

Previous electrophysiology assays performed with OsGTG in Ma et al. (2015) using *Xenopus* oocytes showed an inward current in cells expressing OsGTG and RGA1, after cold treatment. In our experiments, no increase in current was detected when OsGTG and RGA1 were added together into the lipid bilayer assay. However, to

confirm this result, further study is required. It would be interesting to perform the electrophysiology assay after a cold treatment, to test whether RGA1 can increase the channel activity of OsGTG under stress conditions. Ma et al. (2015) proposed that OsGTG could function or be part of a Ca^{2+} channel. This was based in the reduced Ca^{2+} resting level and the reduced increase of Ca^{2+} upon cold treatment observed in the rice *gtg* mutant. In this thesis, it was shown that OsGTG was not able to transport Ca^{2+}, as no channel activity was observed when calcium gluconate was present in the single-channel planar lipid bilayer assay. In addition, OsGTG was more permeable to Cl^- than Ca^{2+} when the currents were analysed using an asymmetrical gradient of $CaCl_2$. A possible explanation could be that as we have shown that OsGTG functions as an anion channel regulating pH in the ER and Golgi (Table 4.7), then the lack of GTG/GPHR in the rice mutant could produce an impairment of the ER and Golgi. This could lead to defects in plasma membrane Ca^{2+} channels, since some of those channels are synthesised through the ER-Golgi network (Roden and Kupershmidt, 1999, Taylor et al., 2009, Lazniewska and Weiss, 2017). Therefore, the reduction of Ca^{2+} concentration observed in the *gtg* mutant (Ma et al., 2015) could be due to a reduction of plasma membrane Ca^{2+} channels due to a defect in the ER and Golgi function produced by the lack of the anion channel GTG/GPHR.

As previously mentioned, the CHO *gphr* mutant line exhibited an increase of 0.35-0.50 in pH at the Golgi and TGN. The pH was measured expressing, in the WT and *gphr* mutant CHO lines, pHluorin fused to the target signal GPP130 for *cis* Golgi, to GnTI, for the *medial-trans* Golgi and to TGN38 for the TGN (Maeda et al., 2008). pH analysis in Arabidopsis WT and *gtg1gtg2* mutant also using pHluorin targeted to different organelles showed an increase of pH at the ER and *cis* Golgi in the mutant (chapter 4). The ER and *cis* Golgi pH in WT were 7.26 and 6.74 respectively, whereas the *gtg1gtg2* mutant exhibited an ER pH of 7.38 and a *cis* Golgi pH of 6.81. No differences in pH values was detected at the *trans* Golgi and PVC between the WT and *gtg1gtg2* mutant (Adam, Terry, Williams, unpublished). Furthermore, AtGTG1 and OsGTG were able to complement the defective pH of the *gtg1gtg2* mutant. This indicates that in plants, GTG/GPHRs are able to regulate endomembrane pH in a similar manner as the mammalian GTG/GPHR.

To corroborate the finding that GTG/GPHRs play a role in the endomembrane system, the intracellular localisation of the proteins was also determined. GTG/GPHRs have been reported to localise in various organelles in different organisms (Table 1.4).

In Arabidopsis, GTG has been observed at the plasma membrane (Pandey et al., 2009) or at the ER and Golgi (Jaffé et al., 2012). In rice and wheat they have been localised at the plasma membrane and ER (Ma et al., 2015, Dong et al., 2019). The localisation of OsGTG described in this thesis resembles the localisation reported for AtGTG1 in Jaffé et al. (2012). In transient expression in tobacco leaves, AtGTG1 and OsGTGs localised at the ER and Golgi. The localisation of OsGTG was corroborated by the use of HDEL::RFP marker for ER, ManI::RFP for *cis* Golgi and ST::RFP for *trans* Golgi localisation. OsGTG co-localised with all three organelle markers. Interestingly, no co-localisation was observed when OsGTG was co-expressed with the plasma membrane LT16b::mOrange marker. The data from this thesis confirm that the localisation of OsGTG is in the endomembrane system mainly at the ER and Golgi, similar to AtGTG1 localisation. The localisation of GTG/GPHR in the endomembrane system has also been observed in the animal kingdom, since it was found at the Golgi in mammalians cells and at the ER and Golgi in *Drosophila* (Maeda et al., 2008, Charroux and Royet, 2014), supporting the role of this protein in these organelles.

The conservation of function between Arabidopsis and rice GTGs was confirmed by the fact that OsGTG was able to rescue the defective root length, fresh weight and hypocotyl growth of the Arabidopsis *gtg1gtg2* double mutant (chapter 3). In addition, OsGTG rescued the defective cell shape and reduced ER body number in the *gtg1gtg2* double mutant. OsGTG also restored the higher pH observed in the ER and Golgi of the *gtg1gtg2* mutant. These results confirm a conserved function between Arabidopsis and rice GTGs. Previous work carried out in our laboratory demonstrated that CeGTG1 was also able to rescue the defective root and hypocotyl phenotype of *gtg1gtg2* mutant, suggesting a conserved function across different kingdoms (Wong, 2014). This conservation of function in GTG/GPHR has also been observed between vertebrate and *Drosophila* since the human and hamster GTG/GPHRs were able to restore the defective growth phenotype of the *Drosophila GPHR*$^{-}$ mutant (Charroux and Royet, 2014). It would be interesting to study whether the mammalian GTG/GPHR can rescue the defective phenotype of Arabidopsis *gtg1gtg2*, to further confirm the conservation of function between kingdoms.

Furthermore, similar growth, development and fertility defects have been observed for Arabidopsis *gtg1gtg2* and rice *gtg* mutants. Arabidopsis *gtg1gtg2* mutant exhibited shorter root and hypocotyl, an increased number of stems and a reduced rosette diameter, silique length and seed yield (Jaffé et al., 2012). Rice *gtg* mutant displayed a

reduced height, an increase of leaves, tillers and panicles, and a reduction of grain formation. The involvement of GTG/GPHRs in growth, development and fertility has been shown in other organisms. The skin-specific mice *gphr* mutants exhibited high mortality, slower growth and a defective skin barrier with skin inflammation, hair loss and a defect in earlobes and genitals (Tarutani et al., 2012). The *Drosophila GPHR*$^{-}$ mutant also displayed high mortality and a reduction of growth of the pupae and adults, with smaller wings, reduced cell size and cell number in the adults compared with WT flies (Charroux and Royet, 2014). The *C. elegans gphr* double mutant exhibited reduced egg laying and a reduction in hatching compared with WT. None of the eggs that hatched reached an adult stage (Wong, 2014). This indicates that GTG/GPHRs are involved in growth, development and fertility, and this function is also conserved between animals and plants. These results, together with the fact the OsGTG, AtGTG1 and HsGPHR exhibited channel activity and involvement in pH regulation, are a strong indication that the function of GTG/GPHRs is conserved across kingdoms.

In this thesis, the importance of the 9th and 187th amino acids residues in the function and localisation of GTG was also studied. In the 9th amino acid position, the OsGTG sequence in the Rice Genome Annotation Project database contains a glycine; however, a glutamic acid was found to be a conserved residue in that position in plant GTG/GPHRs. When amplified from rice in this project, the residue was a glutamic acid and so both versions of OsGTG were cloned for investigation. In addition, the 187th amino acid residue was found to be involved in cold tolerance in rice since OsGTG with lysine in that position was able to rescue the cold sensitivity of the rice *gtg* mutant whereas OsGTG with methionine was not (Ma et al., 2015). In this thesis, neither glutamic acid nor glycine in the 9th residue and neither lysine nor methionine in the 187th affected the function of the protein since all the OsGTG versions were able to rescue the defective root length, fresh weight and hypocotyl growth of the mutant. Electrophysiology assays showed that the 9th amino acid mutation from glycine to glutamic acid did not affect the *in vitro* characteristics of the channel since both OsGTG versions exhibited similar single-channel activity, with similar conductance and selectivity. In addition, the current produced from both proteins was inhibited by DIDS. This polymorphism is located in the N-terminus part of the protein and is part of the first transmembrane domain, according to the predicted topology, and it does not seem to affect the pore or gating properties of the channel. Furthermore, both proteins were also able to restore the defective pH of the *gtg1gtg2* mutant. Interestingly, higher Golgi localisation was found in plant cells that expressed OsGTGe than in cells expressing

OsGTGg. When OsGTGg was expressed in Arabidopsis, not many 'Golgi-like structures' were observed, whereas an abundance of Golgi bodies was observed when OsGTGe was expressed. When this was quantified, it was evident that OsGTGe localised at the ER and Golgi whereas OsGTGg localised predominantly at the ER and rarely at the Golgi. The fact that the mutation is close to the N-terminus of the protein suggests that it could be part of a peptide sequence that retains GTG in the Golgi. This suggests that this polymorphism found in OsGTG could play a role in the localisation of the protein. The fact that one amino acid difference can alter the function of the protein has been proposed previously for GTG/GPHR. As just mentioned, in Ma et al. (2015) it was suggested that the change of one single amino acid in the 187th residue was involved in cold tolerance in rice. In *Drosophila* a point mutation in the third transmembrane domain of GTG/GPHR sequence, that changes a conserved proline into a leucine, was responsible for the defects in growth and development observed in the *GPHR*$^{-}$ mutant flies (Charroux and Royet, 2014). Most of the flies that contained leucine in that position died at late larvae stage and the flies that managed to reach adulthood displayed a small size in comparison to the WT flies (Charroux and Royet, 2014).

Although the data in this thesis demonstrate that OsGTG functions as an anion channel that regulates endomembrane pH, previous work in rice has suggested that OsGTG (called COLD1) could be involved in cold tolerance (Ma et al., 2015). Genome sequence analysis of several rice cultivars revealed that the GTG/COLD1 sequence in the cold tolerant *japonica* varieties contains a lysine in the 187th amino acid residue whereas in the cold sensitive *indica* varieties there is a methionine in the same position. It was observed that rice *gtg* mutant plants expressing OsGTG/COLD1 with lysine in that position were more cold tolerant than the mutants expressing OsGTG/COLD1 with methionine instead. Furthermore, a rice *gtg* mutant plant was shown to be less cold tolerant than WT plants (Ma et al., 2015). In this thesis, the capacity of GTG to be involved in cold tolerance was studied using Arabidopsis plants. It was observed that, although the Arabidopsis *gtg1gtg2* mutant exhibited a reduced rosette diameter, number of leaves and stem length in comparison to WT plants after cold treatment, this reduction of growth was also observed in plants that were kept at normal conditions. This indicates that GTG/GPHRs play a more significant role in general growth rather than specifically in cold tolerance. In addition, *gtg1gtg2* mutant plants expressing OsGTG with lysine or methionine in the 187th amino acid position showed a similar growth pattern to WT plants, and this was observed both in control conditions and when

exposed to low temperature. No increase in cold tolerance was observed in the plants expressing OsGTG with lysine in the 187th residue in comparison to the lines expressing OsGTG with methionine. It is important to mention that the rice *gtg* mutant used in Ma et al. (2015) was shorter than the WT and the transgenic lines, even in the plants that were not under cold treatment. A more detailed analysis of the same rice *gtg* mutant in this thesis has shown that the mutant indeed displayed a defect in growth and development since it was observed that *gtg* was shorter than WT and produced more leaves, tillers and panicles and also exhibited a reduced seed yield. This defect in growth observed in rice *gtg* mutant could affect the capacity of the plant to deal with cold stress, leading to the low cold tolerant phenotype observed in the rice *gtg* mutant previously. Unfortunately, we were not able to carry out the same cold treatment for the rice mutant, but this would be useful to test further in the future.

6.2. GTGs are involved in ER and Golgi regulation

Since it was observed that OsGTG localised at the ER and Golgi, it was important to understand the role that the protein plays in those organelles. As discussed throughout this thesis, AtGTG1 and OsGTG act as anion channels regulating ER and Golgi pH (Adam, Terry and Williams, unpublished; Dorey, 2019), in a similar manner to mammalian GTG/GPHR (Maeda et al., 2008). The maintenance of the correct pH is critical for the function of the organelles since some enzymes and proteins require a specific pH to function (Demaurex, 2002). pH homeostasis in the organelles that are involved in the secretory pathway is regulated by proton pumps and transporters (Martinière et al., 2013a, Shen et al., 2013, Schumacher, 2014). The accurate pH of the organelles is maintained by the influx and efflux of protons (Demaurex, 2002). At the Golgi, the regulation of pH involves V-ATPase and exchanges such as NHX and ClC (Fecht-Bartenbach et al., 2007, Marmagne et al., 2007, Bassil et al., 2011a). However, since the ion/H^+ exchanges are not an energetically favourable method to reduce the electrochemical gradient without the loss of protons, it is possible that GTG/GPHR provides the influx of anions required in the Golgi for the reduction of the electrochemical gradient maintaining the concentration of protons. A model for pH regulation in the Golgi is shown in Figure 6.1 A.

V-ATPase and H^+-PPase are thought to regulate the pH of the ER (Herman et al., 1994, Kuo et al., 2005). Not many channels have been identified in the ER solely for Cl^-. In tobacco plants, a Cl^-/H^+ antiporter that regulates luminal pH has been found (Sun et

al., 2018). It is possible that GTG/GPHR could function as a novel Cl^- channel at the ER that regulates membrane potential and pH without the loss of protons (Figure 6.1 B). Since ER is a storage organelle for Ca^{2+} (Vitale and Denecke, 1999, Schwarz and Blower, 2016, Stefano and Brandizzi, 2018), alteration in Ca^{2+} regulation can cause an ER stress response that produces impairment in protein folding and accumulation of unfolded proteins (Xu et al., 2005). In the *gtg* rice mutant a reduction of Ca^{2+} concentration in the cytoplasm, and a reduction of the Ca^{2+} increase after cold stress was observed (Ma et al., 2015). This alteration in Ca^{2+} homeostasis can affect the Ca^{2+} regulation in the ER and produce an ER stress response. Analysis of the Ca^{2+} concentration in *gtg1gtg2* using Ca^{2+} sensors, such as Aequorin, Chameleon or R-GECO would help us understand whether Ca^{2+} homeostasis is altered in the Arabidopsis mutant and whether this can affect the Ca^{2+} uptake in the ER causing an ER stress response.

Since GTG functions as an anion channel that regulates endomembrane pH, it is possible that in the *gtg1gtg2* mutant the V-ATPase is not functioning properly due to the lack of counterion balance. It has been shown that inhibition of the V-ATPase activity by concanamycin A produces a reduction of hypocotyl length in dark-grown seedlings (Fecht-Bartenbach et al., 2007, Brüx et al., 2008). This defect was also observed in mutants of the V-ATPase, such as *det3,* that showed a dwarf phenotype, including a reduced hypocotyl length, and *vha-c* mutant, that exhibited a reduced root and hypocotyl growth (Schumacher et al., 1999, Padmanaban et al., 2004, Brüx et al., 2008). Inhibition of the TGN-localised isoform VHA-a1 also produced a reduction of cell expansion and hypocotyl length (Brüx et al., 2008).

V-ATPase is also involved in male gametophyte development. The V-ATPase mutant *vha*, exhibited a defect in Golgi morphology in the pollen leading to a defect in pollen tube elongation (Dettmer et al., 2005). It would be interesting to check the level of V-ATPase proton transport activity in the *gtg1gtg2* mutant to examine whether the growth and pollen defects observed in the mutant are caused by impairment of this proton pump.

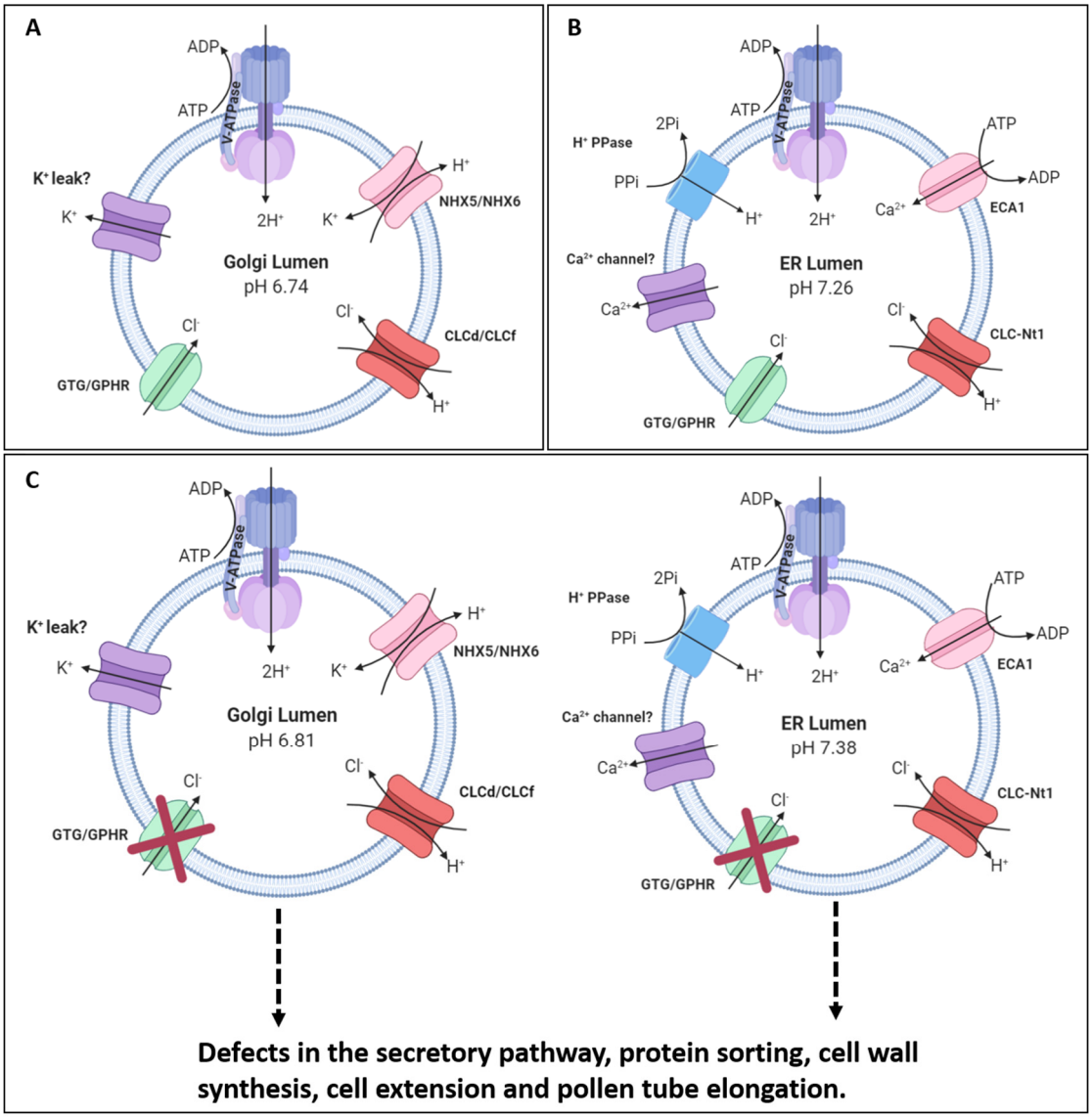

Figure 6.1. GTG/GPHR is involved in Golgi and ER pH regulation in plants

A) Diagram of important proton pumps and ion channels involved in Golgi pH regulation in plants: the V-ATPase proton pump (Marshansky et al., 2014); the NHX family of K^+/H^+ exchanges (Bassil et al., 2011a); the ClC family of Cl^-/H^+ exchanges; the GTG/GPHR family of anion channels and the K^+ leak channels. B) Diagram of important proton pumps and ion channels involved in ER pH and calcium regulation in plants: H^+-PPase (Kuo et al., 2005); V-ATPase (Herman et al., 1994); ECA family of calcium pumps (Liang et al., 1997); the ClC family of Cl^-/H^+ exchanges (Sun et al., 2018); the GTG/GPHR family of anion channel and putative Ca^{2+} channels. C) The lack of GTG/GPHR in Arabidopsis produced an increase in Golgi and ER pH that can lead to defects in the secretory pathway, protein sorting, cell wall formation and pollen tube elongation, causing the growth, development and fertility defects observed in the *gtg1gtg2* knockout.

Cl^- fluxes are also important for pollen germination and pollen tube growth (Tavares et al., 2011, Michard et al., 2017). Anion channels present at the pollen are important for pollen tube growth since the addition of an anion blocker in the pollen produced growth arrest and tube death (Zonia et al., 2002, Gutermuth et al., 2013). Since GTGs are present in the pollen, it is possible that the defects in pollen tube germination and growth observed in the *gtg1gtg2* could be also cause by an anion imbalance in the pollen by the absence of the anion channel GTG/GPHR.

pH homeostasis is important for the correct function of the secretory pathway (Wu et al., 2001). Since *gtg1gtg2* mutant has altered pH at the ER and the Golgi, it is possible that this increase in pH disrupts the gradual acidification that the secretory pathway requires for a correct function, leading to a malfunction of the secretory pathway and protein trafficking (Martinière et al., 2013a, Shen et al., 2013). This malfunction can lead to the defective growth and development phenotype observed in the Arabidopsis *gtg1gtg2* and rice *gtg* mutants (Figure 6.1 C). A correct ER and Golgi function is required for a correct cell wall formation and cell elongation and growth. The main components of the cell wall are hemicellulose and pectin, that are synthesised at the Golgi and transported through the secretory pathway (Zhang and Staehelin, 1992, Worden et al., 2012, Kim and Brandizzi, 2016, Ruiz Rosquete et al., 2017), and cellulose, where the cellulose synthase complexes are assembled at the Golgi and later on transported to the plasma membrane (McFarlane et al., 2014, Polko and Kieber, 2019). Therefore, defects in ER and Golgi pH can lead to organelle dysfunction and, as a result, cell wall components are not synthesised, affecting cell elongation and ultimately growth. Several mutants of the cellulose synthase resulted in reduced root and hypocotyl length due to a decrease in cell elongation (Desnos et al., 1996, Fagard et al., 2000, Beeckman et al., 2002, Caño-Delgado et al., 2003, Paredez et al., 2008, Daras et al., 2009, Pysh et al., 2012). In addition, some of the mutants exhibited a reduced rosette and silique length (Daras et al., 2009, Pysh et al., 2012, Rubio-Díaz et al., 2012), and some produced swollen and distorted hypocotyl epidermal cells in the same manner as the *gtg1gtg2* mutant (Desnos et al., 1996, Fagard et al., 2000, Daras et al., 2009). This defect in growth was also observed in plants with an abnormal pectin localisation and a defect in cell wall, such as the *emb30* mutants (Shevell et al., 2000). Cell wall formation and modification genes, such as xyloglucan endotransglycosylase -3 and 6 and xyloglucan endotransglucosylase/hydrolase-18 were altered in the *gtg1gtg2* mutant (Jaffé et al., 2012). Cell division is also affected by cell wall composition and therefore by the secretory pathway status (Bednarek and Falbel, 2002, Sinclair et al., 2018).

Arabidopsis plants that have affected cell division rate, such as the *scarecrow* and *short-root* mutant, exhibited a reduced rosette and root length growth (Di Laurenzio et al., 1996, Dhondt et al., 2010). Therefore, it is possible that the growth defects displayed by the *gtg1gtg2* could be caused by a defect in cell wall formation and composition produced by pH disruption and ER and Golgi dysfunction.

It is not unusual that the absence of an ion channel can cause a defect in the organelle where that channel plays a role. In Arabidopsis, a mutant of the Mitochondrial Calcium Uniporter, MCU, showed an abnormal mitochondria morphology with altered shape and organisation in comparison with the WT, which showed a normal structure with a uniform matrix (Teardo et al., 2017). A similar observation was reported with the chloroplast localised voltage-dependent Cl^- channel VCCN1. The *vccn1* mutant displayed an abnormal chloroplast morphology, with longer thylakoid stacks in the dark and a longer and curved grana shape in the light (Herdean et al., 2016b). This indicates that ion channels play an important role in organelle morphology. Since GTG/GPHR functions as a channel that localises at the ER and Golgi, it is possible that the absence of this protein can cause defects in those organelles that lead to ER and Golgi disorganisations. Defects in organelle morphology due to the absence of GTG/GPHRs have been previously reported. CHO mutant lines of the Golgi localised GTG/GPHR exhibit Golgi disorganisation with this organelle being more fragmented and dispersed in the mutant (Maeda et al., 2008). In *Drosophila*, where GTG/GPHR localises at the ER and Golgi, defects in the organisation of those organelles were also observed in the *Drosophila GPHR*$^-$ mutant. The ER of the mutant accumulated asymmetrically around the nucleus in comparison with the uniform network observed in the WT, and the Golgi was also more fragmented in the mutant than in the WT flies (Charroux and Royet, 2014). Confocal microscopy analysis of the *gtg1gtg2* Arabidopsis mutant revealed a reduction of ER body number in comparison to the WT. Since ER bodies are ER-derived structures, it is possible that defects in the ER morphology could contribute to the reduction of ER bodies found in the mutant. Further experiments using an electron microscope are required to determine whether the ER and Golgi morphology of the *gtg1gtg2* Arabidopsis mutant are disorganised.

Mutations in channels and carriers can cause defects in growth, development and fertility. The double mutant of NHX1 and NHX2, two tonoplast K^+/H^+ antiporters involved in stomata movements and vacuolar pH regulation (Bassil et al., 2011b, Andrés et al., 2014), showed reduced rosette diameter and reduced stem and cell length.

Stamen filaments were also shorter and silique length was reduced, however pollen viability was not affected (Bassil et al., 2011b). The double mutant of the Golgi and TGN localised NHX5 and NHX6 proteins exhibited defects in vacuolar trafficking, reduced growth with a small rosette diameter and reduced rosette leaf number that were due to a reduction in cell expansion (Bassil et al., 2011a). A mutant of the Cation-Cl^- Cotransporter, CCC, exhibited a shorter-bushy phenotype with shorter inflorescences and a higher number of stems (Colmenero-Flores et al., 2007). In addition, the *ccc* mutant exhibited also a reduced silique length and seed yield although no differences have been found between the WT and the mutant in the flowering day. CCC was shown to be involved in the long distance ion transport through the xylem and it was found that the *ccc* mutant had an altered distribution of Cl^- (Colmenero-Flores et al., 2007). It would be interesting to analyse whether Arabidopsis *gtg1gtg2* and rice *gtg* have differences in the concentration and distribution of Cl^-. In rice, OsCCC regulates ion homeostasis and maintenance of cellular osmotic potential and it is also involved in cell elongation since the rice *ccc* mutant exhibited a reduced root length and shoot elongation (Kong et al., 2011, Chen et al., 2016). Mutations of Cl^- channels can also affect growth and fertility in plants. This was the case for DTX33 and DTX35, two vacuolar Cl^- channels that are involved in cell turgor regulation. It was shown that the *dtx33dtx35* double mutant exhibited a delay in root hair elongation and that the *dtx35* mutant had a reduced pollen tube (Zhang et al., 2017). However, in contrast to *gtg1gtg2* mutant, the *dtx35* did not show reduced pollen germination (Zhang 2017). This above indicates that the lack of ion transporters can alter ion homeostasis causing a strong effect in plant growth and fertility.

6.3. Studying the GTG and Gα interaction

G proteins are heterotrimeric proteins composed of three subunits, α, β and γ that are involved in the transmission of information from outside the cell to the inside (Urano et al., 2013). As described in section 1.5.4.2, GTG/GPHRs have been proposed to interact with the Gα subunit of the G protein in plants. This interaction has been shown by the split-ubiquitin system and Co-IP assays in Arabidopsis and by BiFC and Co-IP assay in rice (Pandey et al., 2009, Ma et al., 2015). However, these methods have been reported to produced unreliable results especially when using overexpressed membrane proteins due to a high likelihood of a false positive (Mackay et al., 2007, Müller and Johnsson, 2008, Kudla and Bock, 2016, Xing et al., 2016). It is also

important to mention that the signal reconstitution in these techniques is due to the spatial proximity of both proteins and not necessarily due to a direct interaction between them. To confirm a positive BiFC results, a combination of one of the proteins of interest with a mutated version of the other protein is recommended as negative control (Kudla and Bock, 2016, Xing et al., 2016). However, in Ma et al. (2015) only a combination of OsBAK1 protein with OsGTG was used as a negative control and therefore further evidence is needed to prove this interaction. In our experimental conditions, OsGTG and rice Gα did not interact in a BiFC assay (Figure 5.19). This result correlates with the intracellular localisation observed for OsGTG, which was at the ER and Golgi but not at the plasma membrane. The BiFC assay performed in our laboratory also did not show an interaction between AtGTG1 and AtGPA1, where in the same experiment a clear interaction was observed between Arabidopsis Gα and Gβ subunits (Adam, Terry, Williams, unpublished). Several proteins have already been demonstrated to interact with the Gα subunit. One example is the phospholipase Dα (PLDα), an enzyme that hydrolyses phospholipids, which interacts with AtGPA1 in a Co-IP assay and its activity can be inhibited by Gα (Zhao and Wang, 2004).

Although GTGs have been previously described as GPCRs, due to the sequence similarity with human GPR89 and due to the interaction of GTGs with G proteins, the evidence from this thesis and other studies do not support this proposal. It is unlikely that GTG/GPHRs function as GPCRs, since HsGPHR, AtGTG1 and OsGTG have been shown to function as anion channel that regulate endomembrane pH (Maeda et al., 2008, Dorey, 2019). However, G proteins can regulate ion channels, both directly, by physical interaction with the protein, and indirectly, via kinases or second messengers (Breitwieser, 1991, Dascal, 2001). This is well-known in mammalians, where Gβγ can activate the K^+ channels GIRKs, and can inhibit the neuronal voltage-dependent Ca^{2+} channels (Dascal, 2001). In plants, G proteins have been shown to regulate ion channels in guard cells. It has been shown that stomatal opening and inward K^+ currents were hyposensitive to ABA in *gpa1*, *agb1* and *agg3* mutants, and also the ABA activation of slow anion channels in guard cells was reduced in those mutants (Wang et al., 2001, Fan et al., 2008, Chakravorty et al., 2011). Gα was shown to also regulate plasma membrane Ca^{2+} permeable channels in pollen cells (Wu et al., 2007). In Ma et al. (2015) a higher current activity was observed after cold stress was applied when the rice Gα subunit was co-expressed with OsGTG in *Xenopus* oocytes, suggesting that Gα can regulate the function of GTG. However, in this thesis, using the single-channel lipid bilayer assay, no additional activation of OsGTG was observed when rice Gα was added

to the system. However, further analysis needs to be carried out to study whether G proteins can regulate the activity of GTG/GPHR under specific stress conditions.

Although a physical interaction between rice GTG and Gα was not observed, an additional study was performed using an Arabidopsis *gtg1gtg2gpa1.4* triple mutant, to test whether GTGs and GPA1 could be involved in the same pathway. The *gtg1gtg2gpa1.4* mutant displayed similar defective growth and fertility as *gtg1gtg2*, such as similar reduced root length, hypocotyl length under low light, rosette diameter, silique length and seed yield. The deletion of AtGPA1 in a *gtg1gtg2* background did not affect those specific characteristics, suggesting that those traits are mainly regulated by GTGs. Interestingly, the *gtg1gtg2gpa1.4* triple mutant exhibited a reduced hypocotyl length with more open cotyledons when they were grown in the dark in comparison to WT, *gpa1.4* and *gtg1gtg2*. This indicates a synergistic interaction between AtGTGs and AtGPA1 to control hypocotyl growth and cotyledon closure in the dark, and that the activity of both proteins regulates these processes. As described in chapter 5, cell wall formation and modification is an important process that controls cell elongation, which is a major process involved in hypocotyl growth in the dark (Gendreau et al., 1997). Furthermore, xyloglucans and pectins, key components of the cell wall, are processed through the Golgi and transported by the secretory pathway (Kim and Brandizzi, 2016, Ruiz Rosquete et al., 2017). Since AtGTG1 has been shown to localise at the ER and the Golgi, and functions as an anion channel that regulates the pH of those organelles, it is possible that the *gtg1gtg2* mutant has a defect in the secretory pathway and protein trafficking that can lead to an impaired cell wall formation. This was corroborated by a microarray study that showed that the *gtg1gtg2* mutant has altered gene expression related to cell wall formation and modification (Jaffé et al., 2012). In addition, the interactome of G proteins has also shown important interaction between Gα and cell wall components, such as xylose (Klopffleisch et al., 2011). Taking all those facts into account, the defect in the *gtg1gtg2gpa1.4* triple mutant could be due to a highly defective cell wall formation that does not permit the correct growth of the hypocotyl.

The absence of Gα can enhance the defects produced by the absence of GTGs. It has been reported that the AtGPA1 mutation produces an enhanced cell division defect in the BR receptor BRI1 mutant. The *gpa1.4bri1-5* double mutant exhibited a stronger reduction of root and hypocotyl growth than the single mutants, indicating a crosstalk between G proteins and the BR pathway (Gao et al., 2008). Plant hormones, such as BR and GA, also play an important role in hypocotyl development and cotyledon closure in

the dark (Gendreau et al., 1997). The open cotyledons phenotype observed in the seedlings grown in the dark has been studied in different mutants where hormone receptors and pathways were effected (Clouse et al., 1996, Li et al., 1996, Wei and Deng, 1996, Gou et al., 2012). The *gtg1gtg2* mutant has altered genes that regulate some plant hormones (Jaffé et al., 2012) and Gα protein is well-known to be involved in different hormonal pathways (Urano et al., 2013). For example, it has been shown that the *gpa1.4* mutant exhibits reduced sensitivity to BR in hypocotyl growth and seed germination (Ullah et al., 2002). These facts together could play a role in the reduced hypocotyl length and the open cotyledon phenotype observed in the *gtg1gtg2gpa1.4* triple mutant in the dark. The *gtg1gtg2gpa1.4* mutant also displayed a reduced height in comparison to WT, *gpa1.4* and *gtg1gtg2.* This defect in growth can also be explained by a defective cell wall formation and composition and an altered hormone balance in the mutant, since for plant height regulation, a balance between hormones, such as BR and GA, is required (Chinnusamy et al., 2010). It is possible that those defects can be enhanced by the deletion of AtGPA1.

In summary, although no clear interaction between GTGs and Gα has been observed, the results obtain in the analysis of the *gtg1gtg2gpa1.4* triple mutant indicate that there is a synergistic interaction between AtGTGs and AtGPA1 to control hypocotyl growth and cotyledon closure in the dark and plant height. This suggests that both proteins could be involved in the regulation of some of the same processes, such as cell elongation and plant growth, producing the defects observed in the *gtg1gtg2gpa1.4* mutant.

6.4. Conclusions and future work

Although several functions have been proposed for the GTG/GPHR family of membrane proteins in the literature, the results of this thesis strongly suggest a fundamental role for these proteins as anion channels regulating endomembrane pH and that this function is conserved among different plant species. However, further work is required to fully characterise these channels. One important step would be to study the 3D structure of the protein by the crystallisation of GTG/GPHR. Crystallisation studies would help to discover specific protein domains, such as the pore region, and further mutagenesis studies will provide information on the residues crucial for the activity of the channel. In addition, using this technique, structural differences could be found between GTG/GPHRs from different kingdoms that could explain the conductance and

selectivity differences observed between organisms. Since in this thesis it has been shown that GTG/GPHR can be successfully synthesised through a cell-free system, this could be a useful tool for future crystallisation studies. Once those important regions are elucidated, CRISPR/Cas9 genome editing technique could be used to mutate those protein residues in different plant species and analyse how the growth and development of those plants are affected. To confirm the conservation of function between mammalian and plant GTGs/GPHRs it would be interesting to express mammalian GPHR into the Arabidopsis *gtg1gtg2* double mutant to test whether it could rescue the defective growth of the mutant.

Since it was shown that the Ca^{2+} levels in the rice *gtg* mutant were reduced (Ma et al., 2015), future studies analysing the Ca^{2+} levels in the Arabidopsis *gtg1gtg2* mutants could be important to understand whether this defect is also observed in other plant species. To address this, several WT and *gtg1gtg2* Arabidopsis mutant plants containing the Ca^{2+} sensor R-GECO1 (Waadt et al., 2017) have been already generated as part of this project. This would contribute to a better understanding of the role of GTG/GPHR in Ca^{2+} homeostasis. In addition, it would be interesting to study at the same time whether other different signalling molecules are affected in the *gtg1gtg2* mutant. Genetically encoded fluorescence indicators (GEFIs) have been developed for several signal molecules, such as ABA, Ca^{2+}, pH and Cl^- that can be used alone or in combination, using 2-in-1-GEFIs (Waadt et al., 2020). It is possible to introduce a combination of those indicators into the same plant to study how those signalling networks function in the cell and how these processes are interconnected. Monitoring different signalling components in Arabidopsis WT and *gtg1gtg2* mutant plants would be useful to understand the role of GTG/GPHR in the regulation of these signals.

Future proteomic, interactomic and metabolomic studies in the WT and *gtg1gtg2* Arabidopsis mutant would be important to study which other proteins and metabolites are affected or regulated by GTG/GPHRs. Preliminary metabolomics work has been performed in our laboratory where the metabolite profile of the WT and *gtg1gtg2* mutant has been analysed. Interesting data have been obtained from this technique, showing that in the *gtg1gtg2* mutant sucrose and nitrogen metabolism were affected, suggesting an impairment of the C/N balance in the mutant. These results can be further corroborated by testing whether those compounds that are reduced in the *gtg1gtg2* mutant can rescue its defective growth when supplied to these plants.

The role of GTG/GPHR in different stress conditions can be also studied. Although it has been proposed that OsGTG is involved in cold stress in rice (Ma et al., 2015), work with Arabidopsis in this thesis did not replicate this result. Therefore, it would be important to test whether GTG/GPHR can be involved in other abiotic and biotic stresses. Arabidopsis and rice GTG mutants and all the transgenic lines generated in this thesis can be subjected to several abiotic stresses including drought, heat and salinity. Also, plants can be infected with several pathogens to study whether GTG/GPHRs are involved in biotic stress.

To study more in depth the reduced hypocotyl growth of the *gtg1gtg2gpa1.4* triple mutant in the dark, several analyses can be carried out. One is the measurement of the number of cells and the length of those cells in the hypocotyl to determine whether the reduced length is due to a defect in cell division and cell elongation. The cell wall composition of the *gtg1gtg2gpa1.4* line in comparison with the WT, *gtg1gtg2* and *gpa1.4* mutants can also be analysed. In addition, to study whether photomorphogenesis is activated in the *gtg1gtg2gpa1.4* triple mutant in the dark, analysis of the expression levels of photosynthetic genes can be performed. The effect of several hormones in the growth of the hypocotyl can also be studied, to determine whether the reduced hypocotyl or the open cotyledons in the dark are due to a defect in hormone pathways, and to test whether those phenotypes can be rescued by the presence of those hormones in the growth media. The expression level of several hormone biosynthesis genes can also be measured in the different lines to understand whether the hormone pathway in the *gtg1gtg2gpa1.4* mutant is different than in the WT, *gtg1gtg2* and *gpa1.4* mutants.

Overall this thesis has provided a deeper understanding of the role of the GTG/GPHRs in plants and has produced many useful tools that will allow further investigation into this family.

References

Accardi, A. & Miller, C. 2004. Secondary active transport mediated by a prokaryotic homologue of ClC Cl- channels. *Nature,* 427**,** 803-807.

Acheampong, A. K., Hu, J., Rotman, A., Zheng, C., Halaly, T., Takebayashi, Y., Jikumaru, Y., Kamiya, Y., Lichter, A., Sun, T.-P. & Or, E. 2015. Functional characterization and developmental expression profiling of gibberellin signalling components in Vitis vinifera. *Journal of Experimental Botany,* 66**,** 1463-1476.

Adamski, J. M., Cargnelutti, D., Sperotto, R. A., Terra, T. F., Rosa, L. M. G., Cruz, R. P., Fett, J. P. & Navabi, A. 2016. Identification and physiological characterization of two sister lines ofindicarice (Oryza sativaL.) with contrasting levels of cold tolerance. *Canadian Journal of Plant Science,* 96**,** 197-214.

Agarwal, P. K., Agarwal, P., Reddy, M. K. & Sopory, S. K. 2006. Role of DREB transcription factors in abiotic and biotic stress tolerance in plants. *Plant Cell Reports,* 25**,** 1263-1274.

Agi, T. 2000. Analysis of the genome sequence of the flowering plant *Arabidopsis thaliana*. *Nature,* 408**,** 796-815.

Alboresi, A., Gestin, C., Leydecker, M.-T., Bedu, M., Meyer, C. & Truong, H.-N. 2005. Nitrate, a signal relieving seed dormancy in Arabidopsis. *Plant, Cell & Environment,* 28**,** 500-512.

Alonso, J. M., Stepanova, A. N., Leisse, T. J., Kim, C. J., Chen, H., Shinn, P., Stevenson, D. K., Zimmerman, J., Barajas, P. & Cheuk, R. 2003. Genome-wide insertional mutagenesis of Arabidopsis thaliana. *Science,* 301**,** 653-657.

Alvarez, S., Roy Choudhury, S., Hicks, L. M. & Pandey, S. 2013. Quantitative proteomics-based analysis supports a significant role of GTG proteins in regulation of ABA response in *Arabidopsis* roots. *Journal of Proteome Research,* 12**,** 1487-1501.

An, G., Lee, S., Kim, S.-H. & Kim, S.-R. 2005. Molecular Genetics Using T-DNA in Rice. *Plant and Cell Physiology,* 46**,** 14-22.

Ando, M., Akiyama, M., Okuno, D., Hirano, M., Ide, T., Sawada, S., Sasaki, Y. & Akiyoshi, K. 2016. Liposome chaperon in cell-free membrane protein synthesis: one-step preparation of KcsA-integrated liposomes and electrophysiological analysis by the planar bilayer method. *Biomaterials Science,* 4**,** 258-264.

Andrés, Z., Pérez-Hormaeche, J., Leidi, E. O., Schlücking, K., Steinhorst, L., Mclachlan, D. H., Schumacher, K., Hetherington, A. M., Kudla, J., Cubero, B. & Pardo, J. M. 2014. Control of vacuolar dynamics and regulation of stomatal aperture by tonoplast potassium uptake. *Proceedings of the National Academy of Sciences,* 111**,** E1806-E1814.

Aoi, W. & Marunaka, Y. 2014. Importance of pH Homeostasis in Metabolic Health and Diseases: Crucial Role of Membrane Proton Transport. *BioMed Research International,* 2014**,** 598986.

Azpiroz, R., Wu, Y., Locascio, J. C. & Feldmann, K. A. 1998. An Arabidopsis brassinosteroid-dependent mutant is blocked in cell elongation. *The Plant Cell Online,* 10**,** 219-230.

Backliwal, G., Hildinger, M., Hasija, V. & Wurm, F. M. 2008. High-density transfection with HEK-293 cells allows doubling of transient titers and removes need for a priori DNA complex formation with PEI. *Biotechnology and Bioengineering,* 99**,** 721-727.

Baltscheffsky, M., Schultz, A. & Baltscheffsky, H. 1999. H+-proton-pumping inorganic pyrophosphatase: a tightly membrane-bound family. *FEBS Letters,* 452**,** 121-127.

Banfield, D. K. 2011. Mechanisms of protein retention in the Golgi. *Cold Spring Harbor perspectives in biology,* 3**,** a005264-a005264.

Barro-Soria, R., Aldehni, F., Almaça, J., Witzgall, R., Schreiber, R. & Kunzelmann, K. 2010. ER-localized bestrophin 1 activates Ca2+-dependent ion channels TMEM16A and SK4 possibly by acting as a counterion channel. *Pflügers Archiv - European Journal of Physiology,* 459**,** 485-497.

Bassil, E., Ohto, M.-A., Esumi, T., Tajima, H., Zhu, Z., Cagnac, O., Belmonte, M., Peleg, Z., Yamaguchi, T. & Blumwald, E. 2011a. The Arabidopsis Intracellular Na^+/H^+ Antiporters NHX5 and NHX6 Are Endosome Associated and Necessary for Plant Growth and Development. *The Plant Cell,* 23**,** 224-239.

Bassil, E., Tajima, H., Liang, Y.-C., Ohto, M.-A., Ushijima, K., Nakano, R., Esumi, T., Coku, A., Belmonte, M. & Blumwald, E. 2011b. The Arabidopsis Na+/H+ antiporters NHX1 and NHX2 control vacuolar pH and K+ homeostasis to regulate growth, flower development, and reproduction. *The Plant Cell Online,* 23**,** 3482-3497.

Bayer, E. M., Sparkes, I., Vanneste, S. & Rosado, A. 2017. From shaping organelles to signalling platforms: the emerging functions of plant ER–PM contact sites. *Current Opinion in Plant Biology,* 40**,** 89-96.

Bednarek, S. Y. & Falbel, T. G. 2002. Membrane trafficking during plant cytokinesis. *Traffic,* 3**,** 621-629.

Beeckman, T., Przemeck, G. K. H., Stamatiou, G., Lau, R., Terryn, N., De Rycke, R., Inzé, D. & Berleth, T. 2002. Genetic complexity of cellulose synthase a gene function in arabidopsis embryogenesis. *Plant Physiology,* 130**,** 1883-1893.

Benítez-Rangel, E., López-Méndez, M. C., García, L. & Guerrero-Hernández, A. 2015. DIDS (4,4'-Diisothiocyanatostilbene-2,2'-disulfonate) directly inhibits caspase activity in HeLa cell lysates. *Cell death discovery,* 1**,** 15037-15037.

Berjukow, S., Döring, F., Froschmayr, M., Grabner, M., Glossmann, H. & Hering, S. 1996. Endogenous calcium channels in human embryonic kidney (HEK293) cells. *British journal of pharmacology,* 118**,** 748-754.

Berthomieu, P., Conéjéro, G., Nublat, A., Brackenbury, W. J., Lambert, C., Savio, C., Uozumi, N., Oiki, S., Yamada, K., Cellier, F., Gosti, F., Simonneau, T., Essah, P. A., Tester, M., Véry, A.-A., Sentenac, H. & Casse, F. 2003. Functional analysis of AtHKT1 in Arabidopsis shows that Na(+) recirculation by the phloem is crucial for salt tolerance. *The EMBO journal,* 22**,** 2004-2014.

Betts, M. J. & Russell, R. B. 2003. Amino acid properties and consequences of substitutions. *Bioinformatics for geneticists,* 317**,** 289.

Beyenbach, K. W. & Wieczorek, H. 2006. The V-type H^+ ATPase: molecular structure and function, physiological roles and regulation. *Journal of Experimental Biology,* 209**,** 577-589.

Bezanilla, F. 2008. Ion Channels: From Conductance to Structure. *Neuron,* 60**,** 456-468.

Boevink, P., Oparka, K., Cruz, S. S., Martin, B., Betteridge, A. & Hawes, C. 1998. Stacks on tracks: the plant Golgi apparatus traffics on an actin/ER network†. *The Plant Journal,* 15**,** 441-447.

Bolle, C., Schneider, A. & Leister, D. 2011. Perspectives on Systematic Analyses of Gene Function in Arabidopsis thaliana: New Tools, Topics and Trends. *Current genomics,* 12**,** 1-14.

Bortesi, L. & Fischer, R. 2015. The CRISPR/Cas9 system for plant genome editing and beyond. *Biotechnology Advances,* 33**,** 41-52.

Boudsocq, M., Willmann, M. R., Mccormack, M., Lee, H., Shan, L., He, P., Bush, J., Cheng, S.-H. & Sheen, J. 2010. Differential innate immune signalling via Ca(2+) sensor protein kinases. *Nature,* 464**,** 418-422.

Breitwieser, G. E. 1991. G protein-mediated ion channel activation. *Hypertension,* 17**,** 684-692.

Breygina, M. A., Matveeva, N. P. & Ermakov, I. P. 2009. The role of Cl− in pollen germination and tube growth. *Russian Journal of Developmental Biology,* 40**,** 157-164.

Brüx, A., Liu, T.-Y., Krebs, M., Stierhof, Y.-D., Lohmann, J. U., Miersch, O., Wasternack, C. & Schumacher, K. 2008. Reduced V-ATPase activity in the trans-Golgi network causes oxylipin-dependent hypocotyl growth inhibition in Arabidopsis. *The Plant Cell Online,* 20**,** 1088-1100.

Buch-Pedersen, M. J., Pedersen, B. P., Veierskov, B., Nissen, P. & Palmgren, M. G. 2008. Protons and how they are transported by proton pumps. *Pflügers Archiv - European Journal of Physiology,* 457**,** 573.

Bugaj, V., Alexeenko, V., Zubov, A., Glushankova, L., Nikolaev, A., Wang, Z., Kaznacheyeva, E., Bezprozvanny, I. & Mozhayeva, G. N. 2005. Functional Properties of Endogenous Receptor- and Store-operated Calcium Influx Channels in HEK293 Cells. *Journal of Biological Chemistry,* 280**,** 16790-16797.

Caño-Delgado, A., Penfield, S., Smith, C., Catley, M. & Bevan, M. 2003. Reduced cellulose synthesis invokes lignification and defense responses in *Arabidopsis thaliana*. *The Plant Journal,* 34**,** 351-362.

Capurro, V., Gianotti, A., Caci, E., Ravazzolo, R., Galietta, L. J. V. & Zegarra-Moran, O. 2015. Functional analysis of acid-activated Cl- channels: Properties and mechanisms of regulation. *Biochimica Et Biophysica Acta-Biomembranes,* 1848**,** 105-114.

Carlson, E. D., Gan, R., Hodgman, C. E. & Jewett, M. C. 2012. Cell-Free Protein Synthesis: Applications Come of Age. *Biotechnology advances,* 30**,** 1185-1194.

Carnell, L. & Moore, H. P. 1994. Transport via the regulated secretory pathway in semi-intact PC12 cells: role of intra-cisternal calcium and pH in the transport and sorting of secretogranin II. *The Journal of cell biology,* 127**,** 693-705.

Cary, A. J., Che, P. & Howell, S. H. 2002. Developmental events and shoot apical meristem gene expression patterns during shoot development in Arabidopsis thaliana. *The Plant Journal,* 32**,** 867-877.

Casey, J. R., Grinstein, S. & Orlowski, J. 2009. Sensors and regulators of intracellular pH. *Nature Reviews Molecular Cell Biology,* 11**,** 50.

Castro Marín, I., Loef, I., Bartetzko, L., Searle, I., Coupland, G., Stitt, M. & Osuna, D. 2011. Nitrate regulates floral induction in Arabidopsis, acting independently of light, gibberellin and autonomous pathways. *Planta,* 233**,** 539-552.

Chakravorty, D., Gookin, T. E., Milner, M. J., Yu, Y. & Assmann, S. M. 2015. Extra-Large G Proteins Expand the Repertoire of Subunits in Arabidopsis Heterotrimeric G Protein Signaling. *Plant Physiol,* 169**,** 512-29.

Chakravorty, D., Trusov, Y., Zhang, W., Acharya, B. R., Sheahan, M. B., Mccurdy, D. W., Assmann, S. M. & Botella, J. R. 2011. An atypical heterotrimeric G-protein γ-subunit is involved in guard cell K^+ channel regulation and morphological development in *Arabidopsis thaliana*. *The Plant Journal,* 67**,** 840-851.

Chanroj, S., Lu, Y., Padmanaban, S., Nanatani, K., Uozumi, N., Rao, R. & Sze, H. 2011. Plant-Specific Cation/H+ Exchanger 17 and Its Homologs Are Endomembrane K+ Transporters with Roles in Protein Sorting. *Journal of Biological Chemistry,* 286**,** 33931-33941.

Chanroj, S., Wang, G., Venema, K., Zhang, M., Delwiche, C. & Sze, H. 2012. Conserved and Diversified Gene Families of Monovalent Cation/H+ Antiporters from Algae to Flowering Plants. *Frontiers in Plant Science,* 3.

Charroux, B. & Royet, J. 2014. Mutations in the Drosophila ortholog of the vertebrate Golgi pH regulator (GPHR) protein disturb endoplasmic reticulum and Golgi organization and affect systemic growth. *Biology open***,** BIO20137187.

Chen, J. G., Gao, Y. & Jones, A. M. 2006a. Differential roles of Arabidopsis heterotrimeric G-protein subunits in modulating cell division in roots. *Plant Physiol,* 141**,** 887-97.

Chen, Y., Ji, F., Xie, H., Liang, J. & Zhang, J. 2006b. The regulator of G-protein signaling proteins involved in sugar and abscisic acid signaling in Arabidopsis seed germination. *Plant Physiology,* 140**,** 302-310.

Chen, Z. C., Yamaji, N., Fujii-Kashino, M. & Ma, J. F. 2016. A Cation-Chloride Cotransporter Gene Is Required for Cell Elongation and Osmoregulation in Rice. *Plant Physiology,* 171**,** 494-507.

Cheng, N.-H., Pittman, J. K., Shigaki, T., Lachmansingh, J., Leclere, S., Lahner, B., Salt, D. E. & Hirschi, K. D. 2005. Functional association of Arabidopsis CAX1 and CAX3 is required for normal growth and ion homeostasis. *Plant physiology,* 138**,** 2048-2060.

Chilton, M.-D., Drummond, M. H., Merlo, D. J., Sciaky, D., Montoya, A. L., Gordon, M. P. & Nester, E. W. 1977. Stable incorporation of plasmid DNA into higher plant cells: the molecular basis of crown gall tumorigenesis. *Cell,* 11**,** 263-271.

Chinnusamy, V., Zhu, J.-K. & Sunkar, R. 2010. Gene Regulation During Cold Stress Acclimation in Plants. *Methods in molecular biology (Clifton, N.J.),* 639**,** 39-55.

Choudhury, S. & Pandey, S. 2016. The role of PLDα1 in providing specificity to signal-response coupling by heterotrimeric G-protein components in Arabidopsis. *The Plant Journal,* 86**,** 50-61.

Churchill, K. A. & Sze, H. 1984. Anion-Sensitive, H^+Pumping ATPase of Oat Roots. *Direct Effects of Cl[−], NO₃[−], and a Disulfonic Stilbene,* 76**,** 490-497.

Clough, S. J. & Bent, A. F. 1998. Floral dip: a simplified method for *Agrobacterium*-mediated transformation of *Arabidopsis thaliana*. *The Plant Journal,* 16**,** 735-743.

Clouse, S. D., Langford, M. & Mcmorris, T. C. 1996. A brassinosteroid-insensitive mutant in Arabidopsis thaliana exhibits multiple defects in growth and development. *Plant Physiology,* 111**,** 671-678.

Colmenero-Flores, J. M., Franco-Navarro, J. D., Cubero-Font, P., Peinado-Torrubia, P. & Rosales, M. A. 2019. Chloride as a Beneficial Macronutrient in Higher Plants: New Roles and Regulation. *International Journal of Molecular Sciences,* 20**,** 4686.

Colmenero-Flores, J. M., Martínez, G., Gamba, G., Vázquez, N., Iglesias, D. J., Brumós, J. & Talón, M. 2007. Identification and functional characterization of cation–chloride cotransporters in plants. *The Plant Journal,* 50**,** 278-292.

Cooper, G. M. 2000. *The Cell - A Molecular Approach 2nd Edition*, Sunderland (MA): Sinauer Associates.

Cournia, Z., Allen, T. W., Andricioaei, I., Antonny, B., Baum, D., Brannigan, G., Buchete, N.-V., Deckman, J. T., Delemotte, L., Del Val, C., Friedman, R., Gkeka, P., Hege, H.-C., Hénin, J., Kasimova, M. A., Kolocouris, A., Klein, M. L., Khalid, S., Lemieux, M. J., Lindow, N., Roy, M., Selent, J., Tarek, M., Tofoleanu, F., Vanni, S., Urban, S., Wales, D. J., Smith, J. C. & Bondar, A.-N. 2015. Membrane Protein Structure, Function, and Dynamics: a Perspective from Experiments and Theory. *The Journal of membrane biology,* 248**,** 611-640.

Crawford, N. M. & Glass, A. D. M. 1998. Molecular and physiological aspects of nitrate uptake in plants. *Trends in Plant Science,* 3**,** 389-395.

Cubero-Font, P., Maierhofer, T., Jaslan, J., Rosales, Miguel a., Espartero, J., Díaz-Rueda, P., Müller, Heike m., Hürter, A.-L., Al-Rasheid, Khaled a. S., Marten, I., Hedrich, R., Colmenero-Flores, José m. & Geiger, D. 2016. Silent S-Type Anion Channel Subunit SLAH1 Gates SLAH3 Open for Chloride Root-to-Shoot Translocation. *Current Biology,* 26**,** 2213-2220.

Cui, Y., Jiang, N., Xu, Z. & Xu, Q. 2020. Heterotrimeric G protein are involved in the regulation of multiple agronomic traits and stress tolerance in rice. *BMC Plant Biology,* 20**,** 90.

Curtis, M. D. & Grossniklaus, U. 2003. A Gateway Cloning Vector Set for High-Throughput Functional Analysis of Genes in Planta. *Plant Physiology,* 133**,** 462-469.

Cutler, S. R., Rodriguez, P. L., Finkelstein, R. R. & Abrams, S. R. 2010. Abscisic acid: emergence of a core signaling network. *Annu Rev Plant Biol,* 61**,** 651-79.

Dametto, A., Sperotto, R. A., Adamski, J. M., Blasi, E. A., Cargnelutti, D., De Oliveira, L. F., Ricachenevsky, F. K., Fregonezi, J. N., Mariath, J. E., Da Cruz, R. P., Margis, R. & Fett, J. P. 2015. Cold tolerance in rice germinating seeds revealed by deep RNAseq analysis of contrasting indica genotypes. *Plant Sci,* 238**,** 1-12.

Daras, G., Rigas, S., Penning, B., Milioni, D., Mccann, M. C., Carpita, N. C., Fasseas, C. & Hatzopoulos, P. 2009. The thanatos mutation in *Arabidopsis thaliana* cellulose synthase 3 (AtCesA3) has a dominant-negative effect on cellulose synthesis and plant growth. *New Phytologist,* 184**,** 114-126.

Dascal, N. 2001. Ion-channel regulation by G proteins. *Trends in Endocrinology & Metabolism,* 12**,** 391-398.

De Angeli, A., Monachello, D., Ephritikhine, G., Frachisse, J. M., Thomine, S., Gambale, F. & Barbier-Brygoo, H. 2006. The nitrate/proton antiporter AtCLCa mediates nitrate accumulation in plant vacuoles. *Nature,* 442**,** 939-942.

De Angeli, A., Zhang, J., Meyer, S. & Martinoia, E. 2013. AtALMT9 is a malate-activated vacuolar chloride channel required for stomatal opening in Arabidopsis. *Nature Communications,* 4**,** 1804.

Dechorgnat, J., Nguyen, C. T., Armengaud, P., Jossier, M., Diatloff, E., Filleur, S. & Daniel-Vedele, F. 2010. From the soil to the seeds: the long journey of nitrate in plants. *Journal of Experimental Botany,* 62**,** 1349-1359.

Deckstein, J., Van Appeldorn, J., Tsangarides, M., Yiannakou, K., Muller, R., Stumpf, M., Sukumaran, S. K., Eichinger, L., Noegel, A. A. & Riyahi, T. Y. 2015. The Dictyostelium discoideum GPHR Ortholog Is an Endoplasmic Reticulum and Golgi Protein with Roles during Development. *Eukaryotic Cell,* 14**,** 41-54.

Delgado-Cerezo, M., Sanchez-Rodriguez, C., Escudero, V., Miedes, E., Fernandez, P. V., Jorda, L., Hernandez-Blanco, C., Sanchez-Vallet, A., Bednarek, P. & Schulze-Lefert, P. 2012. Arabidopsis heterotrimeric G-protein regulates cell wall defense and resistance to necrotrophic fungi. *Mol Plant,* 5.

Demaegd, D., Foulquier, F., Colinet, A.-S., Gremillon, L., Legrand, D., Mariot, P., Peiter, E., Van Schaftingen, E., Matthijs, G. & Morsomme, P. 2013. Newly characterized Golgi-localized family of proteins is involved in calcium and pH homeostasis in yeast and human cells. *Proceedings of the National Academy of Sciences,* 110**,** 6859-6864.

Demaurex, N. 2002. pH Homeostasis of Cellular Organelles. *Physiology,* 17**,** 1-5.

Desnos, T., Orbovic, V., Bellini, C., Kronenberger, J., Caboche, M., Traas, J. & Hofte, H. 1996. *Procuste1* mutants identify two distinct genetic pathways controlling hypocotyl cell elongation, respectively in dark- and light-grown *Arabidopsis* seedlings. *Development,* 122**,** 683-693.

Dettmer, J., Hong-Hermesdorf, A., Stierhof, Y.-D. & Schumacher, K. 2006. Vacuolar H+-ATPase Activity Is Required for Endocytic and Secretory Trafficking in Arabidopsis. *The Plant Cell Online,* 18**,** 715-730.

Dettmer, J., Schubert, D., Calvo-Weimar, O., Stierhof, Y.-D., Schmidt, R. & Schumacher, K. 2005. Essential role of the V-ATPase in male gametophyte development. *The Plant Journal,* 41**,** 117-124.

Dhondt, S., Coppens, F., De Winter, F., Swarup, K., Merks, R. M. H., Inzé, D., Bennett, M. J. & Beemster, G. T. S. 2010. SHORT-ROOT and SCARECROW regulate leaf growth in Arabidopsis by stimulating S-phase progression of the cell cycle. *Plant Physiology,* 154**,** 1183-1195.

Di Laurenzio, L., Wysocka-Diller, J., Malamy, J. E., Pysh, L., Helariutta, Y., Freshour, G., Hahn, M. G., Feldmann, K. A. & Benfey, P. N. 1996. The *SCARECROW* gene regulates an asymmetric cell division that is essential for generating the radial organization of the *Arabidopsis* root. *Cell,* 86**,** 423-433.

Diatloff, E., Peyronnet, R., Colcombet, J., Thomine, S., Barbier-Brygoo, H. & Frachisse, J.-M. 2010. R type anion channel: a multifunctional channel seeking its molecular identity. *Plant signaling & behavior,* 5**,** 1347-1352.

Dickson, K., Pedi, V. & Long, L. S. B. 2014. Structure and insights into the function of a Ca2+-activated Cl− channel. *Nature,* 516**,** 213.

Diévart, A. & Clark, S. E. 2004. LRR-containing receptors regulating plant development and defense. *Development,* 131**,** 251-261.

Ding, L., Pandey, S. & Assmann, S. M. 2008. *Arabidopsis* extra-large G proteins (XLGs) regulate root morphogenesis. *The Plant Journal,* 53**,** 248-263.

Dong, H., Yan, S., Liu, J., Liu, P. & Sun, J. 2019. TaCOLD1 defines a new regulator of plant height in bread wheat. *Plant Biotechnology Journal,* 17**,** 687-699.

Dong, J., Tang, D., Gao, Z., Yu, R., Li, K., He, H., Terzaghi, W., Deng, X. W. & Chen, H. 2014. Arabidopsis DE-ETIOLATED1 Represses Photomorphogenesis by Positively Regulating Phytochrome-Interacting Factors in the Dark. *The Plant Cell,* 26**,** 3630-3645.

Dorey, A. 2019. *Arabidopsis and C. elegans GTG/GPHRs have a conserved role across kingdoms as anion channels.* University of Southampton.

Dubiella, U., Seybold, H., Durian, G., Komander, E., Lassig, R., Witte, C.-P., Schulze, W. X. & Romeis, T. 2013. Calcium-dependent protein kinase/NADPH oxidase activation circuit is required for rapid defense signal propagation. *Proceedings of the National Academy of Sciences,* 110**,** 8744-8749.

Dubouzet, J. G., Sakuma, Y., Ito, Y., Kasuga, M., Dubouzet, E. G., Miura, S., Seki, M., Shinozaki, K. & Yamaguchi-Shinozaki, K. 2003. OsDREB genes in rice, Oryza sativa L., encode transcription activators that function in drought-, high-salt- and cold-responsive gene expression. *The Plant Journal,* 33**,** 751-763.

Duncan, R. R., Westwood, P. K., Boyd, A. & Ashley, R. H. 1997. Rat Brain p64H1, Expression of a New Member of the p64 Chloride Channel Protein Family in Endoplasmic Reticulum. *Journal of Biological Chemistry,* 272**,** 23880-23886.

Dupree, P. & Sherrier, D. J. 1998. The plant Golgi apparatus. *Biochimica et Biophysica Acta (BBA) - Molecular Cell Research,* 1404**,** 259-270.

Dutta, R. & Robinson, K. R. 2004. Identification and Characterization of Stretch-Activated Ion Channels in Pollen Protoplasts. *Plant Physiology,* 135**,** 1398-1406.

Edwards, J. C. & Kahl, C. R. 2010. Chloride channels of intracellular membranes. *FEBS Letters,* 584**,** 2102-2111.

Edwards, J. C., Tulk, B. & Schlesinger, P. H. 1998. Functional Expression of p64, an Intracellular Chloride Channel Protein. *The Journal of Membrane Biology,* 163**,** 119-127.

Elmore, J. M. & Coaker, G. 2011. The Role of the Plasma Membrane H+-ATPase in Plant–Microbe Interactions. *Molecular Plant,* 4**,** 416-427.

Elter, A., Hartel, A., Sieben, C., Hertel, B., Fischer-Schliebs, E., Lüttge, U., Moroni, A. & Thiel, G. 2007. A Plant Homolog of Animal Chloride Intracellular Channels (CLICs) Generates an Ion Conductance in Heterologous Systems. *Journal of Biological Chemistry,* 282**,** 8786-8792.

Engel, A. & Gaub, H. E. 2008. Structure and mechanics of membrane proteins. *Annu Rev Biochem,* 77**,** 127-48.

Ettorre, M., Verzè, G., Caldrer, S., Johansson, J., Calcaterra, E., Assael, B. M., Melotti, P., Sorio, C. & Buffelli, M. 2014. Electrophysiological evaluation of Cystic Fibrosis Conductance Transmembrane Regulator (CFTR) expression in human monocytes. *Biochimica et Biophysica Acta (BBA) - General Subjects,* 1840**,** 3088-3095.

Evers, J. B., Van Der Krol, A. R., Vos, J. & Struik, P. C. 2011. Understanding shoot branching by modelling form and function. *Trends in Plant Science,* 16**,** 464-467.

Fagard, M., Desnos, T., Desprez, T., Goubet, F., Refregier, G., Mouille, G., Mccann, M., Rayon, C., Vernhettes, S. & Höfte, H. 2000. *PROCUSTE1* encodes a cellulose synthase required for normal cell elongation specifically in roots and dark-grown hypocotyls of *Arabidopsis*. *The Plant Cell Online,* 12**,** 2409-2423.

Fan, C., Xing, Y., Mao, H., Lu, T., Han, B., Xu, C., Li, X. & Zhang, Q. 2006. GS3, a major QTL for grain length and weight and minor QTL for grain width and thickness in rice, encodes a putative transmembrane protein. *Theoretical and Applied Genetics,* 112**,** 1164-1171.

Fan, L.-M., Zhang, W., Chen, J.-G., Taylor, J. P., Jones, A. M. & Assmann, S. M. 2008. Abscisic acid regulation of guard-cell K^+ and anion channels in Gβ- and RGS-deficient *Arabidopsis* lines. *Proceedings of the National Academy of Sciences,* 105**,** 8476-8481.

Fecht-Bartenbach, J. V. D., Bogner, M., Dynowski, M. & Ludewig, U. 2010. CLC-b-Mediated NO3-/H+ Exchange Across the Tonoplast of Arabidopsis Vacuoles. *Plant and Cell Physiology,* 51**,** 960-968.

Fecht-Bartenbach, J. V. D., Bogner, M., Krebs, M., Stierhof, Y.-D., Schumacher, K. & Ludewig, U. 2007. Function of the anion transporter AtCLC-d in the trans-Golgi network. *The Plant Journal,* 50**,** 466-474.

Ferjani, A., Segami, S., Horiguchi, G., Muto, Y., Maeshima, M. & Tsukaya, H. 2011. Keep an Eye on PPi: The Vacuolar-Type H^+-Pyrophosphatase Regulates Postgerminative Development in Arabidopsis. *The Plant Cell,* 23**,** 2895-2908.

Ferrero-Serrano, Á. & Assmann, S. M. 2016. The α-subunit of the rice heterotrimeric G protein, RGA1, regulates drought tolerance during the vegetative phase in the dwarf rice mutant d1. *Journal of Experimental Botany,* 67**,** 3433-3443.

Fields, S. & Song, O.-K. 1989. A novel genetic system to detect protein–protein interactions. *Nature,* 340**,** 245-246.

Finbow, M. E. & Harrison, M. A. 1997. The vacuolar H+-ATPase: a universal proton pump of eukaryotes. *The Biochemical journal,* 324 (Pt 3)**,** 697-712.

Finkelstein, R. R., Gampala, S. S. L. & Rock, C. D. 2002. Abscisic acid signaling in seeds and seedlings. *The Plant Cell Online,* 14**,** S15-S45.

Fitzsimmons, R., Amin, N. & Uversky, V. N. 2016. Understanding the roles of intrinsic disorder in subunits of hemoglobin and the disease process of sickle cell anemia. *Intrinsically disordered proteins,* 4**,** e1248273-e1248273.

Franco-Navarro, J. D., Brumós, J., Rosales, M. A., Cubero-Font, P., Talón, M. & Colmenero-Flores, J. M. 2016. Chloride regulates leaf cell size and water relations in tobacco plants. *Journal of experimental botany,* 67**,** 873-891.

Franco-Navarro, J. D., Rosales, M. A., Cubero-Font, P., Calvo, P., Álvarez, R., Diaz-Espejo, A. & Colmenero-Flores, J. M. 2019. Chloride as a macronutrient increases water-use efficiency by anatomically driven reduced stomatal conductance and increased mesophyll diffusion to CO2. *The Plant Journal,* 0.

Friddin, M. S., Smithers, N. P., Beaugrand, M., Marcotte, I., Williamson, P. T. F., Morgan, H. & De Planque, M. R. R. 2013. Single-channel electrophysiology of cell-free expressed ion channels by direct incorporation in lipid bilayers. *Analyst,* 138**,** 7294-7298.

Fuchs, I., Stölzle, S., Ivashikina, N. & Hedrich, R. 2005. Rice K+ uptake channel OsAKT1 is sensitive to salt stress. *Planta,* 221**,** 212-221.

Fujikawa, Y. & Kato, N. 2007. Split luciferase complementation assay to study protein–protein interactions in Arabidopsis protoplasts. *The Plant Journal,* 52**,** 185-195.

Gao, Y., Wang, S., Asami, T. & Chen, J.-G. 2008. Loss-of-function mutations in the Arabidopsis heterotrimeric G-protein α subunit enhance the developmental defects of brassinosteroid signaling and biosynthesis mutants. *Plant and cell physiology,* 49**,** 1013-1024.

Garfinkel, D. J. & Nester, E. W. 1980. Agrobacterium tumefaciens mutants affected in crown gall tumorigenesis and octopine catabolism. *Journal of bacteriology,* 144**,** 732-743.

Gaxiola, R. A., Palmgren, M. G. & Schumacher, K. 2007. Plant proton pumps. *FEBS Letters,* 581**,** 2204-2214.

Gehl, C., Waadt, R., Kudla, J., Mendel, R. R. & Hansch, R. 2009. New GATEWAY vectors for high throughput analyses of protein-protein interactions by bimolecular fluorescence complementation. *Mol Plant,* 2**,** 1051-8.

Gendreau, E., Traas, J., Desnos, T., Grandjean, O., Caboche, M. & Hofte, H. 1997. Cellular Basis of Hypocotyl Growth in Arabidopsis thaliana. *Plant Physiology,* 114**,** 295-305.

Ghosh, A., Khandelwal, N., Kumar, A. & Bera, A. K. 2017. Leucine-rich repeat-containing 8B protein is associated with the endoplasmic reticulum Ca^{2+} leak in HEK293 cells. *Journal of Cell Science,* 130**,** 3818-3828.

Gilliham, M. & Tester, M. 2005. The Regulation of Anion Loading to the Maize Root Xylem. *Plant Physiology,* 137**,** 819-828.

Gjetting, S. K., Ytting, C. K., Schulz, A. & Fuglsang, A. T. 2012. Live imaging of intra- and extracellular pH in plants using pHusion, a novel genetically encoded biosensor. *Journal of Experimental Botany,* 63**,** 3207-3218.

Gomord, V., Denmat, L.-A., Fitchette-Lainé, A.-C., Satiat-Jeunemaitre, B., Hawes, C. & Faye, L. 1997. The C-terminal HDEL sequence is sufficient for retention of secretory proteins in the endoplasmic reticulum (ER) but promotes vacuolar targeting of proteins that escape the ER. *The Plant Journal,* 11**,** 313-325.

Goren, M. A. & Fox, B. G. 2008. Wheat germ cell-free translation, purification, and assembly of a functional human stearoyl-CoA desaturase complex. *Protein Expression and Purification,* 62**,** 171-178.

Gou, X., Yin, H., He, K., Du, J., Yi, J., Xu, S., Lin, H., Clouse, S. D. & Li, J. 2012. Genetic Evidence for an Indispensable Role of Somatic Embryogenesis Receptor Kinases in Brassinosteroid Signaling. *PLOS Genetics,* 8**,** e1002452.

Gräslund, S., Nordlund, P., Weigelt, J., Hallberg, B. M., Bray, J., Gileadi, O., Knapp, S., Oppermann, U., Arrowsmith, C., Hui, R., Ming, J., Dhe-Paganon, S., Park, H.-W., Savchenko, A., Yee, A., Edwards, A., Vincentelli, R., Cambillau, C., Kim, R., Kim, S.-H., Rao, Z., Shi, Y., Terwilliger, T. C., Kim, C.-Y., Hung, L.-W., Waldo, G. S., Peleg,

Y., Albeck, S., Unger, T., Dym, O. & Prilusky, J. 2008. Protein production and purification. *Nature Methods,* 5**,** 135-146.

Graves, A. R., Curran, P. K., Smith, C. L. & Mindell, J. A. 2008. The Cl-/H+ antiporter ClC-7 is the primary chloride permeation pathway in lysosomes. *Nature,* 453**,** 788-792.

Gregory, R. J., Cheng, S. H., Rich, D. P., Marshall, J., Paul, S., Hehir, K., Ostedgaard, L., Klinger, K. W., Welsh, M. J. & Smith, A. E. 1990. Expression and characterization of the cystic fibrosis transmembrane conductance regulator. *Nature,* 347**,** 382-386.

Griffing, L. R., Lin, C., Perico, C., White, R. R. & Sparkes, I. 2017. Plant ER geometry and dynamics: biophysical and cytoskeletal control during growth and biotic response. *Protoplasma,* 254**,** 43-56.

Grigston, J. C., Osuna, D., Scheible, W.-R., Liu, C., Stitt, M. & Jones, A. M. 2008. D-Glucose sensing by a plasma membrane regulator of G signaling protein, AtRGS1. *FEBS letters,* 582**,** 3577-3584.

Guo, F.-Q., Young, J. & Crawford, N. M. 2003. The nitrate transporter AtNRT1.1 (CHL1) functions in stomatal opening and contributes to drought susceptibility in Arabidopsis. *The Plant cell,* 15**,** 107-117.

Guo, X., Liu, D. & Chong, K. 2018. Cold signaling in plants: Insights into mechanisms and regulation. *Journal of Integrative Plant Biology,* 60**,** 745-756.

Gutermuth, T., Lassig, R., Portes, M.-T., Maierhofer, T., Romeis, T., Borst, J.-W., Hedrich, R., Feijó, J. A. & Konrad, K. R. 2013. Pollen tube growth regulation by free anions depends on the interaction between the anion channel SLAH3 and calcium-dependent protein kinases CPK2 and CPK20. *The Plant Cell,* 25**,** 4525-4543.

Gutha, L. R. & Reddy, A. R. 2008. Rice DREB1B promoter shows distinct stress-specific responses, and the overexpression of cDNA in tobacco confers improved abiotic and biotic stress tolerance. *Plant Molecular Biology,* 68**,** 533.

Hackenberg, D., Mckain, M. R., Lee, S. G., Roy Choudhury, S., Mccann, T., Schreier, S., Harkess, A., Pires, J. C., Wong, G. K.-S., Jez, J. M., Kellogg, E. A. & Pandey, S. 2017. Gα and regulator of G-protein signaling (RGS) protein pairs maintain functional compatibility and conserved interaction interfaces throughout evolution despite frequent loss of RGS proteins in plants. *New Phytologist,* 216**,** 562-575.

Hagen, A. R., Hagen, A. R., Barabote, R. D. & Saier, M. H. 2005. The bestrophin family of anion channels: identification of prokaryotic homologues. *Molecular Membrane Biology,* 22**,** 291-302.

Hardke, J. T. & Service, U. O. a. C. E. 2013. *Arkansas Rice Production Handbook*, Cooperative Extension Service, University of Arkansas.

Hartzell, C., Putzier, I. & Arreola, J. 2004. Calcium-activated chloride channels. *Annual Review of Physiology,* 67**,** 719-758.

Haseloff, J., Siemering, K. R., Prasher, D. C. & Hodge, S. 1997. Removal of a cryptic intron and subcellular localization of green fluorescent protein are required to mark transgenic Arabidopsis plants brightly. *Proceedings of the National Academy of Sciences,* 94**,** 2122-2127.

Hassan, K. A., Galea, M., Wu, J., Mitchell, B. A., Skurray, R. A. & Brown, M. H. 2006. Functional effects of intramembranous proline substitutions in the staphylococcal multidrug transporter QacA. *FEMS Microbiology Letters,* 263**,** 76-85.

Hawes, C., Kiviniemi, P. & Kriechbaumer, V. 2015. The endoplasmic reticulum: A dynamic and well-connected organelle. *Journal of Integrative Plant Biology,* 57**,** 50-62.

He, B. & Soderlund, D. M. 2010. Human Embryonic Kidney (HEK293) Cells Express Endogenous Voltage-Gated Sodium Currents and Na(v)1.7 Sodium Channels. *Neuroscience letters,* 469**,** 268.

Heo, J. B., Sung, S. & Assmann, S. M. 2012. Ca2+-dependent GTPase, extra-large G protein 2 (XLG2), promotes activation of DNA-binding protein related to vernalization 1 (RTV1), leading to activation of floral integrator genes and early flowering in Arabidopsis. *J Biol Chem,* 287**,** 8242-53.

Hepler, P. K. 2005. Calcium: A Central Regulator of Plant Growth and Development. *The Plant Cell,* 17**,** 2142-2155.

Herdean, A., Nziengui, H., Zsiros, O., Solymosi, K., Garab, G., Lundin, B. & Spetea, C. 2016a. The Arabidopsis Thylakoid Chloride Channel AtCLCe Functions in Chloride Homeostasis and Regulation of Photosynthetic Electron Transport. *Frontiers in Plant Science,* 7.

Herdean, A., Teardo, E., Nilsson, A. K., Pfeil, B. E., Johansson, O. N., Unnep, R., Nagy, G., Zsiros, O., Dana, S., Solymosi, K., Garab, G., Szabo, I., Spetea, C. & Lundin, B. 2016b. A voltage-dependent chloride channel fine-tunes photosynthesis in plants. *Nature Communications,* 7**,** 11.

Heredia, A., Jiménez, A. & Guillén, R. 1995. Composition of plant cell walls. *Zeitschrift für Lebensmittel-Untersuchung und Forschung,* 200**,** 24-31.

Herman, E. M., Li, X., Su, R. T., Larsen, P., Hsu, H. & Sze, H. 1994. Vacuolar-Type H+ -ATPases Are Associated with the Endoplasmic Reticulum and Provacuoles of Root Tip Cells. *Plant physiology,* 106**,** 1313-1324.

Herpers, B. & Rabouille, C. 2004. mRNA Localization and ER-based Protein Sorting Mechanisms Dictate the Use of Transitional Endoplasmic Reticulum-Golgi Units Involved in Gurken Transport in Drosophila Oocytes. *Molecular Biology of the Cell,* 15**,** 5306-5317.

Hochmal, A. K., Schulze, S., Trompelt, K. & Hippler, M. 2015. Calcium-dependent regulation of photosynthesis. *Biochimica et Biophysica Acta (BBA) - Bioenergetics,* 1847**,** 993-1003.

Hoekema, A., Hirsch, P., Hooykaas, P. & Schilperoort, R. 1983. A binary plant vector strategy based on separation of *vir*-and T-region of the *Agrobacterium tumefaciens* Ti-plasmid.

Houston, K., Tucker, M. R., Chowdhury, J., Shirley, N. & Little, A. 2016. The Plant Cell Wall: A Complex and Dynamic Structure As Revealed by the Responses of Genes under Stress Conditions. *Frontiers in Plant Science,* 7.

Hu, C.-D., Chinenov, Y. & Kerppola, T. K. 2002. Visualization of Interactions among bZIP and Rel Family Proteins in Living Cells Using Bimolecular Fluorescence Complementation. *Molecular Cell,* 9**,** 789-798.

Hu, R., Zhu, Y., Wei, J., Chen, J., Shi, H., Shen, G. & Zhang, H. 2017. Overexpression of PP2A-C5 that encodes the catalytic subunit 5 of protein phosphatase 2A in Arabidopsis confers better root and shoot development under salt conditions. *Plant, Cell & Environment,* 40**,** 150-164.

Huang, C. & Chang, A. 2011. pH-dependent cargo sorting from the Golgi. *The Journal of biological chemistry,* 286**,** 10058-10065.

Huang, J., Taylor, J. P., Chen, J.-G., Uhrig, J. F., Schnell, D. J., Nakagawa, T., Korth, K. L. & Jones, A. M. 2006. The Plastid Protein THYLAKOID FORMATION1 and the Plasma Membrane G-Protein GPA1 Interact in a Novel Sugar-Signaling Mechanism in Arabidopsis. *The Plant Cell,* 18**,** 1226-1238.

Huang, X., Qian, Q., Liu, Z., Sun, H., He, S., Luo, D., Xia, G., Chu, C., Li, J. & Fu, X. 2009. Natural variation at the DEP1 locus enhances grain yield in rice. *Nat Genet,* 41**,** 494-497.

Hwang, I. & Sheen, J. 2001. Two-component circuitry in Arabidopsis cytokinin signal transduction. *Nature,* 413**,** 383.

Ichimura, K., Mizoguchi, T., Yoshida, R., Yuasa, T. & Shinozaki, K. 2000. Various abiotic stresses rapidly activate Arabidopsis MAP kinases ATMPK4 and ATMPK6. *The Plant Journal,* 24**,** 655-665.

Illergård, K., Kauko, A. & Elofsson, A. 2011. Why are polar residues within the membrane core evolutionary conserved? *Proteins: Structure, Function, and Bioinformatics,* 79**,** 79-91.

Ivakov, A., Flis, A., Apelt, F., Fünfgeld, M., Scherer, U., Stitt, M., Kragler, F., Vissenberg, K., Persson, S. & Suslov, D. 2017. Cellulose Synthesis and Cell Expansion Are Regulated by Different Mechanisms in Growing Arabidopsis Hypocotyls. *The Plant Cell,* 29**,** 1305-1315.

Ivakov, A. & Persson, S. 2013. Plant cell shape: modulators and measurements. *Frontiers in plant science,* 4**,** 439-439.

Izawa, Y., Takayanagi, Y., Inaba, N., Abe, Y., Minami, M., Fujisawa, Y., Kato, H., Ohki, S., Kitano, H. & Iwasaki, Y. 2010. Function and Expression Pattern of the α Subunit of the Heterotrimeric G Protein in Rice. *Plant and Cell Physiology,* 51**,** 271-281.

Jaffé, F. W., Freschet, G.-E. C., Valdes, B. M., Runions, J., Terry, M. J. & Williams, L. E. 2012. G protein–coupled receptor-type G proteins are required for light-dependent seedling growth and fertility in *Arabidopsis*. *The Plant Cell Online,* 24**,** 3649-3668.

Jangam, A. P., Pathak, R. R. & Raghuram, N. 2016. Microarray analysis of rice *d1* (RGA1) mutant reveals the potential role of G-protein alpha subunit in regulating multiple abiotic stresses such as drought, salinity, heat, and cold. *Frontiers in Plant Science,* 7.

Javadpour, M. M., Eilers, M., Groesbeek, M. & Smith, S. O. 1999. Helix packing in polytopic membrane proteins: role of glycine in transmembrane helix association. *Biophysical journal,* 77**,** 1609-1618.

Jentsch, T. J. 2008. CLC Chloride Channels and Transporters: From Genes to Protein Structure, Pathology and Physiology. *Critical Reviews in Biochemistry and Molecular Biology,* 43**,** 3-36.

Jentsch, T. J. 2016. VRACs and other ion channels and transporters in the regulation of cell volume and beyond. *Nature Reviews Molecular Cell Biology,* 17**,** 293-307.

Jentsch, T. J. & Günther, W. 1997. Chloride channels: An emerging molecular picture. *BioEssays,* 19**,** 117-126.

Jeon, J.-S., Lee, S., Jung, K.-H., Jun, S.-H., Jeong, D.-H., Lee, J., Kim, C., Jang, S., Lee, S., Yang, K., Nam, J., An, K., Han, M.-J., Sung, R.-J., Choi, H.-S., Yu, J.-H., Choi, J.-H., Cho, S.-Y., Cha, S.-S., Kim, S.-I. & An, G. 2000. T-DNA insertional mutagenesis for functional genomics in rice. *The Plant Journal,* 22**,** 561-570.

Jeong, D.-H., An, S., Park, S., Kang, H.-G., Park, G.-G., Kim, S.-R., Sim, J., Kim, Y.-O., Kim, M.-K., Kim, S.-R., Kim, J., Shin, M., Jung, M. & An, G. 2006. Generation of a flanking sequence-tag database for activation-tagging lines in japonica rice. *The Plant Journal,* 45**,** 123-132.

Jha, S. K., Sharma, M. & Pandey, G. K. 2016. Role of Cyclic Nucleotide Gated Channels in Stress Management in Plants. *Current Genomics,* 17**,** 315-329.

Johnsson, N. & Varshavsky, A. 1994. Split ubiquitin as a sensor of protein interactions in vivo. *Proceedings of the National Academy of Sciences,* 91**,** 10340-10344.

Johnston, C. A., Taylor, J. P., Gao, Y., Kimple, A. J., Grigston, J. C., Chen, J. G., Siderovski, D. P., Jones, A. M. & Willard, F. S. 2007. GTPase acceleration as the rate-limiting step in Arabidopsis G protein-coupled sugar signaling. *Proc Natl Acad Sci U S A,* 104**,** 17317-22.

Jones, J. C., Duffy, J. W., Machius, M., Temple, B. R. S., Dohlman, H. G. & Jones, A. M. 2011. The Crystal Structure of a Self-Activating G Protein α Subunit Reveals Its Distinct Mechanism of Signal Initiation. *Science signaling,* 4**,** ra8-ra8.

Jung, K.-H., Hur, J., Ryu, C.-H., Choi, Y., Chung, Y.-Y., Miyao, A., Hirochika, H. & An, G. 2003. Characterization of a Rice Chlorophyll-Deficient Mutant Using the T-DNA Gene-Trap System. *Plant and Cell Physiology,* 44**,** 463-472.

Kalmbach, R., Chizhov, I., Schumacher, M. C., Friedrich, T., Bamberg, E. & Engelhard, M. 2007. Functional Cell-free Synthesis of a Seven Helix Membrane Protein: In situ Insertion of Bacteriorhodopsin into Liposomes. *Journal of Molecular Biology,* 371**,** 639-648.

Kanaoka, M. M. & Higashiyama, T. 2015. Peptide signaling in pollen tube guidance. *Current Opinion in Plant Biology,* 28**,** 127-136.

Karimi, M., Inzé, D. & Depicker, A. 2002. GATEWAY™ vectors for *Agrobacterium*-mediated plant transformation. *Trends in plant science,* 7**,** 193-195.

Kato, C., Mizutani, T., Tamaki, H., Kumagai, H., Kamiya, T., Hirobe, A., Fujisawa, Y., Kato, H. & Iwasaki, Y. 2004. Characterisation of heterotrimeric G protein complexs in rice plasma membrane. *Plant J,* 38.

Kawahara, Y., De La Bastide, M., Hamilton, J. P., Kanamori, H., Mccombie, W. R., Ouyang, S., Schwartz, D. C., Tanaka, T., Wu, J., Zhou, S., Childs, K. L., Davidson, R. M., Lin, H., Quesada-Ocampo, L., Vaillancourt, B., Sakai, H., Lee, S. S., Kim, J., Numa, H., Itoh, T., Buell, C. R. & Matsumoto, T. 2013. Improvement of the Oryza sativa Nipponbare reference genome using next generation sequence and optical map data. *Rice,* 6**,** 4.

Kawakami, K., Umena, Y., Kamiya, N. & Shen, J.-R. 2009. Location of chloride and its possible functions in oxygen-evolving photosystem II revealed by X-ray crystallography. *Proceedings of the National Academy of Sciences,* 106**,** 8567-8572.

Keuskamp, D. H., Pollmann, S., Voesenek, L. a. C. J., Peeters, A. J. M. & Pierik, R. 2010. Auxin transport through PIN-FORMED 3 (PIN3) controls shade avoidance and fitness during competition. *Proceedings of the National Academy of Sciences,* 107**,** 22740-22744.

Kim, S.-J. & Brandizzi, F. 2016. The plant secretory pathway for the trafficking of cell wall polysaccharides and glycoproteins. *Glycobiology,* 26**,** 940-949.

Kimura, K., Okumura, M. & Yamasaki, S.-I. 2004. Effects of chloride and sulfate application on root growth of rice. *Soil Science and Plant Nutrition,* 50**,** 395-402.

Kiselyov, K., Chen, J., Rbaibi, Y., Oberdick, D., Tjon-Kon-Sang, S., Shcheynikov, N., Muallem, S. & Soyombo, A. 2005. TRP-ML1 Is a Lysosomal Monovalent Cation Channel That Undergoes Proteolytic Cleavage. *Journal of Biological Chemistry,* 280**,** 43218-43223.

Kling, R. C., Lanig, H., Clark, T. & Gmeiner, P. 2013. Active-state models of ternary GPCR complexes: determinants of selective receptor-G-protein coupling. *PLoS One,* 8**,** e67244.

Klopffleisch, K., Phan, N., Augustin, K., Bayne, R. S., Booker, K. S., Botella, J. R., Carpita, N. C., Carr, T., Chen, J. G., Cooke, T. R., Frick-Cheng, A., Friedman, E. J., Fulk, B., Hahn, M. G., Jiang, K., Jorda, L., Kruppe, L., Liu, C., Lorek, J., Mccann, M. C., Molina, A., Moriyama, E. N., Mukhtar, M. S., Mudgil, Y., Pattathil, S., Schwarz, J., Seta, S., Tan, M., Temp, U., Trusov, Y., Urano, D., Welter, B., Yang, J., Panstruga, R., Uhrig, J. F. & Jones, A. M. 2011. Arabidopsis G-protein interactome reveals connections to cell wall carbohydrates and morphogenesis. *Mol Syst Biol,* 7**,** 532.

Kluge, C., Seidel, T., Bolte, S., Sharma, S. S., Hanitzsch, M., Satiat-Jeunemaitre, B., Roß, J., Sauer, M., Golldack, D. & Dietz, K.-J. 2004. Subcellular distribution of the V-ATPase complex in plant cells, and in vivo localisation of the 100 kDa subunit VHA-a within the complex. *BMC Cell Biology,* 5**,** 29.

Knight, H. & Knight, M. R. 2001. Abiotic stress signalling pathways: specificity and cross-talk. *Trends in Plant Science,* 6**,** 262-267.

Köhler, B. & Raschke, K. 2000. The Delivery of Salts to the Xylem. Three Types of Anion Conductance in the Plasmalemma of the Xylem Parenchyma of Roots of Barley. *Plant Physiology,* 122**,** 243-254.

Komatsu, S., Konishi, H. & Hashimoto, M. 2007. The proteomics of plant cell membranes. *J Exp Bot,* 58**,** 103-12.

Kong, X.-Q., Gao, X.-H., Sun, W., An, J., Zhao, Y.-X. & Zhang, H. 2011. Cloning and functional characterization of a cation–chloride cotransporter gene OsCCC1. *Plant Molecular Biology,* 75**,** 567-578.

Kornreich, B. G. 2007. The patch clamp technique: Principles and technical considerations. *Journal of Veterinary Cardiology,* 9**,** 25-37.

Krebs, M., Beyhl, D., Görlich, E., Al-Rasheid, K. a. S., Marten, I., Stierhof, Y.-D., Hedrich, R. & Schumacher, K. 2010. Arabidopsis V-ATPase activity at the tonoplast is required for efficient nutrient storage but not for sodium accumulation. *Proceedings of the National Academy of Sciences,* 107**,** 3251-3256.

Krogh, A., Larsson, B., Von Heijne, G. & Sonnhammer, E. L. 2001. Predicting transmembrane protein topology with a hidden Markov model: application to complete genomes. *Journal of molecular biology,* 305**,** 567-580.

Krouk, G. 2016. Hormones and nitrate: a two-way connection. *Plant Molecular Biology,* 91**,** 599-606.

Krysan, P. J., Young, J. C. & Sussman, M. R. 1999. T-DNA as an insertional mutagen in *Arabidopsis*. *The Plant Cell,* 11**,** 2283-2290.

Krysan, P. J., Young, J. C., Tax, F. & Sussman, M. R. 1996. Identification of transferred DNA insertions within Arabidopsis genes involved in signal transduction and ion transport. *Proceedings of the National Academy of Sciences,* 93**,** 8145-8150.

Kudla, J., Batistič, O. & Hashimoto, K. 2010. Calcium Signals: The Lead Currency of Plant Information Processing. *The Plant Cell,* 22**,** 541-563.

Kudla, J. & Bock, R. 2016. Lighting the Way to Protein-Protein Interactions: Recommendations on Best Practices for Bimolecular Fluorescence Complementation Analyses. *The Plant Cell,* 28**,** 1002-1008.

Kuo, S. Y., Chien, L. F., Van, R. C., Yan, K. H., Liu, P. F., Chang, W. C., Wang, J. K. & Pan, R. L. 2005. Purification and subunit determination of H^+-pyrophosphatase from endoplasmic reticulum-enriched vesicles of mung bean seedlings. *Plant Science,* 169**,** 847-853.

Kuruma, A. & Hartzell, H. C. 2000. Bimodal control of a Ca^{2+}-activated Cl^- channel by different Ca^{2+} signals. *The Journal of general physiology,* 115**,** 59-80.

Lan, W.-Z., Wang, W., Wang, S.-M., Li, L.-G., Buchanan, B. B., Lin, H.-X., Gao, J.-P. & Luan, S. 2010. A rice high-affinity potassium transporter (HKT) conceals a calcium-permeable cation channel. *Proceedings of the National Academy of Sciences of the United States of America,* 107**,** 7089-7094.

Lang, F., Foller, M., Lang, K. S., Lang, P. A., Ritter, M., Gulbins, E., Vereninov, A. & Huber, S. M. 2005. Ion channels in cell proliferation and apoptotic cell death. *Journal of Membrane Biology,* 205**,** 147-157.

Lazniewska, J. & Weiss, N. 2017. Glycosylation of voltage-gated calcium channels in health and disease. *Biochimica et Biophysica Acta (BBA) - Biomembranes,* 1859**,** 662-668.

Lease, K. A., Wen, J., Li, J., Doke, J. T., Liscum, E. & Walker, J. C. 2001. A Mutant Arabidopsis Heterotrimeric G-Protein β Subunit Affects Leaf, Flower, and Fruit Development. *The Plant Cell,* 13**,** 2631-2641.

Lecourieux, D., Lamotte, O., Bourque, S., Wendehenne, D., Mazars, C., Ranjeva, R. & Pugin, A. 2005. Proteinaceous and oligosaccharidic elicitors induce different calcium signatures in the nucleus of tobacco cells. *Cell Calcium,* 38**,** 527-538.

Lee, H. K., Cho, S. K., Son, O., Xu, Z., Hwang, I. & Kim, W. T. 2009. Drought Stress-Induced Rma1H1, a RING Membrane-Anchor E3 Ubiquitin Ligase Homolog, Regulates Aquaporin Levels via Ubiquitination in Transgenic Arabidopsis Plants. *The Plant Cell,* 21**,** 622-641.

Li, B., Byrt, C., Qiu, J., Baumann, U., Hrmova, M., Evrard, A., Johnson, A. a. T., Birnbaum, K. D., Mayo, G. M., Jha, D., Henderson, S. W., Tester, M., Gilliham, M. & Roy, S. J. 2016. Identification of a Stelar-Localized Transport Protein That Facilitates Root-to-Shoot Transfer of Chloride in Arabidopsis. *Plant Physiology,* 170**,** 1014-1029.

Li, J., Nagpal, P., Vitart, V., Mcmorris, T. C. & Chory, J. 1996. A role for brassinosteroids in light-dependent development of Arabidopsis. *Science,* 272**,** 398-401.

Li, J., Yang, H., Ann Peer, W., Richter, G., Blakeslee, J., Bandyopadhyay, A., Titapiwantakun, B., Undurraga, S., Khodakovskaya, M., Richards, E. L., Krizek, B., Murphy, A. S., Gilroy, S. & Gaxiola, R. 2005. Arabidopsis H^+-PPase AVP1 Regulates Auxin-Mediated Organ Development. *Science,* 310**,** 121-125.

Li, J. F., Zhang, D. & Sheen, J. 2014a. Cas9-based genome editing in Arabidopsis and tobacco. *Methods Enzymol,* 546**,** 459-72.

Li, K., Gao, Z., He, H., Terzaghi, W., Fan, L.-M., Deng, Xing w. & Chen, H. 2015. Arabidopsis DET1 Represses Photomorphogenesis in Part by Negatively Regulating DELLA Protein Abundance in Darkness. *Molecular Plant,* 8**,** 622-630.

Li, L., Li, M., Yu, L., Zhou, Z., Liang, X., Liu, Z., Cai, G., Gao, L., Zhang, X., Wang, Y., Chen, S. & Zhou, J.-M. 2014b. The FLS2-Associated Kinase BIK1 Directly Phosphorylates the NADPH Oxidase RbohD to Control Plant Immunity. *Cell Host & Microbe,* 15**,** 329-338.

Li, S., Liu, Y., Zheng, L., Chen, L., Li, N., Corke, F., Lu, Y., Fu, X., Zhu, Z., Bevan, M. W. & Li, Y. 2012. The plant-specific G protein gamma subunit AGG3 influences organ size and shape in Arabidopsis thaliana. *New Phytol,* 194**,** 690-703.

Li, Y.-B., Rogers, S. W., Tse, Y. C., Lo, S. W., Sun, S. S. M., Jauh, G.-Y. & Jiang, L. 2002. BP-80 and homologs are concentrated on post-Golgi, probable lytic prevacuolar compartments. *Plant and Cell Physiology,* 43**,** 726-742.

Liang, F., Cunningham, K. W., Harper, J. F. & Sze, H. 1997. ECA1 complements yeast mutants defective in Ca^{2+} pumps and encodes an endoplasmic reticulum-type Ca^{2+}-ATPase in *Arabidopsis thaliana*. *Proceedings of the National Academy of Sciences,* 94**,** 8579-8584.

Lichtenthaler, H. K. 1998. The Stress Concept in Plants: An Introduction. *Annals of the New York Academy of Sciences,* 851**,** 187-198.

Liu, J., Ding, P., Sun, T., Nitta, Y., Dong, O., Huang, X., Yang, W., Li, X., Botella, J. R. & Zhang, Y. 2013. Heterotrimeric G proteins serve as a converging point in plant defense signaling activated by multiple receptor-like kinases. *Plant Physiol,* 161**,** 2146-58.

Liu, W., Wu, C., Fu, Y., Hu, G., Si, H., Zhu, L., Luan, W., He, Z. & Sun, Z. 2009. Identification and characterization of HTD2: a novel gene negatively regulating tiller bud outgrowth in rice. *Planta,* 230**,** 649-658.

Liu, Y., Yu, L., Qu, Y., Chen, J., Liu, X., Hong, H., Liu, Z., Chang, R., Gilliham, M., Qiu, L. & Guan, R. 2016. GmSALT3, Which Confers Improved Soybean Salt Tolerance in the Field, Increases Leaf Cl- Exclusion Prior to Na+ Exclusion But Does Not Improve Early Vigor under Salinity. *Frontiers in Plant Science,* 7.

Llopis, J., Mccaffery, J. M., Miyawaki, A., Farquhar, M. G. & Tsien, R. Y. 1998. Measurement of cytosolic, mitochondrial, and Golgi pH in single living cells with green fluorescent

proteins. *Proceedings of the National Academy of Sciences of the United States of America,* 95**,** 6803-6808.

Londo, J. P., Chiang, Y.-C., Hung, K.-H., Chiang, T.-Y. & Schaal, B. A. 2006. Phylogeography of Asian wild rice, Oryza rufipogon, reveals multiple independent domestications of cultivated rice, Oryza sativa. *Proceedings of the National Academy of Sciences,* 103**,** 9578-9583.

Lu, J. & Boron, W. F. 2007. Reversible and irreversible interactions of DIDS with the human electrogenic Na/HCO3 cotransporter NBCe1-A: role of lysines in the KKMIK motif of TM5. *American Journal of Physiology-Cell Physiology,* 292**,** C1787-C1798.

Lu, Y., Chanroj, S., Zulkifli, L., Johnson, M. A., Uozumi, N., Cheung, A. & Sze, H. 2011. Pollen tubes lacking a pair of K^+ transporters fail to target ovules in *Arabidopsis*. *The Plant Cell Online,* 23**,** 81-93.

Lurin, C., Geelen, D., Barbier-Brygoo, H., Guern, J. & Maurel, C. 1996. Cloning and functional expression of a plant voltage-dependent chloride channel. *The Plant cell,* 8**,** 701-711.

Lv, Y., Guo, Z., Li, X., Ye, H., Li, X. & Xiong, L. 2016. New insights into the genetic basis of natural chilling and cold shock tolerance in rice by genome-wide association analysis. *Plant Cell Environ,* 39**,** 556-70.

Lyons, J. C., Ross, B. D. & Song, C. W. 1993. Enhancement of hyperthermia effect in vivo by amiloride and dids. *International Journal of Radiation Oncology*Biology*Physics,* 25**,** 95-103.

Ma, H., Yanofsky, M. F. & Meyerowitz, E. M. 1990. Molecular cloning and characterization of GPAI, a G protein α subunit gene from Arabidopsis thaliana. *Proc. Natl. Acad. Sci,* 87**,** 3821-3825.

Ma, Y., Dai, X., Xu, Y., Luo, W., Zheng, X., Zeng, D., Pan, Y., Lin, X., Liu, H., Zhang, D., Xiao, J., Guo, X., Xu, S., Niu, Y., Jin, J., Zhang, H., Xu, X., Li, L., Wang, W., Qian, Q., Ge, S. & Chong, K. 2015. COLD1 Confers Chilling Tolerance in Rice. *Cell*.

Ma, Y., Szostkiewicz, I., Korte, A., Moes, D., Yang, Y., Christmann, A. & Grill, E. 2009. Regulators of PP2C phosphatase activity function as abscisic acid sensors. *Science,* 324**,** 1064-1068.

Mackay, J. P., Sunde, M., Lowry, J. A., Crossley, M. & Matthews, J. M. 2007. Protein interactions: is seeing believing? *Trends in Biochemical Sciences,* 32**,** 530-531.

Maeda, Y., Ide, T., Koike, M., Uchiyama, Y. & Kinoshita, T. 2008. GPHR is a novel anion channel critical for acidification and functions of the Golgi apparatus. *Nat Cell Biol,* 10**,** 1135-1145.

Manishankar, P. & Kudla, J. 2015. Cold tolerance encoded in one SNP. *Cell,* 160**,** 1045-6.

Mao, J., Wang, L., Fan, A., Wang, J., Xu, B., Jacob, T. J. & Chen, L. 2007. Blockage of volume-activated chloride channels inhibits migration of nasopharyngeal carcinoma cells. *Cell Physiol Biochem,* 19**,** 249-58.

Maple, J. & Møller, S. G. 2007. Mutagenesis in Arabidopsis. *Circadian Rhythms.* Springer.

Marmagne, A., Vinauger-Douard, M., Monachello, D., De Longevialle, A. F., Charon, C., Allot, M., Rappaport, F., Wollman, F.-A., Barbier-Brygoo, H. & Ephritikhine, G. 2007. Two members of the Arabidopsis CLC (chloride channel) family, AtCLCe and AtCLCf, are associated with thylakoid and Golgi membranes, respectively. *Journal of experimental botany,* 58**,** 3385-3393.

Marschner, H. 1995. *Mineral Nutrition of Higher Plants,* London: Academic Press, ELsevier Ltd. .

Marshansky, V., Rubinstein, J. L. & Grüber, G. 2014. Eukaryotic V-ATPase: Novel structural findings and functional insights. *Biochimica et Biophysica Acta (BBA)-Bioenergetics,* 1837**,** 857-879.

Martinière, A., Bassil, E., Jublanc, E., Alcon, C., Reguera, M., Sentenac, H., Blumwald, E. & Paris, N. 2013a. *In vivo* intracellular pH measurements in tobacco and *Arabidopsis* reveal an unexpected pH gradient in the endomembrane system. *The Plant Cell*

Martinière, A., Desbrosses, G., Sentenac, H. & Paris, N. 2013b. Development and properties of genetically encoded pH sensors in plants. *Frontiers in Plant Science,* 4.

Marty, F. 1999. Plant Vacuoles. *The Plant Cell,* 11**,** 587-599.

Maruta, N., Trusov, Y., Brenya, E., Parekh, U. & Botella, J. R. 2015. Membrane-localized extra-large G proteins and Gbg of the heterotrimeric G proteins form functional complexes engaged in plant immunity in Arabidopsis. *Plant Physiol,* 167**,** 1004-16.

Masclaux-Daubresse, C., Daniel-Vedele, F., Dechorgnat, J., Chardon, F., Gaufichon, L. & Suzuki, A. 2010. Nitrogen uptake, assimilation and remobilization in plants: challenges for sustainable and productive agriculture. *Annals of Botany,* 105**,** 1141-1157.

Mason, M. G. & Botella, J. R. 2000. Completing the heterotrimer: Isolation and characterization of an Arabidopsis thaliana G protein γ-subunit cDNA. *Proc. Natl. Acad. Sci,* 97**,** 14784-14788.

Mason, M. G. & Botella, J. R. 2001. Isolation of a novel G-protein γ-subunit from Arabidopsis thaliana and its interaction with Gβ. *Biochimica et Biophysica Acta (BBA) - Gene Structure and Expression,* 1520**,** 147-153.

Matsushima, R., Hayashi, Y., Yamada, K., Shimada, T., Nishimura, M. & Hara-Nishimura, I. 2003a. The ER Body, a Novel Endoplasmic Reticulum-Derived Structure in Arabidopsis. *Plant and Cell Physiology,* 44**,** 661-666.

Matsushima, R., Kondo, M., Nishimura, M. & Hara-Nishimura, I. 2003b. A novel ER-derived compartment, the ER body, selectively accumulates a β-glucosidase with an ER-retention signal in Arabidopsis. *The Plant Journal,* 33**,** 493-502.

Matulef, K. & Maduke, M. 2005. Side-dependent inhibition of a prokaryotic ClC by DIDS. *Biophysical journal,* 89**,** 1721-1730.

Maxson, M. E. & Grinstein, S. 2014. The vacuolar-type H+ATPase at a glance – more than a proton pump. *Journal of Cell Science,* 127**,** 4987-4993.

Mcainsh, M. R. & Hetherington, A. M. 1998. Encoding specificity in Ca2+ signalling systems. *Trends in Plant Science,* 3**,** 32-36.

Mcfarlane, H. E., Döring, A. & Persson, S. 2014. The Cell Biology of Cellulose Synthesis. *Annual Review of Plant Biology,* 65**,** 69-94.

Mcfarlane, H. E., Lee, E. K., Van Bezouwen, L. S., Ross, B., Rosado, A. & Samuels, A. L. 2017. Multiscale Structural Analysis of Plant ER–PM Contact Sites. *Plant and Cell Physiology,* 58**,** 478-484.

Mcgavin, W. J., Mitchell, C., Cock, P. J. A., Wright, K. M. & Macfarlane, S. A. 2012. Raspberry leaf blotch virus, a putative new member of the genus Emaravirus, encodes a novel genomic RNA. *Journal of General Virology,* 93**,** 430-437.

Mckay, M. J., Afrose, F., Koeppe Ii, R. E. & Greathouse, D. V. 2018. Helix formation and stability in membranes. *Biochimica et Biophysica Acta (BBA) - Biomembranes*.

Michard, E., Simon, A. A., Tavares, B., Wudick, M. M. & Feijó, J. A. 2017. Signaling with Ions: The Keystone for Apical Cell Growth and Morphogenesis in Pollen Tubes. *Plant Physiology,* 173**,** 91-111.

Michielse, C. B., Hooykaas, P. J., Van Den Hondel, C. A. & Ram, A. F. 2008. *Agrobacterium*-mediated transformation of the filamentous fungus *Aspergillus awamori*. *Nature protocols,* 3**,** 1671-1678.

Miesenböck, G., De Angelis, D. A. & Rothman, J. E. 1998. Visualizing secretion and synaptic transmission with pH-sensitive green fluorescent proteins. *Nature,* 394**,** 192.

Miller, A. J., Fan, X., Orsel, M., Smith, S. J. & Wells, D. M. 2007. Nitrate transport and signalling. *Journal of Experimental Botany,* 58**,** 2297-2306.

Minor, D. L. 2010. An Overview of Ion Channel Structure. *In:* BRADSHAW, R. A. & DENNIS, E. A. (eds.) *Handbook of Cell Signaling (Second Edition).* San Diego: Academic Press.

Mitsuda, N., Enami, K., Nakata, M., Takeyasu, K. & Sato, M. H. 2001. Novel type Arabidopsis thaliana H+-PPase is localized to the Golgi apparatus. *FEBS Letters,* 488**,** 29-33.

Miura, K. & Furumoto, T. 2013. Cold Signaling and Cold Response in Plants. *International Journal of Molecular Sciences,* 14**,** 5312-5337.

Moroni, A., Gazzarrini, S., Cerana, R., Colombo, R., Sutter, J.-U., Difrancesco, D., Gradmann, D. & Thiel, G. 2000. Mutation in Pore Domain Uncovers Cation- and Voltage-Sensitive Recovery from Inactivation in KAT1 Channel. *Biophysical Journal,* 78**,** 1862-1871.

Müller, J. & Johnsson, N. 2008. Split-ubiquitin and the split-protein sensors: chessman for the endgame. *ChemBioChem,* 9**,** 2029-2038.

Nagano, A. J., Maekawa, A., Nakano, R. T., Miyahara, M., Higaki, T., Kutsuna, N., Hasezawa, S. & Hara-Nishimura, I. 2009. Quantitative Analysis of ER Body Morphology in an Arabidopsis Mutant. *Plant and Cell Physiology,* 50**,** 2015-2022.

Nakamura, N., Tanaka, S., Teko, Y., Mitsui, K. & Kanazawa, H. 2005. Four Na+/H+ Exchanger Isoforms Are Distributed to Golgi and Post-Golgi Compartments and Are Involved in Organelle pH Regulation. *Journal of Biological Chemistry,* 280**,** 1561-1572.

Nakano, R., Yamada, K., Bednarek, P., Nishimura, M. & Hara-Nishimura, I. 2014. ER bodies in plants of the Brassicales order: biogenesis and association with innate immunity. *Frontiers in Plant Science,* 5.

Nakazaki, A., Yamada, K., Kunieda, T., Sugiyama, R., Hirai, M. Y., Tamura, K., Hara-Nishimura, I. & Shimada, T. 2019. Leaf Endoplasmic Reticulum Bodies Identified in Arabidopsis Rosette Leaves Are Involved in Defense against Herbivory. *Plant Physiology,* 179**,** 1515-1524.

Nallamsetty, S. & Waugh, D. S. 2007. A generic protocol for the expression and purification of recombinant proteins in Escherichia coli using a combinatorial His6-maltose binding protein fusion tag. *Nature Protocols,* 2**,** 383-391.

Nebenführ, A., Gallagher, L. A., Dunahay, T. G., Frohlick, J. A., Mazurkiewicz, A. M., Meehl, J. B. & Staehelin, L. A. 1999. Stop-and-Go Movements of Plant Golgi Stacks Are Mediated by the Acto-Myosin System. *Plant Physiology,* 121**,** 1127-1141.

Nelson, B. K., Cai, X. & Nebenführ, A. 2007. A multicolored set of in vivo organelle markers for co-localization studies in Arabidopsis and other plants. *The Plant Journal,* 51**,** 1126-1136.

Ng, C. K. Y. & Mcainsh, M. R. 2003. Encoding specificity in plant calcium signalling: hot-spotting the ups and downs and waves. *Annals of botany,* 92**,** 477-485.

Nilius, B., Eggermont, J., Voets, T., Buyse, G., Manolopoulos, V. & Droogmans, G. 1997. Properties of volume-regulated anion channels in mammalian cells. *Progress in Biophysics and Molecular Biology,* 68**,** 69-119.

Noman, A., Kanwal, H., Khalid, N., Sanaullah, T., Tufail, A., Masood, A., Sabir, S.-U.-R., Aqeel, M. & He, S. 2017. Perspective research progress in cold responses of *Capsella bursa-pastoris*. *Frontiers in Plant Science,* 8.

Nomura, S.-I. M., Kondoh, S., Asayama, W., Asada, A., Nishikawa, S. & Akiyoshi, K. 2008. Direct preparation of giant proteo-liposomes by in vitro membrane protein synthesis. *Journal of Biotechnology,* 133**,** 190-195.

Nonogaki, H. 2014. Seed dormancy and germination—emerging mechanisms and new hypotheses. *Frontiers in Plant Science,* 5**,** 233.

Nordeen, M. H., Jones, S. M., Howell, K. E. & Caldwell, J. H. 2000. GOLAC: an endogenous anion channel of the Golgi complex. *Biophysical Journal,* 78**,** 2918-2928.

Numata, M. & Orlowski, J. 2001. Molecular Cloning and Characterization of a Novel (Na+,K+)/H+ Exchanger Localized to the trans-Golgi Network. *Journal of Biological Chemistry,* 276**,** 17387-17394.

Oda, K., Kamiya, T., Shikanai, Y., Shigenobu, S., Yamaguchi, K. & Fujiwara, T. 2016. The Arabidopsis Mg Transporter, MRS2-4, is Essential for Mg Homeostasis Under Both Low and High Mg Conditions. *Plant and Cell Physiology,* 57**,** 754-763.

Odell, J. T., Nagy, F. & Chua, N.-H. 1985. Identification of DNA sequences required for activity of the cauliflower mosaic virus 35S promoter.

Offermanns, S. 2003. G-proteins as transducers in transmembrane signalling. *Progress in Biophysics and Molecular Biology,* 83**,** 101-130.

Ohgaki, R., Van Ijzendoorn, S. C. D., Matsushita, M., Hoekstra, D. & Kanazawa, H. 2010. Organellar Na^+/H^+ exchangers: novel players in organelle pH regulation and their emerging functions. *Biochemistry,* 50**,** 443-450.

Okamoto, H., Gobel, C., Capper, R. G., Saunders, N., Feussner, I. & Knight, M. R. 2009. The alpha-subunit of the heterotrimeric G-protein affects jasmonate responses in Arabidopsis thaliana. *J Exp Bot,* 60**,** 1991-2003.

Omasits, U., Ahrens, C. H., Müller, S. & Wollscheid, B. 2013. Protter: interactive protein feature visualization and integration with experimental proteomic data. *Bioinformatics***,** btt607.

Ooi, A., Wong, A., Esau, L., Lemtiri-Chlieh, F. & Gehring, C. 2016. A Guide to Transient Expression of Membrane Proteins in HEK-293 Cells for Functional Characterization. *Frontiers in Physiology,* 7.

Ooms, G., Hooykaas, P. J., Van Veen, R. J., Van Beelen, P., Regensburg-Tuïnk, T. J. & Schilperoort, R. A. 1982. Octopine Ti-plasmid deletion mutants of *Agrobacterium tumefaciens* with emphasis on the right side of the T-region. *Plasmid,* 7**,** 15-29.

Ooms, G., Klapwijk, P., Poulis, J. & Schilperoort, R. 1980. Characterization of Tn904 insertions in octopine Ti plasmid mutants of *Agrobacterium tumefaciens*. *Journal of bacteriology,* 144**,** 82-91.

Ortega-Amaro, M. A., Rodríguez-Hernández, A. A., Rodríguez-Kessler, M., Hernández-Lucero, E., Rosales-Mendoza, S., Ibáñez-Salazar, A., Delgado-Sánchez, P. & Jiménez-Bremont, J. F. 2015. Overexpression of AtGRDP2, a novel glycine-rich domain protein, accelerates plant growth and improves stress tolerance. *Frontiers in Plant Science,* 5.

Osterbur-Badhey, M. L., Bertalovitz, A. C. & Mcdonald, T. V. 2017. Express with caution: Epitope tags and cDNA variants effects on hERG channel trafficking, half-life and function. *Journal of cardiovascular electrophysiology,* 28**,** 1070-1082.

Østergaard, L. & Yanofsky, M. F. 2004. Establishing gene function by mutagenesis in Arabidopsis thaliana. *The Plant Journal,* 39**,** 682-696.

Ouyang, S., Zhu, W., Hamilton, J., Lin, H., Campbell, M., Childs, K., Thibaud-Nissen, F., Malek, R. L., Lee, Y., Zheng, L., Orvis, J., Haas, B., Wortman, J. & Buell, C. R. 2007. The TIGR Rice Genome Annotation Resource: improvements and new features. *Nucleic Acids Research,* 35**,** D883-D887.

Overvoorde, P., Fukaki, H. & Beeckman, T. 2010. Auxin Control of Root Development. *Cold Spring Harbor Perspectives in Biology,* 2**,** a001537.

Padmanaban, S., Lin, X., Perera, I., Kawamura, Y. & Sze, H. 2004. Differential Expression of Vacuolar H+ATPase Subunit c Genes in Tissues Active in Membrane Trafficking and Their Roles in Plant Growth as Revealed by RNAi. *Plant Physiology,* 134**,** 1514-1526.

Pandey, S. 2019. Heterotrimeric G-Protein Signaling in Plants: Conserved and Novel Mechanisms. *Annual Review of Plant Biology,* 70**,** 213-238.

Pandey, S., Chen, J. G., Jones, A. M. & Assmann, S. M. 2006. G-protein complex mutants are hypersensitive to abscisic acid regulation of germination and postgermination development. *Plant Physiol,* 141**,** 243-56.

Pandey, S., Nelson, D. C. & Assmann, S. M. 2009. Two novel GPCR-type G proteins are abscisic acid receptors in *Arabidopsis*. *Cell,* 136**,** 136-148.

Pandey, S., Zhang, W. & Assmann, S. M. 2007. Roles of ion channels and transporters in guard cell signal transduction. *FEBS Letters,* 581**,** 2325-2336.

Paredez, A. R., Persson, S., Ehrhardt, D. W. & Somerville, C. R. 2008. Genetic evidence that cellulose synthase activity influences microtubule cortical array organization. *Plant Physiology,* 147**,** 1723-1734.

Paroutis, P., Touret, N. & Grinstein, S. 2004. The pH of the secretory pathway: measurement, determinants, and regulation. *Physiology,* 19**,** 207-215.

Pasantes-Morales, H. 2016. Channels and Volume Changes in the Life and Death of the Cell. *Molecular Pharmacology,* 90**,** 358-370.

Perico, C. & Sparkes, I. 2018. Plant organelle dynamics: cytoskeletal control and membrane contact sites. *New Phytologist,* 220**,** 381-394.

Phee, B.-K., Shin, D. H., Cho, J.-H., Kim, S.-H., Kim, J.-I., Lee, Y.-H., Jeon, J.-S., Bhoo, S. H. & Hahn, T.-R. 2006. Identification of phytochrome-interacting protein candidates in Arabidopsis thaliana by co-immunoprecipitation coupled with MALDI-TOF MS. *PROTEOMICS,* 6**,** 3671-3680.

Picollo, A. & Pusch, M. 2005. Chloride/proton antiporter activity of mammalian CLC proteins ClC-4 and ClC-5. *Nature,* 436**,** 420-423.

Piñeros, M. A., Cançado, G. M. A., Maron, L. G., Lyi, S. M., Menossi, M. & Kochian, L. V. 2008. Not all ALMT1-type transporters mediate aluminum-activated organic acid responses: the case of ZmALMT1 – an anion-selective transporter. *The Plant Journal,* 53**,** 352-367.

Pittman, J. 2012. Multiple Transport Pathways for Mediating Intracellular pH Homeostasis: The Contribution of H+/ion Exchangers. *Frontiers in Plant Science,* 3.

Planes, M. D., Niñoles, R., Rubio, L., Bissoli, G., Bueso, E., García-Sánchez, M. J., Alejandro, S., Gonzalez-Guzmán, M., Hedrich, R., Rodriguez, P. L., Fernández, J. A. & Serrano, R. 2015. A mechanism of growth inhibition by abscisic acid in germinating seeds of Arabidopsis thaliana based on inhibition of plasma membrane H+-ATPase and decreased cytosolic pH, K+, and anions. *Journal of experimental botany,* 66**,** 813-825.

Polko, J. K. & Kieber, J. J. 2019. The regulation of cellulose biosynthesis in plants. *The Plant Cell,* 31**,** 282-296.

Pollok, B. A. & Heim, R. 1999. Using GFP in FRET-based applications. *Trends in Cell Biology,* 9**,** 57-60.

Poroca, D. R., Pelis, R. M. & Chappe, V. M. 2017. ClC Channels and Transporters: Structure, Physiological Functions, and Implications in Human Chloride Channelopathies. *Frontiers in pharmacology,* 8**,** 151-151.

Pysh, L., Alexander, N., Swatzyna, L. & Harbert, R. 2012. Four alleles of AtCESA3 form an allelic series with respect to root phenotype in *Arabidopsis thaliana*. *Physiologia Plantarum,* 144**,** 369-381.

Qin, X., Jin, X., Zhou, K., Li, H., Wang, Q., Li, W. & Wang, Q. 2019. EsGPCR89 regulates cerebral antimicrobial peptides through hemocytes in Eriocheir sinensis. *Fish & Shellfish Immunology,* 95**,** 151-162.

Raghavendra, A. S., Gonugunta, V. K., Christmann, A. & Grill, E. 2010. ABA perception and signalling. *Trends in Plant Science,* 15**,** 395-401.

Rahayu, Y. S., Walch-Liu, P., Neumann, G., Römheld, V., Von Wirén, N. & Bangerth, F. 2005. Root-derived cytokinins as long-distance signals for NO3−-induced stimulation of leaf growth. *Journal of Experimental Botany,* 56**,** 1143-1152.

Ratajczak, R., Hinz, G. & Robinson, D. G. 1999. Localization of pyrophosphatase in membranes of cauliflower inflorescence cells. *Planta,* 208**,** 205-211.

Remans, T., Nacry, P., Pervent, M., Filleur, S., Diatloff, E., Mounier, E., Tillard, P., Forde, B. G. & Gojon, A. 2006. The Arabidopsis NRT1.1 transporter participates in the signaling pathway triggering root colonization of nitrate-rich patches. *Proceedings of the National Academy of Sciences,* 103**,** 19206-19211.

Rentel, M. C. & Knight, M. R. 2004. Oxidative stress-induced calcium signaling in Arabidopsis. *Plant Physiology,* 135**,** 1471-1479.

Richard-Molard, C., Krapp, A., Brun, F., Ney, B., Daniel-Vedele, F. & Chaillou, S. 2008. Plant response to nitrate starvation is determined by N storage capacity matched by nitrate uptake capacity in two Arabidopsis genotypes. *Journal of Experimental Botany,* 59**,** 779-791.

Rivinoja, A., Kokkonen, N., Kellokumpu, I. & Kellokumpu, S. 2006. Elevated Golgi pH in breast and colorectal cancer cells correlates with the expression of oncofetal carbohydrate T antigen. *Journal of cellular physiology,* 208**,** 167-174.

Rivinoja, A., Pujol, F. M., Hassinen, A. & Kellokumpu, S. 2011. Golgi pH, its regulation and roles in human disease. *Annals of Medicine,* 0**,** 1-13.

Robinson, D. G., Haschke, H.-P., Hinz, G., Hoh, B., Maeshima, M. & Marty, F. 1996. Immunological detection of tonoplast polypeptides in the plasma membrane of pea cotyledons. *Planta,* 198**,** 95-103.

Roden, D. M. & Kupershmidt, S. 1999. From genes to channels: normal mechanisms. *Cardiovascular Research,* 42**,** 318-326.

Rodriguez, M. C. S., Petersen, M. & Mundy, J. 2010. Mitogen-activated protein kinase signaling in plants. *Annual review of plant biology,* 61**,** 621-649.

Rodriguez, R. E., Debernardi, J. M. & Palatnik, J. F. 2014. Morphogenesis of simple leaves: regulation of leaf size and shape. *Wiley Interdisciplinary Reviews: Developmental Biology,* 3**,** 41-57.

Roelfsema, M. R. G. & Hedrich, R. 2005. In the light of stomatal opening: new insights into 'the Watergate'. *New Phytologist,* 167**,** 665-691.

Roelfsema, M. R. G., Levchenko, V. & Hedrich, R. 2004. ABA depolarizes guard cells in intact plants, through a transient activation of R- and S-type anion channels. *Plant Journal,* 37**,** 578-588.

Rognes, S. E. 1980. Anion regulation of lupin asparagine synthetase: Chloride activation of the glutamine-utilizing reactions. *Phytochemistry,* 19**,** 2287-2293.

Rojas, F., Silvester, E., Young, J., Milne, R., Tettey, M., Houston, D. R., Walkinshaw, M. D., Pérez-Pi, I., Auer, M., Denton, H., Smith, T. K., Thompson, J. & Matthews, K. R. 2019. Oligopeptide Signaling through TbGPR89 Drives Trypanosome Quorum Sensing. *Cell,* 176**,** 306-317.e16.

Romeis, T., Ludwig, A. A., Martin, R. & Jones, J. D. G. 2001. Calcium-dependent protein kinases play an essential role in a plant defence response. *The EMBO Journal,* 20**,** 5556-5567.

Rosano, G. L. & Ceccarelli, E. A. 2014. Recombinant protein expression in Escherichia coli: advances and challenges. *Frontiers in Microbiology,* 5**,** 172.

Rosenbaum, D. M., Rasmussen, S. G. & Kobilka, B. K. 2009. The structure and function of G-protein-coupled receptors. *Nature,* 459**,** 356-363.

Rubio-Díaz, S., Pérez-Pérez, J. M., González-Bayón, R., Muñoz-Viana, R., Borrega, N., Mouille, G., Hernández-Romero, D., Robles, P., Höfte, H., Ponce, M. R. & Micol, J. L. 2012. Cell expansion-mediated organ growth is affected by mutations in three EXIGUA genes. *PLOS ONE,* 7**,** e36500.

Rubio, V., Bustos, R., Irigoyen, M. L., Cardona-López, X., Rojas-Triana, M. & Paz-Ares, J. 2008. Plant hormones and nutrient signaling. *Plant Molecular Biology,* 69**,** 361.

Ruiz Rosquete, M., Davis, D. J. & Drakakaki, G. 2017. The plant Trans-Golgi Network. Not just a matter of distinction. *Plant Physiology*.

Saichuk, J., Center, L. S. U. A., Service, L. C. E. & Station, L. a. E. 2009. *Louisiana Rice Production Handbook*, Louisiana State University Agricultural Center.

Saito, S. & Uozumi, N. 2019. Guard Cell Membrane Anion Transport Systems and Their Regulatory Components: An Elaborate Mechanism Controlling Stress-Induced Stomatal Closure. *Plants,* 8**,** 9.

Sakmann, B. & Neher, E. 1984. PATCH CLAMP TECHNIQUES FOR STUDYING IONIC CHANNELS IN EXCITABLE-MEMBRANES. *Annual Review of Physiology,* 46**,** 455-472.

Scheel, O., Zdebik, A. A., Lourdel, S. & Jentsch, T. J. 2005. Voltage-dependent electrogenic chloride/proton exchange by endosomal CLC proteins. *Nature,* 436**,** 424-427.

Schläppi, M. R., Jackson, A. K., Eizenga, G. C., Wang, A., Chu, C., Shi, Y., Shimoyama, N. & Boykin, D. L. 2017. Assessment of five chilling tolerance traits and GWAS mapping in rice using the USDA mini-core collection. *Frontiers in Plant Science,* 8.

Schoberer, J., Liebminger, E., Vavra, U., Veit, C., Grünwald-Gruber, C., Altmann, F., Botchway, S. W. & Strasser, R. 2019. The Golgi Localization of GnTI Requires a Polar Amino Acid Residue within Its Transmembrane Domain. *Plant Physiology,* 180**,** 859-873.

Schroeder, J. I. & Keller, B. U. 1992. Two types of anion channel currents in guard-cells with distinct voltage regulation. *Proceedings of the National Academy of Sciences of the United States of America,* 89**,** 5025-5029.

Schumacher, K. 2014. pH in the plant endomembrane system—an import and export business. *Current Opinion in Plant Biology,* 22**,** 71-76.

Schumacher, K., Vafeados, D., Mccarthy, M., Sze, H., Wilkins, T. & Chory, J. 1999. The Arabidopsis det3 mutant reveals a central role for the vacuolar H(+)-ATPase in plant growth and development. *Genes & development,* 13**,** 3259-3270.

Schwarz, D. S. & Blower, M. D. 2016. The endoplasmic reticulum: structure, function and response to cellular signaling. *Cellular and molecular life sciences : CMLS,* 73**,** 79-94.

Schwarz, G. & Mendel, R. R. 2006. Molybdenum cofactor biosynthesis and molybdenum enzymes. *Annual Review of Plant Biology,* 57**,** 623-647.

Seed, J. R. & Wenck, M. A. 2003. Role of the long slender to short stumpy transition in the life cycle of the african trypanosomes. *Kinetoplastid biology and disease,* 2**,** 3-3.

Serjeant, G. R. 1997. Sickle-cell disease. *The Lancet,* 350**,** 725-730.

Shakiba, E., Edwards, J. D., Jodari, F., Duke, S. E., Baldo, A. M., Korniliev, P., Mccouch, S. R. & Eizenga, G. C. 2017. Genetic architecture of cold tolerance in rice (Oryza sativa) determined through high resolution genome-wide analysis. *PLoS One,* 12**,** e0172133.

Shen, J., Zeng, Y., Zhuang, X., Sun, L., Yao, X., Pimpl, P. & Jiang, L. 2013. Organelle pH in the Arabidopsis Endomembrane System. *Molecular Plant,* 6**,** 1419-1437.

Shevell, D. E., Kunkel, T. & Chua, N.-H. 2000. Cell wall alterations in the Arabidopsis emb30 mutant. *The Plant Cell Online,* 12**,** 2047-2059.

Shirley, B. W., Hanley, S. & Goodman, H. M. 1992. Effects of ionizing radiation on a plant genome: analysis of two Arabidopsis transparent testa mutations. *The Plant Cell Online,* 4**,** 333-347.

Shlyonsky, V., Dupuis, F. & Gall, D. 2014. The OpenPicoAmp: an open-source planar lipid bilayer amplifier for hands-on learning of neuroscience. *PLOS ONE,* 9**,** e108097.

Shpak, E. D., Berthiaume, C. T., Hill, E. J. & Torii, K. U. 2004. Synergistic interaction of three ERECTA-family receptor-like kinases controls Arabidopsis organ growth and flower development by promoting cell proliferation. *Development,* 131**,** 1491-1501.

Sinclair, R., Rosquete, M. R. & Drakakaki, G. 2018. Post-Golgi Trafficking and Transport of Cell Wall Components. *Frontiers in Plant Science,* 9.

Sinha, A. K., Jaggi, M., Raghuram, B. & Tuteja, N. 2011. Mitogen-activated protein kinase signaling in plants under abiotic stress. *Plant Signaling & Behavior,* 6**,** 196-203.

Sitaraman, K. & Chatterjee, D. K. 2009. High-Throughput Protein Expression Using Cell-Free System. *In:* DOYLE, S. A. (ed.) *High Throughput Protein Expression and Purification: Methods and Protocols.* Totowa, NJ: Humana Press.

Sondergaard, T. E., Schulz, A. & Palmgren, M. G. 2004. Energization of Transport Processes in Plants. Roles of the Plasma Membrane H⁺-ATPase. *Plant Physiology,* 136**,** 2475-2482.

Song, J., Li, J., Sun, J., Hu, T., Wu, A., Liu, S., Wang, W., Ma, D. & Zhao, M. 2018. Genome-Wide Association Mapping for Cold Tolerance in a Core Collection of Rice (Oryza sativa L.) Landraces by Using High-Density Single Nucleotide Polymorphism Markers From Specific-Locus Amplified Fragment Sequencing. *Frontiers in Plant Science,* 9.

Sonnhammer, E. L., Von Heijne, G. & Krogh, A. A hidden Markov model for predicting transmembrane helices in protein sequences. Ismb, 1998. 175-182.

Sottosanto, J. B., Gelli, A. & Blumwald, E. 2004. DNA array analyses of Arabidopsis thaliana lacking a vacuolar Na+/H+ antiporter: impact of AtNHX1 on gene expression. *The Plant Journal,* 40**,** 752-771.

Sparkes, I., Runions, J., Hawes, C. & Griffing, L. 2009a. Movement and Remodeling of the Endoplasmic Reticulum in Nondividing Cells of Tobacco Leaves. *The Plant Cell,* 21**,** 3937-3949.

Sparkes, I. A., Ketelaar, T., De Ruijter, N. C. A. & Hawes, C. 2009b. Grab a Golgi: Laser Trapping of Golgi Bodies Reveals in vivo Interactions with the Endoplasmic Reticulum. *Traffic,* 10**,** 567-571.

Sparkes, I. A., Runions, J., Kearns, A. & Hawes, C. 2006. Rapid, transient expression of fluorescent fusion proteins in tobacco plants and generation of stably transformed plants. *Nature Protocols,* 1**,** 2019-2025.

Stateczny, D., Oppenheimer, J. & Bommert, P. 2016. G protein signaling in plants: minus times minus equals plus. *Curr Opin Plant Biol,* 34**,** 127-135.

Staudt, C., Gilis, F., Tevel, V., Jadot, M. & Boonen, M. 2016. A conserved glycine residue in the C-terminal region of human ATG9A is required for its transport from the endoplasmic reticulum to the Golgi apparatus. *Biochemical and Biophysical Research Communications,* 479**,** 404-409.

Stefano, G. & Brandizzi, F. 2018. Advances in Plant ER Architecture and Dynamics. *Plant Physiology,* 176**,** 178-186.

Suharsono, U., Fujisawa, Y., Kawasaki, T., Iwasaki, Y., Satoh, H. & Shimamoto, K. 2002. The heterotrimeric G protein alpha subunit acts upstream of the small GTPase Rac in disease resistance of rice. *Proc Natl Acad Sci U S A,* 99**,** 13307-12.

Sun, H., Shen, L., Qin, Y., Liu, X., Hao, K., Li, Y., Wang, J., Yang, J. & Wang, F. 2018. CLC-Nt1 affects potato virus Y infection via regulation of endoplasmic reticulum luminal pH. *New Phytol,* 220**,** 539-552.

Swarbreck, S. M., Colaço, R. & Davies, J. M. 2013. Plant Calcium-Permeable Channels. *Plant Physiology,* 163**,** 514-522.

Sze, H. & Chanroj, S. 2018. Plant Endomembrane Dynamics: Studies of K+/H+Antiporters Provide Insights on the Effects of pH and Ion Homeostasis. *Plant Physiology,* 177**,** 875-895.

Sze, H., Li, X. & Palmgren, M. G. 1999. Energization of plant cell membranes by H^+-pumping ATPases: regulation and biosynthesis. *The Plant Cell,* 11**,** 677-689.

Taddese, B., Upton, G. J., Bailey, G. R., Jordan, S. R., Abdulla, N. Y., Reeves, P. J. & Reynolds, C. A. 2014. Do plants contain g protein-coupled receptors? *Plant Physiol,* 164**,** 287-307.

Takahashi, N., Wang, X., Tanabe, S., Uramoto, H., Jishage, K., Uchida, S., Sasaki, S. & Okada, Y. 2005. ClC-3-independent Sensitivity of Apoptosis to Cl- Channel Blockers in Mouse Cardiomyocytes. *Cellular Physiology and Biochemistry,* 15**,** 263-270.

Takai, K., Sawasaki, T. & Endo, Y. 2010. Practical cell-free protein synthesis system using purified wheat embryos. *Nature Protocols,* 5**,** 227-238.

Tanaka, T., Antonio, B. A., Kikuchi, S., Matsumoto, T., Nagamura, Y., Numa, H., Sakai, H., Wu, J., Itoh, T., Sasaki, T., Aono, R., Fujii, Y., Habara, T., Harada, E., Kanno, M., Kawahara, Y., Kawashima, H., Kubooka, H., Matsuya, A., Nakaoka, H., Saichi, N., Sanbonmatsu, R., Sato, Y., Shinso, Y., Suzuki, M., Takeda, J.-I., Tanino, M., Todokoro, F., Yamaguchi, K. & Yamamoto, N. 2008. The Rice Annotation Project Database (RAP-DB): 2008 update. *Nucleic Acids Res,* 36.

Tarutani, M., Nakajima, K., Uchida, Y., Takaishi, M., Goto-Inoue, N., Ikawa, M., Setou, M., Kinoshita, T., Elias, P. M., Sano, S. & Maeda, Y. 2012. GPHR-dependent functions of the Golgi apparatus are essential for the formation of lamellar granules and the skin barrier. *Journal of Investigative Dermatology,* 132**,** 2019-2025.

Tavares, B., Domingos, P., Dias, P. N., Feijó, J. A. & Bicho, A. 2011. The essential role of anionic transport in plant cells: the pollen tube as a case study. *Journal of Experimental Botany,* 62**,** 2273-2298.

Taylor, C. W., Prole, D. L. & Rahman, T. 2009. Ca(2+) channels on the move. *Biochemistry,* 48**,** 12062-12080.

Teakle, N. L. & Tyerman, S. D. 2010. Mechanisms of Cl- transport contributing to salt tolerance. *Plant, Cell & Environment,* 33**,** 566-589.

Teardo, E., Carraretto, L., Wagner, S., Formentin, E., Behera, S., De Bortoli, S., Larosa, V., Fuchs, P., Lo Schiavo, F., Raffaello, A., Rizzuto, R., Costa, A., Schwarzländer, M. & Szabò, I. 2017. Physiological Characterization of a Plant Mitochondrial Calcium Uniporter in Vitro and in Vivo. *Plant Physiology,* 173**,** 1355-1370.

Thompson, R. J., Nordeen, M. H., Howell, K. E. & Caldwell, J. H. 2002. A large-conductance anion channel of the Golgi complex. *Biophysical Journal,* 83**,** 278-289.

Thung, L., Trusov, Y., Chakravorty, D. & Botella, J. R. 2012. Gγ1+Gγ2+Gγ3=Gβ: the search for heterotrimeric G-protein γ subunits in arabidopsis is over. *J Plant Physiology,* 169.

Toei, M., Saum, R. & Forgac, M. 2010. Regulation and isoform function of the V-ATPases. *Biochemistry,* 49**,** 4715-4723.

Tomashek, J. J. & Brusilow, W. S. A. 2000. Stoichiometry of Energy Coupling by Proton-Translocating ATPases: A History of Variability. *Journal of Bioenergetics and Biomembranes,* 32**,** 493-500.

Toru, E., Takashi, S., Masamitsu, S., Masaaki, I., Eiji, A., Toshihiko, U., Osamu, N. & Susumu, T. 2010. Development of an Insect Cell-Free System. *Current Pharmaceutical Biotechnology,* 11**,** 279-284.

Tracy, F. E., Gilliham, M., Dodd, A. N., Webb, A. a. R. & Tester, M. 2008. NaCl-induced changes in cytosolic free Ca2+ in Arabidopsis thaliana are heterogeneous and modified by external ionic composition. *Plant, Cell & Environment,* 31**,** 1063-1073.

Tripathi, N. K. 2016. Production and Purification of Recombinant Proteins from Escherichia coli. *ChemBioEng Reviews,* 3**,** 116-133.

Trusov, Y., Chakravorty, D. & Botella, J. R. 2012. Diversity of heterotrimeric G-protein γ subunits in plants. *BMC Research Notes,* 5**,** 608.

Trusov, Y., Zhang, W., Assmann, S. M. & Botella, J. R. 2008. Gγ1+Gγ2 ≠ Gβ: heterotrimeric G protein Gγ-deficient mutants do not recapitulate all phenotypes of Gβ-deficient mutants. *Plant Physiol,* 147.

Tsay, Y.-F., Schroeder, J. I., Feldmann, K. A. & Crawford, N. M. 1993. The herbicide sensitivity gene CHL1 of arabidopsis encodes a nitrate-inducible nitrate transporter. *Cell,* 72**,** 705-713.

Tsuboi, T., Takeo, S., Iriko, H., Jin, L., Tsuchimochi, M., Matsuda, S., Han, E.-T., Otsuki, H., Kaneko, O., Sattabongkot, J., Udomsangpetch, R., Sawasaki, T., Torii, M. & Endo, Y. 2008. Wheat germ cell-free system-based production of malaria proteins for discovery of novel vaccine candidates. *Infection and immunity,* 76**,** 1702-1708.

Tuteja, N. 2007. Abscisic Acid and Abiotic Stress Signaling. *Plant Signaling & Behavior,* 2**,** 135-138.

Ueda, T., Uemura, T., Nakano, A. & Suda, Y. 2014. Dynamic Behavior of the trans-Golgi Network in Root Tissues of Arabidopsis Revealed by Super-Resolution Live Imaging. *Plant and Cell Physiology,* 55**,** 694-703.

Ueguchi-Tanaka, M., Fujisawa, Y., Kobayashi, M., Ashikari, M., Iwasaki, Y., Kitano, H. & Matsuoka, M. 2000. Rice dwarf mutant d1, which is defective in the α subunit of the heterotrimeric G protein, affects gibberellin signal transduction. *Proceedings of the National Academy of Sciences,* 97**,** 11638-11643.

Ullah, H. 2003. The beta-Subunit of the Arabidopsis G Protein Negatively Regulates Auxin-Induced Cell Division and Affects Multiple Developmental Processes. *The Plant Cell Online,* 15**,** 393-409.

Ullah, H., Chen, J.-G., Temple, B., Boyes, D. C., Alonso, J. M., Davis, K. R., Ecker, J. R. & Jones, A. M. 2003. The β-Subunit of the Arabidopsis G protein negatively regulates auxin-induced cell division and affects multiple developmental processes. *Plant Cell,* 15.

Ullah, H., Chen, J.-G., Wang, S. & Jones, A. M. 2002. Role of a heterotrimeric G protein in regulation of Arabidopsis seed germination. *Plant Physiology,* 129**,** 897-907.

Ullah, H., Chen, J.-G., Young, J. C., Im, K.-H., Sussman, M. R. & Jones, A. M. 2001. Modulation of Cell Proliferation by Heterotrimeric G Protein in Arabidopsis. *Science,* 292**,** 2066-2069.

Urano, D., Chen, J. G., Botella, J. R. & Jones, A. M. 2013. Heterotrimeric G protein signalling in the plant kingdom. *Open Biol,* 3**,** 120186.

Urano, D., Miura, K., Wu, Q., Iwasaki, Y., Jackson, D. & Jones, A. M. 2016. Plant Morphology of Heterotrimeric G Protein Mutants. *Plant Cell Physiol,* 57**,** 437-45.

Urano, D., Phan, N., Jones, J. C., Yang, J., Huang, J., Grigston, J., Philip Taylor, J. & Jones, A. M. 2012. Endocytosis of the seven-transmembrane RGS1 protein activates G-protein-coupled signalling in Arabidopsis. *Nature Cell Biology,* 14**,** 1079-1088.

Utsunomiya, Y., Samejima, C., Fujisawa, Y., Kato, H. & Iwasaki, Y. 2012. Rice transgenic plants with suppressed expression of the beta subunit of the heterotrimeric G protein. *Plant Signal Behav,* 7**,** 443-6.

Utsunomiya, Y., Samejima, C., Takayanagi, Y., Izawa, Y., Yoshida, T., Sawada, Y., Fujisawa, Y., Kato, H. & Iwasaki, Y. 2011. Suppression of the rice heterotrimeric G protein beta-subunit gene, RGB1, causes dwarfism and browning of internodes and lamina joint regions. *Plant J,* 67**,** 907-16.

Vahisalu, T., Kollist, H., Wang, Y.-F., Nishimura, N., Chan, W.-Y., Valerio, G., Lamminmäki, A., Brosché, M., Moldau, H. & Desikan, R. 2008. SLAC1 is required for plant guard cell S-type anion channel function in stomatal signalling. *Nature,* 452**,** 487-491.

Valenzuela, S. M., Martin, D. K., Por, S. B., Robbins, J. M., Warton, K., Bootcov, M. R., Schofield, P. R., Campbell, T. J. & Breit, S. N. 1997. Molecular Cloning and Expression of a Chloride Ion Channel of Cell Nuclei. *Journal of Biological Chemistry,* 272**,** 12575-12582.

Vandenbussche, F., Verbelen, J. P. & Van Der Straeten, D. 2005. Of light and length: regulation of hypocotyl growth in *Arabidopsis*. *Bioessays,* 27**,** 275-84.

Villa-Komaroff, L., Guttman, N., Baltimore, D. & Lodishi, H. F. 1975. Complete translation of poliovirus RNA in a eukaryotic cell-free system. *Proceedings of the National Academy of Sciences of the United States of America,* 72**,** 4157-4161.

Vitale, A. & Denecke, J. 1999. The Endoplasmic Reticulum—Gateway of the Secretory Pathway. *The Plant Cell,* 11**,** 615-628.

Vivian-Smith, A. & Koltunow, A. M. 1999. Genetic analysis of growth-regulator-induced parthenocarpy in *Arabidopsis*. *Plant Physiology,* 121**,** 437-452.

Waadt, R., Köster, P., Andrés, Z., Waadt, C., Bradamante, G., Lampou, K., Kudla, J. & Schumacher, K. 2020. Dual-reporting transcriptionally linked genetically encoded fluorescent indicators resolve the spatiotemporal coordination of cytosolic abscisic acid and second messenger dynamics in Arabidopsis. *The Plant Cell***,** tpc.00892.2019.

Waadt, R., Krebs, M., Kudla, J. & Schumacher, K. 2017. Multiparameter imaging of calcium and abscisic acid and high-resolution quantitative calcium measurements using R-GECO1-mTurquoise in Arabidopsis. *New Phytologist,* 216**,** 303-320.

Waadt, R., Schmidt, L. K., Lohse, M., Hashimoto, K., Bock, R. & Kudla, J. 2008. Multicolor bimolecular fluorescence complementation reveals simultaneous formation of alternative CBL/CIPK complexes in planta. *Plant J,* 56**,** 505-16.

Walch-Liu, P., Neumann, G., Bangerth, F. & Engels, C. 2000. Rapid effects of nitrogen form on leaf morphogenesis in tobacco. *Journal of Experimental Botany,* 51**,** 227-237.

Walter, M., Chaban, C., Schütze, K., Batistic, O., Weckermann, K., Näke, C., Blazevic, D., Grefen, C., Schumacher, K., Oecking, C., Harter, K. & Kudla, J. 2004. Visualization of protein interactions in living plant cells using bimolecular fluorescence complementation. *The Plant Journal,* 40**,** 428-438.

Walter, P. 1989. The Membranes of a Eukaryotic Cell. *American Zoologist,* 29**,** 501-510.

Wang, D., Liu, J., Li, C., Kang, H., Wang, Y., Tan, X., Liu, M., Deng, Y., Wang, Z., Liu, Y., Zhang, D., Xiao, Y. & Wang, G. L. 2016. Genome-wide Association Mapping of Cold Tolerance Genes at the Seedling Stage in Rice. *Rice (N Y),* 9**,** 61.

Wang, L., Xu, Y. Y., Ma, Q. B., Li, D., Xu, Z. H. & Chong, K. 2006. Heterotrimeric G protein alpha subunit is involved in rice brassinosteroid response. *Cell Res,* 16**,** 916-22.

Wang, Q., Guan, Y., Wu, Y., Chen, H., Chen, F. & Chu, C. 2008a. Overexpression of a rice OsDREB1F gene increases salt, drought, and low temperature tolerance in both Arabidopsis and rice. *Plant Molecular Biology,* 67**,** 589-602.

Wang, S., Assmann, S. M. & Fedoroff, N. V. 2008b. Characterization of the Arabidopsis heterotrimeric G protein. *J Biol Chem,* 283**,** 13913-22.

Wang, S., Narendra, S. & Fedoroff, N. 2007. Heterotrimeric G protein signaling in the Arabidopsis unfolded protein response. *Proc Natl Acad Sci U S A,* 104**,** 3817-22.

Wang, X.-Q., Ullah, H., Jones, A. M. & Assmann, S. M. 2001. G protein regulation of ion channels and abscisic acid signaling in Arabidopsis guard cells. *Science,* 292**,** 2070-2072.

Wang, Y., Xu, L., Pasek, D. A., Gillespie, D. & Meissner, G. 2005. Probing the role of negatively charged amino acid residues in ion permeation of skeletal muscle ryanodine receptor. *Biophysical journal,* 89**,** 256-265.

Warton, K., Tonini, R., Fairlie, W. D., Matthews, J. M., Valenzuela, S. M., Qiu, M. R., Wu, W. M., Pankhurst, S., Bauskin, A. R., Harrop, S. J., Campbell, T. J., Curmi, P. M. G., Breit, S. N. & Mazzanti, M. 2002. Recombinant CLIC1 (NCC27) Assembles in Lipid Bilayers via a pH-dependent Two-state Process to Form Chloride Ion Channels with Identical Characteristics to Those Observed in Chinese Hamster Ovary Cells Expressing CLIC1. *Journal of Biological Chemistry,* 277**,** 26003-26011.

Wege, S., De Angeli, A., Droillard, M.-J., Kroniewicz, L., Merlot, S., Cornu, D., Gambale, F., Martinoia, E., Barbier-Brygoo, H., Thomine, S., Leonhardt, N. & Filleur, S. 2014. Phosphorylation of the vacuolar anion exchanger AtCLCa is required for the stomatal response to abscisic acid. *Science Signaling,* 7**,** ra65-ra65.

Wei, N. & Deng, X. W. 1996. The Role of the COP/DET/FUS Genes in Light Control of Arabidopsis Seedling Development. *Plant Physiology,* 112**,** 871-878.

Weiss, C. A., Garnaat, C. W., Mukai, K., Hu, Y. & Ma, H. 1994. Isolation of cDNAs encoding guanine nucleotide-binding protein β-subunit homologues from maize (ZGB1) and Arabidopsis (AGB1). *Proc. Natl. Acad. Sci,* 91**,** 9554-9558.

Wen, Z. & Kaiser, B. N. 2018. Unraveling the Functional Role of NPF6 Transporters. *Frontiers in Plant Science,* 9.

White, P. J. & Broadley, M. R. 2001. Chloride in Soils and its Uptake and Movement within the Plant: A Review. *Annals of Botany,* 88**,** 967-988.

Wilkins, K. A., Matthus, E., Swarbreck, S. M. & Davies, J. M. 2016. Calcium-Mediated Abiotic Stress Signaling in Roots. *Front Plant Sci,* 7**,** 1296.

Wingfield, P. T. 2015. Overview of the purification of recombinant proteins. *Current protocols in protein science,* 80**,** 6.1.1-6.1.35.

Woloszynska, M., Gagliardi, O., Vandenbussche, F., De Groeve, S., Alonso Baez, L., Neyt, P., Le Gall, S., Fung, J., Mas, P., Van Der Straeten, D. & Van Lijsebettens, M. 2018. The Elongator complex regulates hypocotyl growth in darkness and during photomorphogenesis. *Journal of Cell Science,* 131**,** jcs203927.

Wong, N. 2014. *Is there a conserved function for the GTG/GPHR family of membrane proteins?* , University of Southampton.

Worden, N., Park, E. & Drakakaki, G. 2012. Trans-Golgi Network—An Intersection of Trafficking Cell Wall ComponentsF. *Journal of Integrative Plant Biology,* 54**,** 875-886.

Wu, H., Carvalho, P. & Voeltz, G. K. 2018. Here, there, and everywhere: The importance of ER membrane contact sites. *Science,* 361**,** eaan5835.

Wu, M. M., Grabe, M., Adams, S., Tsien, R. Y., Moore, H.-P. H. & Machen, T. E. 2001. Mechanisms of pH Regulation in the Regulated Secretory Pathway. *Journal of Biological Chemistry,* 276**,** 33027-33035.

Wu, Y., Xu, X., Li, S., Liu, T., Ma, L. & Shang, Z. 2007. Heterotrimeric G-protein participation in Arabidopsis pollen germination through modulation of a plasmamembrane hyperpolarization-activated Ca2+-permeable channel. *New Phytol,* 176**,** 550-9.

Wurm, F. M. 2004. Production of recombinant protein therapeutics in cultivated mammalian cells. *Nature Biotechnology,* 22**,** 1393-1398.

Xing, S., Wallmeroth, N., Berendzen, K. W. & Grefen, C. 2016. Techniques for the Analysis of Protein-Protein Interactions in Vivo. *Plant Physiology,* 171**,** 727-758.

Xiong, X., Xu, D., Yang, Z., Huang, H. & Cui, X. 2013. A single amino-acid substitution at lysine 40 of an *Arabidopsis thaliana* α-tubulin causes extensive cell proliferation and expansion defects. *Journal of Integrative Plant Biology,* 55**,** 209-220.

Xu, C., Bailly-Maitre, B. & Reed, J. C. 2005. Endoplasmic reticulum stress: cell life and death decisions. *The Journal of clinical investigation,* 115**,** 2656-2664.

Yadav, R. B., Burgos, P., Parker, A. W., Iadevaia, V., Proud, C. G., Allen, R. A., O'connell, J. P., Jeshtadi, A., Stubbs, C. D. & Botchway, S. W. 2013. mTOR direct interactions with Rheb-GTPase and raptor: sub-cellular localization using fluorescence lifetime imaging. *BMC Cell Biology,* 14**,** 3.

Yadav, S. K. 2010. Cold stress tolerance mechanisms in plants. A review. *Agronomy for Sustainable Development,* 30**,** 515-527.

Yamada, K., Nagano, A. J., Ogasawara, K., Hara-Nishimura, I. & Nishimura, M. 2009. The ER body, a new organelle in Arabidopsis thaliana, requires NAI2 for its formation and accumulates specific beta-glucosidases. *Plant signaling & behavior,* 4**,** 849-852.

Yang, A., Dai, X. & Zhang, W. H. 2012. A R2R3-type MYB gene, OsMYB2, is involved in salt, cold, and dehydration tolerance in rice. *J Exp Bot,* 63**,** 2541-56.

Ying-Hua, D., Ya-Li, Z., Shen, Q.-R. & Song-Wei, W. 2006. Nitrate effect on rice growth and nitrogen absorption and assimilation at different growth stages. *Pedosphere,* 16**,** 707-717.

Yoshida, H. & Nagato, Y. 2011. Flower development in rice. *Journal of Experimental Botany,* 62**,** 4719-4730.

Yu, J., Wang, J., Lin, W., Li, S., Li, H., Zhou, J., Ni, P., Dong, W., Hu, S., Zeng, C., Zhang, J., Zhang, Y., Li, R., Xu, Z., Li, S., Li, X., Zheng, H., Cong, L., Lin, L., Yin, J., Geng, J., Li, G., Shi, J., Liu, J., Lv, H., Li, J., Wang, J., Deng, Y., Ran, L., Shi, X., Wang, X., Wu, Q., Li, C., Ren, X., Wang, J., Wang, X., Li, D., Liu, D., Zhang, X., Ji, Z., Zhao, W., Sun, Y., Zhang, Z., Bao, J., Han, Y., Dong, L., Ji, J., Chen, P., Wu, S., Liu, J., Xiao, Y., Bu, D., Tan, J., Yang, L., Ye, C., Zhang, J., Xu, J., Zhou, Y., Yu, Y., Zhang, B., Zhuang, S., Wei, H., Liu, B., Lei, M., Yu, H., Li, Y., Xu, H., Wei, S., He, X., Fang, L., Zhang, Z., Zhang, Y., Huang, X., Su, Z., Tong, W., Li, J., Tong, Z., Li, S., Ye, J., Wang, L., Fang, L., Lei, T., Chen, C., Chen, H., Xu, Z., Li, H., Huang, H., Zhang, F., Xu, H., Li, N., Zhao, C., Li, S., Dong, L., Huang, Y., Li, L., Xi, Y., Qi, Q., Li, W., Zhang, B., Hu, W., et al. 2005. The Genomes of Oryza sativa: A History of Duplications. *PLOS Biology,* 3**,** e38.

Yu, Y. & Assmann, S. M. 2015. The heterotrimeric G-protein beta subunit, AGB1, plays multiple roles in the Arabidopsis salinity response. *Plant Cell Environ,* 38**,** 2143-56.

Zakharian, E. 2013. Recording of Ion Channel Activity in Planar Lipid Bilayer Experiments. *Methods in molecular biology (Clifton, N.J.),* 998**,** 109-118.

Zeiger, L. T. a. E. 2006. *Plant Physiology*, Sinaurer Associates, Inc.

Zemella, A., Thoring, L., Hoffmeister, C. & Kubick, S. 2015. Cell-Free Protein Synthesis: Pros and Cons of Prokaryotic and Eukaryotic Systems. *ChemBioChem,* 16**,** 2420-2431.

Zhang, G. F. & Staehelin, L. A. 1992. Functional Compartmentation of the Golgi Apparatus of Plant Cells Immunocytochemical Analysis of High-Pressure Frozen-and Freeze-Substituted Sycamore Maple Suspension Culture Cells. *Plant physiology,* 99**,** 1070-1083.

Zhang, H. & Forde, B. G. 2000. Regulation of Arabidopsis root development by nitrate availability. *J Exp Bot,* 51**,** 51-9.

Zhang, H., Gao, Z., Zheng, X. & Zhang, Z. 2012. The role of G-proteins in plant immunity. *Plant Signal Behav,* 7**,** 1284-8.

Zhang, H., Zhao, F.-G., Tang, R.-J., Yu, Y., Song, J., Wang, Y., Li, L. & Luan, S. 2017. Two tonoplast MATE proteins function as turgor-regulating chloride channels in Arabidopsis. *Proceedings of the National Academy of Sciences,* 114**,** E2036-E2045.

Zhang, L., Guo, X., Qin, Y., Feng, B., Wu, Y., He, Y., Wang, A. & Zhu, J. 2020. The chilling tolerance divergence 1 protein confers cold stress tolerance in processing tomato. *Plant Physiology and Biochemistry,* 151**,** 34-46.

Zhang, L., Hu, G., Cheng, Y. & Huang, J. 2008. Heterotrimeric G protein alpha and beta subunits antagonistically modulate stomatal density in Arabidopsis thaliana. *Dev Biol,* 324**,** 68-75.

Zhang, M., Ye, J., Xu, Q., Feng, Y., Yuan, X., Yu, H., Wang, Y., Wei, X. & Yang, Y. 2018a. Genome-wide association study of cold tolerance of Chinese indica rice varieties at the bud burst stage. *Plant Cell Reports,* 37**,** 529-539.

Zhang, Q., Chen, Q., Wang, S., Hong, Y. & Wang, Z. 2014. Rice and cold stress: methods for its evaluation and summary of cold tolerance-related quantitative trait loci. *Rice (New York, N.Y.),* 7**,** 24-24.

Zhang, Q., Jiang, N., Wang, G.-L., Hong, Y. & Wang, Z. 2013. Advances in Understanding Cold Sensing and the Cold-Responsive Network *Adv Crop Sci Tech,* 1.

Zhang, T., Xu, P., Wang, W., Wang, S., Caruana, J. C., Yang, H.-Q. & Lian, H. 2018b. *Arabidopsis* G-protein β subunit AGB1 interacts with BES1 to regulate brassinosteroid signaling and cell elongation. *Frontiers in plant science,* 8**,** 2225-2225.

Zhang, Y., Chen, C., Jin, X.-F., Xiong, A.-S., Peng, R.-H., Hong, Y.-H., Yao, Q.-H. & Chen, J.-M. 2009. Expression of a rice DREB1 gene, OsDREB1D, enhances cold and high-salt tolerance in transgenic Arabidopsis. *BMB reports***,** 486-492.

Zhao, J., Barkla, B. J., Marshall, J., Pittman, J. K. & Hirschi, K. D. 2008a. The *Arabidopsis cax3* mutants display altered salt tolerance, pH sensitivity and reduced plasma membrane H^+-ATPase activity. *Planta,* 227**,** 659-669.

Zhao, J., Qin, J.-J., Song, Q., Sun, C.-Q. & Liu, F.-X. 2016. Combining QTL mapping and expression profile analysis to identify candidate genes of cold tolerance from Dongxiang common wild rice (Oryza rufipogon Griff.). *Journal of Integrative Agriculture,* 15**,** 1933-1943.

Zhao, J. & Wang, X. 2004. Arabidopsis Phospholipase Dα1 Interacts with the Heterotrimeric G-protein α-Subunit through a Motif Analogous to the DRY Motif in G-protein-coupled Receptors. *Journal of Biological Chemistry,* 279**,** 1794-1800.

Zhao, X.-Q., Wang, W.-S., Zhang, F., Zhang, T., Zhao, W., Fu, B.-Y. & Li, Z.-K. 2013. Temporal profiling of primary metabolites under chilling stress and its association with seedling chilling tolerance of rice (Oryza sativa L.). *Rice (New York, N.Y.),* 6**,** 23-23.

Zhao, Y., Inayat, S., Dikin, D. A., Singer, J. H., Ruoff, R. S. & Troy, J. B. 2008b. Patch clamp technique: Review of the current state of the art and potential contributions from nanoengineering. *Proceedings of the Institution of Mechanical Engineers, Part N: Journal of Nanoengineering and Nanosystems,* 222**,** 1-11.

Zhou, J.-J. & Luo, J. 2018. The PIN-FORMED Auxin Efflux Carriers in Plants. *International journal of molecular sciences,* 19**,** 2759.

Zhu, H., Li, G. J., Ding, L., Cui, X., Berg, H., Assmann, S. M. & Xia, Y. 2009. Arabidopsis extra large G-protein 2 (XLG2) interacts with the Gbeta subunit of heterotrimeric G protein and functions in disease resistance. *Mol Plant,* 2**,** 513-25.

Zhu, J., Ren, Y., Wang, Y., Liu, F., Teng, X., Zhang, Y., Duan, E., Wu, M., Zhong, M., Hao, Y., Zhu, X., Lei, J., Wang, Y., Yu, Y., Pan, T., Bao, Y., Wang, Y. & Wan, J. 2019. OsNHX5-mediated pH homeostasis is required for post-Golgi trafficking of seed storage proteins in rice endosperm cells. *BMC Plant Biology,* 19**,** 295.

Zhu, J. K. 2016. Abiotic Stress Signaling and Responses in Plants. *Cell,* 167**,** 313-324.

Zonia, L., Cordeiro, S., Tupý, J. & Feijó, J. A. 2002. Oscillatory chloride efflux at the pollen tube apex has a role in growth and cell volume regulation and is targeted by inositol 3,4,5,6-tetra*kis*phosphate. *The Plant Cell,* 14**,** 2233.